

Durham E-Theses

Modelling, dynamics and control of a permanent magnet generator for wind power applications.

Westlake, Alexander

How to cite:

Westlake, Alexander (1996) *Modelling, dynamics and control of a permanent magnet generator for wind power applications.*, Durham theses, Durham University. Available at Durham E-Theses Online:
<http://etheses.dur.ac.uk/1642/>

Use policy

The full-text may be used and/or reproduced, and given to third parties in any format or medium, without prior permission or charge, for personal research or study, educational, or not-for-profit purposes provided that:

- a full bibliographic reference is made to the original source
- a [link](#) is made to the metadata record in Durham E-Theses
- the full-text is not changed in any way

The full-text must not be sold in any format or medium without the formal permission of the copyright holders.

Please consult the [full Durham E-Theses policy](#) for further details.

Academic Support Office, Durham University, University Office, Old Elvet, Durham DH1 3HP
e-mail: e-theses.admin@dur.ac.uk Tel: +44 0191 334 6107
<http://etheses.dur.ac.uk>

**Modelling, Dynamics and Control
of a
Permanent Magnet Generator
for
Wind Power Applications**

The copyright of this thesis rests with the author. No quotation from it should be published without the written consent of the author and information derived from it should be acknowledged.

Alexander Westlake

B.Sc. (Dunelm)

School of Engineering
University of Durham



A thesis submitted in partial fulfilment of the requirements
of the Council of the University of Durham for the Degree
of Doctor of Philosophy (Ph.D.).

April 1996

23 JAN 1998

Declaration

I hereby declare that this thesis is a record of work undertaken by myself, that it has not been the subject of any previous application for a degree, and that all sources of information have been duly acknowledged.

© Copyright 1996, Univesity of Durham

The copyright of this thesis rests with the University of Durham. No quotation from it should be published without the written consent of the University of Durham, and information derived from it should be acknowledged.

Abstract

This thesis describes the modelling, simulation and performance assessment of a novel multi-pole, permanent magnet, synchronous generator that goes some way to reducing both the cost and the noise of wind turbine generation. The small pole pitch of the permanent magnet generator allows 50 Hz a.c. voltages to be generated at low rotational speeds. This low speed operation enables the generator to be connected directly to the wind turbine thereby eliminating the need for the usual gearbox.

Two modes of operation typically exist for the operation of grid connected wind turbines: fixed speed and variable speed operation. Both modes are discussed and detailed simulation models developed in the thesis. The associated design interactions and constraints are analysed for each mode to produce an effective method for designing such direct drive generating systems.

Once the optimum design criteria have been established, a range of generators with ratings from 200 kW to 1.5 MW for fixed and variable speed operation are designed. Cost comparisons are carried out to establish which mode of operation is best suited to the direct drive, permanent magnet, synchronous generator. The thesis concludes that the fixed speed operation of the multi-pole, permanent magnet, synchronous generator leads to designs with considerable cost reductions and performance improvements over the conventional induction generator and gearbox arrangement but does not lead to weight reductions. Furthermore the variable speed operation of such a generator would also lead to cost, weight and performance improvements over the variable speed operated induction generator and gearbox arrangement. The question as to whether variable speed operation of the permanent magnet generator is better than the fixed speed case is partially answered in terms of the weight and performance advantages of the variable speed design. However the cost advantage is difficult to quantify due to the uncertainties over the price of the IGBT technology chosen for the switching devices of the inverter.

This thesis is dedicated to my family and friends.

Acknowledgments

Firstly I would like to acknowledge the assistance, support and encouragement provided by my supervisors Dr. J.R. Bumby and Prof. E. Spooner.

Thanks must then be given to Dr. G. Catto and Dr. A.C. Williamson for accommodating me during several visits to UMIST and letting me carry out some experiments on their test rig which were very useful in increasing both my understanding of permanent magnet generators and in validating my simulation models.

Finally special mention must be made to thank Dave Grey for letting me bounce ideas off him, John Glover for knowing far more about UNIX than I ever will and Steve Robinson and Martin Bradley for providing both the entertainment and some useful advice.

Contents

Abstract	i
Dedication	ii
Acknowledgments	iii
Contents	iv
List of Figures	xiii
List of Tables	xxi
Abbreviations	xxii
1 Introduction	1
1.1 The emergence of wind power as an economic renewable	2
1.1.1 Why invest in renewables over conventional power plant?	3
1.1.2 Comparison of the renewable technologies for electricity generation .	9
1.1.3 Current Status and future trends in wind power	11
1.2 The history of wind turbine development	12
1.2.1 Horizontal (HAWT) versus vertical axis wind Turbines (VAWT) . .	12
1.2.2 Blade design: material, number, diameter, pitchable, orientation . .	14
1.2.3 Synchronous or Induction Generator	15
1.2.4 Sizing and siting	16
1.2.5 Control Strategies	16
1.2.6 Tower design	18
1.2.7 The definitive design	19
1.3 The Aim of this thesis	19

1.4	The Design of Permanent Magnet Generators	21
1.4.1	Modular Stator Construction	23
1.4.2	Damping requirements of a multi-pole, permanent magnet, synchronous generator	23
1.4.3	Further design implications of removing the gearbox from the wind turbine drive train	24
1.5	Thesis Outline	25
2	Wind Turbine Modelling	27
2.1	Wind distribution near ground level	29
2.1.1	Yearly distribution modelling and energy capture prediction	29
2.1.2	Typical performance characteristic	30
2.1.3	Turbulent timescale wind modelling	31
2.1.4	Discrete model of the turbulent wind	33
2.1.5	MATLAB with SIMULINK	34
2.1.6	SIMULINK implementation of the discrete point wind speed model	34
2.1.7	Spectral model of the turbulent wind	35
2.1.8	Validation of the point wind speed and spectral methods against measured wind data	39
2.2	Wind Turbine Aerodynamics	40
2.2.1	Power from the wind calculation	42
2.2.2	Induction Lag	43
2.2.3	Additional effects to include in the discrete wind speed method	44
2.2.4	Overall SIMULINK implementation for the discrete wind speed method	46
2.2.5	Additions to the spectral method	46
2.2.6	Complete Wind Spectrum Model	51
2.2.7	Implementation and comparison of the methods to model the wind interaction with the blades	52
2.2.8	Choice of wind model	57
2.3	Power Limiting Methods	57
2.3.1	Typical Pitch Actuators	58
2.3.2	Modelling Pitch Actuators	59
2.3.3	The Pitch Controller	60

2.4	The full wind turbine model	61
2.4.1	Implementation on Simulink	61
2.5	Pitch controller design and validation	62
2.5.1	Simplified transfer function representation	63
2.5.2	PI controller values	64
2.5.3	PI controller performance	64
2.5.4	Validation against the measured power curve of a Vestas 500 kW turbine	66
2.5.5	Implications of pitch control	66
2.6	Concluding remarks	67
3	Permanent Magnet Synchronous Generator: Design, Modelling and simulation validation	68
3.1	The Permanent Magnet Generator	69
3.1.1	Physical Description of a Three Phase Synchronous Generator . . .	70
3.1.2	The development of a multi-pole, permanent magnet, synchronous generator	72
3.1.3	Ferrimagnetism and achievable multi-pole, synchronous generator rotor designs	72
3.1.4	Rotor construction and design	76
3.1.5	Modular Stator Construction	77
3.1.6	Generator magnetic circuit analysis	77
3.1.7	Generator magnetic and electrical operation	78
3.1.8	Compliant Mounting	81
3.2	The Generator Parameters	84
3.2.1	Overall design procedure	84
3.2.2	WINDGEN2 - A fixed speed permanent magnet design suite	85
3.2.3	Tier Number	85
3.2.4	Overall Values for a 455 kW rated generator	86
3.2.5	Per Unit System	86
3.2.6	Implementation on EXCEL	87
3.3	Full Permanent Magnet Generator Model	89
3.3.1	Electrical Behaviour - Five Winding Model	90
3.3.2	Conversion to modelling the Permanent Magnet Generator	92

3.3.3	Synchronous generator connected to an infinite bus system	93
3.3.4	Development of the simulation model of the permanent magnet generator	95
3.4	Methods of Analysis	96
3.4.1	Non-Linear Simulation	97
3.4.2	The theory behind linearisation	100
3.5	Preliminary results for the 455 kW rated generator	101
3.5.1	Eigenvalues	102
3.5.2	Stator results	102
3.5.3	Rotor results	104
3.5.4	Axis current results	105
3.6	Permanent Magnet Model Validation and practical implementation	106
3.6.1	The Test Rig	107
3.6.2	Parameter measurement for the 750 VA, 400 VA and 2.75 kVA generators and DC motor	109
3.6.3	Modelling Methodology	110
3.6.4	Step Response of the 750 VA testrig	112
3.6.5	Synchronisation transients of the 750 VA testrig with a 2mm airgap	113
3.6.6	Synchronisation of the 2.75 kW generator	117
3.6.7	Parameter validation for a modular constructed generator	118
3.6.8	Final comments on validation results	119
3.7	Conclusions	119
4	Performance of the Fixed Speed Permanent Magnet Generator	120
4.1	Basic performance of a 455 kW generator	121
4.1.1	Method of attack	121
4.1.2	The General Behaviour of the Compliant Mounting	121
4.1.3	The choice of design values for k and c	125
4.2	Design Constraints with parameter variation	127
4.2.1	Variation with generator ratings	127
4.2.2	Damping coefficient and Spring Stiffness	128
4.2.3	Effect of varying the number of tiers	128
4.2.4	Key design interactions as generator rating varies	129

4.2.5	Concluding remarks	130
4.3	Synchronisation of a 455 kW generator	131
4.3.1	Synchronisation of a 455 kW wind turbine in windy conditions . . .	136
4.4	Response of the 455 kW rated generator to simulated wind data	138
4.4.1	Below to above rated wind speed operation - power limiting	139
4.4.2	Above rated wind speed performance	142
4.4.3	Cut out performance	144
4.4.4	Wind turbine performance with a stiff stator	146
4.4.5	Wind turbine performance with low damping ratio, ζ	148
4.5	Conclusions	150
5	Modelling a Variable Speed Wind Turbine	151
5.1	The advantages of variable speed operation	152
5.1.1	Energy capture from variable speed control	153
5.1.2	Power Quality	155
5.1.3	Generator design	155
5.1.4	Further advantages	158
5.2	Realising the advantages of variable speed operation	158
5.2.1	Tracking the C_p curve for C_{pmax}	159
5.2.2	Power flow control	160
5.3	Variable Speed Wind Turbine Modelling	161
5.3.1	Variable speed wind turbine model library	161
5.3.2	Modelling aims and method of attack	162
5.3.3	Wind Turbine Modelling	163
5.3.4	Rectifier Theory	163
5.3.5	Generator and capacitor compensated rectifier theory	165
5.3.6	Generator and rectifier combined model	169
5.3.7	Deriving the C_{pmax} tracking control law	173
5.3.8	DC link modelling	176
5.3.9	Inverter configurations	177
5.3.10	Inverter modelling	178
5.3.11	Harmonic output and voltage control	180
5.3.12	Overall inverter to grid representation	183

5.3.13	Implementation on Simulink	187
5.4	The parameters of the variable speed system	190
5.4.1	Overall design procedure	191
5.4.2	WINDVARD, WINDVARP, WINDVOUT - A variable speed permanent magnet design suite	192
5.4.3	Tier Number	193
5.4.4	The choice of dc link capacitance	193
5.4.5	Variation with generator ratings	194
5.4.6	Data post-processing	194
5.5	Further control issues for a variable speed wind generator	196
5.5.1	Reactive power control for an embedded generator	196
5.5.2	Further control issues in variable speed operation	198
5.5.3	Overall proposed control scheme	201
5.6	Concluding remarks	202
6	Variable Speed Results	203
6.1	Tracking C_{pmax} with the control ratio, K_{Vdc} , constant	205
6.1.1	Control scheme	205
6.1.2	Step response with no control of the control ratio, K_{Vdc}	206
6.1.3	Best values for PI controller	211
6.1.4	Discussion	212
6.2	Tracking C_{pmax} with K_{Vdc} constant and V_{dc} limited to 1100 Volts	213
6.2.1	Step response with no control of the control ratio, K_{Vdc}	213
6.3	Maintaining V_1 constant as V_{dc} varies	214
6.3.1	Control Scheme	215
6.3.2	Controlling K_{Vdc} to keep $V(1)$ constant	215
6.3.3	Discussion	218
6.4	Maintaining Q constant as V_{dc} varies	218
6.4.1	Control scheme to include a reactive power setpoint	218
6.4.2	Constant Q results	219
6.5	The effect of pitch action on variable speed operation	219
6.5.1	Suitable pitch control for variable speed operation	220
6.5.2	Step up and step down result	220

6.6	Response of the 458 kW rated generator to simulated wind data	221
6.6.1	Below rated wind speed response	222
6.6.2	Below to above rated wind speed response	227
6.6.3	Above rated wind speed results	231
6.6.4	Cut-out wind speed results	234
6.6.5	Capacitance variation	237
6.7	Conclusions	238
7	Comparison between fixed and variable speed operation of the permanent magnet generator	240
7.1	A comparison of energy capture	241
7.1.1	Application to yearly energy delivered to the grid	244
7.1.2	Discussion	244
7.2	The grid connection performance comparison	245
7.2.1	Reactive power flow for simulated wind speed of AMWS 9 m/s . . .	245
7.2.2	Real power quality for simulated wind speed of AMWS 9 m/s	246
7.2.3	Voltage regulation for simulated wind speed of AMWS 9 m/s	247
7.3	Comparison of design values and cost	248
7.3.1	Comparison of generator weight	248
7.3.2	Comparison of resulting capital cost	249
7.4	Comparison against the gearbox and induction generator configuration . . .	250
7.4.1	Induction generator plus gearbox model	250
7.4.2	Induction generator plus gearbox performance	253
7.4.3	Comparison of the transient performance	256
7.4.4	Comparison on weight, cost and reliability	258
7.5	Design comparison of the fixed and variable speed wind turbines	261
7.5.1	Fixed speed operation	261
7.5.2	Variable speed operation	262
7.6	Conclusions	263
8	Conclusions and further work	264
8.1	Chapter summary and key conclusions	264
8.1.1	Key conclusions	268
8.2	Suggestions for further work	268

8.2.1	Enhancements to the wind turbine model	269
8.2.2	Fixed speed operation	270
8.2.3	Variable speed operation	270
8.3	Original contribution	271
8.3.1	Wind Modelling	271
8.3.2	Fixed speed generator modelling and performance	271
8.3.3	Wind turbine driving the fixed speed, permanent magnet, generator model	272
8.3.4	Variable speed wind generator modelling and performance	272
8.4	Benefits and final conclusions	272
A	Wind Modelling Equations	282
A.1	Discrete Point Wind Model Equations	282
A.2	Spectral method equations	284
A.2.1	Spectral point wind speed equations	284
A.2.2	Derivation of time domain equivalent of the spatial filter	285
A.2.3	Power in the wind	286
A.2.4	Induction Lag	286
A.2.5	Rotational Sampling	287
B	The derivation of the governing equations of a permanent magnet, syn- chronous generator	289
B.1	Per Units	289
B.1.1	Electrical per units	289
B.1.2	Mechanical per units	290
B.2	Five winding governing equations	291
B.3	Three winding governing equations	292
B.3.1	Derivation of expressions for pi_d and pi_q	293
B.3.2	Electromagnetic Torque	294
B.4	Initial Conditions	295
B.4.1	Initial values of i_d and i_q	295
B.4.2	Initial value of τ_{ag}	297
B.4.3	Initial value of δ_r and δ_s	297

C The theory behind linearisation **298**

 C.1 Linearising the governing equations of a synchronous machine 298

 C.2 Linearising the three winding model 300

D The theory of a variable speed operated generator **302**

 D.1 Power flow by the phasor method 302

 D.2 Time stepping solution of the capacitor compensated E-core and rectifier . 306

E The derivation of the governing equations of an induction generator plus gearbox **308**

 E.1 Governing equations 308

 E.2 Initial conditions 309

List of Figures

1.1	Typical 300 kW turbines (Source: Private Photograph of Ovenden Moor Wind Farm, Uk)	2
1.2	The energy spectrum of wind speed fluctuations in the atmosphere	8
1.3	Typical medium sized horizontal axis wind turbine	13
1.4	Fixed speed wind turbine simulation library	21
1.5	Variable speed wind turbine simulation library	22
1.6	Two Permanent Magnet Generator Designs	22
2.1	The dynamics of a pitch regulated wind turbine	27
2.2	Raleigh Distribution	30
2.3	A Typical Output Power Curve and the Power Coefficient	31
2.4	Rotational sampling of the free wind stream by the rotating blades	32
2.5	Simulation of the Wind	33
2.6	Wind speed time series library	35
2.7	The Von Karman Spectrum and Dryden Approximation for $\bar{U} = 15$, $L = 200$	37
2.8	The Dryden Transfer function block	38
2.9	Generating an effective point wind speed by spectral modelling	38
2.10	Wind histories from point and spectral methods versus real wind data	39
2.11	Spectrum of real wind speed data versus spectral simulation	40
2.12	Wind turbine model library	41
2.13	Evaluating the shaft power from the wind	43
2.14	Induction Lag of a typical wind turbine	43
2.15	Wind Shear for a typical wind turbine	45
2.16	Tower shadow and blade imbalance	46
2.17	Converting the discrete point wind speed to shaft torque	47
2.18	The actual and spatially filtered windspeed	48

2.19	The Effect of Rotational Sampling on the Wind Spectrum	49
2.20	The Model of Rotational Sampling of the Wind Spectrum	50
2.21	The Simulink Model of the spectral Method	52
2.22	The time history of the point windspeed	53
2.23	The induced hub torque without tower shadow	53
2.24	The power spectral density of the induced rotational torque variation	54
2.25	The induced hub torque with tower shadow	55
2.26	The induced hub torque with and without induction lag	55
2.27	The spectral density of the point and spectral methods	56
2.28	The power spectral density of the total hub torque	57
2.29	A typical pitch actuator system	58
2.30	Modelling the actuator dynamics	59
2.31	Pitch demand	60
2.32	Pitch Actuation	61
2.33	The Simulink implementation of a wind turbine modelled using the spectral method	62
2.34	Transfer function of a typical wind turbine	63
2.35	The simulated windspeed and corresponding power spectrum	64
2.36	The aerodynamic torque with and without rotational effects included	65
2.37	The pitch actuator response	66
2.38	The simulated power curve against measured power curve and corresponding pitch action	67
3.1	Typical 4-pole synchronous machine (Source: Synchronous Machines) . . .	70
3.2	Typical B-H curves for two different Nickel-Zinc based ferrites (Source: Elec- tric Machines)	74
3.3	Typical B-H curves for a Barium based ferrite (Source: Electric Machines) .	74
3.4	Rotor and Stator Arrangement	76
3.5	Equivalent Circuit of a Permanent Magnet Generator	78
3.6	Stator phasor diagram for deriving winding connection	80
3.7	Damper windings in Permanent Magnet Generators	81
3.8	Compliant Mounting configurations	82
3.9	The tiered approach	86

3.10	Generator parameter spreadsheet	89
3.11	The $dq0$ frame of reference	90
3.12	The five winding model	91
3.13	The three winding model	92
3.14	Definition of angles	94
3.15	The system configuration	94
3.16	The phasor diagram of the system	95
3.17	A schematic representation of full non-linear simulation	98
3.18	Eigenvalues	102
3.19	The Variation of the High Frequency Eigenvalue as stiffness and damping are varied	103
3.20	The Time Response for the Stator angle for a 1 p.u. step change in input torque	103
3.21	The Variation of the Low Frequency Eigenvalue as stiffness and damping are varied	104
3.22	The time response for the generator power angle, δ , for a 1 p.u. step change in input torque	105
3.23	The variation of the middle frequency eigenvalue as stiffness and damping are varied	106
3.24	Overall Layout of the Test Rig	108
3.25	Electrical Circuit of the system side of the Test Rig	109
3.26	The DC motor model	111
3.27	The full Simulink model of the testrig	111
3.28	Experimental step response of a 750 VA testrig with and without damping .	112
3.29	Eigenvalue analysis of the testrig	113
3.30	Damped and undamped step response of the 750 VA rated generator	113
3.31	Current Transient on synchronisation from $\delta = 40$ degrees, $\dot{\delta} = -6$	115
3.32	Simulated current transient for synchronisation from delta = 180 degrees, DC motor included	115
3.33	Measured current transient for synchronisation from delta = 180 degrees, DC motor included	116
3.34	Simulated current and stator transient for synchronisation from delta = 40 degrees, DC motor included	117

3.35	Simulated and measured current transients for synchronisation from $\delta = 40$ degrees, DC motor included	118
4.1	Mass, spring and damper representation of the generator	122
4.2	The variation of the low and high frequency eigenvalues as stiffness and damping are varied for both the no load and the full load operating condition . .	124
4.3	The time response for the generator power angle and stator angle for a 1 p.u. step change in input torque with the generator initially at no load	125
4.4	Mode 1 and 2 - Variation with tier number	129
4.5	The variation of the key generator parameters with rating	130
4.6	Time response of the stator	131
4.7	The energy transfers during synchronisation	132
4.8	Typical synchronisation transients with spring stiffness $k = 0.5$ p.u. as the damping coefficient is varied for an initial δ of 40 degrees and $d\delta/dt = 22$ rads/s	134
4.9	Synchronisation envelope for constant damping coefficient as spring stiffness is varied	135
4.10	Synchronisation envelope for constant spring stiffness as damping coefficient is varied	136
4.11	Performance on synchronisation of a 455 kW wind turbine	137
4.12	Control action for synchronisation of a 455 kW wind turbine	137
4.13	Simulated wind speed and the corresponding power spectrum	140
4.14	The power coefficient and input torque information	141
4.15	The 455 kW rated generator performance	141
4.16	The pitch controller performance	142
4.17	The real and reactive power flows and voltage regulation	143
4.18	Simulated wind speed and the corresponding power spectrum	143
4.19	The resulting power coefficient and input torque information	144
4.20	The pitch controller performance	145
4.21	Simulated wind speed and the corresponding power spectrum	145
4.22	The pitch controller performance	146
4.23	The resulting power coefficient and input torque information	147
4.24	The 455 kW rated generator performance	147

4.25	The real and reactive power flows and voltage regulation	148
4.26	The 455 kW rated generator performance	149
4.27	The real and reactive power flows and voltage regulation	149
5.1	Variable speed system configuration	152
5.2	C_p versus tip speed ratio for zero degrees blade pitch	153
5.3	Power output versus cumulative hours at that power level	154
5.4	Material Costs versus frequency and control scheme	157
5.5	Constant Windspeed Curves and operational strategies for a variable speed turbine	159
5.6	Variable Speed Modelling Interfaces	160
5.7	Schematic of the variable speed wind turbine model	162
5.8	Modular Electrical Arrangement for the AC/Dc Power Interface	164
5.9	Equivalent Circuit for Capacitance Compensated Rectifier	165
5.10	Current out of the E-core	166
5.11	Current injected into the dc link	167
5.12	Voltage waveform across the tuning capacitance	167
5.13	Current out of the E-core after step down in V_{dc}	168
5.14	Current injected into the dc link after step down in V_{dc}	168
5.15	Voltage waveform across the tuning capacitance after step down in V_{dc} . . .	169
5.16	SIMULINK model for generator rotor equation	170
5.17	SIMULINK model for the injected dc link current	171
5.18	Airgap power as rotor speed varies for constant V_{dc}	172
5.19	Maximum current from the E-core	172
5.20	Mechanical power in as rotor speed varies for constant windspeed	174
5.21	Vdc setpoint versus shaft speed for optimal C_{pmax} tracking	175
5.22	Variable Speed Control Architecture for constant control ratio	176
5.23	DC link SIMULINK model	177
5.24	Equivalent Circuit for Inverter	179
5.25	Potential Waveforms	180
5.26	Voltage Reversals for Selective Harmonic Elimination	182
5.27	Switching angles for the elimination of the 5 th and 7 th harmonics with control of the fundamental by means of voltage reversal	184

5.28	Variation of the 11 th and 13 th harmonics versus control ratio with elimination of the 5 th and 7 th harmonics using three switching angles	185
5.29	Phasor diagram of the inverter connected to the infinite bus	186
5.30	SIMULINK model of the inverter and its controllers	187
5.31	SIMULINK implementation of the V_{dc} setpoint controller	188
5.32	Variable speed wind turbine model	189
5.33	Extended power curves for accurate interpolation	190
5.34	Variable speed generator parameter spreadsheet	195
5.35	Grid Connection Configuration	197
5.36	Power Control Scheme	198
5.37	Maintaining V_{dc} constant during pitch control	200
5.38	V_{dc} control during pitch control	200
5.39	Overall Control Scheme	202
6.1	Step increase and corresponding input torque	206
6.2	The resulting power coefficient and tip speed ratio	207
6.3	Module airgap and mechanical power	208
6.4	The input power, airgap power, rotor speed and dc link voltage	209
6.5	Inverter and dc link current and output power and overall power loss	210
6.6	Measured and dc link setpoint voltage	210
6.7	Reactive Power and voltage regulation	211
6.8	Module airgap and mechanical power	213
6.9	The input power, airgap power, rotor speed and dc link voltage	214
6.10	Response of Q , V_1 and $K_{V_{dc}}$ for step change in wind speed from 8 m/s to 12 m/s	215
6.11	Response of Q , V_1 and $K_{V_{dc}}$ for step change in wind speed from 8 m/s to 12 m/s	217
6.12	Response of Q , V_1 and $K_{V_{dc}}$ for step change in wind speed from 8 m/s to 15 m/s	219
6.13	Response of P_m and P_{ag} for step up then step down in windspeed from 12 to 13 m/s	221
6.14	Simulated wind speed with AMWS of 9 m/s and the corresponding input torque	223

6.15	The resulting power coefficient and tip speed ratio	224
6.16	Module airgap and mechanical power	224
6.17	The input power, airgap power, rotor speed and dc link voltage	225
6.18	Inverter and dc link current and output power and overall power loss	225
6.19	Measured and dc link setpoint voltage	226
6.20	Reactive power and $K_{V_{dc}}$ setpoint	226
6.21	Simulated wind speed with AMWS of 12 m/s and the corresponding input torque	228
6.22	The resulting power coefficient and tip speed ratio	228
6.23	Module airgap and mechanical power	229
6.24	Pitch control and actuator response	230
6.25	Reactive Power and voltage regulation	230
6.26	Simulated wind speed with AMWS of 18 m/s and the corresponding input torque	231
6.27	The resulting power coefficient and tip speed ratio	232
6.28	Module airgap and mechanical power	232
6.29	Pitch control and actuator response	233
6.30	Reactive Power and voltage regulation	233
6.31	Simulated wind speed with AMWS of 25 m/s and the corresponding input torque	234
6.32	The resulting power coefficient and tip speed ratio	235
6.33	Module airgap and mechanical power	235
6.34	Pitch control and actuator response	236
6.35	Reactive Power and voltage regulation	237
6.36	Airgap Transfer Table	239
7.1	Windspeed time history input to the models	241
7.2	The airgap power for the fixed and variable speed case	242
7.3	The loss mechanisms for the fixed and variable speed case	242
7.4	The delivered power for the fixed and variable speed case	243
7.5	Reactive power comparison between fixed and variable speed case for wind speed with AMWS of 9 m/s	246

7.6	Voltage regulation comparison between fixed and variable speed case for wind speed with AMWS of 9 m/s	247
7.7	Weight comparison between the fixed and variable speed case	248
7.8	Cost comparison between the fixed and variable speed case	249
7.9	Induction generator and gearbox model representation	250
7.10	SIMULINK model of the induction generator plus gearbox	252
7.11	SIMULINK model of wind turbine driven induction generator plus gearbox	253
7.12	Induction generator plus gearbox step response	254
7.13	Wind speed and and corresponding power spectra	254
7.14	Power coefficient, aerodynamic torque and corresponding power spectrum	255
7.15	Induction generator slip, low and high speed shaft rotational speeds and tip speed ratio	256
7.16	Mechanical power input, real power out to the grid and power loss	257
7.17	Weight comparison between fixed and variable speed case and industrial standard model	259
7.18	Weight comparison between fixed and variable speed case and industrial standard model	260
A.1	SIMULINK model for the spatial filter	286
A.2	SIMULINK model for the induction lag	287
B.1	The phasor diagram for single wind turbine infinite bus system	296
D.1	Phasor diagram of the E-core and tuning capacitor circuit	303

List of Tables

1.1	Summary of electricity production costs (1992 Estimates)	7
1.2	Summary of electricity production costs (1992 Estimates)	11
1.3	The thesis wind turbine design	20
2.1	Turbulence Intensity	36
2.2	Coefficient values for the rotational sampling effect	51
2.3	Pitch PI controller values	64
3.1	Winding connection arrangement for 455 kW rated generator	80
3.2	The 455 kW Generator Parameters	87
3.3	Test rig parameters	110
3.4	Per unit test rig parameters	110
3.5	Parameter validation	119
4.1	Generator Parameters	128
5.1	Energy capture comparison between fixed and variable speed operation . .	155
5.2	Variable speed generator Parameters	194
6.1	PI controller values for power angle controller	212
6.2	Energy capture analysis for the 458 kW rated variable speed generator . . .	227
6.3	Energy capture analysis for the 458 kW rated variable speed generator . . .	230
6.4	Energy capture analysis for the 458 kW rated variable speed generator . . .	234
6.5	Performance comparison between dc link with a capacitance of 4000 μF versus 8000 μF	237
7.1	A comparison of energy capture	241
7.2	A comparison of delivered energy and revenue	243

7.3 Comparison of yearly energy delivered to the grid and resulting revenues . . 244

7.4 Induction generator plus gearbox values 255

7.5 Comparison of performance in the windy environment 257

7.6 Comparison of yearly energy capture 258

7.7 Comparison of cost versus net present value 260

List of Abbreviations

AMWS	Average mean wind speed
GRE	Glass reinforced epoxy
GRP	Glass reinforced polyester
HAWT	Horizontal Axis Wind Turbine
IGBT	Insulated Gate Bipolar Transistor
MOSFET	Metal Oxide Semiconductor Field Effect Transistor
NdFeB	Neodymium-Iron-Boron
NFFO	Non-fossil Fuel Obligation
NREL	National Renewable Energy Laboratory, USA.
OD	Outer Diameter
PI	Proportional plus Integral
PD	Proportional plus Derivative
PWM	Pulse Width Modulation
SHE	Selective Harmonic Elimination
SPWM	Sinusoidal Pulse Width Modulation
TCHD	Total Current Harmonic Distortion
TSR	Tip Speed Ratio
UMIST	University of Manchester, Institute of Technology
VAWT	Vertical Axis Wind Turbine
WECS	Wind Energy Conversion System

Notation

Throughout the text the following conventions are used,

- All values are in per units except those whose units are specified individually.
- Lower case symbols denote instantaneous values and upper case values indicate r.m.s values for all electrical parameters, i.e. voltages and currents.

WIND TURBINE NOTATION.

A	The swept area of the turbine blades, m^2
A_{1r}	Blade imbalance magnitude, Nm
A_{3r}	Deterministic torque magnitude, Nm
a	Spatial filter coefficient
a_t	Break point of the Von Karman spectrum
a_{3r}	Stochastic torque frequency spread, rads/s
b_t	Gain of the Von Karman spectrum
b_{3r}	Stochastic torque component, Nm
C_p	The power coefficient
C_{pnom}	The power coefficient at nominal wind speed
C_{pmax}	The maximum value of power coefficient at zero blade pitch
D	The diameter of the turbine blades, m
H	Wind turbine hub height above the ground, m
h	Height above the ground, m
i	Turbulence intensity
J	Inertia, $kg\ m^2$
J_{gen}	Generator Inertia, $kg\ m^2$
J_{hub}	Hub Inertia, $kg\ m^2$
J_{in}	Inner Inertia, $kg\ m^2$
J_{out}	Outer Inertia, $kg\ m^2$
J_r	Rotor Inertia, $kg\ m^2$
J_s	Stator Inertia, $kg\ m^2$
K_v	Factor determining the value of $S_u(w)$

L	Turbulent length scale, m
M	Mass, kg
M_b	Blade mass, kg
P_{nom}	Nominal turbine power, Watts
R	Blade radius, m
R_g	Blade radius of gyration, m
$S_u(w)$	Power spectrum describing the free wind stream
T_v	Factor determining the value of $S_u(w)$
U	The mean free stream velocity of the wind, $m\ s^{-1}$
U_H	The wind speed at the hub height, $m\ s^{-1}$
U_m	Annual average wind speed, $m\ s^{-1}$
U_{nom}	Nominal design wind speed, $m\ s^{-1}$
U_w	The rated wind speed of the turbine, $m\ s^{-1}$
W_{AV}	Transfer function of spatial filter
W_{FS}	First order approximation to Von Karman spectrum
α	Factor determining shape of $S_u(w)$
β	Factor determining shape of $S_u(w)$
γ_s	Turbulence decay factor
λ	Spatial filter coefficient
μ	Factor determining shape of $S_u(w)$
ρ	The density of air, $kg\ m^{-3}$
σ_u	The standard deviation of the wind speed, $m\ s^{-1}$
τ	Time decay of induction lag effect, secs
β	Blade pitch angle, degrees

MAGNET SYSTEMS NOTATION.

A_g	Airgap Area, m^2
A_m	Magnet Area, m^2
B	Magnetic flux density, Tesla
B_g	Peak airgap magnetic flux density, Tesla
B_{rem}	Remanent magnetic flux density, Tesla

H	Magnetic field intensity, A/m
l_g	Airgap length, m
l_m	Magnet length, m
q	Leakage factor
R	Rotor radius, m
L	Rotor length, m
$S\hat{E}L$	Peak electric loading, Amps
V_m	Magnet volume, m^3
μ_r	Relative permeability
μ_0	Permeability of free space

FIXED SPEED GENERATOR MODELLING NOTATION.

c	The spring damping of the compliant mounting, per unit
E	The excitation voltage, per unit
En	Kinetic energy relative to synchronous speed, per unit
$En_{k_{syn}}$	Potential energy stored in airgap, per unit
En_k	Potential energy stored in compliant mounting, per unit
$En_{initial}$	Initial energy prior to synchronisation, per unit
H_r	The rotor inertia constant, per unit
H_s	The stator inertia constant, per unit
I	Line current, amps
i_d	The instantaneous d-axis current, per unit
i_f	The field winding current, per unit
i_{kd}	The d-axis damper current, per unit
i_{kq}	The q-axis damper current, per unit
i_q	The instantaneous q-axis current, per unit
$K\phi_f$	The flux generated by the permanent magnets, per unit
k	The spring stiffness of the compliant mounting, per unit
k_{syn}	The synchronising power coefficient, per unit
L_d	The total d-axis inductance to the grid, per unit
L_f	The field winding inductance, per unit

L_{kd}	The d-axis damper winding inductance, per unit
L_{kq}	The q-axis damper winding inductance, per unit
L_q	The total q-axis inductance to the grid, per unit
n_p	The number of pole pairs
p_e	The electrical output power, per unit
p_m	The mechanical input power, per unit
R	The total resistance to the grid, per unit
r	The radius at which spring and damper act, m
r_f	The field winding resistance, per unit
r_{kd}	The d-axis damper resistance, per unit
r_{kq}	The q-axis damper resistance, per unit
r_l	The line resistance, per unit
r_t	The transformer resistance, per unit
V_b	The system voltage, per unit
$v_{d,q,0}$	The $dq0$ -axis voltages, per unit
$v_{a,b,c}$	The abc phase voltage, per unit
X_d	The total d-axis reactance to the grid, per unit
X_q	The total q-axis reactance to the grid, per unit
δ	The generator power angle, $rads$
$\dot{\delta}$	The rate of change of generator power angle, $rads\ s^{-1}$
δ_r	The generator rotor angle, $rads$
$\dot{\delta}_r$	The rate of change of generator rotational speed, $rads\ s^{-1}$
δ_s	The stator angle, $rads$
$\dot{\delta}_s$	The stator angular speed, $rads\ s^{-1}$
γ	Coil phase band for the permanent magnet generator
ψ_d	The d-axis flux linkage, per unit
ψ_q	The q-axis flux linkage, per unit
τ_{ag}	The electromagnetic airgap torque, per unit
τ_m	The mechanical driving torque, per unit
ω	The synchronous angular speed, $rads\ s^{-1}$
ω_d	The damped frequency of oscillation, $rads$
ω_n	The natural frequency of oscillation, $rads$

C_{ac}	AC side tuning capacitance, μF
C_{dc}	DC link capacitance, μF
$E_{a,b,c}$	Excitation phase voltages, Volts
E_f	E-core module excitation voltages, Volts
F_{loss}	Rated E-core iron loss, Watts
K_{Vdc}	Inverter voltage control ratio
$L_{a,b,c}$	Total phase inductances to the rectifier, Ω
L_e	Transmission line inductance
I_c	Module AC current, Amps
I_{dc}	DC link current, Amps
I_{cap}	DC link capacitor current, Amps
I_{comp}	Complex component of E-core current, Amps
I_{inv}	Inverter current, Amps
I_{lim}	Maximum current per module
I_{real}	Real component of E-core current, Amps
n	Harmonic order
n_m	Number of stator modules
P	Real power into the grid, Watts
P_{ac}	Airgap power transfer, Watts
P_{copper}	Power dissipation in E-core resistance, Watts
P_{dc}	DC link power transfer, Watts
P_{diode}	Power loss in E-core rectifier diodes, Watts
P_{in}	Power transfer into E-core, Watts
P_{iron}	Core loss in E-core at a specific frequency, Watts
P_{max}	Max power transfer across E-core, Watts
P_{out}	Transmitted dc link power per E-core, Watts
Q	Reactive power into the grid, VARs
$R_{a,b,c}$	Total phase resistances to the rectifier, Ω
R_e	Transmission line resistance
V_{Cac}	Voltage across tuning capacitor, Volts
V_{dc}	DC link voltage, Volts
V_{Lc}	Voltage across E-core inductance, Volts

V_{line}	Line voltage on forward side of rectifier, Volts
V_{R_c}	Voltage across E-core resistance, Ω
V_{sys}	System voltage, Volts
V_1	Fundamental of the terminal voltage, Volts
X_s	Total reactance to the grid, Ω
α	Inverter firing angle, degrees
ϕ	Phase angle between E-core voltage and current, <i>rads</i>
ψ	Phase angle between E-core voltage and real component of E-core current, <i>rads</i>
ζ	Phase angle between E-core current and real component of E-core current, <i>rads</i>

INDUCTION GENERATOR PLUS GEARBOX MODELLING NOTATION.

c_{hs}	High speed shaft damping coefficient, $Nm\ rads\ s^{-1}$
c_{ls}	Low speed shaft damping coefficient, $Nm\ rads\ s^{-1}$
J_{Hs}	Total high speed inertia, $kg\ m^2$
J_{ls}	Total low speed inertia, $kg\ m^2$
k_{hs}	High speed shaft spring stiffness, $Nm\ rads$
k_{ls}	Low speed shaft spring stiffness, $Nm\ rads$
N	Gearbox ratio
<i>slip</i>	Induction generator slip
T_{qls}	High speed shaft load torque, Nm
T_{qls}	Low speed torque, Nm
$T_{q_{rtr}}$	Rotor torque, Nm
$T_{q_{spcv}}$	Torque-speed curve coefficient, $Nm\ slip^{-1}$
τ_d	Induction generator time constant
ω_{ls}	Low speed shaft rotational speed, $rads\ s^{-1}$
ω_{ld}	High speed shaft rotational speed, $rads\ s^{-1}$

Chapter 1

Introduction

The generation of electricity from renewable energy sources, such as the wind, incurs no input fuel costs. Therefore, the initial capital and subsequent operational and maintenance costs dominate the lifetime cost of the electricity generated. Conventional power stations, on the other hand, have fuel costs which can form a significant proportion of the total cost of the electricity produced. Hence the optimisation of designs to reduce capital cost and the development of control strategies to improve operating performance are most likely to lead to better economic attractiveness of renewable energy power stations.

This thesis is concerned with the modelling, dynamics and control of a new design of multi-pole, permanent magnet, synchronous generator for use with wind turbines. Such a multi-pole generator allows 50 Hz to be generated from the low rotational speed of the wind turbine blades and results in the elimination of the usual step-up gearbox, leading to cost and noise reductions. Wind turbines are typically operated at fixed or variable speed and both methods of connecting the generator to the grid for such operation are considered. Control strategies for achieving efficient operation and to satisfy the grid connection criteria of the wind turbines are devised and their performance simulated to determine which mode of operation is the most effective and economical.

Horizontal axis wind turbines are examined and, in particular, stand alone, three blade, partial span pitch controlled turbines connected directly to the distribution network. This type of configuration is becoming fairly industry standard [1]. Several sizes of turbine, from 200 kW to 1.5 MW, are analysed and a picture of a typical wind farm comprising several



Figure 1.1: Typical 300 kW turbines (Source: Private Photograph of Ovenden Moor Wind Farm, Uk)

300 kW turbines is shown in Figure 1.1.

The beginning of this first chapter offers a comparison between wind power and the other leading contenders for the renewable energy crown, such as biomass, wave power and hydro-electric power, to justify the research into reducing the cost of wind turbine technology further and bring it into the realm of economic reality. The historic development of modern wind turbines is presented and their likely contribution to the energy mix is discussed. The reasons for using the type of wind turbine, described in the previous paragraph, as a benchmark to test the performance of the multi-pole, permanent magnet, synchronous generator are then presented. The main goals of the thesis are stated and the ways in which such a generator can be designed to fulfill these goals are briefly introduced. Finally an outline of the whole thesis is given to show the overall methods of attack used to successfully complete these goals.

1.1 The emergence of wind power as an economic renewable

Many articles have been written about the emergence of wind power as one of the foremost renewables but the book by Golding [2] and an article by Musgrove [3] perhaps best outline

1.1 _____ The emergence of wind power as an economic renewable

this rise. Wind turbines have been in operation for over a thousand years with the earliest evidence of their use being found in the Middle East and Afghanistan. In the 18th century wind power was the main prime mover but with the advent of the steam revolution, the internal combustion engine, and the increasing reliance on electric power systems, wind power was quickly displaced.

These new technologies relied on fossil fuels, such as coal and gas, and as demand for them grew they became progressively more available and cheap. However since 1973 this trend of declining fuel prices has been sharply reversed and an awareness of the detrimental environmental effect of burning fossil fuels has grown increasingly strong. This led to major research and development programs in America and Europe into alternative fuel sources and the coining of the term ‘renewable energy’ which is now used to describe benign energy sources whose primary energy inputs are renewable in the lifetime of mankind. Initially renewable energy researchers considered wave energy, direct solar radiation, hydro and tidal energy the most feasible. However, after further research [4], wind power was seen to be one of the most promising renewables and prototype windmills to generate electricity were developed. These early prototypes paved the way for the modern wind turbine. Today other renewable technologies, such as biogas and waste-to-fuel plants, are creating considerable interest and compete with wind power for development.

The key advantages and drawbacks of renewables, and in particular wind power, over conventional plant in terms of reducing environmental impact and cost will now be discussed. Once the need for renewables in the energy mix has been identified, a cost comparison of the leading renewables will be presented to justify wind as one of the most promising for further investigation. Finally the current worldwide status will be outlined and future price predictions included to indicate how well this new design must perform in order to push forward the current era of wind turbine technology.

1.1.1 Why invest in renewables over conventional power plant?

The industrialised nations of the world are energy intensive and any increase in electricity generation must be carefully planned to ensure good reliability of supply. Unfortunately the reliance on fossil fuels in the past has had a detrimental environmental impact and, urged on by popular support, the UK government signed the Rio Accord and introduced

1.1 _____ The emergence of wind power as an economic renewable

the Non-Fossil Fuel Obligation Act (NFFO). This act offered subsidies to renewable energy developments, thus encouraging new technologies and their inclusion in the utilities generation mix. However legislation alone should not guide investment in renewables and both sound economics and ease of implementation must be considered. The result of the subsidies has been a gradual driving down of the cost of generated electricity from renewable sources of energy and, in particular, the development of wind power plant has been a notable success [5] [6].

WIND POWER: THE UTILITIES DREAM TICKET? Most of the traditional power industries have learnt that big is not always beautiful and that large centralised power stations are not always the most cost effective way of delivering electricity to the customer. There is widespread recognition that utilities must diversify their resource base, distribute generating units over wide geographical areas and build smaller power plants closer to population centers and thus reduce transmission costs. In this scenario new energy technologies, such as wind power, are coming into their own.

Many utilities are also turning to natural gas as a means of minimising environmental impact. A combination of wind power and natural gas can help utilities address environmental concerns and minimise the risks associated with changing fuel prices and supply [7]. The slightly higher capital cost but low operating costs of wind power plant fit well into a plant investment plan that includes natural gas power stations which have a low capital cost and higher operating cost. Utilities can use wind to hedge against future price and deliverability uncertainties associated with gas. Furthermore natural gas turbines can come on line quickly and compensate for the intermittent nature of wind power. Other schemes matching diesel with wind have similar benefits but a slightly worse environmental cost.

ENVIRONMENTAL COMPARISON BETWEEN CONVENTIONAL AND RENEWABLE TECHNOLOGIES. Even though electrical energy is the most benign form of energy, its production relies heavily on the use of thermal resource. This leads to environmental problems of a varied nature: the key ones being CO_2 , NO_x and SO_x emissions, depletion of natural resources and visual impact. Wind power is renewable and the environmental impact, at present, is mainly limited to noise and visual intrusion with a slight disturbance of the natural habitat and minimal CO_2 emissions during manufacture. A comparison of the CO_2 emissions for the main fuel cycles can be found in [8]. Noise and visual intrusion can be very contentious issues as summary articles of reports from the me-

1.1 _____ The emergence of wind power as an economic renewable

dia suggest [9] [10]. These two problems cannot be ignored and special consideration must be shown in siting and sizing wind farms [11].

There are two main sources of noise in the wind turbine: mechanical noise from the drive train and generator and aerodynamic noise from the rotating blades [12]. Mechanical noise could be reduced by eliminating the gearbox but the aerodynamic noise from the blade moving through the air is more difficult to eliminate. Work is being carried out to develop quieter blades. Alternatively aerodynamic noise can be reduced by allowing the turbine rotor to rotate at a speed appropriate to the windspeed by connecting the generator to the grid via a frequency converter, i.e. operate the generator at lower rotational speeds in low wind speeds to maintain the optimum tip speed ratio. Improvements as much as 5-7 dB(A) can be achieved by ensuring tip speeds of less than 60 m/s [13]. These two aspects are dealt with later in the thesis. The size of a turbine and its siting also contribute to the perceived noise emitted by the turbine and this can be optimised through careful and sympathetic developments.

Complaints about visual intrusion mainly arise because developers of wind farms want to place them in the windiest sites, which are often the most beautiful areas of the countryside. Guidelines have been issued and visits organised for county planning offices [14] [15] to ensure the right balance between the environment and profit. However the risk wind technologists face, if unsympathetic development is carried out, is the same as that experienced by the nuclear industry when bad press led to public uncertainty and scepticism about the benefits of the technology. This must be avoided if this infant industry is to survive as the incumbent giants like coal, oil, gas and nuclear will exploit bad publicity at every opportunity to maintain their market share. One solution is to ensure wind farms are placed in areas already used by man. This has two major benefits: firstly there would be little visual intrusion over and above what is already there and secondly these sites would be close to load centres and have lower transmission losses. Recent studies also show that uniformity within a wind farm is an important factor in improving visual intrusion [11], i.e. ensuring that the same type, colour, direction of rotation and height of the turbines is maintained within the wind farm. Furthermore it seems that the public is more willing to accept three blade turbines than two blade turbines because they always portray the same visual impression as the blades rotate.

COST COMPARISON. Renewables have a more valuable contribution to make in less-

1.1 _____ The emergence of wind power as an economic renewable

ening the environmental impact of electricity generation when compared with fossil fuel technologies. However the question must be asked: are they cost effective? The answer is a complicated one depending on the level at which fossil fuel plant is levied for their associated environmental impact and the way in which the value of an intermittent renewable, such as wind power, can be credited. Furthermore there are two forms of wind power development predominant today: commercially, in a utility context, and privately, for the alleviation of fuel costs and surplus export to the local grid. Therefore the economic argument must focus on both forms of development. However periphery issues, such as the benefit to the local community, must also be included when considering the advantage of a wind development over conventional power plant.

An economic evaluation of wind in a utility context, involves a comparison between the total cost of wind turbines and the value of the wind power generated. This concept of 'value' is determined by the savings from decreased fuel consumption and the changes in the purchase of conventional equipment. Chowdhury [16] studied a system with about 6 % wind penetration, the ratio of variable wind power to firm conventional power, and concluded that savings over a ten year period amounted to \$55m for operating costs and \$105m in construction costs (1990 dollars). The operating costs of the wind turbines were neglected for this study because, as wind is a relatively new technology, the operating data and experience is limited. For a dispersed wind farm situation, where the dispersal acts to smooth some of the variability of the wind power, the figures are even more impressive.

Taking into account the factors mentioned above, the cost of the electricity generation over the lifetime of current wind and fossil fuel plant can be estimated. These are shown in Table 1.1. Clearly combined cycle gas turbine plant is very cost effective and this explains their popularity at the present time. However if the environmental costs were to be factored into the cost of building a new coal fired or nuclear powered plant, wind power would appear much more economical. However the pool price at the moment is dominated by coal plant, whose capital costs have already been accounted for. It is currently running at about 2 p/kWh, against which wind power cannot compete when selling electricity directly to the pool without the NFFO subsidies. Therefore more research is needed to reduce the costs further.

In terms of development for smaller scale implementation, the economics of wind power become even more attractive as turbines can not only be used exclusively to generate elec-

1.1 _____ The emergence of wind power as an economic renewable

Combined Cycle Gas Turbine	2.5 to 3.0 p/kWh [17]
Coal	3.5 to 4.5 p/kWh [17]
Nuclear	5 to 8.0 p/kWh [17]
Wind	3.5 to 7.0 p/kWh [17]

Table 1.1: Summary of electricity production costs (1992 Estimates)

tricity for the grid but also to displace bought electricity. The economics of this form of wind energy development are the most attractive as utilities sell electricity at commercial rates 3-4 times higher than they buy from independent power producers. Furthermore the owners of land, where wind turbines are to be situated, can increase their return per acre of agricultural land with the additional revenue stream from wind generated electricity.

COMPARISON OF AVAILABILITY. Wind energy is an indirect form of solar energy resulting from an imbalance in the solar radiation incident on the north and south poles which leads to large scale convection currents. An introduction to the complex processes involved can be found in [18]. The total energy received by the sun is huge, with about one percent being converted into the wind. If only one percent of this wind energy could be harnessed economically it would alleviate the need for any fossil fuels to be burnt for energy in the world. The practical problems associated with harnessing all this energy are enormous but allowing for restrictions placed by economics, land use, accessibility and the allowed penetration into the network, 10 % of all of Europe's electricity needs could be provided by wind power by the year 2050 and 50,000 jobs created [19].

Although the wind is not a reliable source of energy from hour to hour, it is statistically much more reliable from year to year. The free stream wind is a wind turbine's raw energy input and therefore understanding its dynamics up to a height of about 100 metres is very important. The free stream wind is stochastic and has several key contributions to its variance at different time scales: the passing of identifiable weather systems (time period (T) of about 4 days), diurnal variations ($T \approx 12$ hours), and atmospheric turbulence (T between approximately 5 minutes and 5 seconds). The energy spectrum of wind speed fluctuations about a mean steady wind in the atmosphere, as developed by Van Der Hoven, can be seen in Figure 1.2 [20]. This diagram shows the energy contained in the wind fluctuations across the full range of typical cyclic periods. For example, take the 4-day peak which has a period of about 100 hours and corresponds to large weather fronts moving across an individual site. Large fluctuations in wind speed occur during this period and there is, therefore, a

1.1 The emergence of wind power as an economic renewable

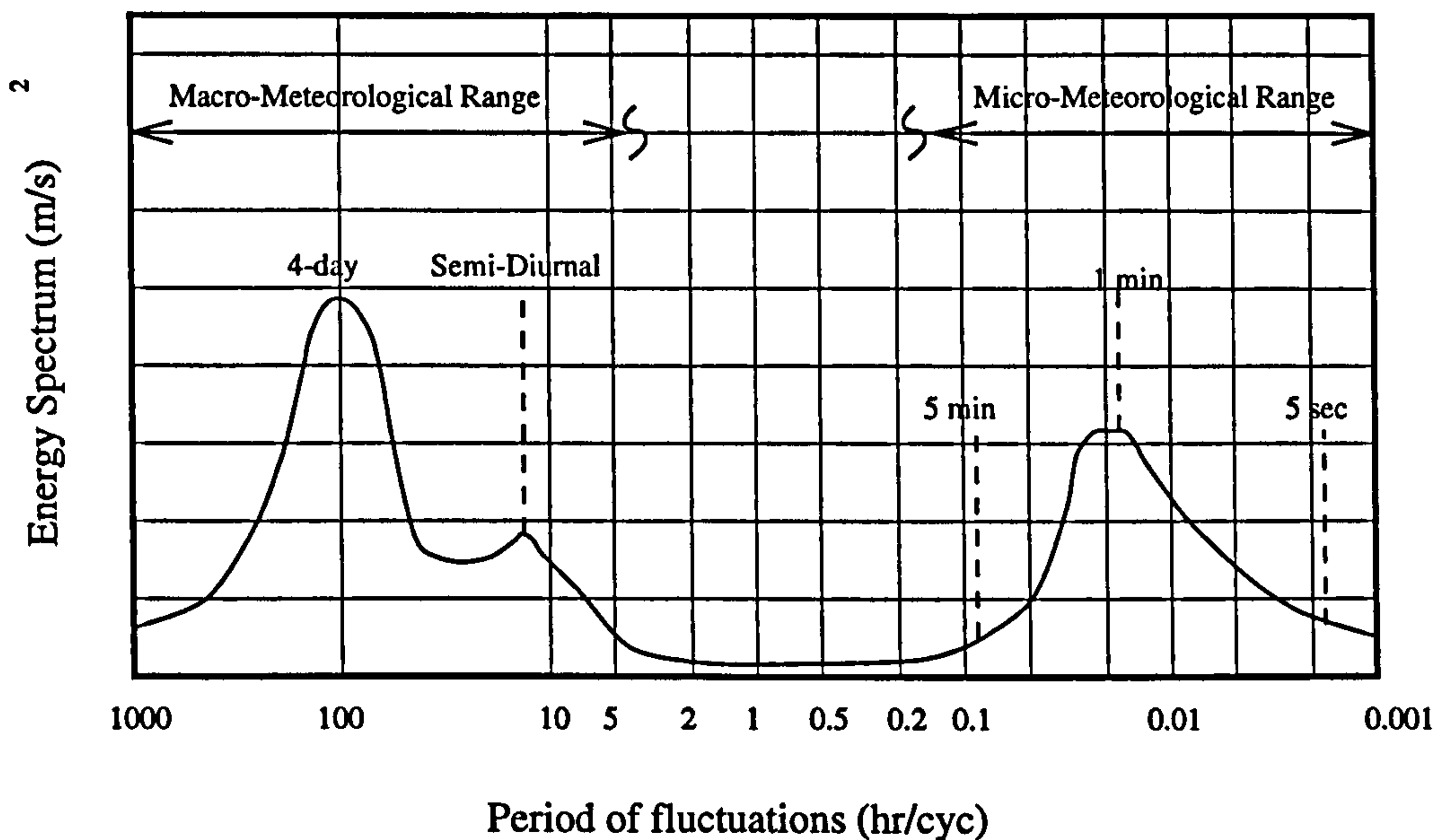


Figure 1.2: The energy spectrum of wind speed fluctuations in the atmosphere

large amount of energy attributable to these fluctuations. At the other extreme, on the micro-meteorological timescale, the bulk of the energy of the fluctuating wind is contained in fluctuations with durations of about one minute in length. This spectrum shows that there is a gap between 0.1 and 5 hours where the wind is virtually steady. Therefore availability estimates can be based on studies with sampling times in this region, typically a five minute reading once an hour. The longer time scale fluctuations are important in determining resource assessments and wind turbine siting, whereas the shorter time scales are important in determining the individual wind turbines performance and this is discussed in greater detail in Chapter 2.

In the UK there is also a pronounced seasonal variation, with higher wind speeds occurring during winter months. This correlates well with electricity demand which also tends to be greater in the winter. This significantly enhances the value of wind energy systems. Yet wind power will never be a 'power on demand' technology and, although wind farm dispersal does add some firm capacity credit, conventional power still has the big advantage of being available whatever the weather. However, research has shown that wind power with storage or diesel backup can provide firm power, typically in isolated regions where grid supplied electricity is expensive, and can prove an economic solution [21] [22].

1.1 _____ The emergence of wind power as an economic renewable

1.1.2 Comparison of the renewable technologies for electricity generation

Several renewable energy technologies exist that produce electricity and these will be discussed firstly in terms of their prospects and constraints [23] on widespread deployment in the UK and secondly in terms of cost.

HYDRO-ELECTRIC POWER. Large scale hydro-electric power plant, with power ratings greater than 5 MW, are already deployed by the generating boards and the available sites are almost fully exploited with a capacity of about 4.3 TWh per year. Small scale hydro-electric power plant, with power ratings upto 5 MW, needs to be researched further to ensure that the currently predicted costs can be achieved. The constraints on siting are considerably eased when compared with large scale hydro, with the only constraints being extraction rates and charges and environmental impact. These obviously vary according to location and thus certain sites may be more favourably developed.

TIDAL POWER. Tidal power is a 'promising but uncertain' technology with further work required to firmly place it as an economically attractive renewable energy supply. This work must focus on the cost effectiveness of the technology. However, if a rise in fuel prices occurred the technology would quickly leap into the 'economically attractive' category. The prospects in the UK are estimated at about 23 TWh/ year from estuaries with costs of less than 5 p/kWh. The constraints for widespread deployment are the high capital costs of projects, such as the Severn Barrage, and the typically long lead times. Public acceptability also has to be courted as projects impose quite large environmental impacts on the estuaries where the barrages are to be sited. Favourable features do exist for barrage projects which can alleviate the adverse impacts and cost such as watersports, fishing facilities and the usual revitalisation of disused waterfronts.

However tidal power is not limited to conventional barrages. A tidal turbine is being developed which is very similar to a wind turbine underwater and the direct drive generator of this thesis could be used for this application [24]. Unfortunately, even though there is a predicted resource of 58 TWh per year the cost at present is 2 to 3 times that of conventionally generated electricity and research needs to be done to make it economic.

WAVE POWER. This technology falls into two categories: large open sea installations (up to 2GW) and small shore mounted installations (below 5MW). The former falls into the 'long shot' category where only an unlikely reduction in costs or a dramatic increase in

1.1 _____ The emergence of wind power as an economic renewable

fuel costs will render it cost effective. The main constraint to development is the unproven nature and expense of the technology. The latter, on the other hand, is more promising and could already be exploited in certain locations. The constraint in this case is the limitation in available sites and again the lack of proven technology. However a 2 MW inshore wave machine, "OSPREY", was recently launched which had a predicted cost of only 4 p/kWh [25]. Unfortunately it sank at its operation mooring point only three weeks after launch due to damage when it was launched. The insurance company will hopefully pay for a another device. This highlights the difficulty of taming the sea to generate electricity economically [26], but, with further development and the placing of a wind turbine on the platform to harness the increased offshore wind speed, this looks to be a promising development.

PHOTOVOLTAICS. Although readily available, photovoltaics fall into the 'long shot' category as far as large scale implementation in the UK is concerned. The cost varies considerably with the key limit on full scale implementation arising from the mismatch between supply in the summer months and demand in the winter months. However a breakthrough seems to have taken place at the Center for Photovoltaic devices and systems at the University of New South Wales where they are predicting costs of 2-3 p/kWh by the end of the decade and the prospects appear more promising [27].

LANDFILL AND SEWAGE GAS. Landfill and sewage gas fuel plants tend to have high efficiencies, recycle methane, one of the most powerful greenhouse gases, and can supply power on demand. Many of these plants have been included in all rounds of the NFFO contracts [5] [6] and this technology will make a useful contribution in the future.

WASTE-TO-FUEL. Waste-to-fuel plants, like the one in South East London [28], tend to face quite hostile opposition to planning applications on the grounds of smell and emission contents and therefore expensive flue gas cleaning is often required. This means that support in the form of NFFO subsidy is required to make the technology economically attractive and only when the capacity of current landfill sites has been used will the technology be able stand on its own. Yet it still provides a very 'green' way of getting rid of waste and producing a large amount of firm generating capacity.

Clearly, of the above technologies, only landfill and sewage gas, waste-to-fuel and small scale hydro-electric power plant are the most likely to be developed into economically viable and useful electricity supplies. Wave power has recently had a setback in that Osprey II sank

1.1 _____ The emergence of wind power as an economic renewable

[26] but could contribute a small amount soon if launching difficulties can be overcome. Geothermal energy also has promise in reducing the overall need for electricity for heating but the efficiency and availability of geothermal power is poor. A summary of the estimated costs to generate electricity by the above renewable plant can be seen in Table 1.2. The different technologies can most effectively be compared by using the concept of the discounted cost per unit of electricity (p/kWh) over the lifetime of the plant.

Wind	3.5 to 7.0 p/kWh [17]
Wave	4 [25] to 16 p/kWh [29]
Solar	25 to 30 p/kWh [30]
Tidal	6.5 p/kWh [31]
Offshore Wind	5.6 to 11.2 [32] p/kWh
Hydro	5 p/kWh [33]

Table 1.2: Summary of electricity production costs (1992 Estimates)

Clearly wind power is one of the more favourable options in terms of predicted cost and, providing the problems of visual intrusion, noise impact and the intermittent nature of the operation of wind turbines can be overcome, wind turbines look to be a major source of electricity in the future.

1.1.3 Current Status and future trends in wind power

Wind power currently makes a valuable contribution to the world energy market. A recently published article [34] quotes worldwide wind generation as surpassing 6 TWh in 1994 with sales of turbines and generated electricity surpassing \$1750 million dollars for the first time. In fact there is such a boom in wind power that Europe will surpass the US in 1995 and the worldwide market could exceed 8,100 MW. Most of this market is concentrated in the first world but small scale projects in Africa and the Americas are becoming increasingly the most economic method for rural electrification as grid extension is too expensive. Furthermore the cost of wind generated electricity is predicted to fall to about 4 p/kWh by the year 2000 in 8 m/s winds due in part to advances in wind turbine design and economies of scale [35]. Also the specific energy yields of wind turbines are improving rapidly due to increases in reliability, better airfoil design, and greater tower height and could pass 1250 kWh per unit swept area per year. Clearly wind power has a very promising future as one of the foremost economical renewable technologies. However these costs and improvements must be put into the context of the historical development of wind turbines so that the reasons

1.2 _____ The history of wind turbine development

why the design advances proposed in this thesis should bring down the current capital costs can be best understood.

1.2 The history of wind turbine development

The two main types of wind turbine are horizontal and vertical axis. Each has its advantages and drawbacks. This thesis concentrates on the horizontal axis turbine. The following history mainly focuses on its development and includes a brief comparison between the two types for completeness.

The initial research into the modern horizontal axis turbine was carried out in America but since then Europe has led the way. The American program started in 1973 and by 1975 the first test bed of the Mod 0 was completed [3]. This 100 kW horizontal axis turbine had twin 38m diameter blades mounted downwind of the tower and was connected to the grid via a synchronous generator. The 4 pole synchronous generator operated at a constant speed for 60Hz generation whilst the rotor operated at 40 rpm so that a 45:1 ratio speed increasing gearbox was needed. Power control in high winds was effected through altering the pitch of the blades. These turbines accumulated thousands of hours of operating data and proved that a turbine equipped with a microprocessor based control system could operate in a stand alone manner. Since then several multi-megawatt turbines and different configurations have been tried and tested, leading to several standard design guidelines. A schematic diagram of a typical medium sized wind turbine can be seen in Figure 1.3. The following sections will talk about the design options presently available.

1.2.1 Horizontal (HAWT) versus vertical axis wind Turbines (VAWT)

The argument over whether the turbine should be vertical or horizontal has remained controversial since the early seventies, but the predominant form of turbine today is horizontal.

The vertical option, typically the modern Darrieus turbine, has a low rotational speed. The main advantage over the horizontal option is the placing of the generator at ground level. This reduces the constraints on weight or size and allows a large, directly connected, synchronous generator to be used [3]. Thus VAWT's do not need a speed increasing gearbox which considerably reduces operation and maintenance costs. Furthermore, because they

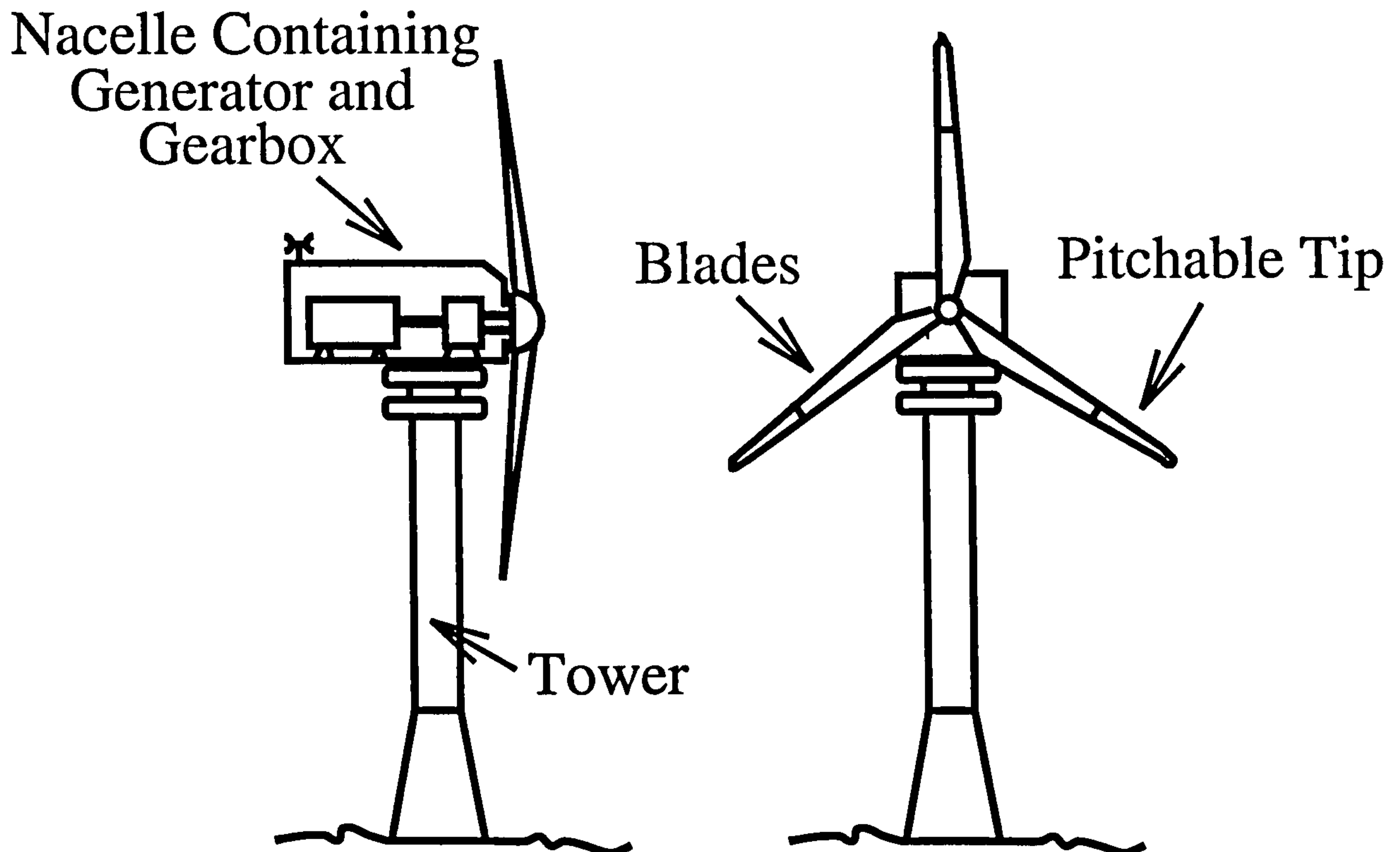


Figure 1.3: Typical medium sized horizontal axis wind turbine

are at ground level, noise emissions can be reduced by shielding the equipment properly. This may allow small scale VAWT's to be situated within the urban environment. The cyclic forces due to blades passing through the wind shear, common to HAWT's, is not a problem in VAWT's because each blade element experiences the same windspeed as it stays at the same height. VAWT's also offer a simpler architecture which may lead to more optimal design and hence lower cost. These claims have yet to be developed into a reliable industry standard turbine and, as there is a vast experience in HAWT design, a VAWT would have to demonstrate very good cost effectiveness to overcome the entry barriers to the worldwide wind market.

A serious drawback associated with VAWT's is that their power cannot be regulated easily as pitching the blades would have to be done cyclically which would involve considerable mechanical complexity [3]. Furthermore they are also less effective at capturing energy from the wind. The permanent magnet synchronous generator would be a viable form of generator for a VAWT but cost comparisons would be needed against a large multi-pole conventional synchronous or induction generator in order to verify this.

1.2 _____ The history of wind turbine development

1.2.2 Blade design: material, number, diameter, pitchable, orientation

A designer of wind turbines must decide on the blade material; whether to mount the blades up or downwind of the tower; how to regulate the power from the blades in high windspeed; and finally the number of blades to be used. There still seems to be no real consensus of opinion on what is the best design but a brief history will now be outlined.

BLADE MATERIAL. The common blade materials are carbon epoxy, glass fibre reinforced epoxy (GRE), glass fibre reinforced polyester (GRP), steel, and wood epoxy with GRP. The cost effectiveness of a material can be calculated by dividing its specific manufacturing cost by its specific strength [36]. A trade off must be maintained between this effectiveness, the blade weight and its fatigue properties.

BLADE NUMBER. The number of blades is an important area for discussion. Three main reasons exist for the choice of blade number and these are cost, aesthetic appearance and dynamic performance. A comprehensive cost comparison of the various design options is given in [36]. The partial span pitch controlled, three blade, wind turbine costs 35 % more than the equivalent partial span pitch controlled, two blade version. The main cost savings, when moving from three to two blade turbines, are due to the reduced overall blade weight leading to lighter tower head weight. Furthermore the two blade wind turbines have a higher optimum tip speed ratio leading to higher frequency of rotation and, together with the low tower head weight, allows a 'softer' and hence lighter tower structure design. However the cyclic load variation is more pronounced with lower blade number and concepts such as the teetered hub, to reduce the impact of this variation, have been used but these tend to increase the complexity of the drive train. From a visual view point three blades appear more aesthetic than one or two because the overall shape does not vary [11] as the blades rotate.

BLADE ORIENTATION. There are two orientations for the blades of a wind turbine: either upwind or downwind of the tower. If the blades are mounted upwind the yaw control system must move the blades into the wind and there is less room for movement of the blades before they impact with the tower. Downwind mounted blades do not have this restriction and can therefore be less stiff which can lead to the alleviation of some of the cyclic loading. The blades will also naturally swing to face downwind thus reducing the yaw system rating. However there is a much more pronounced tower shadow effect in downwind

1.2 _____ The history of wind turbine development

turbines and therefore upwind turbines are favoured.

BLADE DIAMETER. The diameter of the blades determines the power produced by the turbine. A larger diameter blade allows more energy capture as the diameter squared but will lead to heavier spars and hub. The generator and drive train will also have to be uprated to cope with the higher power developed. The rotor thrust will also increase and thus affect the nacelle bedplate, yaw system, tower and foundation design.

In light of the arguments presented, an upwind wind turbine design with three GRP blades is adopted for this thesis. However only simple modifications are required to convert the simulation models developed in Chapter 2 for any type of wind turbine blade design.

1.2.3 Synchronous or Induction Generator

The electrical generator converts the mechanical power transmitted along the rotor shaft into electrical energy. For constant speed operation, the generator must rotate at a speed which can produce ac power at the same frequency as the grid i.e. 50 Hz in Europe and 60 Hz in the USA. For variable speed operation, there is more scope for design optimisation and this is discussed in section 1.2.5. Designers usually choose generators which run at 1500 rpm, 1000 rpm or 750 rpm and there is a simple trade off between gearbox and generator costs. Two main types of generators are used in wind turbines: induction and synchronous generators.

INDUCTION GENERATORS. Induction generators have stator windings energised from the electricity at the grid frequency and power is generated when the wind turbine is going slightly faster than synchronous speed i.e. a slip greater than one. Induction generators are robust, relatively inexpensive and are used wherever grid synchronised power is needed and when the grid is substantially larger in power terms than the individual wind turbine or farm output. A major advantage of induction generators is that they enable stall regulated turbines to operate at a constant speed, as a large grid provides a stable frequency.

SYNCHRONOUS GENERATORS. Synchronous generators usually have a small permanent magnet exciter to provide the rotor field current. They require no external frequency control from the grid but tend to be heavier and more expensive than an induction genera-

1.2 _____ The history of wind turbine development

tor running at the same speed. They must be run at a specific speed and careful control of the wind turbine rotor speed is required. They are typically used when the grid is weak or in stand-alone applications. Synchronous generators would be the most suitable for wind turbines which are connected to the distribution network and sited far from load centres and other forms of generation.

The generator used in this thesis is a multi-pole, permanent magnet, synchronous generator and is introduced in section 1.4. The key cost comparison required is between its performance and that of the relatively expensive gearbox and inexpensive induction generator arrangement.

1.2.4 Sizing and siting

Average wind speeds can alter considerably even over a few kilometres, e.g. a hilltop ridge will be windier than a sheltered valley, so the siting of a wind turbine is important. However the prominent sites, although being more productive, can have detrimental effects both in terms of visual impact and reliability. If the windspeed is too great the turbine needs to shed power or even shut down. At a recent incident in Cemmaes several two blade wind turbines suffered catastrophic failures due to winds in excess of 120 mi/hr, the supposed 50 year maximum. The design should have withstood such a windspeed and the exact mode of failure is not known. Perhaps if a less windy site was chosen, the failures would not have occurred and £1.5M damages and £600k per winter month lost revenue would not have been foregone [37].

1.2.5 Control Strategies

Several strategies can be used to control the performance of wind turbines depending on their design. There are two control aims that need to be addressed: speed control and power limiting. In addressing these aims it is desirable that the controller alleviates stress throughout the wind turbine, smoothes the generated power and maximises energy capture. For a typical wind generator, with a drive train including a gearbox, the controller should clearly avoid any resonant frequencies [38].

The aerodynamic performance of the blades is optimum at a single value of blade tip speed

1.2 _____ The history of wind turbine development

and windspeed. The designer has two options: fixed speed operation where the blade performs under non-optimal aerodynamic conditions and variable speed operation where the controller must track the optimum point as the windspeed varies. The first results in a simple electrical system whereas the second requires quite a complex and expensive frequency converter to link the generator to the grid.

The wind available at any site is extremely variable, varying from zero to very high levels in storm conditions. The power train of the turbine is designed for a cost effective intermediate level and hence some form of power limiting is needed. There are two basic methods currently used: stall control where the blade aerofoil falls progressively into stall at high angles of attack when the wind speed is high and partial or full span pitch control where the blade is feathered by a mechanical actuator. A detailed summary of the arguments for and against the technologies is included in [36]. The key points are summarised below.

STALL CONTROL. Stall control results in relatively smooth control of power and a simple hub structure but even with full stall across the blades there can be quite high loads in high windspeeds and the rotor needs to be shut down. Stall controlled rotors must be designed to withstand gust loads as they cannot be shed by changing the blade angle so the hub, drive train and tower must all be designed for these high shock loads.

PITCH CONTROL. The original reasons for pitch control were to assist in the start up and shut down of the turbine and to regulate the power in high speeds. This enabled the rating of the generator and gearbox to be reduced.

Full span pitch control allows the matching of the pitch angle to the incoming speed to give the optimum angle of attack which can lead to increased energy capture. Gust loads can also be shed, if the controller can act fast enough, to alleviate loads on the drive train. A further feature is the ability to park the blades in the feathered position in storm conditions and thus reduce loading on the blades and tower. However the hub is complicated, heavy, larger to accommodate the actuation mechanism and hence more costly than for a stall controlled turbine.

Partial span pitch control gives the benefits of full span pitch whilst avoiding some of the drawbacks. It strikes a compromise between the mechanical simplicity but higher shock loads of stall control and the mechanical complexity and lower loads of full span pitch control. The pitchable section operates in the region of maximum effectiveness, at the blade

1.2 _____ The history of wind turbine development

tip, where aerodynamic moments are greatest. The non-pitchable inboard acts like a stalled rotor. Advantages of such a scheme are that the hub can be simple, there is reduced shock loading when compared with stall rotors, faster pitch rates can be attained leading to lower structural requirements and normal operating brake duty. However the pitch actuation mechanism must be compact and light. Higher loads are experienced in high windspeeds when compared with full span control and some method of transferring a control signal to the actuator is needed. For a constant windspeed HAWT, Leithead [38] concluded that the performance improves with tip rather than full span regulated blades and with three blades than one.

Other forms of blade control are continually being proposed. For instance, a method where, as the wind speed increases, the blades collapse downwind of the tower thus reducing the effective swept area of the rotor [39]. In the extreme condition, the blades are parked horizontally and the design load on the tower is merely the bending moment due to the weight of the blades and the wind load on the tower. This should radically reduce the costs of all the structural components in a wind turbine and dramatically improve the cost effectiveness of wind power. For this thesis, a partial span pitch control mechanism is assumed for the turbine operating at both fixed and variable speed.

1.2.6 Tower design

Two tower designs have been used to date: lattice and tubular. The lattice tower has a more diffuse tower shadow than the tubular design and is cheaper and easier to construct. However it is visually ugly and the tubular tower has come to dominate the European market and is slowly beginning to dominate the US market.

A major effect that determines the power from a wind turbine is the boundary layer of the Earth's surface which is typically several hundred meters deep. Over limited ranges in height, this can be represented by a simple power law [40],

$$\frac{U_h}{U_{10}} = \left(\frac{h}{10} \right)^{\frac{1}{7}} \quad (1.1)$$

The higher the turbine blades the greater the windspeed and hence power out but the tower structure becomes more expensive to construct. Tower design is a complex affair as the tower

must be strong enough to withstand the bending forces induced by the rotor thrust and wind drag and have natural frequencies which must not resonate with the rotation frequency or with the blade passing frequency. ‘Stiff’ towers with high natural frequencies which avoid resonance are expensive and heavy. ‘Soft’ towers which have natural frequencies between the resonant bands are lighter and therefore cheaper but require more care in designing the controller to avoid the lower resonance. This is usually achieved by accelerating the blade through the resonant band as quickly as possible [41].

Although the tower movement will have an impact on both the wind speed as seen by the blades due to fore-aft movement and the stator oscillations these effects are small in comparison with the overall torque produced. As such they can be ignored for this thesis with the main aim being to produce a reasonable model for simulating the performance of the permanent magnet, synchronous generator and developing a good understanding of the required control algorithms. Therefore, from this point onwards, the tower is assumed to be stiff enough that there are no structural interactions. Furthermore the wind turbine blades are also considered to be stiff enough that blade bending does not contribute a sizeable variation in the shaft torque input to the permanent magnet model.

1.2.7 The definitive design

The ‘best’ configuration of turbine may not exist. The key criterion for a wind turbine design is to assess its suitability to the actual location and then to optimise the costs. However an appreciation of the different factors and how they interact should help this process. Interactive designs where tower, blades and hub are all more flexible with variable speed control are being designed to minimise the cost of wind turbines. A review of future developments in wind turbine technology is given in [1]. However this thesis is concerned mainly with the electrical generating aspects and the typical and fairly cost effective turbine structure using the key components listed in Table 1.3 is modelled.

1.3 The Aim of this thesis

The aim of this thesis is to model a directly connected, multi-pole, permanent magnet, synchronous generator and examine its performance to show that this design of generator

Number of blades	3
Blade type	Stiff (GRP)
Power control	Active tip pitch control
Safety	Brake tips and low speed brake
Tower type	Stiff steel tubular
Blade orientation	Upwind
Hub type	Rigid
Generator	Permanent magnet synchronous
Gearbox	None (directly connected)

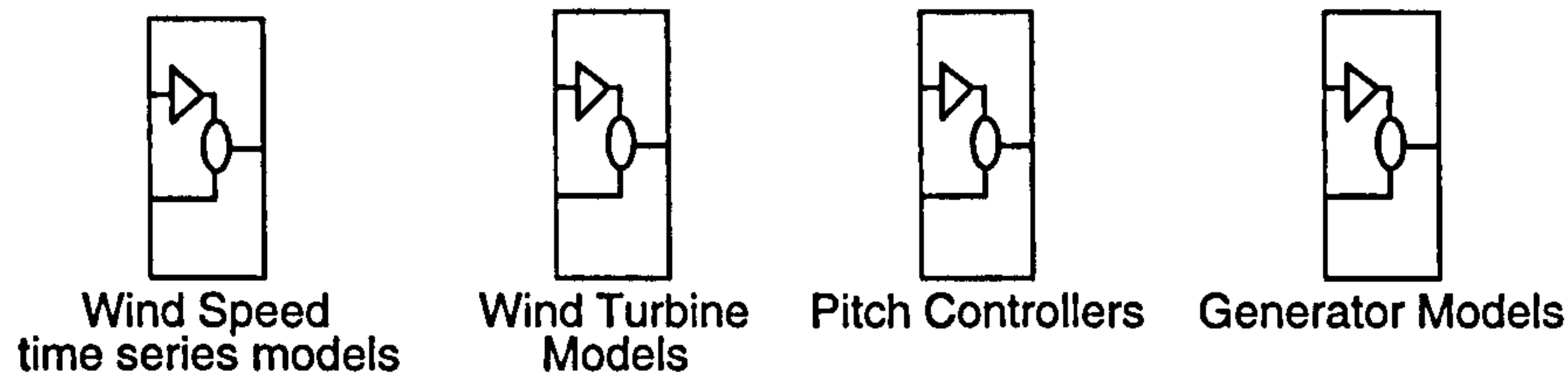
Table 1.3: The thesis wind turbine design

can lead to cost savings and improved performance when compared with current wind turbine systems.

Wind turbines typically rotate at 30 to 50 rpm and the generator, either induction or synchronous, is coupled to the turbine via gears so that it can rotate at 1000 to 1500 rpm for grid connection. However the gearbox brings weight and cost penalties, demands regular maintenance, generates noise and incurs loss. Clearly eliminating the gearbox would improve the attractiveness of wind generation [42]. Direct connection of the generator to the wind turbine requires the generator to have a large number of poles. A multi-pole, synchronous generator fitted with a conventional field winding would have a prohibitively large diameter and be very expensive whereas permanent magnet excitation allows a small pole pitch to be used and can yield cost effective designs [43].

MATLAB with SIMULINK [44] was chosen as the main package used to develop the simulation of the wind turbine. The aim of the simulations was to predict the performance of the generator and show its advantage over standard generator designs. The initial work focussed on the simulation of fixed speed generators with 50 Hz output which can be connected directly to the grid. A simulation library, comprising the key elements of the wind turbine system shown in Figure 1.3, was required for the fixed speed case and the final version is shown in Figure 1.4. Each block contains a library of models that can be used in a SIMULINK program to represent the aspect of wind turbine operation indicated by its title. Software, in the form of Matlab scripts and functions, was written to support this library so that the initial conditions of the blocks could be set up and results analysed.

During the course of the work presented in this thesis, the wind energy industry began to show an interest in variable speed systems with electronic frequency converters. The direct drive generator can be applied to such a situation with cost benefits and performance en-



Fixed Speed Wind Turbine Modelling Library - Version 1.0

Figure 1.4: Fixed speed wind turbine simulation library

hancements. The latter chapters of the thesis address this form of operation and compare its viability with that of the fixed speed case. A similar simulation library for the variable speed case was developed with the key difference between the two libraries being the operation of the generator at variable speed and the inclusion of a frequency converter, and its associated control requirements. This simulation library is shown in Figure 1.5.

1.4 The Design of Permanent Magnet Generators

When designing permanent magnet systems, the choice of which permanent magnet material to use has a critical impact on the design. Expensive, high remanence, rare earth materials, such as the Neodymium-Iron-Boron complex (NdFeB), lead to designs with small magnet volume but high overall costs. Conversely using cheaper ferrite magnets requires greater volume of magnet but lower cost [45]. Furthermore surface mounted NdFeB magnet designs can have a tendency to demagnetise slightly at low load torques because of the flux density they experience. Therefore buried magnet designs using flux concentration, although heavier, are considered to be better [46]. Thus the permissible weight, volume, cost and magnitude of the demagnetising mmf all alter the design of generator. Two typical designs of generator using ferrite and rare earth magnets can be seen in Figure 1.6 (a) and (b).

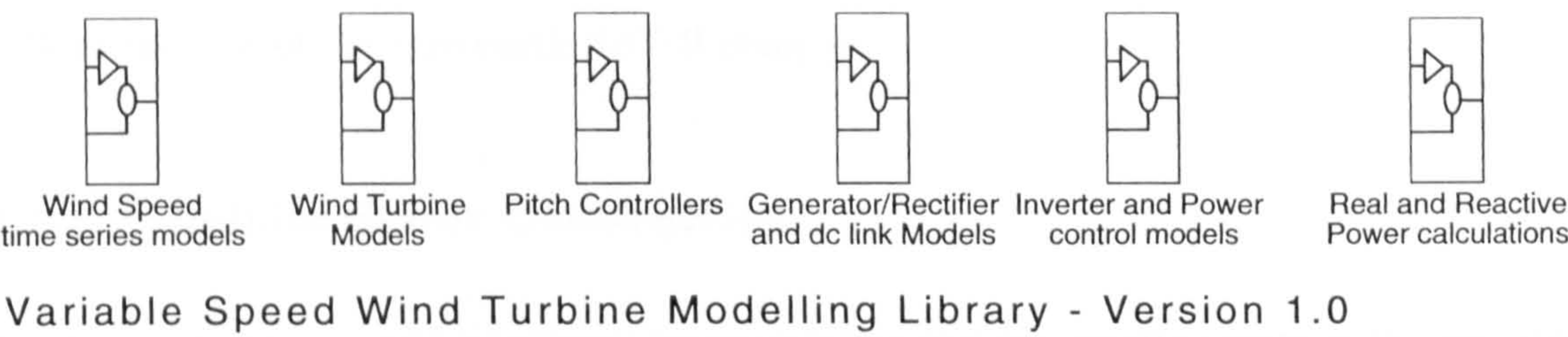


Figure 1.5: Variable speed wind turbine simulation library

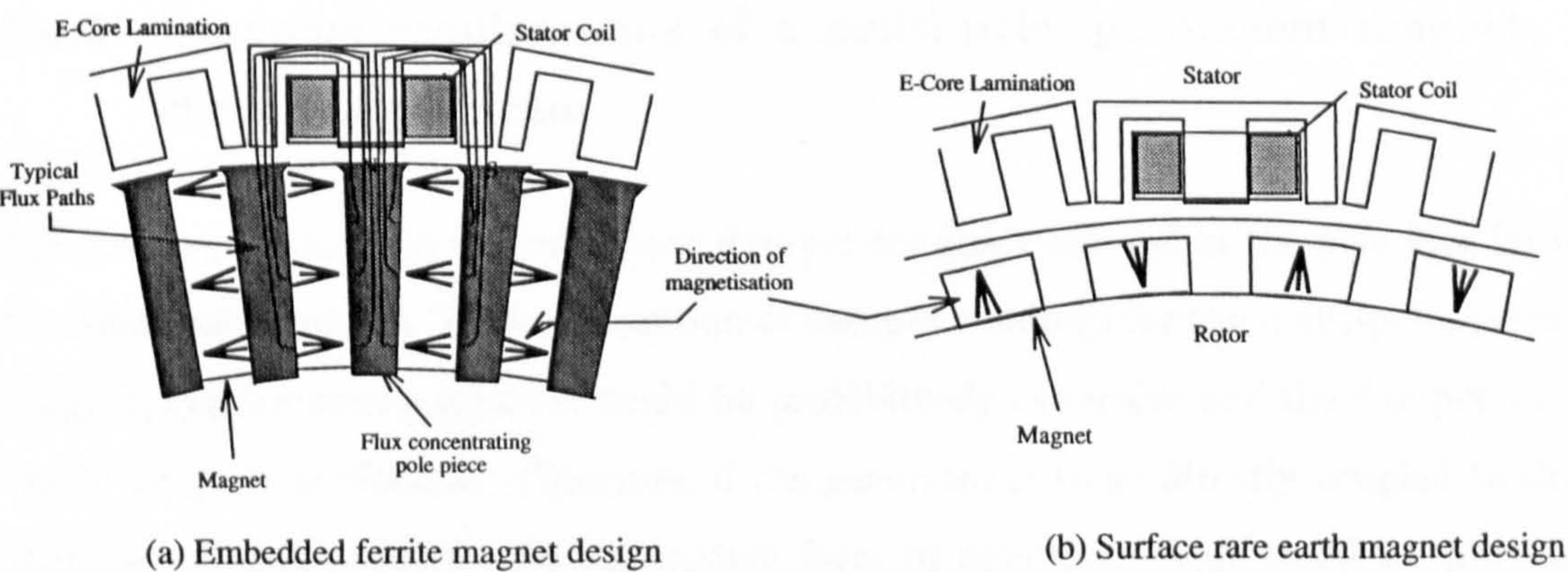


Figure 1.6: Two Permanent Magnet Generator Designs

The concepts behind permanent magnet generators are covered in greater depth in Chapter 3 of this thesis. A comparison of generator costs carried out by Spooner [45] shows that a radial flux design using ferrite magnets as the means of excitation is the most cost effective. This cost effectiveness arises from the design flexibility offered by working with ferrites which allow more optimum magnetic conditions to exist. The ferrite magnets are about 12% of the cost of the rare earth NdFeB complex.

1.4.1 Modular Stator Construction

Further cost savings can be achieved by considering the construction costs of the generator stator [47]. For such a large pole number, permanent magnet, synchronous generator a stator diameter is needed which would exceed the maximum available width of electrical steel sheet. So, unless a modular form is adopted, a segmented core with appropriate structural support would be needed. This would require accurate machining after fabrication and laminations to be fitted in place manually so that they overlap each other. Such a time consuming process would also require a series of complicated and expensive punching dies and hence a modular arrangement suitable for high speed automated manufacture is desirable. The proposed multi-pole generator, discussed in Chapter 3, has a very localised flux in the stator and this makes such a modular arrangement possible [43]. A very large number of separate units can be used which do not detract from the flux distribution greatly.

1.4.2 Damping requirements of a multi-pole, permanent magnet, synchronous generator

Synchronous generators typically have damper windings inserted in the pole face for better transient performance. The construction of damper windings for the multi-pole, permanent magnet, synchronous generator would be prohibitively expensive and the damper windings would be quite ineffective. Therefore, if the generator is to be directly coupled to the grid there is a requirement for an alternative form of damping. This could be provided by compliantly mounting the generator.

If the generator is connected to the grid via a frequency converter, there is no need for a compliant mounting. Generator damping is no longer required for acceptable transient

1.4 _____ The Design of Permanent Magnet Generators

performance because the power out of the generator can be controlled by the inverter and the rotor inertia used as a flywheel to smooth power excursions. This mode of operation is discussed in Chapter 5.

The latter method to achieve acceptable transient performance is expensive but may lead to increased energy capture whilst the former offers a simplicity of construction and design. A comparison between the cost, weight and performance of the fixed and variable speed schemes is included in Chapter 7.

1.4.3 Further design implications of removing the gearbox from the wind turbine drive train

High powered wind turbines rated from 500 to 1500 kW, with large diameter blades and tall towers, are increasingly economic and improve the total power extraction from a site. However large diameter blades have low rotational speeds to limit the tip speeds to about 60 m/s and correspondingly large shaft torques. Standard wind turbines therefore use a step-up gearbox to generate 50 Hz ac from the low speed. Such a gearbox, capable of handling large torques, is very expensive, noisy and requires considerable maintenance. The increased height of the turbine towers, required to place the turbine blades in a higher windspeed regime, leads to the tower head weight being a substantial cost factor [36]. Eliminating the gearbox has many benefits and the direct drive generator is the next logical step in the development of a more economic wind turbine.

As a direct drive wind generator has no need for a gearbox, one of the key constraints placed on reducing system cost is removed, providing the new permanent magnet generator is cheaper and lighter than the induction generator plus gearbox. However the overall effect of removing the gearbox is greater than merely reducing the cost of the drive train. Many designs of wind turbines have suffered from excitation of the drive train oscillation modes by the unsteady and cyclic oscillations inherent in wind systems. Typically the drive train oscillation modes are lightly damped to avoid any excessive power loss in the drive train and the excitation of these modes has led to unwanted excursions in the power flow into the grid and increased wear on the gearbox. This excitation has been counteracted by mounting the gearbox on a suspension, teetering the hub and introducing quill shafts to add some damping to the system [48] [49] [50] [41]. However problems exist and further operating

experience is required to prove them economical or reliable [37].

1.5 Thesis Outline

The preceding sections have introduced the need for some fundamental changes to the design of wind turbines so that they may compete against conventional fossil fuel and nuclear technology in terms of environmental impact and more importantly in terms of good economic sense. The need to reduce cost is addressed by eliminating the gearbox and the effect of this change on wind turbine design is the main thrust of this thesis. The chapters are structured such that the method of attack and key results for the fixed and then variable speed operation of the direct drive, multi-pole, permanent magnet, synchronous generator are outlined in order to make a comparison with a conventional gearbox driven induction generator design.

To understand more fully the methods of simulating wind turbines, the second chapter of this thesis describes in detail the development of a model for a fixed speed, horizontal axis wind turbine. The modelling of the free wind stream, the blade interaction with the wind and the developed torque driving the generator is discussed first. Then a comparison against published wind turbine performance is included to validate the approach taken. Finally the modelling of other aspects of the wind turbine system, such as the pitch controller, is outlined and validated.

The next chapter describes the development and validation of a simulation model for the multi-pole, permanent magnet, synchronous generator operating at fixed speed. The pertinent theory of permanent magnets and electrical machine design is outlined first and then the final design of the permanent magnet generator is presented [51]. The use of a compliant mounting, to act instead of damper windings, is introduced and its manufacturing limits discussed. WINDGEN2, a suite of programs written by others in the Wind Energy Group at Durham University that allows the user to design a fixed speed permanent magnet generator of any rating, is then described. The per unit system used in the simulations and how the values can be extracted from the results of WINDGEN2 are detailed. This is followed by the d, q -axis modelling of the permanent magnet generator and the compliant mounting using SIMULINK. Finally the validation of the generator model against a small test rig at UMIST is presented.

The fourth chapter contains results for the fixed speed case and discusses the design interaction necessary to match the compliant mounting to the parameters of the permanent magnet generator and in particular the d - and q - axis reactance. The basic operation of the compliantly mounted permanent magnet wind generator is discussed for a 455 kW rated design which is the median of the typical ‘best’ designs commercially available at present. These operational characteristics are then extended to cover a range of generator ratings from 200 kW to 1.5 MW for step and ramp changes, under synchronisation and then for gusting and severe storm conditions.

In Chapter 5 the case for allowing wind turbines to run at variable speed is presented in terms of increased energy capture, load alleviation, power smoothing and noise reduction. Several schemes for the frequency converter connection are identified and the modelling effort for the selected scheme is described. Finally the control mechanisms and desired performance of the scheme is outlined.

The key results for the variable speed operation of the multi pole permanent magnet generator are presented in Chapter 6 for several different control schemes to show their dynamic interaction and assess how they can be designed. Once an acceptable overall control scheme is developed the operation of the variable speed wind turbine is presented for wind speeds above and below rated.

Chapter 7 contains a detailed comparison between the fixed and variable speed cases of operating the direct drive, multi-pole, permanent magnet, synchronous generator in terms of cost, weight and performance. Then both cases are compared with the gearbox driven induction generator design to see which is best. Finally key design constraints for the further development of both the fixed and variable speed cases are presented and avenues for improvement discussed.

Chapter 8 concludes the thesis and describes some further work which the author feels would be profitable to pursue. Several appendices are then included which contain the key equations of the models. Appendix A contains the relevant equations for the modelling of the wind turbine dynamics, Appendices B and C contain the relevant equations for the fixed speed permanent magnet generator model modelling and linearisation, Appendix D contains the equations for the variable speed permanent magnet generator model and Appendix E contains the modelling equations for the gearbox plus induction generator arrangement.

Chapter 2

Wind Turbine Modelling

To understand how electricity can be generated from the wind effectively requires a knowledge of the full spectrum of engineering disciplines. This chapter covers the development and validation of a simulation model for a complete wind energy conversion system (WECS). The interfaces between the wind and the blades, the developed blade torque and the tower structure and finally the pitch controller and blades are discussed with special reference to a typical 455 kW turbine of similar design to the Howden HWP300 [52]. The scheme of these interlinking dynamics can be seen in Figure 2.1. Perfect yaw control is assumed so that the turbine is always facing into the direction of wind.

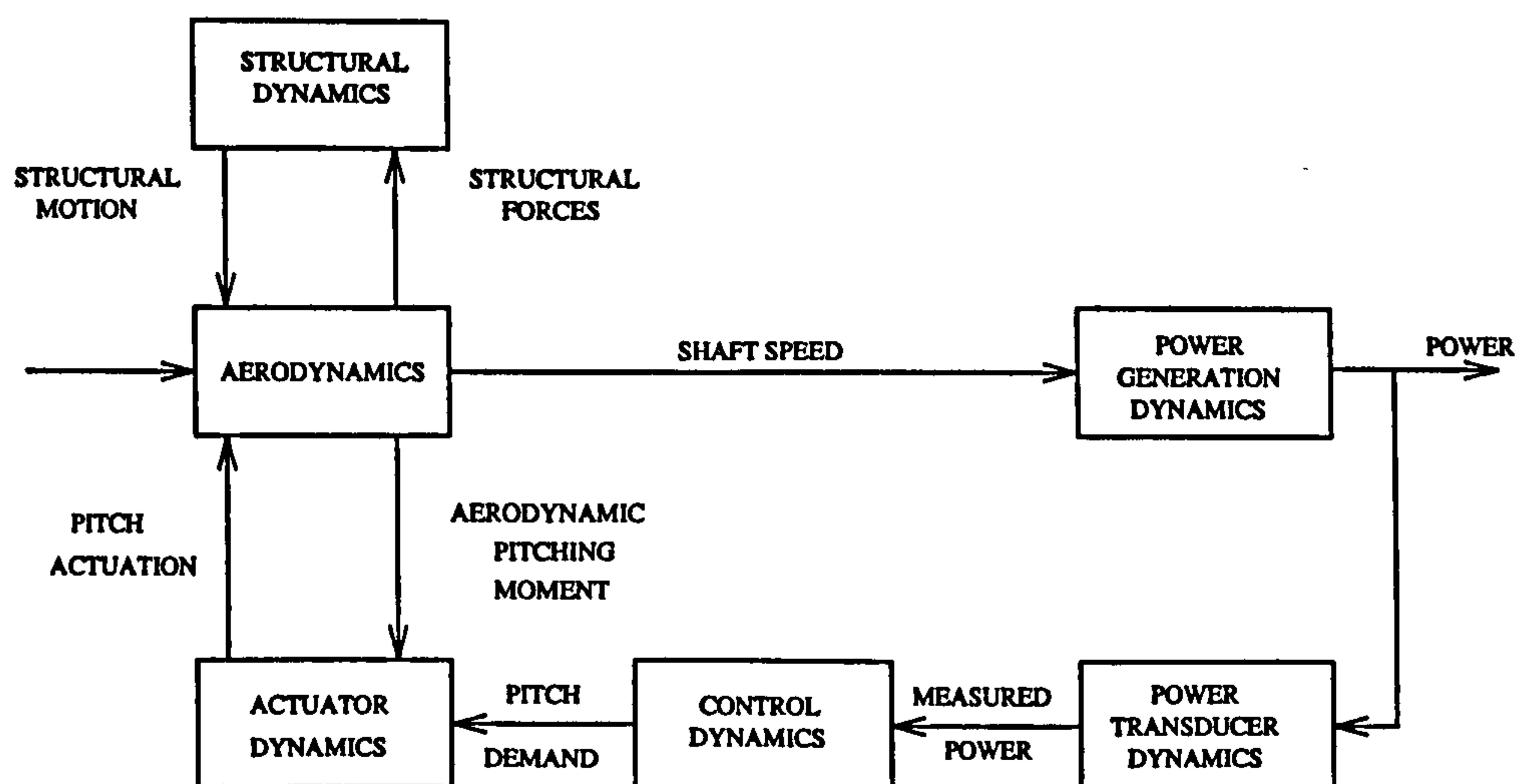


Figure 2.1: The dynamics of a pitch regulated wind turbine

In the first section of this chapter, the wind distribution near ground level is explored and two methods for modelling the turbulence, gusting and transient effects of the free

wind stream compared. The first method assumes that the same point wind speed acts throughout the wind stream and that the wind speed is made up from discrete elements with noise superimposed upon them consistent with that experienced by a typical wind turbine. This is then used to evaluate the power of the free wind stream experienced by the wind turbine. The second method is very similar except now the point wind speed is built up using spectral techniques to derive a point wind speed with the same spectrum as would be experienced by a wind turbine. The key simulation models for each method are presented and validation runs of these models are undertaken to compare the output with real measured wind data. These simulation models are contained in the 'Wind speed time series models' sub-library of the 'Fixed Speed Wind Turbine Modelling Library' shown in Figure 1.4.

The second section of the chapter goes on to examine the wind interaction with the rotating blades which is the integral part of any WECS as this is the mechanism whereby power is extracted from the wind and converted into useful torque. Again both the discrete and spectral point wind speed methods are compared and conclusions made as to which method is most suitable for the test bed simulation of the permanent magnet synchronous generator. The simulation models developed in this section are contained in the sub-library 'Wind Turbine Models' again shown in Figure 1.4.

Pitch control is considered to be the most appropriate power control method for the reasons given in section 1.2.5 and the pitch controller of a typical WECS is outlined, the modelling associated with it discussed, and the development of the 'Pitch Controllers' library shown in Figure 1.4 described. The pitch controller comprises an industry standard PI control algorithm and a model for the actuator dynamics. The design and validation of the PI controller and pitch actuator is outlined and a few sample results presented.

The last section of this chapter summarises the chosen methods for modelling the wind interaction with the wind turbine and presents the overall Simulink model necessary for such a simulation.

2.1 Wind distribution near ground level

The free wind stream is the raw energy input to a wind turbine and as such it is crucial to understand its dynamics upto a height of about 100 metres. The energy spectrum of fluctuations in the free wind stream has already been presented in section 1.1.1 and it is now necessary to consider the timescales associated with modelling the wind for the assessment of wind turbine performance.

There are two key timescales. Firstly an analysis of the wind speed is usually carried out at a proposed site for a wind turbine or farm which takes into account all the variations likely over a year to establish the overall energy capture. Secondly turbulent models are used to establish the dynamic performance of a given wind turbine design to show that it will be safe in all wind conditions. These two timescales require different modelling techniques and both are required in this thesis to analyse the performance of the direct drive wind turbine design.

2.1.1 Yearly distribution modelling and energy capture prediction

To evaluate the total energy capture of a wind turbine requires a prediction of the number of hours a turbine operates in a certain mean wind speed regime and the power output of the wind turbine for that mean wind speed.

WIND DISTRIBUTION. The large spectral gap between the diurnal contribution and atmospheric turbulence allows a wind energy analysis where the latter is considered to be a stationary process [53]. Probability distributions such as the Weibull function can then be used to evaluate the number of hours the wind turbine experiences a mean wind speed at a site. The Rayleigh distribution, which is a special case of the Weibull function with shape factor 2, is a simple single parameter function that is widely used to describe the wind [54]. When preparing such estimates it is usually implicitly assumed that the distribution is the same from year to year although this may not be true.

The Rayleigh distribution provides a reasonable approximation over flat terrain and states that the probability, $p(U)$, that the wind speed exceeds a certain value, U , is given by,

$$p(U) = \exp \left[-\frac{\pi}{4} \left(\frac{U}{U_m} \right)^2 \right] \quad (2.1)$$

2.1 Wind distribution near ground level

where U_m is the annual average wind speed. This equation implies that wind speeds in excess of U_m occur for 46 % of the year whereas wind speeds above $2.4 U_m$ occur for less than 1% of the year. A graphical representation of the Raleigh distribution can be seen in Figure 2.2 for a site with a mean average wind speed of 8 m/s.

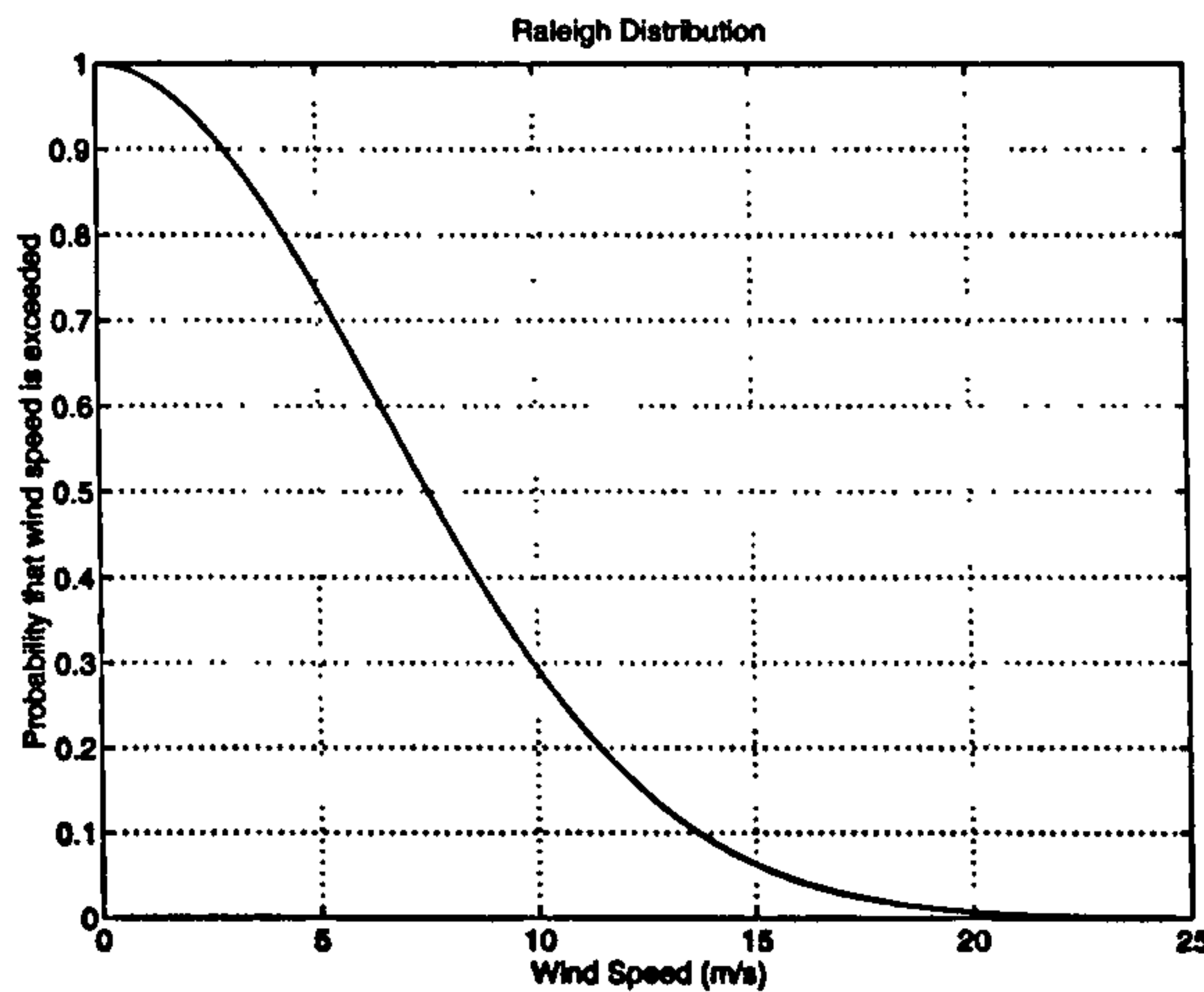


Figure 2.2: Raleigh Distribution

At any given wind speed, U , the power in the wind, P , per unit area is simply the product of the kinetic energy per unit mass and the mass flow rate. This leads to the expression for the power present in the free wind stream,

$$P = \frac{1}{2} \rho U^3 \text{ per unit area} \quad (2.2)$$

Combining the results from equation 2.1 with equation 2.2 gives the free stream energy during one year. It is now necessary to understand the effectiveness of a wind turbine at extracting this energy.

2.1.2 Typical performance characteristic

According to equation 2.2, the power available in the wind increases as the cube of the windspeed. High windspeed is not encountered often enough to make it economic to extract the total energy available during the year. Over-engineering is thus kept to a minimum by rating the generator for an optimum windspeed and then using some form of aerodynamic power limiting above this windspeed. Two forms of aerodynamic limiting are commonly used - stall regulation where the rotor falls progressively into stall as the wind speed increases

and pitch regulation where the power is shedded by feathering a portion of the blades. Excessive wear and fatigue of the turbine is also avoided by having a cut-in wind speed below which it is uneconomical to run the turbine as most of the captured energy is dissipated in overcoming the losses of the turbine. Typical cut-in and cut-out wind speed are 5 and 25 m/s respectively [55].

The desired power curve for such operation can be seen in Figure 2.3 (a). Above rated windspeed the pitch controller maintains power at the rated value and below rated wind speed the performance of the wind turbine is determined by the typical variation of the power coefficient shown in Figure 2.3 (b). The power coefficient is discussed in greater detail in section 2.2. Pitch control is also beneficial in helping with the start-up and shut-down of the turbine. It is currently the predominant form of regulation today and is selected for the wind turbine model.

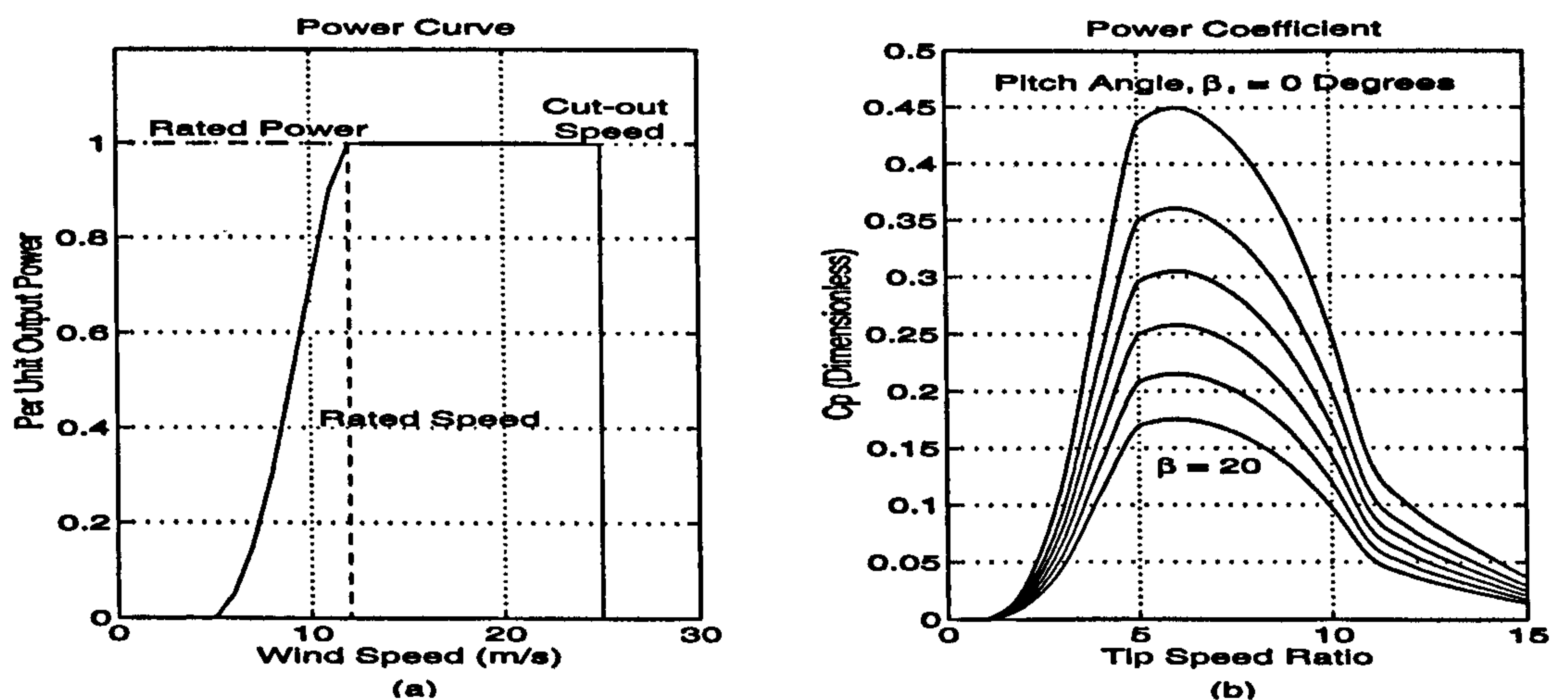


Figure 2.3: A Typical Output Power Curve and the Power Coefficient

To carry out an energy analysis requires the value of the energy present in the free wind stream to be modified by the performance curve of Figure 2.3 (a). Such an energy capture analysis is presented in Chapter 5 when comparing the fixed and variable speed operation of the direct drive wind turbine.

2.1.3 Turbulent timescale wind modelling

This section is devoted to the complex subject of the simulation of the wind itself and how the type of model impacts on the type of results achieved. Turbulent timescale wind was

initially modelled by adding up a set of discrete component parts in the wind, i.e. turbulence, gusting, ramping components, to establish a point wind speed at any given time and assume that this value acted over the whole wind turbine swept area. This allowed the design engineer to test the wind turbines performance for specific transient conditions. However experience with actual wind turbines proved that this method, although easy to implement, had some fairly serious drawbacks because of the failing to take into account blade rotation [56] [57]. As an individual blade rotates it samples a cross-section of the the whole free wind stream. The turbulence present in the wind takes a finite time to pass the turbine and therefore the blade samples this turbulence at a frequency proportional to its rotational speed. This alters the effective frequency spectrum of the developed shaft torque in such a way which is not included in the discrete point wind speed model. A representation of this process can be seen in Figure 2.4. Spectral techniques were, therefore, developed which can account for blade rotation, wind shear and tower shadow and model the wind speeds in the entire swept area of the blades [58]. The spectral method is based on using cross-correlation between two point wind speeds within the swept area to generate a spectrum for turbulence in the whole swept area. This spectrum is then converted into an effective point wind speed which has the correct spectral characteristics as would be present in measured wind data. Both techniques have been implemented and a comparison carried out between them to see which method is best for the performance assessment of the direct drive wind turbine.

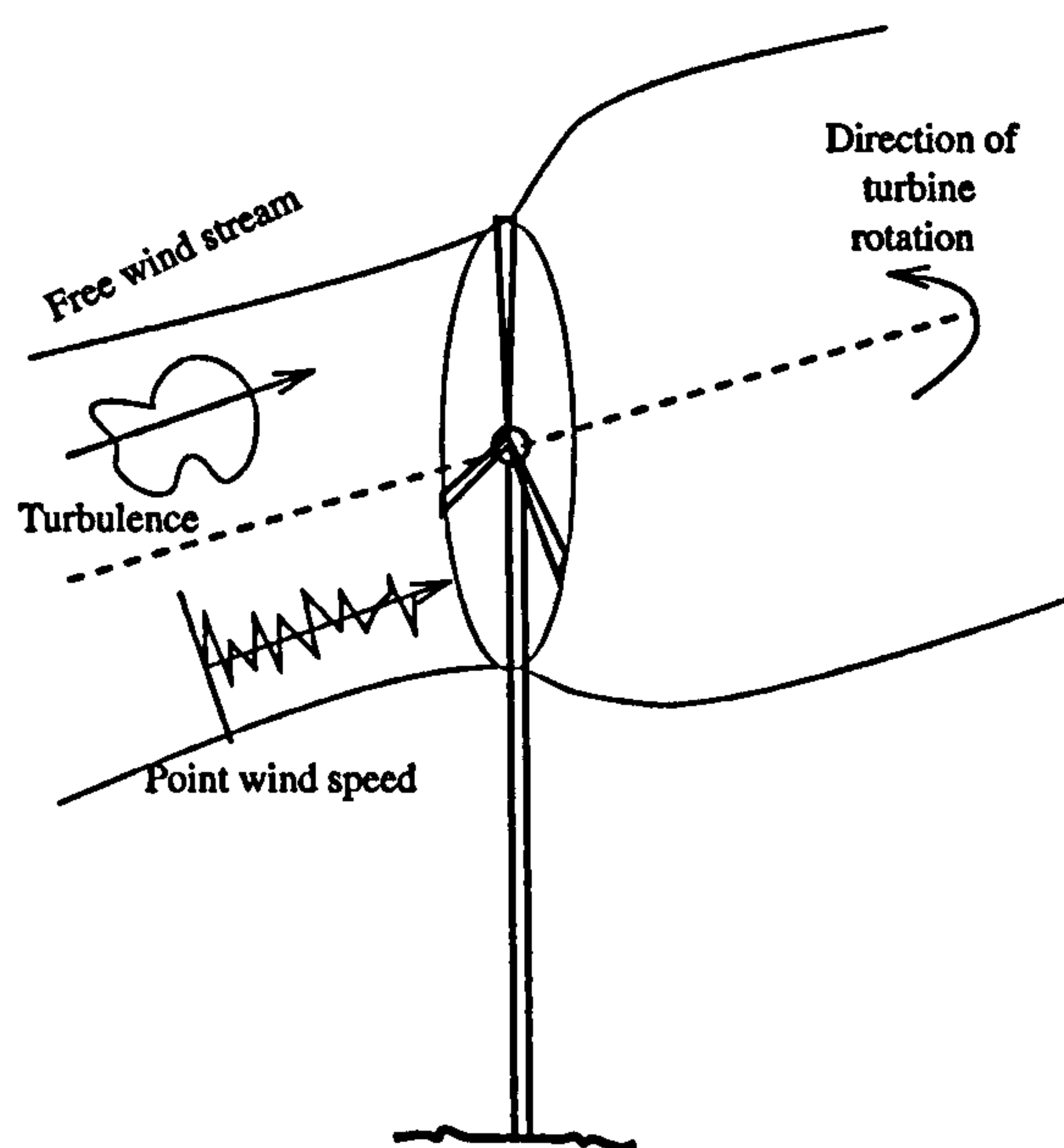


Figure 2.4: Rotational sampling of the free wind stream by the rotating blades

2.1 _____ Wind distribution near ground level

2.1.4 Discrete model of the turbulent wind

In the discrete model for generating a point wind speed time series the wind is broken down into four components as can be seen in Figure 2.5: a base component which corresponds to the underlying strength of the wind, a noisy component representing turbulence, a ramp component which relates to a gradual increase in the base speed and a component representing gusting. The total wind speed at any time is given by the addition of all four components.

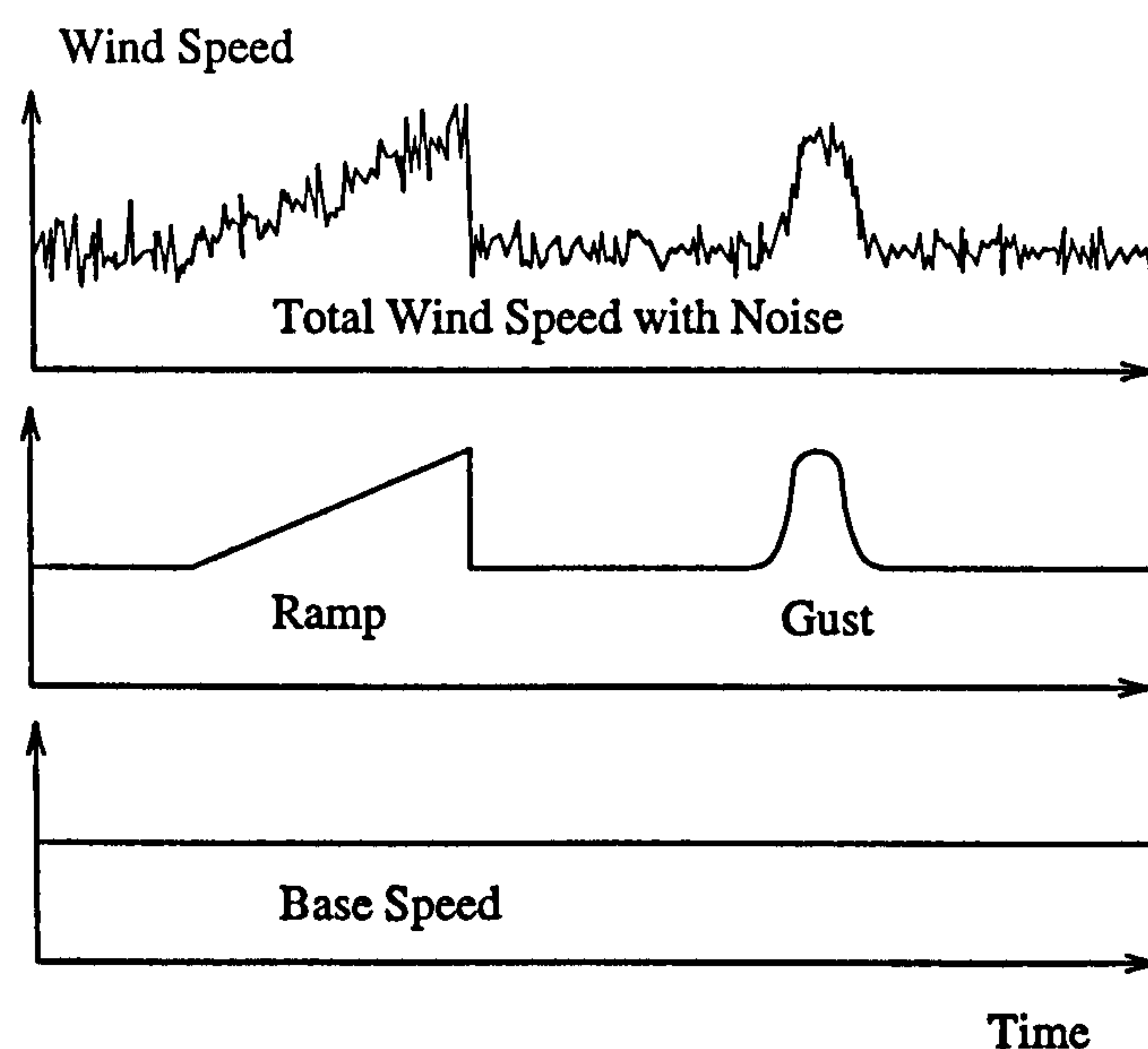


Figure 2.5: Simulation of the Wind

The graphs are shown as variations in time. However wind varies as a multidimensional, multivariate process in all directions and therefore the point wind speed model is inherently inaccurate. To improve the accuracy requires either a detailed dynamic blade model which maps the interaction of the wind stream and finite sections of the turbine blades into hub torque which is a function of time only [59] or the use of a power spectral methods. Work is being done to eliminate the inaccuracies from the point wind speed model but O. Wasynczuk [60] reports that the correlation between the assumed point windspeed model and accurate wind data is reasonably good. The wind equations are listed in Appendix A and are taken from work carried out by Anderson [40]. This is implemented on SIMULINK by inputting a vector of values for time and the corresponding values for the point wind speed calculated by a MATLAB script, *windspeed.m*, which carries out the above discrete method. Before the spectral method can be introduced it is necessary to expand on SIMULINK [44] to clarify

to the reader how models can be developed to represent both algebraic and differential equations.

2.1.5 MATLAB with SIMULINK

SIMULINK [44] is a dynamic modelling package which allows quick and easy simulation of complex n^{th} order differential equations and control systems. It is written by Math Works and front ends MATLAB, the matrix laboratory program, and as such the results from any script written for MATLAB to execute complex algebraic vector calculations can easily be input into SIMULINK models. The package solves the full non-linear set of differential equations that govern the system by using a fifth order Runge-Kutta-Fehlberg technique with adaptive step size control. The Control Systems Toolbox extension package allows full system linearisation to be performed and propagation of the solution for any continuous input time history. Hence time responses of the linearised version can be checked against the full non-linear version and conclusions may be drawn as to which values to use for the best performance of the system.

From this point on in the thesis several block diagrams of SIMULINK systems will be presented, which represent different aspects of the wind turbine, pitch controller, permanent magnet generator and frequency converter. The process of building these individual models from their governing equations and how they are glued together to form complete system models will also be explained and the models then used to derive an understanding of the operation of the direct drive permanent magnet generator in the windy environment.

2.1.6 SIMULINK implementation of the discrete point wind speed model

The 'Wind speed time series models' library shown in Figure 1.4 expands to give the library of blocks shown in Figure 2.6. The first block is the implementation of the discrete method as the wind time series history is calculated prior to running the simulations by the script, *windsped.m*. The spectral blocks will now be developed.

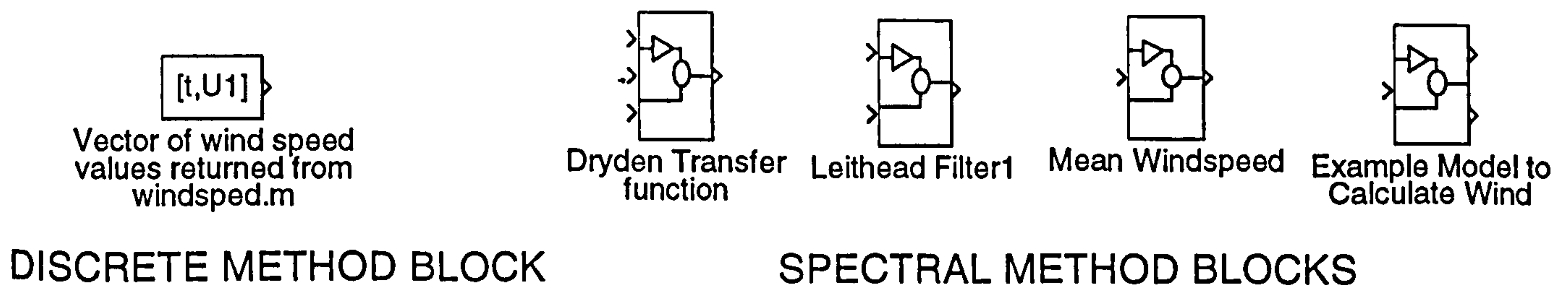


Figure 2.6: Wind speed time series library

2.1.7 Spectral model of the turbulent wind

The second method, mentioned earlier, is concerned with more accurately representing the fact that the free wind stream is a three dimensional wind field. The work of Kristensen and Frandsen [57] and Leithead [58] is particularly relevant and will be discussed now. This work is based on determining an expression for the spectrum of the wind field from the correlation between two distinct points within the free wind stream [41] and hence deriving a method of generating an effective wind speed which is spectrally correct. Therefore it is crucial to develop a good understanding of the likely variance of the wind speed experienced by the rotor and a model for the turbulent spectrum. The key equations and development of a model to generate an effective point wind speed with the correct spectral characteristic is now outlined with the full derivation included in Appendix A.

WIND SPEED VARIANCE. An estimate for the probable standard deviation of the wind speed as experienced by the rotor can be found from Connell's [56] turbulence intensity, i , which he defines as,

$$i = \frac{\sigma_u}{\bar{U}} \quad (2.3)$$

where σ_u is the standard deviation and \bar{U} is the mean windspeed. Connell presents the values in Table 2.1 as representative as the terrain and turbulence structure vary.

A value of 0.2 covers the situations above the horizontal line and is used for the evaluation of

the standard deviation of the turbulent wind spectrum for any mean wind speed according to equation 2.3 because it covers the areas where wind turbines are most likely to be sited.

TURBULENCE AT A POINT. There are numerous models for representing the power spectrum of turbulent windspeed, $S_u(\omega)$ about an average windspeed (\bar{U}). They are generally of the form,

$$S_u(\omega) = \frac{K_v |\omega|^\mu}{[1 + (\omega T_v)^\alpha]^\beta} \quad (2.4)$$

The factors K_v and T_v depend on such factors as the surface roughness, turbulence intensity and mean windspeed of a site. The powers α , β and μ depend on which spectrum is used. The most commonly used examples are the Von Karman [41], Davenport [61], Dryden [62], and Kaimal [63] spectra. From a considerable literature search the Von Karman spectra, although perhaps slightly inaccurate due to the assumption about turbulent length scales, is the most popular and is used in this work,

$$S_u(\omega) = 0.475 \sigma_u^2 \frac{L \bar{U}^{-1}}{[1 + (\omega L \bar{U} - 1)^2]^{\frac{5}{6}}} \quad (2.5)$$

This spectrum is centered on the average windspeed, \bar{U} , with a standard deviation, σ_u , given by equation 2.3 and a turbulent length scale L . The turbulent length scale can be considered as the length of typical eddies in the free wind stream. This is quite difficult to estimate but Frandsen suggests a good approximation [64] to be,

$$L = 6.5h \quad (2.6)$$

where h is the height above ground at which the wind is measured and is usually taken to be the hub height of the wind turbine.

MODELLING THE VON KARMAN SPECTRUM. The Dryden spectrum can be

Terrain Type	Turbulence Structure		
	Stable	Neutral	Unstable
Simple	0.08	0.15	≤ 0.4
Gentle Complex	0.12	0.2	0.4
Moderate	0.18	0.3	0.5
Severe Complex	0.25	0.35	0.5

Table 2.1: Turbulence Intensity

used to approximate the Von Karman spectrum as the Dryden spectrum is more easily modelled [65]. The Dryden spectrum has a transfer function given in equation 2.7 and the values of b_t and a_t are selected to closely fit the Von Karman spectrum.

$$W_{FS} = \frac{b_t}{s + a_t} \quad (2.7)$$

A series of Dryden spectra are generated to give a best fit approximation to the Von Karman spectrum over the range of windspeeds required with the turbulent length scale, L , given by equation 2.6. The value of a_t is found from the break point on the Von Karman spectrum and the value of b_t is found from the initial gain. The value of b_t must be modified so that the standard deviation of the wind speed is consistent with that presented in equation 2.3. This is achieved by passing a white noise signal through a block representing the Dryden spectrum and increasing b_t until the required standard deviation is achieved. This gives the variation of b_t and a_t against mean wind speed and these variations are implemented as two look-up tables. Typical plots of the two spectra for a mean wind speed of 15 m/s and turbulent length scale of 200m (equivalent to a 200 kW turbine), can be seen in Figure 2.7. The Von Karman spectrum is a smooth curve as it is generated numerically and the Dryden spectrum is generated by using MATLAB's Fast Fourier Transfer routine on the filtered white noise. The spectrum of the white noise closely follows the Von Karman spectrum. The dryden transfer function and white noise generator are implemented on SIMULINK by the blocks shown in Figure 2.8.

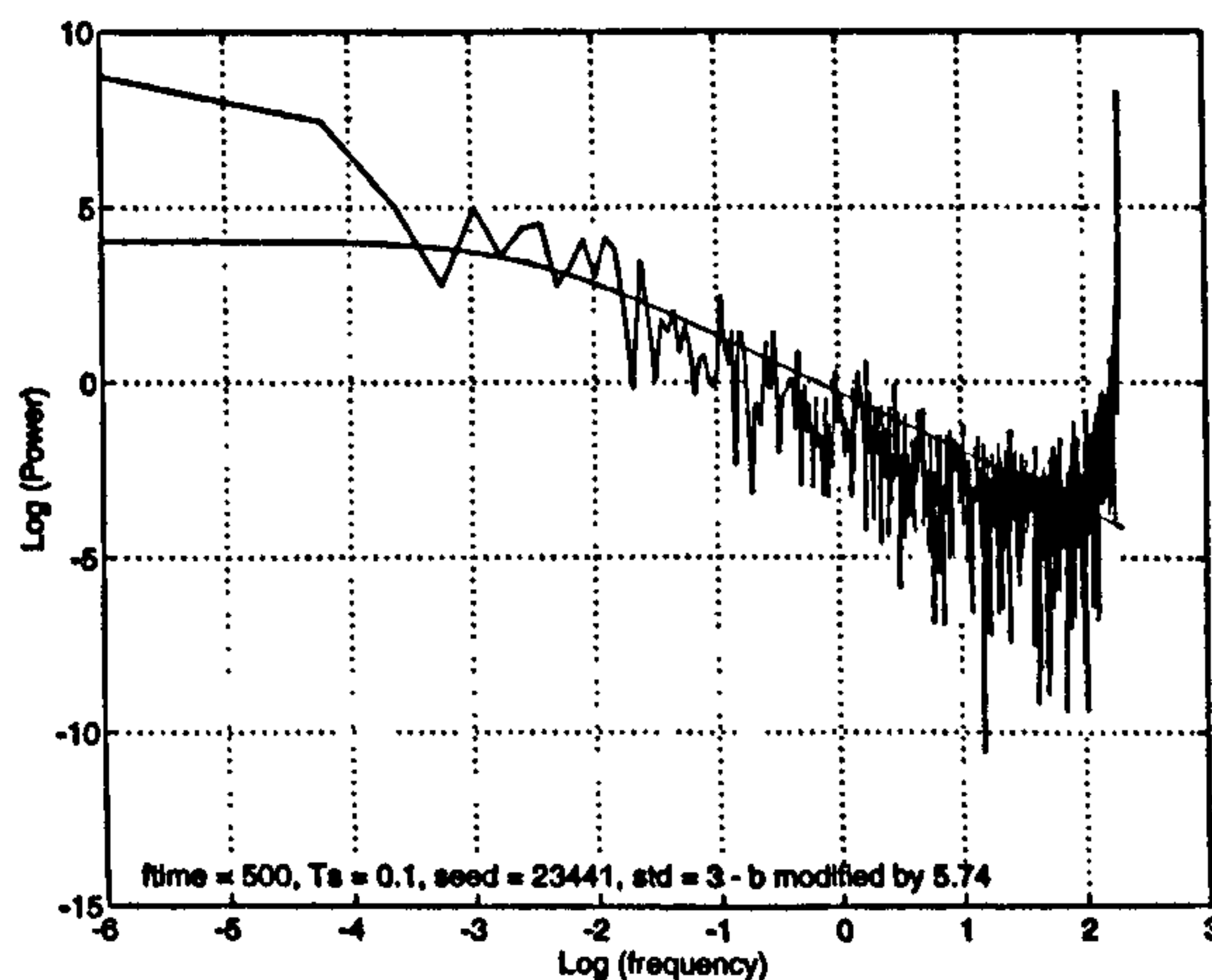


Figure 2.7: The Von Karman Spectrum and Dryden Approximation for $\bar{U} = 15$, $L = 200$

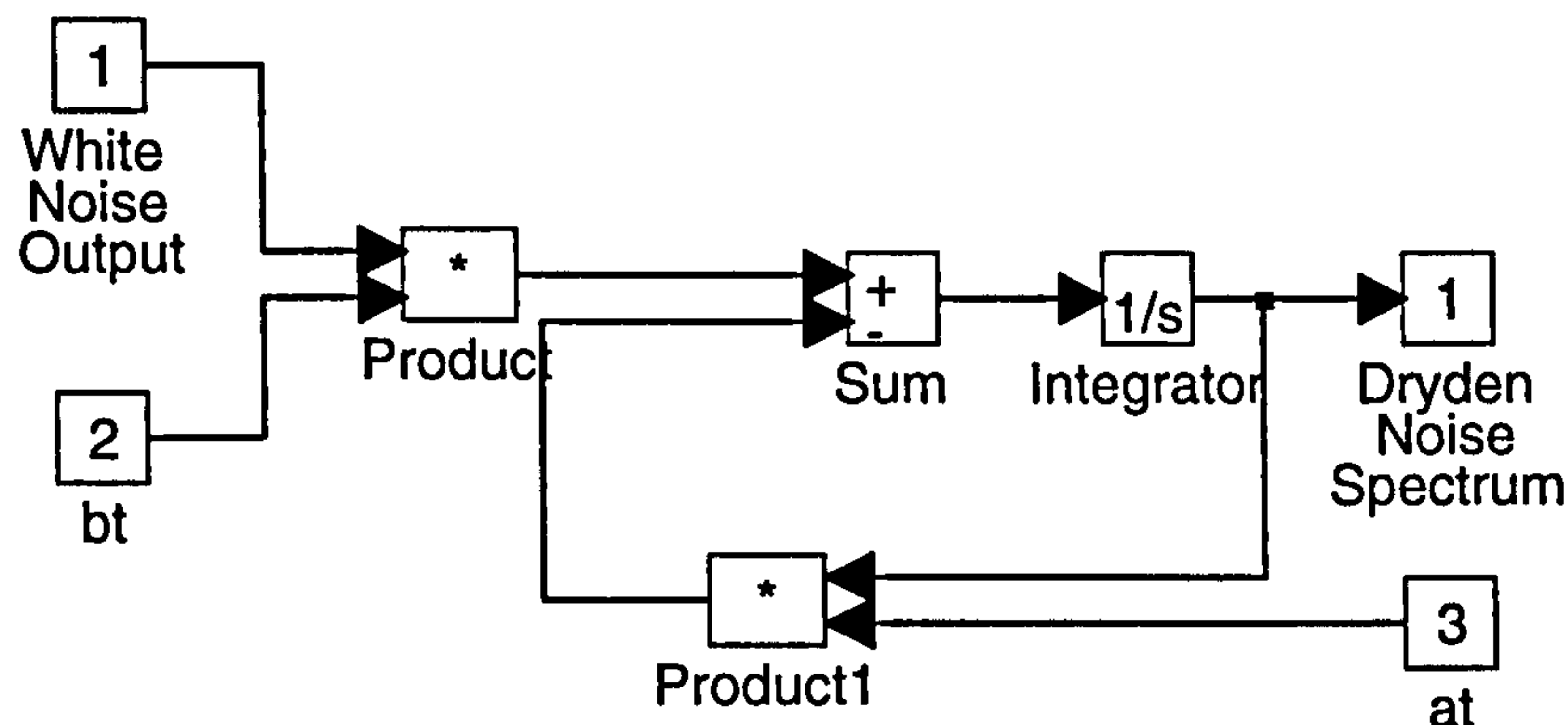


Figure 2.8: The Dryden Transfer function block

FROM TURBULENCE TO AN EFFECTIVE POINT WIND SPEED. Now that a method for evaluating an approximation to the Von Karman spectrum has been outlined it is necessary to show how this can be used to generate an effective point wind speed time history. This is done by the SIMULINK model shown in Figure 2.9.

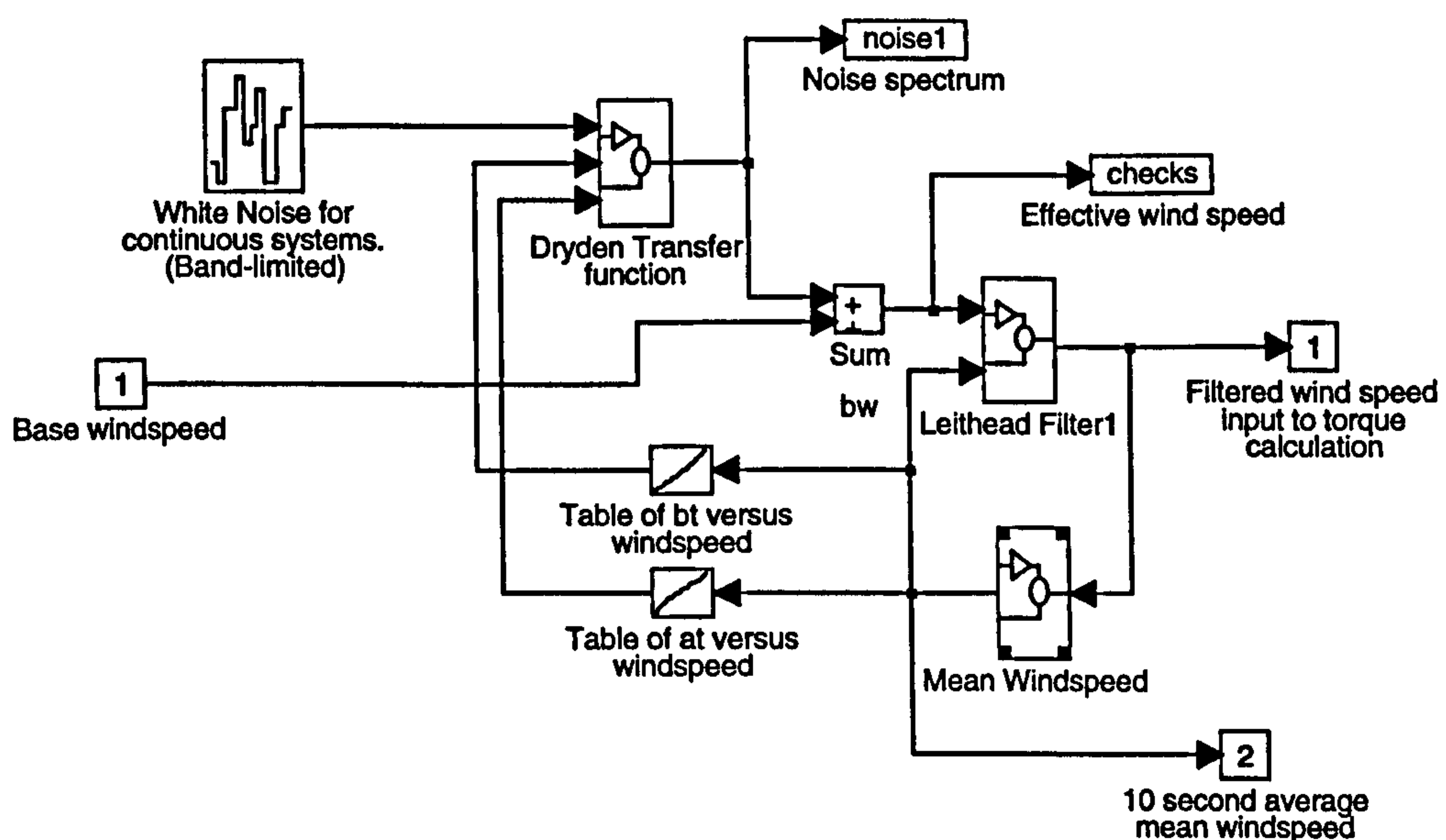


Figure 2.9: Generating an effective point wind speed by spectral modelling

The output from the white noise is spectrally filtered according to the Dryden approximation given by the values from the functions of b_t and a_t indexed by the mean windspeed and this value is added to the base wind speed to give the effective point wind speed. The mean windspeed is calculated over an averaging time of 10 seconds. To show the effective wind speed contains the correct spectral variation as real wind data it is necessary to validate

2.1 _____ Wind distribution near ground level

the output spectrum of the variable transfer function. The 'Leithead filter' block is the implementation of the spatial filter which represents the disk averaging by the rotation of the wind turbine blades and this is dealt with in section 2.2.2.

2.1.8 Validation of the point wind speed and spectral methods against measured wind data

It is when the output from the discrete and spectral derived point wind speed methods are validated against real wind data or need to be used as an input to the simulation of a wind turbine that the key differences between the two methods show up. The discrete point wind speed model is very labour intensive to set up as the individual gusts, ramps must be entered into the program which sets up the wind history to match it against the measured wind speed whereas the spectral method may not introduce exactly the same variations but will introduce the right spectral information. This is the important factor when determining the dynamic performance of the wind turbine and its control schemes.

A comparison of the type of wind history from the discrete and spectral point wind speed methods and real wind data for an average mean wind speed (AMWS) of 14.1 m/s can be seen in Figure 2.10. This real wind data was provided by the National Renewable Energy Laboratory (USA) and was recorded on a 42 m wind measurement mast [66].

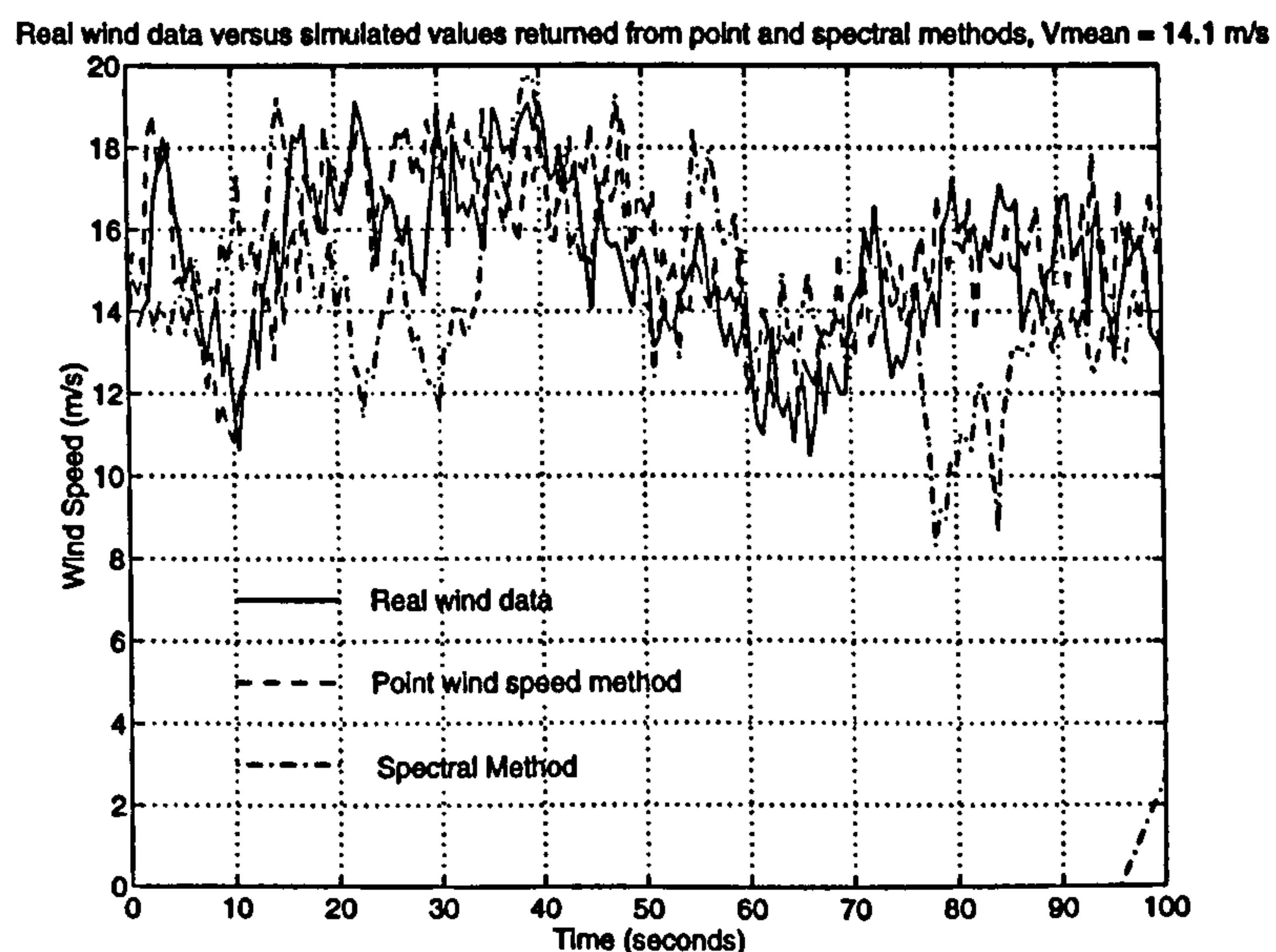


Figure 2.10: Wind histories from point and spectral methods versus real wind data

Clearly the point wind speed model can be constructed so that it follows the variation

of the real wind data. However it is a time consuming process and the spectral method gives reasonable correlation. A further comparison between the spectrum returned from the spectral method and that of the real wind speed data can be seen in Figure 2.11. It is important that the spectrum is the same as the real wind as this will ensure the same control action is necessary [58].

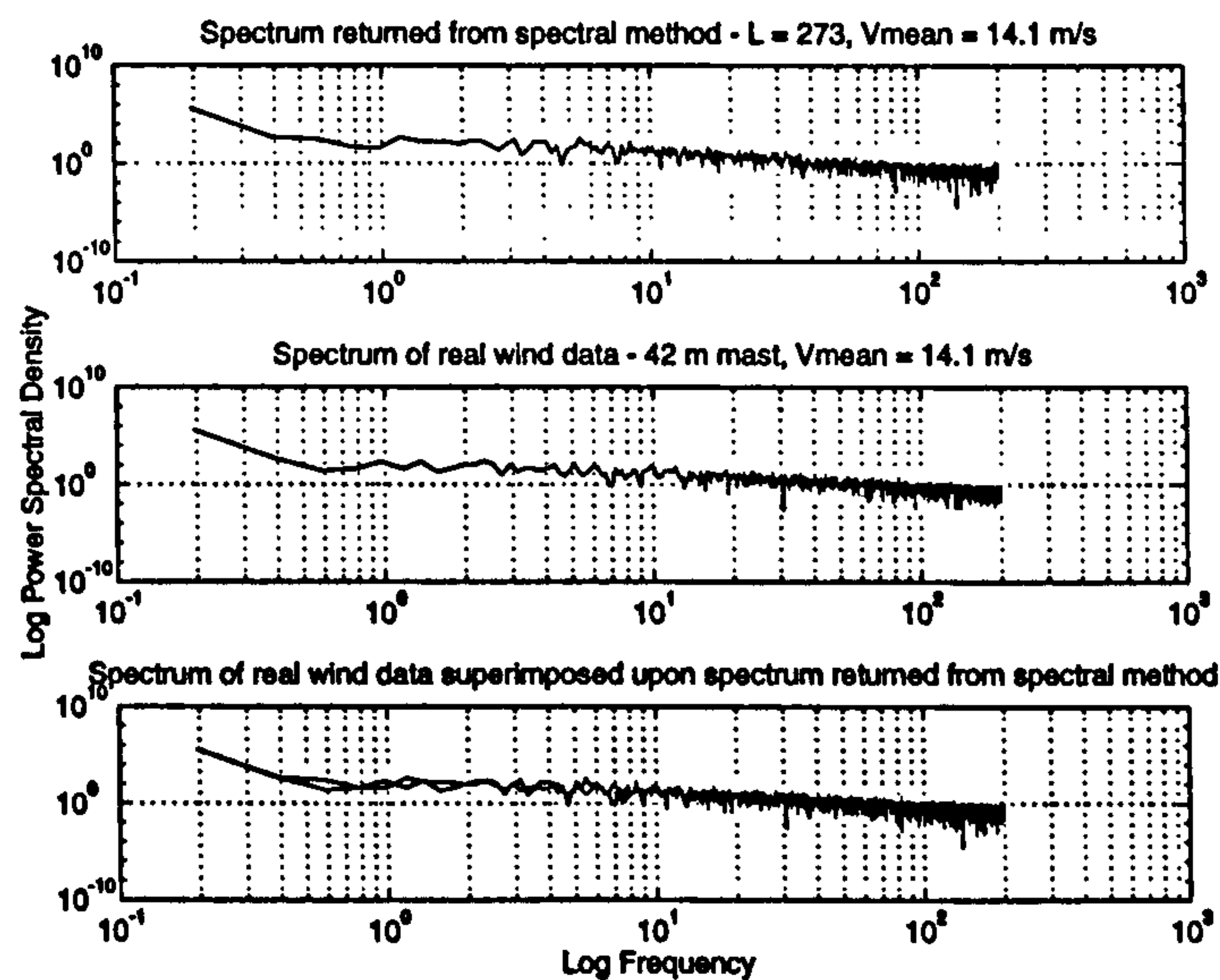


Figure 2.11: Spectrum of real wind speed data versus spectral simulation

Clearly good correlation is achieved between the spectra of the spectral method and from the real wind speed data. The previous two figures show that both the point wind speed and the spectral method can produce the correct free wind stream but the former is very time consuming to set up and for reasons which are made clear in the next section can lead to large inaccuracies in the developed shaft torque.

2.2 Wind Turbine Aerodynamics

The development of suitable models for the wind speed at a point in the free wind stream has been discussed in the previous section. It is now necessary to consider how the wind turbine blades interact with that free wind stream and outline which aerodynamic effects are the most important to include to ensure the key control criteria of the wind turbine can be met.

The physical approach to modelling the wind interaction with the blades involves finding

the net hub torque from the sum of the aerodynamic forces exerted on finite sections of the rotating blades [59]. The torque developed by each section is dependent on the local rotational velocity, the local windspeed and the sections geometry. A three dimensional wind model including the effects of rotational sampling and blade modes is required. This is very calculation intensive and so a simplified approach has been proposed [65] and this is described in the next few sections.

This section considers the complex question of wind turbine aerodynamics and, in particular, methods for simulating the wind interaction with the blades so as to get realistic values for the derived hub torque. The discrete and spectral point wind speed methods, presented in the previous section to obtain wind speed time histories, are extended to include the key effects introduced by the rotating blades to get an accurate shaft torque. The ‘Wind turbine model’ library shown in Figure 1.4 expands to reveal the blocks shown in Figure 2.12.

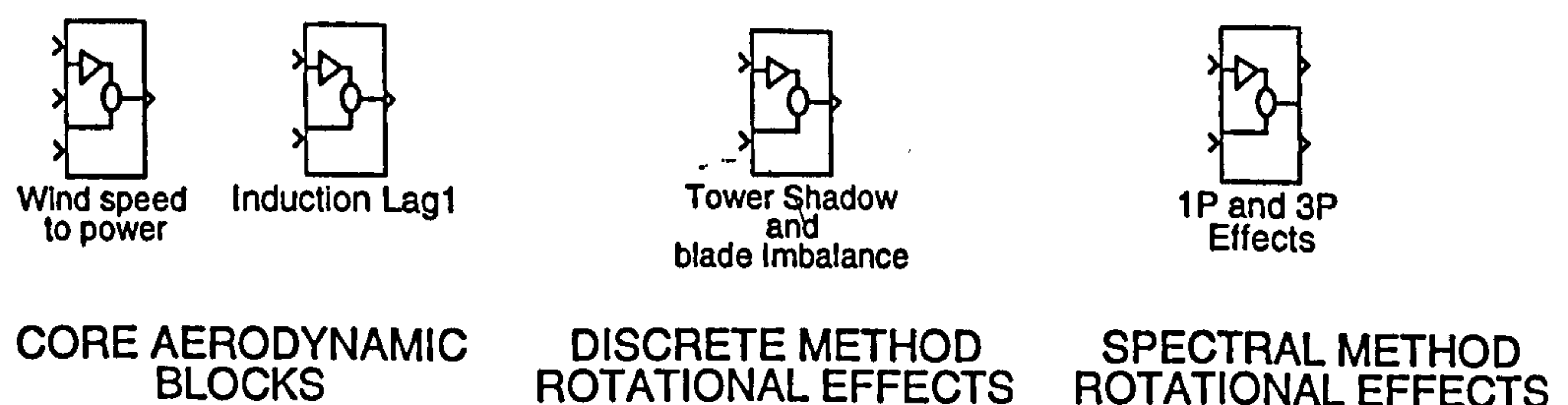


Figure 2.12: Wind turbine model library

Both the discrete and spectral methods are methods which allow the power in the wind to be determined from a point wind speed which is assumed to act throughout the wind stream and therefore there are some core blocks which are present in both simulation models. The differences between the two methods come about from the assumptions used to generate the point wind speed time history as described in the previous section and from differences in the modelling of the wind interaction with the blades. The differences in modelling the interaction of the wind with the turbine blades is now discussed and the results returned by

each method are then compared so that a choice can be made as to which method is likely to offer the best accuracy.

2.2.1 Power from the wind calculation

The first core block present in the wind turbine simulation is the block to calculate the power in the wind. The simplest method of modelling the interaction of the wind with the blades of the wind turbine is to assume that the same point windspeed acts throughout the wind field and that the power transmitted to the hub shaft is simply that from equation 2.2 modified by some factor known as the power coefficient. This power coefficient is dependent on the speed of the wind and the pitch of the blades [40]. The power coefficient can be seen graphically in Figure 2.1(b) and is incorporated into equation 2.2 to give,

$$P = \frac{1}{2} C_p \rho A U^3 \quad (2.8)$$

The wind speed is either generated by the simple discrete method or by the more complex spectral method which gives an effective point wind speed for the whole wind stream. This effective wind speed is used to induce the same spectral torque in the hub shaft as would the three dimensional windspeed acting over all the elements of the rotor [58]. Furthermore the spectral method method allows for the fact that the turbulence present in the free wind stream is rotationally sampled and this leads to important frequency spikes in the power spectrum of the induced torque which are not apparent in the discrete point wind speed method.

The merit of the point windspeed method is that it gives a quick and easy method for investigating the performance of the compliant mounting. The C_p curves are implemented as a look-up table referenced by both the tip speed ratio and the current pitch angle. The resulting power is converted into per unit torque by dividing by the turbine speed and per unit torque base. This has been implemented on SIMULINK and can be seen in Figure 2.13.

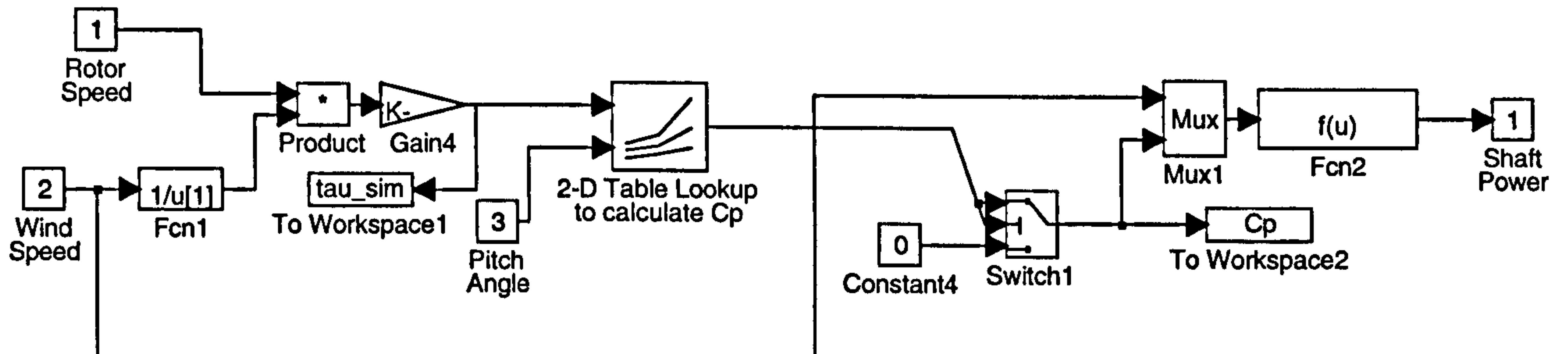


Figure 2.13: Evaluating the shaft power from the wind

2.2.2 Induction Lag

The second core block in both wind turbine models simulates the effect of induction lag. This transient effect must be included in both the discrete and spectral point wind speed methods. When the pitch on the blade or the windspeed changes there is a finite time delay whilst the airflow downstream from the turbine adjusts to suit. Stig-Øye [67] showed that the complex wake takes time to attain the required form with a time constant related to the windspeed. This can be seen in Figure 2.14.

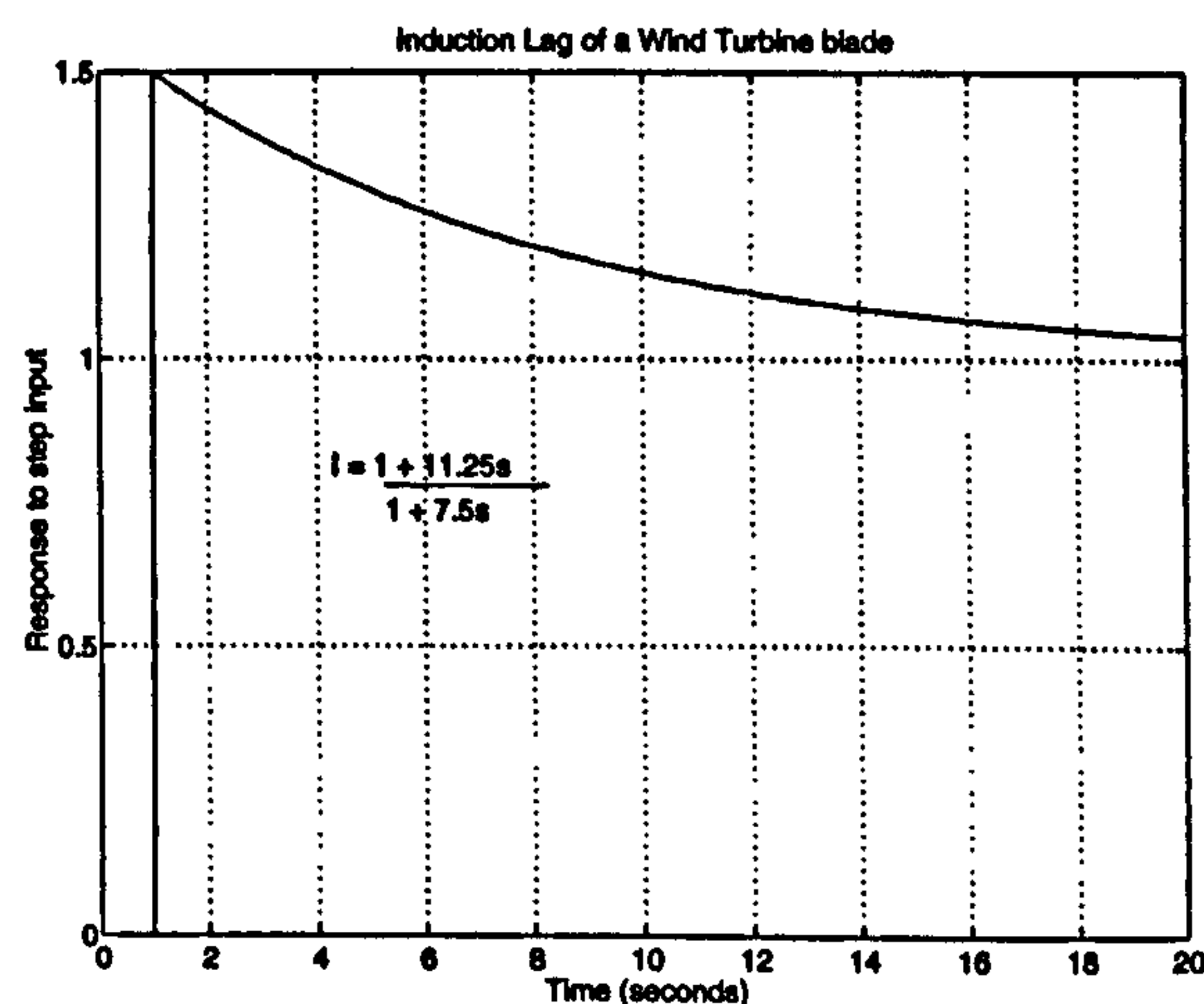


Figure 2.14: Induction Lag of a typical wind turbine

Typically there is an overshoot in the response of the blade flapwise bending moment of

about 50 % which then decays with a time constant roughly equal to the windspeed (m/s). The shaft torque also shows a similar response. This can be modelled by control lead-lag system of the form,

$$I = \frac{1 + As}{1 + \tau s} \quad (2.9)$$

This effect was initially considered only in the case of the spectral method but it has been included in the point windspeed model because it is an important transient effect which both methods should and can contain.

2.2.3 Additional effects to include in the discrete wind speed method

If the windspeed is only modelled at a single point, several key dynamic transients in the derived hub torque are neglected. These deterministic effects should be introduced into the discrete point wind speed method to get a more accurate torque input to the permanent magnet synchronous generator model. These additional effects are contained in the ‘Tower Shadow and Blade Imbalance’ block shown in Figure 2.12.

DETERMINISTIC EFFECTS. The hub torque induced by the wind contains certain deterministic variations due to the rotation of the blades. The first deterministic effect for both upwind and downwind wind turbines is a phenomena known as tower shadow [68]. Tower shadow in downwind turbines is easy to understand as it is fairly obvious that the tower will block the air flow in the region immediately downwind of the tower and hence as the blade goes through this region there will be a loss in driving force. These variations in driving force can lead to excess fatiguing of the blade. Tower shadow can be added to the point wind speed model by representing it as a pure sinusoidal torque variation,

$$T_{ts} = A \sin(\omega_{bp} t) \quad (2.10)$$

where T_{ts} is the torque variation that must be added to the overall torque, A is the amplitude of the variation and ω_{bp} is the blade passing frequency. For an upwind tower the effect is less apparent but still occurs due to the wind flow reversing after hitting the tower and causing a region of lower pressure. This has been implemented on SIMULINK and is referenced

on the block diagram of Figure 2.14. The tower shadow is calculated in per unit terms and is therefore added to the per unit torque from the wind to give the total per unit shaft torque. The amplitude of the tower shadow is scaled with windspeed such that the standard deviation introduced by it in above rated wind speeds is about 10 % of the rated torque of the turbine and this is a typical level for such a wind turbine [65]. In below rated wind speeds the torque amplitude is scaled down with the cube of the windspeed.

The second deterministic effect is wind shear. There exists a boundary layer between the surface of the earth and the free stream velocity at a great height. This velocity profile can be seen in Figure 2.15. The boundary layer has been described mathematically [40] by,

$$U_h = \frac{h}{H}^{\frac{1}{7}} U_H \quad (2.11)$$

where U_h is the wind speed at height h and U_H is the wind speed measured at the hub height, H .

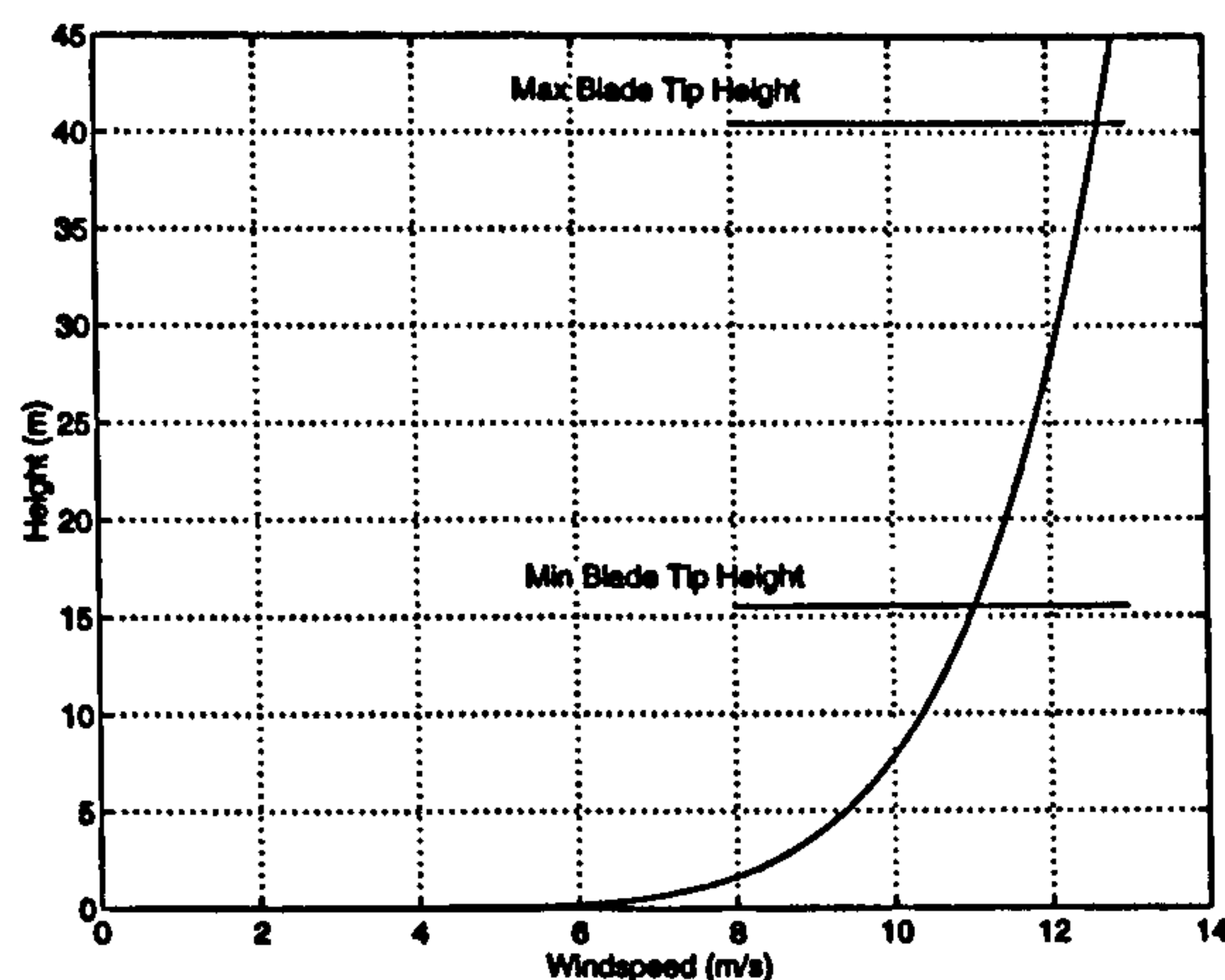


Figure 2.15: Wind Shear for a typical wind turbine

Wind shear introduces oscillations in the blade speed because there is more torque on the blades in the up position because the wind is stronger further away from ground level and less torque on the lower blades for the same reason. The effect of wind shear on the induced torque is more noticeable for a two blade turbine as for a three blade turbine and increases with turbine diameter. For the wind turbine described in this report the deviation in driving torque as the blade rotates is calculated to be less than 0.25% and is thus neglected for the discrete point wind speed model.

IMPLEMENTATION. The additional effects contained in the 'Tower shadow and blade imbalance' block which generate a suitable torque variation to add to the torque derived from the point wind speed can be seen in Figure 2.16.

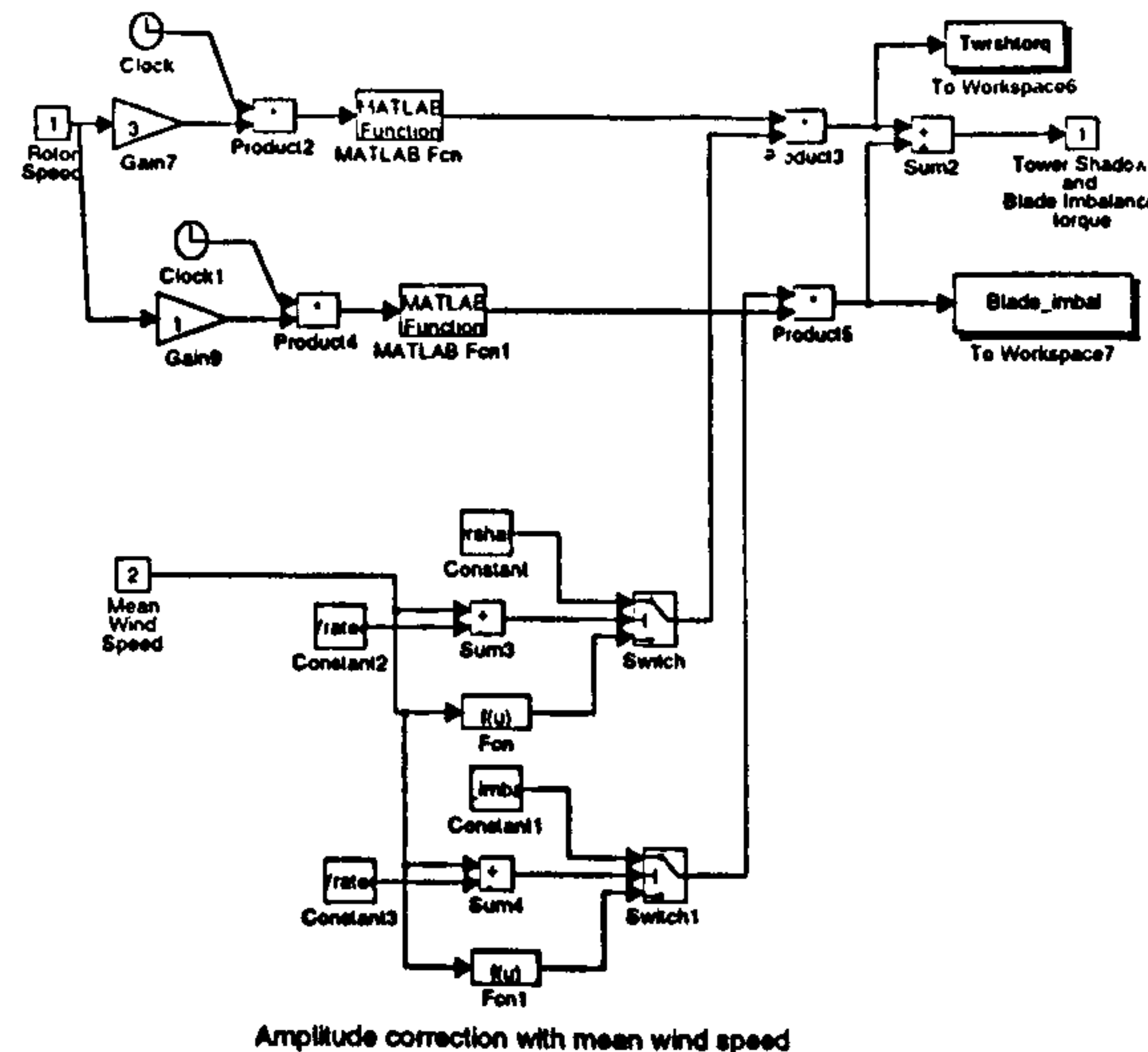


Figure 2.16: Tower shadow and blade imbalance

The blocks above the caption 'Amplitude correction with mean windspeed' are explained in greater detail in section 2.2.5 as they have been derived from the spectral method. Essentially the blocks ensure that the tower shadow and blade imbalance are scaled sensibly as the mean wind speed varies so that in low wind speeds the torque variation is maintained at a level corresponding to a 10 % increase in the standard deviation of the torque input to the generator model.

2.2.4 Overall SIMULINK implementation for the discrete wind speed method

The method of deriving the shaft torque from the discrete point wind speed model has been implemented on SIMULINK and can be seen in Figure 2.17. The wind velocity profile is generated by a MATLAB script prior to simulation runtime. The rotor speed and pitch angle are generated during the simulation run.

2.2.5 Additions to the spectral method

The method for deriving the torque for the spectral method is very similar to the point windspeed model except now an effective wind speed representing the three dimensional

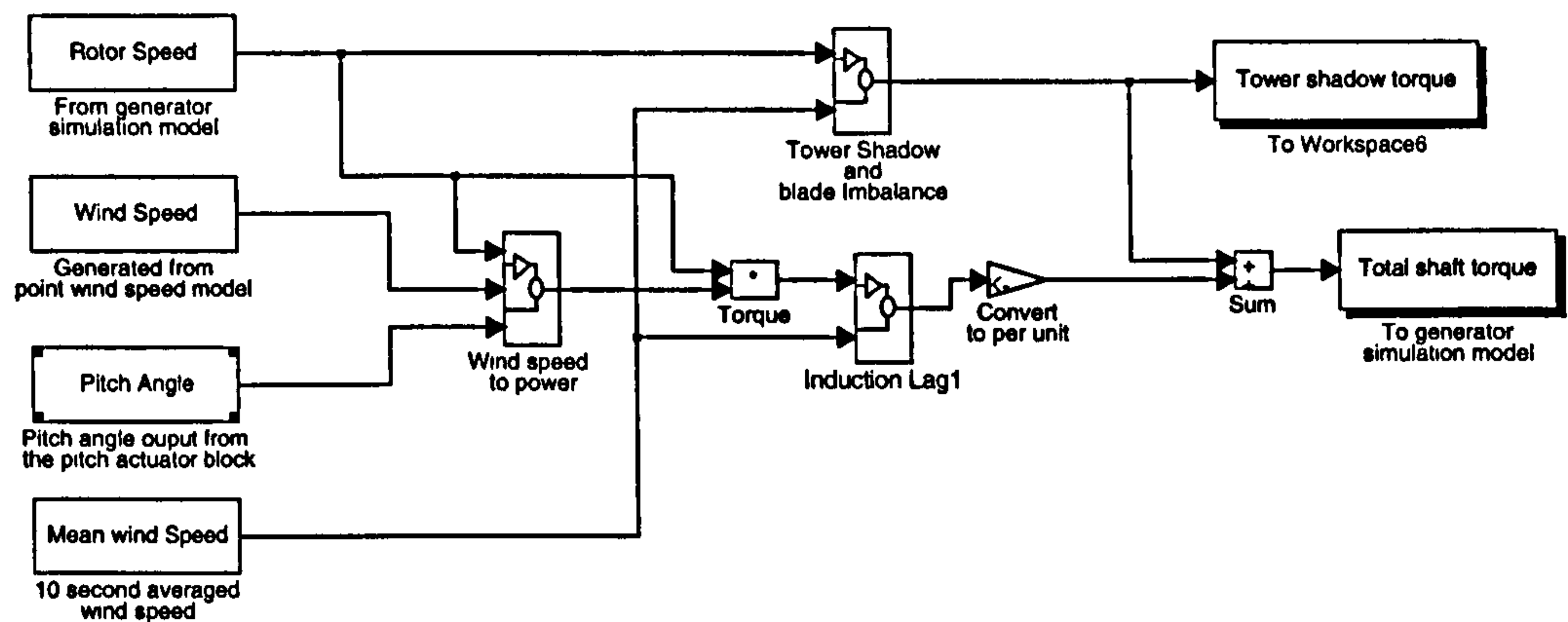


Figure 2.17: Converting the discrete point wind speed to shaft torque

wind speed is used [58]. This means that the correct spectral information is retained and the same equation for the mechanical input power can be used. However there are a few modifications that must be made to account correctly for the rotational sampling and disk averaging of the free wind stream by the rotating blades. The theory and implementation of a SIMULINK model for these two phenomena will now be presented and a method for quantifying their effect discussed.

DISK AVERAGING. The wind turbine experiences an average of the free stream wind speed over the rotor disc and this effect can be modelled by a spatial filter [69] of the form,

$$W_{AV} = \frac{(\sqrt{2} + \lambda s)}{(\sqrt{2} + \sqrt{a}\lambda s)(1 + \frac{\lambda s}{\sqrt{a}})} \quad (2.12)$$

This spatial filter is derived by using the cross spectrum of wind speed between two points in the wind field to evaluate the power spectrum of the driving torque. The value of a is taken as 0.55 and λ is given by the following expression,

$$\lambda = \frac{\gamma_s R}{U} \quad (2.13)$$

where γ_s is the decay factor of the turbulence and is taken to be 1.3. Hence the total wind spectrum is found by combining equation 2.7 and equation 2.12,

$$W_T = W_{FS} * W_{AV} \quad (2.14)$$

This filter which is dependent on the value of the mean wind speed can be seen in the SIMULINK block diagram shown in Figure A.1 in Appendix A. The effective point wind speed is averaged by the variable transfer function, W_{AV} . The effect of the spatial filter on the input wind speed from the spectral method can be seen in Figure 2.18.

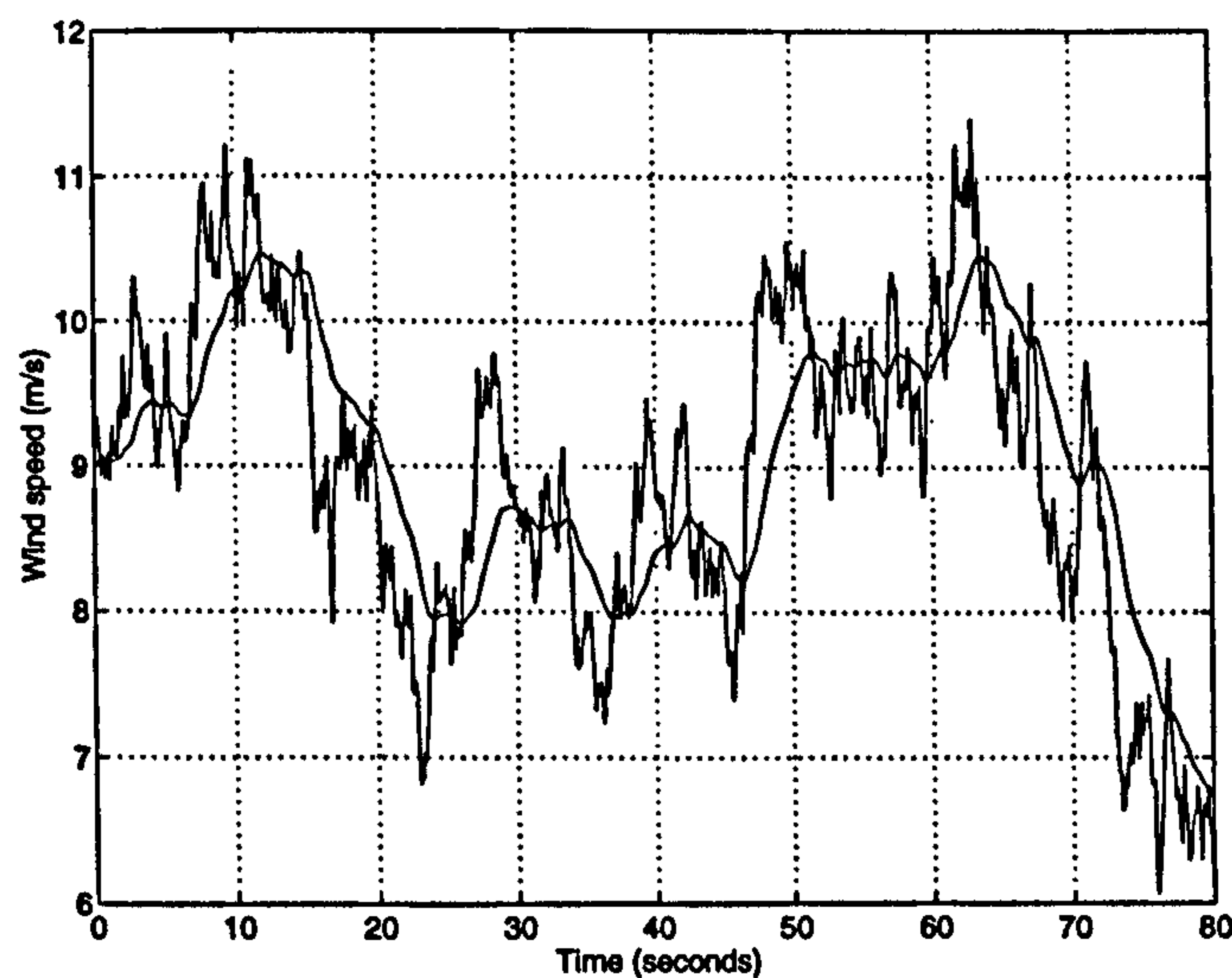


Figure 2.18: The actual and spatially filtered windspeed

MODELLING THE EFFECTS OF ROTATIONAL SAMPLING. As the wind turbine rotates it samples the wind field at its rotational frequency. This has the effect of introducing spectral peaks at multiples of the blade passing frequency and shifting the whole spectra towards higher frequencies [56]. This effect can be seen in Figure 2.19. The three curves have been generated numerically by the method presented in [57] and represent the effect of rotational sampling experienced by a typical wind turbine. The factors α and β referred to on the diagram are dimensionless quantities that determine the shape of the spectrum and are defined as,

$$\alpha = \frac{R}{L} \quad (2.15)$$

$$\beta = \frac{\bar{U}}{L\omega_r} \quad (2.16)$$

So for a given wind turbine design the predicted power spectrum of the shaft torque can be derived. Clearly as α increases the radius of the swept area increases and the amount of rotational sampling increases when compared with the spectrum at the hub, which is given by $\alpha = 0$.

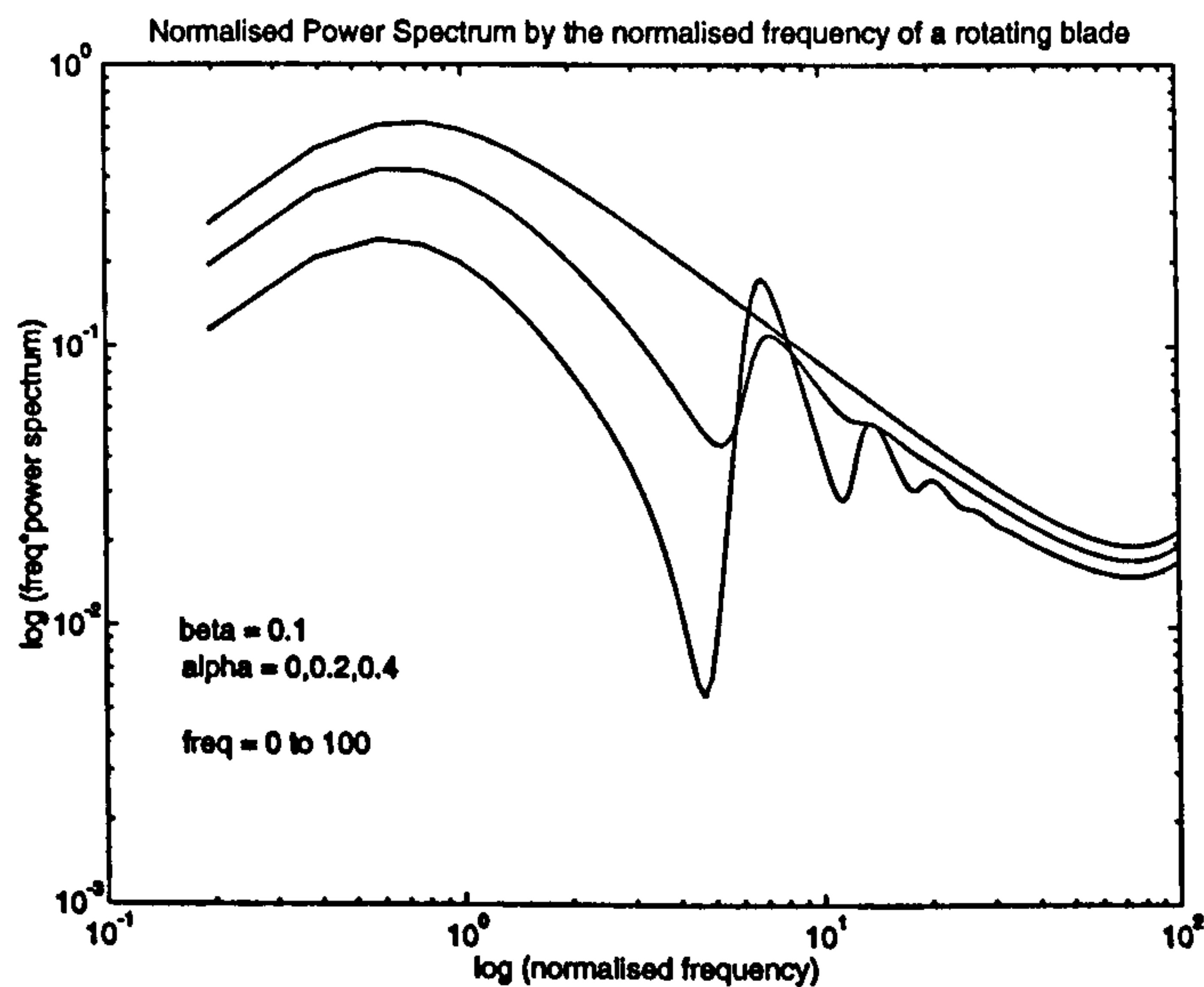


Figure 2.19: The Effect of Rotational Sampling on the Wind Spectrum

The largest spectral peak is at the rotational frequency of the blades, $1\omega_r$ and the relative size of the others depends on the turbulence and the rotor configuration. A small anemometer would experience no rotational sampling effect. The action of the blade chopping through the turbulence is the main cause of rotational sampling with the other terms, wind shear and tower shadow, contributing a small proportion.

By altering the shaft torque derived from the effective point wind speed model the net hub torque can be modified to include a principle component at $3\omega_r$, the blade passing frequency, to represent the rotational sampling. In a steady wind field the $1\omega_r$ components have no correlation and are, therefore, almost completely cancelled in the hub torque except a component attributable to blade imbalance. The $3\omega_r$ loads have some degree of correlation and hence do not cancel out [65]. It is easiest to implement the rotational sampling and blade imbalance effects as additive torques to the hub torque produced from the effective wind speed model and the following sections will outline how this can be done.

BLADE IMBALANCE. Blade imbalance covers such factors as engineering imperfections in the blades, offsets in blade position and even the build up of detritus. An imbalance torque is set up centered at $1\omega_r$. As it is mainly deterministic in nature the imbalance can be represented by,

$$u_{1r}(t) = A_{1r} \sin 1\omega_r t \quad (2.17)$$

IMPLEMENTATION. The power spectrum of the rotational sampling model must contain a spike at $3\omega_r$ to represent the deterministic components due to rotational sampling, tower shadow and wind shear and a broader spectrum to indicate the spreading effect of the stochastic part from turbulence in the wind. Furthermore a sin generator is required at $1\omega_r$ to represent blade imbalance. The model used to obtain this effective spectrum can be seen in Figure 2.20.

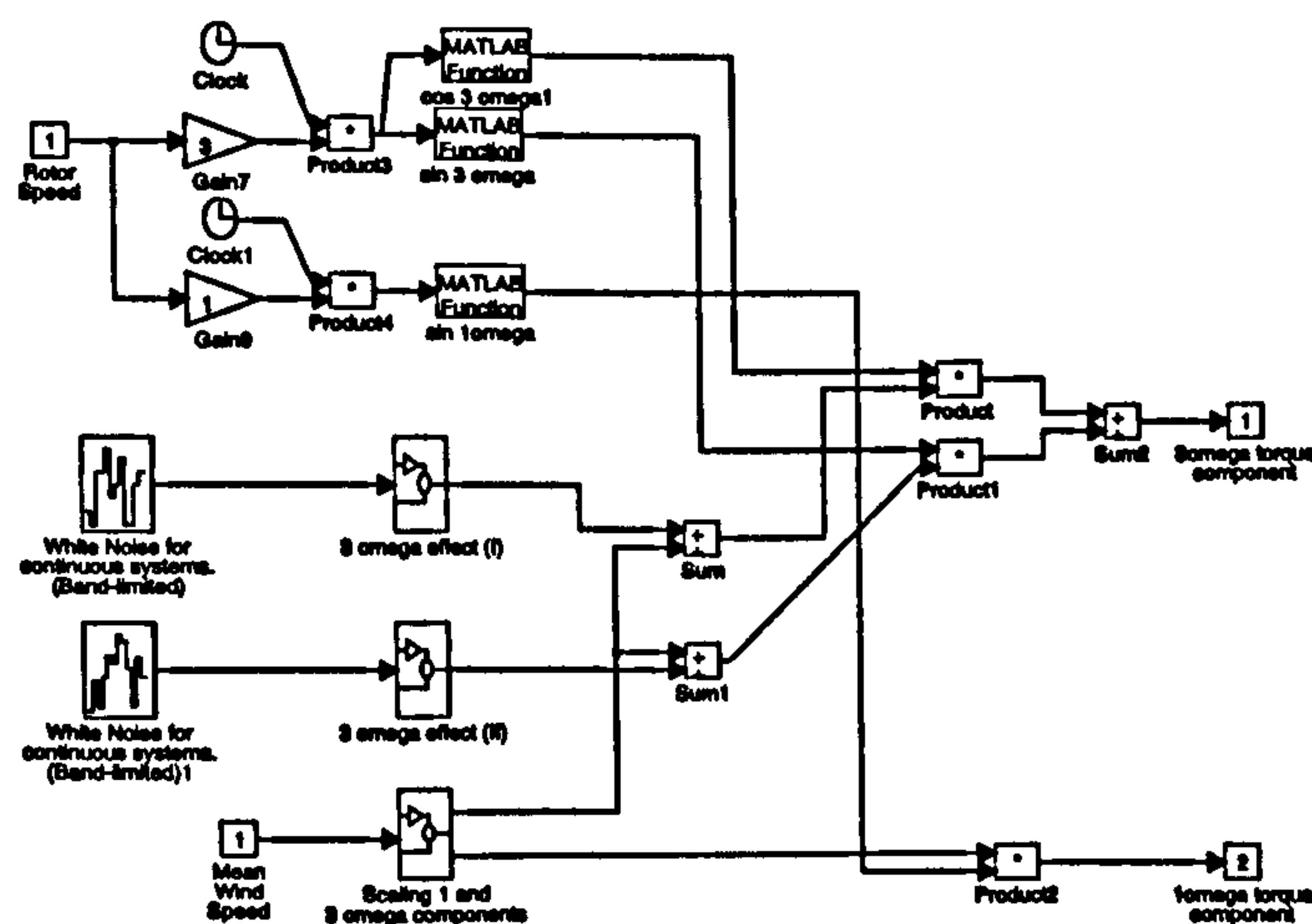


Figure 2.20: The Model of Rotational Sampling of the Wind Spectrum

The white noise generator gives the desired spread about $3\omega_r$ and the cos and sin generators give the desired spectral peak for the $1\omega_r$ and $3\omega_r$ effects. The magnitudes of the spectral components must be chosen to give good agreement with the spectral plot from representative site data.

QUANTIFYING THE ROTATIONAL EFFECTS. The standard deviation due to rotational effects at both $3\omega_r$ and $1\omega_r$ can be assumed to be equal to 10% of the rated aerodynamic torque with the ratio between the variances being 9:1 [70]. It is also assumed that this figure is constant above rated windspeed and reduces with the cube of the windspeed

below rated windspeed. Furthermore it is necessary to quantify what is the percentage contribution of the deterministic and stochastic components to the rotational sampling at $3\omega_r$. A reasonable approximation is to assume a ratio which gives 80% stochastic and 20% deterministic contributions. Evaluating the power spectrum of the $1\omega_r$ and the $3\omega_r$ equations and, using the ratios of the variances, values for the constants can be found. A program which automatically calculates these values from the data for the wind turbine has been written and the values it returns are shown in Table 2.2.

A_{3r}	Deterministic Component	3181.98
a_{3r}	Stochastic frequency spread	1.5
b_{3r}	Stochastic component	11.90E3
A_{1r}	Deterministic Component	3622.43

Table 2.2: Coefficient values for the rotational sampling effect

Again, as for the discrete point wind speed case, the standard deviation introduced by the rotational sampling of the free wind stream and other deterministic effects is assumed constant above rated wind speed but must be scaled for below rated wind speeds. The factors given in Table 2.2 are therefore scaled down as the cube of the windspeed to maintain a reasonable level of standard deviation.

2.2.6 Complete Wind Spectrum Model

Putting the ideas from the previous sections into context the overall spectral scheme for taking the wind speed to the torque driving the generator can be seen in Figure 2.21. The spatially filtered and mean wind speed values are input to the model, having been previously generated by the separate model shown in Figure 2.9. This pre-simulation run only needs to be carried out once for each windspeed and the values for the spatially filtered and mean wind speeds are stored as vectors in the MATLAB workspace. This reduces the computation time considerably. The corresponding power coefficient for the spatially filtered wind speed is substituted into the power equation to give the shaft power. This shaft power is then converted into shaft torque and passed through the filter representing the induction lag effect. The $3\omega_r$ and $1\omega_r$ torque disturbances are added to the shaft torque through a first order filter and then this total shaft torque is passed to the sixth order generator block.

As has been shown SIMULINK allows the user to group large sections of the individual functional icons together to allow for clearer representation of simulation models. This has

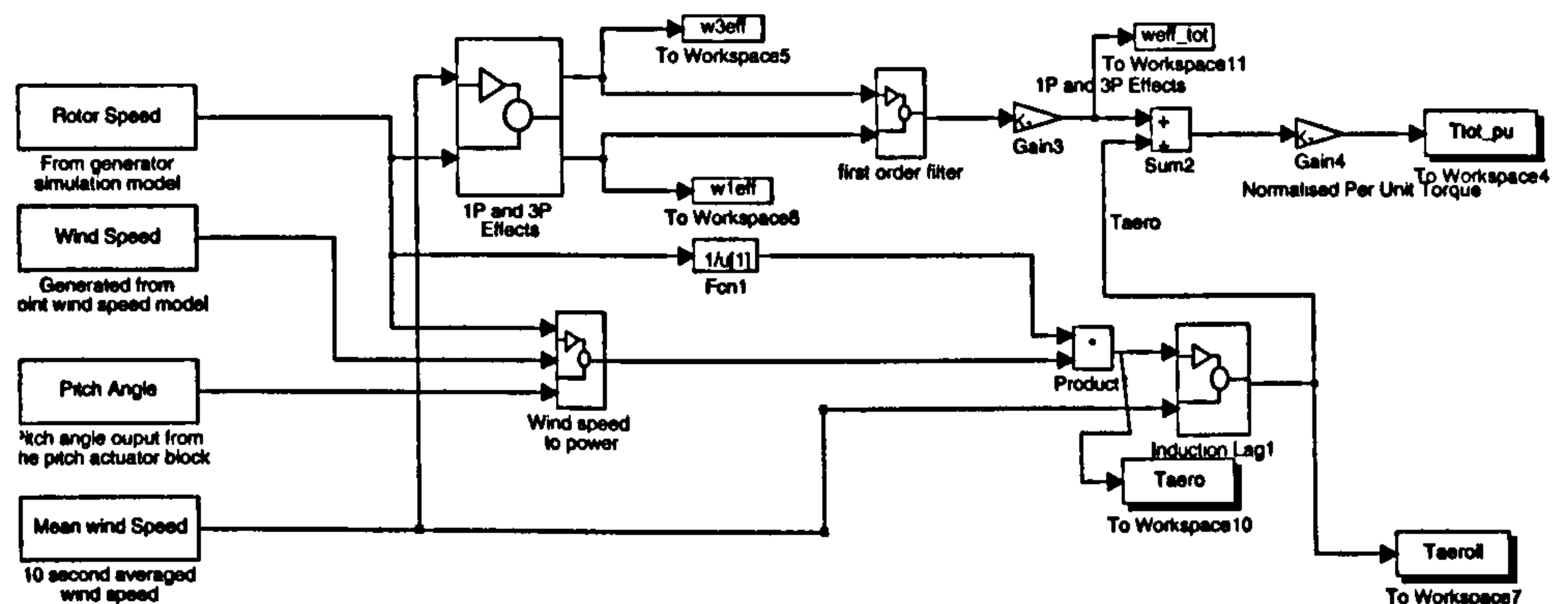


Figure 2.21: The Simulink Model of the spectral Method

been carried out for the diagram shown in Figure 2.21. There is only one real difference to the model shown in Figure 2.17 for the discrete wind speed model and that is the block to represent the rotational effects which contains the group of icons shown in Figure 2.20. The 1P and 3P effects are summed through a first order filter, converted to per unit value and then added to the hub shaft torque. The net hub torque is then used to drive the generator.

2.2.7 Implementation and comparison of the methods to model the wind interaction with the blades

It is now appropriate to compare the results from the discrete and spectral point wind speed methods to justify the two approaches and evaluate which should be the method used subsequently in the thesis. For a clear comparison the pitch controller, which is examined in the next section, is not included and therefore a below rated wind speed time series is used as input to the model. The effect of the sixth order generator is included to complete the link from shaft torque to shaft rotational speed to give the correct variation in the tip speed ratio. However for the fixed speed case the rotational speed is almost constant.

DISCRETE METHOD RESULTS. The windspeed time history for the comparison can be seen in Figure 2.22. The fifty seconds of wind data is user generated with noise representing the turbulence at the measurement point imposed upon it with a spectrum as described earlier in section 2.1.4. It has been generated to match the wind speed time series

returned from the spectral method for a hub height of 30 metres and mean wind speed of 9 m/s.

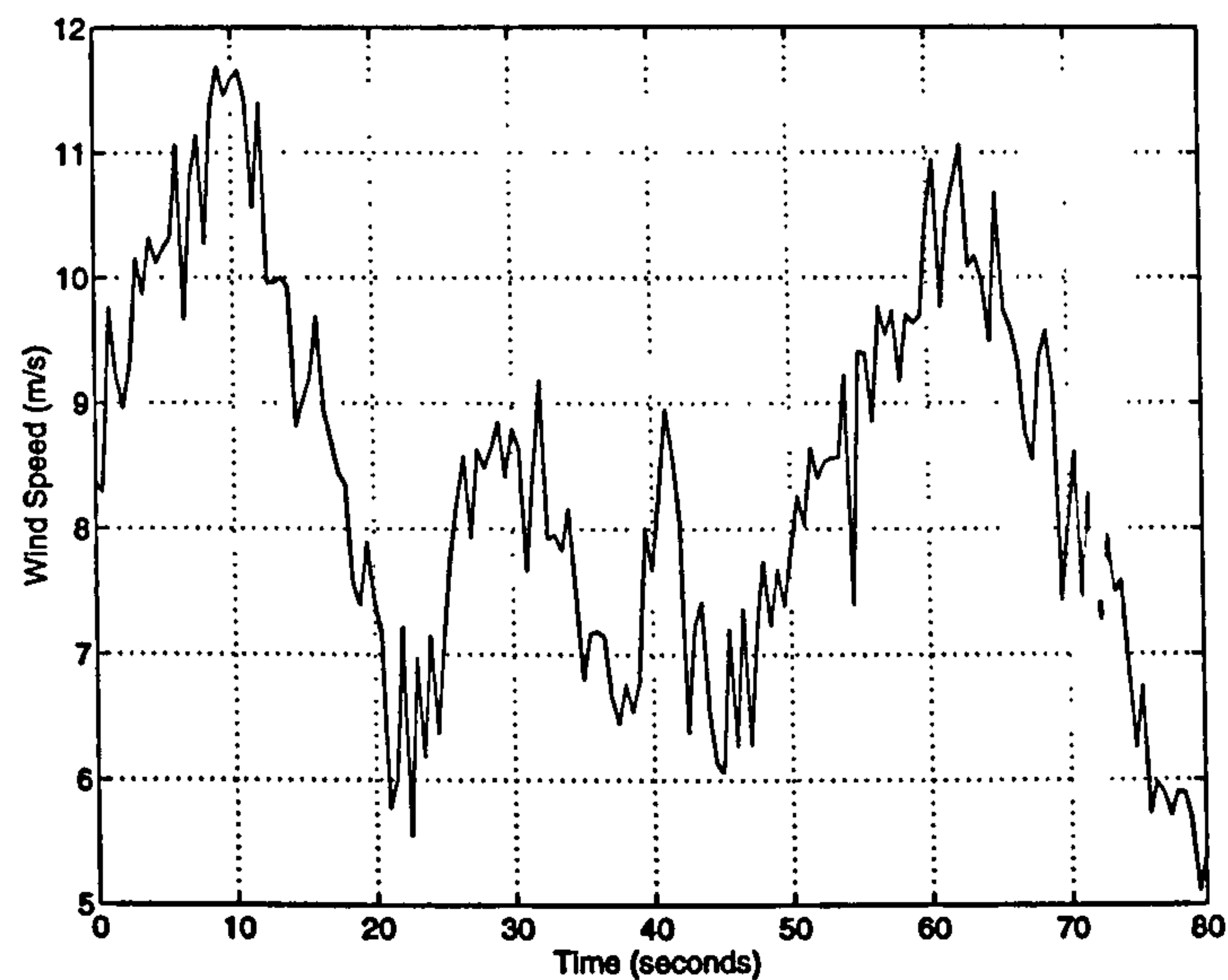


Figure 2.22: The time history of the point windspeed

Time series and corresponding power spectral density for the induced hub torque without the deterministic effects can be seen in Figure 2.23 for a 455 kW wind turbine generator as described in Chapter 3. There is no appreciable signal at $3\omega_r$ and most of the energy occurs at low frequencies. This is in contrast to the work presented by both Frandsen and Leithead who have studied the effect of rotational sampling as explained earlier.

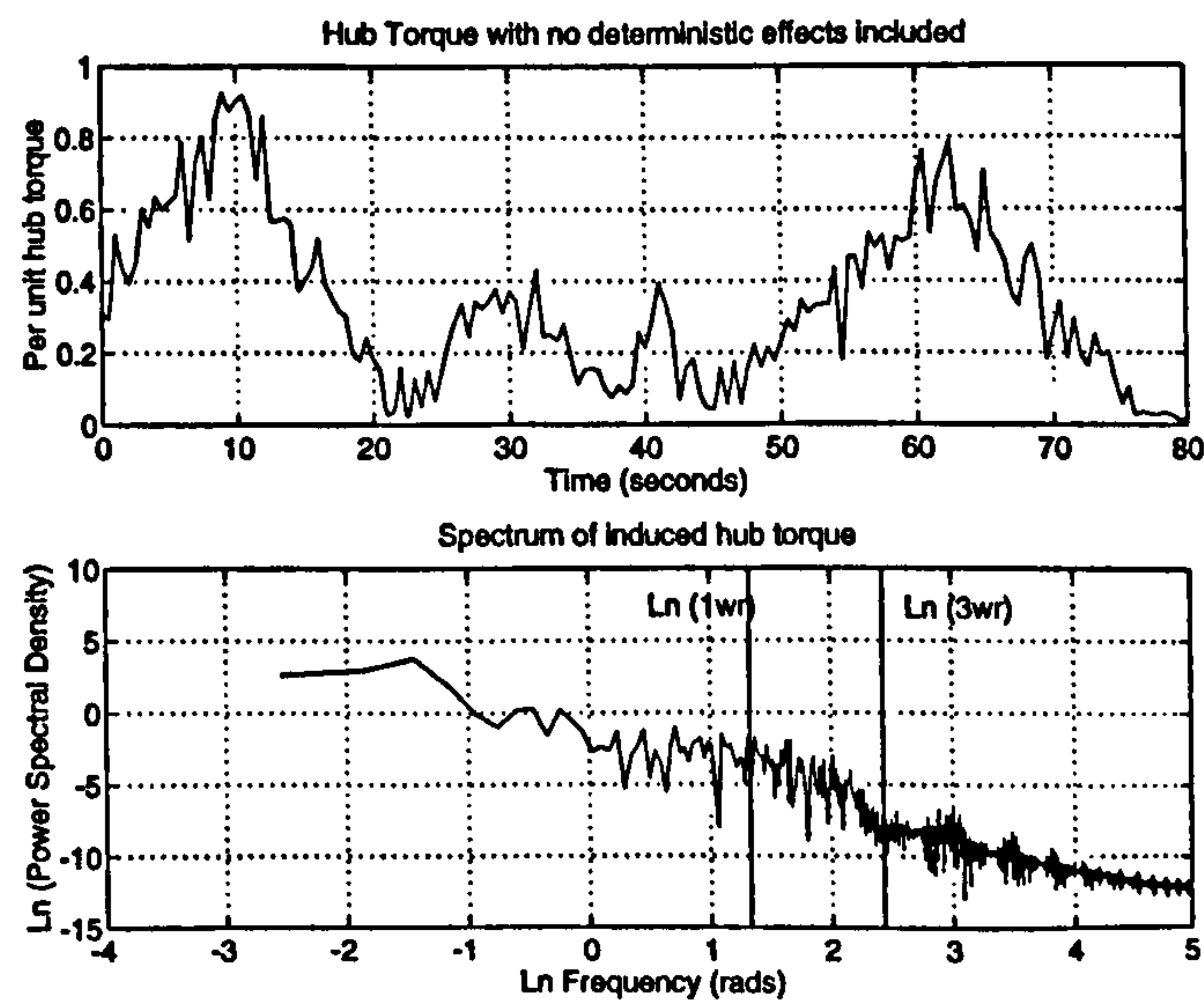


Figure 2.23: The induced hub torque without tower shadow

The torque variations due to rotational sampling and deterministic effects, such as tower shadow and blade imbalance, are introduced to the point windspeed model explicitly using a sin wave generator at $3\omega_r$ and at $1\omega_r$ with amplitudes consistent with a 10% increase in standard deviation. These torque variations have the spectra of the form seen in Figure 2.24.

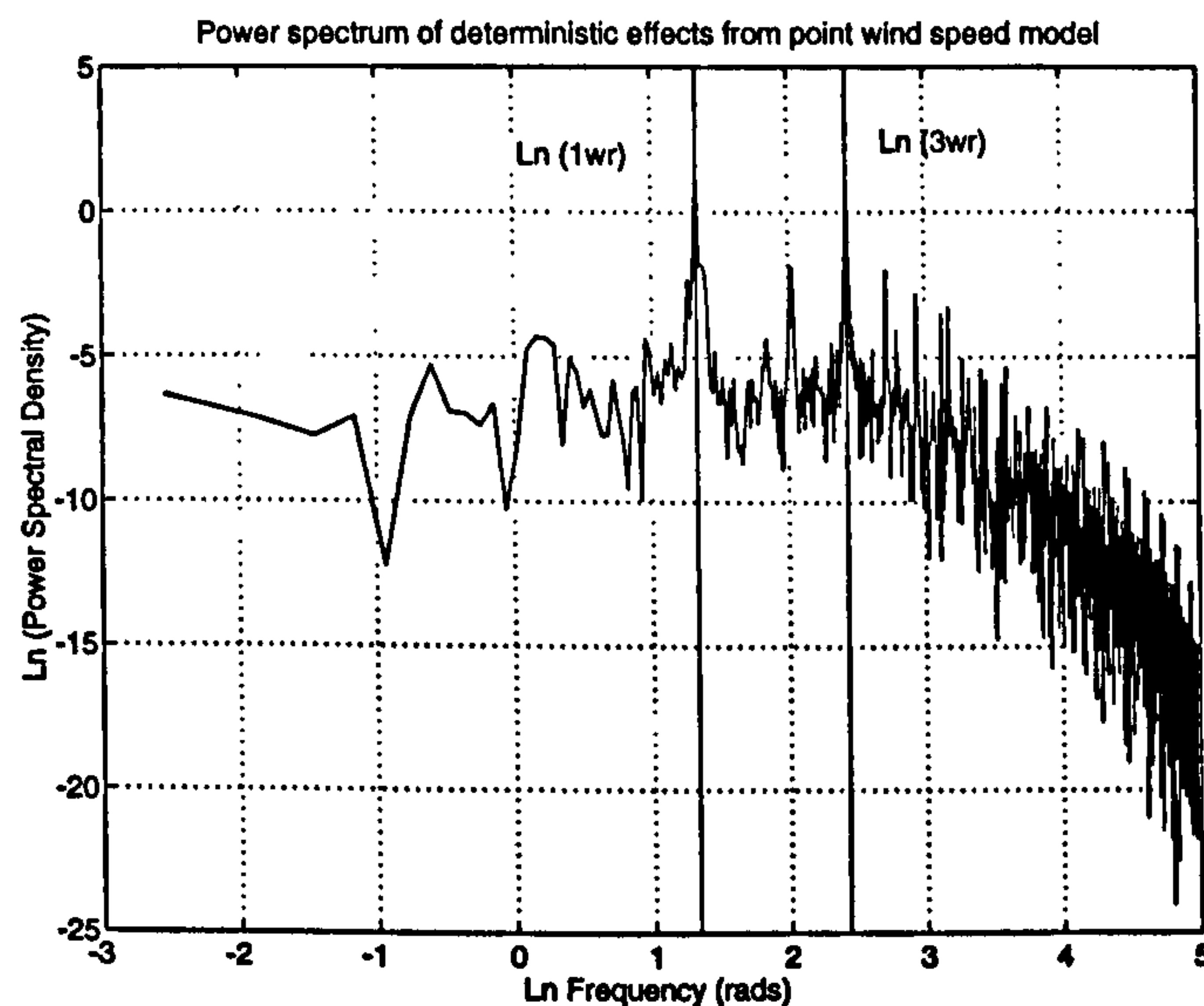


Figure 2.24: The power spectral density of the induced rotational torque variation

Combining Figure 2.23 and Figure 2.24 to give the overall spectrum due to the wind data and the superimposed rotational torque gives the torque variation and power spectral density of the induced hub torque. This can be seen in Figure 2.25 and it is clear that the effect of introducing rotational effects almost completely swamps the Von Karman noise in the data.

A spectral peak is now introduced at one and three times the blade passing frequency but there is no shift in power from the lower frequencies to the higher as reported by Leithead and so a spectral implementation is needed. The discrete point wind speed method can also include the induction lag effect as well as deterministic effects. This has been implemented and the results can be seen in Figure 2.26. The effect of induction lag is to make the variation of the hub torque increase and the standard deviation increases by 35 %.

SPECTRAL METHOD RESULTS. The need for the spectral method can be reinforced by assessing the spectral density of the point wind speed input produced by the discrete method and that produced from the spectral method. This is shown in Figure 2.27 and

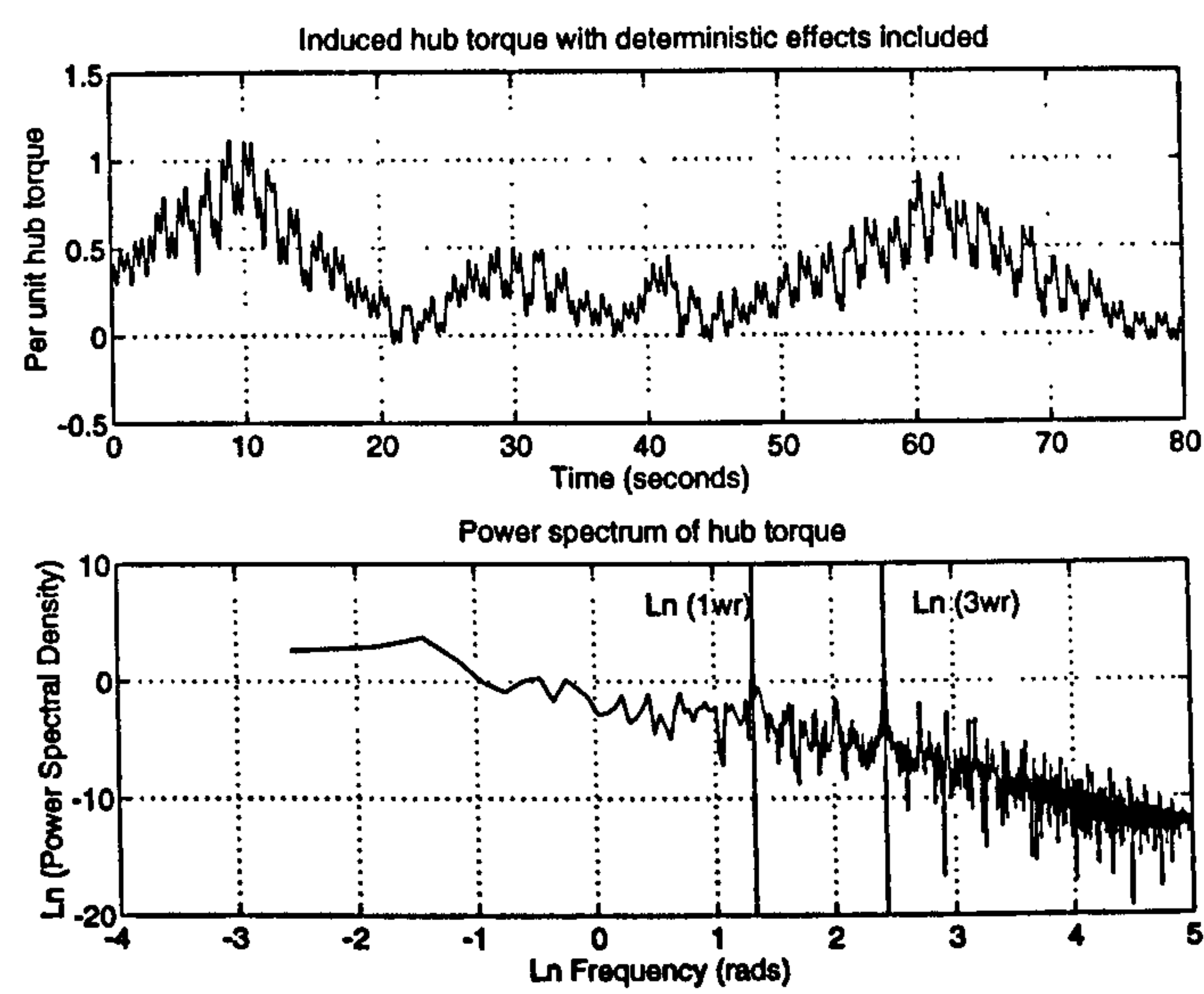


Figure 2.25: The induced hub torque with tower shadow

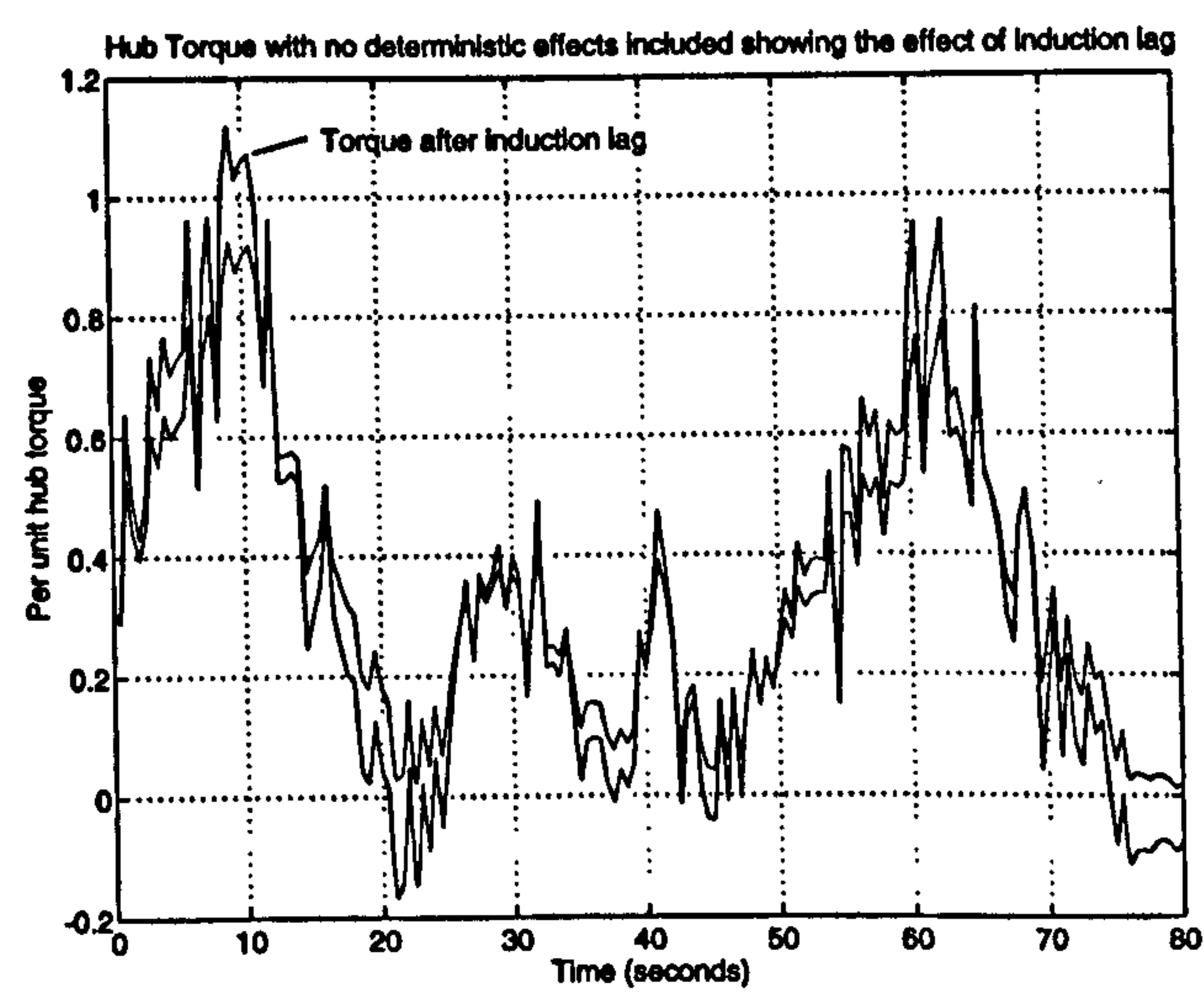


Figure 2.26: The induced hub torque with and without induction lag

there is a marked difference. The spectrum of the wind speed time history produced by the discrete method starts with roughly the same amplitude and variation as the spectrum produced by the spectral method but as the frequency increases the two spectra diverge with the discrete method showing an incorrect drop off in energy at higher frequencies.

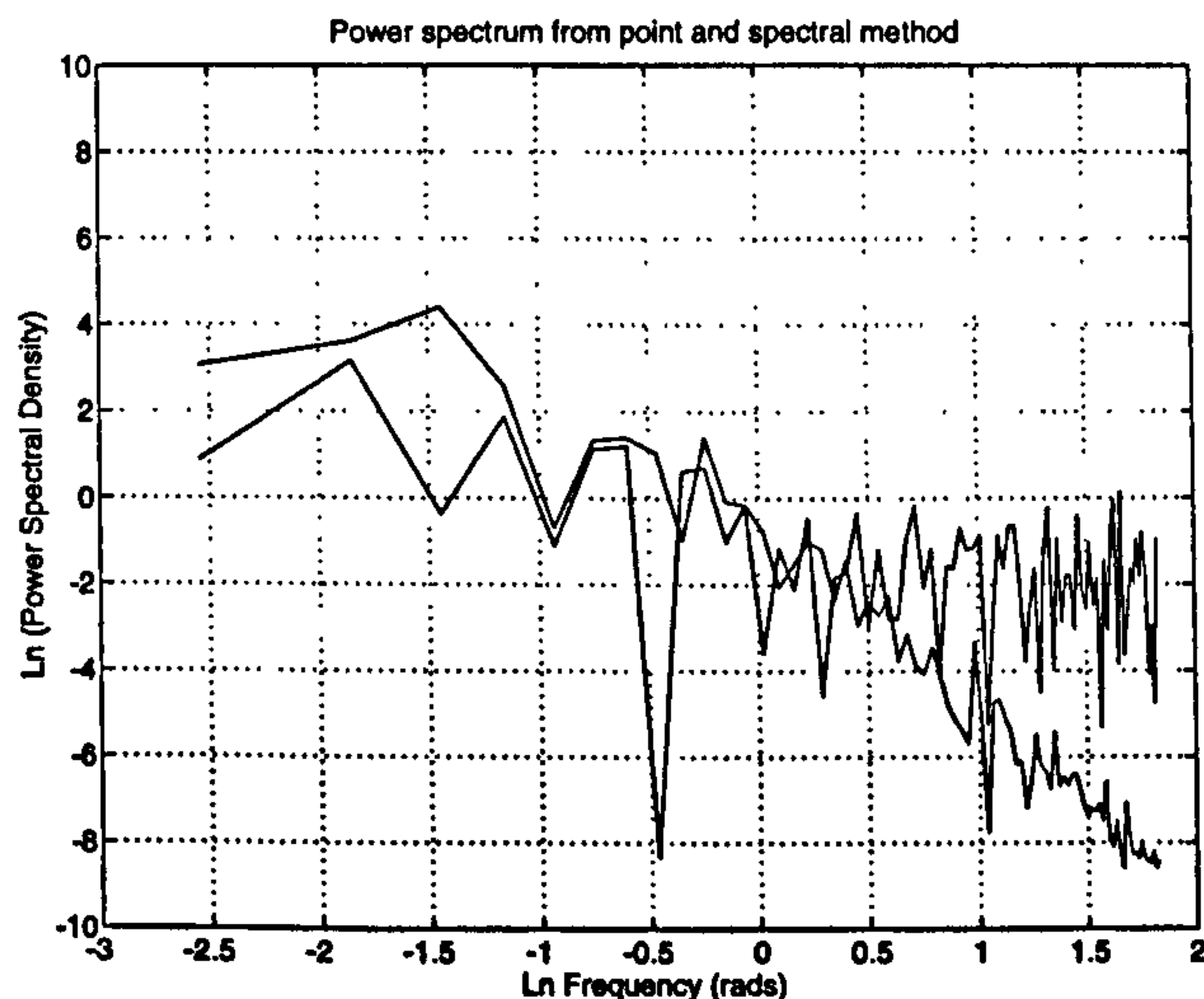


Figure 2.27: The spectral density of the point and spectral methods

Disk averaging leads to an even larger discrepancy between the two spectra as more power is shifted to the higher frequency components in the wind. This cannot be accommodated in the discrete method as easily as tower shadow, blade imbalance and the induction lag effects can and therefore the spectral method is required. The implementation of the full spectral method on SIMULINK requires considerably more complexity than for the simple discrete method and the run times are slower. Some sample results have been obtained for the 455 kW wind turbine and these are now presented.

The power spectral density of the total per unit torque can be seen in Figure 2.28. Comparing the spectrum with the one shown in Figure 2.25 for the total hub torque predicted by the discrete point speed model it is clear that the spectrum predicted by the spectral method has more energy at the higher frequencies and better definition of the $3\omega_r$ rotational spike. These spectral characteristics are typical of those derived from measured hub torque time histories and therefore the spectral method seems to be the better method for deriving hub torque.

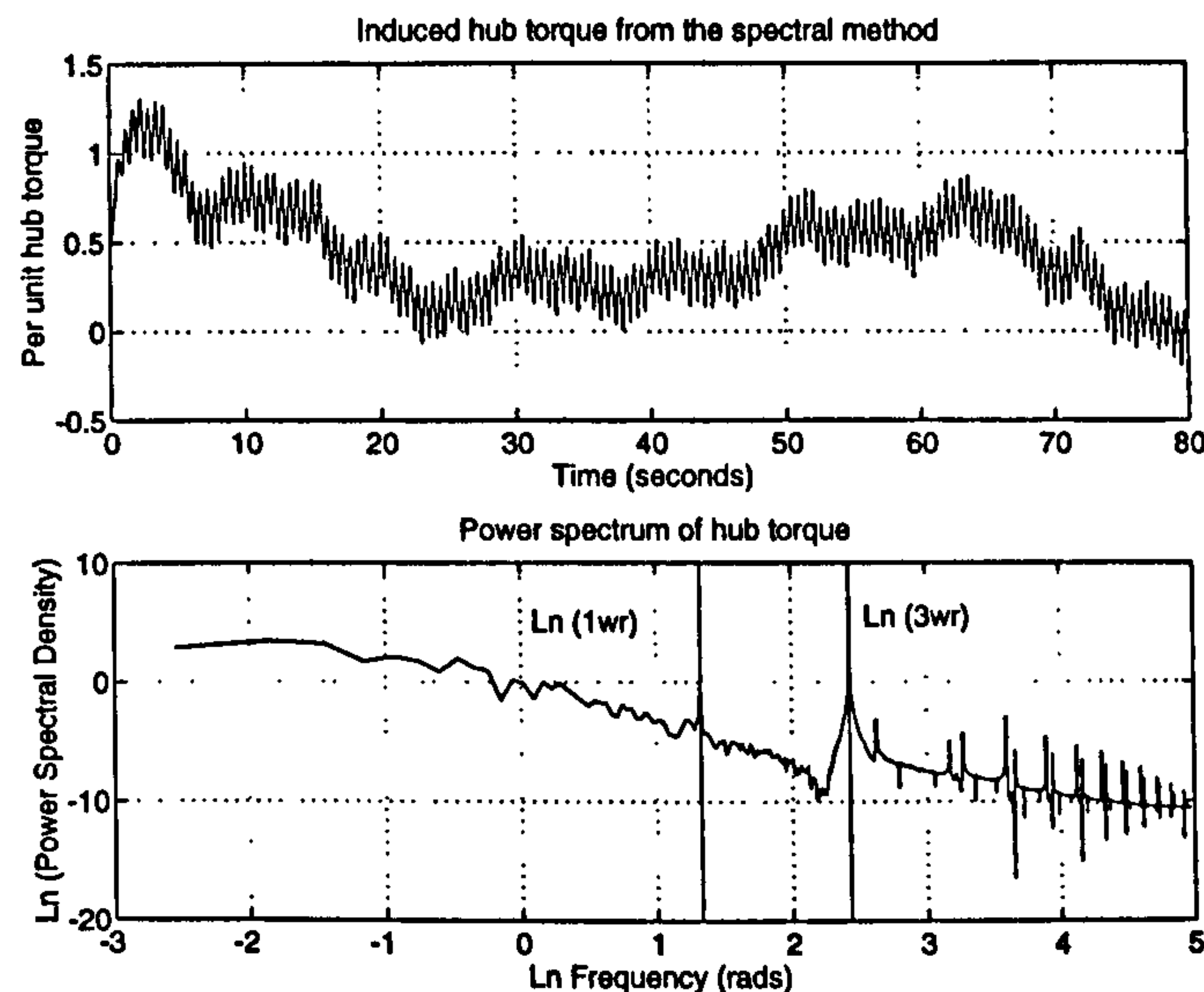


Figure 2.28: The power spectral density of the total hub torque

2.2.8 Choice of wind model

Overall the discrete method for deriving a point windspeed and corresponding hub torque is easier to implement, understand and gives quicker simulation run times than the spectral method yet it fails to introduce the correct form of spectrum at higher frequencies. Therefore throughout the rest of this thesis the discrete point wind speed model is only used for the step responses which are included to demonstrate the action of the different controllers on the key dynamic interactions within the fixed and variable speed cases. The spectral method is used for all simulations of the generator in the windy environment to demonstrate the operational performance of the fixed and variable speed cases.

2.3 Power Limiting Methods

The next integral part of the wind turbine model that needs to be explained is how can the input power to the wind turbine be limited. As explained earlier there are two common ways to limit the aerodynamic power. The first is to use passive regulation where the rotor blades are designed to stall progressively as the windspeed increases above rated. The second, and preferred, method is active regulation where the blades are feathered to maintain constant torque. The blades are continually adjusted above rated wind speed to limit the power input to the wind turbine and the adjustment is usually made in response to power measurement.

The whole of the blades may be pitched, full-span pitch regulation, or only the tips may be pitched, part span pitch regulation.

The next sections outline a typical pitch actuator and control system model and introduce the role pitch control has to play in the context of the directly coupled, permanent magnet, generator situation. Some sample results are presented for the fixed speed case and the pitch controller performance is validated by comparison against the measured power curve of the 500 kW rated Vesta wind turbine [55].

2.3.1 Typical Pitch Actuators

One of the most common forms of pitch actuator comprises a ball screw and ball nut arrangement as can be seen in Figure 2.29 [71].

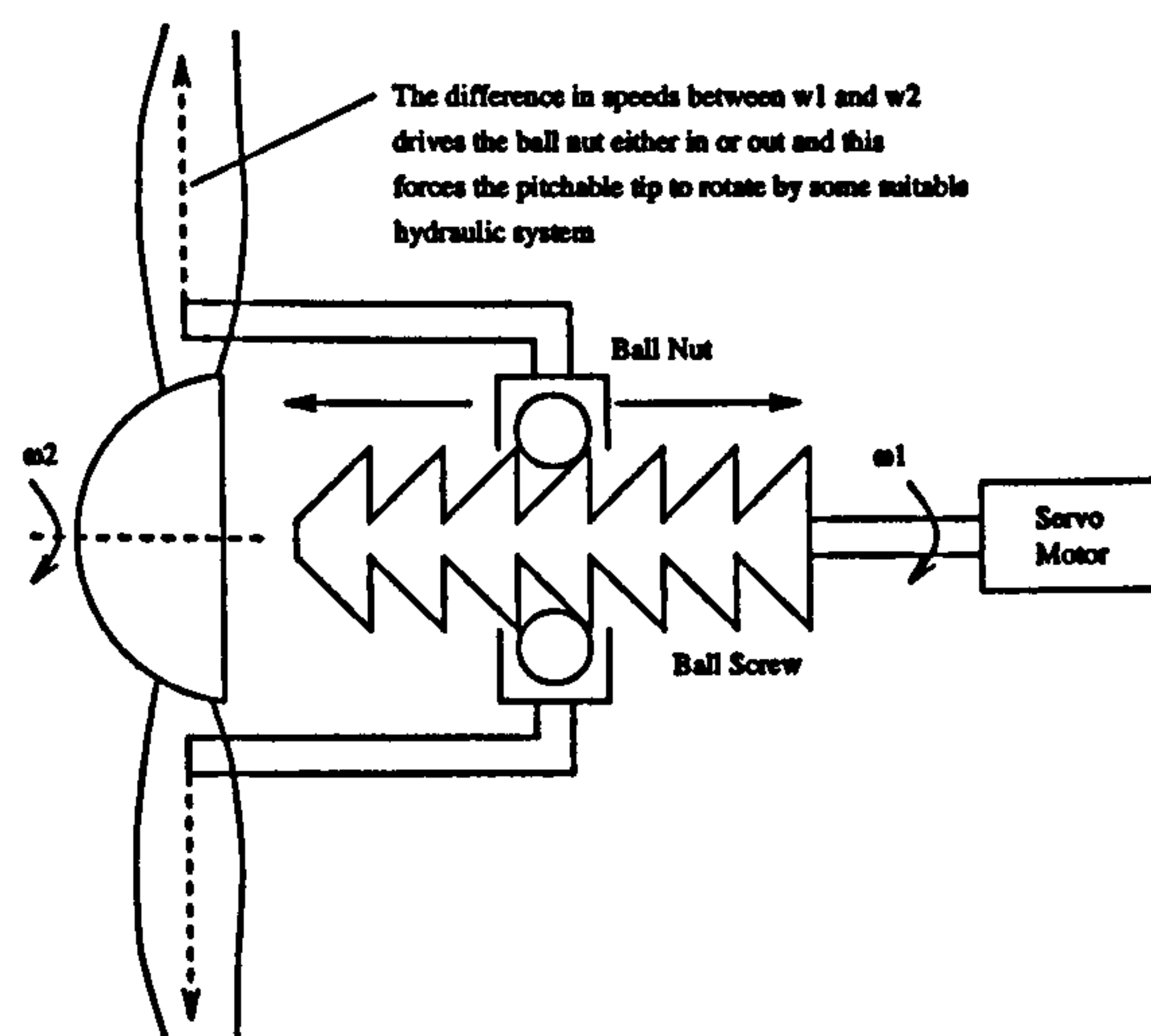


Figure 2.29: A typical pitch actuator system

The servo motor drives the ball screw at a speed governed by some power measurement and control interpretation. This speed is close to the speed the rotor actually rotates at. When a gust occurs to take the turbine into a region of above rated windspeed the speed of the rotor will increase. As this speed increases a difference in speed, $\omega_2 - \omega_1$, arises which forces the ball screw to move in the direction of the thread and a suitable hydraulic system forces the pitch of the movable span to be altered. This in turn brings the rotor speed to the rated level and no further action is required. It is desirable for the actuator to be simple and robust yet it must also satisfy the condition of low power consumption for this would detract from the efficiency of the WECS. As the inertia of the blades is large and the actuator should not

consume too much power the actuator has limited capabilities. Its dynamics are non-linear with limits on both the pitch rate and acceleration which are easily reached. Typical values for the saturation levels of the actuator torque are ± 20 kNm which is equivalent to a pitch acceleration of $\pm 90 \text{ deg s}^{-2}$ and for the pitch rate ± 10 to $\pm 15 \text{ deg s}^{-1}$ [70].

2.3.2 Modelling Pitch Actuators

As outlined in the previous section the pitch demand is used to drive the servo motor and as such must be amplified to give a useful voltage driving level. The servo-motor is represented by a first order delay with a simple feedback loop forcing the motor to the required speed. The acceleration is integrated to find the speed of the ball nut and this is converted into a pitch angle by a further integration. A model of the system described in the previous section can be seen in Figure 2.30 [70].

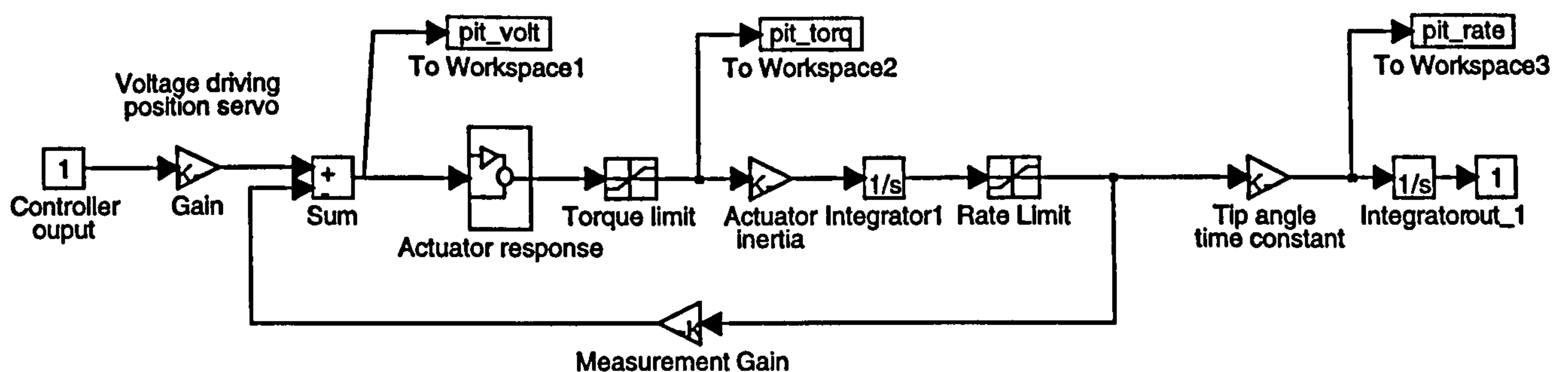


Figure 2.30: Modelling the actuator dynamics

This model is quite complicated and specific to a given machine design and manufacturer but it introduces the correct level of pitch response which can be used to assess the performance of the permanent magnet generator. The full pitch actuator model is used in all subsequent simulations as it also predicts the duty of the pitch controller in terms of its non-linear saturation performance.

2.3.3 The Pitch Controller

So far the dynamics of typical pitch actuators have been discussed. However the key element in achieving good power and structural load limiting is a well designed control algorithm. Typically PI control of the measured electrical power out is used to derive the pitch demand. The method for generating the pitch demand signal can be seen in Figure 2.31. The per unit power and torque are the same quantity for the fixed speed case and the difference between the actual torque and rated torque is used to derive the pitch demand. The switch controls whether there is any pitch action required or not and this can either be dependent on a measurement of wind speed or the torque itself. A relay is used to ensure that there is a small hysteresis loop in switching pitch control on and off to stop any fluttering of the blades around rated wind speed.

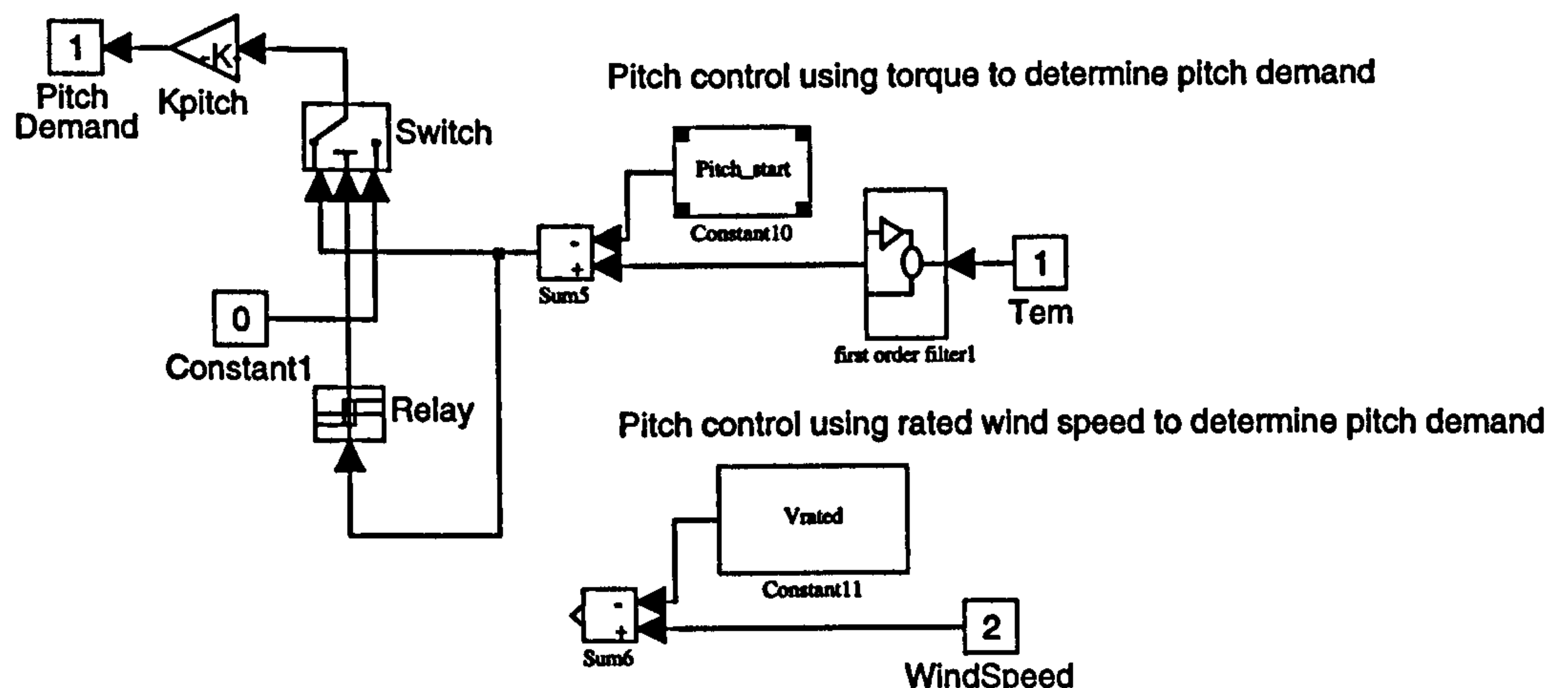


Figure 2.31: Pitch demand

This pitch demand is then passed to a PID controller which works on the difference between the desired pitch angle and the measured pitch angle. This can be seen in Figure 2.32. This pitch control and actuator model has been reasonably successful but work is needed to quantify the improvements that can be made with say more complex classical control techniques as in [72] or in more advance techniques as in [71].

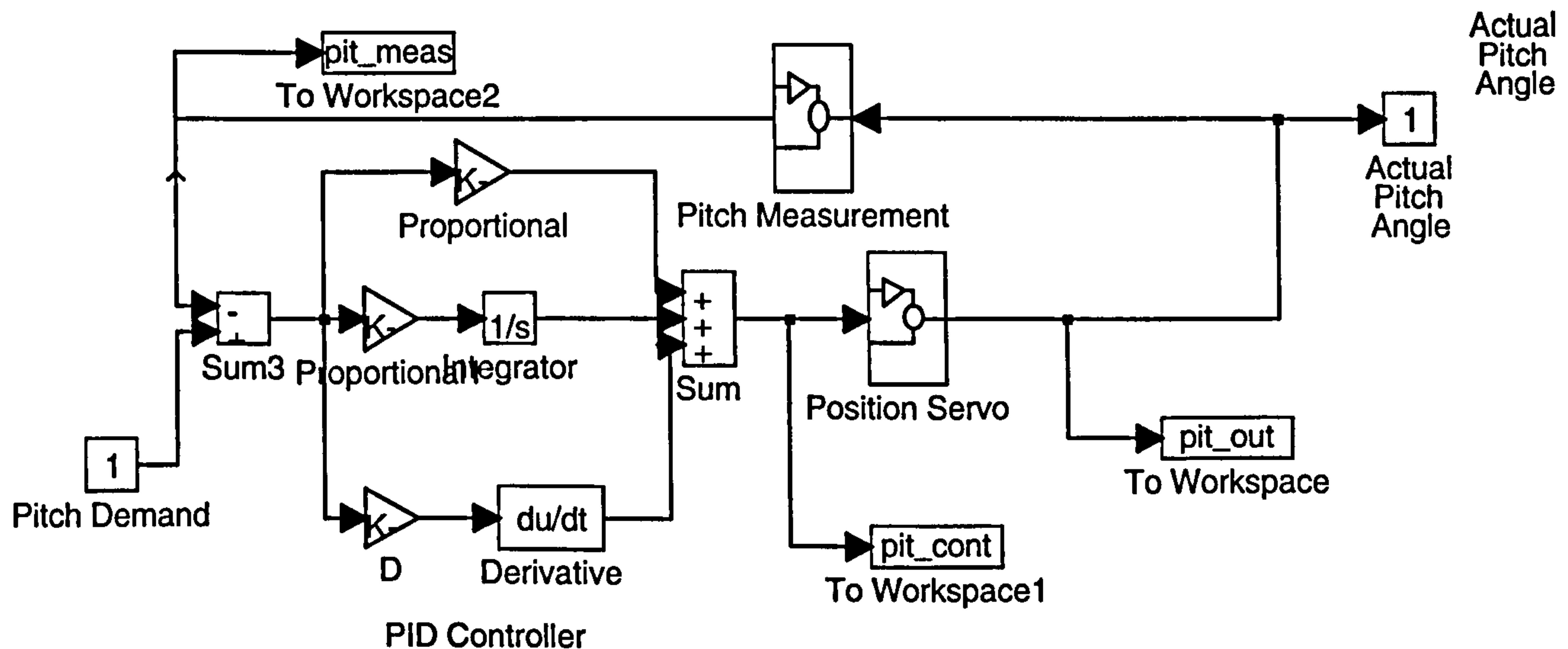


Figure 2.32: Pitch Actuation

2.4 The full wind turbine model

Now that each component has been discussed it is necessary to bring them all together to outline the chosen model of a wind turbine operating at fixed speed and to discuss its simulation on SIMULINK.

2.4.1 Implementation on Simulink

The time history of the spatially filtered point wind speed derived by the spectral method and its corresponding mean are the inputs to the model. The power coefficient is derived from the point windspeed and the blade pitch angle. This results in a value for the shaft power from the wind. The power is converted to shaft torque by dividing by the shaft speed and this is then passed through the block representing induction lag. The resulting torque is summed together with the torque of the combined rotational effects and converted to a per unit value of generator driving torque. This per unit torque drives the permanent magnet generator model comprising the rotor, stator and d,q-axis currents differential equations. The difference between the resulting electromagnetic air gap torque and rated torque is converted into a pitch demand by a fixed gain. If the windspeed is above rated this pitch demand is used as the input to the pitch controller and actuator. The overall model for the wind turbine can be seen in Figure 2.33.

give as small an aerodynamic over-torque as possible during a full simulation run.

Normally for PID control design the transfer function is first obtained and then an ideal integral compensator (PI) designed to limit the steady state error and an ideal derivative compensator (PD) designed to improve the transient response [73]. For the pitch actuator there are definite limits on the pitch rate and therefore not much can be gained from increasing the transient response. Hence this section concentrates on the design of a PI controller of the type shown in Figure 2.32 with the derivative gain set to zero.

2.5.1 Simplified transfer function representation

A simplified transfer block diagram of a wind turbine can be derived from the models presented earlier and this can be seen in Figure 2.34. The transfer functions representing pitch actuation, induction lag and generator dynamics can be obtained by defining the required inputs and outputs to each of the blocks and extracting the linearised state space equivalent using the 'Linmod' function. This can be converted to transfer function form using the 'tf2ss' function of the Control Systems Toolbox. Classic PI design techniques can then be used to estimate reasonable values for the PI controller for a given operating condition. However the values returned for the PI controller do not actually give the expected performance and the main reason for this is that the system is highly non-linear. Non-linear control techniques could be applied to the problem [74] but it was just as easy to tune the controller through simulation runs due to the ease and speed of use of Simulink. Further work could be carried out in this area and this is discussed in Chapter 8.

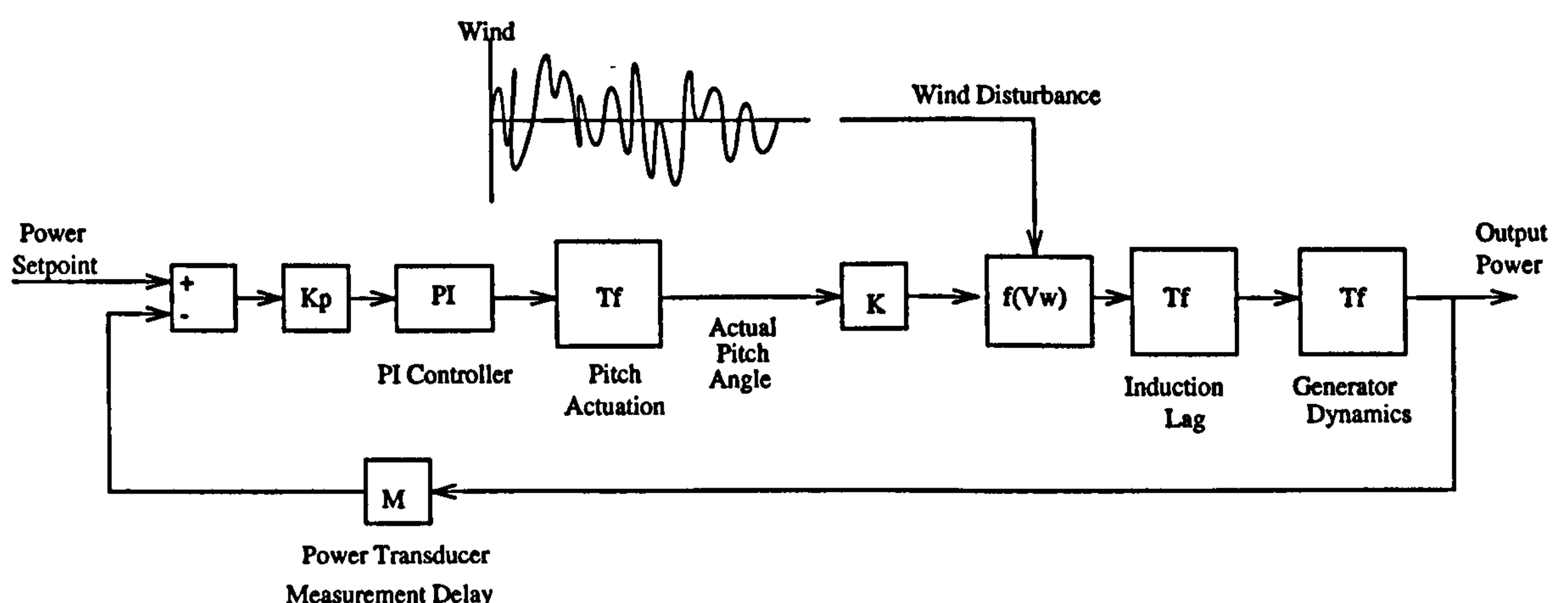


Figure 2.34: Transfer function of a typical wind turbine

2.5.2 PI controller values

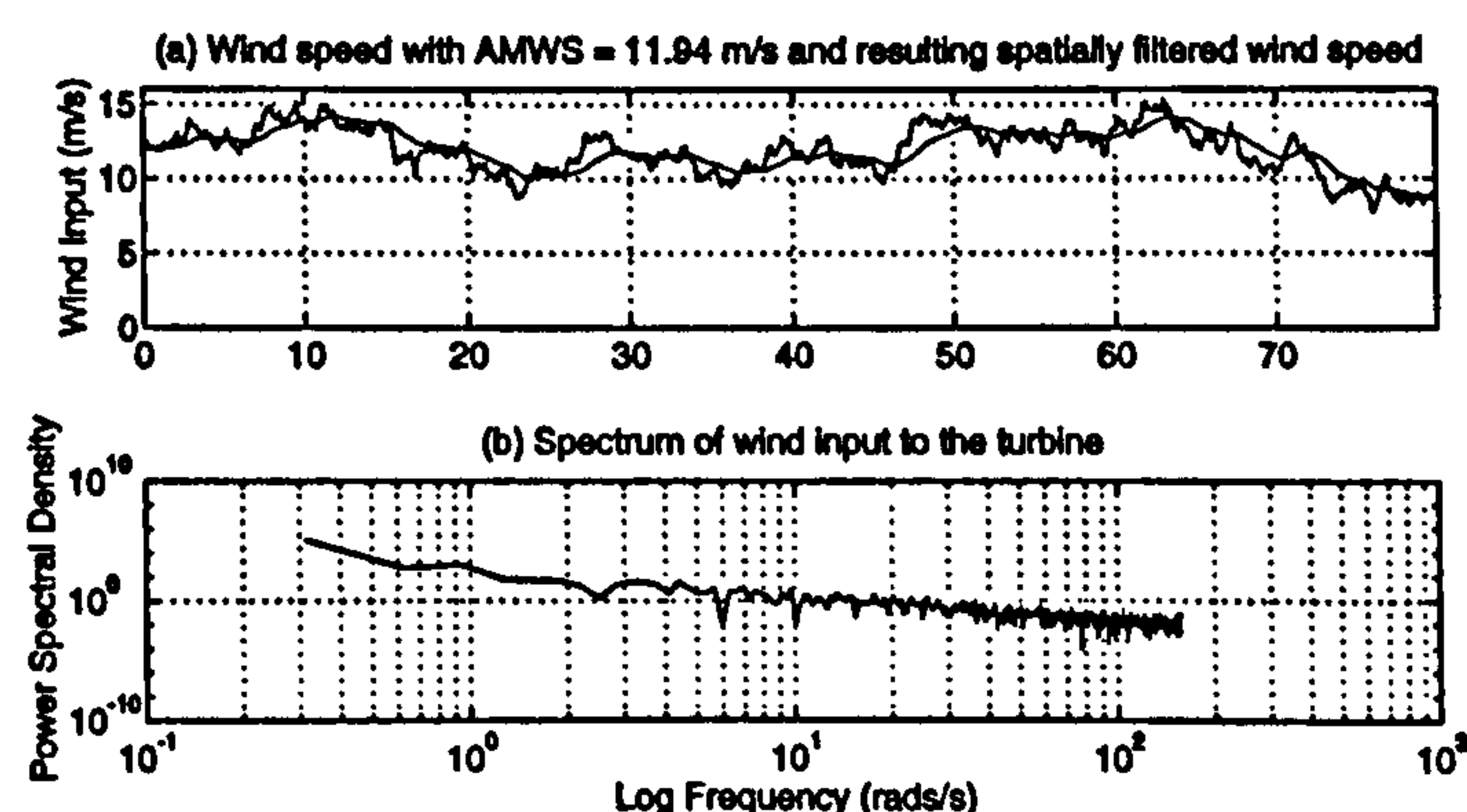
The best values for the PI controller to drive the full pitch actuator model are given in Table 2.3. The values PaProp, PaInt and PaDer are the gains of the proportional, integration and derivative branches of the PID controller shown in Figure 2.32. The gain Kpitch was set to ensure that the pitch demand is adequate to drive the pitch actuator to the required level.

PaProp	0.15
PaInt	0.1
PaDer	0
Kpitch	20

Table 2.3: Pitch PI controller values

2.5.3 PI controller performance

The simulated input wind to the model and the corresponding power spectrum, as described earlier, can be seen in Figure 2.35. The simulated windspeed has an AMWS of 11.94 m/s and was generated by the spectral method. The run identifiers, corresponding to the gains of the pitch controller and showing whether rotational effects have been included, can also be seen on the figure.



Run Identifier: Prop = 0.15, Int = 0.1, Der = 0, Kpitch = 20, Omeff_include = 1

Figure 2.35: The simulated windspeed and corresponding power spectrum

The power coefficient, aerodynamic torque power input before and after induction lag effects,

the total shaft torque including all rotational effects and the corresponding power spectrum can be seen in Figure 2.36. It is clear that as the torque increases above the rated value of 1 p.u. the pitch actuator acts so as to try to maintain constant power out. The pitch actuation could be improved upon by examining the effect of introducing a more adaptive form of control or by using non-linear techniques. The classical controller limits the power to 36 % above its rated value which is comparable with the performance of the Richborough 1 MW wind turbine [75]. The pitch actuator never limits the power strictly to one per unit torque by measuring T_{em} and so perhaps some alternative signal or mix of signals is needed to adequately limit the peak torque. This is discussed further in Chapter 8.

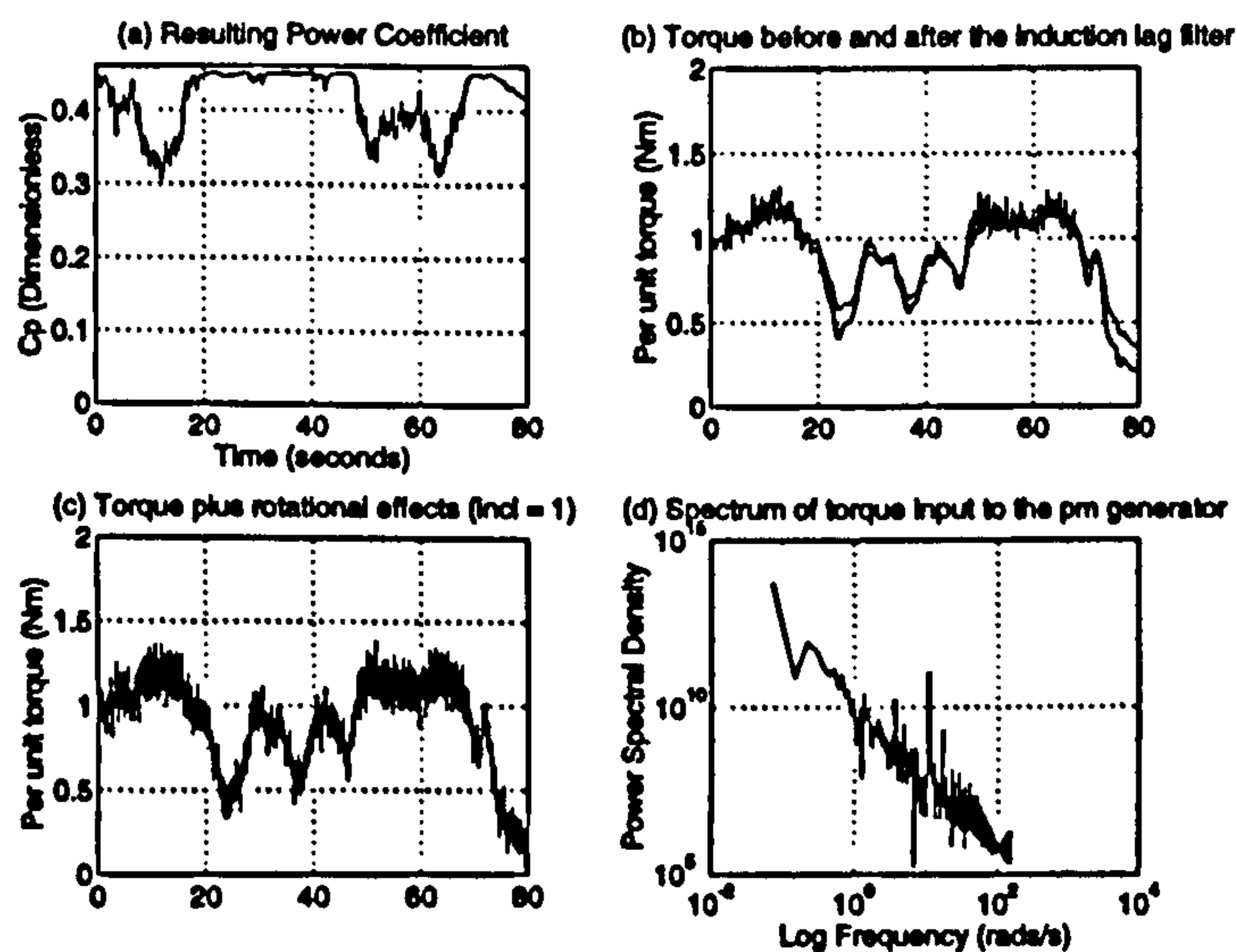


Figure 2.36: The aerodynamic torque with and without rotational effects included

PITCH CONTROLLER AND ACTUATOR VALIDATION. The response of the pitch controller can be seen in Figure 2.37. The characteristic saturation of both pitch rate and acceleration torque are typical of this type of controller and the performance correlates well with that presented in [65]. Furthermore the pitch demand fluctuates considerably which indicates the power out from the generator is fluctuating a lot, but this is slightly smoothed in the actual pitch angle due to the non-linearities and inertias involved in pitch actuation. This is desirable in terms of the reduced fatigue loading on the actuator mechanism. The pitch actuator and controller are considered to be representative of such part span, pitch control systems. Certainly the key dynamic effects are visible and this is adequate to test the performance of the direct drive, permanent magnet, synchronous generator.

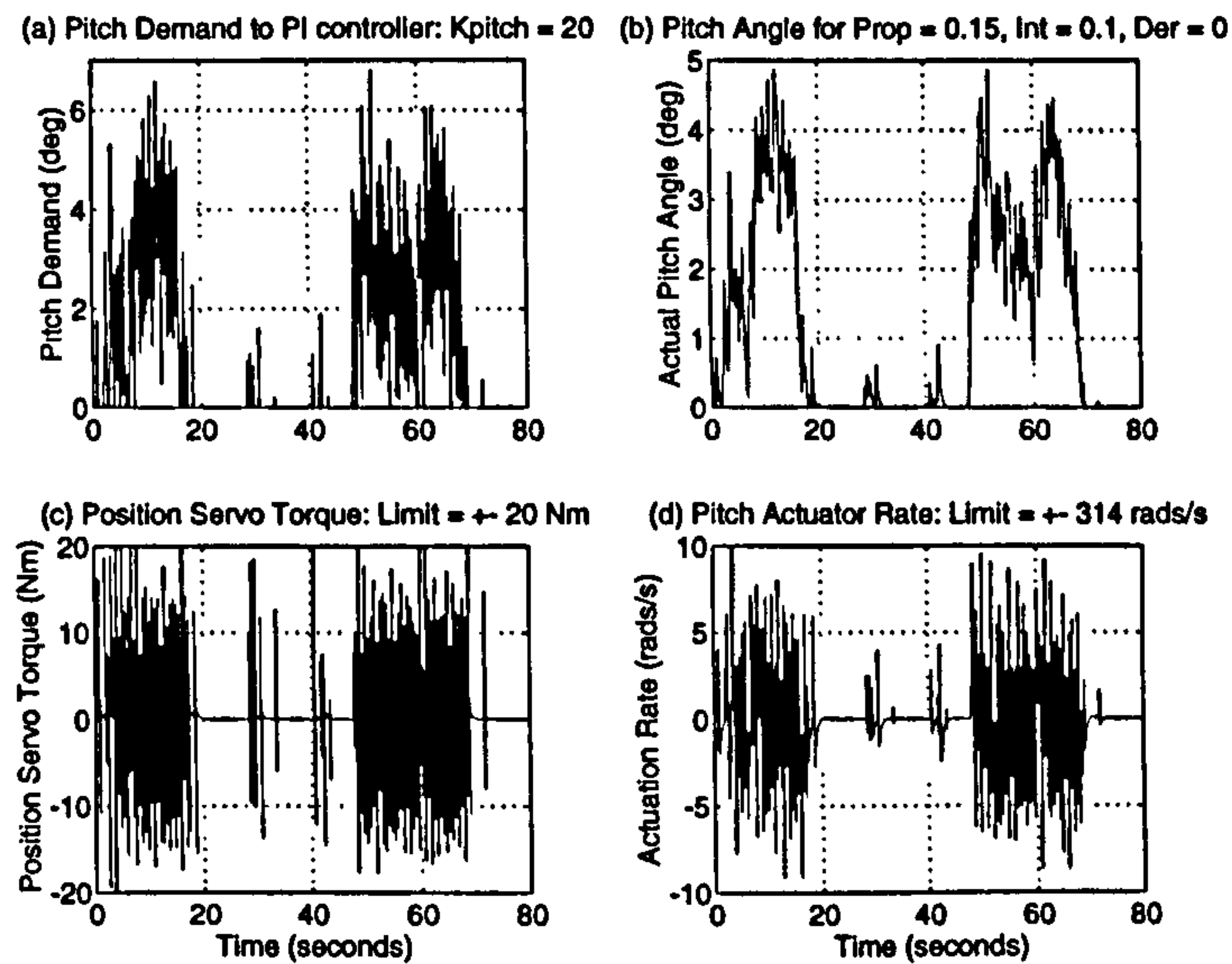


Figure 2.37: The pitch actuator response

2.5.4 Validation against the measured power curve of a Vestas 500 kW turbine

To validate the C_p curves and the level of action of the pitch controller and the wind turbine further a comparison has been made against the measured power curve of a Vestas 500 kW turbine [55]. The windspeed was ramped up using the ramp element of the discrete point wind speed model from 5 to 30 m/s with no tower shadow or blade imbalance effects included. The resulting output power against wind speed can be seen in the top half of Figure 2.38. There is good agreement between the two curves except that the simulated curve, which extends all the way to 30 m/s, has a higher final value and this is because the generator was slightly over-rated when compared with the 500 kW rated Vestas.

The bottom part of Figure 2.38 shows the corresponding level of blade pitch required. At the cut out speed of 25 m/s the blade pitch demand is set to 90 degrees but the actual blade pitch angle takes about 1 seconds to reach this value due to the limit on the pitch angle rate.

2.5.5 Implications of pitch control

The methodology behind simulating the pitch actuator of the wind turbine has now been described. The pitch actuator is the only control handle that exists for a direct drive, fixed

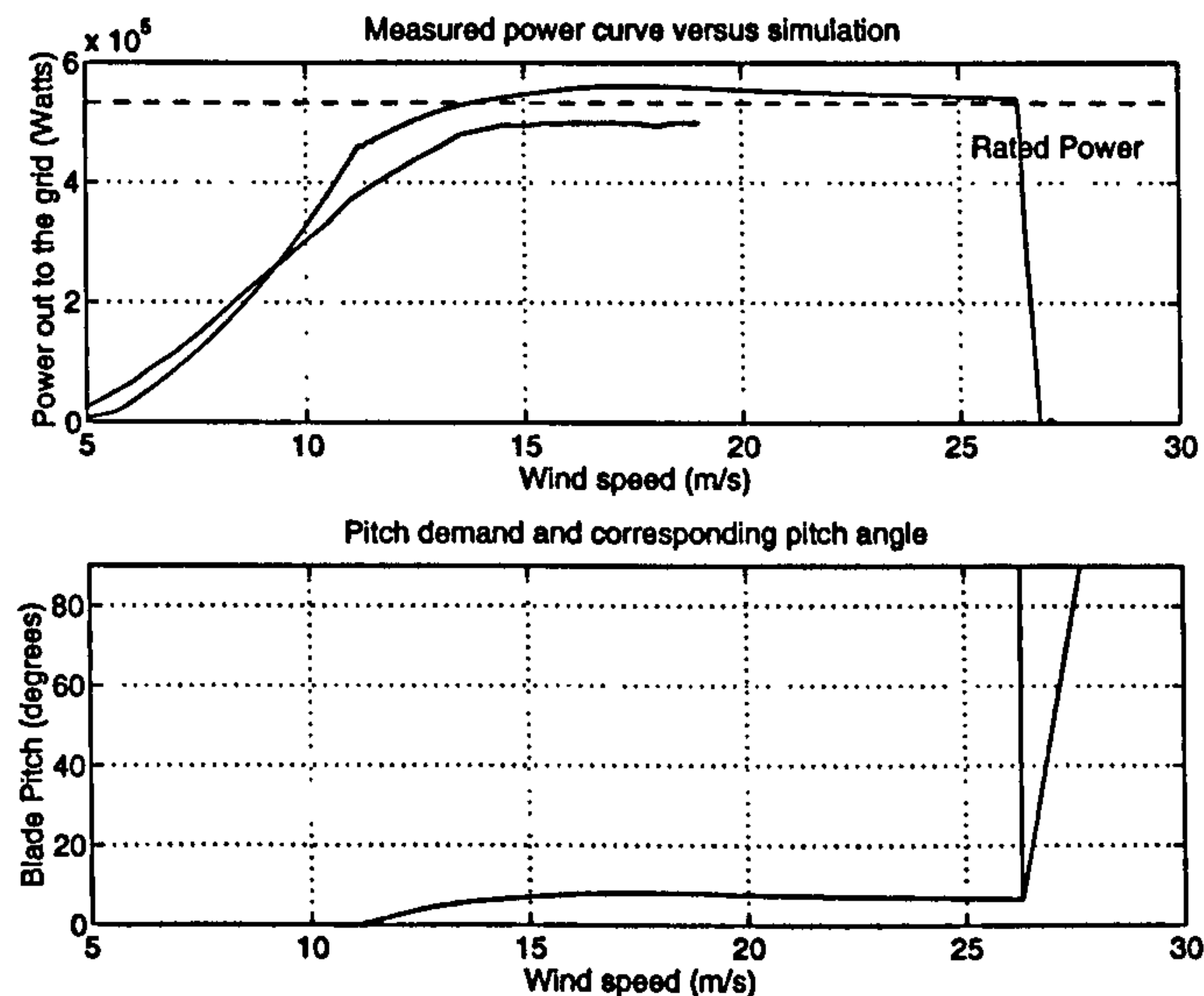


Figure 2.38: The simulated power curve against measured power curve and corresponding pitch action

speed, wind turbine and as such its control is very important. A brief introduction into PI control has been outlined and further work is reported in chapter 4. The impact of pitch control on the variable speed case also has control implications and these are discussed in chapter six. The full model of the pitch actuator is used for all the simulations presented hereafter for the turbine operating in the windy environment.

2.6 Concluding remarks

It has been shown in this chapter that a wind turbine model has been implemented and validated which typifies the current industry standard. This model will be used to quantify the benefits obtainable from a constant or variable speed operated permanent magnet generator. The discrete point wind speed method will be used for all step responses and the spectral method whenever the performance in the wind situation is presented. The full model of pitch actuation will be used in all subsequent simulations. The only piece left to fit into the wind turbine simulation is the model of the multi-pole, permanent magnet, synchronous generator and this is dealt with in the next chapter. Further issues which increase the accuracy of the wind turbine model and allow access to other dynamic interactions, for instance blade and tower displacements, are discussed in Chapter 8 but as explained in Chapter 1 all structural components are considered stiff.

Chapter 3

Permanent Magnet Synchronous Generator: Design, Modelling and simulation validation

This chapter describes the work which has been done to model a multi-pole, permanent magnet, synchronous generator for use in a wind turbine connected to large power systems. Firstly the layout of a conventional synchronous generator is described and then the advantages of using permanent magnet excitation are outlined. The historical development of a multi-pole, permanent magnet, synchronous generator by Spooner and Williamson [47] is described and the current state of the art examined.

The second section describes a computer program, WINDGEN2 [76], which calculates the key parameters of such multi-pole, permanent magnet, synchronous generators. The design methodology and key design drivers are introduced to give an understanding of how this new form of generator can best be matched to the torque input from the blade interaction with the wind.

The third section starts with a detailed analysis of the five winding model of a synchronous generator. The model developed is in the d, q -axis frame of reference and the methodology behind simulating such a generator connected to an infinite bus is described. This five winding model is reduced to a three winding model that represents the permanent magnet synchronous generator. The governing equations are then linearised to show how values of

the generator parameters which satisfy the design constraints can be obtained. The method for linking the eigenvalues, returned from the linearisation, with step response results from full non-linear simulation is then presented. The physical realisation of these results is discussed.

The fourth section outlines a test rig, comprising a dc motor and permanent magnet generator, and the test procedures used to validate the simulation model. The permanent magnet generator undergoes several electro-mechanical transients and the recorded angular movement of the stator and rotor and the output current are compared against those from the simulation model. The agreement reached between the test and simulation results is discussed to determine the validity of the simulation model.

The final section of the chapter reviews the work and gives a clear indication of how the model can be integrated into a full wind turbine simulation.

3.1 The Permanent Magnet Generator

Wind turbines typically rotate at 30 to 50 rpm and the generator, either induction or synchronous, is coupled to the turbine via gears so that it can rotate at 1000 or 1500 rpm for grid connection. However the gearbox brings weight and cost penalties, demands regular maintenance, generates noise and incurs loss. Clearly eliminating the gearbox would improve the attractiveness of wind generation [42].

Direct connection of the generator to the wind turbine requires the generator to have a large number of poles. A multi-pole generator fitted with a conventional field winding would have a prohibitively large diameter and be very expensive whereas permanent magnet excitation allows a small pole pitch to be used and can yield cost effective designs [45]. This next section starts with a brief description of a conventional synchronous generator and shows why it would be unsuitable for the direct drive application. Then the development of ferrite permanent magnets and in particular their application to synchronous generators is outlined. Finally a discussion of the damping requirements for such a generator in terms of its transient stability is presented.

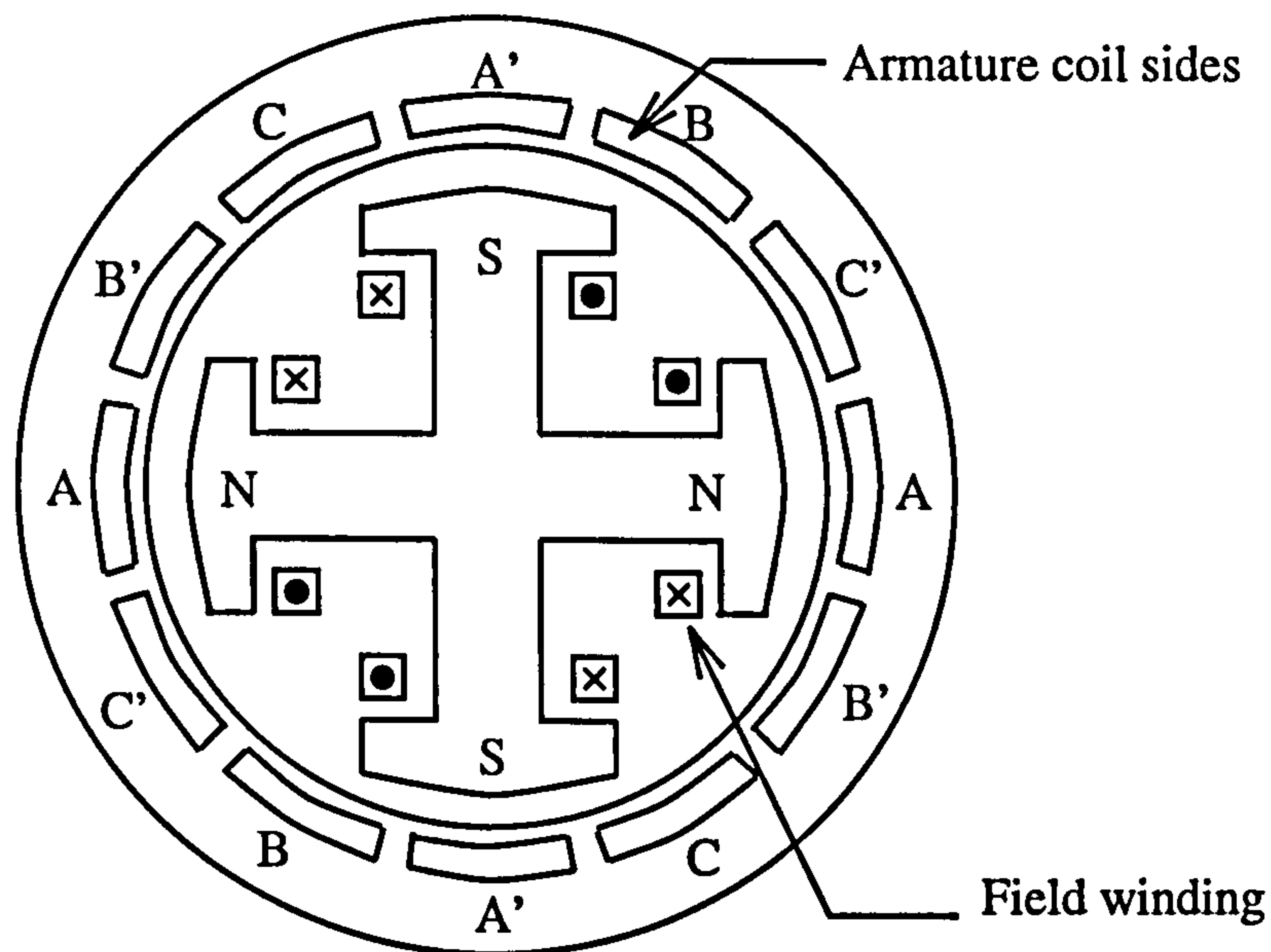


Figure 3.1: Typical 4-pole synchronous machine (Source: Synchronous Machines)

3.1.1 Physical Description of a Three Phase Synchronous Generator

A synchronous machine is a rotating apparatus that is usually part of a power system and a schematic can be seen in Figure 3.1. It consists of two parts: a set of armature coils and a field winding in relative motion. For constructional convenience and economic reasons the armature winding is usually located in the stator and the rotor contains the field winding [77]. When the field is supplied by a direct current and is rotated by the prime mover, for instance a steam turbine, alternating currents are induced in the armature.

SYNCHRONOUS SPEED. The synchronous speed of a synchronous machine is the speed at which the machine normally runs under balanced steady state conditions and is given by,

$$\omega_r = \frac{2}{p} \omega_s \text{ rads/s} \quad (3.1)$$

where ω_r is the rotational speed of the shaft, ω_s is the angular frequency of the supply and p is the number of poles. The number of poles of a synchronous machine is therefore determined by the mechanical speed and the electric frequency at which the machine is intended to operate and to get high frequency generation from low rotational speeds requires a high pole number. Furthermore to connect a synchronous generator to the grid requires that the generator be run at this synchronous speed with the same phase sequence and voltage magnitude as the grid at the instant of closing the synchronising breaker otherwise

large transient oscillation may occur.

TYPICAL CONSTRUCTION. A salient pole rotor construction is typically used for low speed multi-pole applications and two or four pole cylindrical rotor construction for high speed applications. Each pole is usually made up of a set of windings and insulation with a minimum pole pitch of about 150 mm. There must be as many complete sets of armature coils as the number of pole pairs, symmetrically distributed around the stator, and each set consisting of three coils 120 electrical degrees apart. The balanced steady state voltages are therefore always 120 degrees apart in phase regardless of the speed.

TORQUE PRODUCTION. The magnetic flux produced by the field winding is normally rotating at synchronous speed with respect to the stator. The fundamental of the magnetic field produced by the balanced three phase armature currents rotates at synchronous speed and so is stationary with respect to the field. The magnetic fields are constant in amplitude and stationary with respect to each other and a steady electromagnetic torque is produced from the tendency of the two fields to align. In the case of a generator this torque opposes the mechanical torque applied from the prime mover [77].

DAMPER WINDINGS. Most salient pole synchronous machines are equipped with damper or amortisseur windings, which usually consist of a set of copper or brass bars set in the pole face slots and connected at the end of the machine to form a cage winding. If the rotor speed departs from the steady synchronous value, the short circuited path linking the gap flux behaves with reference to the travelling wave stator field as the cage winding of an induction generator. Slip frequency currents are induced and the resulting I^2R loss dissipates some of the swing energy, developing a torque roughly proportional to slip. At negative slip damping torque acts to reduce speed and vice versa for positive torque. Thus a damper winding aids the transient stability of a generator fitted with one. Furthermore damper windings can reduce over voltages under short circuit. However the induced current in the damper winding during transients alters the flux path and hence the reactance of the machine and leads to higher short circuit currents.

WINDING ARRANGEMENT. The armature windings of a typical synchronous machine can have a single or double layer, a variable number of slots spanned by each coil (slot pitch), integral or fractional slot windings and either full or short pitch windings. These factors affect the number and magnitude of the harmonics present in the generated voltage,

3.1 --- The Permanent Magnet Generator

alter its magnitude and can ease the end connections. The typical pole pitch of a conventional field winding in a 455 kW generator is of the order 200 mm to accommodate the copper and suitable insulation and, for say a 168 pole direct coupled generator, would give a rotor outer diameter of 10.7 meters [45]. This would be far too large to fit into a standard size nacelle, which typically is only 10 % of the blade diameter, and therefore such a conventional generator construction can not be easily used for a direct drive generator. An alternative form of providing the excitation is required and this leads to the development of multi-pole, permanent magnet, synchronous generators.

3.1.2 The development of a multi-pole, permanent magnet, synchronous generator

Permanent magnet machines are typically designed for specific applications in devices upto a few kilowatts and therefore the large scale permanent magnet machines proposed in this thesis are a departure from the current situation. Larger scale machines have been designed, built and run successfully [45] and careful consideration of manufacturing constraints [78] and their operating experience have led to the design described in this thesis as one of the most cost effective for a multi-pole, permanent magnet, synchronous generator. The following sections outline the key design steps for the rotor and stator of such a generator.

3.1.3 Ferrimagnetism and achievable multi-pole, synchronous generator rotor designs

As has already been mentioned in section 1.4 the use of ferrite magnets for providing the excitation in permanent magnet synchronous generators is more cost effective than using other permanent magnets like rare earth or ferromagnets. The theory of ferrimagnetism and design of suitable magnetic systems can be found in any book on electrical machines [79] [80] and the key design ideas are included here for clarity. Firstly the characteristics of typical ferrite magnets are outlined and the impact they have on the rotor design introduced. Then the actual proposed rotor construction is introduced.

FERRITE MAGNETS. Ferrite magnets are manufactured by sintering oxides of iron and another material together in correct proportions at about 1300 degrees. The resulting

ferrite is chemically homogeneous and mechanically hard. If a ferrite is placed in a magnetic field the molecular magnetic moments align with a resultant magnetic field strength about one fifth of the maximum of pure iron [79]. Ferrites are cheap, light and come in a wide variety of standard shapes. Furthermore they are reasonably good electrical insulators and hence eddy currents tend to be less of a problem.

Typical B-H curves for two different Nickel-Zinc based ferrite magnets can be seen in Figure 3.2. Figure 3.2 (a) is suitable for the case where the ferrite magnet experiences alternating magnetic field intensities and Figure 3.2 (b) for the case where the ferrite magnet experiences a constant magnetic field intensity. Both figures show that, as the molecules align with field intensity, it becomes increasingly difficult for further magnetisation and saturation occurs. Temperature can also affect ferrimagnetism in that higher temperatures disrupt the stability of the alignment of the two molecules and the magnetism reduces. The effect of temperature on the B-H characteristic is shown for the ferrite of Figure 3.2 (a). It is therefore usual practice to design ferrite magnet systems for a given operating temperature and saturation. The B-H curves are highly non-linear but can be approximated by a linear relation upto saturation and this linearisation leads to the definition of the relative permeability, μ_r , and an expression for B as,

$$B = \mu_r \mu_0 H \quad (3.2)$$

When the ferrite magnet of Figure 3.2 (b) is excited with a very low frequency alternating supply, the field intensity goes from $-H$ to $+H$ and the cycle shown is set up. B lags behind H and this lagging is termed hysteresis. The enclosed area is the energy lost in the cycle and the resulting magnetism at $H = 0$ is termed the remanence of the material. This remanence, B_{rem} , is permanent provided not too great a negative H is applied and leads to the idea of using permanent ferrite magnets to provide excitation in synchronous machines.

GENERAL DESIGN CONSIDERATIONS. A magnetic system that can produce flux in an air gap but requires no exciting coil and hence no dissipation of electrical power has obvious attractions. Barium, Strontium, and the modern Neodymium-Iron-Boron ferrites form good permanent magnets that can be manufactured in large sizes, are suitable for assembly into a rotor structure and can withstand large demagnetising fields. A typical characteristic curve can be seen in Figure 3.3.

It is the second quadrant of the loop, the demagnetisation curve, that is of interest in the

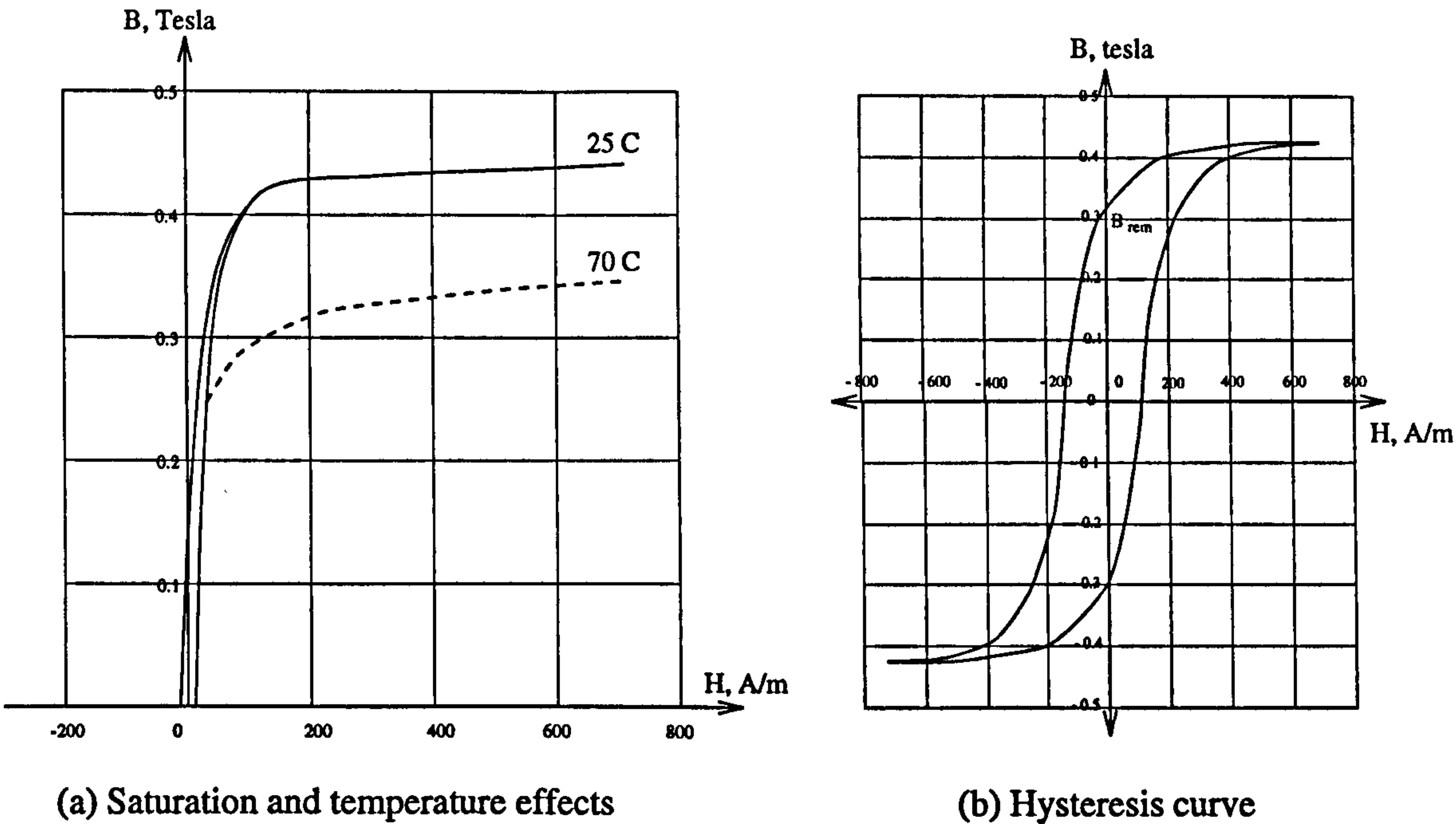


Figure 3.2: Typical B-H curves for two different Nickel-Zinc based ferrites (Source: Electric Machines)

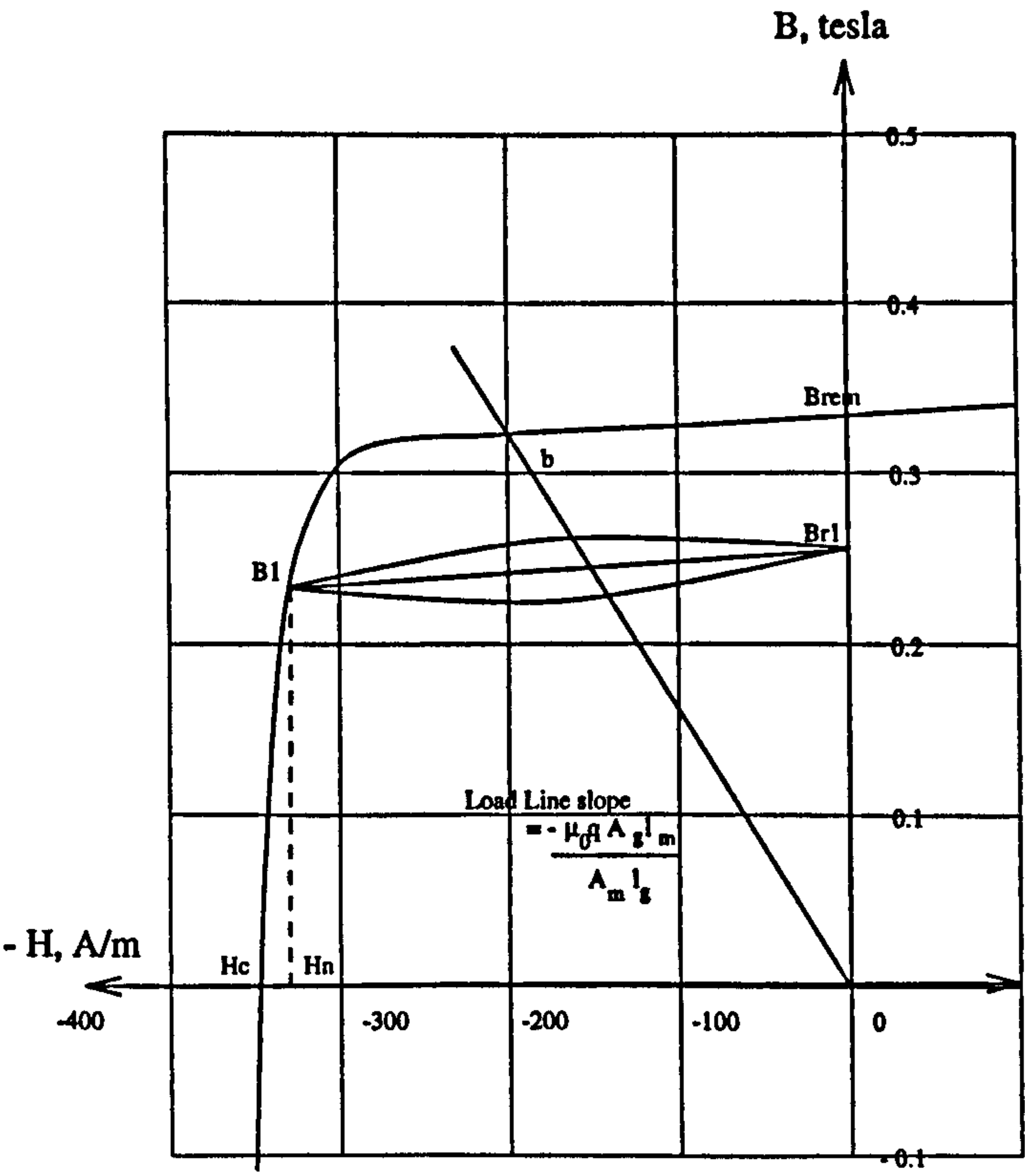


Figure 3.3: Typical B-H curves for a Barium based ferrite (Source: Electric Machines)

design of permanent magnet systems. Suppose a ferrite magnet with the characteristic of Figure 3.3 has a field intensity applied to it of $-H_n$. The flux density will fall to B_1 and when this field is removed the flux density will return along a minor hysteresis loop to B_{r1} . If this process is repeated and providing the field intensity doesn't exceed $-H_n$ then the magnet will follow the minor hysteresis loop and can be considered reasonably permanent. The loop can be approximated by a straight line which has a slope called the recoil permeability, μ_{rec} . This slope is almost the same as that of the original B-H curve at B_{rem} . If the field intensity $-H_n$ is exceeded a new and lower recoil line will be established. It is essential that H_c is not exceeded otherwise the magnet will be demagnetised and this is one of the key constraints in the design of permanent magnet systems.

RADIAL FLUX PERMANENT MAGNET ROTORS. When designing radial flux permanent magnet systems a few key principles need to be followed. The magnetic circuit must be designed to use the magnet at its optimum operating point whilst at the same time concentrating the flux in the airgap to a suitable level for producing power and using the minimum amount of material. The load line, ob, for a simple system comprising a section of barium ferrite magnet, iron core and airgap in a closed loop is shown on Figure 3.3. The slope of the line is defined by the physical dimensions of the magnet and airgap and this determines at what point on the loop from B_1 to B_{r1} the magnet is operating at. A similar approach using equivalent circuits can be derived and analysed for the magnetic system of radial flux machines and used to derive useful expressions which govern their design. One key expression relates the output power of a cylindrical machine to the peak airgap flux density and peak stator electric loading distributions [80],

$$P = \frac{\pi}{\sqrt{2}} k_w \omega D^2 L \hat{B}_g \hat{A} \quad (3.3)$$

where k_w relates to the technical details of the windings. The stator electric loading is limited by temperature rise and peak air gap flux density is limited by saturation. If \hat{B}_g is to be in the usual range found in large electrical machines, 0.8 to 1.1 T, then the magnet material should have a remanent flux density of at least 1 T. However, for systems using low cost ferrite magnet with a B_{rem} of only 0.37 T, a flux concentrating scheme can be used. The development of a rotor that gives acceptable flux concentration will now be discussed.

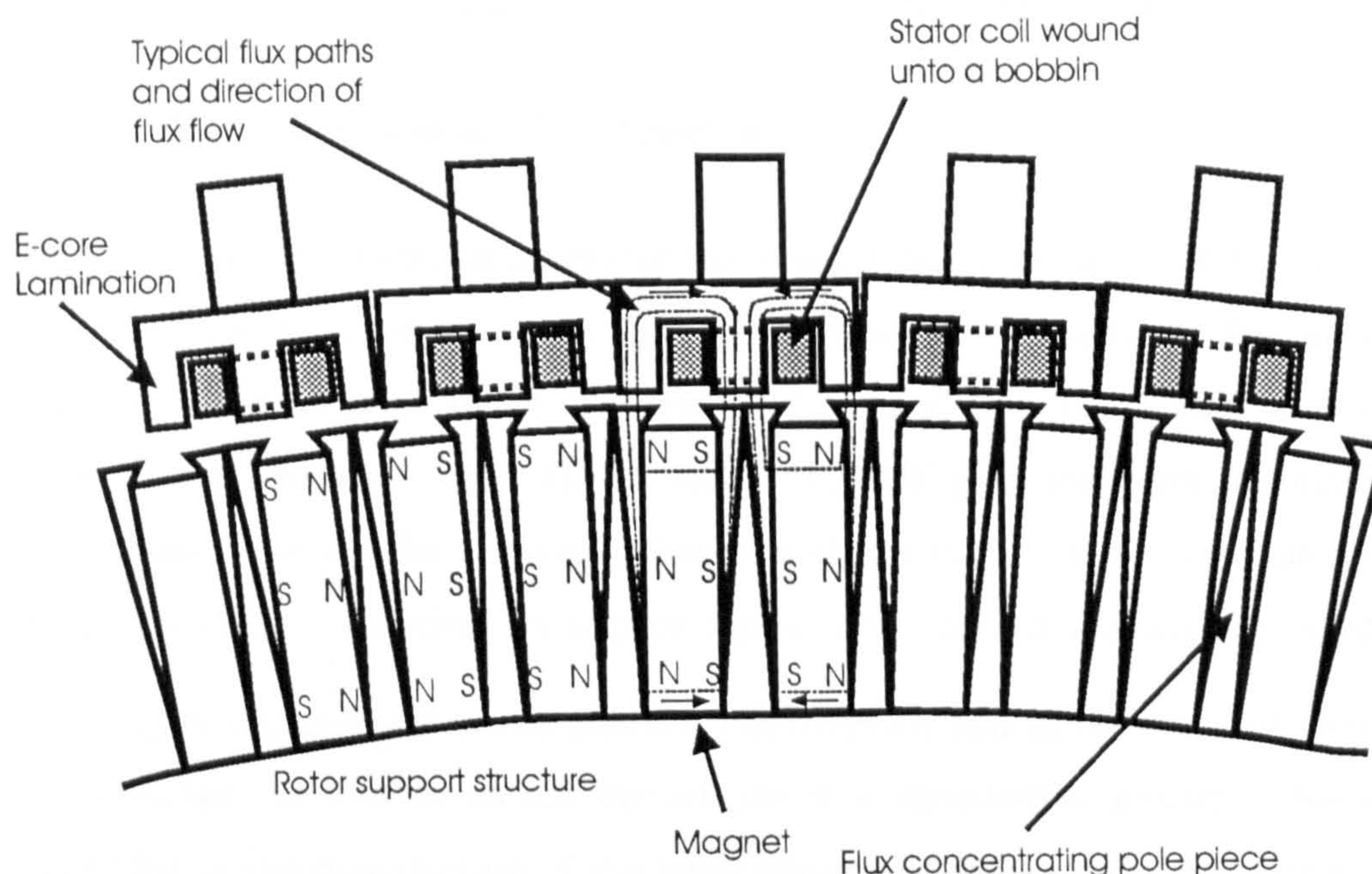


Figure 3.4: Rotor and Stator Arrangement

3.1.4 Rotor construction and design

The use of a permanent magnet rotor to provide the field is the key element that enables the wind turbine to be directly coupled to the generator thereby allowing the overall system to be considerably less bulky than could be achieved using a conventionally wound generator.

ROTOR CONSTRUCTION. Figure 3.4 shows the general form of the magnetic circuit used to obtain an airgap flux density of about 1.0 Tesla and a pole pitch of 45 mm using cheap ferrite magnets with a remanence of less than 0.4 Tesla [42]. For a 455 kW rated generator there are 166 poles which allow 50 Hz to be generated directly from the low speed of the wind turbine rotor. The small pole pitch allows the generator to fit into a conventional sized nacelle with an outer diameter of the stator of 2.396 metres. The magnets are based on the industrial standard size 25 by 100 by 150 mm and therefore for the 45 mm pole pitch the pole pieces are 20 mm wide. A modular construction is used for assembling the rotor magnets together whereby each rotor module consists of two by one wide of the above industrial size magnet blocks surrounded on either side by half the width of steel of the flux concentrating pole piece. Constructing the pole piece shape out of several tapered laminations of steel allows the same module construction to be used in a range of generator sizes from 200 kW to 1500 kW [43]. The flux paths that show how flux concentration can be achieved are also shown on Figure 3.4.

3.1.5 Modular Stator Construction

Unlike a large conventional generator the space restrictions imposed by such a high pole number mean that a normal two layered lap winding is unsuitable for the stator and a coarser arrangement as shown in Figure 3.4 is required. The E-core laminations which make up the stator are 75 by 41 mm for the 455 kW generator with slot dimensions of 19 by 32 mm. The smaller the airgap between stator surface and rotor pole pieces the less magnet material is required for a given flux density and a 2 mm airgap is used.

The E-core arrangement allows modular construction and as the flux paths within the core are localised the E-cores do not disturb the flux distribution greatly. This gives greater flexibility in the manufacture of the laminations and support of the stator as they can be cut from upto 3.2m sheet steel without the need for a segmented design. If segmentation of the structure is needed the tooling and construction costs increase dramatically. Now, unlike a conventional generator where many of the forces are resisted by internal stress within the core, the force on the individual E-cores must be borne by their own support structure. A scheme of fixing the E-cores to hollow rectangular beams supported by a disc at each end as shown in Figure 3.4 is preferred [81]. The rotor modules are also supported by a similar beam structure.

3.1.6 Generator magnetic circuit analysis

The overall design procedure is presented in section 3.2 for the direct drive, permanent magnet, synchronous generator but a brief introduction to the analysis of the complicated magnetic system is included here. In a continuous stator machine, the EMF is proportional to the rotating wave of airgap flux. With the modular machine, however, the flux wave changes shape as the rotor poles move past the modules due to the coarse slotting and the gaps[81]. The procedure for a given rotor and stator module is to firstly determine the equivalent circuit and then evaluate how much flux is generated in the airgap. An equivalent circuit for a rotor and stator module of the permanent magnet generator in this thesis can be seen in Figure 3.5. Figure 3.5 (a) is only a diagrammatic representation as in a real generator the E-core pitch and pole pitch would not be an exact ratio of each other to prevent cogging. This magnetic circuit can then be used to determine the EMF generated in the E-core and the d, q -axis reactances which are necessary for the full non-

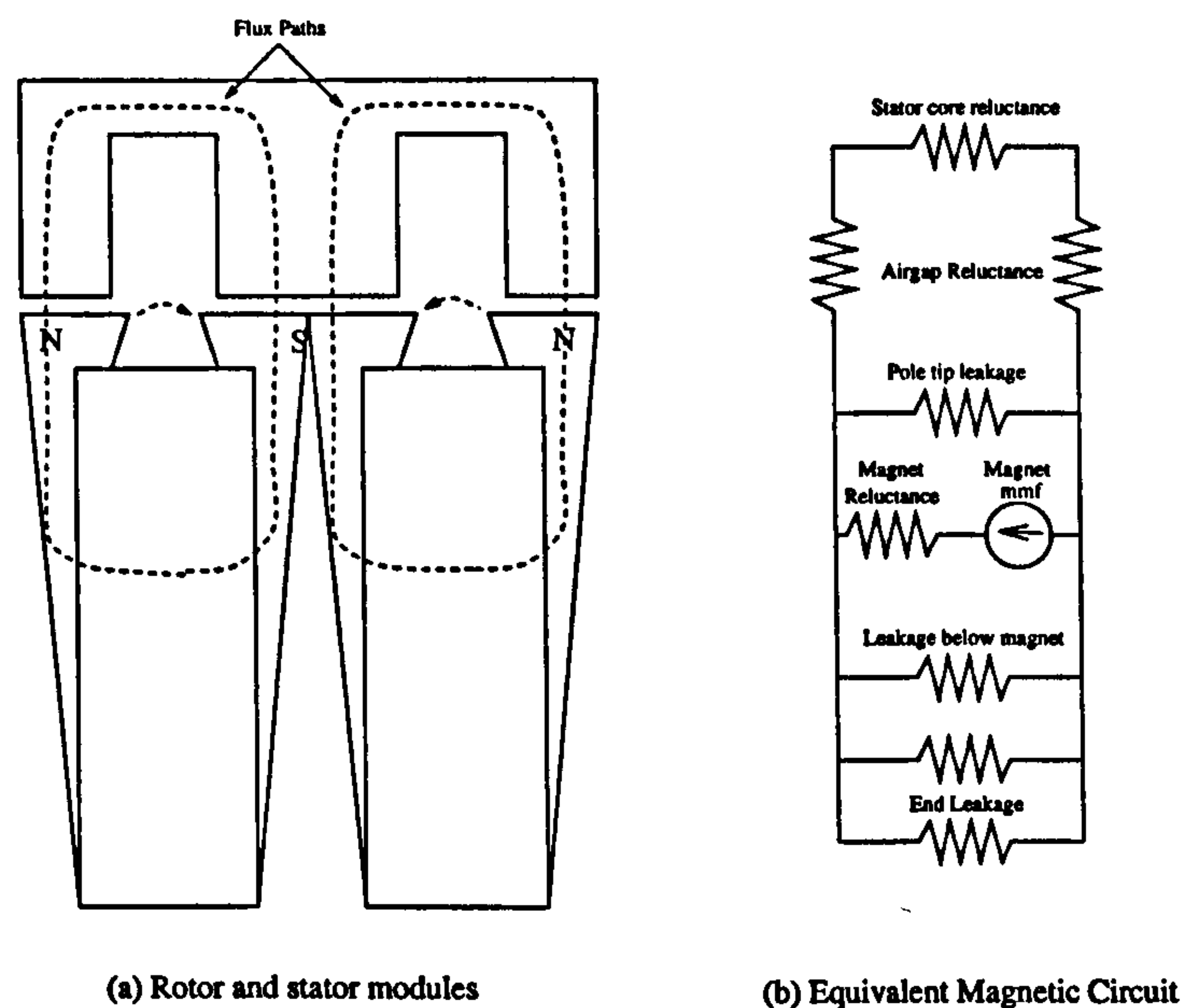


Figure 3.5: Equivalent Circuit of a Permanent Magnet Generator

linear simulation and linearisation presented later in the chapter. This procedure takes into account the change in air gap reluctance as the rotor moves by considering a short arc of the machine at several rotor positions. The resulting set of flux linkages can be used to calculate the fundamental and harmonic flux linkage variations from which the EMF components can be found.

3.1.7 Generator magnetic and electrical operation

Now that the rotor and stator construction details have been discussed and the principles used to derive the key parameters outlined it is necessary to briefly describe the mechanism by which the generator operates.

WINDING ARRANGEMENT. Unlike a conventional generator which usually has a three phase winding of the form portrayed in Figure 3.1, the coils of the three phase winding of the modular permanent magnet generator are distributed around the stator and connected as a fractional slot winding [43]. Each coil is wound onto a single E-core module which makes coil construction and connection very simple. The fundamental of the induced EMF in adjacent coils differs in phase according to the number of coils, N_c , and the number of poles, $2p$, by,

$$\phi = \frac{2\pi p}{N_c} \quad (3.4)$$

The coil connections for creating a three phase output can then be found from the phasor diagram of Figure 3.6. Coils from 0 to 60 degrees are connected in series to form part of phase A with coils between 0 to 240 degrees connected in reverse to form the rest of phase A. These two groups can be connected in series or parallel with each other. Phase B and C are formed similarly but rotated by 120 and 240 degrees respectively. Adding EMFs in this way is equivalent to adding coil EMFs within a phase band of an integral winding: consequently the usual distribution factor applies:

$$k_d = \frac{\sin \frac{1}{2}n\gamma}{g' \sin \frac{1}{2}(n\gamma/g')} \quad (3.5)$$

Substituting the value for the phase band, γ , of 60 degrees and the slots per pole and phase, g' , leads to the following expression for the distribution factor of the fundamental of the fractional slot wound permanent magnet generator,

$$k_d = \frac{3}{N_c \sin(180/N_c)} \quad (3.6)$$

The distribution factor is a measure of the amount the fundamental is reduced from that amount it would be if the phase of all the coil EMFs was the same. Triplen harmonics are eliminated by the terminal connection with all other harmonics reduced from evaluating Equation 3.5 and inserting the order, n , of the harmonic.

The winding arrangement table for the 455 kW rated generator introduced in section 3.2.4 can be seen in Table 3.1. The phase of the coil and the direction of its contribution to the phase voltage are indicated. The winding arrangement table assumes that the top left hand entry is the top dead center E-core and each subsequent row entry is mounted at the next clockwise E-core position. At the end of each row, the next clockwise E-core position is given by the first position in the next row down.

This pattern of winding arrangement is repeated for the second and third tier of the generator stator with the pattern being shifted through 120 degrees clockwise from tier to tier. This rotation reduces the noise generated by the vibration of the E-core structural support

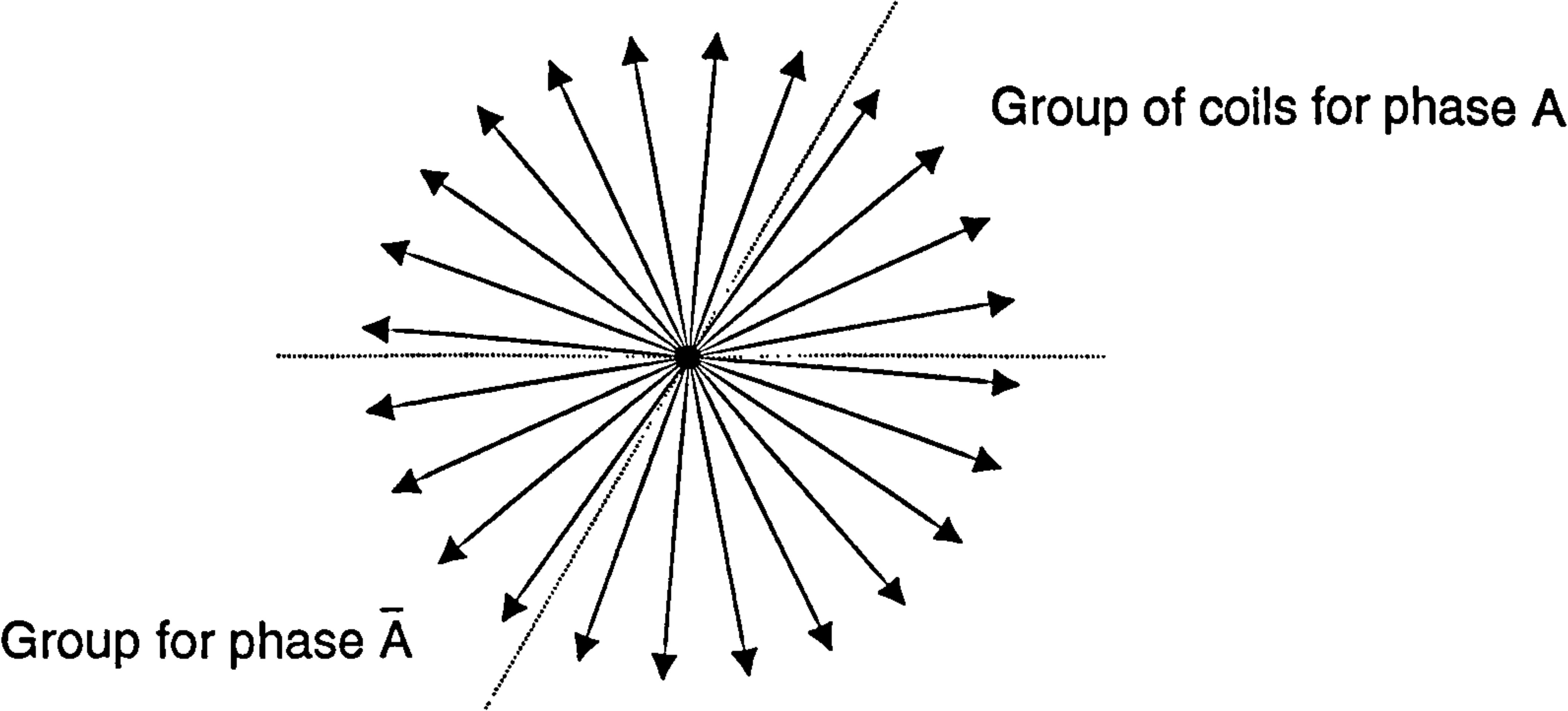


Figure 3.6: Stator phasor diagram for deriving winding connection

A	A	-B	-B	C	C	-A	-A	B	B
-C	-C	A	A	-B	-B	-B	C	C	-A
-A	B	B	-C	-C	A	A	-B	-B	C
C	C	-A	-A	B	B	-C	-C	A	A
-B	-B	C	C	-A	-A	-A	B	B	-C
-C	A	A	-B	-B	C	C	-A	-A	B
B	B	-C	-C	A	A	-B	-B	C	C
-A	-A	B	B	-C	-C	-C	A	A	-B
-B	C	C	-A	-A	B	B	-C	-C	A

Table 3.1: Winding connection arrangement for 455 kW rated generator

due to electromagnetic forces.

WINDING CONNECTION AND HARMONICS. The coils of the phase winding are connected to minimise the harmonic distortion of the terminal voltage. The coils are connected in a fractional slot winding of order $\frac{13}{12}$ over the three tiers. A fractional slot winding leads to a reduction in slot harmonics and breaks the link between slot number and multiples of pole number which increases design flexibility. The coils of each tier are connected in series to make an individual group and then the groups from the individual tiers are paralleled together. This gives a line to line voltage at the terminal of the generator of about 2.2 kV.

The program, WINDGEN2, calculates the level of the harmonics of the terminal voltage of the above winding upto the 43rd order. This is done by fourier analysis and has been checked

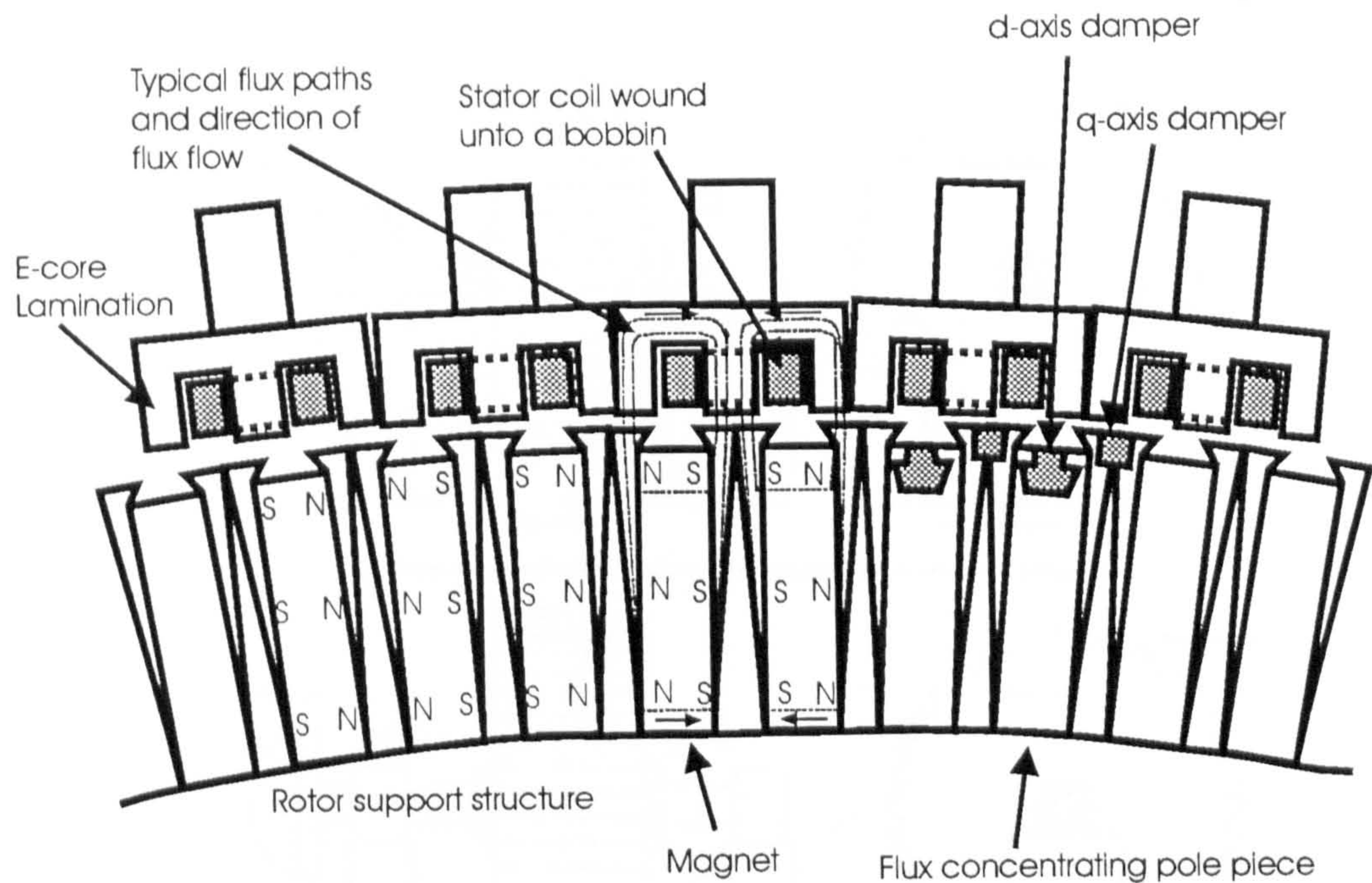


Figure 3.7: Damper windings in Permanent Magnet Generators

against a harmonic analysis of the output waveforms of a small test rig with reasonable agreement. The total harmonic distortion of the line voltage of the rig upto the ninth harmonic was 1.26 % and compares favourably with that returned by WINDGEN2 for the small test rig [81].

3.1.8 Compliant Mounting

The synchronising torque of a generator is required to overcome the natural oscillations of a synchronous machine connected to the grid about its load angle during transient conditions but without damper windings these oscillations tend to last for sometime and could lead to stability problems. Likewise the oscillations introduced due to wind gusting must also be damped out. As mentioned previously most machines incorporate some form of damper winding for this purpose. However in the proposed rotor design there is insufficient space for an effective damper winding. The diagram in Figure 3.7 illustrates this point and also demonstrates the fact that the positioning of such damper windings takes up magnet space, detracts from the magnetic circuit and would prove costly to construct. The conductors sketched in would typically need to be closed by a short circuit ring at each end of the rotor to form a cage winding.

Hence an alternative form of damping of the rotor is required and the proposed solution is to provide mechanical damping through the use of a compliantly mounted stator. This

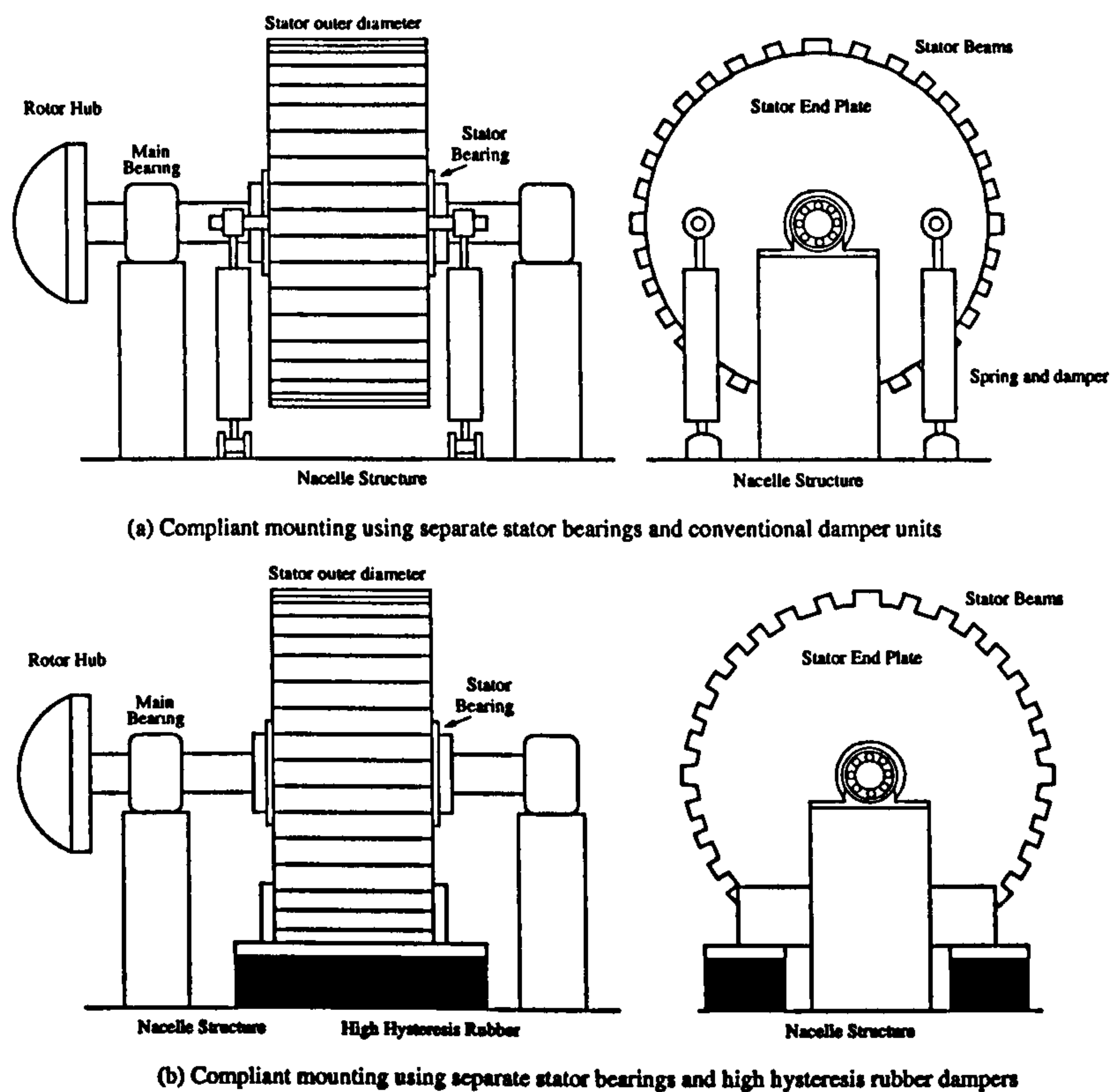


Figure 3.8: Compliant Mounting configurations

method of damping was explored by Kirtley with respect to the stability of superconducting machines [82] and is also already used in some wind turbines to absorb energy from the mechanically excited oscillations of the gearbox. The stator now rotates with respect to the stiff floor of the nacelle and damping is provided either by conventional oil filled dashpots or preferably through the use of a high hysteresis rubber mounting.

POSSIBLE CONFIGURATIONS. There are several possible configurations for such a compliant mounting, two of which can be seen in Figure 3.8. In Figure 3.8 (a) the stator is mounted on separate bearings with two spring damper units at each end. This may prove more expensive than electrical damping because of the extra bearings and other components. In Figure 3.8 (b) the stator is mounted on a rubber support which should be cheap and inexpensive to make. The only possible drawbacks being the stress at the bracket linking the rubber to the stator end plate [47] and the resistance of the chosen rubber material to degradation of its performance with time and environmental conditions.

In Case A the stator ring and end cage must be stiff enough not to sag between the bearings otherwise the airgap distance would be compromised. One benefit is that the damper is not required to support the load and the type of damper envisaged is quite standard. Active

suspension would be possible with such a scheme but the possible benefits of smoother power flow into the grid would have to outweigh the cost of a solenoid and resistive dump.

In Case B the rubber must be able to support the stator and also be able to provide the necessary damping. The rubber must be able to absorb the required energy and a suitable cooling system may be needed. The rubber would also have to show consistent performance with temperature and use.

BENEFITS OF A COMPLIANT SUSPENSION. Several advantages follow from the use of a compliant suspension. Firstly, the key advantage of using such a compliant suspension is that there is relative freedom to choose the stiffness and damping of the suspension to meet any desired transient performance criteria. This is not the case for a conventional damper winding as electrical and magnetic considerations are the prime concern. This is explained in greater detail in section 3.5 and Chapter 4.

Secondly, the angular swing is not limited by the pole pitch because the mechanical restorative force acts for all deflections of the generator upto the limit of the spring extension. The electrical synchronising torque, on the other hand, depends on the position of the generator on its characteristic power angle curve.

Thirdly, damping is now provided to any subsequent oscillations proportional, by some means depending on the damping arrangement used, to the angular speed of the stator. In a conventional generator, the damping provided by damper windings depends on the current flowing in the winding as explained in section 3.1.1. However the current which would flow in the damper winding of such a multi-pole, permanent magnet generator during transient conditions would be small and ineffective [83]. This is due to the high resistance of such a damper winding and the low EMF introduced in the damper winding during transient conditions.

Finally, the generator can accept unbalanced current without loss and hence electrical transients can be more readily absorbed. The first point that the mechanical restorative force is not limited by pole pitch is the key reason why compliant suspension is really the only cost effective method for ensuring good performance of a fixed speed, multi-pole, permanent magnet, synchronous generators.

3.2 The Generator Parameters

Now that the multi-pole, permanent magnet, synchronous generator has been introduced it is necessary to outline the derivation of the parameters for the wind turbine, the permanent magnet generator and the compliant mounting. Firstly the design procedure for a medium sized wind turbine rated at 455 kW is outlined. Several design drivers are identified and these are used to derive designs of generator ratings from 200 kW to 1.5 MW, a typical range for wind power applications. The per unit system and post-processing using EXCEL of a generator design program, WINDGEN2, is then introduced.

3.2.1 Overall design procedure

Given a desired rating of generator, the nominal windspeed at a site and the performance coefficient data for the wind turbine blades, then the required diameter of the blades is found by rearranging equation 2.8 for the power in the wind to give,

$$\text{diameter} = \sqrt{\frac{8P_{nom}}{\rho V_{nom}^3 C_{p_{nom}} \pi}} \quad (3.7)$$

The maximum rotational speed of a wind turbine is constrained by the tip speed which should be typically between 50 and 70 m/s for optimum performance [41]. Hence, for a given nominal wind speed and the calculated diameter, a particular rotational speed is given by,

$$\frac{50}{\text{diameter}} \geq \omega_r \leq \frac{70}{\text{diameter}} \quad (3.8)$$

This then fixes the number of pole pairs required to give 50 Hz generation and, using the magnetic circuit described in section 3.1.4, the outside diameter of the rotor. The maximum number of E-cores is given by dividing the circumference of the rotor by the standard E-core width of 75 mm and arranging the winding connections to give a satisfactory output voltage.

3.2.2 WINDGEN2 - A fixed speed permanent magnet design suite

A program, WINDGEN2, that enables a full range of permanent magnet generators to be designed has been written by other members of the Wind Energy Research Group at Durham. The required specification in terms of the wind turbine blade diameter, design and mean windspeed at hub height and coefficient of performance data are entered first and a nominal power rating is found for 50 Hz grid connection. Then the generator is specified in terms of standard module size for both the rotor and stator from a selection which satisfy the design constraints of demagnetisation current, required frequency of operation and electric loading. Once the basic design is entered a magnetic circuit is carried out to find the values of generator reactance, resistance and the generated emf and a fourier analysis carried out to assess the harmonic content of the terminal voltage. The program then evaluates the thermal loading of a whole generator ring and requires the user to specify the number of rings to satisfy the minimum thermal loading. Finally a prediction of the generator performance at nominal frequency and voltage is carried out to ascertain the designs effectiveness. WINDGEN2 also returns values for the masses of the key generator parts as weight is a crucial design criteria in wind turbines as a low tower head weight leads to a lighter tower structure and overall cost savings. The returned values for the weights are used to calculate the inertia of the generators rotary parts.

3.2.3 Tier Number

The thermal loading on the E-cores imposes a limit on the allowable current in the coils. To ensure a suitable E-core current involves either increasing the depth of the slots and hence allowing more turns per E-core or altering the size of wire used. This leads to an increase in the power out of a given module but also changes the insulation and current carrying requirements and can lead to an inefficient design.

Alternatively the tiered system shown in Figure 3.9 could be used. The tiers share the driving torque and hence less current flows through the windings although the total power out is the same. Decreasing the number of tiers increases the per unit value of X_d and X_q and can lead to poor designs. Increasing the number of tiers, on the other hand, increases the weight of the generator and there is a trade-off between tower head weight and electrical performance. The efficiency of a tiered generator depends on the loading of the generator

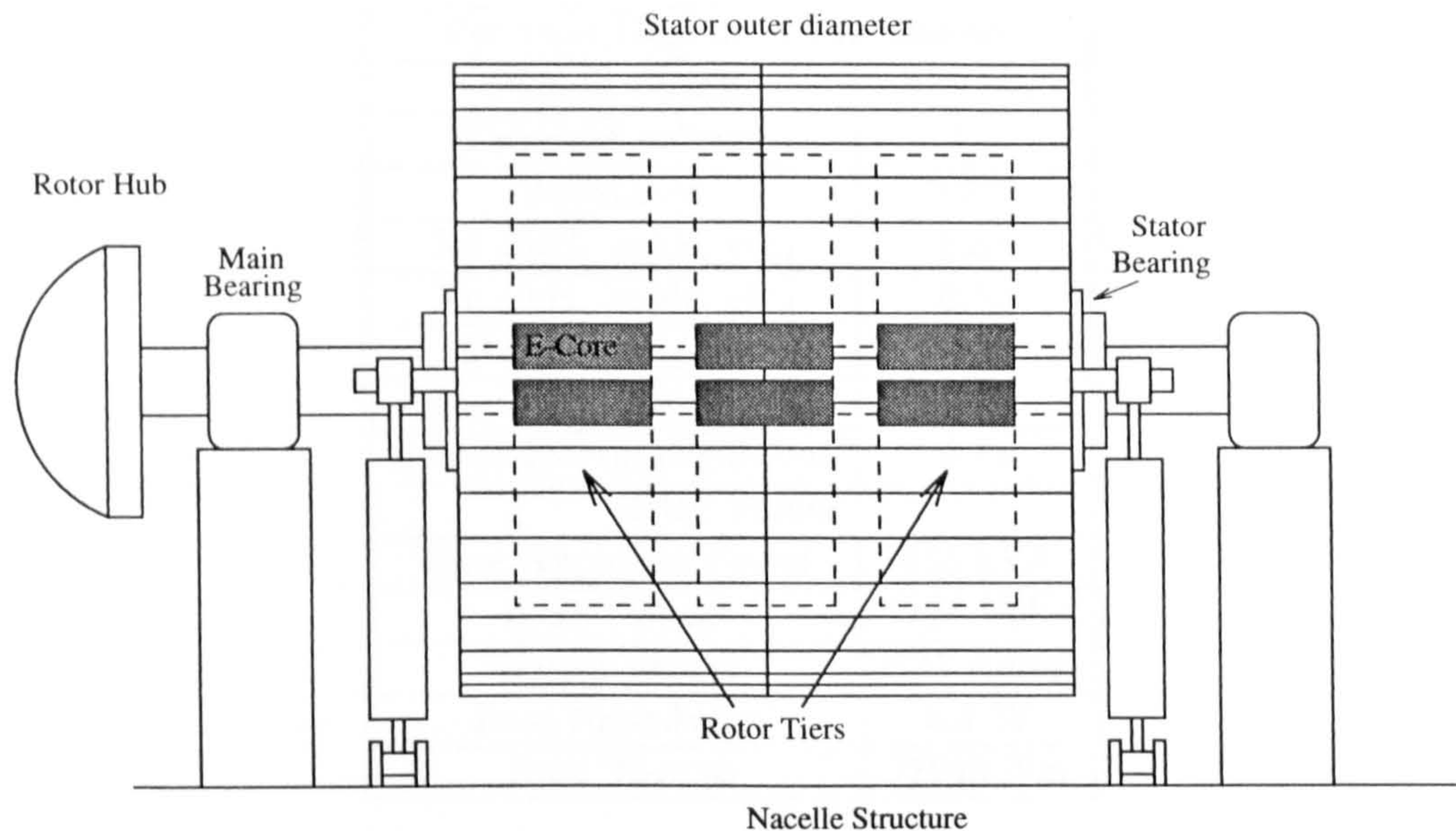


Figure 3.9: The tiered approach

but is about 96 % at full load which compares well with a conventional generator.

3.2.4 Overall Values for a 455 kW rated generator

This section outlines some key results for a 455 kW rated wind generator, the main parameters of which are given in the Table 3.2. The inertia of the rotor is much larger than that of the stator as it includes both the inertia of the generator rotor and the inertia of the turbine blades. The impedance of the grid and the unit transformer are included in the value of R , X_d and X_q . The r.m.s. base values used in the per unit normalisation are also included in Table 1.

3.2.5 Per Unit System

A per unit system is essentially a system of dimensionless parameters occurring in a set of wholly or partially dimensionless equations. This helps simplify the calculations as the dimensionless groups are usually derived by a process of normalisation in which one physical parameter is divided by another of the same dimension. These base quantities are chosen because of the ways in which they characterise key features of the system. The magnitudes of some of the base quantities can be chosen quite freely but then the subsequent bases must be chosen in accordance with the rules of the system. Normally the principle per unit

Per Unit Generator Parameters	
Overall rating	455 kW
Terminal voltage	1.0
Resistance	0.023
Xd (incl. cable, etc)	0.54
Xq (incl. cable, etc)	0.52
Number of poles	166
Rotor inertia coefficient	2.90
Stator Inertia coefficient	0.15
Base Values	
Base Apparent Power	455 kVA
Base Voltage	1128 Volts
Base Current	134 Amps
Base Impedance	8.4 W
Base Torque	72215 Nm

Table 3.2: The 455 kW Generator Parameters

variables assume unit magnitude under rated conditions. The principle bases are derived in Appendix C and the post-processing of the rest of the design variables is now outlined.

3.2.6 Implementation on EXCEL

The output of WINDGEN2 contains values for all the electrical values of the generator and the weights of its key components. However the main part of the rotor inertia is the blades of the wind turbine itself. Therefore it was necessary to carry out some post processing of the WINDGEN2 output on EXCEL [84] to determine all the component inertias.

BLADE WEIGHT AND INERTIA CALCULATION. In the thesis the aerodynamic performance of the blade is approximated by the coefficient of performance as described in an earlier section. However a realistic simulation of the wind turbine also requires a value for the rotor inertia. The inertia of the blade depends on its weight distribution and length. Harrison [36] has produced an exhaustive report into the costing of modern commercially available horizontal axis wind turbine designs and the results from his model are used for the blade weights for any diameter upto 70 metres. The inertia of the blade is calculated assuming a radius of gyration at a third of the length of the blades. This is assumed from the typical weight profile of a blade - heavier at the hub due to the thicker chord there than at the tip. The total inertia of the three blades is thus,

$$J_r = 3M_b R_g^2 \quad (3.9)$$

GENERATOR ROTOR INERTIA CALCULATION. The rotor is essentially made up of two thick walled cylinders connected by some structural supports. The outer cylinder comprises the pole pieces and magnetic material and the inner cylinder is the low speed shaft connecting the generator rotor to the wind turbine hub. The rotor structural weight is assumed to be distributed equally in the radial direction and therefore is divided by two and the mass is lumped with that of the inner and outer cylinders. The equation for the inertia of the two cylinders is thus,

$$J = \frac{M + \frac{M'}{2}}{2} (r_{out}^2 + r_{in}^2) \quad (3.10)$$

Hence the total generator inertia is given by,

$$J_{gen} = J_{out} + J_{in} \quad (3.11)$$

TOTAL ROTOR INERTIA. The total rotor inertia is found from adding the inertia of the generator to the inertia of the rotor blades and adding a further amount to represent the rotor hub,

$$J_{tot} = J_{rot} + J_{gen} + J_{hub} \quad (3.12)$$

STATOR INERTIA CALCULATION. The stator weight is returned from WINDGEN2 and the same equation for the inertia of a thick walled cylinder is used to calculate the stator inertia. The inertia of the spring and damper unit is assumed negligible.

EXCEL IMPLEMENTATION. The above equations used to extract usable values from WINDGEN2 and the relationships between the actual masses and the per unit values have been implemented on a spreadsheet using Microsoft Excel [84]. The values in bold face are typed into the spreadsheet, shown in Figure 3.10, from the printed output of WINDGEN2 for the given rating of generator design. The values required for the simulation are then updated automatically using equations (3.9) to (3.12) and those presented in Appendix B for the per unit system. This simplifies the procedure for evaluating the necessary parameters for the Simulink models to run as just a few key values from the printed output from WINDGEN2

3 GRP Blades, Design Vw=12							
Generator Rating, kW	200	455	455	500	750	1000	1500
Rated Rotational Speed	44.80	36.10	36.10	30.60	29.10	24.40	20.00
Blade Diameter	24.00	35.00	35.00	39.00	46.00	55.00	63.40
Blade Weight	0.79	1.71	1.71	2.18	3.64	5.71	8.41
Blade Inertia at Rgy = 0.5L	8.49E+04	3.94E+05	3.94E+05	6.21E+05	1.45E+06	3.24E+06	6.34E+06
Check using rod	1.13E+05	5.25E+05	5.25E+05	8.28E+05	1.93E+06	4.32E+06	8.45E+06
Check with Rgy = Rod/3	3.77E+04	1.75E+05	1.75E+05	2.76E+05	6.42E+05	1.44E+06	2.82E+06
Hub Diameter	1.20	1.75	1.75	1.95	2.30	2.75	3.17
Hub Weight	0.59	1.29	1.29	1.63	2.73	4.29	6.30
Hub Inertia	8.49E+01	3.94E+02	3.94E+02	6.21E+02	1.45E+03	3.24E+03	6.34E+03
Number of Tiers	2.00	3.00	2.00	3.00	3.00	4.00	5.00
Rotor OD1	1.74	2.17	2.17	2.54	2.62	3.19	3.92
Rotor ID1	1.54	1.97	1.97	2.34	2.42	2.99	3.72
Total Rotor Weight	3.14E+03	5.83E+03	3.99E+03	7.36E+03	7.44E+03	1.17E+04	1.81E+04
Number of Poles	134	166	166	196	206	248	302
Module Weight	7.40	7.40	7.40	7.40	7.40	7.40	7.40
Total Module Mass	1.98E+03	3.69E+03	2.46E+03	4.35E+03	4.57E+03	7.34E+03	1.12E+04
Shaft Diameter	1.20	1.60	1.60	2.00	2.20	2.60	3.40
Shaft Length	1.00	1.40	1.00	1.40	1.40	1.80	2.20
Shaft Weight	2.35E+02	4.40E+02	3.14E+02	6.50E+02	6.05E+02	9.20E+02	1.47E+03
Rotor Outer Weight	2.44E+03	4.54E+03	3.06E+03	5.58E+03	5.70E+03	9.08E+03	1.39E+04
Rotor Outer Inertia	1.65E+03	4.88E+03	3.30E+03	8.29E+03	9.09E+03	2.17E+04	5.07E+04
Number of Stator Modules	72.00	90.00	90.00	105.00	108.00	132.00	162.00
Shaft OD1	1.20	1.60	1.60	2.00	2.20	2.60	4.14
Shaft ID1	1.18	1.58	1.58	1.98	2.18	2.58	4.12
Shaft Inertia	9.89E+02	3.27E+03	2.34E+03	7.05E+03	8.34E+03	1.79E+04	7.19E+04
Total gen+shaft weight	3.38E+03	6.27E+03	4.30E+03	7.91E+03	8.05E+03	1.27E+04	1.96E+04
Total Inertia	4.04E+04	1.84E+05	1.81E+05	2.92E+05	6.61E+05	1.48E+06	2.94E+06
Per Unit Rotor Inertia	2.13	2.89	2.85	2.82	4.15	4.49	4.24
Power Base	2.09E+05	4.55E+05	4.55E+05	6.33E+05	7.42E+05	1.06E+06	1.50E+06
Stator Outer Diameter	1.92	2.40	2.40	2.76	2.81	3.14	4.14
E - core Depth	0.04	0.06	0.06	0.06	0.04	0.06	0.06
Stator Mass	2.24E+03	4.51E+03	3.28E+03	5.29E+03	4.65E+03	8.89E+03	9.06E+03
Stator Inertia	1.98E+03	6.16E+03	4.49E+03	9.64E+03	8.91E+03	2.11E+04	3.77E+04
Per Unit Stator Inertia	0.10	0.15	0.11	0.20	0.13	0.22	0.28
Vbase	2.29E+02	1.13E+03	1.16E+03	1.16E+03	5.72E+02	1.73E+03	1.16E+03
Ibase	3.04E+02	1.34E+02	1.31E+02	1.54E+02	4.32E+02	2.05E+02	4.34E+02
Zbase	0.75	8.39	8.83	7.53	1.32	8.45	2.67
Per Unit Resistance	0.03	0.02	0.04	0.03	0.05	0.04	0.03
Per Unit Xd	0.45	0.54	0.81	0.54	0.68	0.69	0.58
Per Unit Xq	0.43	0.62	0.77	0.51	0.64	0.66	0.55
Emf	2.29E+02	1.13E+03	1.16E+03	1.16E+03	5.72E+02	1.73E+03	1.16E+03
System Voltage	2.40E+02	1.27E+03	1.27E+03	1.27E+03	6.35E+02	1.91E+03	1.27E+03
Per Unit Emf	1.00	1.00	1.00	1.00	1.00	1.00	1.00
Per unit System Voltage	1.05	1.13	1.10	1.10	1.11	1.10	1.10
Allowable Deflection (Degrees)	3.78	3.09	3.09	2.71	2.67	2.40	1.85
Active Weight	3.51E+03	6.54E+03	4.36E+03	7.69E+03	8.00E+03	1.29E+04	1.98E+04
Structural Weight	2.10E+03	4.23E+03	3.22E+03	5.51E+03	4.69E+03	8.61E+03	8.91E+03
Total Weight	5.61E+03	1.08E+04	7.58E+03	1.32E+04	1.27E+04	2.15E+04	2.87E+04
Cost Ecu / Kg of active material	3.20	2.81	2.81	3.10	3.10	3.12	3.12
Cost Ecu / Kg of structural material	2.36	1.41	1.41	1.80	1.49	1.80	1.23
Total cost	1.62E+04	2.44E+04	1.68E+04	3.21E+04	3.18E+04	5.33E+04	7.26E+04
Cost Ecu/kW	80.98	53.55	36.93	64.19	42.40	53.27	48.42

Figure 3.10: Generator parameter spreadsheet

are required.

3.3 Full Permanent Magnet Generator Model

Firstly the modelling of the electrical and mechanical behaviour of a conventional synchronous machine is described. Then the methodology of reducing the conventional model to represent a permanent magnet machine is outlined. The derivation of the governing equations are presented in Appendix B with the key equations quoted in this section for completeness. The effect of connecting a generator to the transmission grid on the governing

3.3 Full Permanent Magnet Generator Model

equations is also discussed.

3.3.1 Electrical Behaviour - Five Winding Model

Most synchronous generators consist of a three phase armature winding and a field winding. The performance of the machine can be modelled using a phase model but to simulate their performance in the time domain the inductance matrix must be updated at each time interval as the inductances between the field and armature coils depend on the rotor position. In addition the simulation follows the 50 Hz variation in current and voltage and therefore requires a small time step. To overcome these problems it is usual practice to transform the armature equations into a reference frame, $dq0$, rotating at synchronous speed such that all inductances have constant values and the 50 Hz armature voltages map onto d.c. values so allowing larger integration time steps to be taken. A typical reference frame with the quadrature axis leading the direct axis is shown in Figure 3.11.

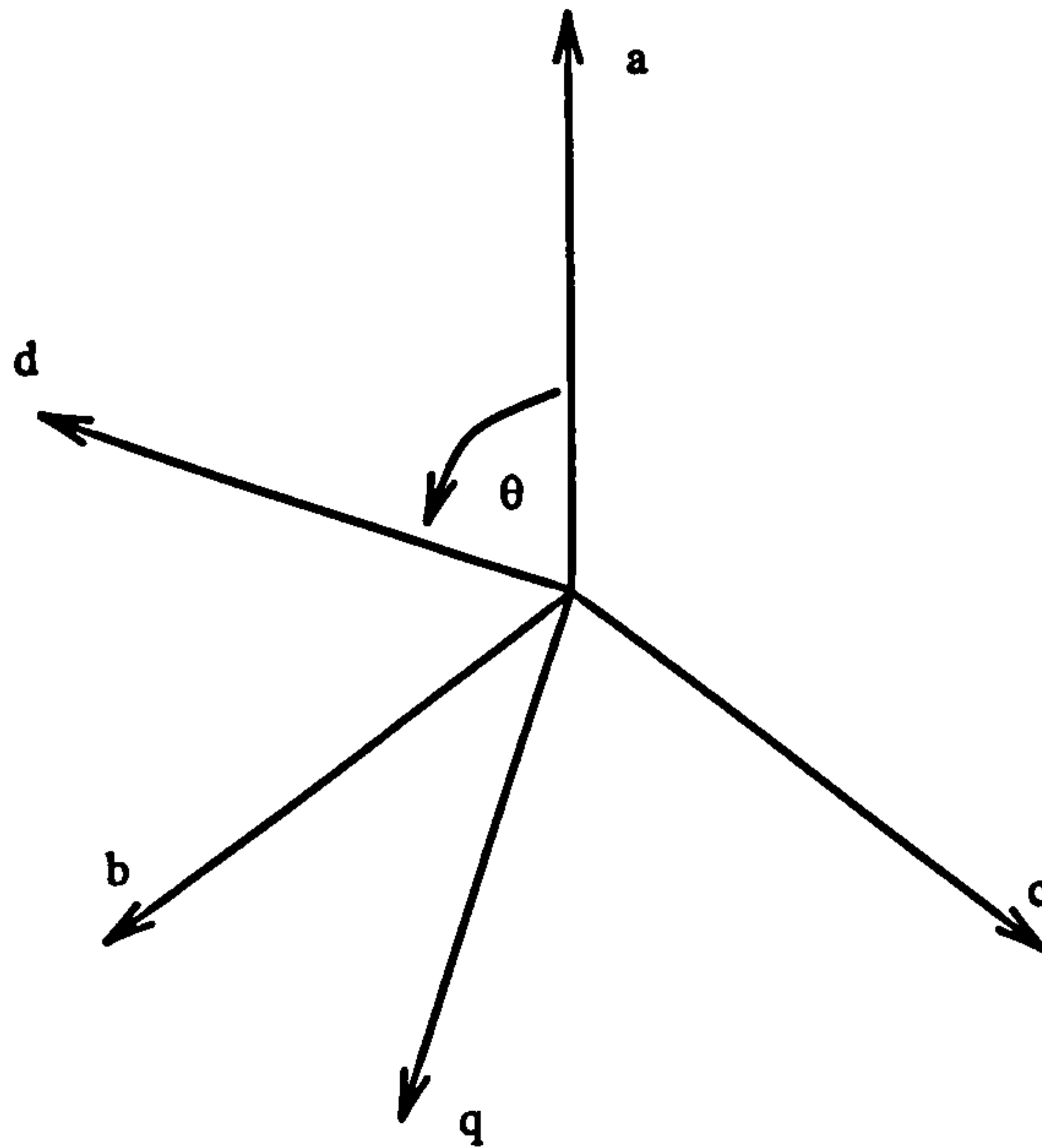


Figure 3.11: The $dq0$ frame of reference

With this notation the instantaneous $dq0$ and abc voltages, currents and fluxes are related by the following transforms,

$$\begin{bmatrix} v_d \\ v_q \\ v_0 \end{bmatrix} = \sqrt{\frac{2}{3}} \times \begin{bmatrix} \cos \theta & \cos(\theta - 120) & \cos(\theta - 240) \\ -\sin \theta & -\sin(\theta - 120) & -\sin(\theta - 240) \\ \frac{1}{\sqrt{2}} & \frac{1}{\sqrt{2}} & \frac{1}{\sqrt{2}} \end{bmatrix} \times \begin{bmatrix} v_a \\ v_b \\ v_c \end{bmatrix} \quad (3.13)$$

with inverse,

$$\begin{bmatrix} v_a \\ v_b \\ v_c \end{bmatrix} = \sqrt{\frac{2}{3}} \times \begin{bmatrix} \cos \theta & -\sin \theta & \frac{1}{\sqrt{2}} \\ \cos(\theta - 120) & -\sin(\theta - 120) & \frac{1}{\sqrt{2}} \\ \cos(\theta - 240) & -\sin(\theta - 240) & \frac{1}{\sqrt{2}} \end{bmatrix} \times \begin{bmatrix} v_d \\ v_q \\ v_0 \end{bmatrix} \quad (3.14)$$

To model the machine the three armature phase coils map onto two coils one on the direct axis and the other on the quadrature axis. The field winding is also represented as a further coil on the direct axis. It is also normal practice to assume two further coils, one on each axis, to represent the effect of the currents in the damper winding as well as minor effects such as eddy currents induced in the pole face and slot wedge region during fault conditions, i.e. to simulate the effect of machine damping. The full five winding model is shown in Figure 3.12. Each coil is both inductive and resistive as per the governing equations in Appendix B.

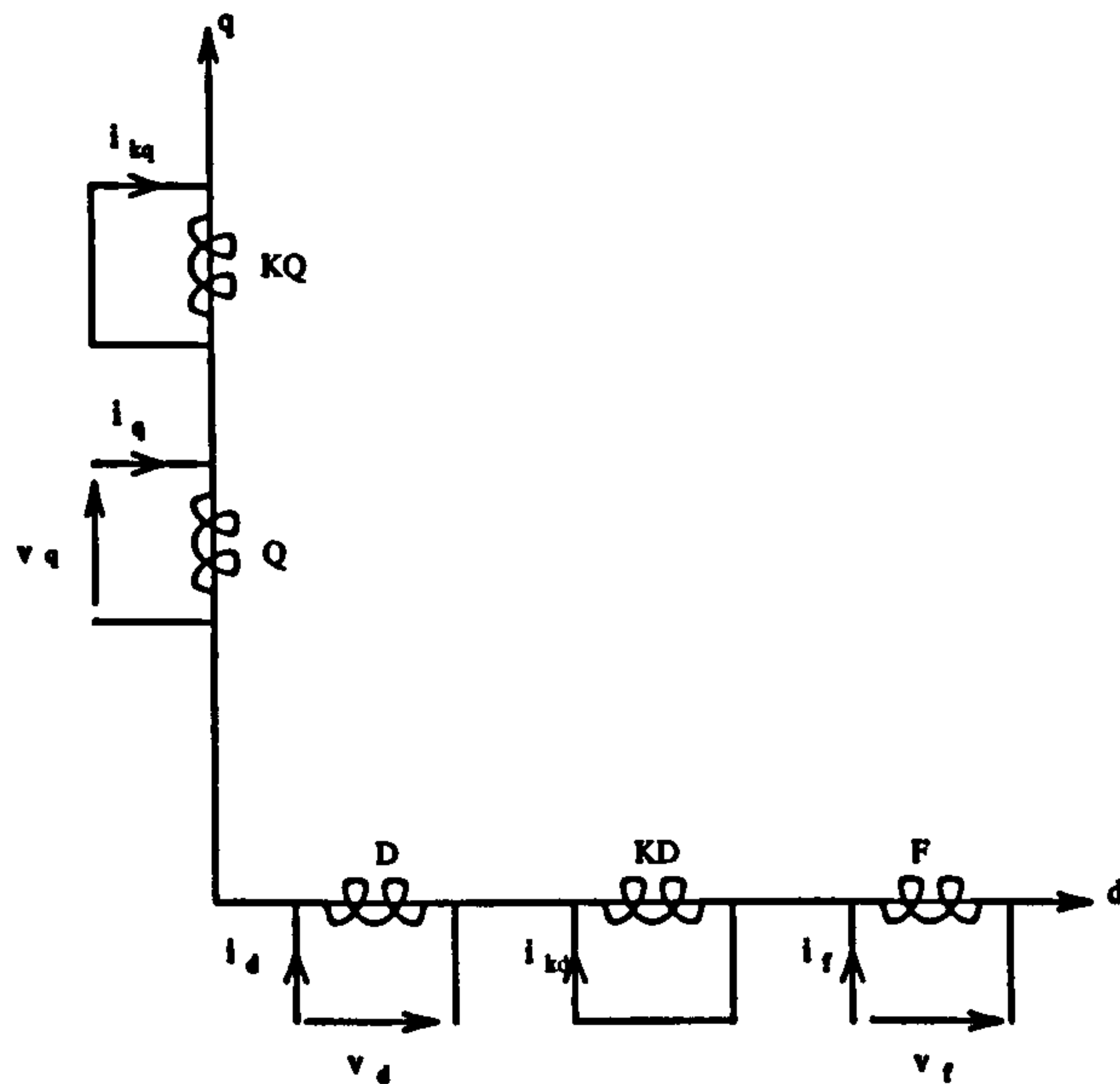


Figure 3.12: The five winding model

The $\sqrt{\frac{2}{3}}$ factor in the transformations relating the $dq0$ axis to the abc phase voltages, equations (3.13) and (3.14), is necessary to ensure that the m.m.f.'s of the three phase winding and two phase winding systems are equal in magnitude. The same factor is used in the current transformations and ensures there is power invariance between the two systems [85].

3.3.2 Conversion to modelling the Permanent Magnet Generator

The permanent magnet machine has a high number of poles and as such has a small pole pitch. Such a small pole pitch precludes the use of conventional damper windings as described in section 3.1. Eliminating the damper windings reduces the electrical model to a more simple three winding model. As there is permanent magnet excitation the field winding can be replaced by a constant fictitious current source [86] [87]. This constant current source models the fact that the flux generated by the permanent magnets is constant. The new model representing the permanent magnet machine can be seen in Figure 3.13.

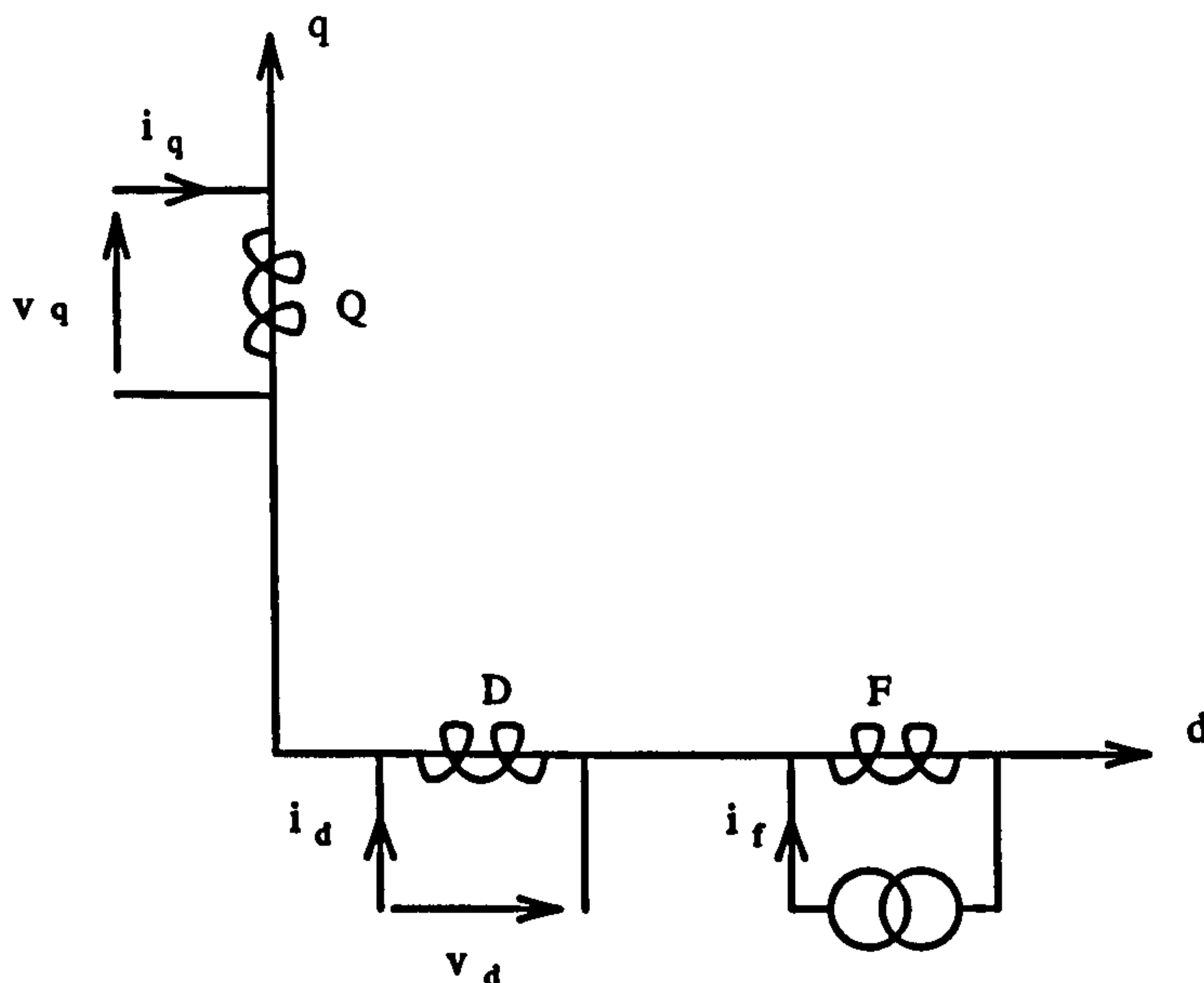


Figure 3.13: The three winding model

Furthermore as there are no damper windings present and it is a multi-pole, permanent magnet, synchronous generator, the effects of the damper and field windings on the d - and q -axis reactance need to be reconsidered. Modelling and measurement of a test rig at UMIST [88] has shown that there will be no alteration to the values of X_d and X_q under transient conditions and therefore a simple model with no change in X_d or X_q can be derived. This has implications in terms of the peak fault current that is likely to flow if there is a 3 phase short circuit at the generator terminals. As the sub-transient and synchronous reactance are the same the fault current will be far smaller than the current produced by an equivalent conventional generator with damper windings. In fact studies show that the peak current for this kind of multi-pole permanent magnet synchronous generator is only about 2 to 3 times rated value. This is a further benefit of removing the damper windings.

3.3 _____ Full Permanent Magnet Generator Model

3.3.3 Synchronous generator connected to an infinite bus system

Typically when a conventional synchronous generator is modelled for connection to an infinite bus the terminal voltage is used as reference and then the load angle of the generator is defined as the angle between the excitation voltage, E , and the terminal voltage. When system effects are considered a further angle must be defined known as the power angle, δ , which takes into account the impedance of the transmission link. This angle is usually defined as the angle between the infinite bus voltage, V_b , and the excitation voltage [89]. Now if, instead of using the load angle and then converting to a power angle to simulate such a generator, the power angle is defined as the angle between the infinite bus voltage phasor and the excitation voltage phasor no angle conversion is required. However the generator reactances and resistances must be corrected to include the impedance of the transmission line so that the generator has the correct performance. This is the approach used in this thesis.

If a stroboscope at mains frequency is used to illuminate a line marked on the end of the shaft of such a generator, the angle the line would move through from the no load condition until stability is lost is 90 degrees. This spatial angle, δ_r , relative to the synchronous rotating reference frame has a one to one mapping to the power angle of the generator. The rotor angle, δ_r , has now been made equivalent to the power angle of the generator.

However there is one further stage to the definition of the system connection. For a compliantly mounted generator there is another angle to consider and this is due to rotation of the stator, δ_s . This angle is defined in Figure 3.14 relative to the rotating reference frame. Clearly an increase in δ_s for a fixed δ_r will reduce the power angle, δ , of the generator. This is the mechanism whereby the stator motion interacts with the electrical response of the generator. Extracting energy from that motion leads to damping of the generator's electrical response. This approach to modelling angle interactions within synchronous generators is akin to that used in multi-machine studies. A rotating reference frame is typically defined and then all generator rotor angles are determined relative to it. If on an isolated system all the generators increased in speed together, they may have rotor angles in excess of 360 degrees. The dependence on absolute rotor angle as a measure of stability when compared with the rotating reference frame is lost. It is the relative angle between the generators that is now important, just as it is the relative angle between the stator and rotor that

3.3 Full Permanent Magnet Generator Model

determines the power angle of a compliantly mounted synchronous generator. All angles are given in electrical radians. Electrical radians are converted to mechanical radians by dividing by the number of pole pairs.

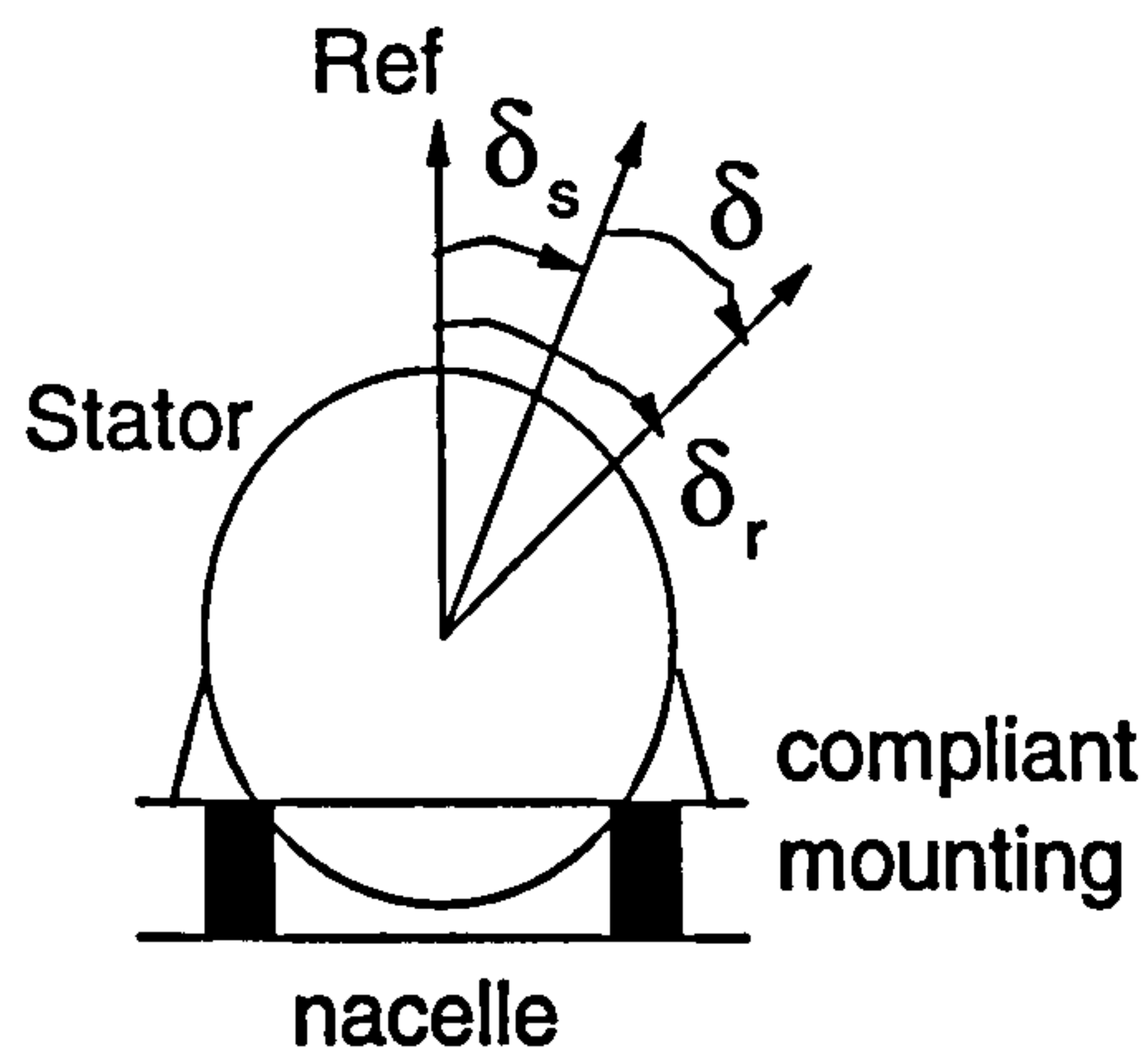


Figure 3.14: Definition of angles

Figure 3.15 shows the generator connected via a transformer to the infinite bus. The phasor diagram representing the above system can be seen in Figure 3.16. The value for the total d - and q -axis resistance and reactance to the grid is the sum of the winding, the transformer and the transmission line resistance and reactance and the angle, δ , is the power angle of the generator.

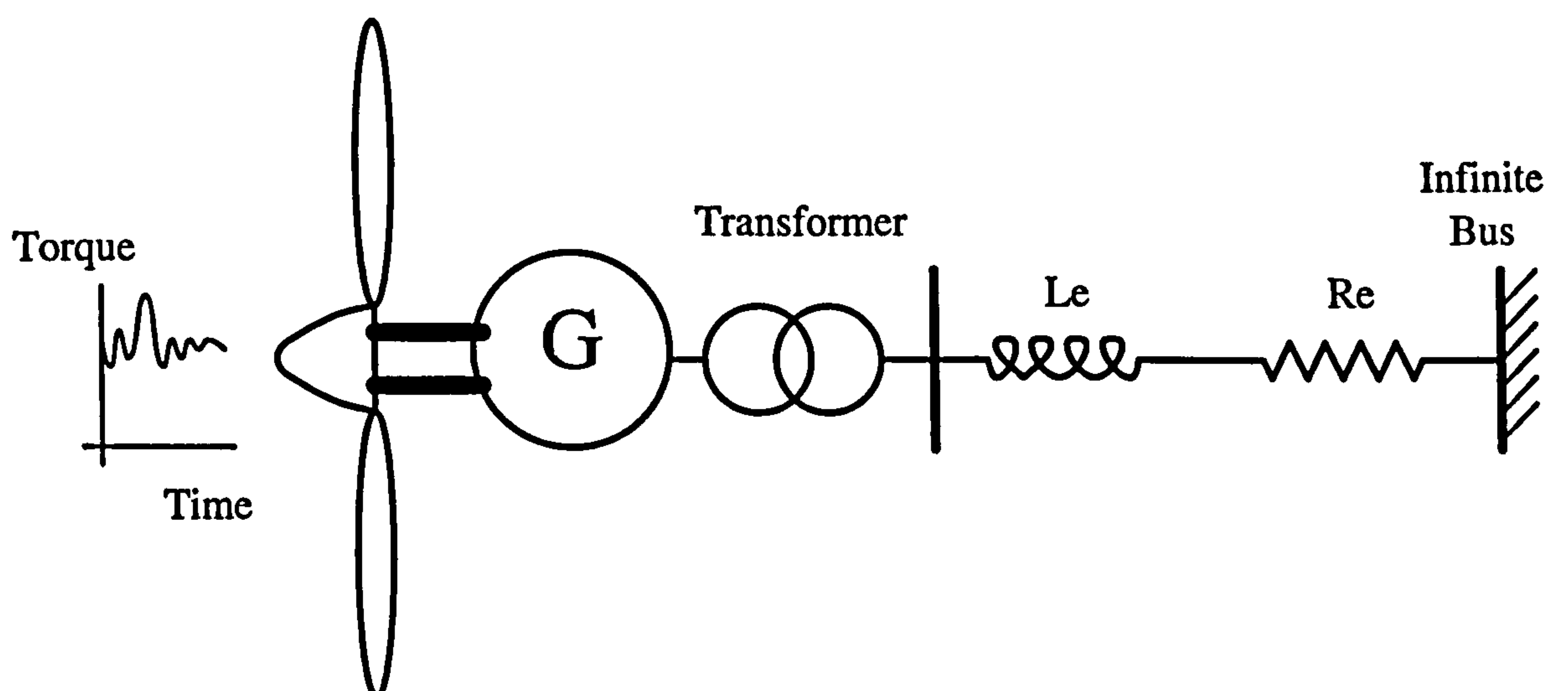


Figure 3.15: The system configuration

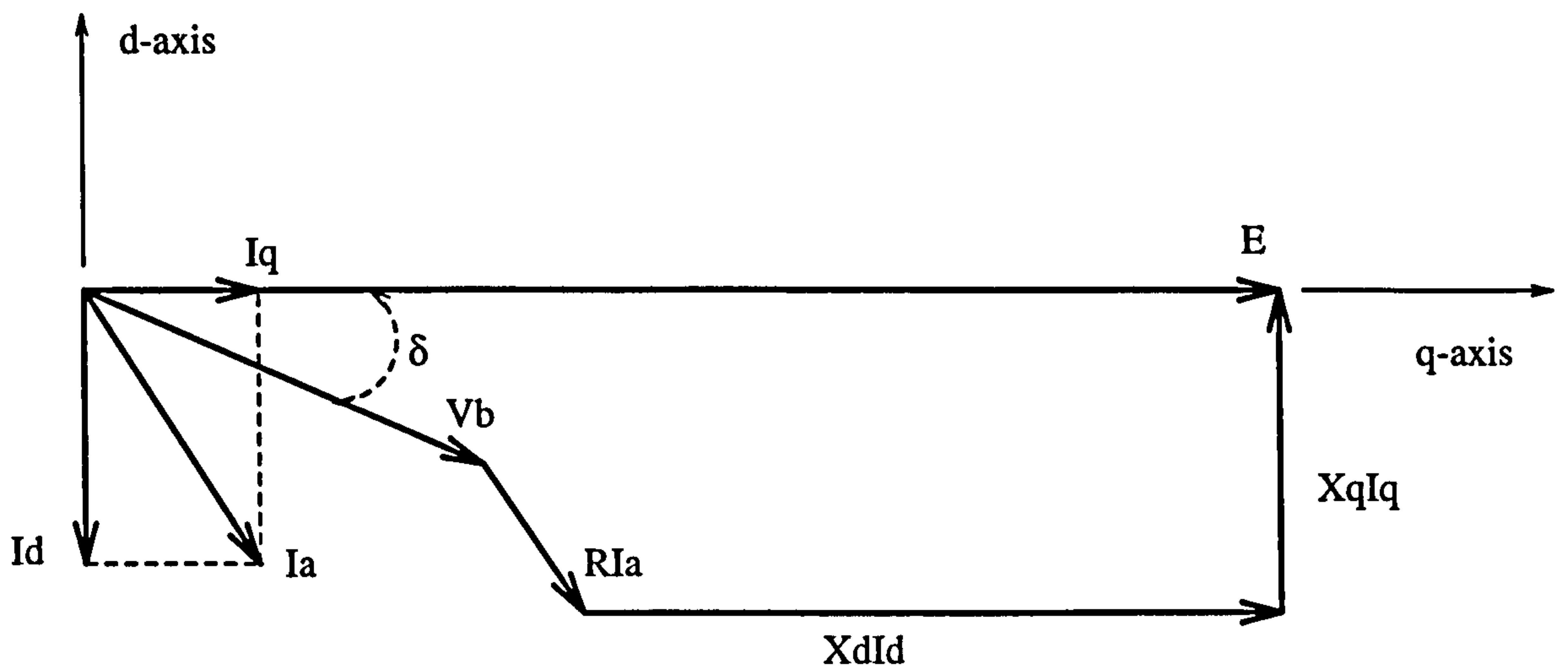


Figure 3.16: The phasor diagram of the system

3.3.4 Development of the simulation model of the permanent magnet generator

Now that the three winding model has been introduced and the system configuration of the multi-pole permanent magnet synchronous generator has been outlined it is necessary to present the key equations for the generator model. A full derivation of these equations is included in Appendix B.

Rotor Movement. For the case of a rotor with a fixed stator the following non-linear second order differential equation holds.

$$\dot{\omega} = \frac{d^2\delta}{dt^2} = \frac{\omega_0}{2H_r}(\tau_m - \tau_{ag} - K_d\dot{\delta}) \quad (3.15)$$

where K_d is a damping term corresponding to friction in the bearings and the like and is usually neglected. τ_{ag} is given by equation B.49 in Appendix B and τ_m is the input mechanical torque from the turbine.

Rotor and Stator Movement. For a machine with the stator allowed some degree of freedom of movement and connected to the frame via some suitable spring and damper system then both the rotor and stator inertias must be considered. Several sets of equations can be derived to describe such a system mathematically. The most useful for the purposes of linking the generator model to the dynamic wind turbine model is one which has rotor speed, $\dot{\delta}_r$, as a state variable. This leads to a linked set of two differential equations,

$$\frac{d^2\delta_r}{dt^2} = \frac{\omega_0}{2H_r}(\tau_m - \tau_{ag}) \quad (3.16)$$

$$\frac{d^2\delta_s}{dt^2} = \frac{\omega_0}{2H_s}(\tau_{ag} - c\frac{d\delta_s}{dt} - k\delta_s) \quad (3.17)$$

where c is the per unit damping coefficient and k is the per unit spring stiffness of the compliant mounting. The generator power angle, δ , is now given by,

$$\delta = \delta_r - \delta_s \quad (3.18)$$

This equation relating the power angle to the rotor and stator angle is very important as it can be used to rearrange equation 3.16 to be in terms of the power angle instead of rotor angle. This is useful in the linearisation process and is discussed in greater detail in section 3.4.2.

ELECTRICAL BEHAVIOUR. The equations of motion for the stator and the rotor are linked to the electrical behaviour through the electromagnetic torque. The electromagnetic torque is dependent on the value of the instantaneous currents, i_d and i_q . The two first order differential equations that govern i_d and i_q can be derived from the voltage equations as,

$$pi_d = -\frac{\omega_0 r_a i_d}{X_d} - \frac{\omega X_d i_d}{X_d} + \frac{\omega_0 \sqrt{3} V_b \sin \delta}{X_d} \quad (3.19)$$

$$pi_q = -\frac{\omega_0 r_a i_q}{X_q} + \frac{\omega(\omega_0 k \phi_f)}{X_q} + \frac{\omega X_d i_d}{X_q} - \frac{\omega_0 \sqrt{3} V_b \cos \delta}{X_q} \quad (3.20)$$

The resulting airgap electromagnetic torque is then given by,

$$\tau_{ag} = \frac{1}{3} ((\omega_0 k \phi_f) i_q + i_d i_q (X_d - X_q)) \quad (3.21)$$

3.4 Methods of Analysis

There are two complimentary types of analysis used: Non-linear simulation and linearisation. The two methods will be described here and over the next two chapters will be applied

to develop models for the permanent magnet generator.

3.4.1 Non-Linear Simulation

The non-linear model of the generator can now be interfaced with the wind turbine model developed in Chapter 2 to produce a full non-linear model of the wind turbine generator system, as shown in Figure 2.33. The first interface variable between the two models is the driving torque, τ_m , at the shaft of the wind turbine. This is calculated at every time interval by dividing the power harnessed from the wind, from equation 2.8, by the rotor speed of the generator, the second interface variable. The final interface variable is the measured output power of the generator which, in the per unit system defined in Appendix B, is the same as τ_{ag} minus the losses due to the armature resistance of the generator. This is used as the input for the pitch controller.

Non-linear simulation of the generator involves converting the two second order differential equations representing the rotor and stator movement, equations 3.16 and 3.17 respectively, into a set of four first order differential equations. This set of equations is linked via the expression for the electromagnetic torque, equation 3.21, which is based on an algebraic expression including the differential equations governing the d - and q -axis currents, equations 3.19 and 3.20 respectively. These are solved using a standard Runge-Kutta integration technique within SIMULINK. A schematic of such a simulation can be seen in Figure 3.17. The 'rotor' equation is equation 3.16 and the 'stator' equation is equation 3.17. Both equations can be integrated twice as they are second order. τ_{ag} is calculated at each time step from the evaluation of equation 3.21 which uses values returned from the integration of equations 3.19 and 3.20 representing the d - and q -axis currents. This is a sixth order model as there are six first order differential equations. When the generator is considered in isolation to the wind turbine the driving torque τ_m can be set to give any required input torque disturbance, e.g. a step increase.

STATE VARIABLES. As the permanent magnet, synchronous generator is represented by six first order differential equations six state variables can be chosen which uniquely define the operation of the generator. The rotor angle is chosen to be the state variable in preference to the power angle for ease of interfacing the resulting rotor speed with the wind turbine model. These state variables are chosen to be,

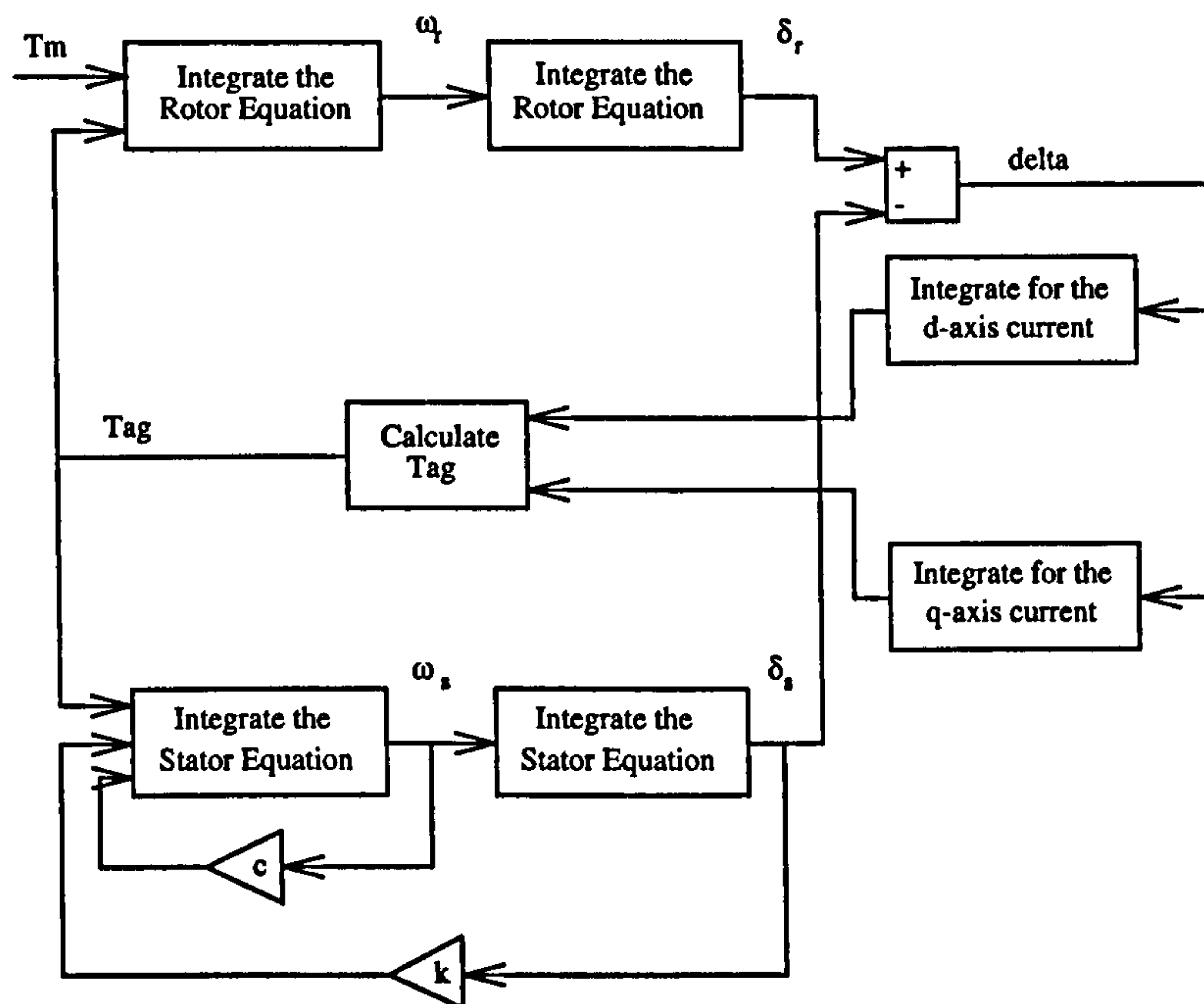


Figure 3.17: A schematic representation of full non-linear simulation

$$x_1 = i_d \quad (3.22)$$

$$x_2 = i_q \quad (3.23)$$

$$x_3 = \delta_r \quad (3.24)$$

$$x_4 = \dot{\delta}_r \quad (3.25)$$

$$x_5 = \delta_s \quad (3.26)$$

$$x_6 = \dot{\delta}_s \quad (3.27)$$

INITIAL OPERATING POINT. Before starting a simulation run it is necessary to evaluate the initial conditions of the generator. The initial values of the state variables for the simulation are found from an analysis of the steady state conditions. At steady state the input mechanical power to the generator must equal the power supplied to the infinite bus, assuming no transmission or stray losses. An initial estimate of the power angle can be found by rearranging the expression for the power supplied to the infinite bus which, for this system, is,

$$P = \frac{EV_b \sin \delta}{X_d} \quad (3.28)$$

By resolving the phasor diagram of the system in the d - and q -axes, expressions governing the initial values for the currents I_d and I_q can then be calculated using this approximation for δ . As a quasi-static initial condition is assumed and, knowing the transformation between the phase values and the d, q -axis currents, expressions for the initial instantaneous currents can be found,

$$x_{10} = i_{d0} = -\sqrt{3}I_{d0} = -\sqrt{3} \left(\frac{EX_q - V_b X_q \cos \delta_0 - V_b r_a \sin \delta_0}{X_d X_q + r_a^2} \right) \quad (3.29)$$

$$x_{20} = i_{q0} = \sqrt{3}I_{q0} = \sqrt{3} \left(\frac{X_d V_b \sin \delta_0 + r_a E - V_b r_a \cos \delta_0}{X_d X_q + r_a^2} \right) \quad (3.30)$$

These two equations are derived in Appendix B. This method gives a slight imbalance between the mechanical driving torque and the electromagnetic torque which can be calculated by substituting the initial values for i_q and i_d into the torque equation, equation 3.18. Therefore an iterative approach is used to alter the calculated value of power angle, δ , to improve the power imbalance until after a few iterations a balanced set of initial conditions is reached.

The initial stator angle is then found from equation 3.17 by setting $\ddot{\delta}_s = \dot{\delta}_s = 0$. The initial rotor angle, δ_r , is then found from equation 3.18. In summary the other initial values for the state variables are found from:

$$x_{40} = x_{60} = 0 \quad (3.31)$$

$$x_{50} = \frac{\tau_{ag}}{k} \quad (3.32)$$

$$x_{30} = \delta_0 + x_{50} \quad (3.33)$$

SIMULATION PROCEDURE. Once the initial conditions have been set the solution for the disturbance caused by the input torque function is found for the required duration of simulation. At each time step the differential equations for the rotor, stator and the d - and q -axis currents are integrated before evaluating the expression for the electromagnetic

torque.

3.4.2 The theory behind linearisation

Synchronous machines are non-linear devices due to the form of the output power equation and the effect of magnetic saturation. Therefore, in order to study problems associated with dynamic stability, a model of the generator linearised about some operating point is generally used. Analysis of the linearised equations of such a generator connected to a infinite bus reveals the natural frequencies and degree of damping of the modes of oscillation of the system [90]. The equations of the compliantly mounted, permanent magnet, synchronous generator can also be linearised similarly. It is important to note that the state variables defined in equations 3.22 to 3.27 are altered for this linearisation so that x_3 is now the power angle, δ , and x_4 , is now $\dot{\delta}$. Analysis of these linearised equations to find the frequencies and corresponding level of damping as various design parameters are altered allows the performance of a compliantly mounted generator to be evaluated. The performance predicted by analysis of the linearised model is then compared against the full non-linear simulation to see how the design actually performs. This is outlined in detail in the next section.

To examine the behaviour of the system when it is perturbed such that the new and old equilibrium states are nearly equal, the system equations are linearised about the quiescent operating point, i.e. first order approximations are made for the system equations. The new linear equations are assumed to be valid near to the quiescent operating point.

The dynamic response of a linear system is determined by its characteristic equation. Both the forced response and the free response are decided by the roots of this equation. From a point of view of stability the free response gives the needed information. If it is stable any bounded input will give a bounded and therefore stable output.

The synchronous machine model developed earlier in the chapter has two types of nonlinearities: product nonlinearities and trigonometric functions. The first order approximations that hold for these are outlined Appendix C. The linearised state space equations can be formulated into the expression,

$$\dot{x}_\Delta = A(x_0)x_\Delta + B(x_0)u \quad (3.34)$$

3.5 Preliminary results for the 455 kW rated generator

where $A(x_0)$ is the plant matrix and $B(x_0)$ is the driving matrix.

LINEARISATION PROCEDURE. The elements of the plant matrix, A , depend upon the initial conditions of the state vector x_0 . The dynamic properties of the system are then determined from the nature of the eigenvalues of the plant matrix using the Control Systems Toolbox [91].

3.5 Preliminary results for the 455 kW rated generator

The eigenvalues of the plant matrix, from equation C.27, determine the natural frequencies and associated damping ratios of the response of the compliantly mounted generator connected to the infinite bus following disturbances, such as a change in input torque. They can therefore be used for preliminary design of the compliant mounting. The performance predicted for all designs by linearisation is then checked against the performance from the full non-linear simulation. The eigenvalues can be negative real, positive real (indicating an unstable system) or in complex conjugate pairs; in the latter case the imaginary part corresponds to the damped frequency of oscillation and the real part the rate of decay (if negative). Six eigenvalues exist for the matrix $[A]$ as it is a sixth order model and these split into three conjugate pairs. The full explanation of the physical meaning of these three conjugate pairs is given in section 4.1.2., but the following results for the 455 kW rated generator are included to introduce both the concept of relating the position of the eigenvalue to the full non-linear simulation and the basic operation of the compliant mounting. The three pairs of eigenvalues occupy different loci on the imaginary plane as the generator parameters vary and are therefore described as the high, middle and low frequency eigenvalues due to their relative position. The high frequency pair of eigenvalues is related to the movement of the stator and the low frequency pair to the movement of the rotor. The middle frequency pair of eigenvalues, with a natural frequency close to 50 Hz, relate to the stator transformer voltages. This pair of eigenvalues disappear if these voltages are neglected in equation B.31 and B.32.



3.5 Preliminary results for the 455 kW rated generator

3.5.1 Eigenvalues

The position of eigenvalues in the complex plane determines the physical behaviour of the systems they represent. Eigenvalue pairs are typically complex conjugates and therefore only the positive eigenvalue is shown with the negative eigenvalue exhibiting mirror image behaviour but with a negative imaginary part. Figure 3.18 shows the relationship between the position of an eigenvalue and the corresponding damped frequency of oscillation, ω_d , and damping ratio, ζ , associated with it.

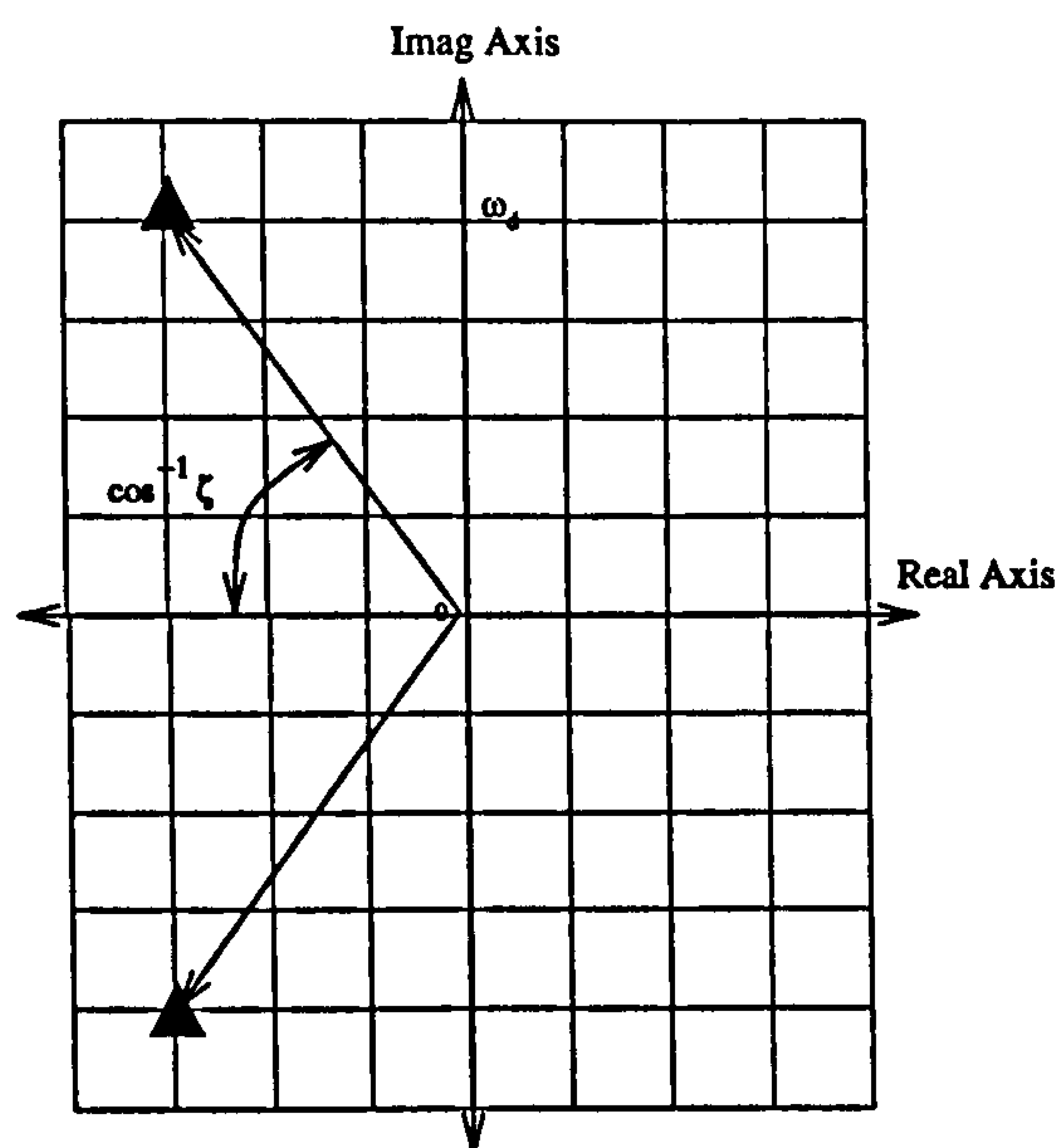


Figure 3.18: Eigenvalues

3.5.2 Stator results

The variation of the positive high frequency eigenvalue and the corresponding time response for the stator for different values of per unit spring stiffness, k , as per unit damping coefficient, c , varies can be seen in Figure 3.19 and Figure 3.20 respectively.

Several key points need to be raised from analysing these plots. Firstly the eigenvalues lie in the left half of the complex plane indicating stable response. For a stiff stator, $k = 10$, the stator movement is restricted and with low damping coefficient, $c = 0.0187$, the position of the eigenvalue would be very close to the imaginary axis which corresponds to low damping ratio. As the damping is increased a point is reached at which the eigenvalue moves onto the real axis and the damped oscillations of the stator are removed from the system as it is now

3.5 Preliminary results for the 455 kW rated generator

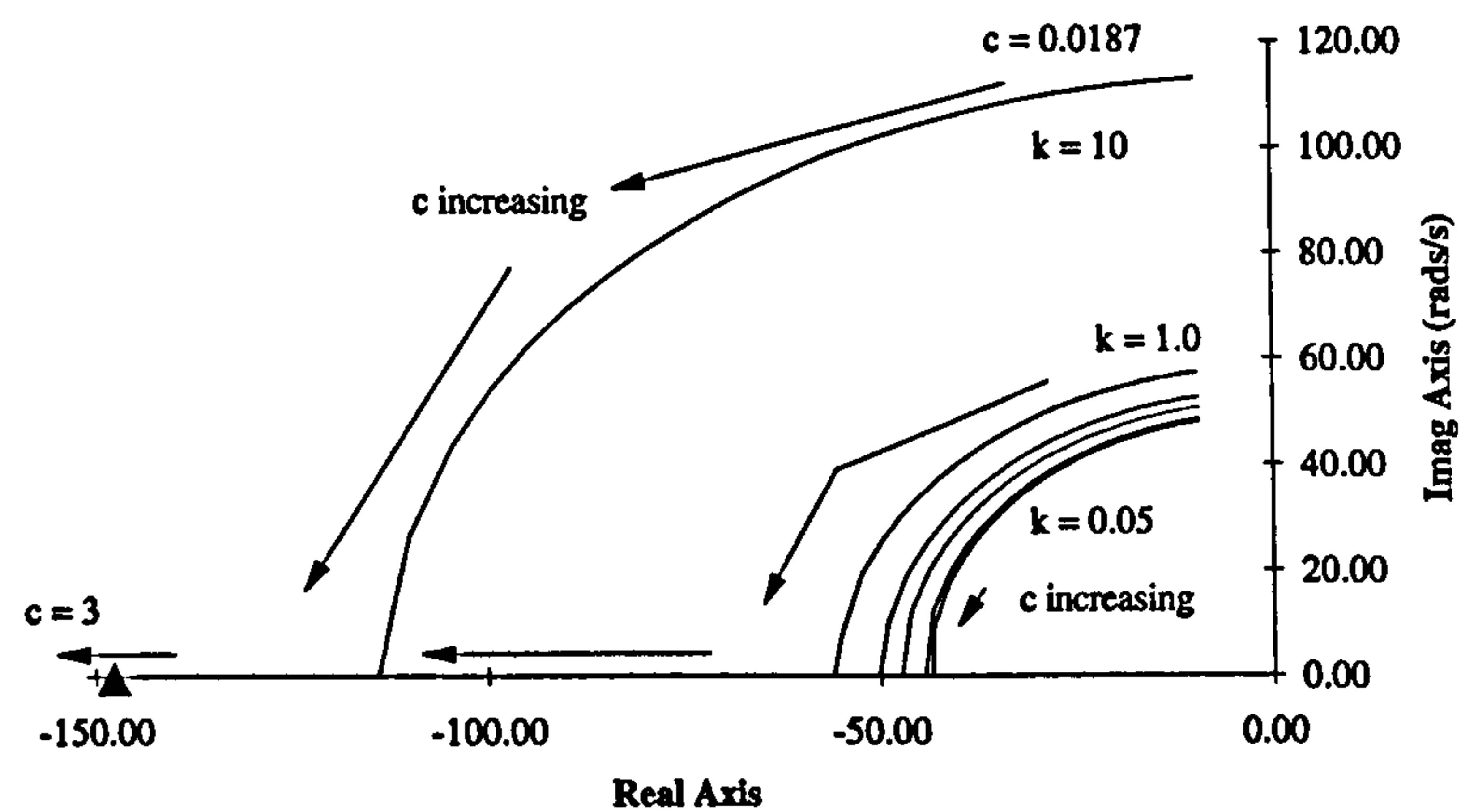


Figure 3.19: The Variation of the High Frequency Eigenvalue as stiffness and damping are varied

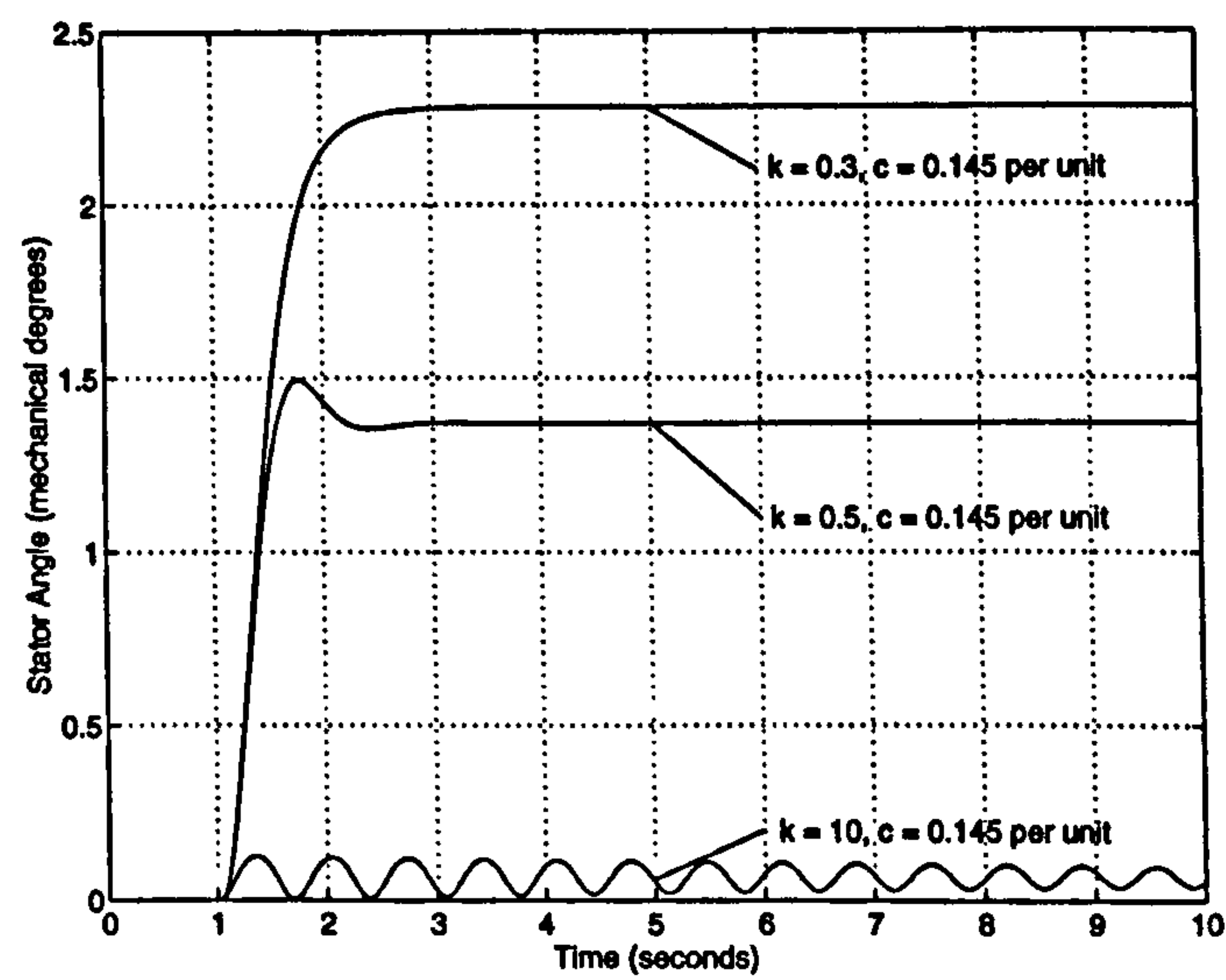


Figure 3.20: The Time Response for the Stator angle for a 1 p.u. step change in input torque

3.5 Preliminary results for the 455 kW rated generator

critically damped. As damping is further increased the position of the eigenvalue remains on the real axis but moves further and further away from the imaginary axis. Clearly there is a wide range of possible responses of the stator depending on the position of the eigenvalue.

3.5.3 Rotor results

A similar argument holds for the transient behaviour of the rotor. However when designing the compliant mounting, it is more useful to determine the effect of varying the parameters of the compliant mounting on the performance of the generator power angle as opposed to that of the rotor because the power angle defines the power out of the generator. The relation between the rotor angle and the generator power angle is defined in equation 3.18 and clearly involves the stator angle. The variation of the low positive frequency eigenvalue and the corresponding time response for the generator power angle for different values of per unit spring stiffness, k , as per unit damping coefficient, c , varies can be seen in Figure 3.21 and Figure 3.22 respectively. The two dashed lines on Figure 3.21 show the required position of the eigenvalue with a damping ratio, ζ , of 0.5 and 0.7 respectively.

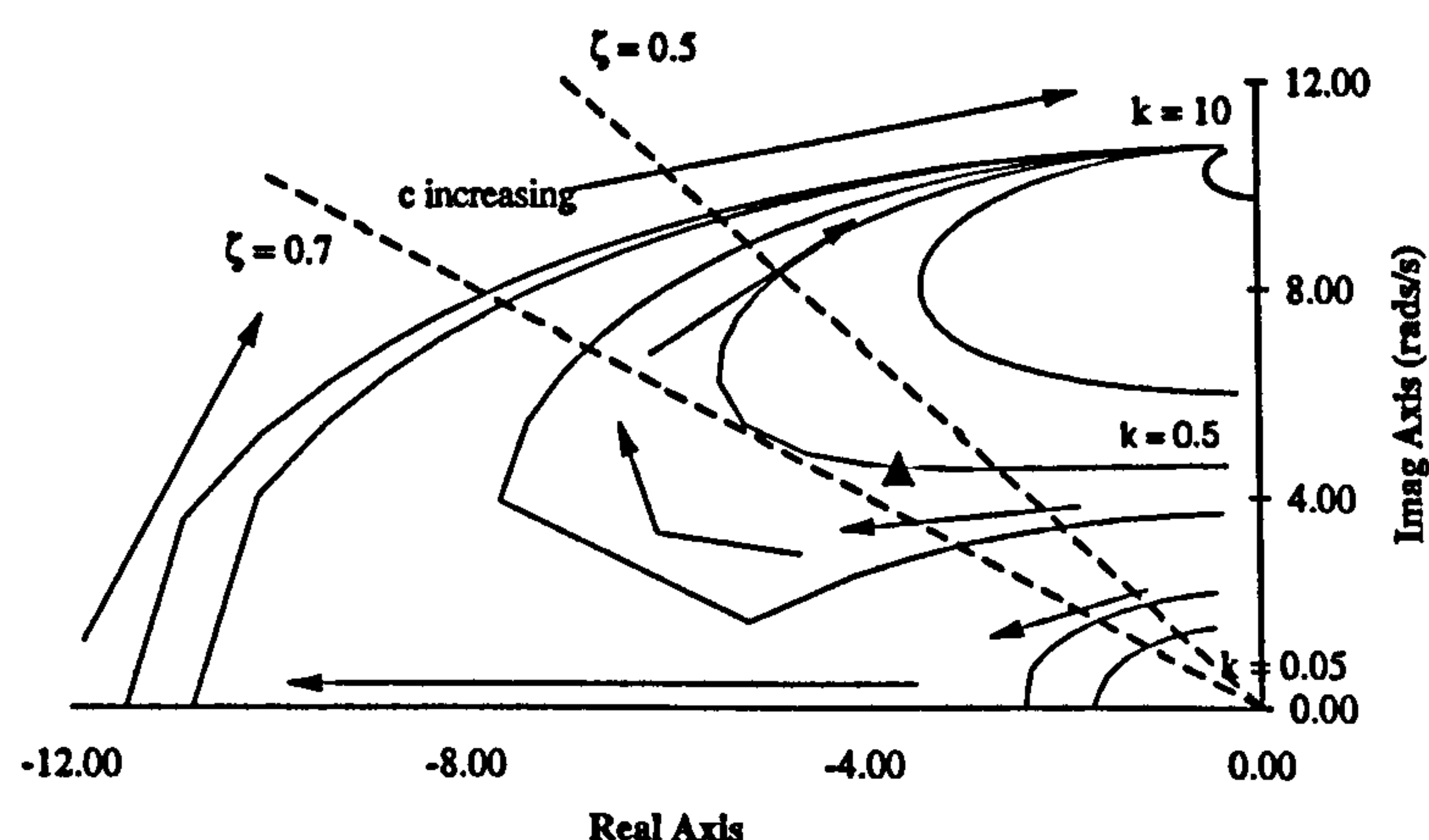


Figure 3.21: The Variation of the Low Frequency Eigenvalue as stiffness and damping are varied

The case with $k = 10$, $c = 0.145$ corresponds to a stiff stator which allows little stator movement and hence little damping of the power angle oscillations. In this case the rotor angle and power angle are virtually the same as the stator angle is very small. Reducing the

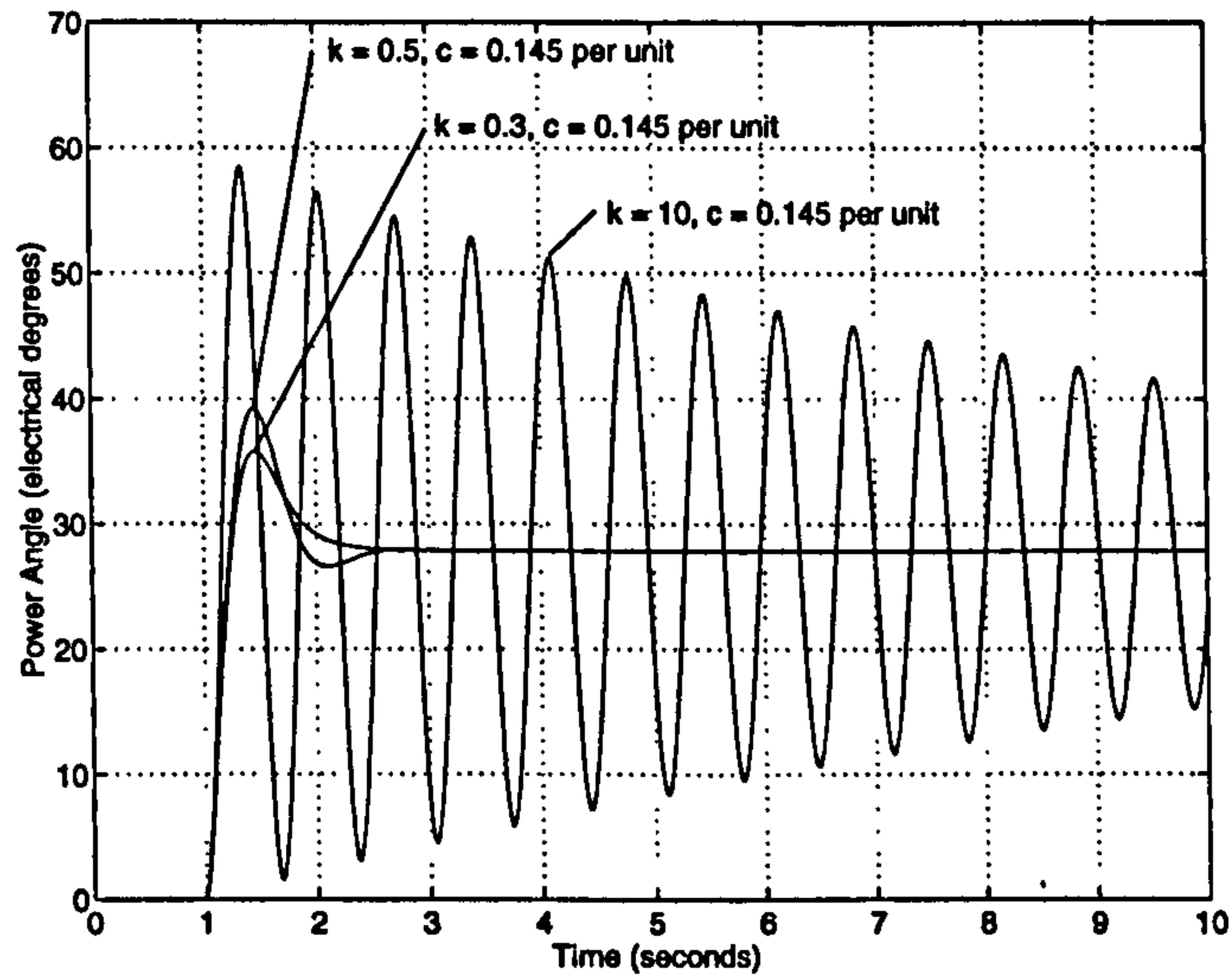


Figure 3.22: The time response for the generator power angle, δ , for a 1 p.u. step change in input torque

spring stiffness allows relative stator movement and damping of the power angle oscillations with values of $k = 0.5$ and $c = 0.145$ giving good transient performance. This response has a damping ratio, ζ , of 0.6 and the position of the corresponding positive eigenvalue of the power angle is shown by Δ on Figure 3.21. This value of damping ratio is better than that of a conventional generator, which typically have a damping ratio of 0.16 at no load approaching 0.2 at full load. The corresponding position of the positive eigenvalue for the stator angle is also denoted on Figure 3.19 by Δ . Thus the desired performance of the power angle requires an overdamped stator response with sufficient angular movement to interact with and extract energy from the power angle oscillations. This is explained in greater detail in Chapter 4.

3.5.4 Axis current results

The positive middle frequency eigenvalue, corresponding to the stator transformer voltages, remains at a position consistent with a 50 Hz variation whatever happens to the parameters of the compliant mounting. This variation is shown in Figure 3.23.

3.6 ——— Permanent Magnet Model Validation and practical implementation

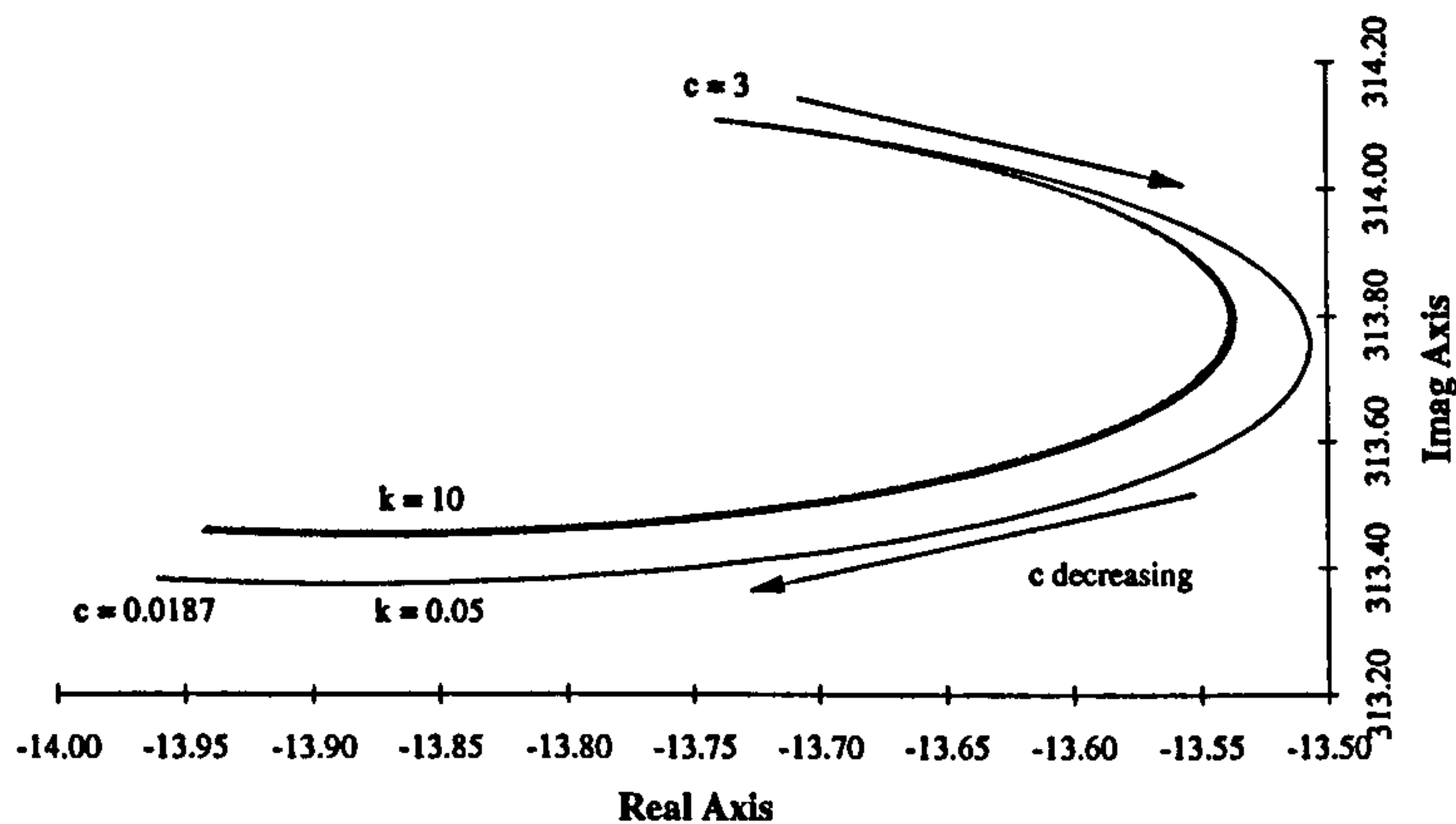


Figure 3.23: The variation of the middle frequency eigenvalue as stiffness and damping are varied

3.6 Permanent Magnet Model Validation and practical implementation

In order to validate the multi-pole, permanent magnet, synchronous generator several experiments were carried out on a test rig at UMIST. In this section the mechanical and electrical configuration of the test rig and the apparatus for measuring and recording data is described. The measurement and validation of the test rig parameters is outlined and a discussion of the practical implementation presented. The modelling methodology for such a test rig is then presented.

Validation results are presented firstly for a generator rated at 750 and 400 VA, depending on the airgap, and secondly for a generator rated at 2.75 kVA. Eigenvalue analysis and full non-linear simulation are used to validate the simulation model using both real and per unit values for the 750 VA rated rig. The parameters for these generators are presented and the results from several runs of synchronising the 400 VA and 2.75 kVA machines to the grid are presented for further validation of the full sixth order Simulink model.

Finally a comparison of the predicted and measured values for a generator with modular construction of the stator and rotor is presented to show that the values returned from WINDGEN2 are correct and consistent.

3.6 ——— Permanent Magnet Model Validation and practical implementation

3.6.1 The Test Rig

The test rig description will be split into three parts: firstly the overall physical layout of the rig is discussed, secondly the measuring devices used on the rig are described and finally the electrical circuit will be outlined.

OVERALL LAYOUT. The overall layout of the rig can be seen in Figure 3.24. The D.C. motor supplies the power requirements of the generator. The total power supplied to the D.C. motor is given by multiplying the dc supply voltage and armature current readings together. The product of the shaft torque and speed is also a measure of the power driving the rotor but now losses within the DC motor have been accounted for. The torque transducer sits around the shaft and the output from it is linked to the torque/speed display device. The generator is mounted on a set of bearings. In between the bearing mounting and the torque transducer is the clutch device which is controlled remotely. The generator has a 13 pole pair rotor and a fifteen E-core winding stator. The air-gap can be adjusted by the introduction of shims under the E-core mounting. The spring and damper system consists of a stiff arm connected to the stator with various holes to allow the spring to be attached at different radii allowing the effective rotational spring stiffness to be varied. The damper originally included for the device was too strong and so has not been used. However a hysteresis rubber mounting and an alternative viscous damper have been used to provide a reasonable level of damping.

OUTPUT DEVICES. There are four main output devices:

1. The FFT analyser: this device is used to generate Bode plots of the system and to record system voltage output and the harmonic content. The Bode plots are found from putting a random signal through the field circuit of the D.C. motor to generate fluctuations in torque. The speed output is measured and a Bode plot of input torque to output speed can be derived. The system voltage is measured across the terminals and a harmonic analysis is carried out.
2. The CRT: this device is used to measure the transient response of the inputs to its two channels. The current from the Hall effect probe circuit was measured using this device for several time responses of the current on synchronisation. The output from the position detector was also linked to the CRT to record stator transients after

3.6 ——— Permanent Magnet Model Validation and practical implementation

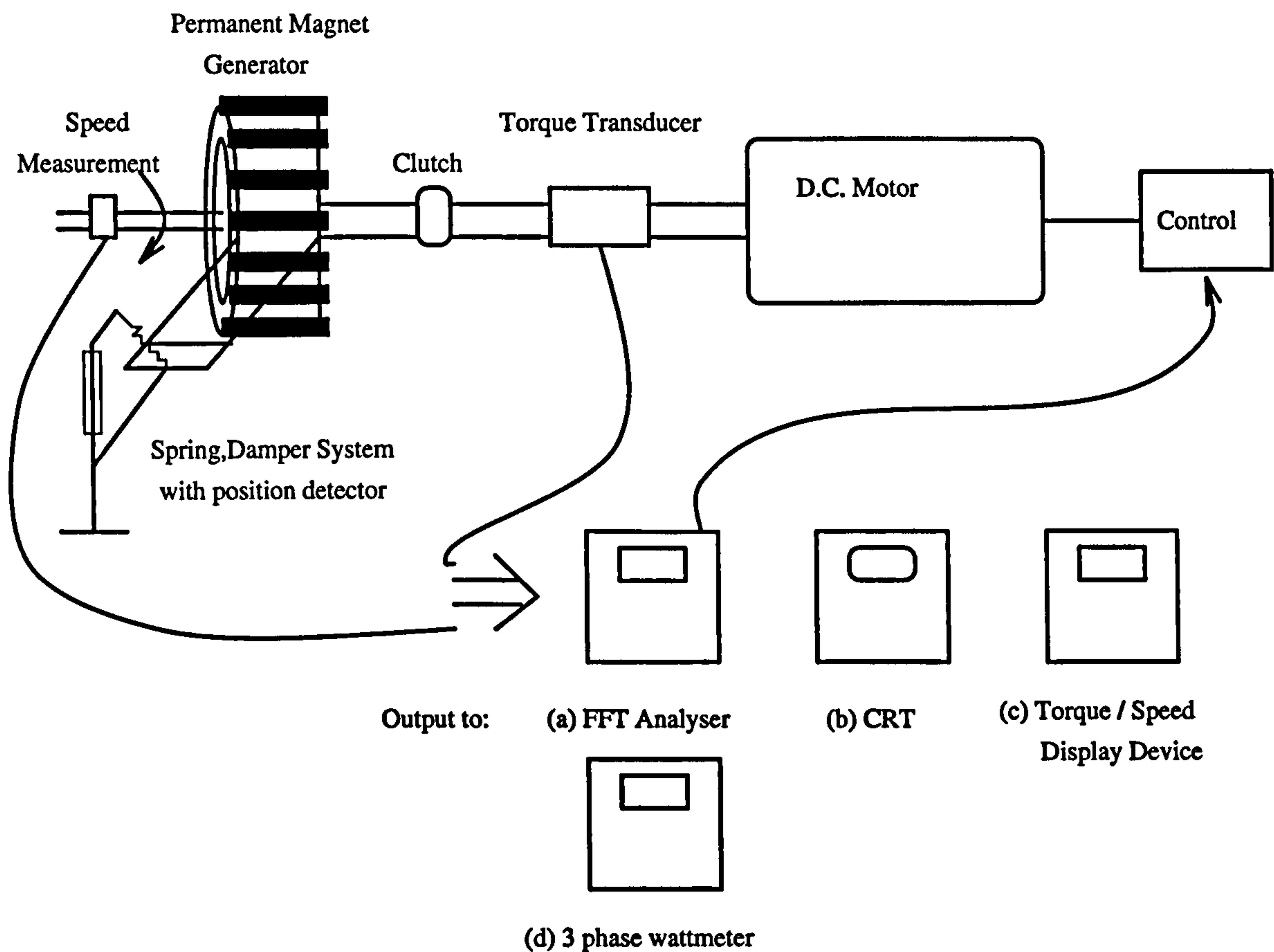


Figure 3.24: Overall Layout of the Test Rig

synchronisation. These results can be seen in section 3.6.4.

- 3. The Torque / Speed Display Device: This display device takes in the output from the torque transducer and speed measurement device and displays it in digital format. The output can be transferred to the CRT for visual display of transients.
- 4. The 3 phase watt meter: This device displays the real and apparent power and r.m.s. voltage and current from the generator in a digital format.

ELECTRICAL CIRCUIT. The electrical circuit of the rig can be seen in Figure 3.25. The generated line voltages and voltage from the variac are connected to either side of the contactor. When the condition for synchronisation are met the contactor is closed. The variac voltage is set to equal the synchronous voltage developed by the machine.

3.6 Permanent Magnet Model Validation and practical implementation

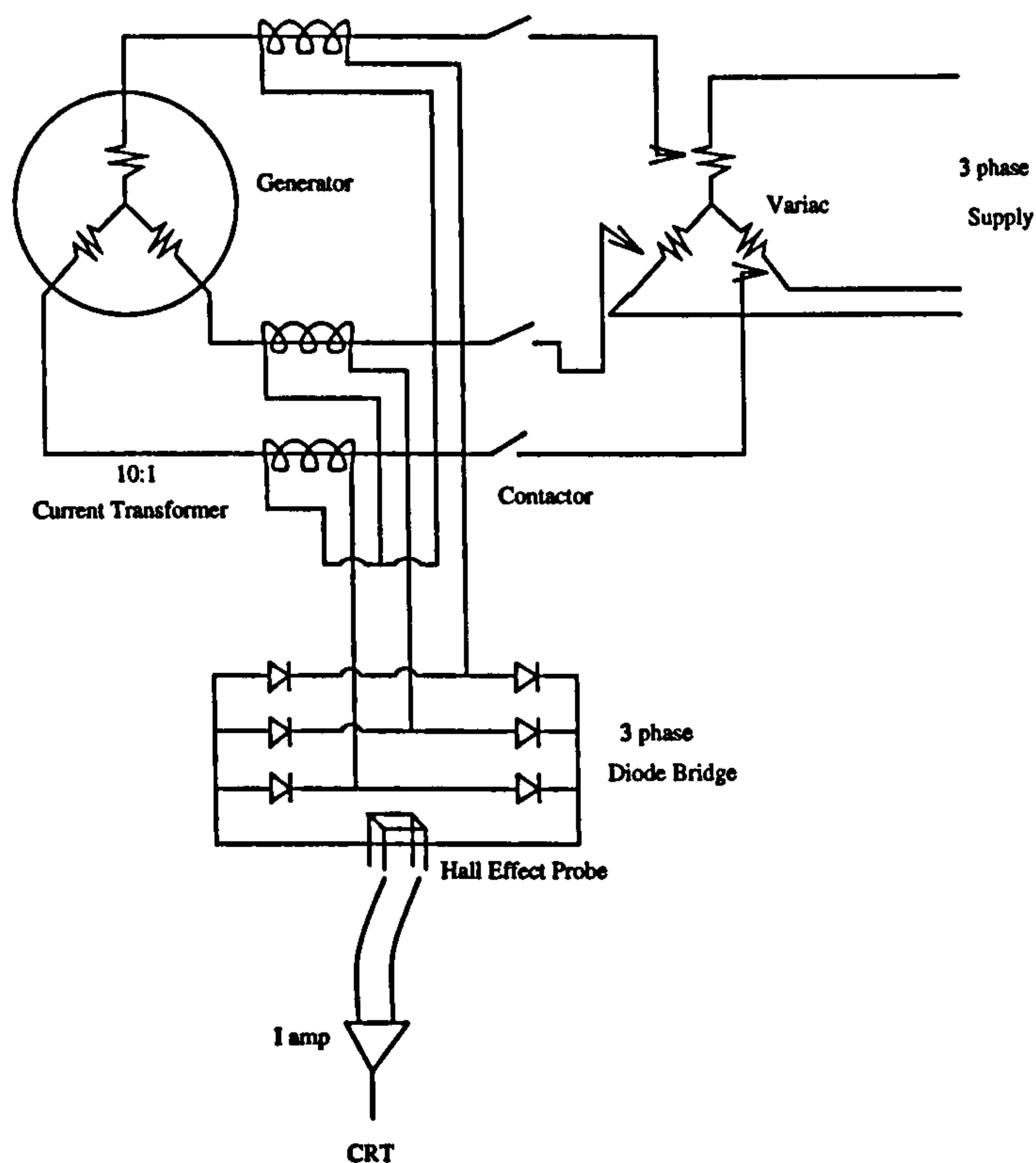


Figure 3.25: Electrical Circuit of the system side of the Test Rig

3.6.2 Parameter measurement for the 750 VA, 400 VA and 2.75 kVA generators and DC motor

The measured parameters for the three generators are given in Table 3.3 and the corresponding per unit values are given in Table 3.4. The real power rating of each generator is assumed to be two thirds of the peak pull out power and is therefore given by,

$$P_{base} = \frac{2E_f V_b}{X_d} \quad (3.35)$$

The apparent power rating of the generator can be calculated by working out the real and reactive power at rated operation and then inserting this value in,

$$S_{base} = \sqrt{P_{base}^2 + Q_{base}^2} \quad (3.36)$$

The base voltage is chosen to be the terminal voltage and all the other per unit values can be derived from these two bases. Each generator is slightly different from the others in terms of the number of turns per stator E-core, rotor magnetic configuration and airgap but

3.6 ——— Permanent Magnet Model Validation and practical implementation

all can be modelled in a very similar manner by the sixth order permanent magnet model introduced in section 3.3.4. The reason for the difference in configuration is that several designs were tested to find out which was the most effective [88].

Terminal voltage, V_t (r.m.s Volts)	82	60	121.2
Stator inertia, J_s (kg/m^2)	2.5	2.6	2.5
Rotor inertia, J_r (kg/m^2)	0.3	0.3	0.3
D.C. motor inertia, J_m (kg/m^2)	0.7	0.7	0.7
D.C. motor armature resistance, R_{dc} (Ω)	1	1	1
D.C. motor flux constant, K_{flux}	1.03	1.03	1.03
D.C. motor field current, I_f (Amps)	1.7	1.7	1.7
D-axis reactance, X_d (Ω)	21.3	15.4	10.8
Q/D-axis reactance ratio	1.07	1.07	1.07
Generator a.c. resistance, R (Ω)	2.4	2.4	5
Rated power, S (VAr)	632	398	2730
Airgap, mm	1.5	2	1

Table 3.3: Test rig parameters

Terminal Voltage, V_t	1 p.u.	1 p.u.	1 p.u.
Stator Inertia, H_s	1.16 p.u.	1.83 p.u.	0.27
Rotor Inertia (with D.C. motor), H_r	0.46 p.u.	0.73 p.u.	0.11
D-axis Reactance, X_d	0.67 p.u.	0.67 p.u.	0.67
Q/D-axis reactance ratio	1.07	1.07	1.07 p.u.
Generator a.c. resistance, R (Ω)	0.08	0.10	0.31
Rated Power, S	1.0 p.u.	1.0 p.u.	1.0 p.u.

Table 3.4: Per unit test rig parameters

The first two columns refer to the same generator with the only difference being the airgap. This generator is referred to as the 750 VA testrig due to its rated apparent power at an airgap of 1 mm. Clearly as the airgap is increased its apparent power rating will reduce but for clarity it is referred to as the same generator with the different airgaps being noted. The third column refers to a more powerful generator rated at about 3 kVA with a better rotor magnet arrangement.

3.6.3 Modelling Methodology

Simulation models for the testrig were developed in both real and per unit values to ensure that the sixth order model outlined in section 3.3 is correct. The first approach to modelling the testrig situation did not include the dc motor, except as a linked inertia, and the results obtained from the simulation were considerably inaccurate. Including a model of

3.6 Permanent Magnet Model Validation and practical implementation

the separately excited dc motor into the simulation led to much better correlation and this resulted in the SIMULINK models of Figure 3.26 and Figure 3.27 respectively. The dc machine introduced a much slower time constant to the rate of change of angular speed than was obtained purely by modelling it as an inertial effect.

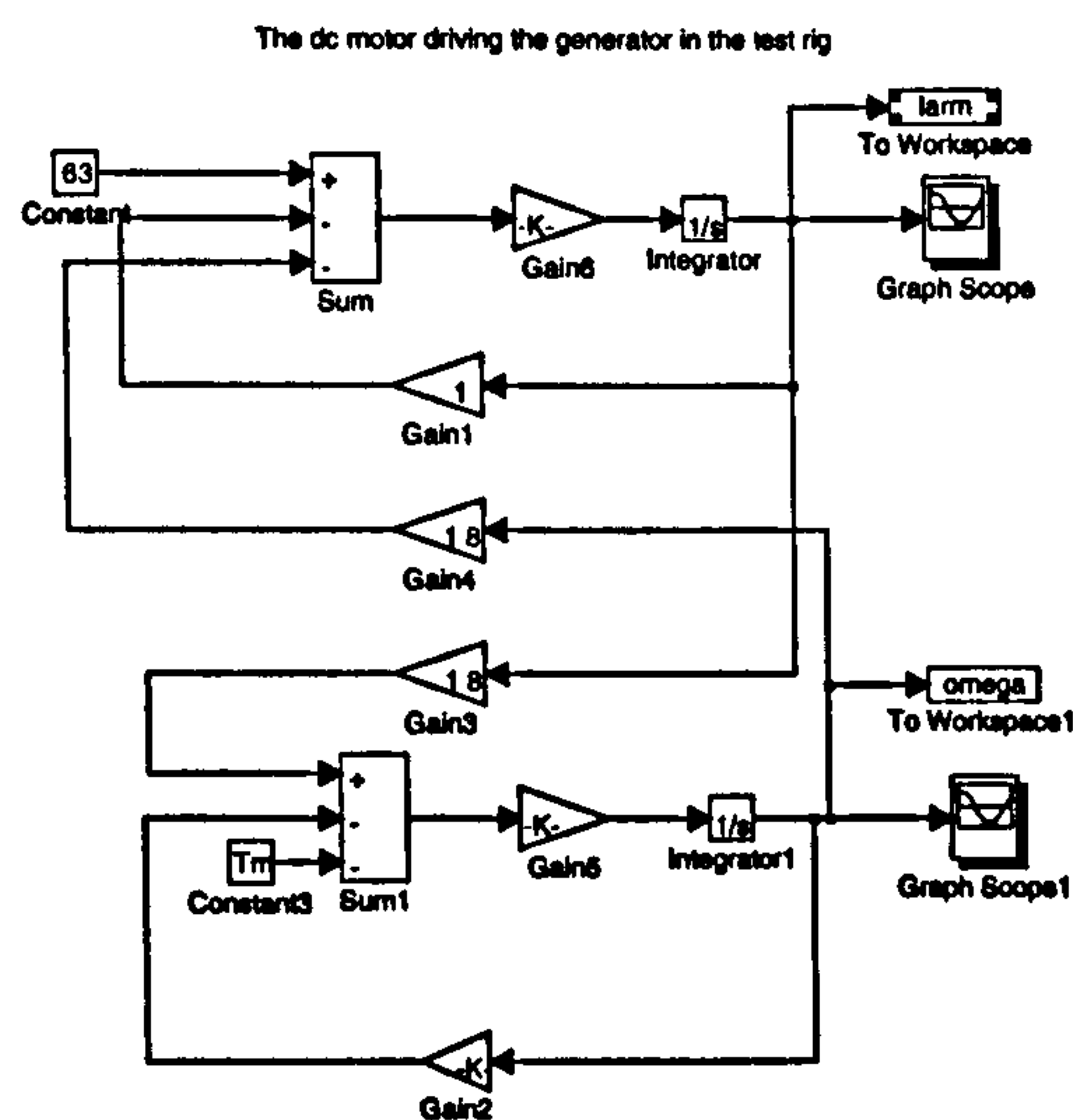


Figure 3.26: The DC motor model

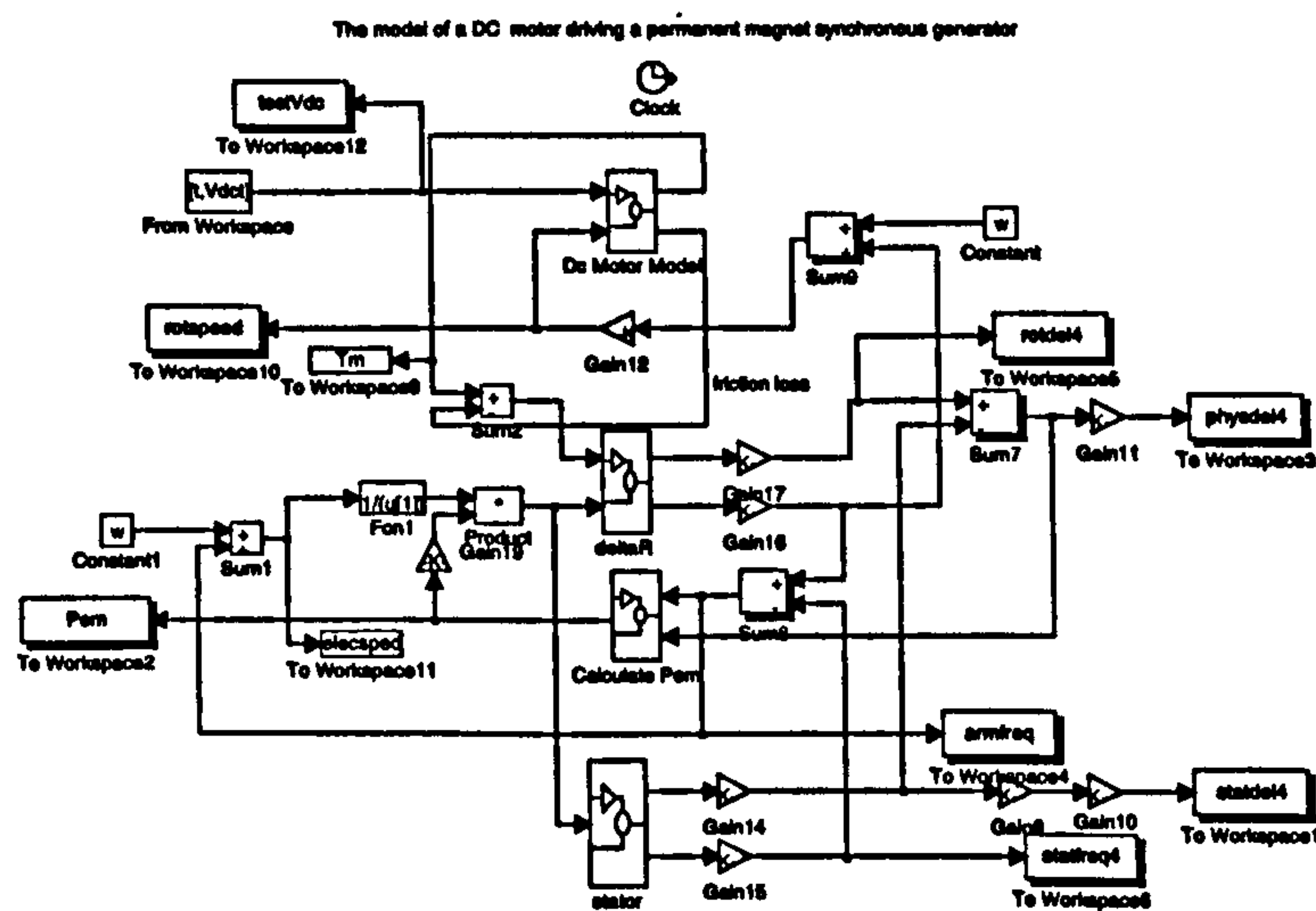


Figure 3.27: The full Simulink model of the testrig

The DC motor provides the input torque to the block representing rotor movement. The three blocks, 'deltaR', 'Calculate Pem' and 'stator', contain the functionality for the sixth order generator model. It was necessary in this case to split the functionality into its constituent parts to evaluate the generator power angle, δ , for ease of connection to the DC motor model which requires the actual shaft speed and not the system frequency as an

3.6 — Permanent Magnet Model Validation and practical implementation

input.

3.6.4 Step Response of the 750 VA testrig

A comparison has been carried out between the step responses of the 750 VA testrig reported in [92] and the response from simulation. Firstly the values for the testrig were found from [88] and, then, an eigenvalue analysis carried out to predict what value of spring stiffness, k , and damping coefficient, c would give the equivalent second order response shown in Figure 3.28 which has a peak overshoot of 50 % and therefore a required damping ratio, ζ , of about 0.8 (from standard second order dynamic theory).

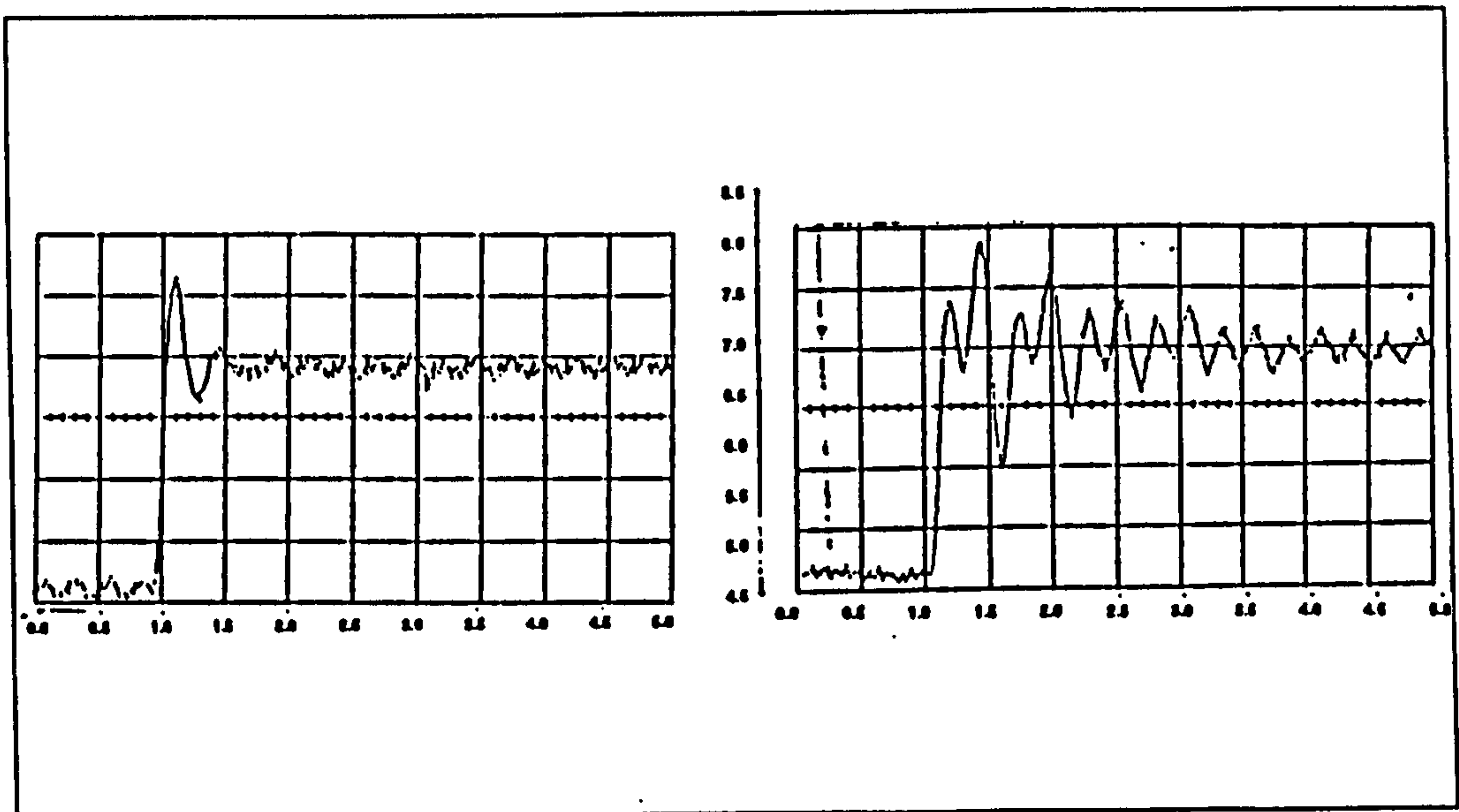


Figure 3.28: Experimental step response of a 750 VA testrig with and without damping

The eigenvalue analysis can be seen in Figure 3.29 for the testrig. The position corresponding to a damping ratio of 0.8 at the correct value of spring stiffness, $k = 450 \text{ N rad}^{-1}$, is marked by Δ . This gives a damping coefficient of $c = 60 \text{ N rad}^{-1} \text{ s}^{-1}$. These values are converted into per unit values and then used in the full simulation to show that the experimental results and the simulation are equivalent. The simulated results for the damped and undamped step response can be seen in Figure 3.30. A value of $c = 2 \text{ N rad}^{-1} \text{ s}^{-1}$ was used for the undamped performance with the same spring stiffness. This value of c represents the small amount of energy dissipation, i.e. damping, in the bearings of the stator mounting. Both the damped and undamped response predicted by the simulation and measured from the test rig are in good agreement in terms of current magnitude and

3.6 ——— Permanent Magnet Model Validation and practical implementation

overall shape. These results show that the full sixth order model is a valid representation of the permanent magnet synchronous generator and that the assumptions made in deriving the model are fair assumptions to make.

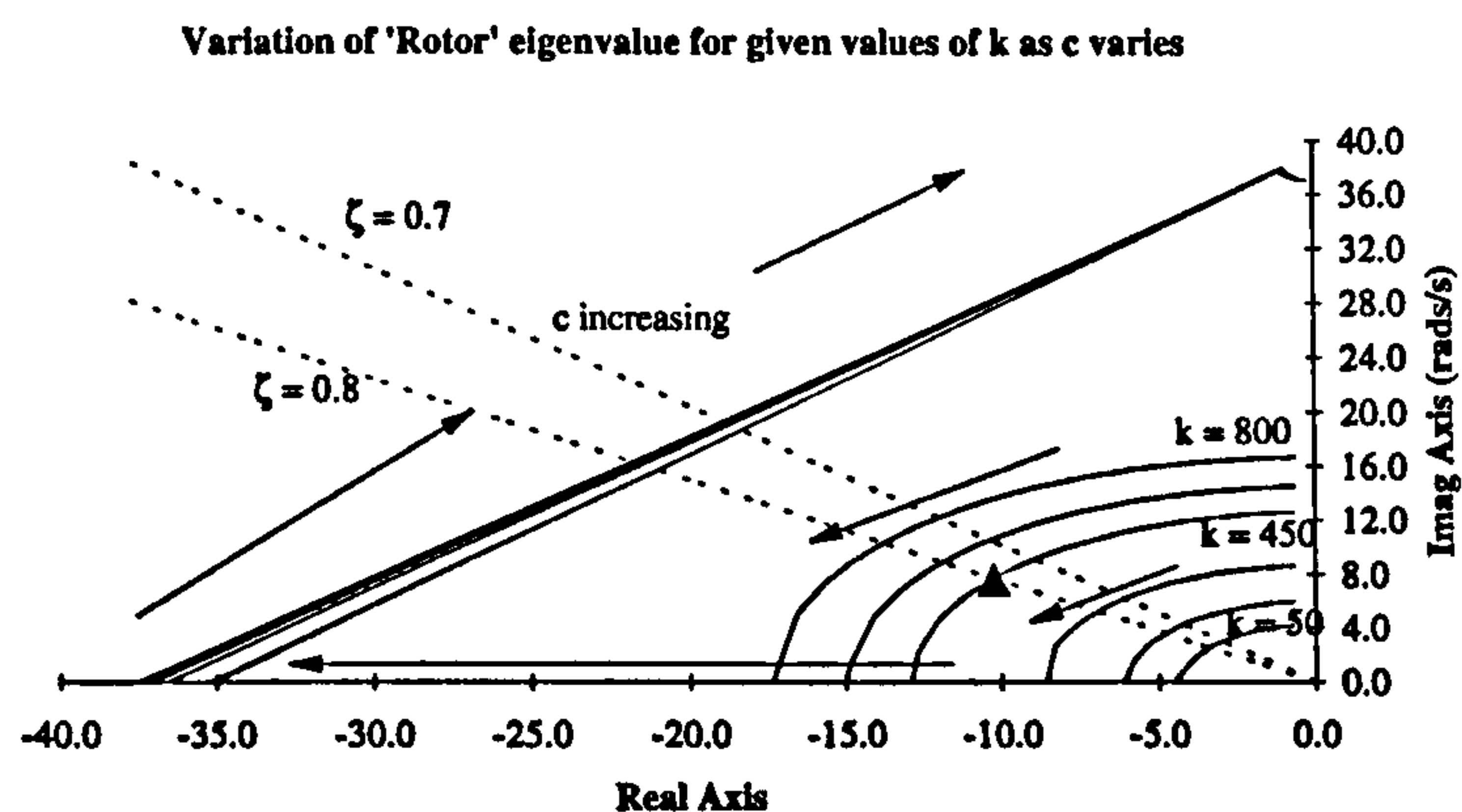


Figure 3.29: Eigenvalue analysis of the testrig

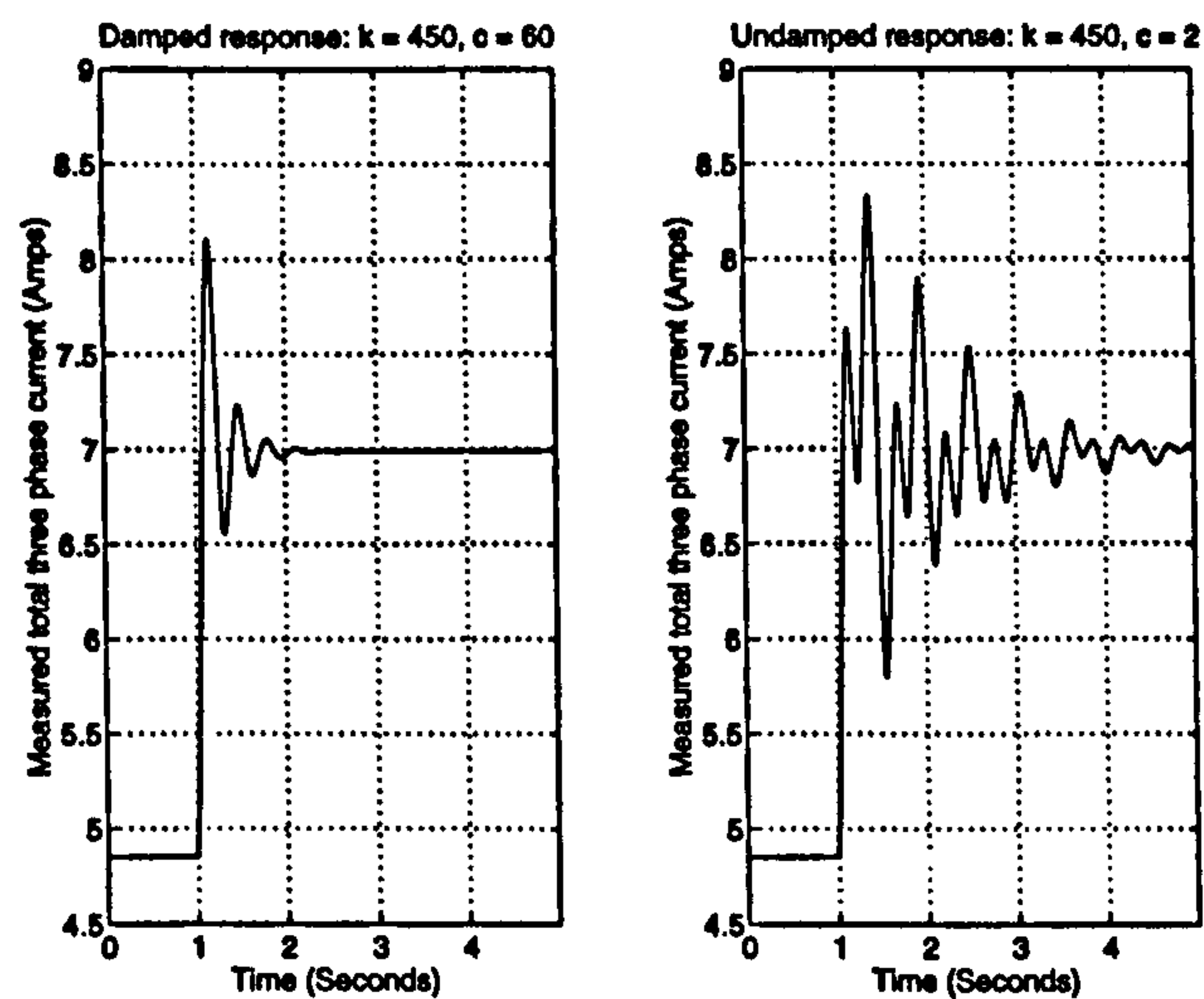


Figure 3.30: Damped and undamped step response of the 750 VA rated generator

3.6.5 Synchronisation transients of the 750 VA testrig with a 2mm airgap

It was also considered appropriate for various measurements of the currents, torques and stator movement for the spring mounted stator configuration to attempt some further validation of the full sixth order Simulink model against the testrig for synchronisation where the initial $\dot{\psi}_{d,q}$ terms are important.

3.6 ——— Permanent Magnet Model Validation and practical implementation

At the instant of synchronising to the grid there was no measured driving torque applied to the generator from the dc motor. The angular speed of the rotor was controlled using the D.C. motor controls and was marginally different to synchronous speed. This allowed the phasor of the generator open circuit terminal voltage and the infinite bus voltage, in this case from a directly connected variac as no transformer existed, to pass one another. The contactor was closed when a certain measured phase mismatch occurred and the machine synchronised. The initial value for the phase mismatch between the infinite bus and the generator terminal voltage was found by using the CRT to display the system voltage and the generated terminal voltage and setting the phase counter to the required angle.

The angle measured is equivalent to the power angle of the generator as no current is flowing into the infinite bus. This can be simulated by setting the power angle to the measured value, the d - and q -axis currents to zero and letting the simulation settle down to the balanced steady state conditions with no power flow from dc motor to the infinite bus. The machine for which these results apply was the 750 VA testrig with a 2mm airgap. The values of the machine parameters are presented in column 2 of Tables 3.3 and 3.4.

LOCKED STATOR RESULTS. The stator was effectively locked in position. Therefore only torque and current measurements were taken. The torque measurement is quite difficult to simulate due to its position in the test rig so only the current transient will be compared for this case. Figure 3.31 shows the simulated current transient and the measured current in the output of the 3 phase bridge by the Hall effect probe as shown in Figure 3.25 for synchronisation from 40 degrees. The current flowing in the three phase bridge can be shown to be equivalent to the envelope of the phase currents being measured, i.e. the magnitude of the combined d, q - axis currents. The d - and q - axis currents are related to the phase currents by the factor $\sqrt{\frac{3}{2}}$ and a factor to take into account the action of the rectifier. Furthermore there is assumed to be a 1.5 Amps loss in current through the current transformers, rectifier and hall probe arrangement [88].

There is some degree of correlation between the two traces both in terms of the magnitude and the occurrence of the peaks. The peaks of the current are due to the swinging of the power angle, δ , as the generator comes into synchronism to the grid. The assumed difference in initial speed mismatch, $\dot{\delta}$, corresponds to a difference in speed of about 1 Hz which was introduced in the experiment to get the system and generator terminal voltage phasors to pass each other at a slow rate.

3.6 _____ Permanent Magnet Model Validation and practical implementation

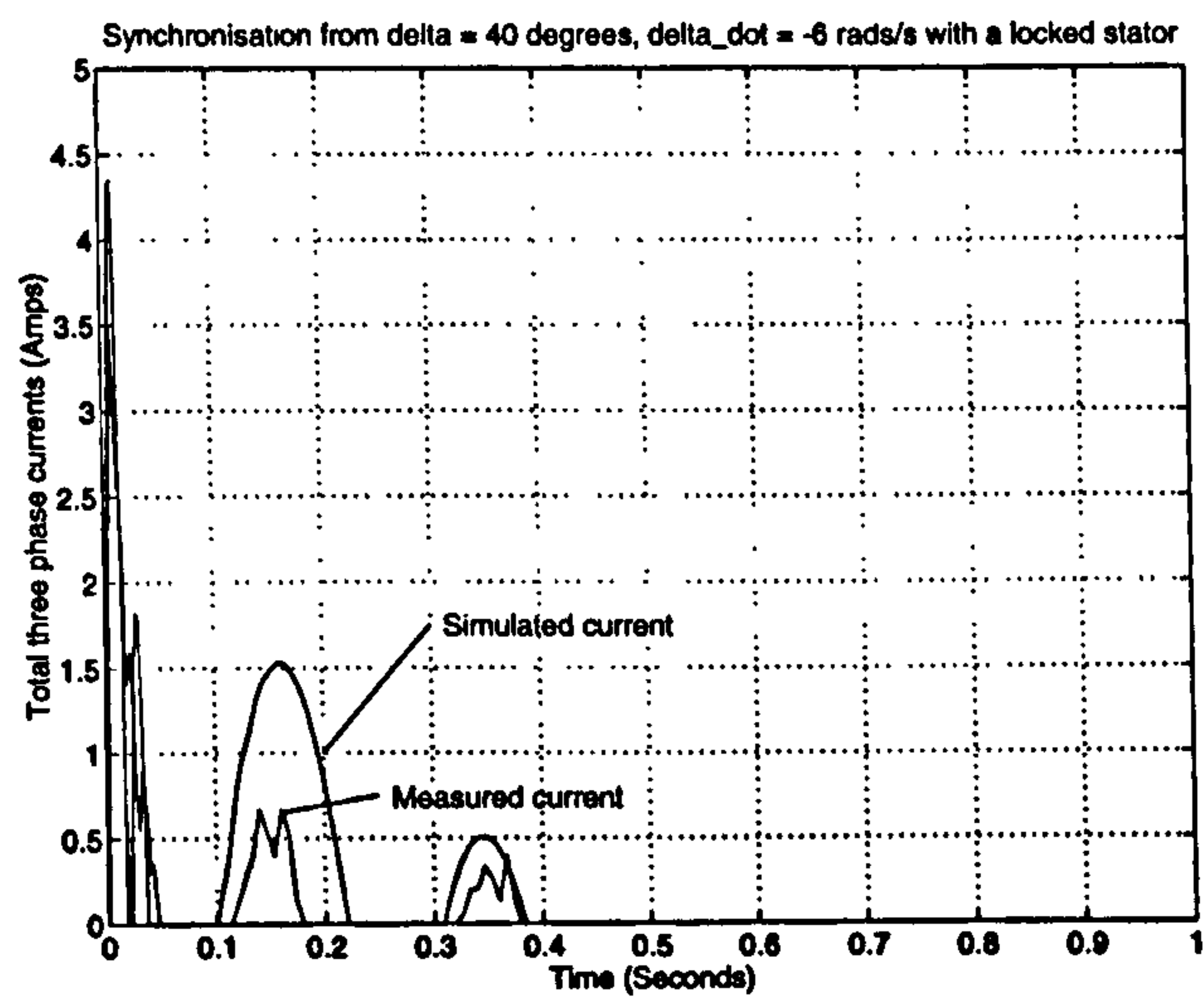


Figure 3.31: Current Transient on synchronisation from $\delta = 40$ degrees, $\dot{\delta} = -6$

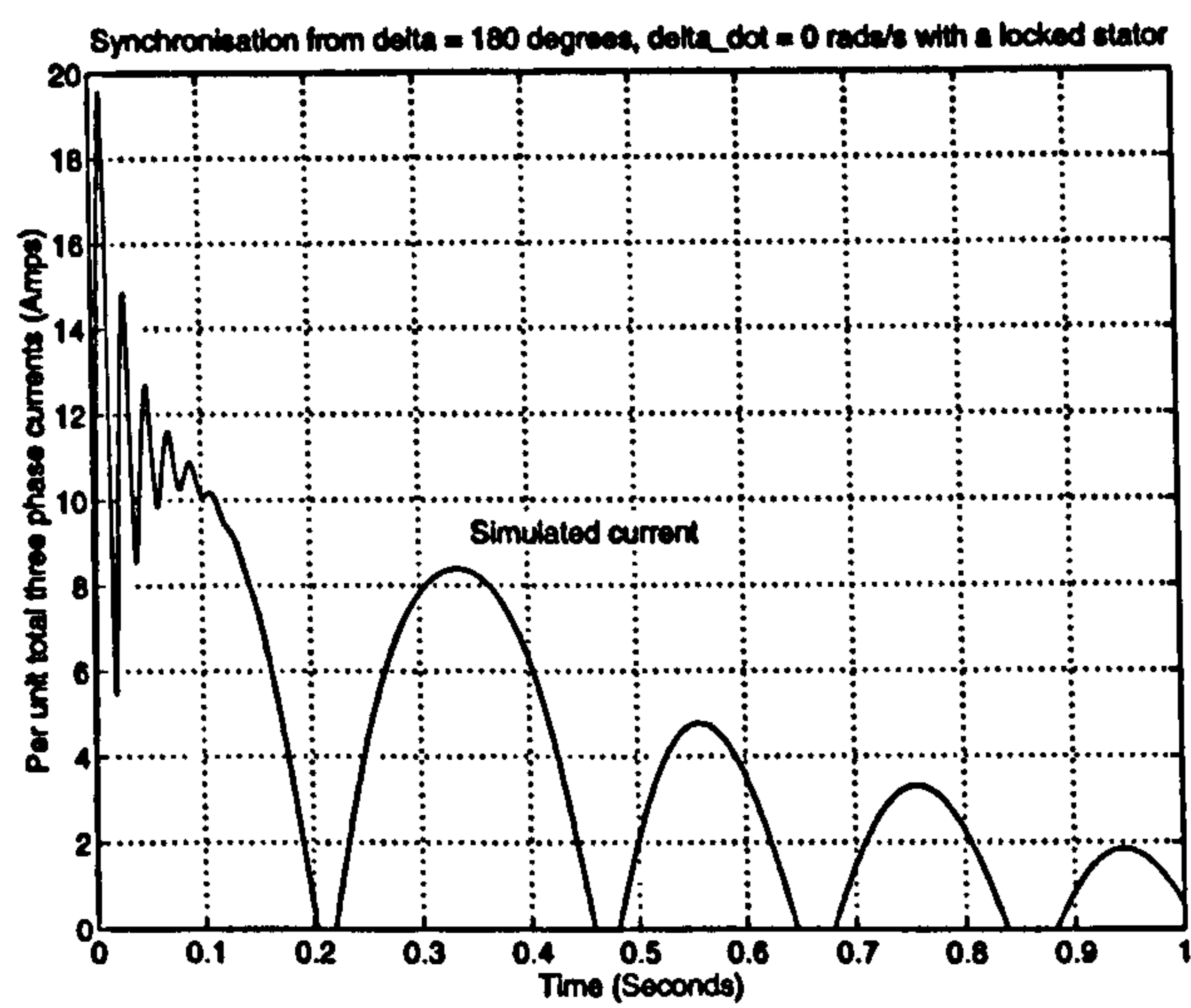


Figure 3.32: Simulated current transient for synchronisation from $\delta = 180$ degrees, DC motor included

3.6 Permanent Magnet Model Validation and practical implementation

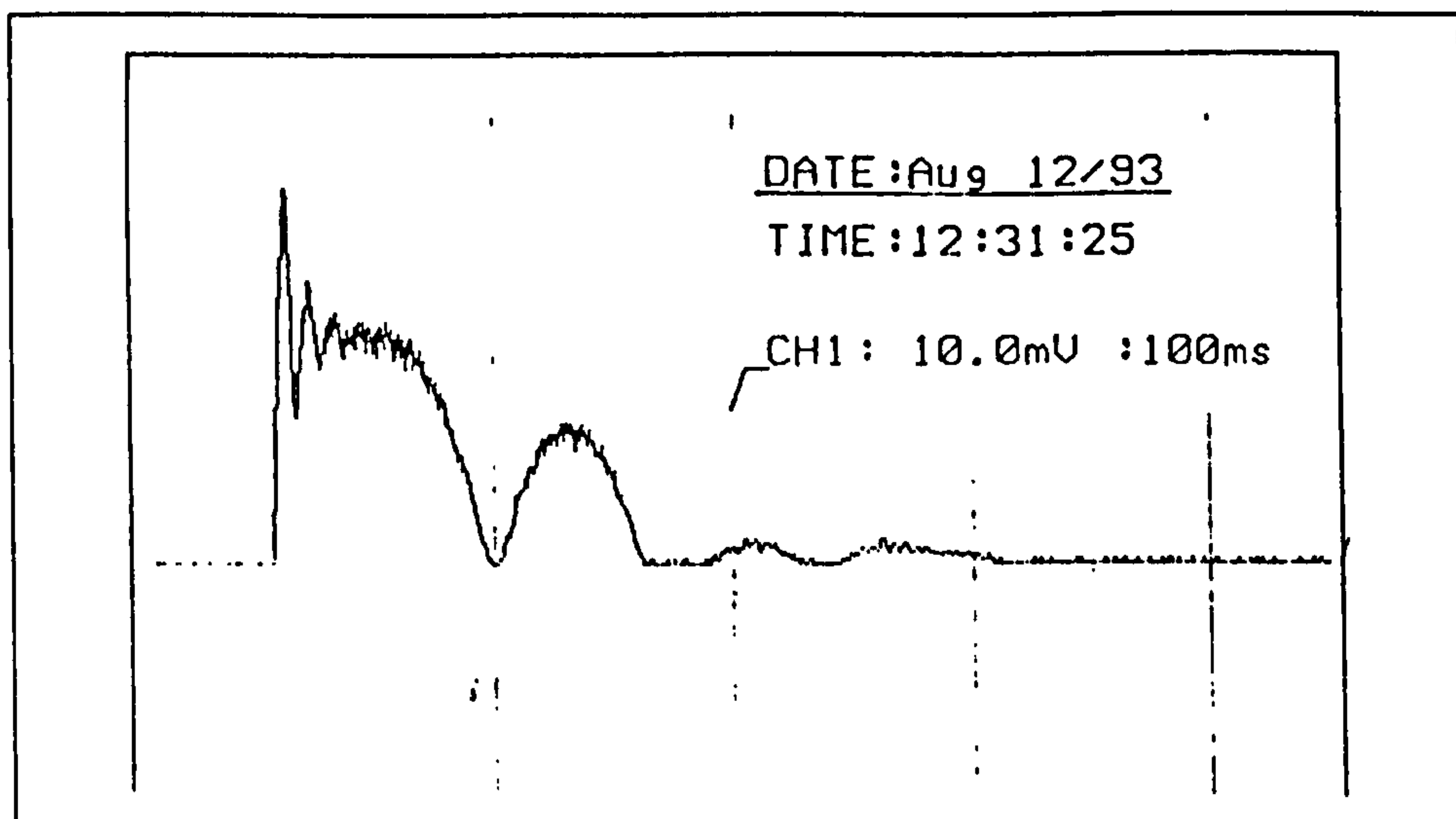


Figure 3.33: Measured current transient for synchronisation from $\delta = 180$ degrees, DC motor included

Running this simulation for the case of synchronisation from 180 degrees, the worst possible scenario, gives the current transient as seen in Figure 3.32. The measured experimental trace can be seen in Figure 3.33. The vertical scale of the measured current transient is 5 Amps per division with a time base of 100 ms per division. The first peaks correlate to within 13 % but subsequently the peaks predicted by the simulation are too large compared with the measured values from experiment. However the shape is comparable and the key things to note from this simulation are the large currents flowing in each phase of the generator. In per unit terms the current is about 8 times the per unit rated value and this could lead to damage of the E-core winding insulation. Furthermore it has been shown that such large currents would lead to demagnetisation at the tips of the embedded magnet pole pieces [88] and a corresponding loss in the performance in terms of a worse voltage profile. Therefore it is important not to synchronise the generator 180 degrees out of phase with the grid even though in terms of stability the generator can still synchronise with such a severe transient.

Overall there is an acceptable correlation between the locked stator case and the simulation for the first and second peaks. Upto this point in the simulation the generator appears only slightly damped as the envelope of the current oscillations would take a long time to die away. This decay occurs because of the fringe losses within the generator and energy loss due to friction in the bearings. There is sudden change in the measured current after the second peak which is most probably due to an effect not modelled by the dc motor driven generator model which continues to decay without a sudden cut off.

3.6 Permanent Magnet Model Validation and practical implementation

STIFF SPRING RESULTS. The stator movement and transient current traces were used for comparison for synchronisation from 40 degrees mismatch and the measured and simulated responses can be seen in Figure 3.34. Again a degree of correlation is found between the results. The reason for use of the stiffer spring compared to the step response shown in Figure 3.30 is the linear distance of the spring from the rotor shaft. The spring was mounted closer to the rotor shaft and therefore had a larger effective rotational stiffness.

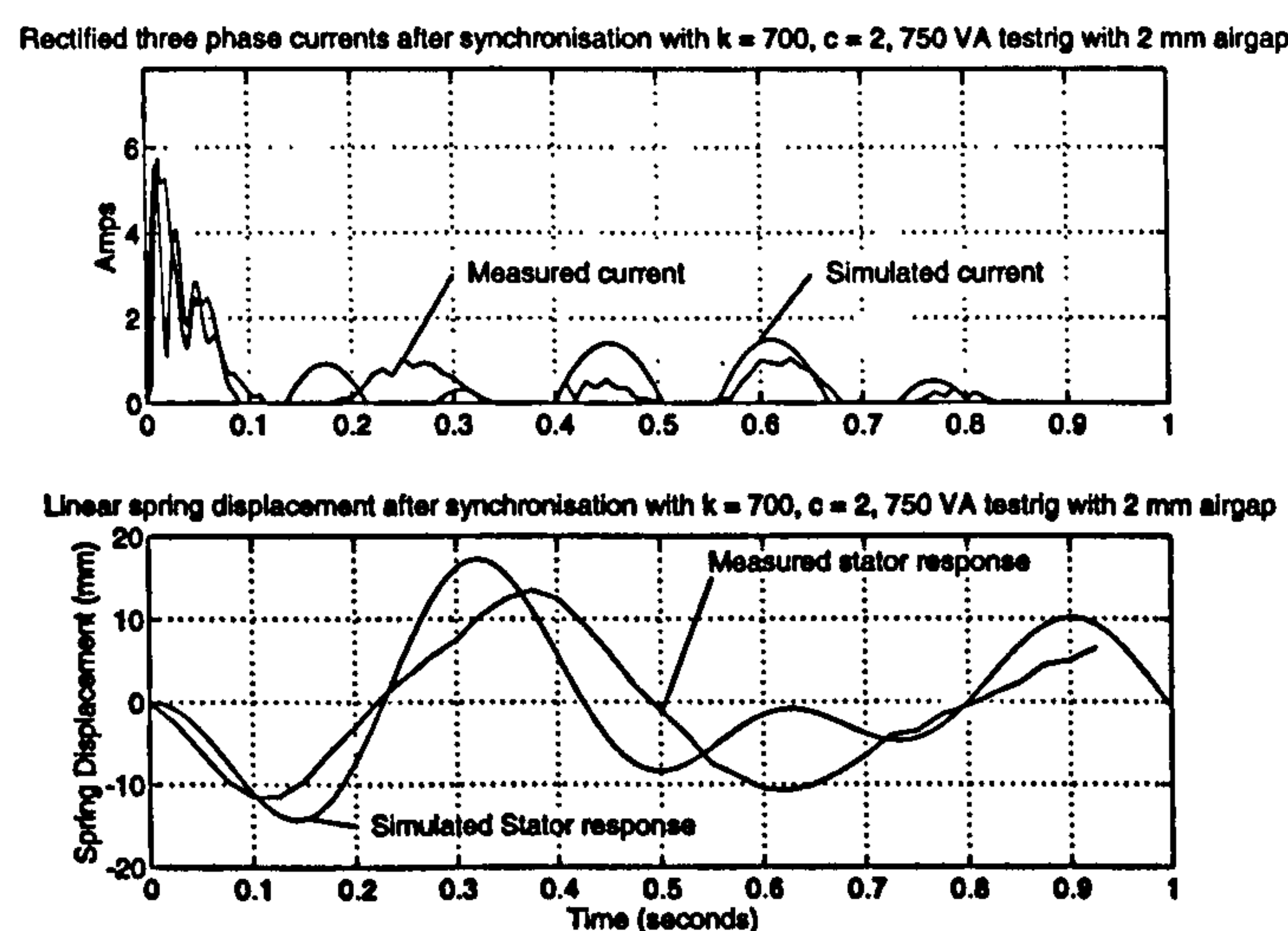


Figure 3.34: Simulated current and stator transient for synchronisation from $\delta = 40$ degrees, DC motor included

The magnitude of both the current and stator movement traces for the measured and simulated responses are in only rough agreement as there are a few discrepancies in terms of their phase and shape. The most likely reason for this discrepancy is the introduction of the position transducer which, although it should not affect the results, does in fact introduce some non-linear damping due to the misalignment of the transducer itself. This was only noted after the experiments had been carried out [88] and the correlation obtained was considered adequate.

3.6.6 Synchronisation of the 2.75 kW generator

Further validation was attempted on a new test rig at UMIST rated at 2.75 kW with the values as given in column 3 of Tables 3.3 and 3.4. The aim was to measure the phase currents on synchronisation as the current envelope results were considered not to be representative of the true current transient effects. The rotor configuration and the amount of magnetic

3.6 Permanent Magnet Model Validation and practical implementation

material in the rig had changed but it was still a 13 pole pair generator. Taking some measurements from the larger rig also provided an opportunity to verify the full sixth order simulation model at a different power level. The measured and simulated phase currents can be seen in Figure 3.35 for a 40 degree mismatch with the stator locked into position.

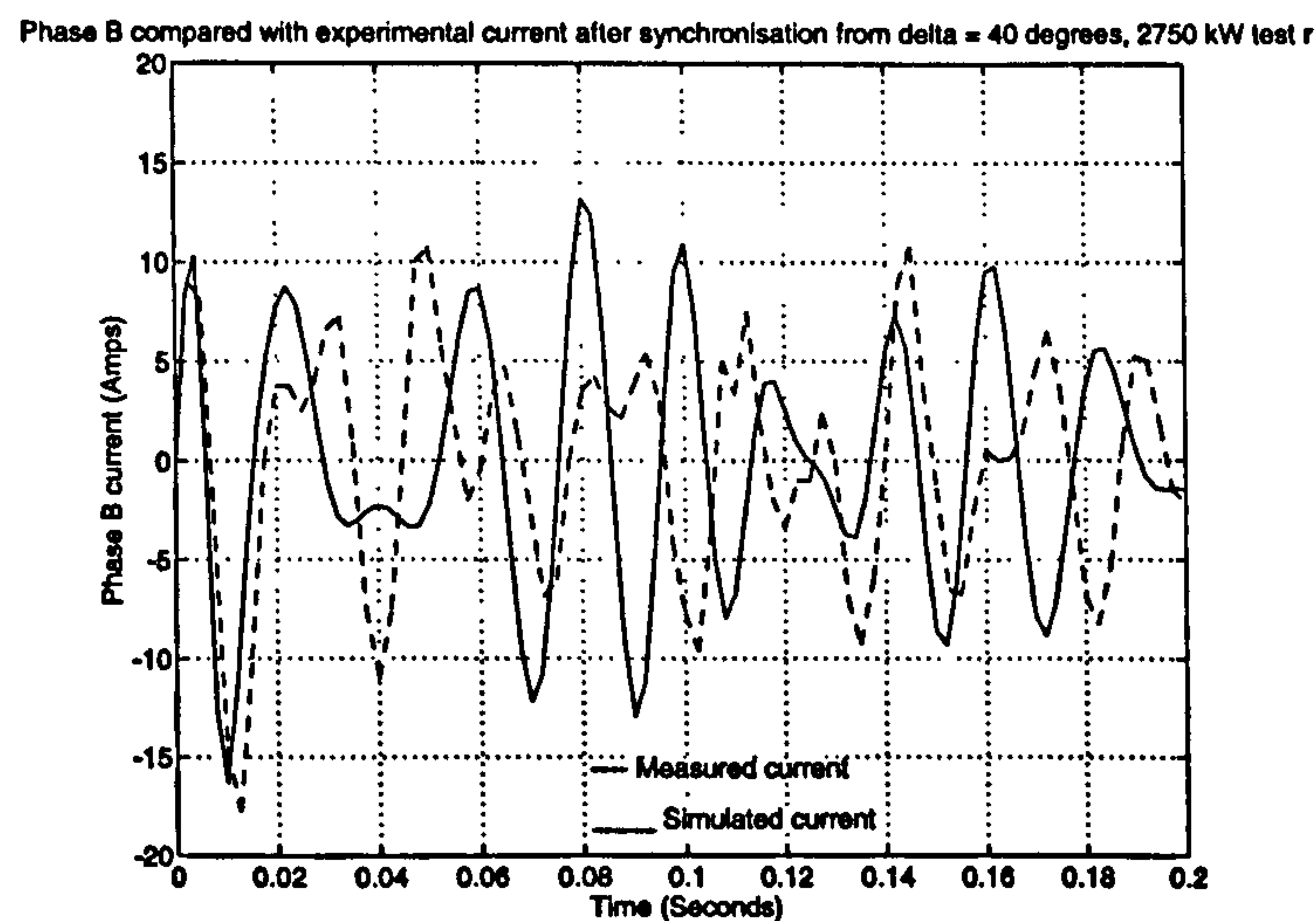


Figure 3.35: Simulated and measured current transients for synchronisation from delta = 40 degrees, DC motor included

The magnitudes of the two currents are very similar but the actual shape and the frequency spectrum present in the measured current trace is different from that of the simulated trace. This does not mean that the sixth order model is incorrect but at the timescale of 0.2 seconds there are many different effects that could be happening which such a model would not begin to pick up - such as the impact of torsional modes of vibration, changes of the conditions at the bus which is unlikely to be considered infinite and the effects of harmonics within the generator. Unless a very detailed set of experiments were carried out this kind of validation would be difficult and the initial premise that measuring phase currents would be better as a validation method proved false. However the fact that the magnitudes are similar is considered to be sufficient for the simulation modelling over the timescales upto 100 seconds.

3.6.7 Parameter validation for a modular constructed generator

Parameter validation is also necessary for the generator with both a modular rotor and stator. This was carried out by Spooner on a 26 pole testrig at UMIST. The measured and

predicted values from WVMAG, the magnetic circuit analysis part of WINDGEN2 which was introduced earlier in the chapter, can be seen in Table 3.5 for the terminal voltage and inductance with the respective error.

	Measured	Simulated	Percentage Error
R.M.S terminal Voltage @ 50 Hz, V_t	24 Volts	24.9 Volts	3.75 %
Inductance	8.9 - 9.6 mH	8.3 mH	7.2 - 15.7 %

Table 3.5: Parameter validation

3.6.8 Final comments on validation results

The simulation model of the testrig has been validated provided the effect of the DC motor is included. Discrepancies do arise and these are probably due to causes made more significant by the small size of the test rig, end effects and space harmonics [88] and the timescales involved. Therefore the validation presented in this section is considered adequate to instill confidence in the results from the sixth order model of a permanent magnet, synchronous generator.

3.7 Conclusions

This chapter has discussed the concept of a multi-pole, permanent magnet, synchronous generator which would be suitable for direct connection to the low speed rotor of a wind turbine and thus eliminate the need for the usual speed increasing gearbox. The derivation of the parameters for both the wind turbine and the generator was outlined and the mathematical modelling and validation of a sixth order simulation model of such a permanent magnet generator presented. The sixth order model has been validated against several ratings of test rig with reasonable correlation. The full model of a three blade wind turbine driving a multi-pole, permanent magnet, generator has now been developed and the operation of such a generator both in terms of the internal dynamic interactions between the rotor and stator and also in the windy environment will be presented in the next chapter.

Chapter 4

Performance of the Fixed Speed Permanent Magnet Generator

The purpose of this chapter is to discuss the performance of the multi-pole, permanent magnet, synchronous generator with a compliant stator mounting for a range of wind turbine ratings from 200 kW to 1.5 MW. The basic parameters of the generators are outlined and the permanent magnet synchronous generator model, developed in the last chapter, is used to investigate the general behaviour of the compliant mounting for a 455 kW rated generator. An eigenvalue technique is used to quantify the generator damping in conjunction with full non-linear simulation to investigate the actual response of the generator. The main aim of the first part of the chapter is to show that the response of the generator is dependent on tuning the characteristics of the compliant mounting to the conditions under which it is operating.

The second part of the chapter considers operational aspects of the generator. Firstly boundaries for successful synchronisation have been developed which show that the turbine is robust to a wide range of conditions of mismatch between the generator and the grid. The response of the wind turbine to simulated wind data, above and below rated windspeed, is presented to show that the compliant mounting operates as expected and to demonstrate the effectiveness of a well designed pitch controller as outlined in Chapter 2. The argument presented in the first part of this chapter to select suitable values for the compliant mounting considers only step responses to the system and the results are analysed to see whether the

good performance to a step input is repeated in response to the stochastic wind input.

4.1 Basic performance of a 455 kW generator

This section outlines some key results for the 455 kW multi-pole, permanent magnet synchronous generator, the main parameters of which are given in Table 3.2. The inertia of the rotor is much larger than that of the stator as it includes both the inertia of the generator rotor and the inertia of the turbine blades. The impedance of the grid and the unit transformer are included in the value of X_d and X_q . The r.m.s. base values in the per unit normalisation are also included in Table 3.2.

4.1.1 Method of attack

The operation of the generator can be understood by using linearisation to identify the generator's modes of oscillation and full non-linear simulation to confirm the predicted performance. Both these methods have already been introduced in Chapter 3 and it is now necessary to extend the preliminary results presented therein.

4.1.2 The General Behaviour of the Compliant Mounting

Six eigenvalues exist for the matrix $[A]$ from section C.2, which represents the interaction between the state variables, and these split into two conjugate pairs representing the rotor and stator movement and two eigenvalues representing the d - and q -axis currents. The two conjugate pairs are referred to as the high frequency and the low frequency eigenvalues due to their relative positions in the complex plane. Each pair of eigenvalues relates to the physical system and the behaviour of the generator to small disturbances can be represented by the equivalent mass, spring and damper system shown in Figure 4.1.

In the figure H_r and H_s represent the rotor and stator inertias respectively whilst c and k are the damping coefficient and equivalent spring stiffness of the compliant stator mounting. The synchronising power coefficient, k_{syn} , is given by,

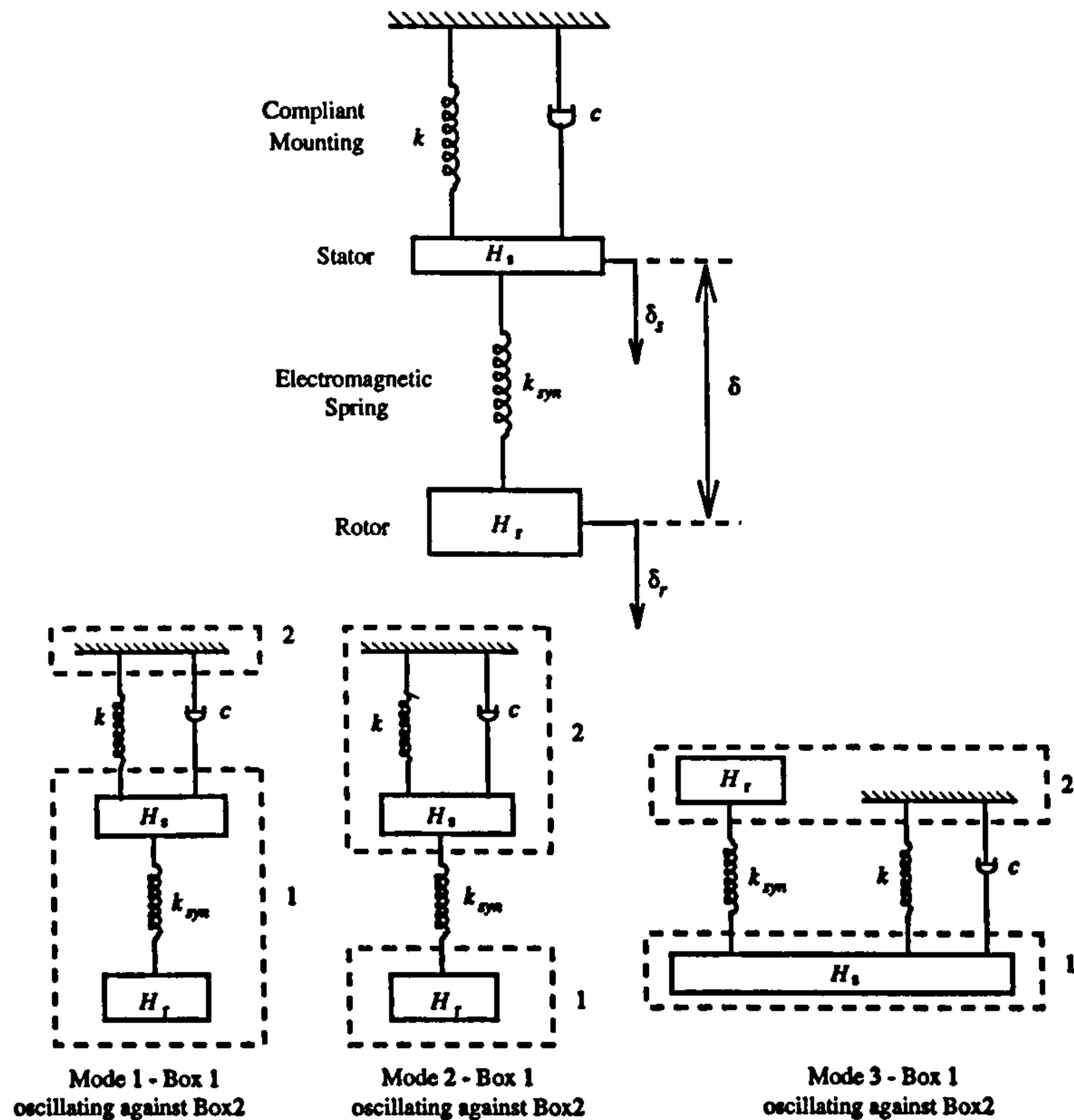


Figure 4.1: Mass, spring and damper representation of the generator

$$k_{syn} = \frac{EV_b}{X_s} \cos \delta_0 \quad (4.1)$$

and represents the electromagnetic spring tying the rotor and the stator together. For the 455 kW generator at no load the synchronising power coefficient, k_{syn} , is equal to 1.84 per unit. This mass, spring and damper system has three possible oscillation modes and these are also shown in Figure 4.1. In mode 1 the rotor and stator try to oscillate together against the anchor point with an undamped natural frequency of,

$$\omega_{1n} \approx \sqrt{\frac{\omega_0 k}{2(H_r + H_s)}} \quad (4.2)$$

If $k < k_{syn}$ and the damping coefficient is not excessive then this oscillation mode will predominate. This is the mode to be encouraged as any torque disturbance on the rotor would cause the rotor and stator to oscillate with the damping coefficient, c , determining the damped behaviour.

However if $k > k_{syn}$, or the damping coefficient is large, then the stator movement is re-

4.1 _____ Basic performance of a 455 kW generator

stricted and mode 2 would tend to dominate. In this mode the rotor is effectively oscillating against the system with the stator movement being negligible. There is very little damping of the rotor oscillations and consequently this mode of oscillation must be avoided if at all possible. It is interesting to note that this oscillation mode would normally be damped by the action of damper windings, these damper windings effectively introducing a "damper" between H_r and H_s . The undamped natural frequency of this mode of oscillation is given by,

$$\omega_{2n} \approx \sqrt{\frac{\omega_0 k_{syn}}{2H_r}} \quad (4.3)$$

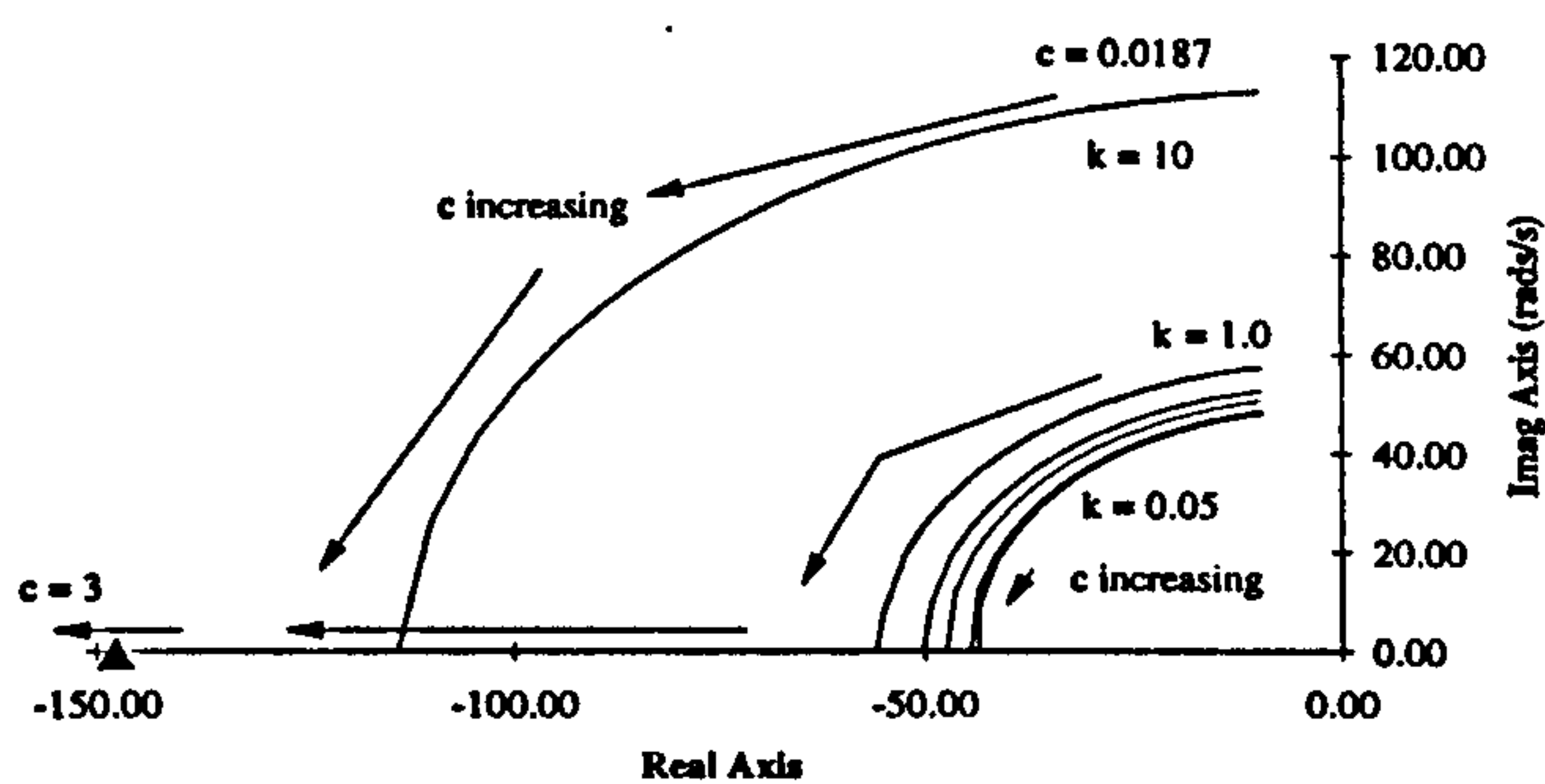
In mode 3 the stator oscillates but with the rotor tending to remain stationary. This high frequency oscillation is quickly damped by the damping coefficient. The undamped frequency of this mode of oscillation is given by,

$$\omega_{3n} \approx \sqrt{\frac{\omega_0(k_{syn} + k)}{2H_s}} \quad (4.4)$$

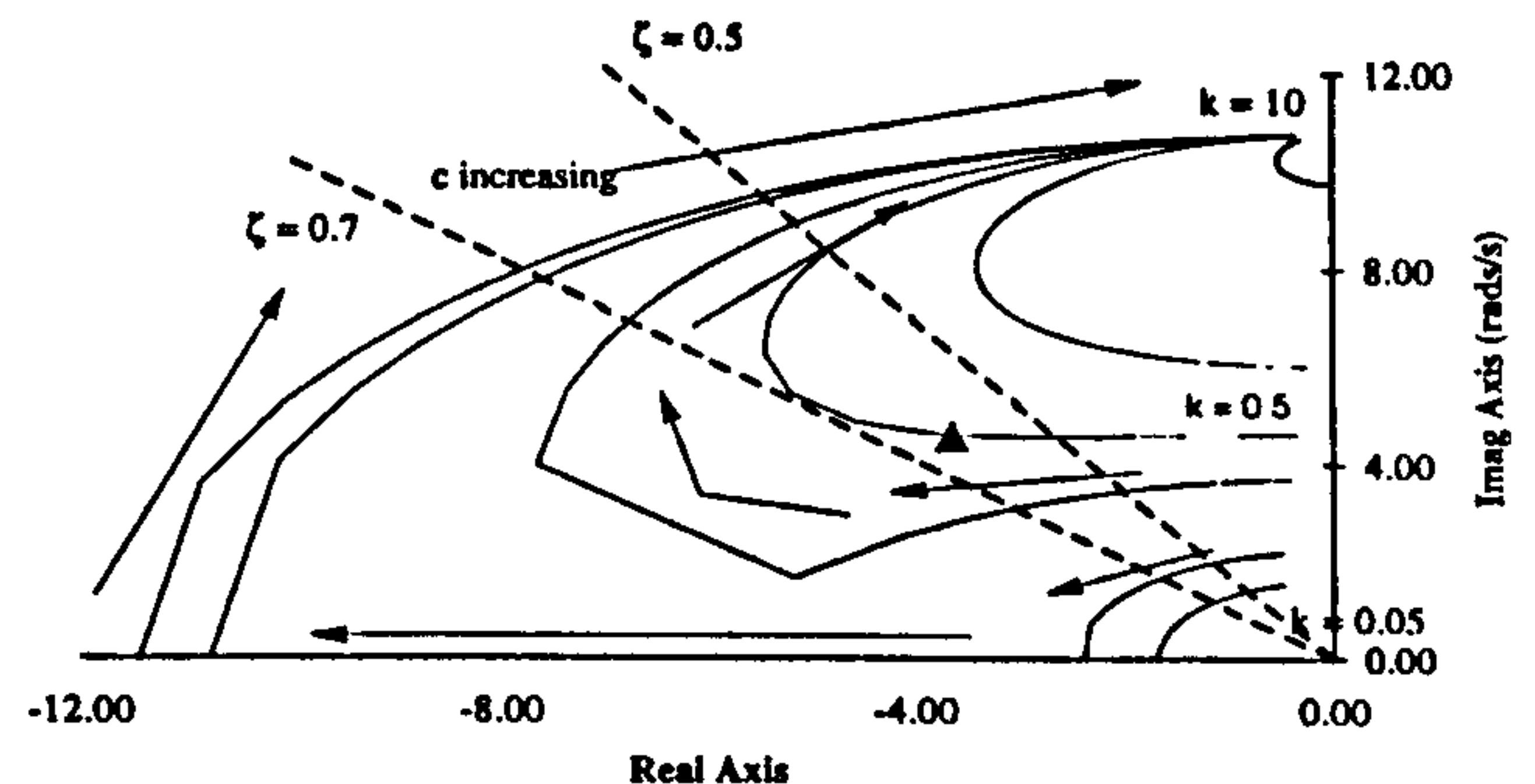
Two of these three oscillation modes will always be present in the response of the generator. Figure 4.2 (a to d) shows the variation of the eigenvalues of the system for different values of spring stiffness, k , and damping coefficient, c , for both the no load and rated load condition.

Figure 4.2 (a and c) predict mode 3 to be always present in the response whilst Figure 4.2 (b and d) shows that the value of the spring stiffness and the stator damping coefficient determines whether mode 1 or mode 2 will be dominant. With the generator on no load, a spring stiffness of $k=10$ p.u. and a damping coefficient of zero the natural frequency of mode 3 calculated from equation 11 is 113 rads/s and this compares well with the 111.8 rads/s obtained from the eigenvalue analysis of Figure 4.2 (a). Mode 3 oscillations are quickly damped such that for a stiffness of 1 p.u. and a damping coefficient of 0.10 p.u. critical damping is obtained.

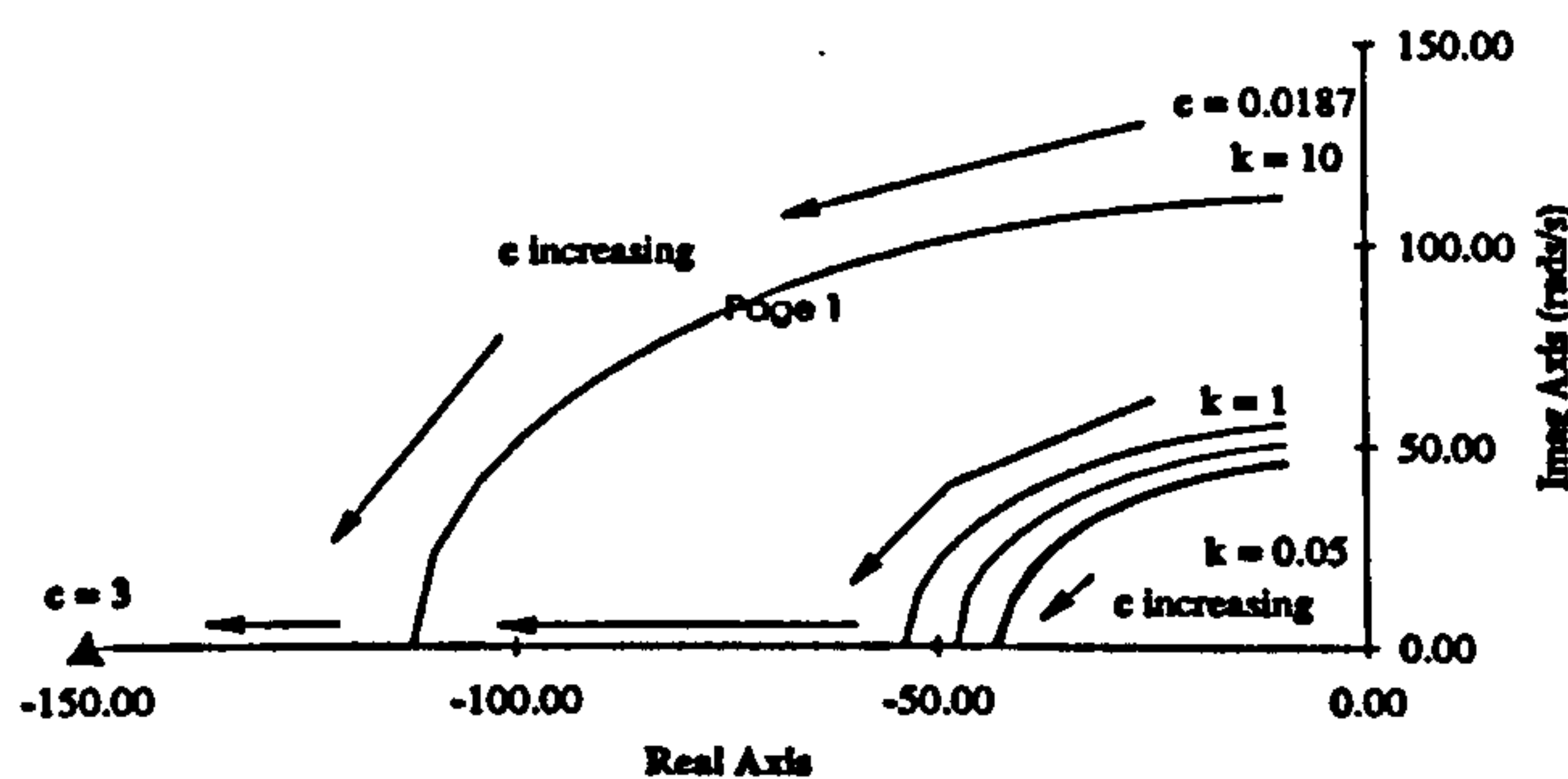
The presence of mode 1 and 2 is more complicated and depends on the stator stiffness and damping coefficient. For $k < 0.2$ p.u., which is much less than k_{syn} , mode 1 will dominate. Figure 4.2 (b) illustrates this and shows that as the damping coefficient, c , is increased the damping of the oscillations increases with critical damping being obtained when the eigenvalue of this mode just becomes real and negative. For values of $k > k_{syn}$, e.g. k



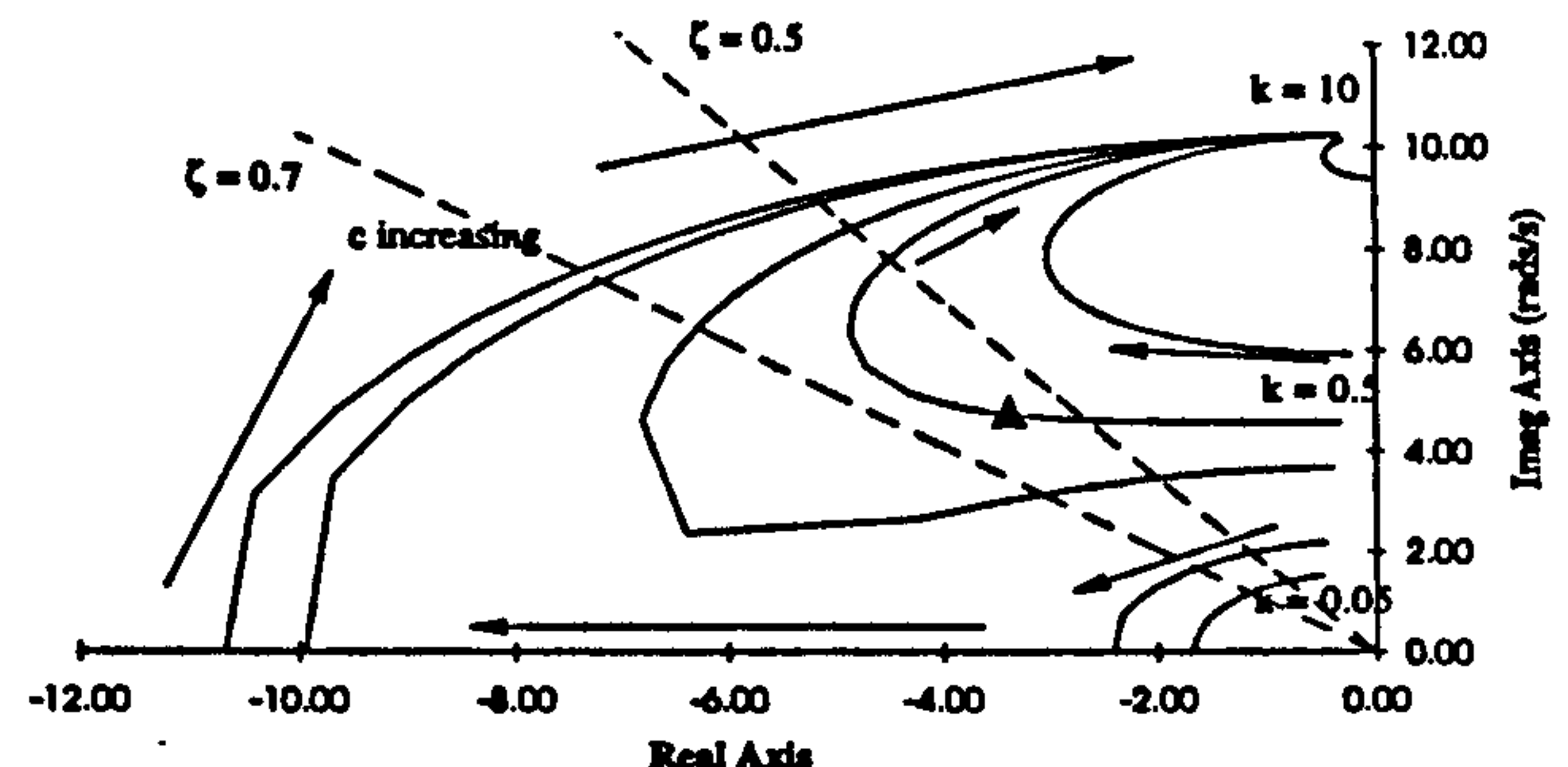
(a) Mode 3 - No load



(b) Mode 1 and 2 - No load



(c) Mode 3 - Full load



(d) Mode 1 and 2 - Full load

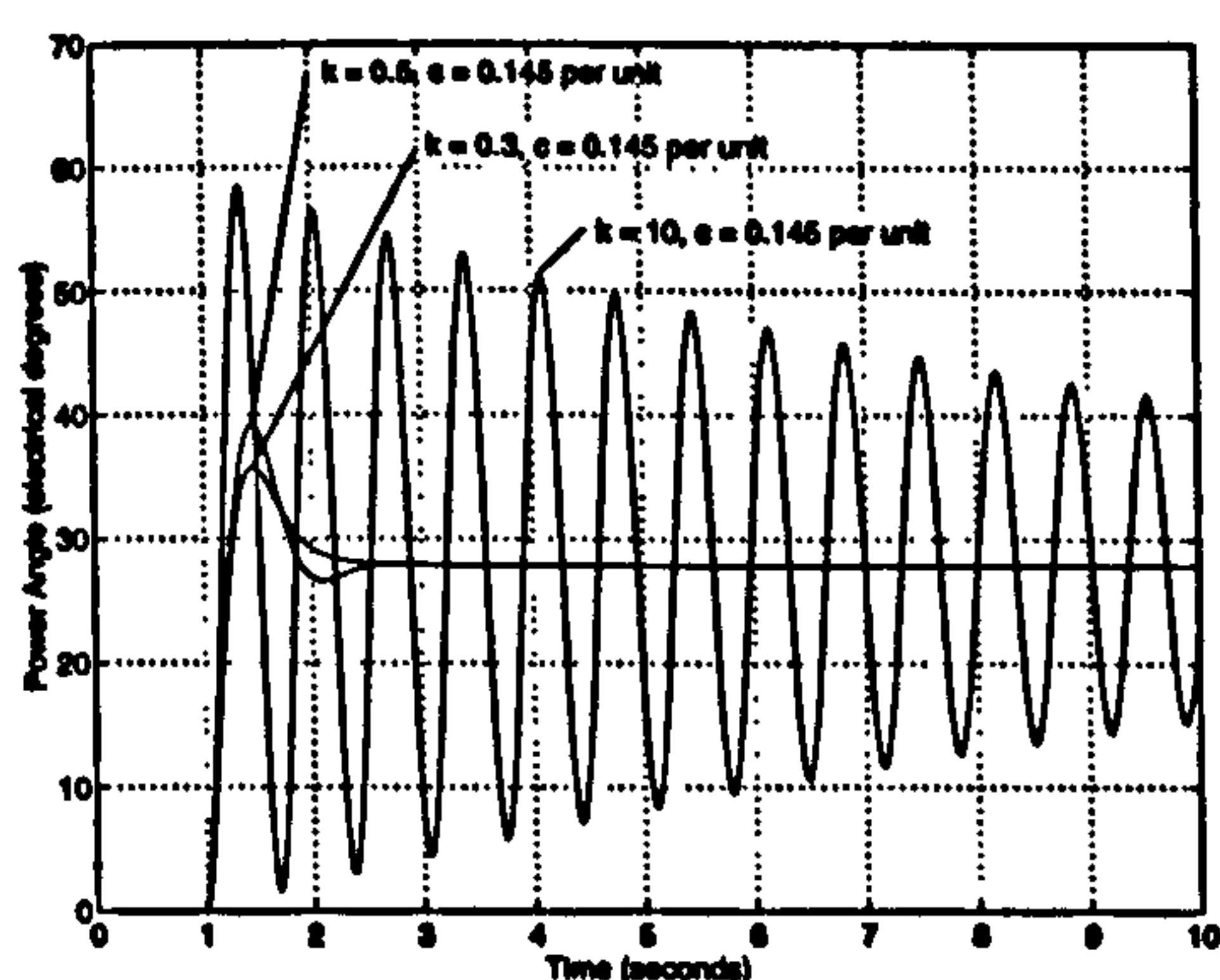
Figure 4.2: The variation of the low and high frequency eigenvalues as stiffness and damping are varied for both the no load and the full load operating condition

= 10 p.u., then mode 2 dominates and no matter what the value of c very little damping of the rotor oscillations is possible as there is now little stator movement. For the range $0.5 > k > 0.2$ p.u. the mode predominating depends on the damping coefficient. With no damping, the oscillation mode is predominantly mode 1 and as c is increased damping of the rotor is initially achieved. As c is increased further, the eigenvalue locus curves back towards the imaginary axis, stator movement is restricted and mode 2 starts to dominate. Eventually the oscillation is totally that of mode 2 with no damping of the rotor oscillations even though the damping coefficient is very large. As the aim of the compliant mounting design is to damp the rotor oscillations it is vital that the design does not have a dominant mode 2 type oscillation.

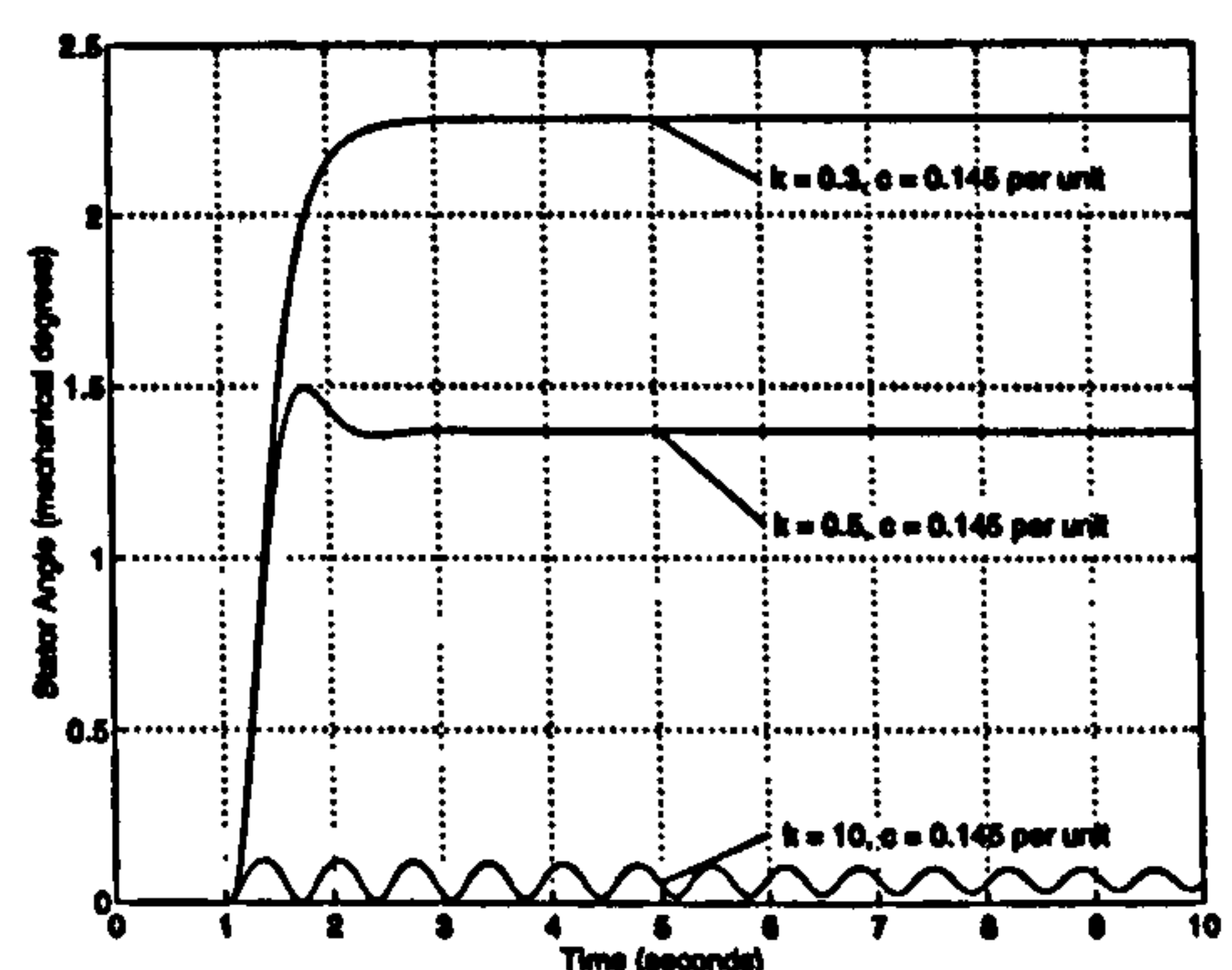
4.1.3 The choice of design values for k and c

The choice of spring stiffness, k , and damping coefficient, c , affects the response of the system. It is necessary to choose appropriate values so that the generator power angle, δ , is suitably damped for a wide range of loading conditions. The first limit on the choice of design values for the compliant mounting is on the spring stiffness. Manufacturing studies of suitable spring assemblies suggest that a maximum allowable movement of the stator is about ± 3 mechanical degrees at a 1.25 meter radius, i.e. at a radius just greater than the outer edge of the stator. The second consideration is on the choice of the damping coefficient, c , as this alters the damping ratio, ζ , of the generator power angle. Critical damping can result in severe mechanical loading and a more flexible system is preferred with a damping ratio of between 0.5 and 0.7.

Power angle and stator angle time response results from the full non-linear simulation can be used to corroborate the oscillation mode argument presented earlier and to find values for the compliant mounting that satisfy the design constraints. Several such time responses for different values of k and c are shown in Figure 4.3 (a and b) for a large step change in input torque of 1 per unit.



(a) Generator Power Angle



(b) Stator Angle

Figure 4.3: The time response for the generator power angle and stator angle for a 1 p.u. step change in input torque with the generator initially at no load

The case with $k = 10$ p.u. corresponds to mode 2 oscillation and hence little damping of power angle oscillations. With a value of $k=0.3$ p.u. and $c=0.145$ p.u. the stator movement and the power angle oscillations are nicely damped but the actual stator movement is perhaps a little too large to accommodate above rated torque operation. It is therefore necessary to increase the stiffness of the stator mounting slightly to allow for above rated

4.1 _____ Basic performance of a 455 kW generator

torque operation whilst remaining within the 3 degrees limit. With this limitation a spring stiffness in the range $0.5 > k > 0.2$ p.u. is desirable. With $k=0.5$ p.u. and $c=0.145$ p.u. acceptable damping of power angle oscillations is retained whilst stator deflection is limited to under 2 mechanical degrees.

It is important that the design of the compliant mounting is non-sensitive to both load changes and changes in the damper parameters which will occur due to wear and variations in the operating temperature. With a spring stiffness of 0.5 p.u. the damping coefficient for a damping ratio of $\zeta=0.61$ at no load is 0.145 per units. The position of the corresponding eigenvalues are marked on Figure 4.2. Lines corresponding to a constant damping ratio of 0.5 and 0.7 are also shown on Figure 4.2. Because of its low synchronous reactance the permanent magnet generator exhibits a stiff connection to the power system with the result that the variation in power angle between no load and rated is about 27.8 electrical degrees. With a constant stator stiffness and damping coefficient this limits the variation of the natural frequency of the eigenvalues to about 0.5% and the damping ratio to about 3 % in the critical region of interest. Indeed as the load changes the value of damping ratio of 0.61 at no load degrades to only 0.59 at full load

In designing the compliant mounting it is necessary to ensure that the low frequency eigenvalue corresponds to mode 1 operation. So as to keep the sensitivity of the system to parameter and load changes as low as possible an operating point that lies on the eigenvalue locus before it curves back on itself towards the y-axis and mode 2 operation is to be preferred. Ideally a locus which bends to intersect the x-axis will have a greater range over which increasing the damping coefficient has a beneficial effect. Unfortunately in this 455 kW design this criterion leads to an optimum spring stiffness of about 0.25 per unit which is slightly too soft for the allowed stator movement.

The limits placed upon the spring stiffness to ensure mode 1 operation has implications for the design of the generator itself. As there is a limit placed on the extension of the spring due to manufacturing constraints of the mounting it is necessary to limit the spring stiffness to a reasonably large value. For mode 1 operation k should be much less than k_{syn} . However as k_{syn} is inversely proportional to X_d the limit on stator movement imposes a limit on synchronous reactance and hence the generator electrical design. This may become of particular importance in the larger generators as the allowable spring deflection is restricted more with the torque rating of the generator.

4.2 _____ Design Constraints with parameter variation

This section has demonstrated the use of a compliant mounting as a means of providing damping to a permanent magnet synchronous generator. A generator performs better with compliant mountings than with conventional damper windings, provided the characteristics of the compliant mounting are tuned to the main parameters of the generator. A single value of spring stiffness and damping coefficient, correctly chosen, will result in a generator with good dynamic performance over a wide range of operating conditions.

In selecting the damping coefficient and stiffness of the compliant mounting it is vital to ensure mode 1 operation (where the rotor and stator oscillate together against the power system with an undamped natural frequency of oscillation dependent on the stiffness of the stator compliant mounting). For this 455 kW generator the stator spring stiffness should lie in the range $0.5 \text{ p.u.} > k > 0.2 \text{ p.u.}$ and the damping coefficient $0.145 > c > 0.153 \text{ p.u.}$ so as to give a damping ratio of about $\zeta = 0.6$.

4.2 Design Constraints with parameter variation

There are only four parameters that can really be varied in an attempt to design the compliant mounting to suit the permanent magnet synchronous generator because the rest are dependent on the wind turbine design, for instance H_r , or have little effect, for instance R . The parameters for a range of generator ratings are now presented and their performance discussed.

4.2.1 Variation with generator ratings

It is now appropriate to consider the change in X_d and X_q as the generator ratings vary for units which are considered to be well designed in light of the arguments presented in the previous sections. The key parameters for a range of generator ratings typically found in wind turbine applications can be seen in Table 4.1.

It can be seen quite easily that increasing the generator rating does in fact alter the values for X_d and X_q only slightly provided an appropriate number of tiers is allowed. More important now is the allowable deflection of the spring and damper unit and this is dependent on the allowed angular rotation and radius of the stator. The allowed angular rotation at rated torque decreases from 3 to 1.85 degrees as the stator outer diameters increase from 2.4 m

4.2 Design Constraints with parameter variation

Rating	200 kW	455 kW	750 kW	1 MW	1.5 MW
R	0.033	0.023	.048	0.043	0.028
X_d	0.45	0.54	0.68	0.69	0.58
X_q	0.43	0.52	0.64	0.66	0.55
H_r	2.13	2.90	4.15	4.49	4.24
H_s	0.10	0.15	0.13	0.22	0.28
Stator OD (m)	1.92	2.40	2.81	3.14	4.14
ω_r (rev/min)	44.8	36.1	29.1	24.4	20
No. of Poles	134	166	206	248	302
No. of Tiers	2	3	3	4	5

Table 4.1: Generator Parameters

at 455 kW to 4.15 m at 1.5 MW.

4.2.2 Damping coefficient and Spring Stiffness

As has already been outlined in Section 4.1.3 good performance is achieved by selecting the damping coefficient to give a damping ratio, ζ , in the range $0.5 < \zeta < 0.7$. Furthermore the spring stiffness must be chosen to ensure mode 1 operation and restrict stator movement to ± 3 mechanical degrees at a radius of 1.25 meters, i.e. at a radius just greater than the outer edge of the stator.

4.2.3 Effect of varying the number of tiers

The limits on the spring stiffness to ensure mode 1 operation have implications for the design of the generator itself. As the extension of the spring is limited, the spring stiffness should be reasonably large, and for mode 1 operation, k should be much less than k_{syn} . However, as k_{syn} is inversely proportional to X_d , the choice of synchronous reactance and overall generator electrical design is restricted.

The number of generator tiers is initially restricted by the electric loading of the stator modules. There are two ways of ensuring suitable electric loading as explained in section 3.2.3. and altering the number of generator tiers was proposed as the better method for this type of permanent magnet generator. Considering the case when all the shaft power of the 455 kW rated generator was transmitted through a single tier, it is clear that rated voltage would be generated at rated speed and therefore there must be a large current flowing in the windings of the individual E-cores to transmit the correct level of power. As the tier number

4.2 Design Constraints with parameter variation

increases the current level in the tiers reduces proportionally and the total shaft power is shared between the tiers equally. The tiers are also connected in parallel and therefore the resistance and reactance also reduce in proportion to the increase in number of tiers. For example, a two tiered generator would have half the reactance of a single tiered generator and a three tiered generator a third, etc, for the same rating of generator.

If the 455 kW generator had two tiers instead of three X_d and X_q would increase by a factor of about 1.5 to the new values of 0.81 p.u. and 0.77 p.u. respectively whilst R would change to 0.039, H_r to 2.85 and H_s to 0.11. The effect on the eigenvalues is shown in Figure 4.4.

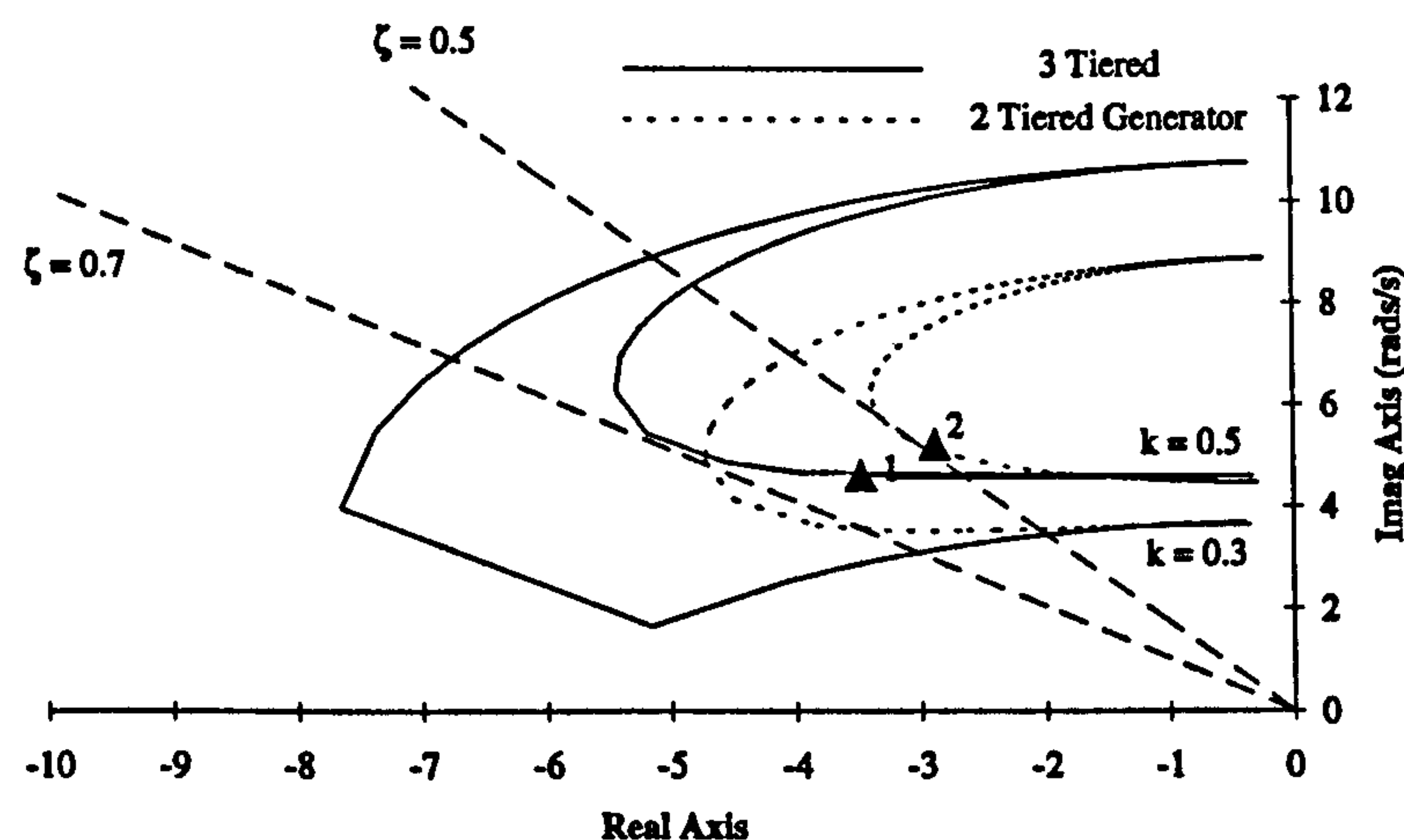


Figure 4.4: Mode 1 and 2 - Variation with tier number

Clearly the two tier design restricts the value of damping to a greater extent than the three tier design. In fact for $k = 0.5$ the performance degrades so much that the damping ratio requirement is just violated and the design would not be suitable. For $k = 0.5$ and $c = 0.145$ the eigenvalues move from Δ_1 to Δ_2 with the decrease in tier number.

4.2.4 Key design interactions as generator rating varies

The key design parameters are X_d , X_q and the stator outer diameter. These are presented in graphical form in Figure 4.5 for a range of generator ratings, which have been designed in light of the arguments presented in the preceding sections.

The values of X_d and X_q change with increase in generator rating but, provided enough

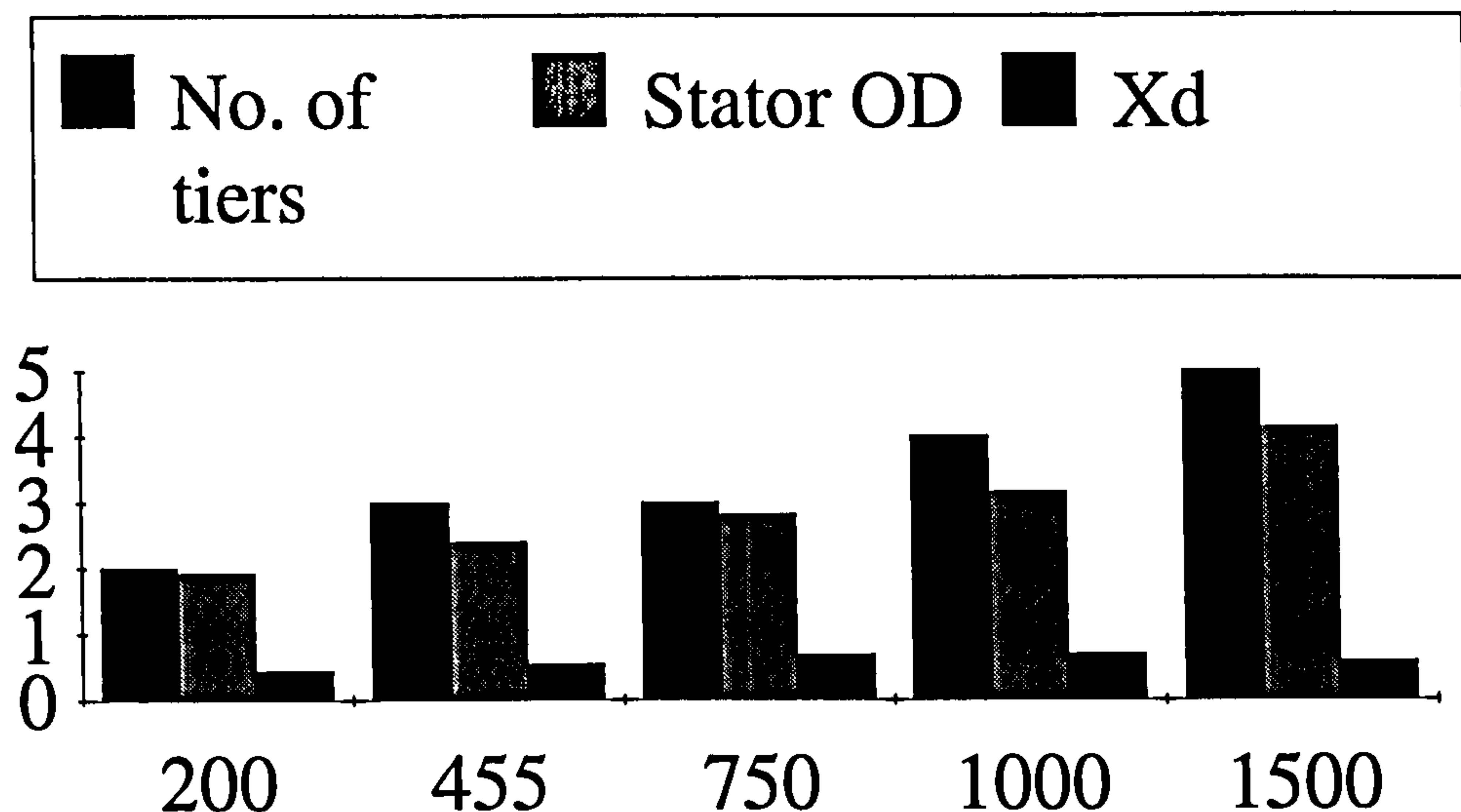


Figure 4.5: The variation of the key generator parameters with rating

tiers are used, k_{syn} has a large value and mode 1 operation is ensured. The stator outer diameter increases with generator rating and so less angular movement in a larger machine will give a similar linear deflection of the spring as for the 200 kW generator. The deflection of the spring and damper unit might then be critical. Figure 4.6 shows several stator angle time responses for a step change in input torque on the 1.5 MW generator. The maximum stator deflection is 1.3 degrees at $k = 0.3$, $c = 0.14$, which corresponds to a damping ratio of 0.7. This is within the limit defined earlier because the increased pole number of the 1.5 MW turbine partially compensates for the increased stator diameter. Furthermore it can be seen that the value of k for a well designed mounting for the 1.5 MW rated generator does not change in per unit terms compared with the value for the mounting of the 455 kW generator and the damping coefficient only varies by 4.5 %.

4.2.5 Concluding remarks

This section has identified several conflicting parameters in the design of a compliantly mounted, permanent magnet, synchronous generator for wind power applications. Firstly sufficient tiers must be used to give a good range for the power angle eigenvalue and, secondly, the spring stiffness must be set to limit the spring's linear deflection. The damping coefficient must then be chosen to give mode 1 operation and ensure good transient performance of the generator to withstand the power angle excursions during wind gusts,

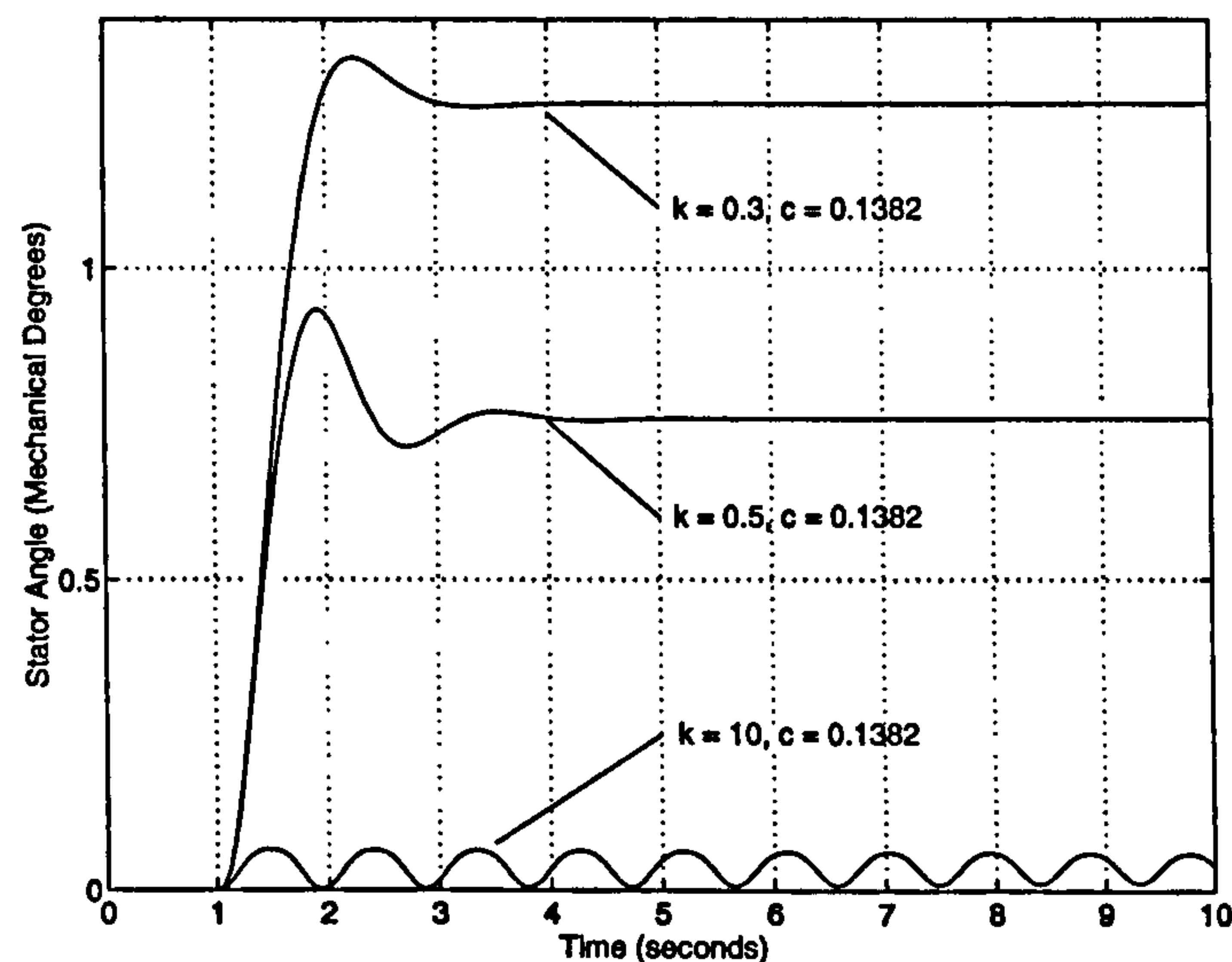


Figure 4.6: Time response of the stator

synchronisation and grid electrical faults. Although the allowed deflection of the spring must be limited for reasons of manufacture the increase in pole number with generator rating and careful design ensures that this limit is not usually reached.

The operation of the compliantly mounted permanent magnet generator has been examined in response to ideal step changes in torque to identify the its key mode of oscillations and design interactions. It is now necessary to consider two key questions concerning the operational performance of the generator. The first question that needs to be answered is will such a generator synchronise to the grid without any control over the excitation and only rudimentary speed control from the pitch controller and the second question is how will the generator perform in a windy environment?

4.3 Synchronisation of a 455 kW generator

The synchronisation problem is particularly interesting as, in addition to the damping properties of the generator, the variable speed nature of the wind turbine and the inability to control the generator excitation makes the behaviour of the generator on synchronisation an important issue. Stable synchronisation is fundamental to the operation of the generator.

During start-up, the wind turbine uses an auxiliary pitch control system to maintain the generator speed close to its synchronous value. This implies that there will be little or no

torque on the generator shaft at the instant of synchronisation but that the generator emf phasor will be both out of phase with, and moving relative to, the system voltage phasor. Both these conditions can be represented in the simulation by varying the initial conditions on the power angle, δ_0 , and the rate of change of power angle, $d\delta_0/dt$. At the instant of synchronisation the stator angle will be zero and the rotor displacement angle equals the power angle. The synchronisation of the 455 kW generator has been studied using this approach and the resultant transient from allowing the system to settle examined to see if pole slipping arose.

The synchronisation process can be quantified by considering the basic mass, spring and damper arrangement of Figure 4.2 and relating this to the equal area criterion. As large excursions of power angle, δ , now occur Figure 4.2 becomes that of Figure 4.7 where the electromagnetic spring, k_1 , has a non-linear characteristic.

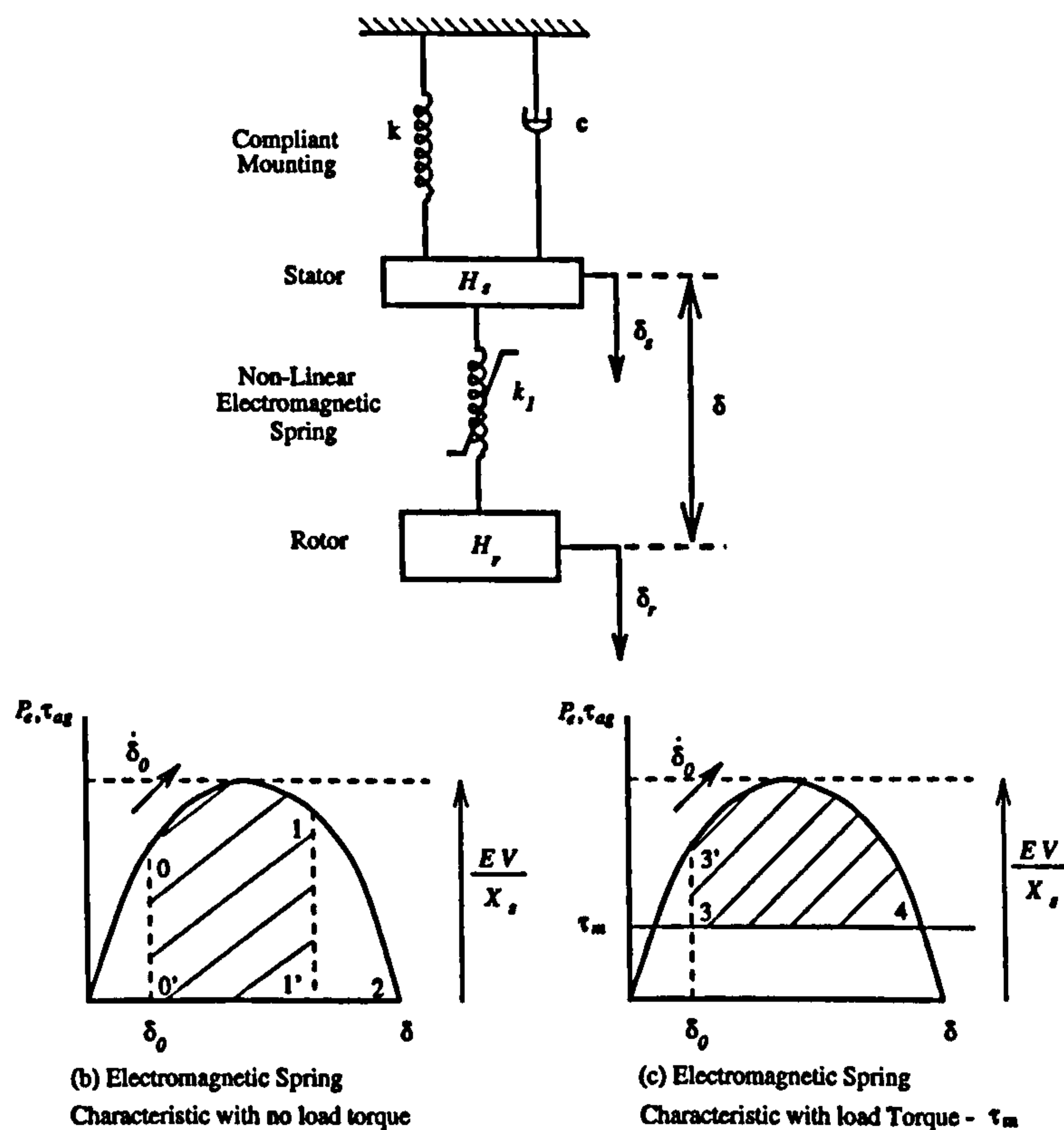


Figure 4.7: The energy transfers during synchronisation

On closing the synchronisation switch the mass, spring and damper system is equivalent to examining the behaviour of Figure 4.7 (b) given the rotor has some initial condition on δ and $d\delta/dt$ of δ_0 and $d\delta_0/dt$ respectively with the stator initial position and velocity both being zero. In addition mode 1 behaviour will dominate because of the selection of k and c

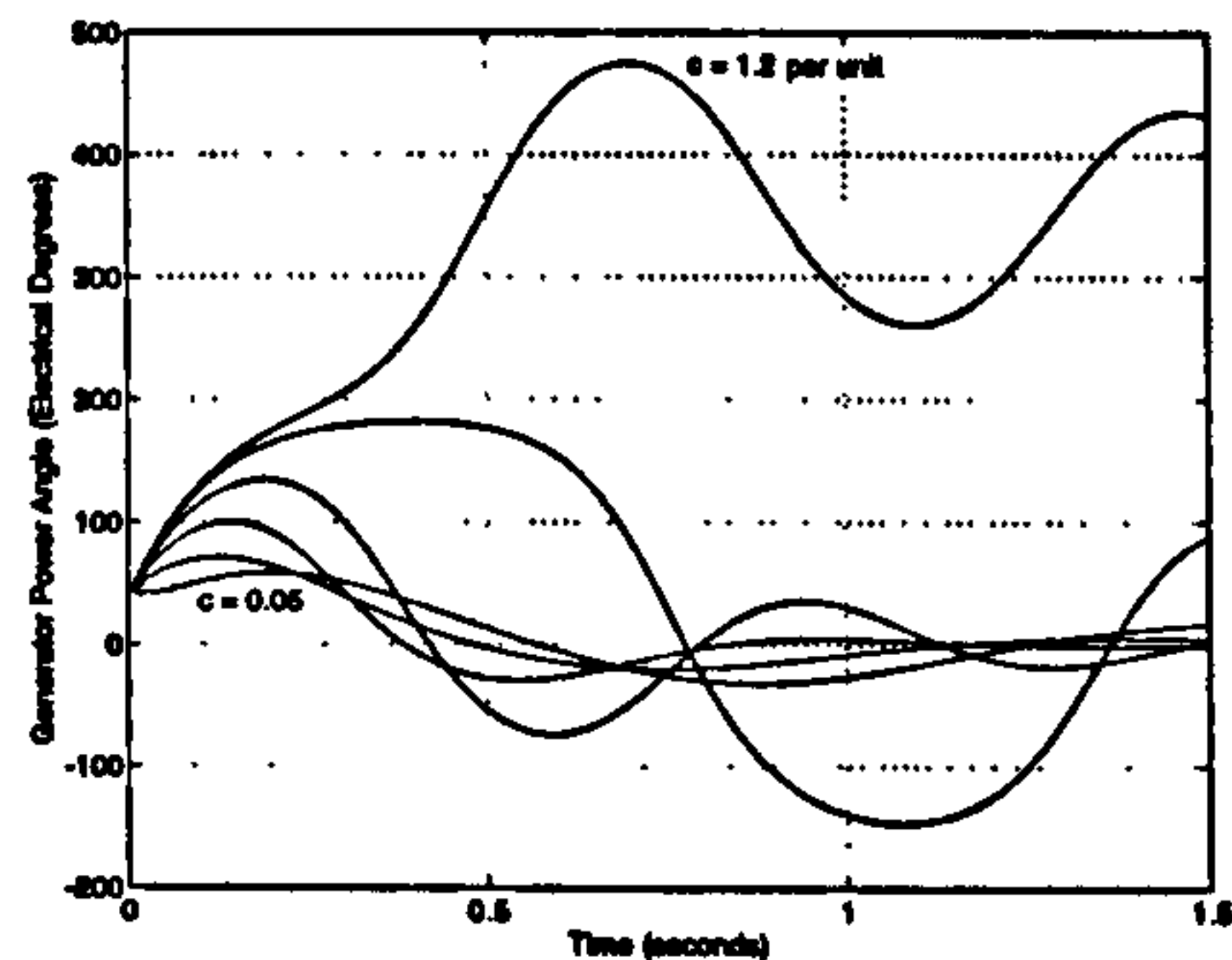
for the compliant mounting. Due to the initial velocity, $d\delta_0/dt$, the rotor will have an excess of kinetic energy relative to the synchronous speed, ΔE . For successful synchronisation this excess energy should not cause pole slipping.

If the stator mounting was very stiff then the excess kinetic energy of the rotor would be absorbed by the non-linear electromagnetic spring, k_1 . The extension of this spring is such that the area 0 0' 1 1' on Figure 4.7 (b) is equal to the excess kinetic energy. In the limit should ΔE be greater than area 0 0' 2 then pole slipping would occur. If stator movement is allowed by reducing k then the excess kinetic energy, ΔE , can be absorbed both in the electromagnetic spring, k_1 , and the stiffness of the compliant mounting, k . In fact the greater the extension of the stator, δ_s , allowed the better as this transfers energy storage from k_1 to k and reduces the excursion in δ . Once $\delta > 90$ degrees the non-linear characteristic of the electromagnetic spring, k_1 , is such that any small increase in energy storage ΔE_s requires a smaller increase in δ_s than δ . Consequently restricting the movement of δ_s is not advisable, either due to an increase in k or c , as this will lead to a reduced energy storage in k and a disproportionate increase in δ as it strives to store this energy. This would ultimately lead to pole slipping and a reduction in the stability boundary. It should be noted that a percentage of the rotor kinetic energy will also be dissipated in the stator damper depending on the degree of stator movement.

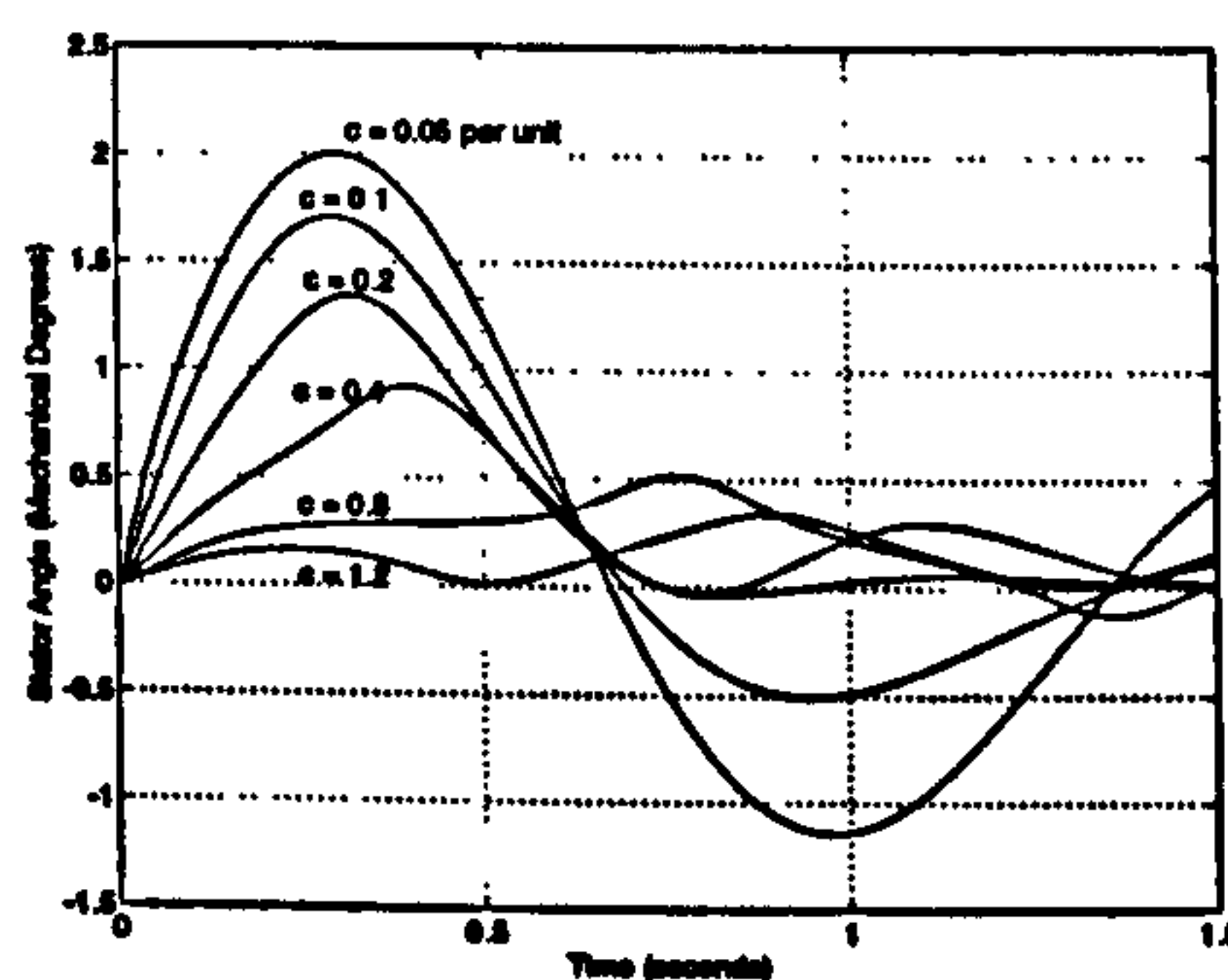
The explanation above has assumed that during the synchronisation process the torque input from the wind turbine is zero. If some torque input, τ_m , is present then Figure 4.7 (c) is valid where the critical area is now 3 3'4. As area 3 3'4 < area 0 0' 2 this would lead to a reduction in the size of the envelope for successful synchronisation relative to the $\tau_m = 0$ case.

Typical power and stator angle responses are shown in Figure 4.8 for synchronisation with a δ mismatch of 40 degrees and an initial $d\delta/dt$ of 22 rads/s for $k = 0.5$ per unit as the damping coefficient is varied.

As the damping is increased the stator movement is restricted until the initial energy, ΔE , is greater than the energy that can be stored in the extension of k and k_1 or dissipated in the damper. At this point pole slipping occurs but the generator synchronises after one pole slip. An energy analysis can be used to verify the results from the simulation. The per unit kinetic energy input relative to synchronous speed is given by,



(a) Generator Power Angle



(b) Stator Angle

Figure 4.8: Typical synchronisation transients with spring stiffness $k = 0.5$ p.u. as the damping coefficient is varied for an initial δ of 40 degrees and $d\delta/dt = 22$ rads/s

$$\Delta E_{initial} = 0.5 \left(\frac{2H_r}{\omega_0} \right) \left(\frac{d\delta}{dt} \right)^2 \quad (4.5)$$

whilst the area 0 0' 2 is,

$$\Delta E_{k_{syn}} = Area = \int_{\delta_0}^{180} \frac{EV_b}{X_d} \sin \delta d\delta = \frac{EV_b}{X_d} (\cos \delta_0 + 1) \quad (4.6)$$

and the energy stored in the compliant mounting is,

$$\Delta E_k = 0.5k\delta_s^2 \quad (4.7)$$

where δ_s is the extension of the stator when δ is 180 degrees. For the case when $\delta_0 = 40$, $d\delta_0/dt = 22$, $k = 0.5$, the energy input, $\Delta_{initial}$, is equal to 4.36 per unit. When the stator damping coefficient $c=0.5$ p.u. the relatively large movement of the stator allows 31% of this energy to be stored in the compliant mounting whilst only 10% is stored in the

electromagnetic spring. Consequently only a relatively small power angle movement is necessary as shown in Figure 4.8. Because of the stator movement the damper is also effective in removing 47% of the energy. However if the stator damping coefficient is increased to $c=0.8$ p.u. then the stator movement is restricted so that 75% of the energy is stored in the electromagnetic spring and only 1% in the compliant mounting. In addition the damper is ineffective removing only 23% of the energy during this first oscillation. This leads to the large, poorly damped, power angle excursion shown.

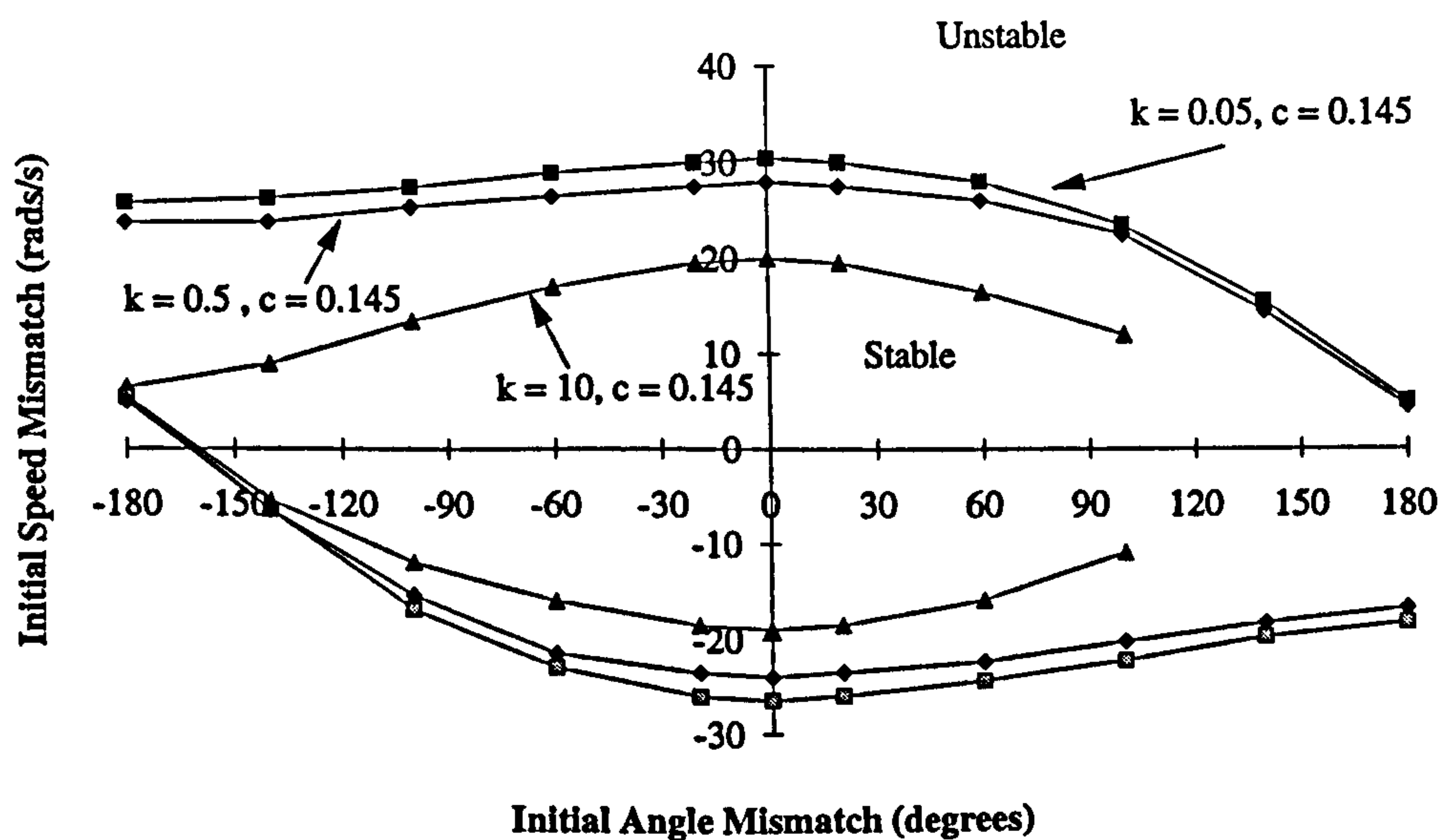


Figure 4.9: Synchronisation envelope for constant damping coefficient as spring stiffness is varied

Figure 4.9 and Figure 4.10 show synchronisation envelopes for different values of spring stiffness and damping coefficient for the 455 kW rated generator with the boundaries representing the conditions at which pole slipping will just occur. In many cases synchronisation will result after one or two pole slips so that by drawing pole slip envelopes a pessimistic estimate for the successful synchronisation boundary is obtained. Figure 4.9 shows how increasing the spring stiffness, and reducing the stator movement, decreases the ability of the turbine to synchronise with the grid without pole slipping. With a stiffness value of $k=0.5$ p.u. the area of synchronisation with no pole slipping is large and acceptable. As explained in section 4.1.3 spring stiffness values much above this value are not favoured. Figure 4.10 shows the envelope for the system as the damping is varied. Again, because the damper restricts stator movement, increasing the damping coefficient decreases the size of the synchronisation envelope but as an effective damper is necessary to damp subsequent

**PAGE
MISSING
IN
ORIGINAL**

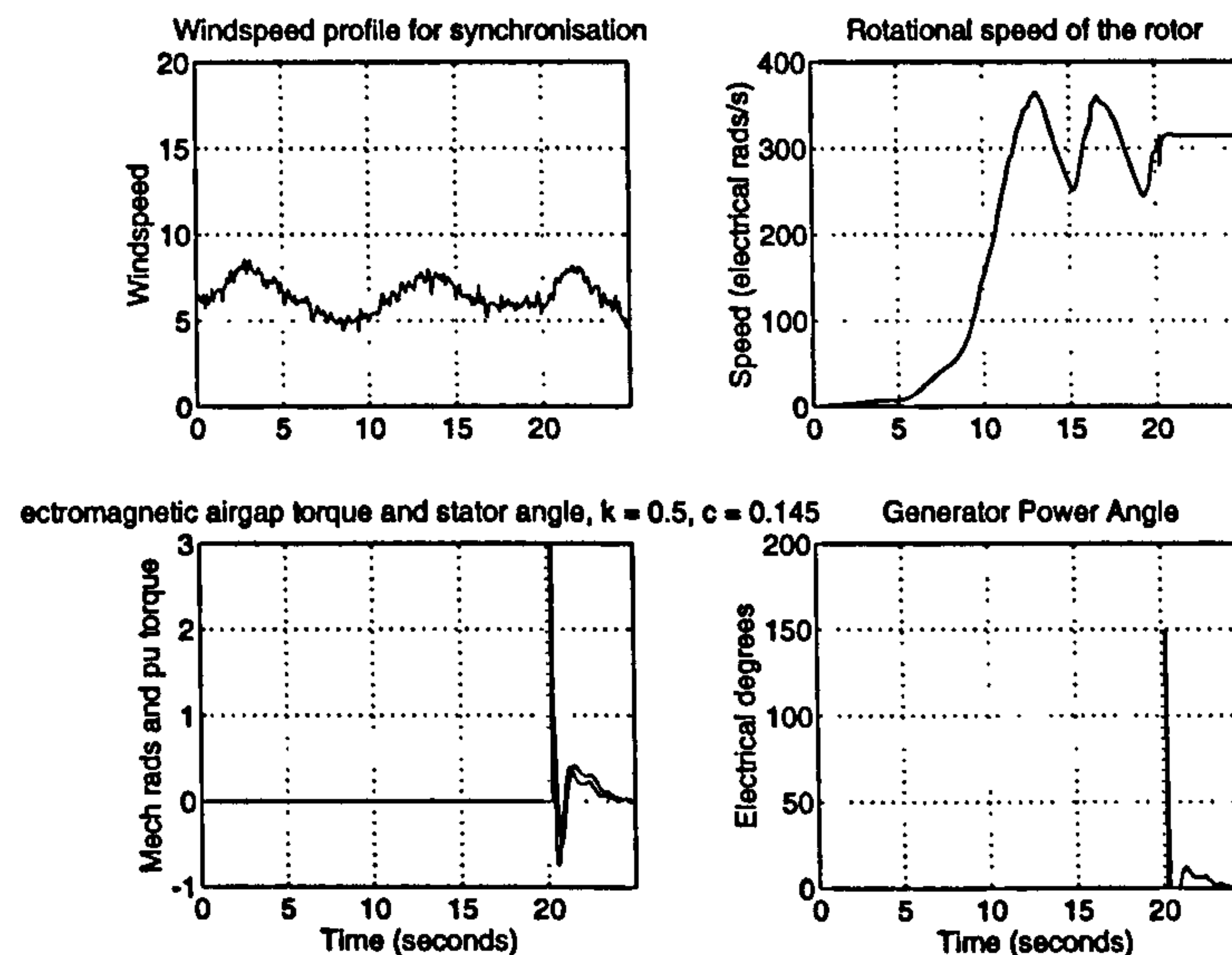


Figure 4.11: Performance on synchronisation of a 455 kW wind turbine

extension constraint. The phase sequence of the generator would be matched to the grid by ensuring the terminal connections of the generator were attached to the correct phases of the grid and that the generator rotated in the correct direction. The blade pitch demand, actual pitch action and the 'synchronise now' control flag for this synchronisation procedure can be seen in Figure 4.12.

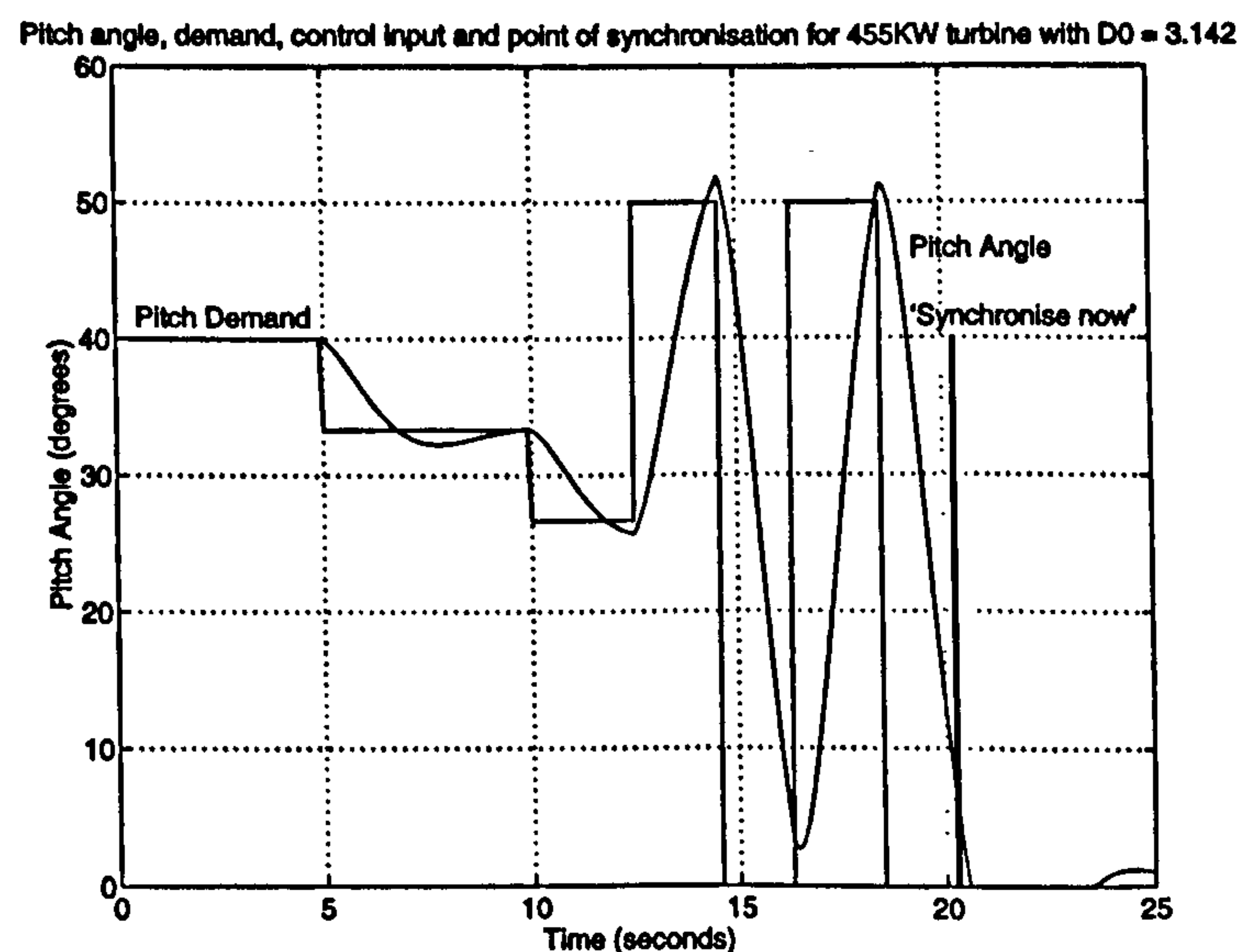


Figure 4.12: Control action for synchronisation of a 455 kW wind turbine

The original aim of pitch control was to assist in the start up and shut down of wind turbines to make it easier to connect them to grid. Only subsequently was it realised that it could

4.4 _____ Response of the 455 kW rated generator to simulated wind data

also be used for power limiting. At the start of this simulation run it is assumed that a preliminary control signal has decided that the wind is strong enough to generate useful power and that the generator should synchronise to the grid. Therefore, as can be seen in Figure 4.12, the pitch of the blades is assumed to start at 40 degrees. The reason for this is to limit the accelerating torque on the blades to within the design constraints placed on them by their economic design [75]. The pitch controller then reduces the pitch demand in discrete 5 degree steps, thus maintaining a low accelerating torque, until synchronous speed is reached. The actual pitch angle follows the pitch demand but is delayed by the time constants and limitations of the pitch actuation system as described in Chapter 2. Once synchronous speed is reached the pitch controller is used to alternate the speed of the turbine blades at 0.1 Hz. When the phase mismatch is within ± 150 degrees and the speed passes through the synchronous value with positive acceleration the 'synchronise now' control flag is set high and the synchronising breaker is closed. A tighter margin on phase mismatch leads to a longer time until the phase of the generator and grid match but less initial torque stressing of the generator. This simulation run through shows it is possible to synchronise such a direct coupled, permanent magnet, synchronous generator provided that the terminal voltage and phase sequence of the generator are designed to match the grid voltage at synchronous speed.

4.4 Response of the 455 kW rated generator to simulated wind data

This section investigates how the compliant mounting interacts with the complete wind turbine system in a typical windy environment and demonstrates the ability of the stator damper system to limit any high frequency power oscillations and rotor movement. Excessive rotor movement could result in loss of synchronism. The pitch controller has the same values as described in Chapter 2, section 2.3.3.

Five simulated wind speeds are generated by the spectral method and used to characterise the performance of the compliantly mounted generator and assess the impact of the pitch controller on the compliant mounting. These five wind speed variations correspond to the following cases:

4.4 _____ Response of the 455 kW rated generator to simulated wind data

1. **Cut in.** This corresponds to the synchronisation case presented in the previous section and clearly the pitch controller ensures the correct point of synchronisation whilst the compliant mounting ensures that the resulting oscillations are stable.
2. **Below rated windspeed.** This is not such an important region for the fixed speed wind turbine but is useful later in comparing the energy capture between the fixed and variable speed operation and the response can be seen in Chapter 7.
3. **Below to above rated windspeed.** This is the key area for the pitch controller as the output power to the grid must be limited to rated value with the compliant mounting ensuring smooth operation.
4. **Above rated windspeed.** Gradually the turbulence becomes stronger in the wind and the pitch controller must act more to maintain constant power out.
5. **Cut out.** Finally this time history demonstrates the fail safe pitching of the blade when the mean wind speed is greater than the designed cut-out value of 25 m/s the pitch controller must shut down the turbine until such time as successful synchronisation can be carried out.

The last three situations are simulated for the 455 kW rated generator with the values for the compliant mounting designed in section 4.1 and the effect of using an ill-designed compliant mounting is demonstrated to show what happens when mode 2 operation occurs (where there is very little movement of the stator). This will vindicate the use of the extra tier to ensure mode 1 operation is possible within the design limits imposed upon the compliant mounting. Furthermore the effect of low damping ratio will also be considered for the case with $k = 0.5$ to stress the need for ensuring the damping coefficient is set to give a damping ratio of $0.7 > \zeta > 0.5$.

4.4.1 Below to above rated wind speed operation - power limiting

The performance of the 455 kW rated generator will be examined in full in this section and only the key results portrayed thereafter. The wind speed time history, its power spectrum, and the run identifiers for this mode of the pitch controller can be seen in Figure 4.13 (a) and (b) respectively. The simulated wind speed has been generated by the spectral method

4.4 _____ Response of the 455 kW rated generator to simulated wind data

presented in Chapter 2. The compliant mounting has a spring stiffness of $k = 0.5$ and a damping coefficient of $c = 0.145$, the values chosen in section 4.1 to give the best transient performance and still remain within the design constraints. The run identifiers for the fixed speed simulation runs contain information for the PID pitch controller and a flag to show whether rotational effects have been included.

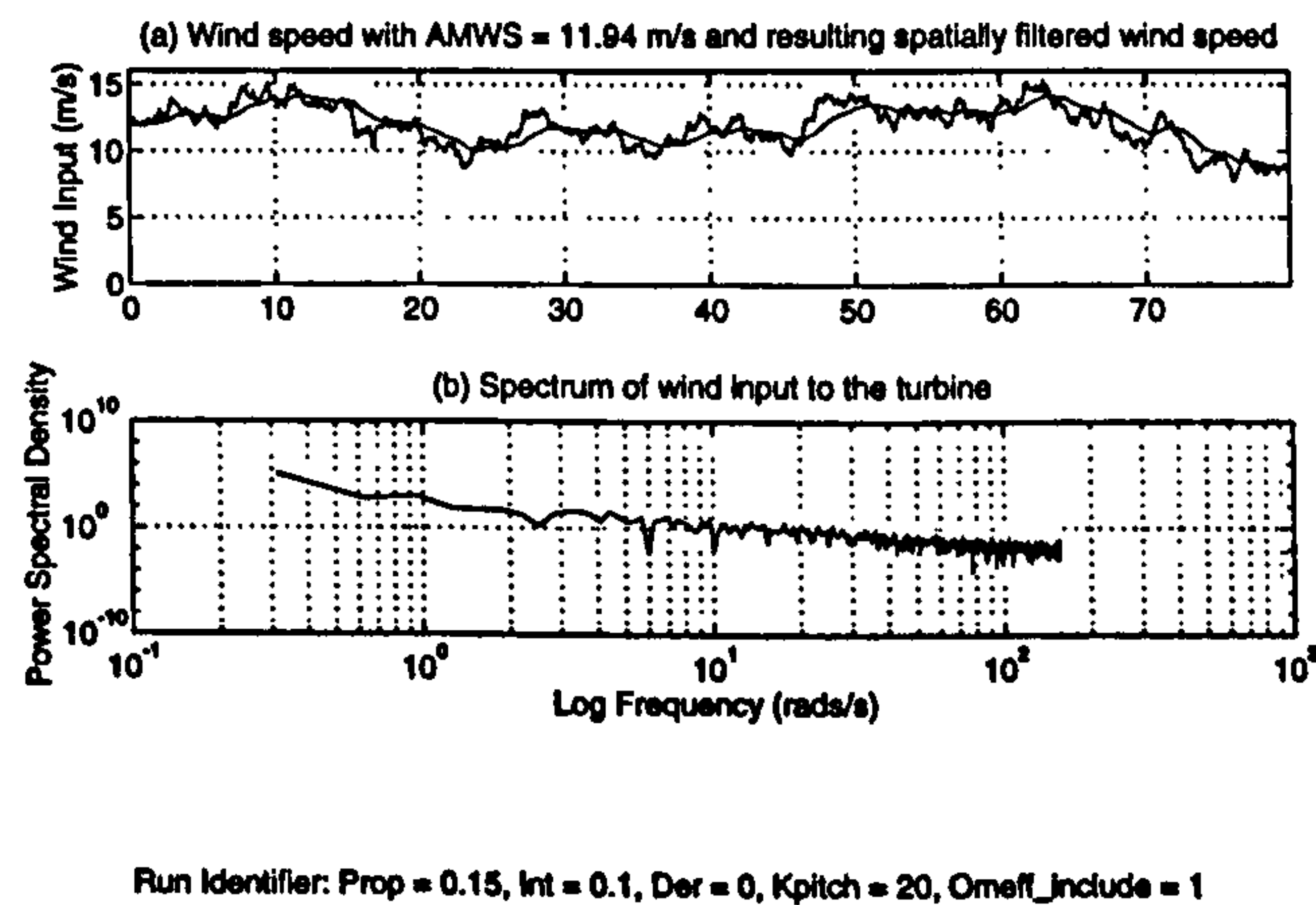


Figure 4.13: Simulated wind speed and the corresponding power spectrum

The resulting power coefficient, aerodynamic torque before and after induction lag, per unit hub torque including rotational effects and the corresponding power spectrum can be seen in Figure 4.14 (a) to (d) respectively. The power coefficient is at 0.45 for much of the simulation run because the tip speed ratio is almost 6 at rated wind speed, 12 m/s, and rotational speed. The power coefficient drops quickly as the wind speed increases from this value because of the shape of the C_p curve and the effect of blade pitch action. The effect of induction lag can be clearly seen in Figure 4.14 (b) where the effect of any variation in the input torque is accentuated by the induction lag effect. Above rated wind speeds, i.e. between 0 and 20 seconds and 50 and 70 seconds the effect of induction lag is swamped by the effect of pitch action. The PI controller limits the peak power output to 30 % above its rated value and this compares favourably with the results presented in [65] which show results for a similar wind speed time history and a 300 kW rated wind turbine with a peak of 35 % over rated power.

The response of the generator power angle and the stator angle can be seen in Figure 4.15 (a) and (b) respectively. The stator movement damps out the typically oscillatory response of

4.4 Response of the 455 kW rated generator to simulated wind data

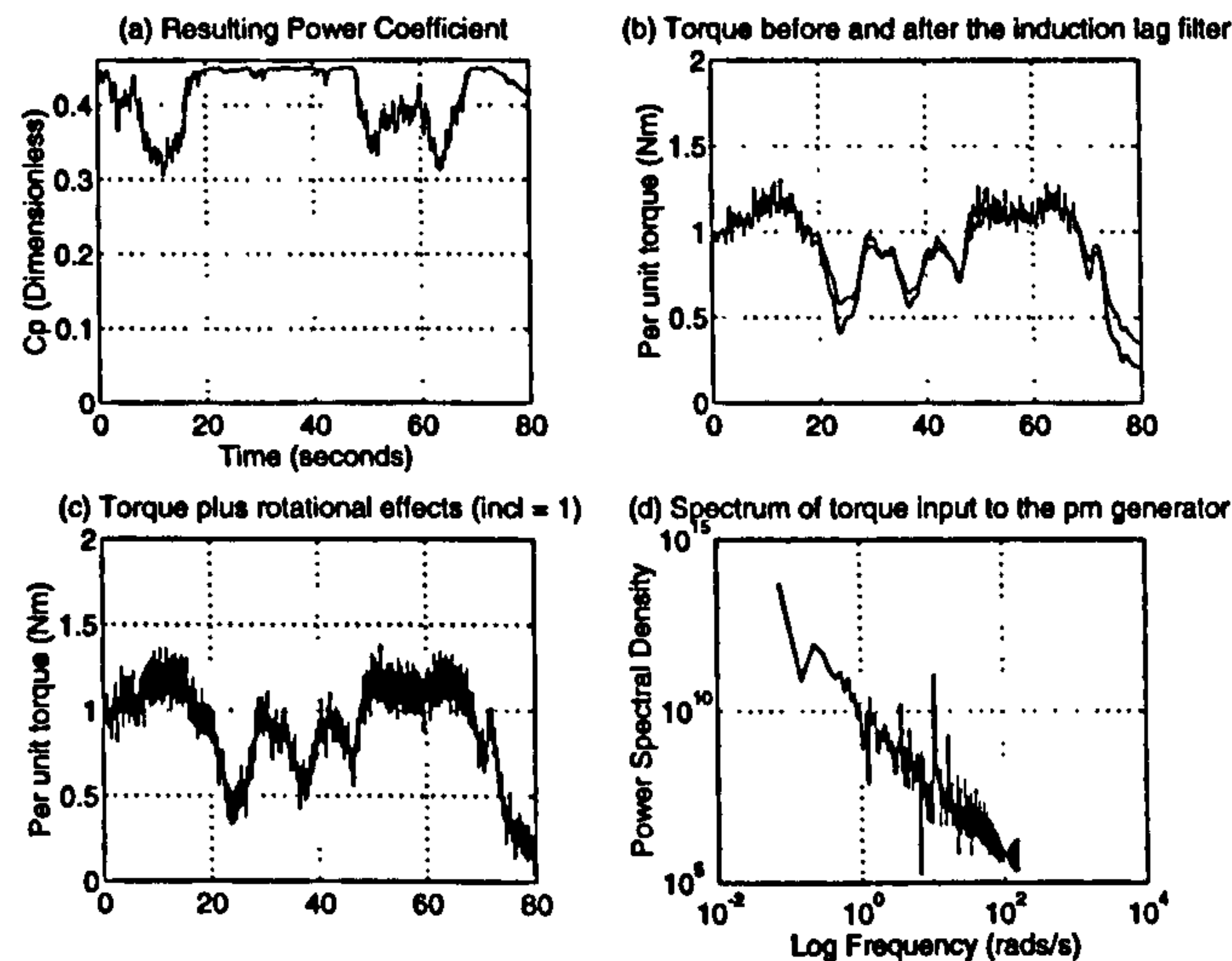


Figure 4.14: The power coefficient and input torque information

the power angle to a change in operating conditions with the maximum deflection of the stator well within the manufacturable range of ± 3 degrees. Figure 4.15 (c) and (d) are included to show that because the output of the generator is assumed to be connected to the infinite bus the rotational speed is fairly constant with a maximum deviation of 0.3 % and therefore the tip speed ratio varies with the inverse of the effective wind speed.

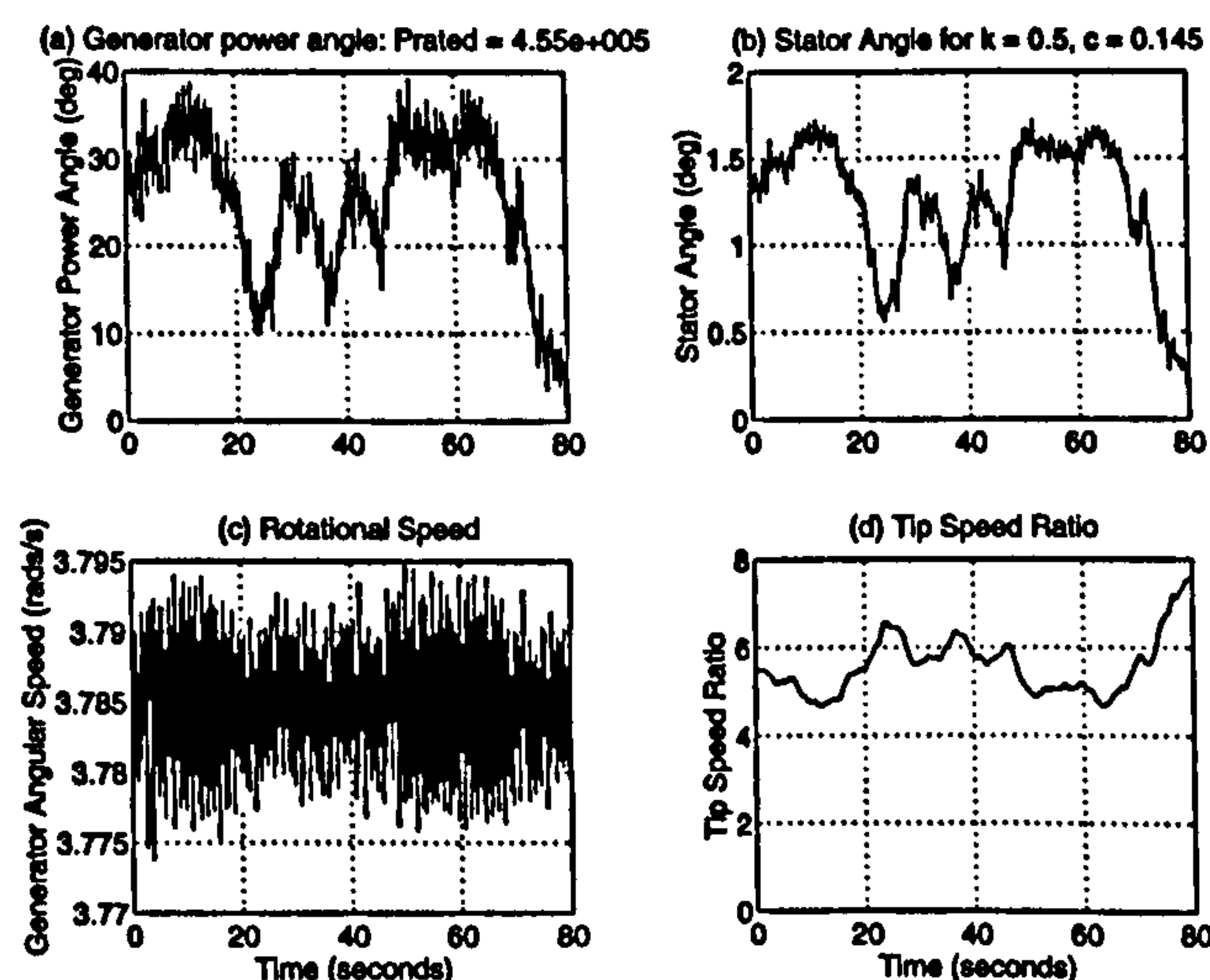


Figure 4.15: The 455 kW rated generator performance

The performance of the pitch controller can be seen in Figure 4.16 (a) to (d). The pitch demand, plot (a), is highly oscillatory because it is derived from a measurement of the power out of the generator which contains oscillations due to the rotational effects induced into the shaft torque by the wind interaction with the blades. These oscillations in pitch

4.4 _____ Response of the 455 kW rated generator to simulated wind data

demand drive the pitch actuator to its limits on acceleration and pitch rate for most of the time and this can be seen in plots (c) and (d). The limits on pitch acceleration and rate do however have a beneficial effect in that the resulting pitch angle is much less oscillatory and this would reduce the amount of fatiguing of the blades and pitch mechanism.

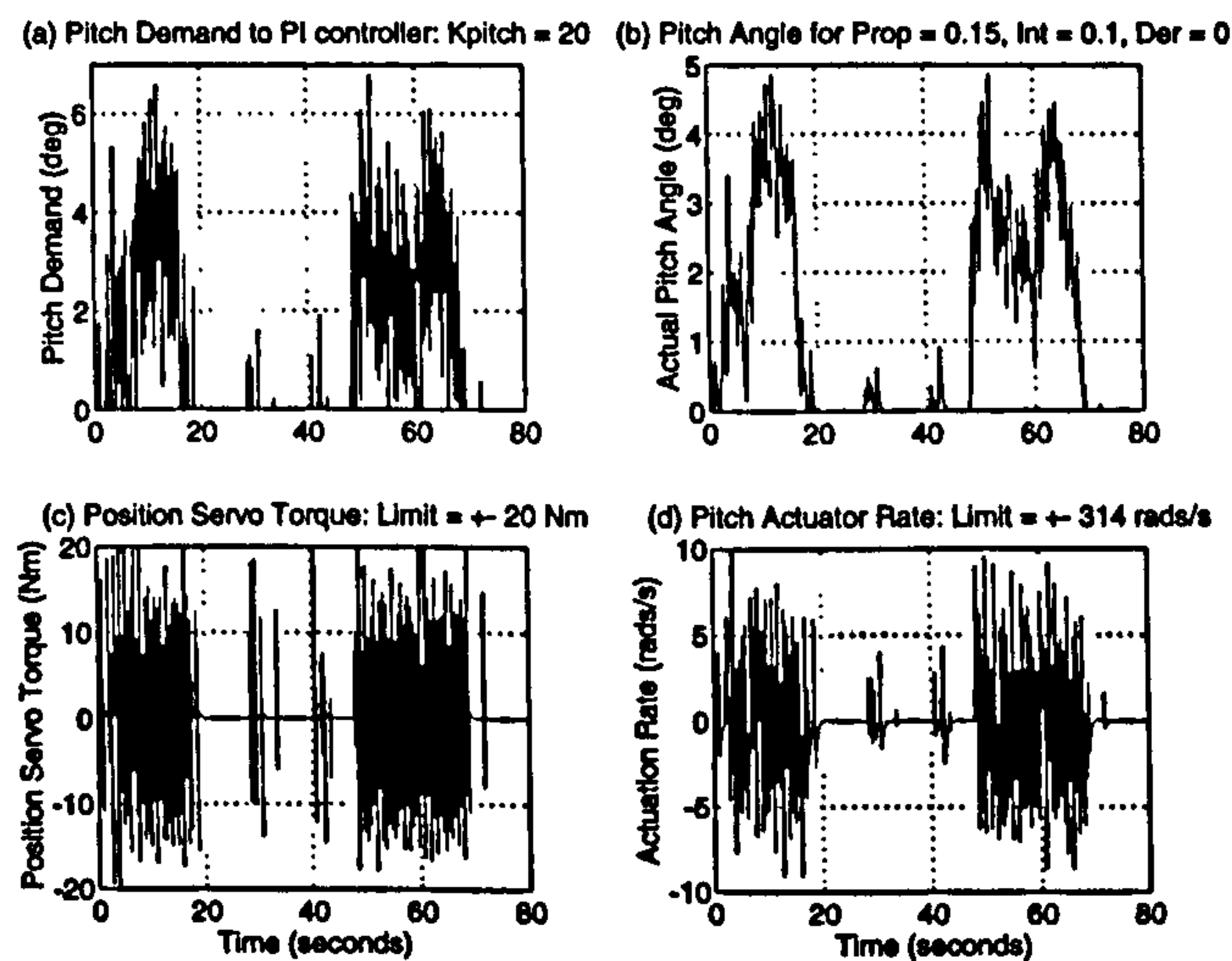


Figure 4.16: The pitch controller performance

The resulting real and reactive power flow into the grid and the voltage regulation can be seen in Figure 4.17. There is no control over the reactive power flow as there is no automatic voltage regulation. However, in this instance, the terminal voltage is maintained at its rated design value of one per unit because of the direct connection to the grid. As the line length increased or the connection became less stiff, i.e. the generator was considered to be an embedded generator in a local distribution network, then this may not be the case and voltage regulation would be an issue.

4.4.2 Above rated wind speed performance

The wind speed time history, its power spectrum, and the run identifiers for this mode of the pitch controller can be seen in Figure 4.18 (a) and (b) respectively. The compliant mounting has the same values as in the previous section.

The resulting power coefficient, aerodynamic torque before and after induction lag, per unit hub torque including rotational effects and the corresponding power spectrum can be seen in Figure 4.19 (a) to (d) respectively. The power coefficient is much reduced when

4.4 _____ Response of the 455 kW rated generator to simulated wind data

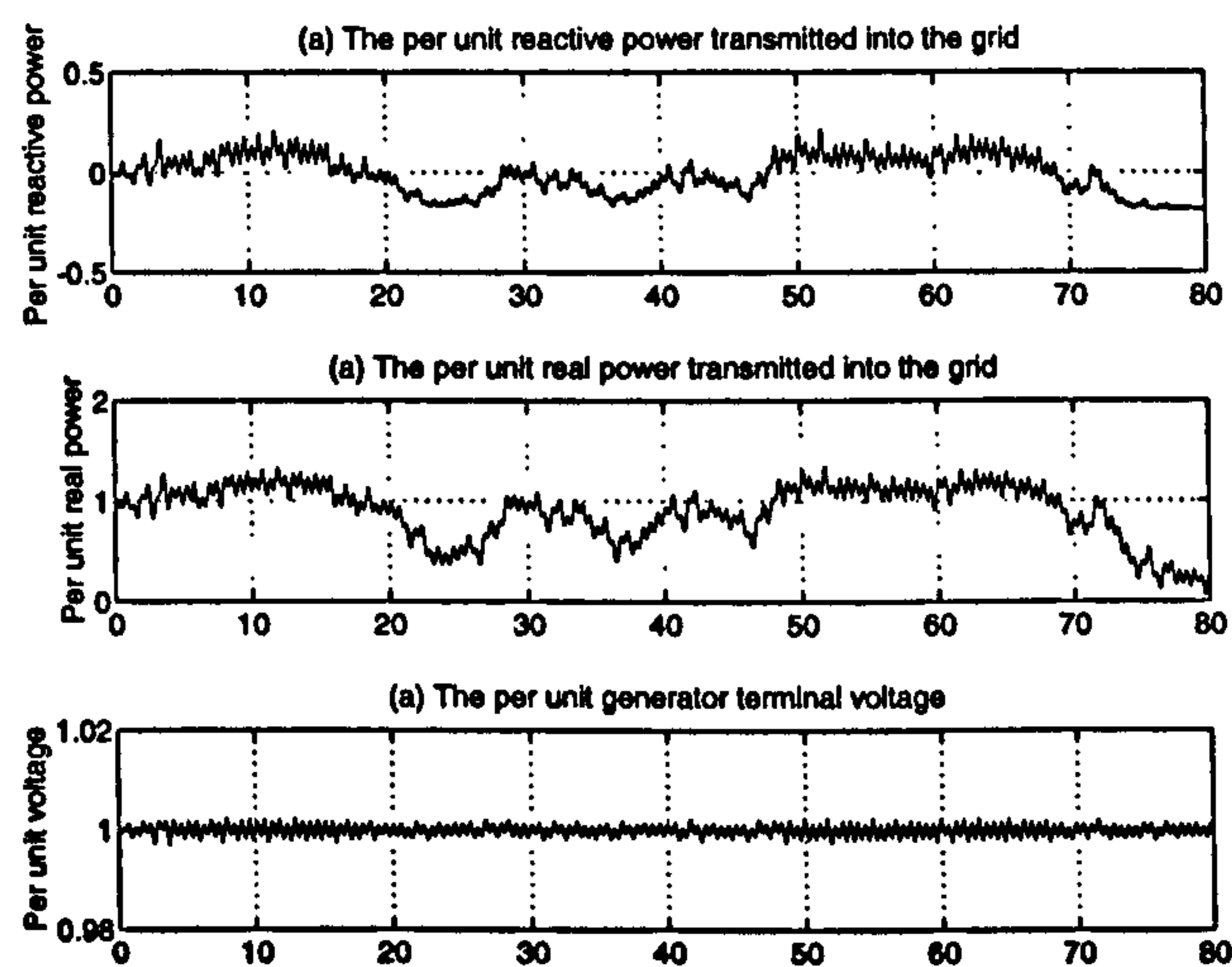


Figure 4.17: The real and reactive power flows and voltage regulation

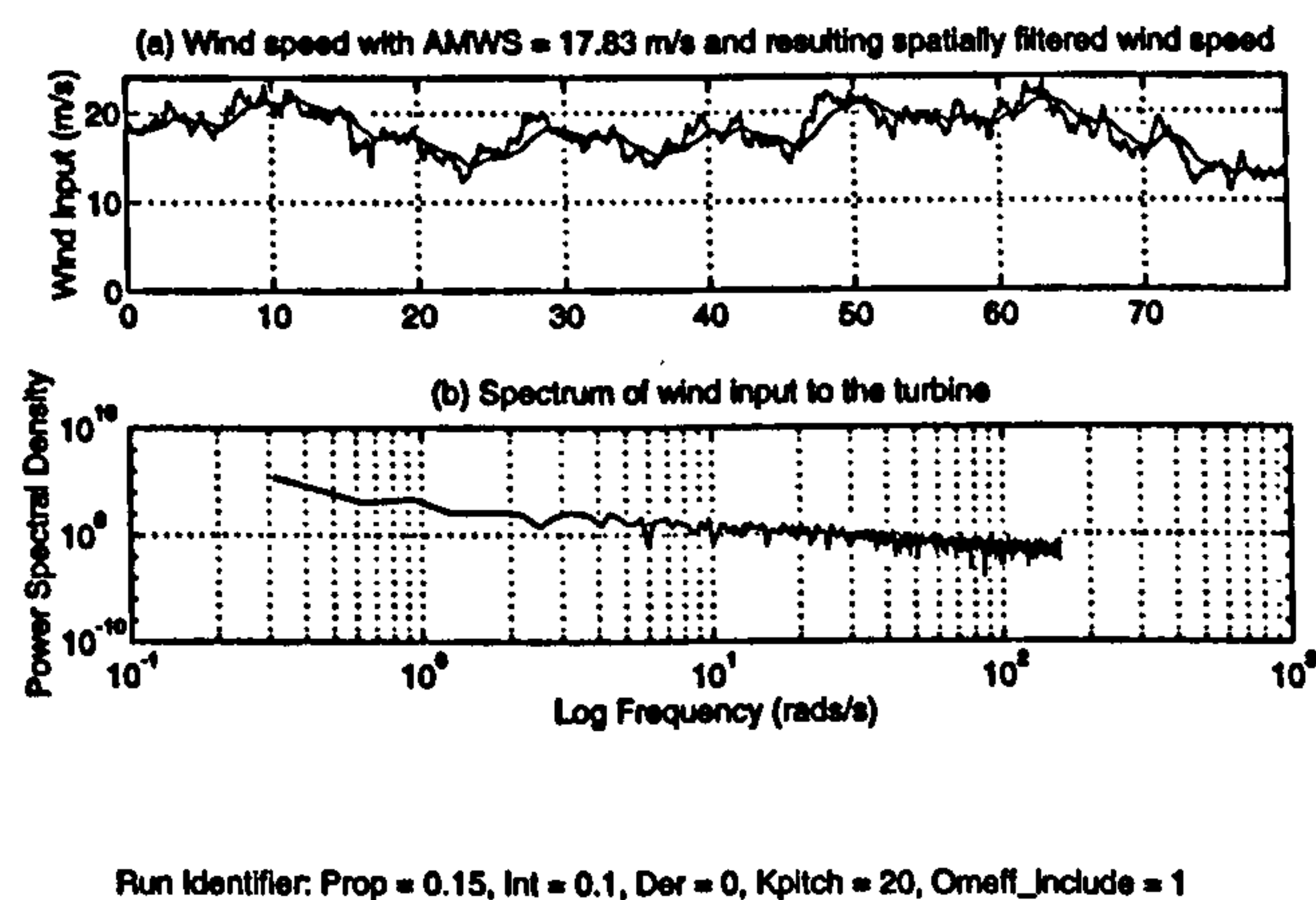


Figure 4.18: Simulated wind speed and the corresponding power spectrum

4.4 _____ Response of the 455 kW rated generator to simulated wind data

compared against the response obtained for the 12 m/s wind speed because of the increased pitch action at this higher wind speed. Again, as there is continual pitch action during this simulation run, the effect of induction lag is difficult to detect because it is swamped by oscillations introduced by the pitching of the blades. The PI controller now limits the peak power output to 45 % above its rated value, which is again consistent with [75].

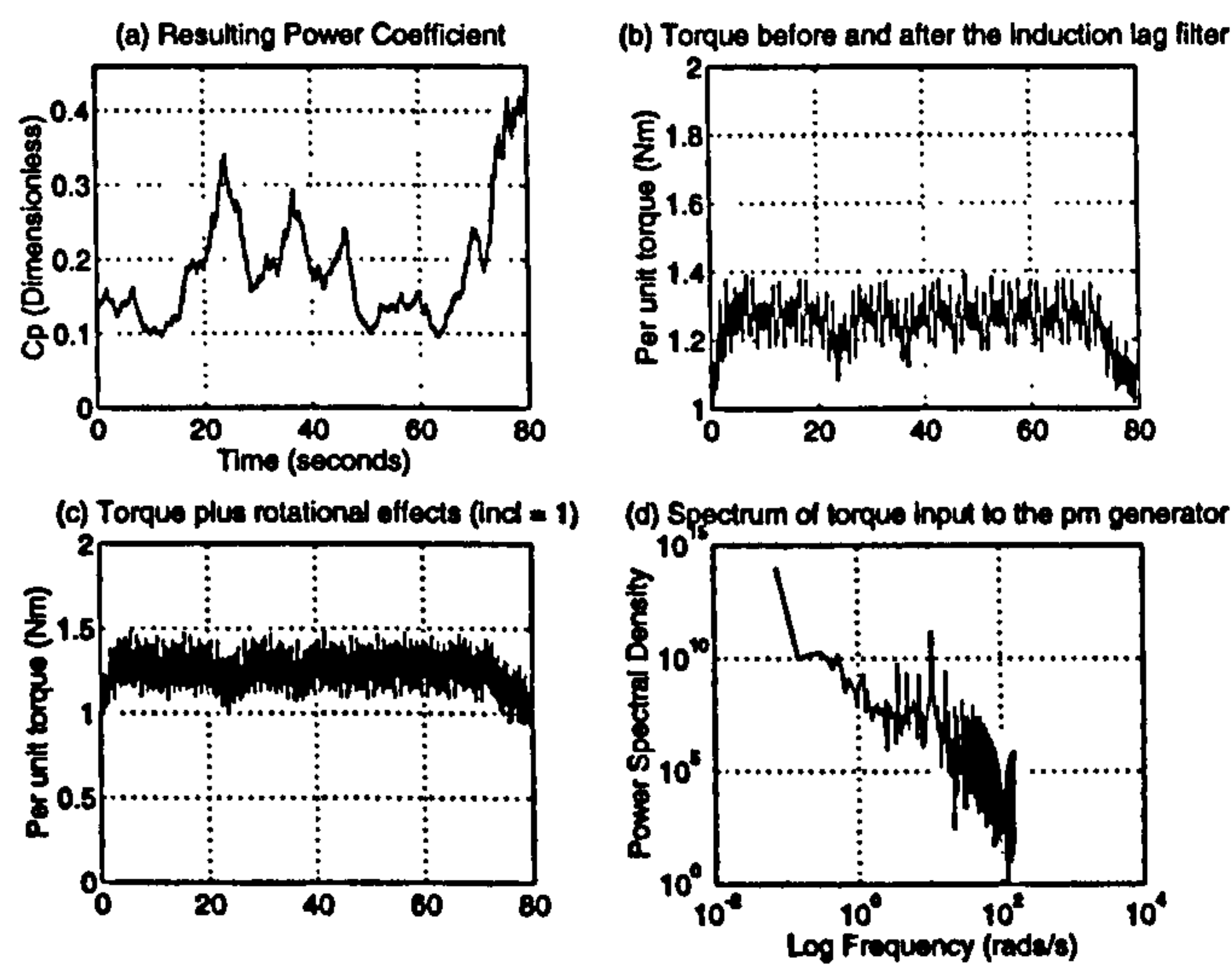


Figure 4.19: The resulting power coefficient and input torque information

The performance of the pitch controller can be seen in Figure 4.20 (a) to (d) respectively. The pitch demand, plot (a), is again highly oscillatory and this is moderated in the pitch angle response, plot (b), by the pitch acceleration and rate limits. The pitch actuator is driven to its limits on acceleration and pitch rate for even more of the time when compared with Figure 4.16 (c) and (d) so as to cope with the increasing strength of the stochastic variations introduced by the rotational effects caused by the turbine blades. The controller values should perhaps be optimised for each wind speed to cope with the non-linear variation of the effect of the pitch angle on the power coefficient [65]. This would lead to consistent peak powers being recorded for each wind speed above rated. However this detailed optimisation of the pitch controller is not crucial to the thesis and so the well designed values for the 12 m/s wind series were used throughout.

4.4.3 Cut out performance

The wind speed time history, its power spectrum, and the run identifiers for this mode of the pitch controller can be seen in Figure 4.21 (a) and (b) respectively. Again all the same

4.4 Response of the 455 kW rated generator to simulated wind data

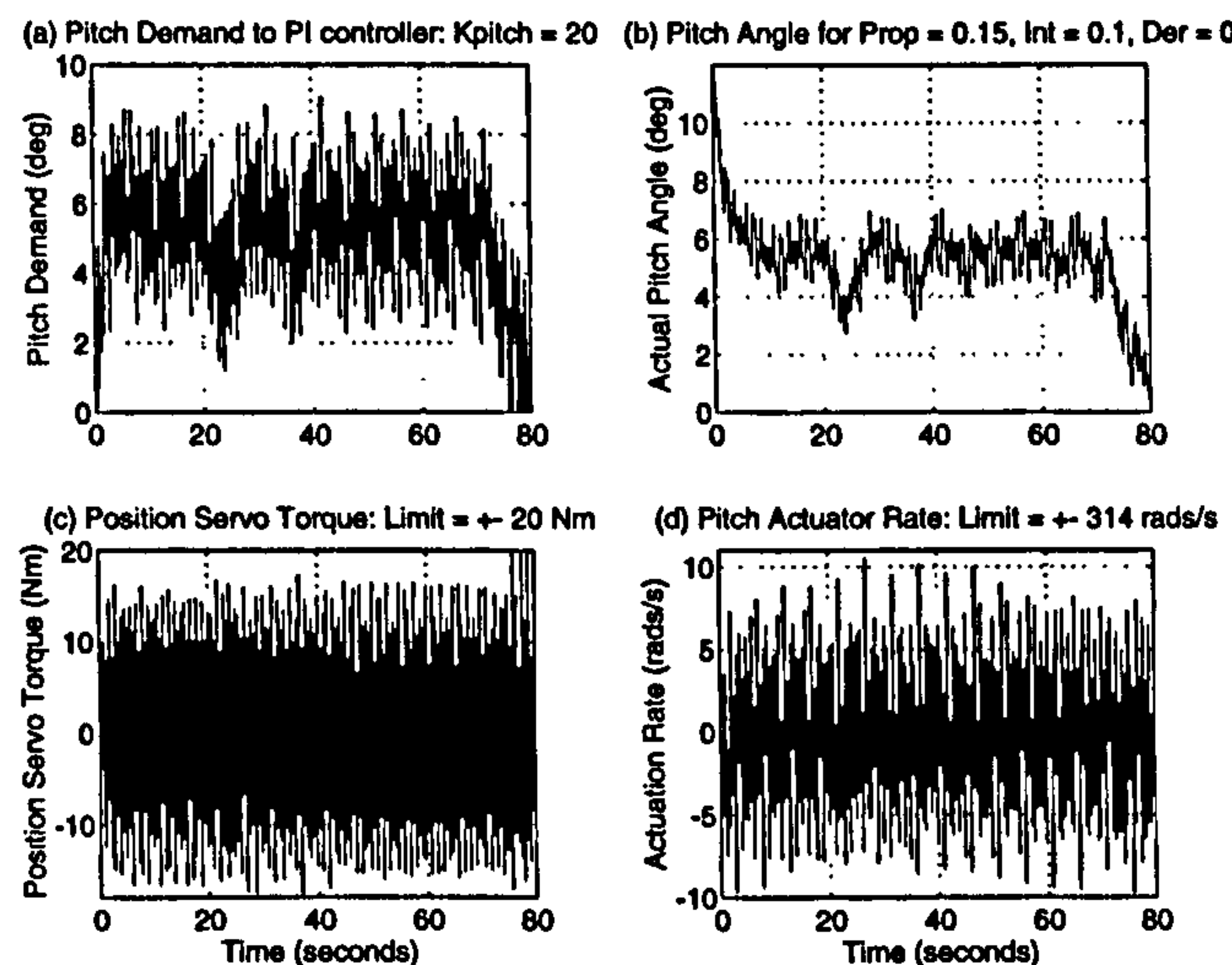


Figure 4.20: The pitch controller performance

values are used for the generator and wind turbine parameters as in the previous sections. The crucial point to note here is that the mean wind speed rises above 25 m/s, the cut-out wind speed, at a simulation time of about 9 seconds and at this point the controller should act to bring the driving torque to zero. If this wind speed persisted a further control action should open the breaker to the grid and allow the turbine to come to a complete stop and the parking brake applied to limit the possibility of damage to the turbine.

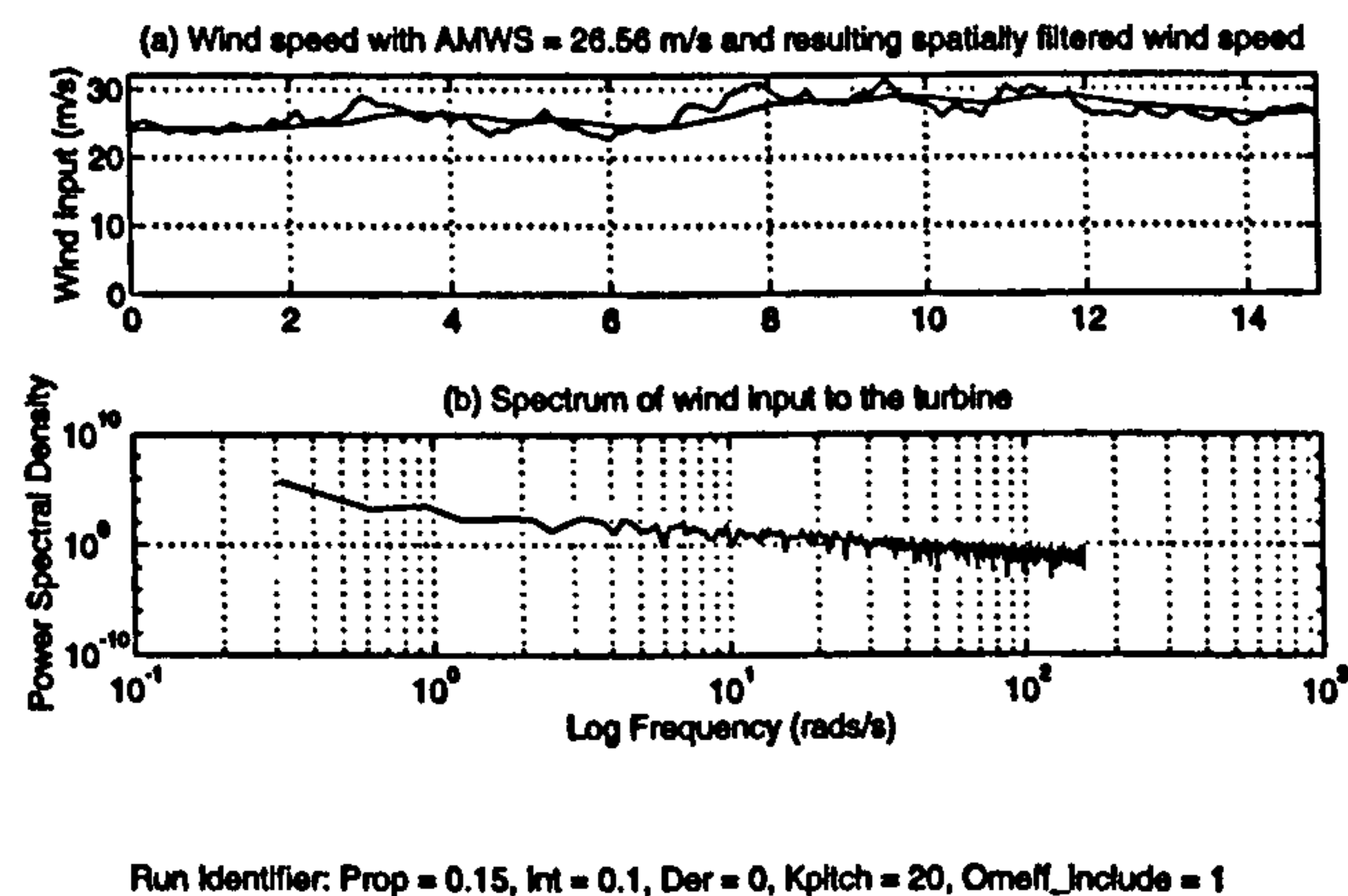


Figure 4.21: Simulated wind speed and the corresponding power spectrum

The performance of the pitch controller can be seen in Figure 4.22 (a) to (d). For the first 9 seconds the pitch rate and acceleration are oscillatory in response to the stochastic variations introduced into the hub torque by the rotation of the wind turbine blades. At a

4.4 _____ Response of the 455 kW rated generator to simulated wind data

time of about 9 seconds the mean wind speed increases above 25 m/s, the cut-out speed, and the fail safe control is activated which sets the pitch demand to 90 degrees, i.e. complete feather. The pitch actuator acts to attain this value within the limits on torque and rate.

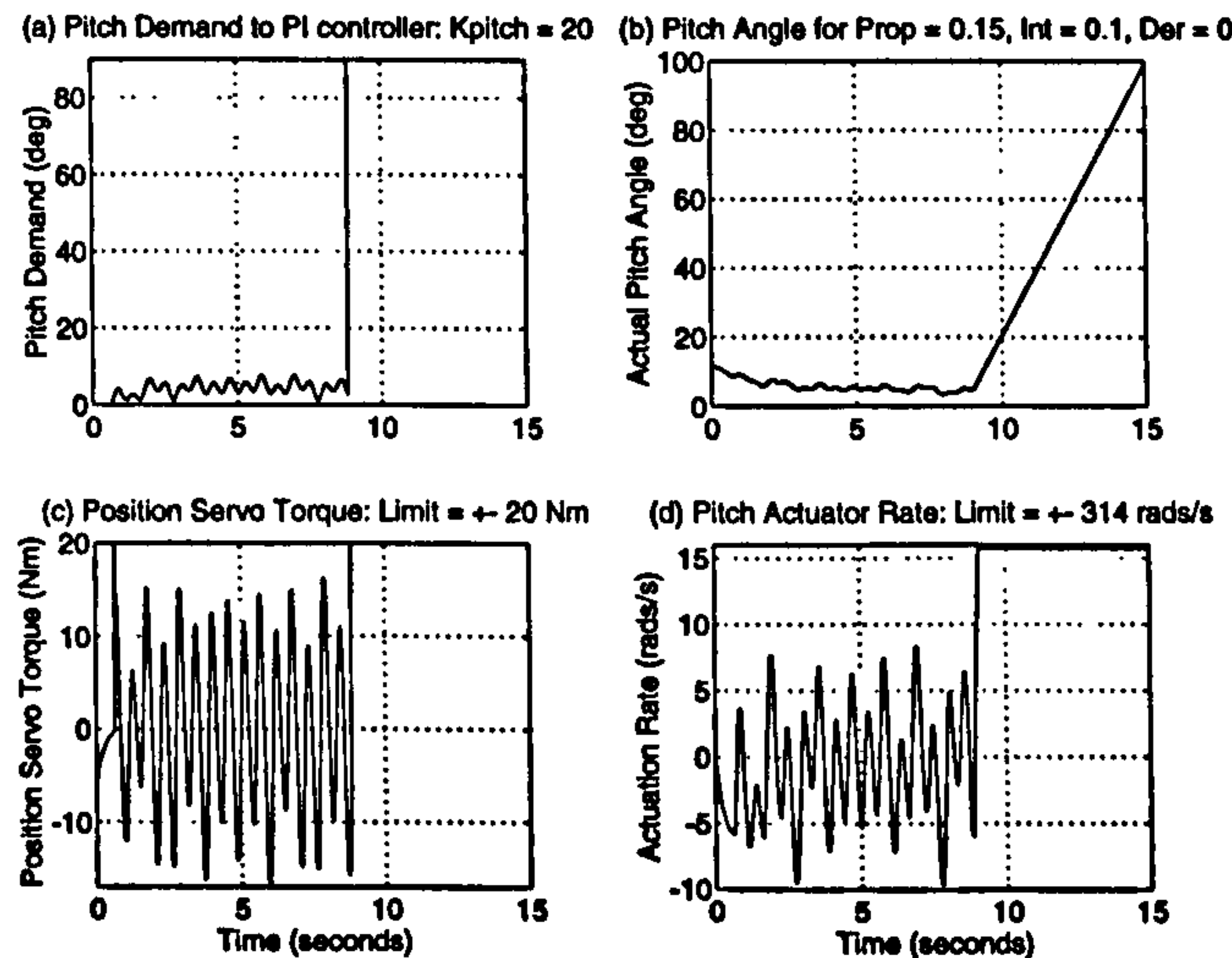


Figure 4.22: The pitch controller performance

The resulting power coefficient, aerodynamic torque before and after induction lag, per unit hub torque including rotational effects and the corresponding power spectrum can be seen in Figure 4.23 (a) to (d) respectively. Once the fail safe control is activated and the pitch angle increases to 90 degrees the power coefficient and torque reduce to zero. The effect of the induction lag on the sudden decrease in aerodynamic driving torque due to this increase in pitch angle leads to a negative overshoot in the post-induction lag torque. The rotational effects are still present in the induced hub torque after the blade pitch has been increased to 90 degrees because the blade is still sampling turbulence and experiencing both blade imbalance and tower shadow effects.

4.4.4 Wind turbine performance with a stiff stator

To demonstrate the effect of the stochastic input of the wind induced shaft torque to a poorly designed compliantly mounted, permanent magnet, synchronous generator a series of simulations were carried out with the spring stiffness, k , set to large values in the range 2 to 10 per unit with the damping coefficient, c , still set to 0.145. This was done for only the first 10 seconds of the 12 m/s time history. The important features to look at are the angular oscillations of the generator power angle and stator angle and the quality of the real

4.4 Response of the 455 kW rated generator to simulated wind data

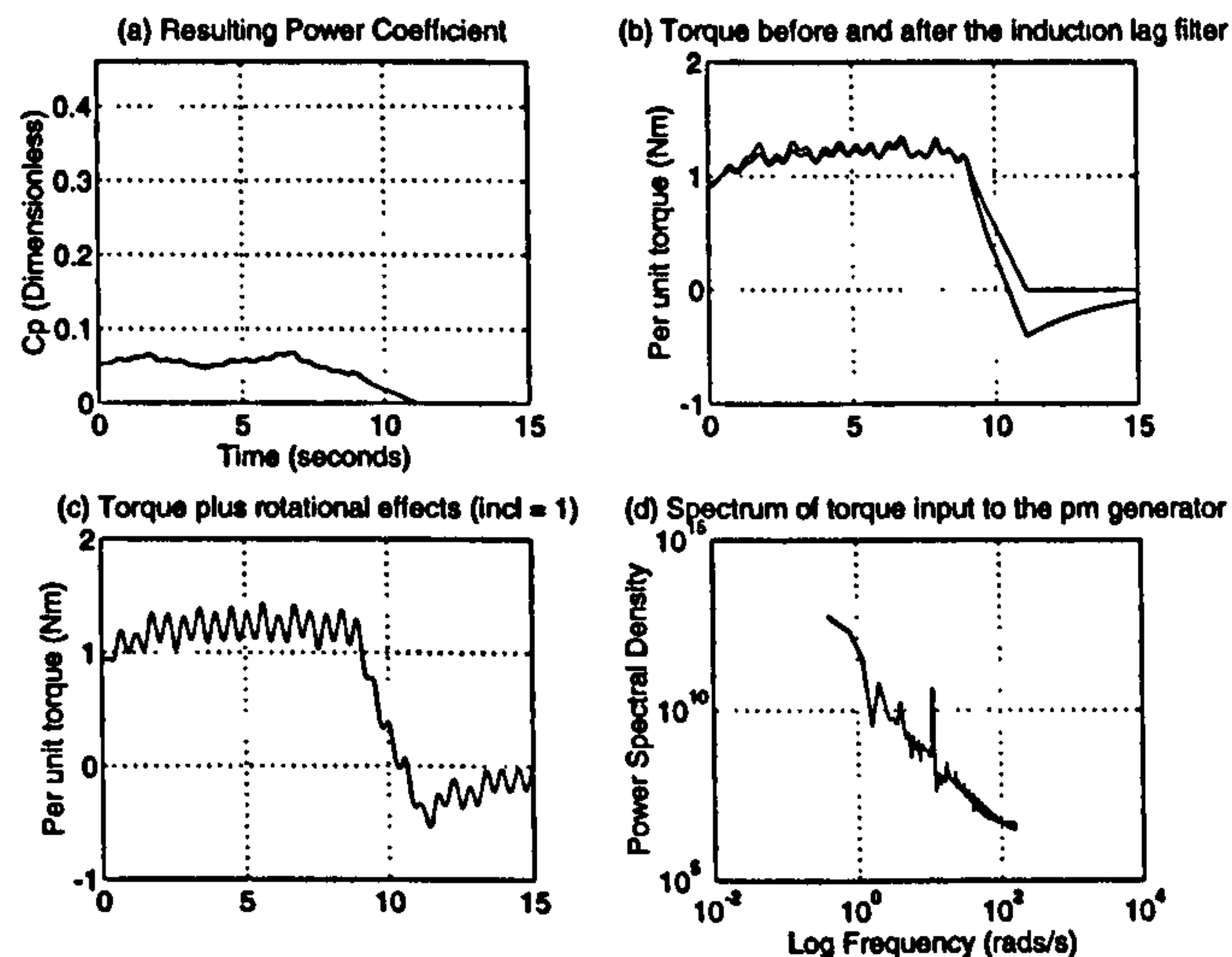


Figure 4.23: The resulting power coefficient and input torque information

and reactive power flow and voltage regulation into the grid. These can be seen in Figure 4.24 (a) and (b) and Figure 4.25 (a) to (c) respectively for the case with $k = 5$ per unit.

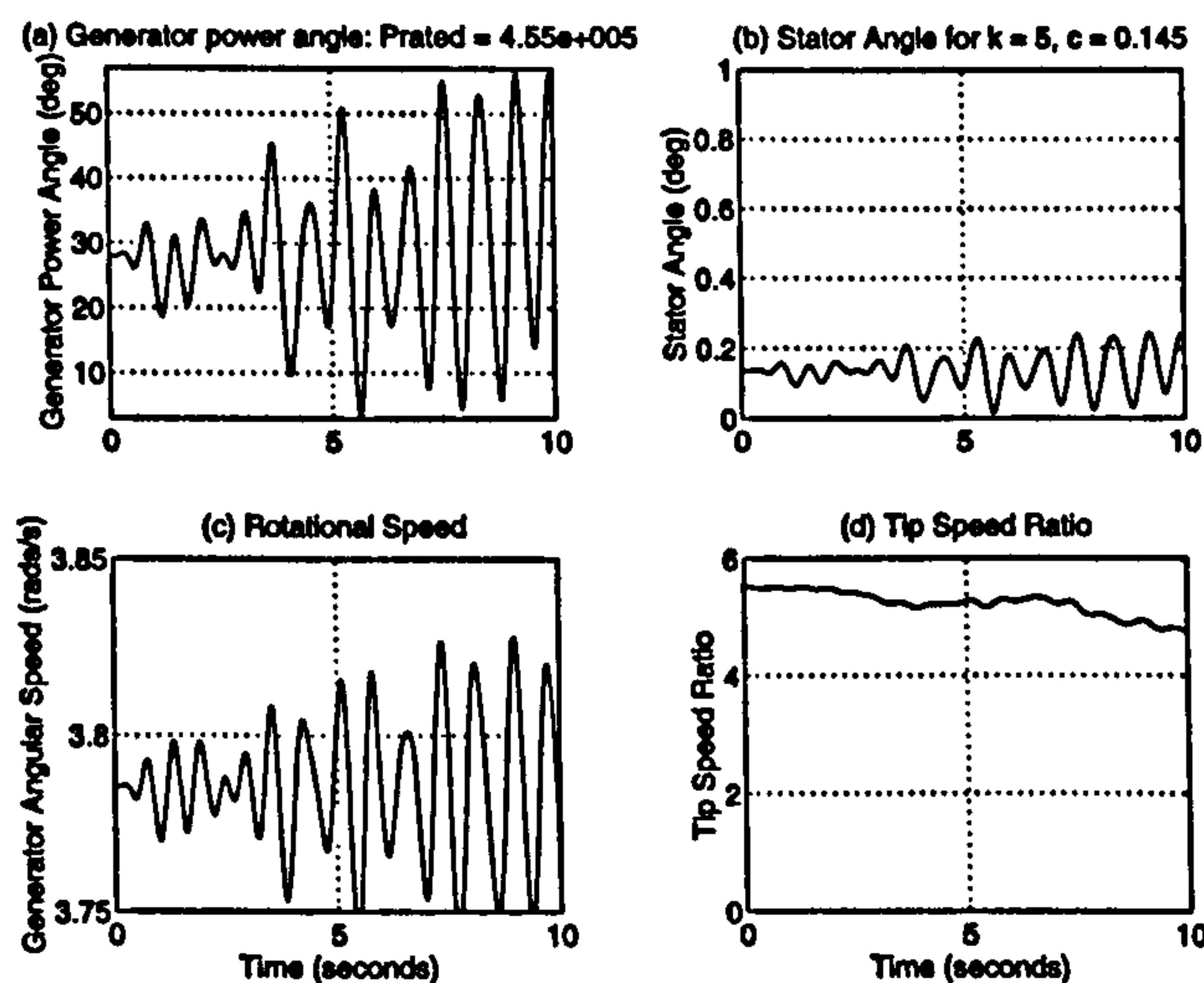


Figure 4.24: The 455 kW rated generator performance

The magnitude of the response of the stator angle is much reduced when compared with the well designed case and there is much less damping of the resulting power angle swings due to the stochastic torque input from the wind. In fact the oscillations of the power angle are dynamically magnified and this leads to unacceptable real power swings against the infinite bus. Looking at the voltage regulation and reactive power flow, the generator terminal voltage is within typical limits for such a grid connected generator, between +6 and -10 % of nominal [93], but if the generator were connected to a weak grid the oscillations could lead

4.4 Response of the 455 kW rated generator to simulated wind data

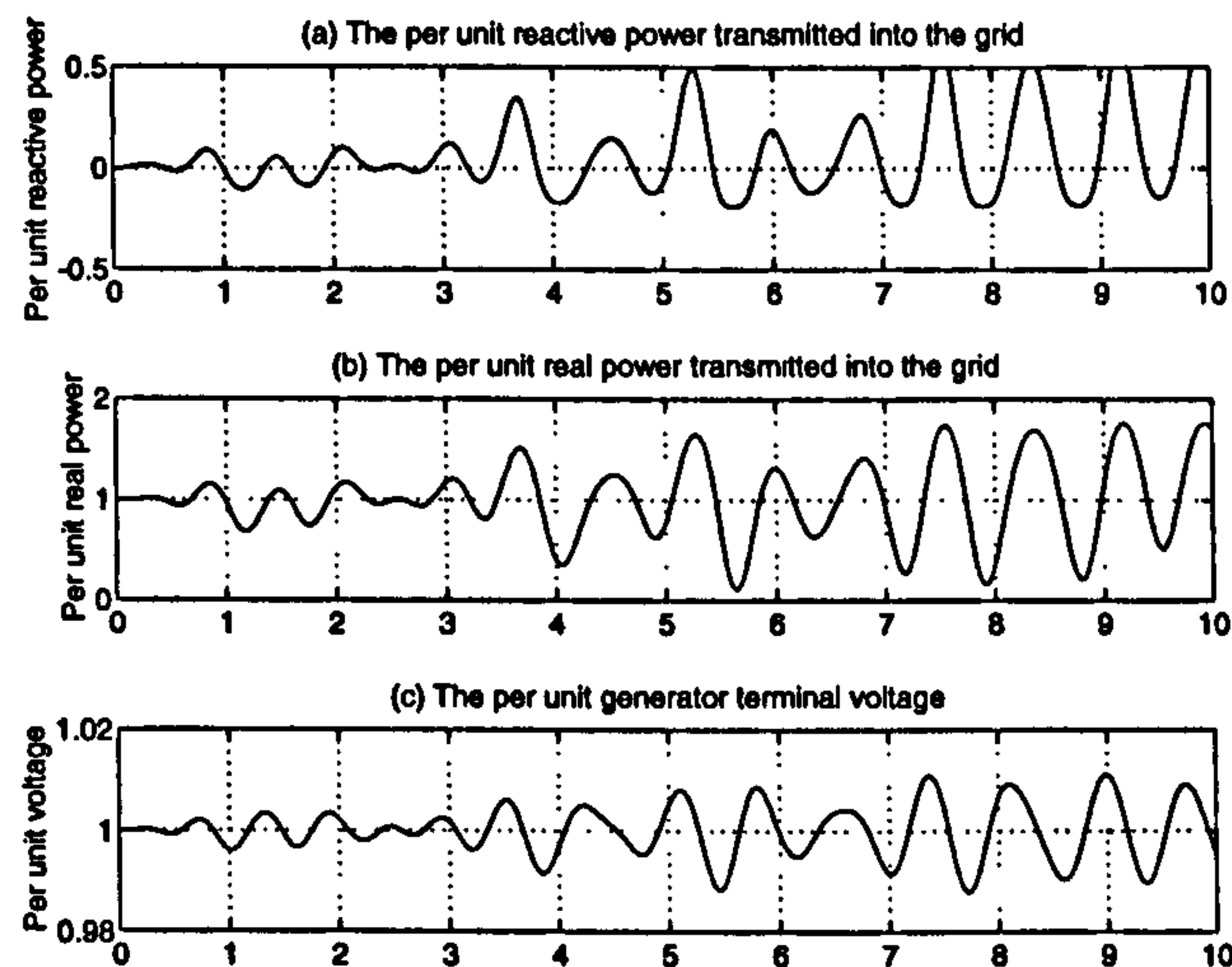


Figure 4.25: The real and reactive power flows and voltage regulation

to unacceptable performance. Certainly if a two tier design generator were used, instead of the three tier design, these large power swings coupled with the larger rated power angle due to the increased reactance could lead to instability. It is therefore important to allow the stator sufficient movement to ensure damping of the machine power angle.

4.4.5 Wind turbine performance with low damping ratio, ζ

The second handle on the design of the compliant mounting is the damping coefficient. To judge whether the design principles stated in section 4.2 are valid for the stochastic response due to the wind the damping coefficient, c , was set to values in the range 0.02 to 0.2 per unit with the spring stiffness, k , set to 0.5. This was done for only the first 10 seconds of the 12 m/s time history. Again the important features to look at are the angular oscillations of the generator power angle and stator angle and the quality of the real and reactive power flow and voltage regulation into the grid. These can be seen in Figure 4.24 (a) and (b) and Figure 4.25 (a) to (c) for the case with $c = 0.05$ per unit which corresponds to $\zeta = 0.018$.

The stator angle response is more oscillatory when compared with the well designed case and there is far less damping of the resulting power angle swings due to the torque input from the wind. The build up of voltage fluctuations would quickly violate the grid connection requirements for embedded generators which states that the variation in terminal voltage must remain between +6 and -10 % of nominal rated voltage [93].

4.4 ——— Response of the 455 kW rated generator to simulated wind data

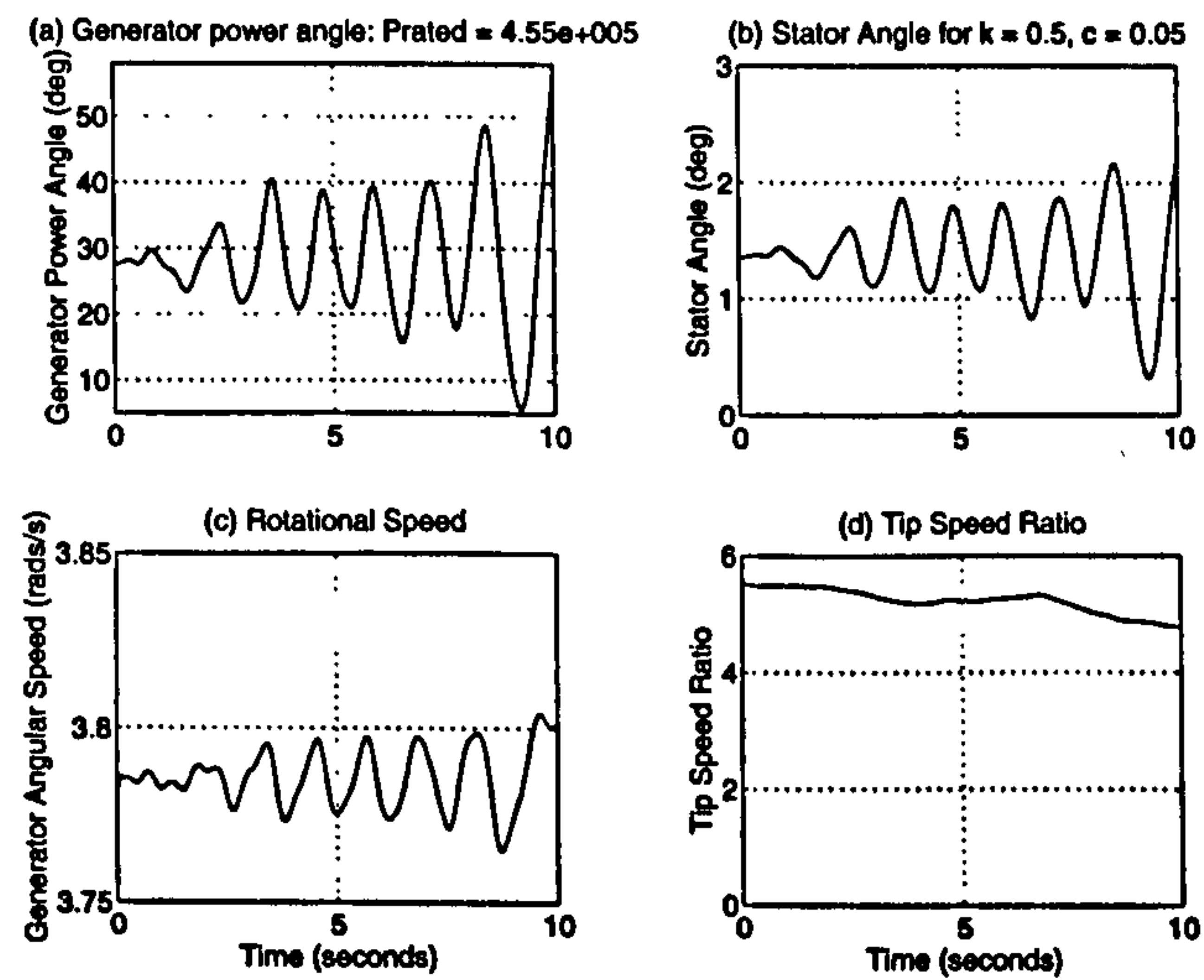


Figure 4.26: The 455 kW rated generator performance

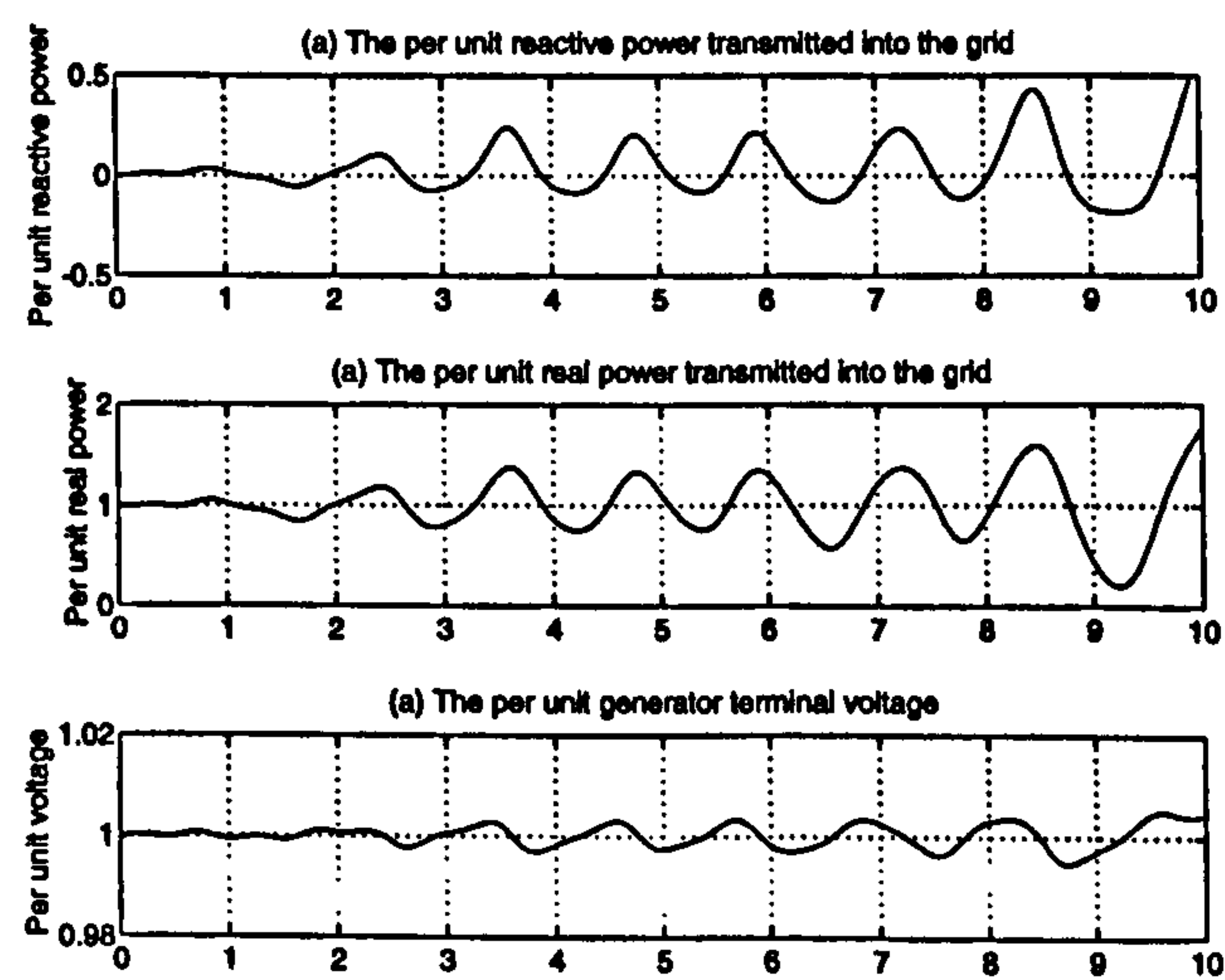


Figure 4.27: The real and reactive power flows and voltage regulation

4.5 Conclusions

This chapter has outlined the performance of a compliantly mounted, permanent magnet, synchronous generator rated at 455 kW and shown that, provided the values of the compliant mounting are matched to the generator design to satisfy the limits imposed by manufacturing and stability constraints, this form of generator is suitable for wind power applications. The focus has been on the performance of a generator rated at 455 kW but the arguments apply to the full range of generators ratings due to the per unit modelling and design strategy. The use of classic design techniques, eigenvalue analysis and step responses, for the compliant mounting have been extended well to the windy environment. A similar level of power limiting is obtained from the permanent magnet generator as for a conventional induction generator plus gearbox arrangement. Furthermore the hypothesis that this kind of permanent magnet generator requires an extra tier than necessary from a consideration of thermal loading alone is borne out by the poor performance of a badly designed compliant mounting in the windy environment. The stiffness and damping ratio selected from the classic techniques translate into good transient performance in the windy environment and therefore the eigenvalue technique is vindicated as a good design procedure for matching the values of the compliant mounting to those of the permanent magnet generator. This concludes the fixed speed section of the thesis and the variable speed modelling of the permanent magnet generator is presented next to determine if this mode of operation will bring cost, weight and performance benefits.

Chapter 5

Modelling a Variable Speed Wind Turbine

As has already been discussed in Chapter 3, direct connection of a fixed speed generator to the wind turbine requires a multi-pole construction with a small pole pitch to fit into a conventional sized nacelle. This leads to a generator design where conventional damper windings are ineffective and for synchronous operation an alternative damping system is required where the stator is mounted compliantly.

The operation of such damping has been discussed in the previous chapters but it is not required if variable speed operation is adopted where the generator voltage is decoupled from the grid via a frequency converter. Furthermore the wind turbine can rotate at a speed appropriate to the actual wind speed. This should result in smoother power flow into the grid, alleviate the mechanical stress throughout the turbine structure, reduce the noise impact and lift the constraint of generating 50 Hz ac [94]. Further design optimisation of the modular permanent magnet generator can then be achieved. A schematic of a representative variable speed configuration can be seen in Figure 5.1.

This chapter introduces the concept of the variable speed operation of the permanent magnet, synchronous generator. Firstly the perceived benefits of such operation, as outlined above, are further elaborated to demonstrate the attractiveness of variable speed operation. Secondly the requirements of a scheme to decouple the generator from the grid and the key features of a suitable control methodology necessary to achieve the perceived benefits

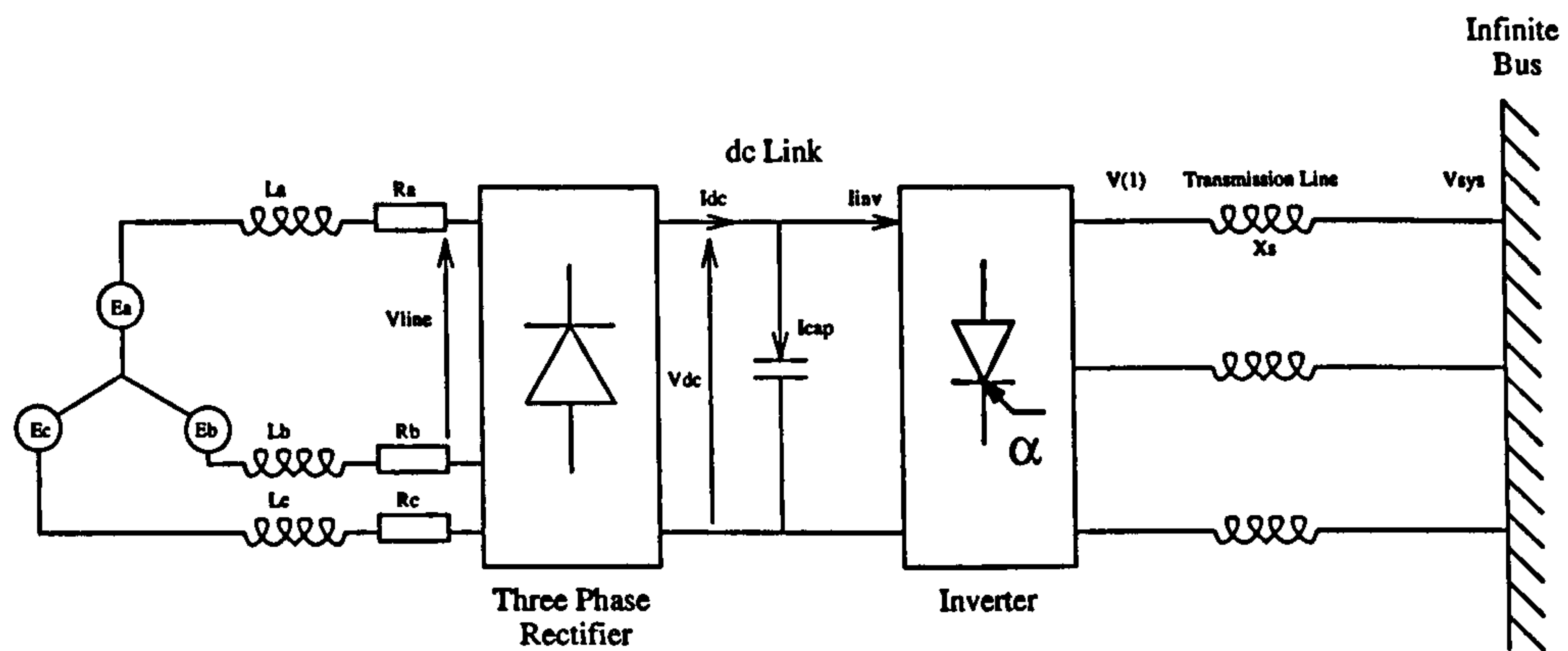


Figure 5.1: Variable speed system configuration

are described. Several schemes exist for decoupling the generator output from the grid to allow the required controlled variations in rotational speed to achieve the basic control aim. Figure 5.1 shows a three phase rectifier and an inverter based on thyristor technology but, for the reasons outlined in section 5.3, a multi-phase rectifier and an inverter using insulated gate bipolar transistor (IGBT) technology is the proposed choice of technology for the frequency converter in this thesis. The reasons for choosing the multi-rectifier and a pulse width modulated (PWM) inverter scheme to control the permanent magnet generator output are discussed. The advantages of such a scheme are presented and the development of suitable simulation models for each of the constituent parts of the scheme is outlined. These models are then pulled together and linked to the models presented in Chapter 2 to create the simulation model of a variable speed, wind turbine driven, permanent magnet generator. Finally a discussion is presented on the derivation of further control strategies for both matching the power input characteristic of the wind turbine blades to the power output transfer of the generator, rectifier and inverter and balancing the requirements for grid connection. These control strategies allow the full potential advantages of variable speed operation to be realised.

5.1 The advantages of variable speed operation

Typically variable speed turbines have small ($\pm 5\%$), medium ($\pm 25\%$) or full unrestricted speed operation. As described previously the wind turbine blades will either be stall regulated or have pitch control to limit the power above rated windspeed and the following discussion applies to a typical three blade pitch regulated wind turbine with full unrestricted

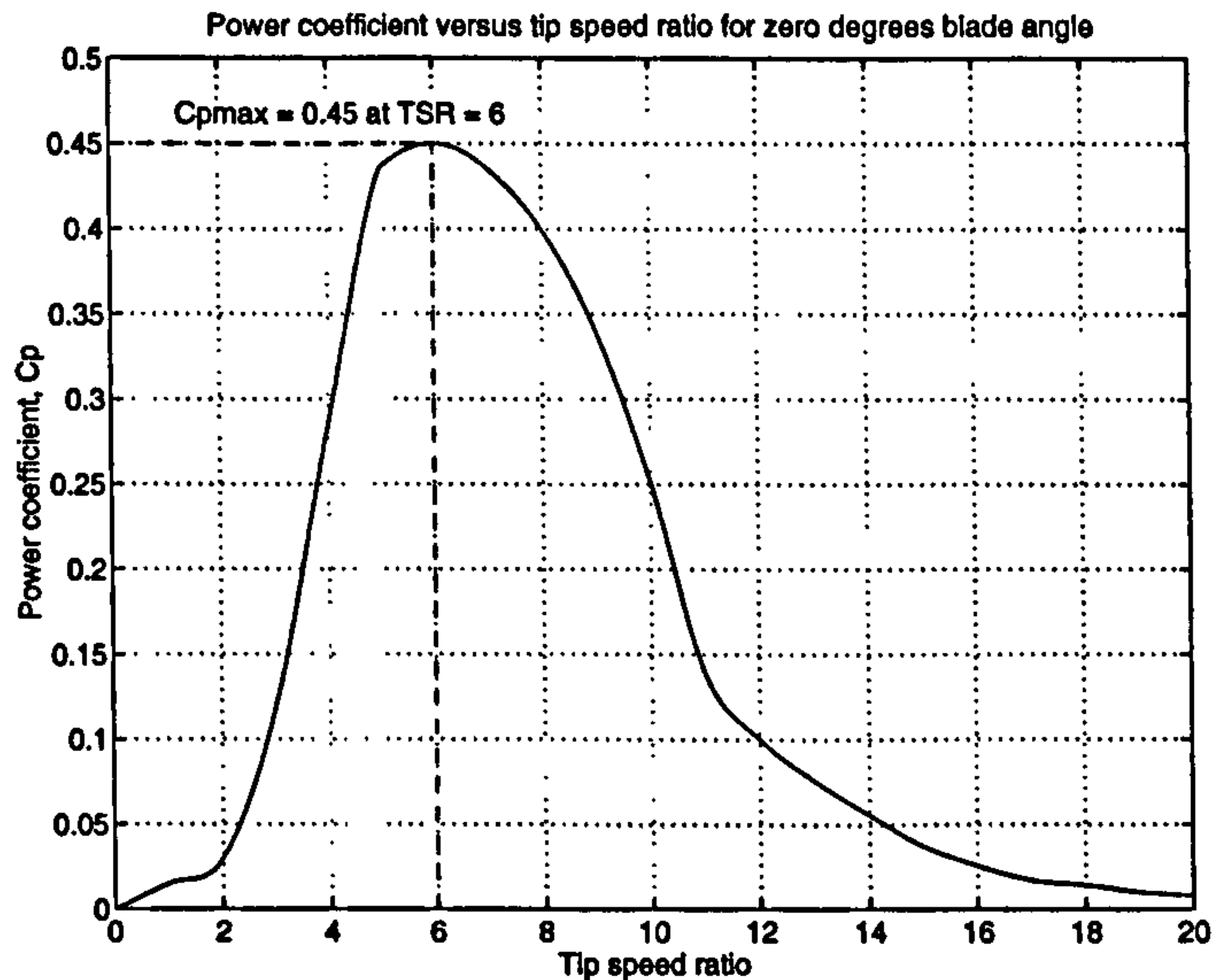


Figure 5.2: C_p versus tip speed ratio for zero degrees blade pitch

speed operation.

5.1.1 Energy capture from variable speed control

The first advantage of variable speed operation of a wind turbine is the greater energy capture by the wind turbine blades because of the ability to alter the rotor speed by some suitable frequency converter arrangement and control strategy. This control strategy should be designed to track the required tip speed ratio to keep the blades operating at the maximum power coefficient, C_{pmax} . A plot of the power coefficient showing C_{pmax} can be seen in Figure 5.2.

The C_p curve has a peak at only one ratio of windspeed and blade angular speed - C_{pmax} typically occurs at a tip speed ratio of six. If the rotor speed could be controlled so that as the windspeed varies the tip speed ratio was maintained at this value then the energy capture by the wind turbine blades would be a maximum. An analysis of the energy capture of a fixed and variable speed wind turbine can be carried out using the Raleigh distribution and C_p curves introduced in section 2.1.1 .

The Raleigh distribution, shown in Figure 2.2, gives the probability that the wind speed will exceed a given value, in this case 8 m/s. This can be used to obtain the cumulative hours a turbine will experience any wind speed. For a fixed speed wind turbine operating below

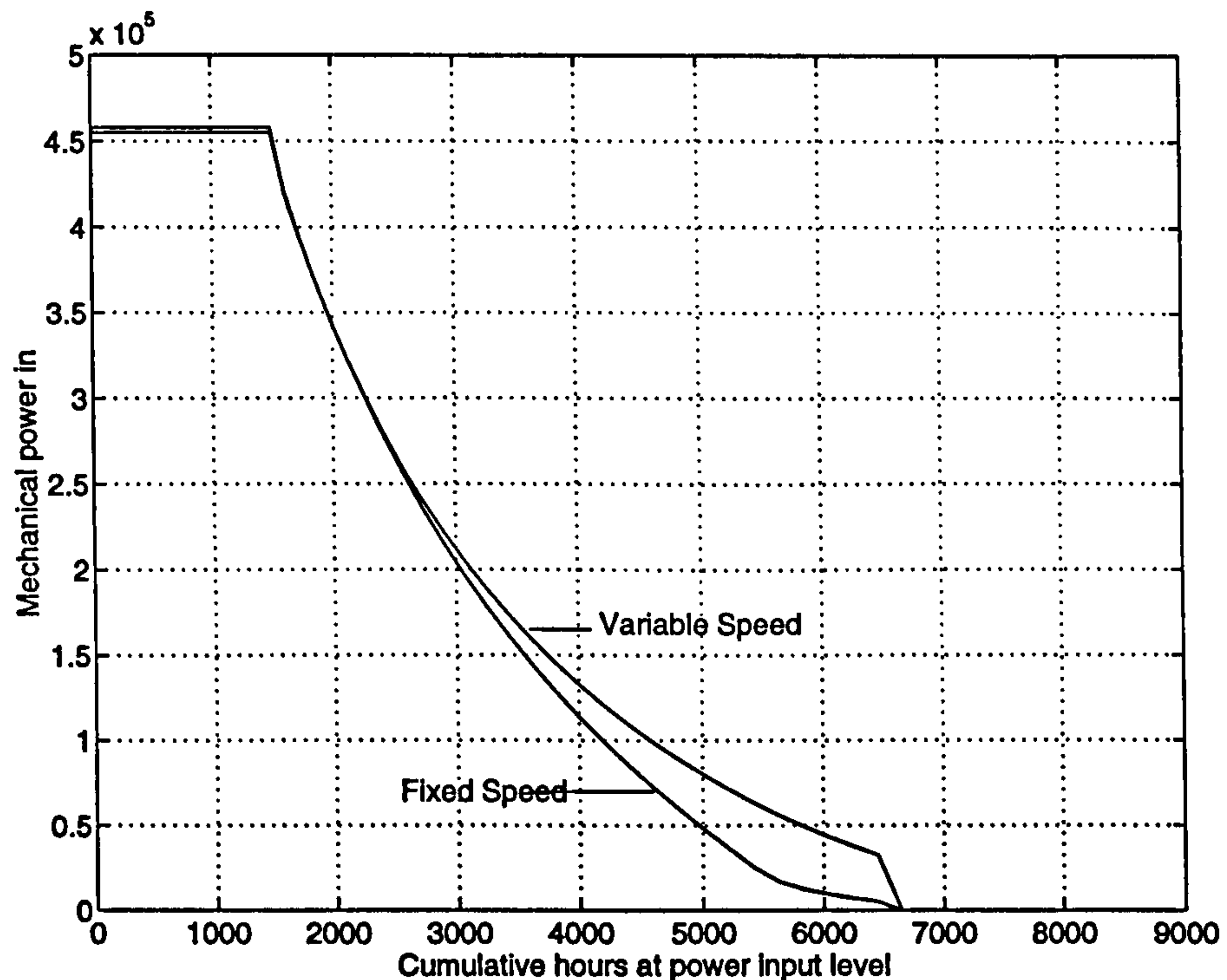


Figure 5.3: Power output versus cumulative hours at that power level

rated windspeed the resulting power is given by equation 2.8 where C_p is determined from the value of tip speed ratio, which is only at its maximum value for one value of wind speed, and assuming the blade is at zero pitch. Power limiting above the rated windspeed, 12 m/s, is assumed to be that of an ideal pitch controller. This leads to the graph of mechanical power input to a fixed speed 455 kW permanent magnet, synchronous generator against the cumulative hours the wind turbine operates at that level during the year shown in Figure 5.3. The total cumulative number of hours in a year is 8760 and the turbine does not operate for every hour of the year because of periods where the wind speed is above the cut-out wind speed, 25 m/s, or below the cut-in wind speed, 5 m/s.

For the variable speed case, below rated windspeed, it is assumed that the turbine has an ideal control response and therefore is always operated at C_{pmax} . Again for above rated wind speed conditions power limiting is assumed to be ideal. This leads to the power input to the variable speed 455 kW permanent magnet, synchronous generator against the cumulative hours the wind turbine operates at that level during the year.

Clearly the variable speed wind turbine operates at higher power levels because of the ability to remain at C_{pmax} . Integrating the area under the graph gives the energy capture over

5.1 --- The advantages of variable speed operation

the year. A comparison of the theoretical maximum energy capture for the variable versus the fixed speed 455 kW rated wind turbine can be seen in Table 5.1 and shows that for the aerofoil assumed in this thesis there is a maximum theoretical increase of about 7 % in energy capture if variable speed operation is used. This is only a theoretical maximum as the requirement to track the C_p curve for C_{pmax} in a turbulent windy environment leads to a reduction in this figure. The engineering challenge is to derive and simulate a cost effective control strategy that minimises this reduction. This is outlined in section 5.2.

Variable Speed	1511 MWhr
Fixed Speed	1411 MWhr
Percent Increase	7.1 %

Table 5.1: Energy capture comparison between fixed and variable speed operation

5.1.2 Power Quality

The second and key advantage of variable speed operation will be the enhanced quality of the power flowing into the grid. Although the output voltage and current of inverters can have a high level of harmonic distortion this can be controlled and the ability to absorb energy in the rotor blade means there will not be such excessive power swings into the grid which would make voltage control difficult. Furthermore the control of the inverter allows the fundamental component of the terminal voltage to be altered and this means that it will be possible to control the reactive power independently of real power flow. For the fixed speed case the terminal voltage of the generator is fixed, as the field and rotational speed are almost constant, and the level of reactive power is purely determined from the state of the system. Several inverters and control methodologies are outlined in sections 5.3.9 to 5.3.13 and results of a thorough investigation presented in chapter 6 for the chosen PWM inverter.

5.1.3 Generator design

The third advantage of variable speed control is also important as it leads to a considerable reduction in the weight of the generator over the fixed speed case. The generator design mentioned in Chapter 3 for the fixed speed design of generator describes a modular arrangement of a large number of separate stator E-cores. This allows a machine of any

5.1 _____ The advantages of variable speed operation

specification to be made from a simple set of module designs using the same set of simple tooling. Matching the design of the generator to the wind turbine is still the same for the variable speed case but there are two key differences between the fixed speed generator design and the design for variable speed operation. Firstly, for the variable speed generator the number of tiers necessary for the dynamic performance of the generator is reduced when compared with the fixed speed case for there is no need to balance the design of the compliant mounting to a suitable level of synchronous reactance. In fact the variable machine design typically has one to two less rotor tiers than the fixed speed case in turbines rated from 200 kW upwards. Secondly the generator does not need to be designed for 50 Hz operation and redesign of the generator is possible. These two ideas are now expanded.

LOW TIER NUMBER. The key benefit of losing the requirement for a compliant mounting is a reduction in the number of tiers as the limit on reducing the number of tiers is now dependent only on the allowable electric loading. In fact, providing the same configuration of rotor module is retained, the variable speed generator typically has one less rotor tier than the fixed speed case in turbines rated from 200 kW upwards. This is illustrated in Figure 5.4 which shows the material costs of building a 455 kW permanent magnet generator as the mode of operation changes from variable to fixed speed at 50 Hz. Clearly the 455 kW variable speed generator would have about a 33 % saving in material costs when compared with the fixed speed case. This cost saving could be used to offset the additional cost of the frequency converter.

DESIGN FREQUENCY. The generator does not need to be designed for 50 Hz operation and redesign of the generator is possible. Figure 5.4 also shows the material costs of building a variable speed 455 kW permanent magnet generator as the design frequency varies. The frequency cannot be reduced too far as the power transfer capability of the tuning circuit, introduced in section 5.3.5, depends to a large extent on the frequency of the generated E-core voltage which is dependent on the designed number of pole pairs for a given rated rotor speed. Increasing the design frequency requires a higher pole number and therefore a heavier rotor but less windings are required per stator E-core to provide the same rated voltage. Therefore a trade off exists between stator and rotor weight as the design frequency increases. There is one further constraint on increasing the design frequency and that is the size of the standard nacelle which is typically of the order 5-10 % of the diameter of the blades. The results indicate that 55 Hz is a good design frequency for the 455 kW

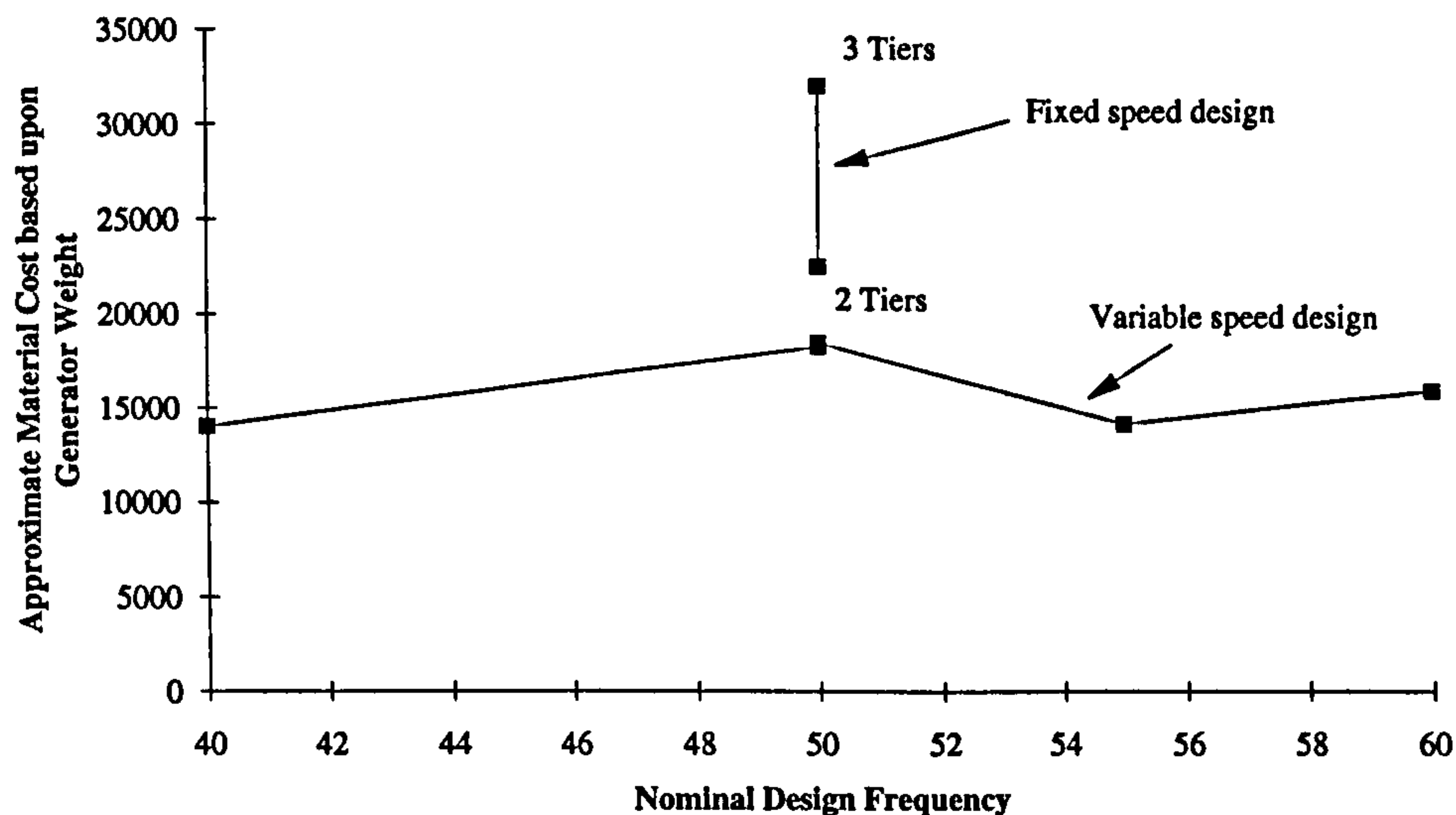


Figure 5.4: Material Costs versus frequency and control scheme

rated generator and is used for all subsequent variable speed generator designs. However equation 3.3 indicates that the power out of a generator is dependent on frequency as well as physical size, achievable magnetic flux density and stator electric loading. Thus increasing the frequency to a much higher value, say 200 Hz, may have an interesting effect on the design. However to achieve 200 Hz operation without reintroducing a gearbox would require about 4 times the number of poles for the low rotational speed of the wind driven rotor. To keep the same rotor diameter, the pole pitch would have to be reduced proportionally and this could lead to constructional difficulties. Whether this could be achieved or not is beyond the scope of this thesis.

FURTHER DESIGN MODIFICATIONS. The preceding argument is based on generator designs with rotor modules comprising two standard $25 \times 100 \times 150$ mm ferrite magnets blocks with flux concentrating pole pieces per module as described in Chapter 3. This design was shown to be well suited to the fixed speed case. When considering the variable speed operation of the generator, further fundamental design modifications can be made to the rotor by altering the number of standard industrial magnet blocks used in each module. For example, doubling the width of the module from one to two magnet blocks would result in a more powerful airgap flux density which would allow a larger airgap to be used for the same rating of generator. A larger airgap would allow greater tolerances to be withstood by the stator support structure and could lead to substantial material cost savings. However the number of poles would decrease for the same diameter of generator

5.2 _____ Realising the advantages of variable speed operation

and hence the frequency of generation would be lower for the same rated rotational speed. For this thesis, the iterations in the design process necessary to understand the performance of such a different generator design is not considered. The standard fixed speed design is, therefore, retained as the basis for the variable speed permanent magnet generator. The model of the variable speed wind turbine, presented in section 5.3, can, however, cater for a generator with a different rotor design: the only change being to alter the power transfer characteristic of the generator and rectifier unit and the calculated rotor inertia. Matching the generator design to the frequency converter is still important and this is outlined in more detail in sections 5.2 and 5.3.

5.1.4 Further advantages

Two further advantages exist for variable speed operation yet their benefits are difficult to quantify. Allowing the wind turbine to rotate at a speed appropriate to the windspeed means that the aerodynamic noise over and above the ambient wind noise is less when compared with the noise generated by the fixed speed case, i.e. at low windspeeds the turbine blades can rotate at a lower speed than for the fixed speed case thus generating less aerodynamic noise [95]. Secondly the ability of the rotor blades to accelerate and absorb some of the power within a wind gust means tower and blade structural design can be optimised. However the variable frequency of operation may mean that structural vibrational modes may be excited and this must be avoided [94].

5.2 Realising the advantages of variable speed operation

The case for variable speed operation over the fixed speed case has been outlined in the previous section in terms of increased energy capture, enhanced power quality, lighter cheaper generators and other more indeterminable advantages. Clearly the inclusion of a frequency converter is key to the variable speed operation of a permanent magnet generator but what is not clear is will the added cost of the rectifier and inverter outweigh the realisable benefits? The implications of this question and the problems associated with realising the benefits of variable speed operation need to be understood and their impact on the design drivers outlined.

5.2 _____ Realising the advantages of variable speed operation

5.2.1 Tracking the C_p curve for C_{pmax}

Ignoring any structural resonance problems, an operational strategy can be found for a pitch regulated turbine by controlling the generator reaction torque using variable speed operation below rated windspeed and pitch control for power limiting above rated windspeed [94]. Below rated speed the aim is to maximize the energy capture by adjusting the rotor speed to keep the optimal tip speed ratio and hence track the C_{pmax} curve, a to b on Figure 5.5. The curves on Figure 5.5 are derived from the C_P curve shown in Figure 5.2 and the equation for the power in the wind, equation 2.8. Instead of plotting the C_P curve against the tip speed ratio, each curve of Figure 5.5 is the power calculated from equation 2.8 at a constant wind speed plotted against rotor speed. For each windspeed, C_p , and hence the power out, is a maximum at only one ratio of windspeed to rotor speed. Above rated speed the pitch angle is controlled to limit the power out and, depending on the performance of the pitch controller, the generator operates at point b. For the case of a stall regulated wind turbine the rotor speed would be varied to limit the power out, b to c on Figure 5.5, as the windspeed varied above rated. So the question is how to balance the mechanical power into the generator and the power transferred out to the grid via the rectifier and inverter so that there is maximum energy capture whilst maintaining rated terminal voltage.

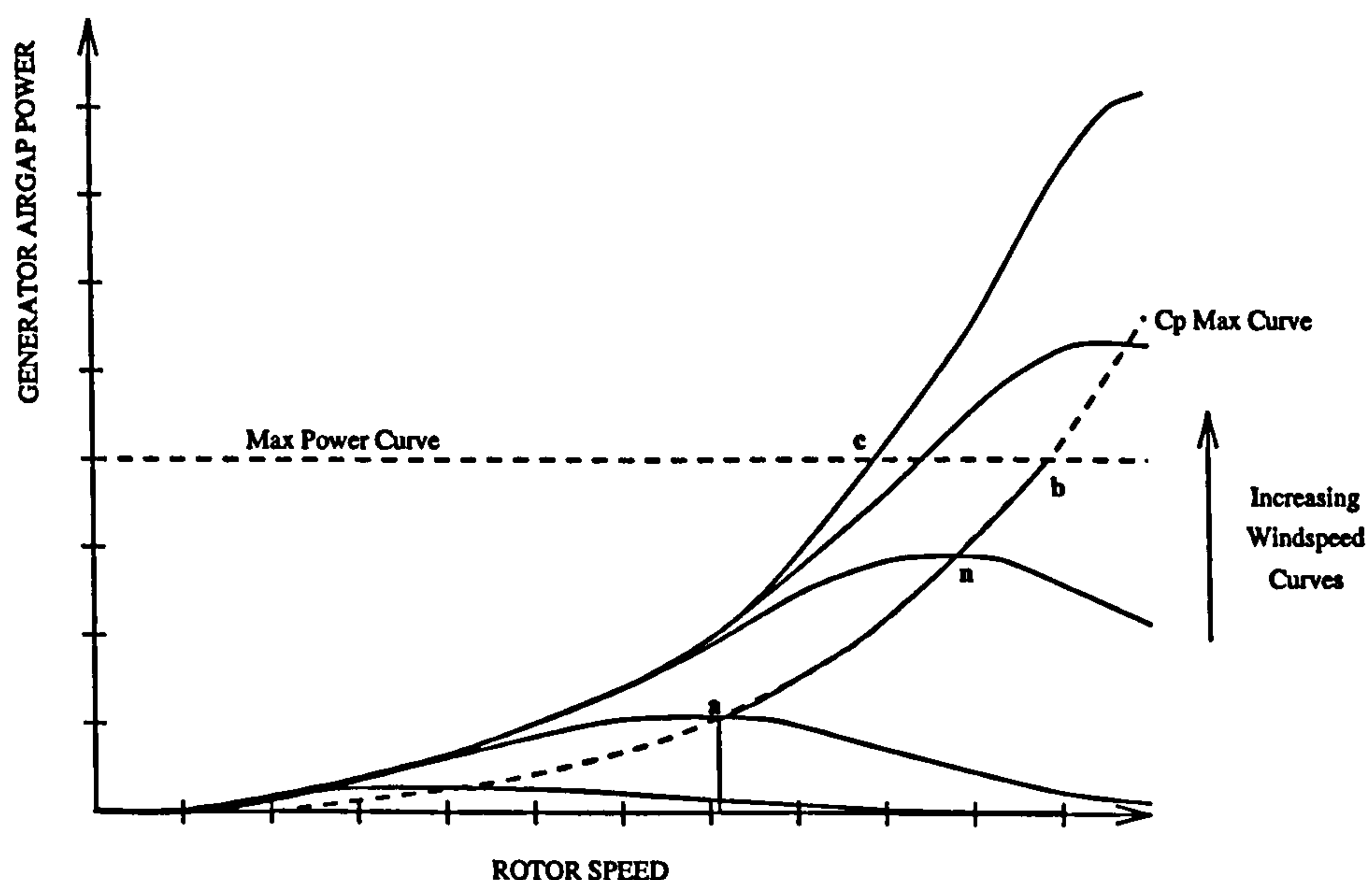


Figure 5.5: Constant Windspeed Curves and operational strategies for a variable speed turbine

5.2.2 Power flow control

Clearly to implement the strategy, outlined in the previous section, the facility must exist within the scheme to separate the power harnessed by the wind turbine to drive the generator from the power transmitted to the grid. The difference in input and output power can then be used to either accelerate or decelerate the rotor to track C_{pmax} . This is achieved by coupling the generator to the grid via a frequency converter, typically comprising a generator, rectifier and inverter. The key interfaces that determine the power flow from the blades to the infinite bus can be seen in Figure 5.6.

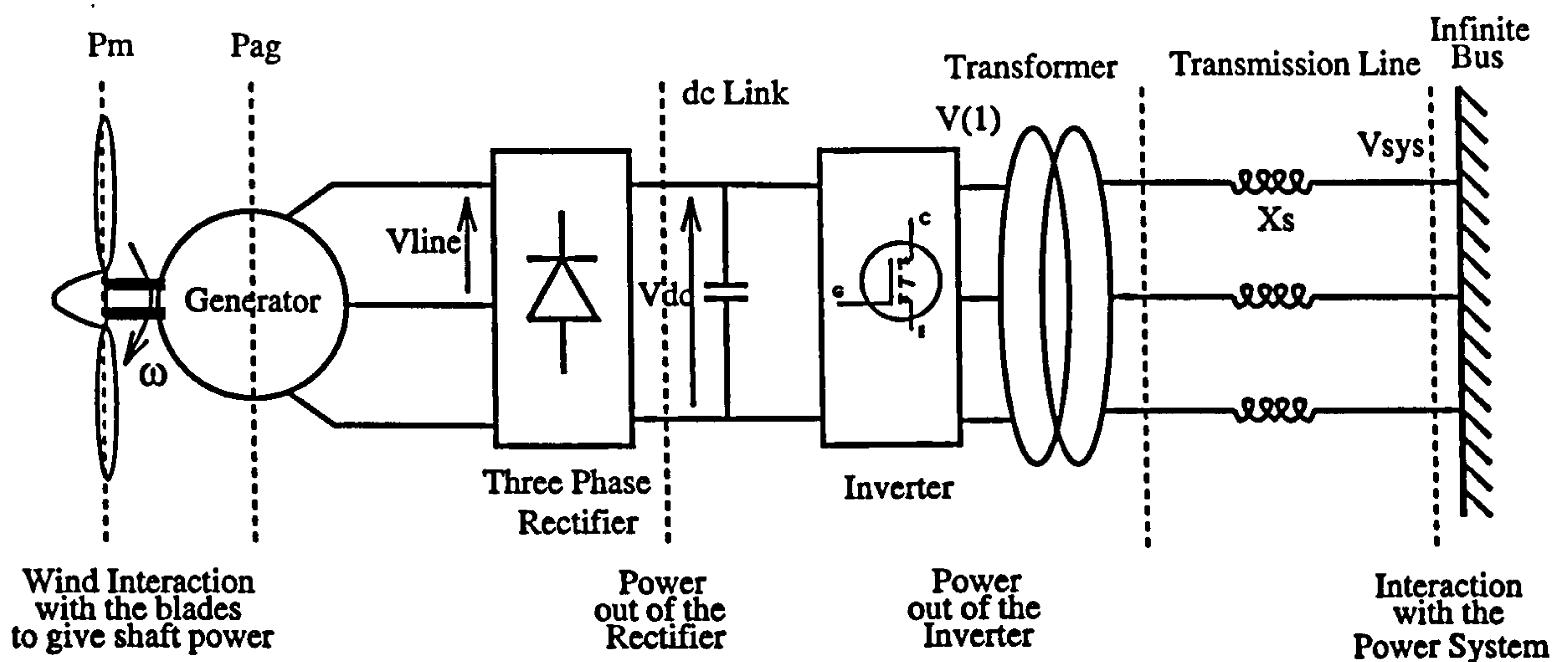


Figure 5.6: Variable Speed Modelling Interfaces

The power into the generator is dependent on the windspeed and rotor speed. For a conventional diode bridge rectifier, the power can only be transmitted via the rectifier into the dc link if the absolute magnitude of the generated voltage is greater than the dc link voltage. Other schemes exist but these are beyond the scope of this thesis. The level of power that flows into the inverter is then dependent on the voltage of the dc link and the current that flows within the link. The power that can be transmitted to the infinite bus is a function of the voltage of the system and the voltage at the terminals of the inverter. The power angle between these two voltages can be varied by delaying the sequence of the firing angles of the inverter with respect to a measured signal of the angle of the infinite bus. The level of the inverter terminal voltage can be controlled either by altering the dc link voltage or by changing the control ratio, K_{Vdc} , of the inverter which is the ratio between the dc link voltage and output voltage of the inverter. The range over which this ratio can be altered depends on the configuration and control of the inverter. If less current is taken out of the

link by the inverter than flows into the link from the rectifier then the voltage across the dc link capacitance will increase and vice versa. Thus a scheme is required which allows the dc link voltage to vary in response to any change in windspeed and thus match the power flow through the generator, rectifier and inverter to the grid to track C_{pmax} . Furthermore as the dc link voltage varies the inverter control ratio must be adjusted to maintain either rated terminal voltage or a reactive power setpoint. The detailed modelling of these concepts is presented in the next section.

5.3 Variable Speed Wind Turbine Modelling

The d, q -axis modelling and fixed speed operation of a multi-pole, permanent magnet, synchronous generator connected directly to the grid has already been described in Chapters 3 and 4. However the modelling necessary for variable speed operation is very different because of the connection to the rectifier and inverter unit. This section outlines those differences and discusses the theory, operation and implementation into simulation models of several frequency converter schemes.

The key interfaces that need to be modelled are shown in Figure 5.6. The power input from the wind is still given by equation 2.8 as the turbine blade design has not changed. The standard method for rectifying the three phase output of a conventional generator is to use a three phase rectifier but the modular design of the permanent magnet, synchronous generator allows a better configuration to be used and the modelling of this is described. Finally the modelling of several kinds of inverter scheme is discussed with particular reference to the power flow into the grid. A full discussion of the operation and theory of the variable speed generator and frequency converter is presented in [96]. Throughout the discussion the SIMULINK models used for the variable speed wind turbine model are introduced as appropriate.

5.3.1 Variable speed wind turbine model library

The simulation library shown in Figure 1.5 contained block libraries for all the key parts of a wind turbine operated at variable speed. It is now necessary to outline the theory behind each of the blocks to arrive at a suitable SIMULINK model. Some of the modelling is the

5.3 Variable Speed Wind Turbine Modelling

same as for the fixed speed case, i.e. the pitch controller and actuator, wind time series and shaft power calculations, etc, but different models will be required for the generator and new models needed to represent the operation of the frequency converter. The final model will have the form shown in Figure 5.7 with the block libraries expanded as required.

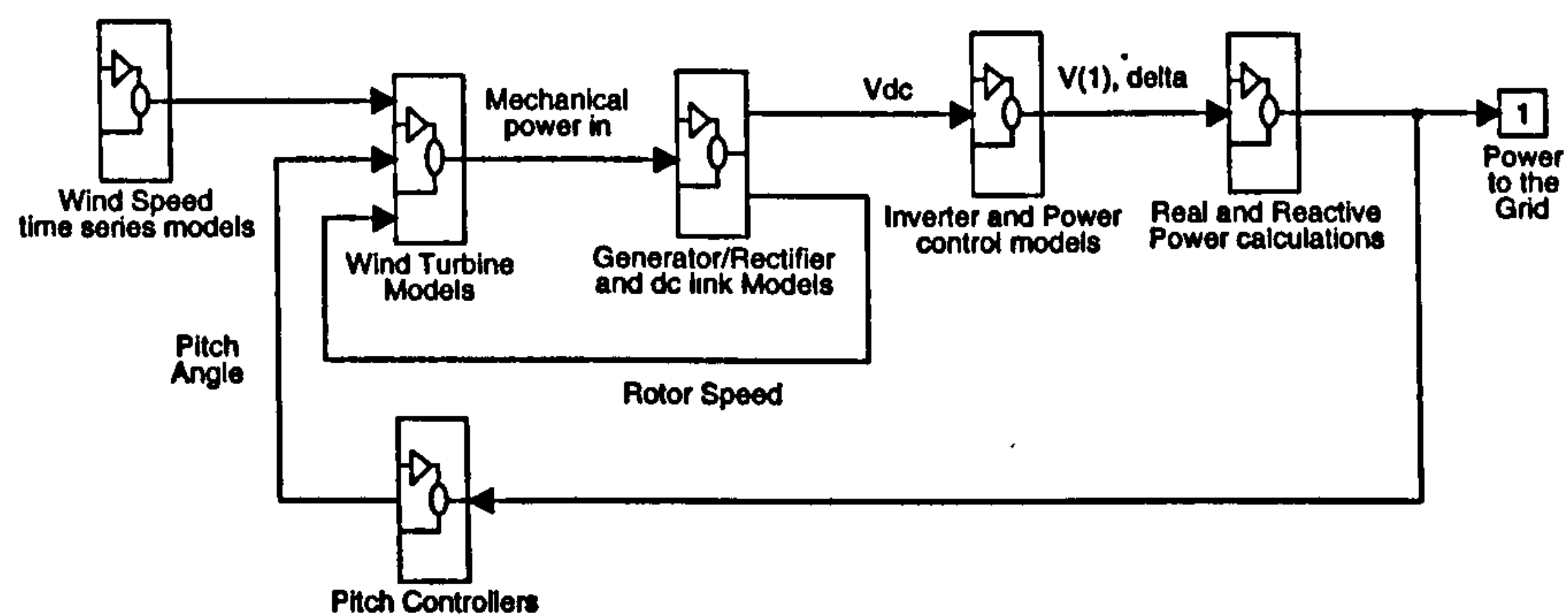


Figure 5.7: Schematic of the variable speed wind turbine model

5.3.2 Modelling aims and method of attack

The aim of developing a MATLAB model of a variable speed wind turbine is to be able to compare the dynamic performance and control requirements of the fixed and variable speed operation in the timescale from 10 to 500 seconds. The performance during this timescale of operation will give an indication as to which is the preferred mode of operation. To achieve this objective it was considered inappropriate to develop an in depth a, b, c phase model of the generator and couple it to a detailed model of the individual diodes and IGBT's of the rectifiers and inverter because of the timescales involved. The time savings alone when considering an inverter scheme with 34 switching instants per cycle, as outlined in section 5.3.9, and the constraint of simulating at least ten times as fast as the fastest oscillating frequency would require a step length an order of magnitude lower than currently used. This would mean that the 80 seconds of results presented in the next chapter would take about 20 hours instead of the 2 hour run time on the 50 MHz 486 at present. A quasi-static approach is, therefore, used where it is assumed that the generator and rectifier and inverter

move from one steady state operating point to another. This ignores all switching transients and is equivalent in principle to a fourth order model of the fixed speed permanent magnet generator where all frequency effects are neglected. The method of attack was to use a full non-linear simulation using the SIMULINK models which will now be described.

5.3.3 Wind Turbine Modelling

The wind turbine modelled is the same three blade, horizontal axis, grid connected, medium sized turbine whose theory of operation was outlined in Chapter 2 and therefore the same Simulink models for the wind turbine can be used. However there are a few slight changes and these will now be addressed.

WIND TIME SERIES AND WIND TURBINE MODELS. The approach for generating the wind speed time histories and for modelling the wind interaction with the blades is the same as for the spectral method proposed in Chapter 2 but now instead of fixed frequency spikes to represent the rotational sampling effects, the sin and cos wave generators shown in Figure 2.20 have the varying frequency of the rotor speed input to them to represent the fact that the rotor is no longer operated at fixed speed. The power transmitted to the hub is still given by,

$$P = 0.5\rho C_p A U^3 \quad (5.1)$$

The C_p curves are again implemented as a look-up table referenced by the tip speed ratio and pitch angle. The developed shaft torque is then given by dividing the hub power by the rotational speed of the shaft, which is no longer fixed. The same pitch controller and actuator as developed in Chapter 2 is used for the variable speed operation to enable a fair comparison to be made.

5.3.4 Rectifier Theory

The proposed E-core arrangement of the multi-pole, permanent magnet, synchronous generator suggests a scheme for rectification where each coil is connected to a single phase diode rectifier bridge and then paralleled onto the dc bus [97]. This is shown in Figure 5.8.

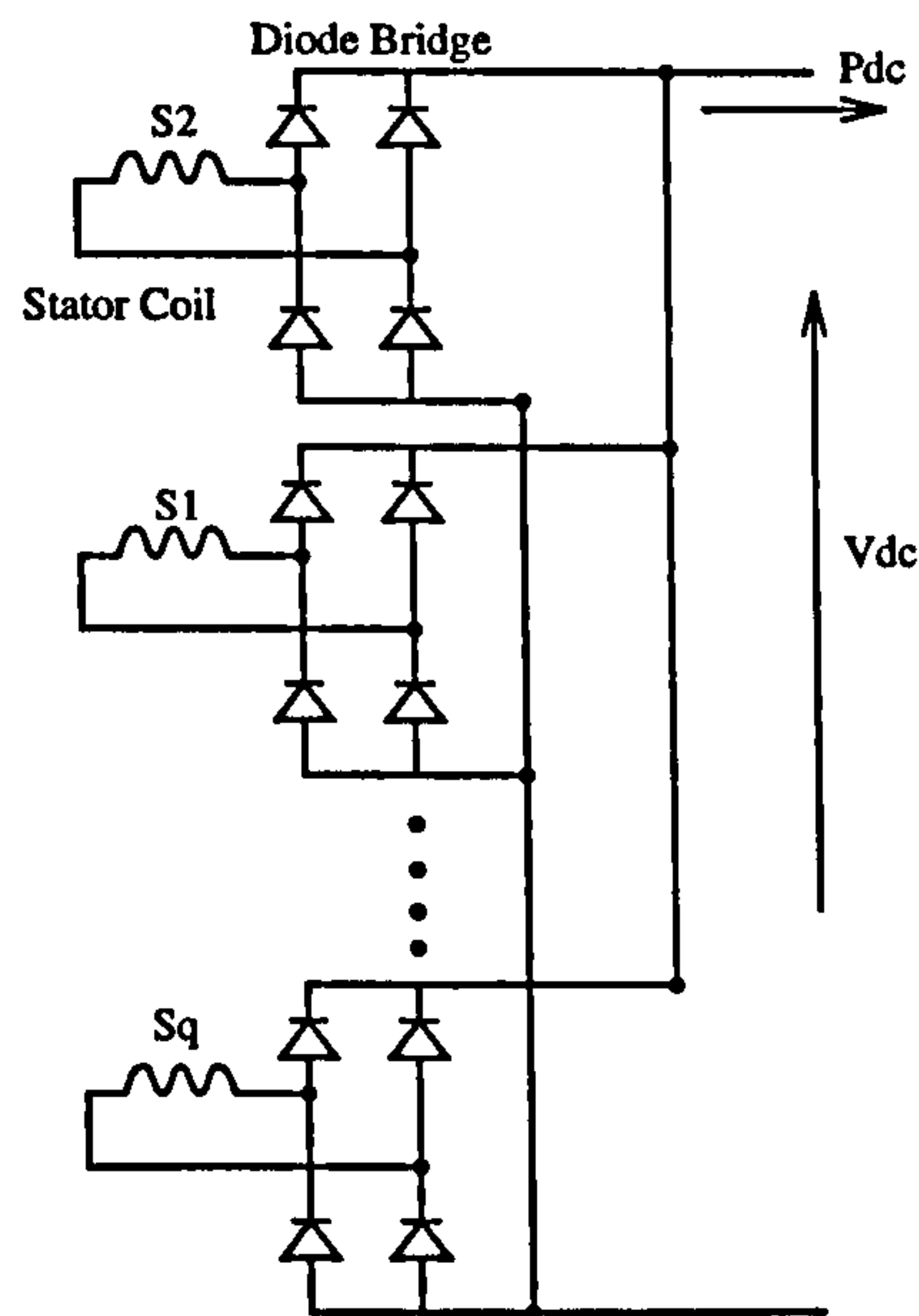


Figure 5.8: Modular Electrical Arrangement for the AC/Dc Power Interface

There are two main advantages of such an arrangement. Although this is an inefficient use of diodes compared with a single three phase bridge, the number of E-cores and diode bridges mean that if one fails the change in the quality of the output dc link voltage would be low. This has important and beneficial maintenance implications. Secondly the dc link voltage would have very little ripple due to the large number of phases and a filter for the dc link would be unnecessary.

The developed terminal voltage across a single E-core in the 455 kW generator is about 420 Volts with the biggest harmonic being the fifth at about 8 %. One major problem does arise from analysis of this E-core arrangement and that is the poor power transfer capability of each E-core and rectifier unit onto the dc link. This poor capability arises because the diodes only transmit power when the absolute magnitude of the voltage across the ac side of the bridge is greater than the voltage of the dc link. The low E-core emf is further reduced by the voltage drop across the inductance, L_c , of the E-core so that, to achieve an acceptable conduction time for the diodes of the bridge, a low dc link voltage is required. Unfortunately to transmit the rated module power of the generator at a low dc link voltage requires a high dc link current. The losses in such an arrangement would be high. One solution to this problem would be to increase the number of tiers, and hence number of modules, of the variable speed generator and effectively lower the required power rating of each module. A high dc link voltage could then be used with less current being

drawn from each of the greater number of modules. However the drawback to this would be an excessively heavy generator. The proposed solution to this problem [101] is to fit a capacitor, C_{ac} , across the diode bridge on the ac side to partially tune out the inductance. This resonant circuit allows much more power to flow. The proposed arrangement for a single E-core and rectifier module can be seen in Figure 5.9.

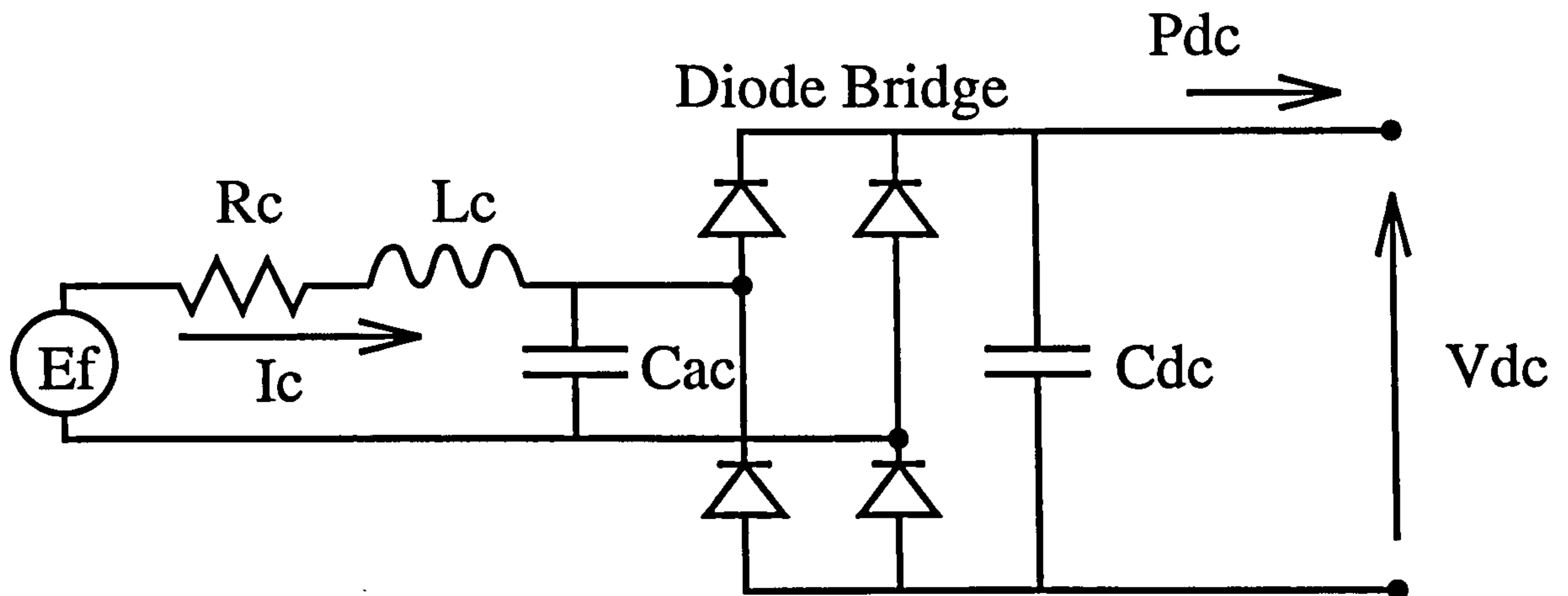


Figure 5.9: Equivalent Circuit for Capacitance Compensated Rectifier

5.3.5 Generator and capacitor compensated rectifier theory

The power transfer capability of the generator and capacitor compensated rectifier depends on the speed of the generator rotor, the level of the dc link voltage and the value of the tuning capacitance. This can be modelled using a full time stepping analysis and three programs (WINDVARD, WINDVARP, and WINDVOUT) are used to derive the steady state power transfer capability for any given rating of wind generator and rectifier as the voltage in the dc link and rotational speed of the rotor are varied. The key equations contained within these programs to determine the steady state performance of the circuit shown in Figure 5.9 are included in Appendix D. The programs output values for the airgap power and the dc link power, from which the injected dc link current can be found.

The output current from the E-core, injected current into the dc link and the corresponding absolute magnitude of the voltage across the tuning capacitor, C_{ac} , from WINDVARP for a module of the 455 kW generator with a capacitance of $33 \mu F$, a fixed dc link voltage of 900 V, at a frequency of 55 Hz can be seen in Figure 5.10, Figure 5.11 and Figure 5.12 respectively. These waveforms have been calculated by time stepping through an exact

solution to the circuit shown in Figure 5.9. The dc link voltage of 900 Volts is calculated to be the maximum dc link voltage level at which meaningful power transfer can occur at 55 Hz. The emf from the E-core is calculated at each time step by the analysis of the equivalent magnetic circuit at the frequency of interest and the dc link voltage is fixed. The waveform of the E-core voltage induced by the travelling magnetomotive force at the generator airgap will not be a pure sinusoid, but will contain odd harmonics. It is necessary to include these harmonics when determining the likely transmitted power levels through the proposed multiple E-core, tuning capacitor and diode bridge arrangement.

Assuming the initial conditions to be zero, the voltage across the tuning capacitor, C_{ac} , initially builds up due to the current flowing during the positive half cycle of the E-core emf. When the voltage across C_{ac} is just greater than the dc link voltage, just enough current flows into the capacitor from the E-core to prolong conduction but the bulk of the current is now injected into the dc link. When the current from the E-core then changes in polarity the diodes switch off. During the negative half cycle, capacitor C_{ac} , discharges back into the E-core and then charges giving rise to a negative voltage across it. When the reverse voltage across C_{ac} is larger in magnitude than the dc link voltage the second leg of the rectifier bridge switches on. This then conducts the bulk of the current flowing from the E-core until I_c again changes in polarity. This action repeats itself until a limit cycle is set up where the charge period and discharge period are in equilibrium and an average mean current is injected into the dc link.

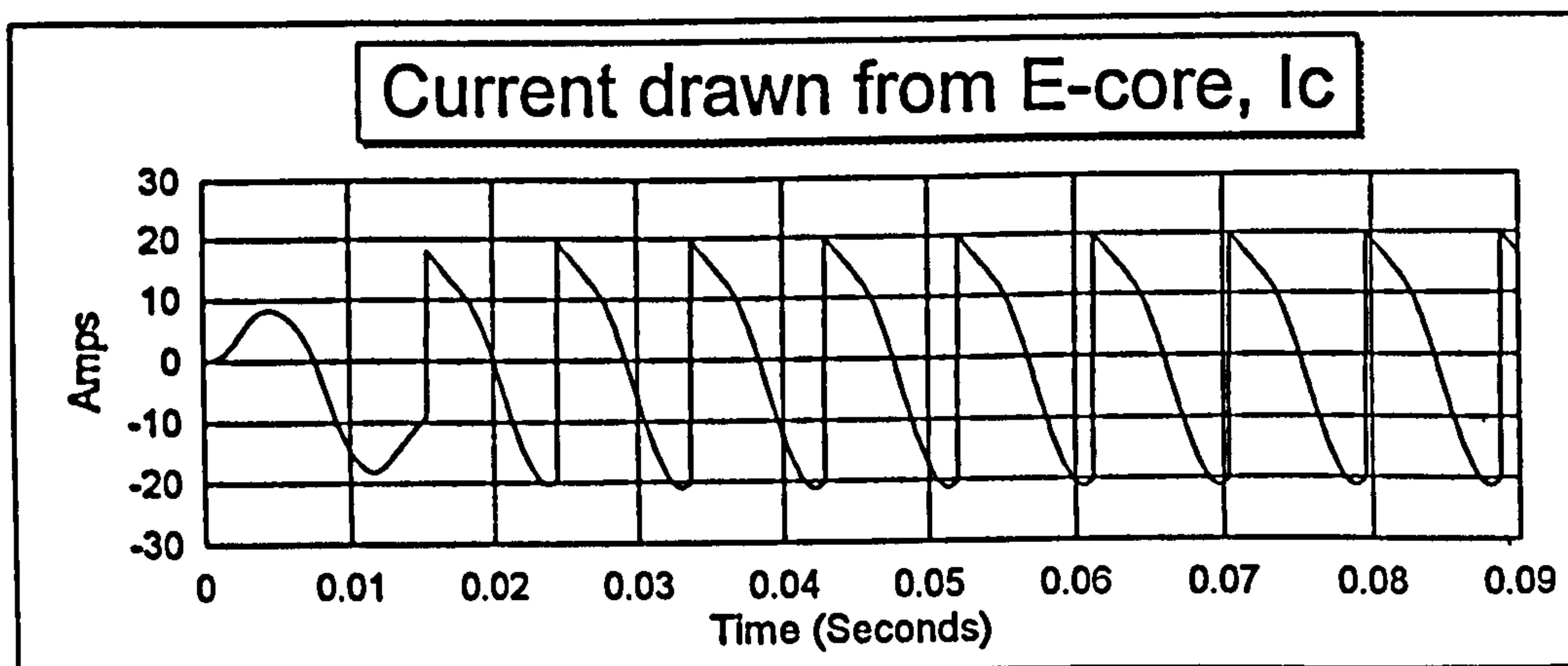


Figure 5.10: Current out of the E-core

Figure 5.10 to Figure 5.12 clearly demonstrate the resonant properties of the circuit of Figure 5.9 in that the dc link voltage at which meaningful levels of power can still be

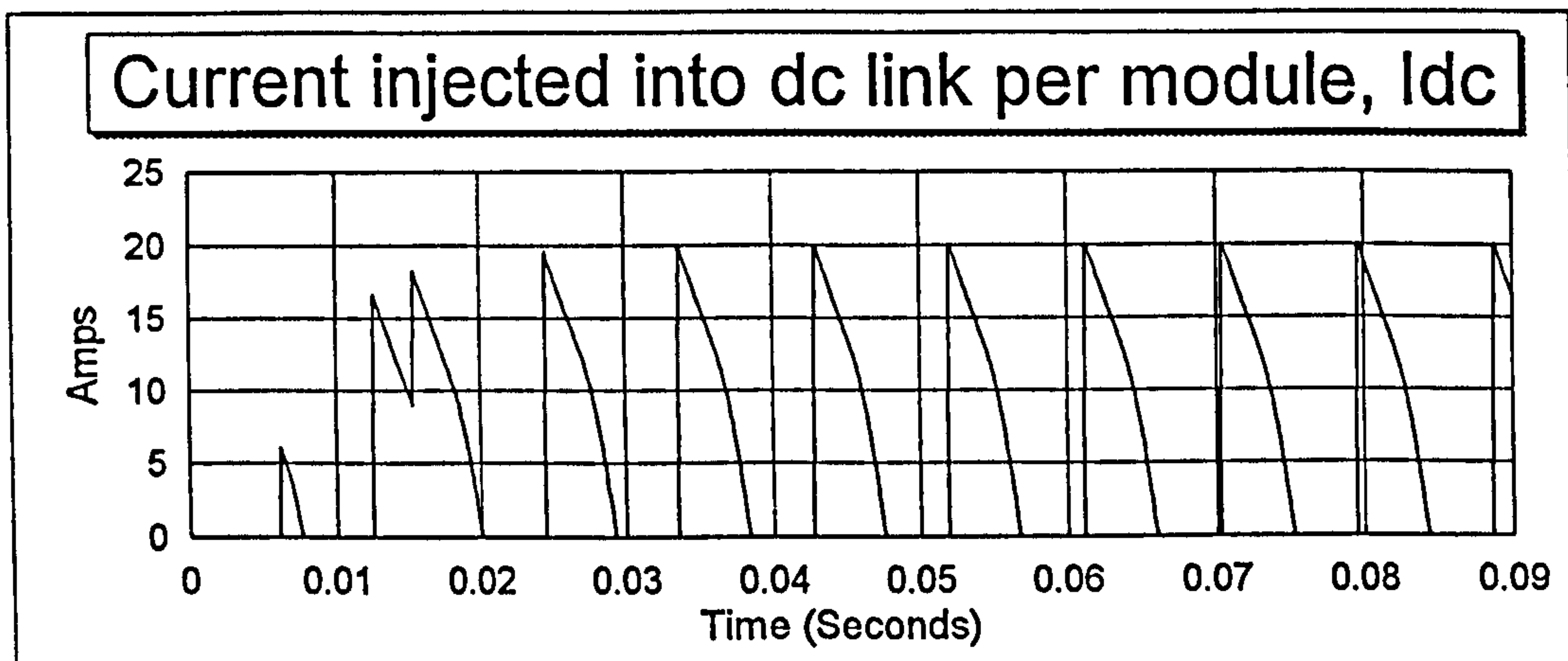


Figure 5.11: Current injected into the dc link

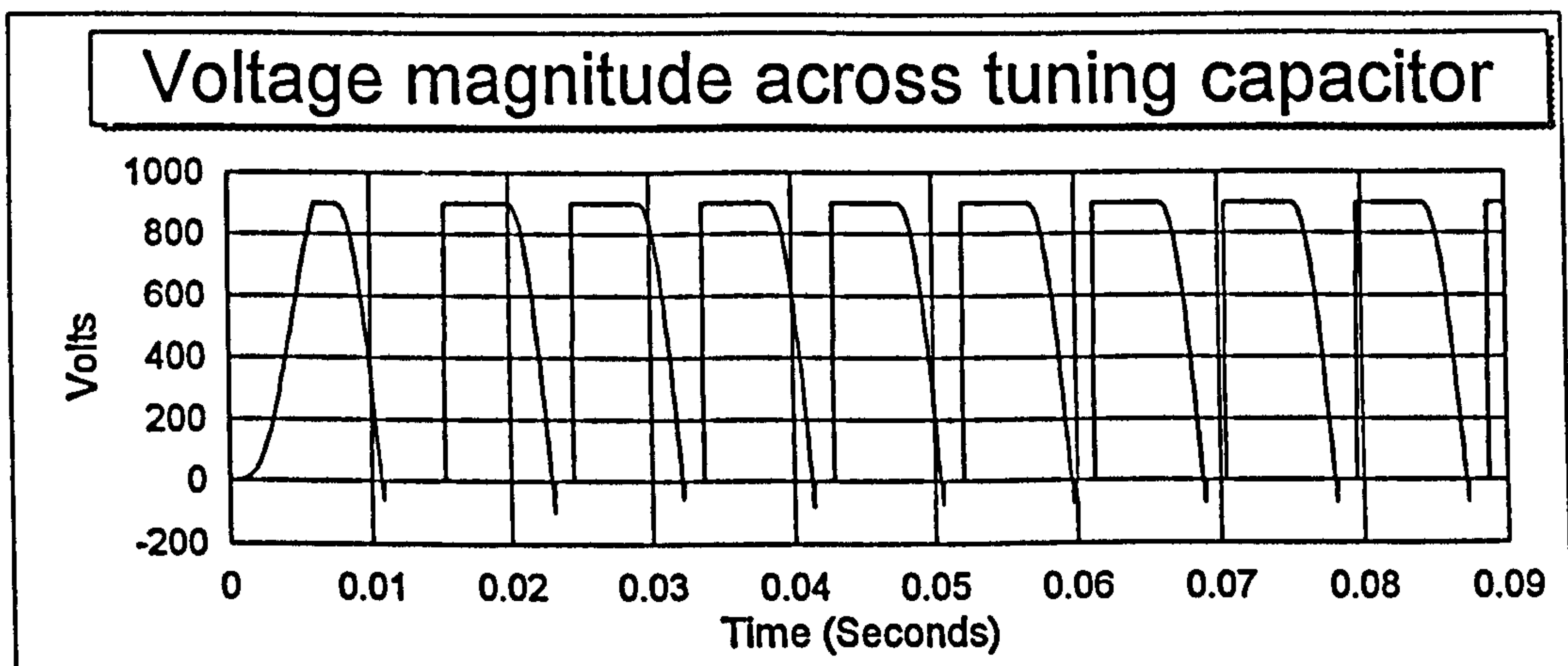


Figure 5.12: Voltage waveform across the tuning capacitance

transmitted is increased to 900 Volts. The E-core voltage for this case is about 567 V a.c. and the overall efficiency from the E-core to the dc link is 91.6 %. This is about 95 % of the efficiency of the fixed speed permanent magnet generator. The analysis of WINDVARP does not consider the mechanical power into the circuit but merely finds the steady state equilibrium point of the circuit of Figure 5.9 at the given frequency and dc link voltage and evaluates all the losses. The equations for this are given in Appendix D.

The step response of the tuning circuit to a reduction in the dc link voltage from 900 Volts to 450 Volts demonstrates the time constants involved in the circuit. The step responses can be seen in Figure 5.13 to Figure 5.15 and indicate a fast settling time, of the order 0.01 seconds. This is very fast compared with the time constant of the mechanical power flow into the generator which is dominated by the inertia of the wind turbine blades. Therefore the interface between the mechanical power into the generator and the airgap power transmitted

via the multi-phase rectifier to the dc link is modelled quasi-statically by considering only the power transfer at the airgap and current injected into the dc link. This approach to modelling the conversion from the mechanical power of the shaft to electrical power flow within the dc link of the variable speed operated generator has sufficient accuracy for performance comparisons against the more accurate model developed in Chapter 3 for the fixed speed generator.

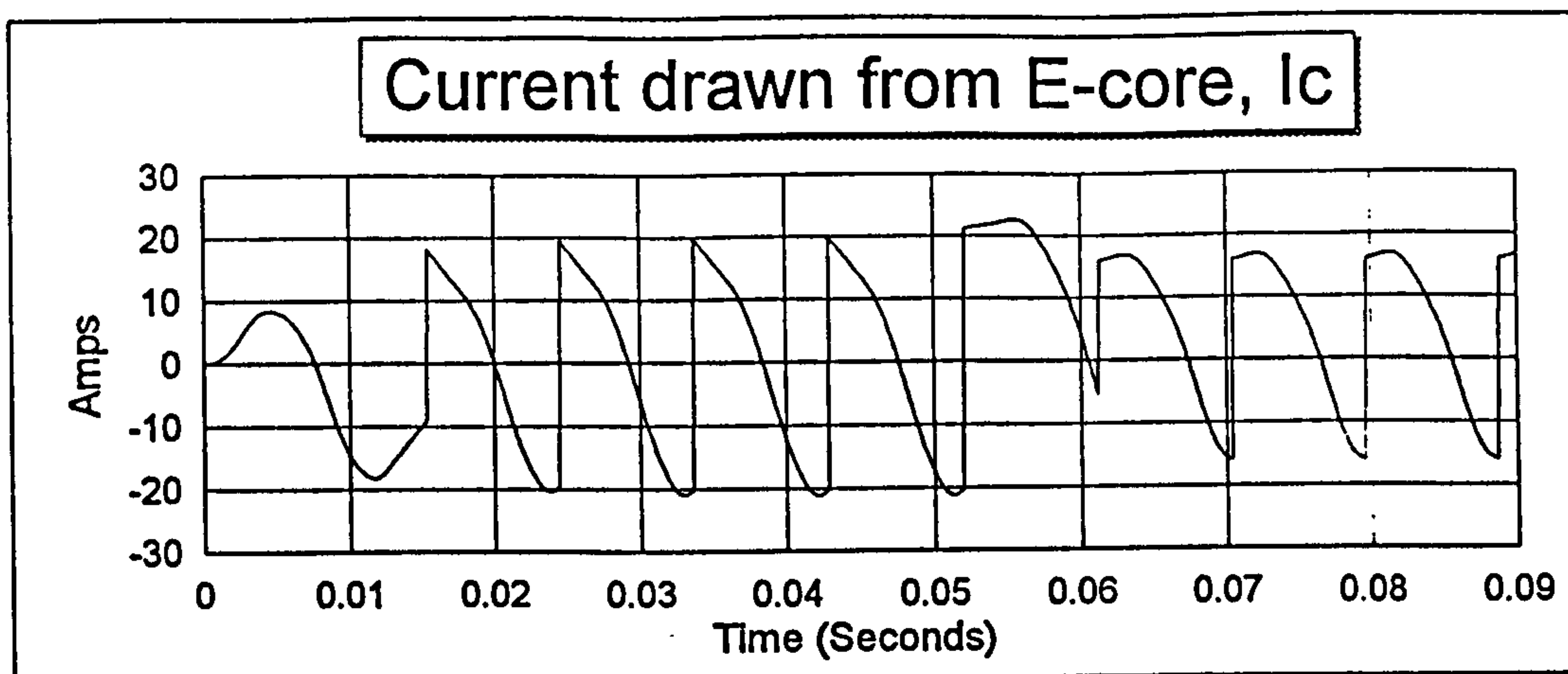


Figure 5.13: Current out of the E-core after step down in V_{dc}

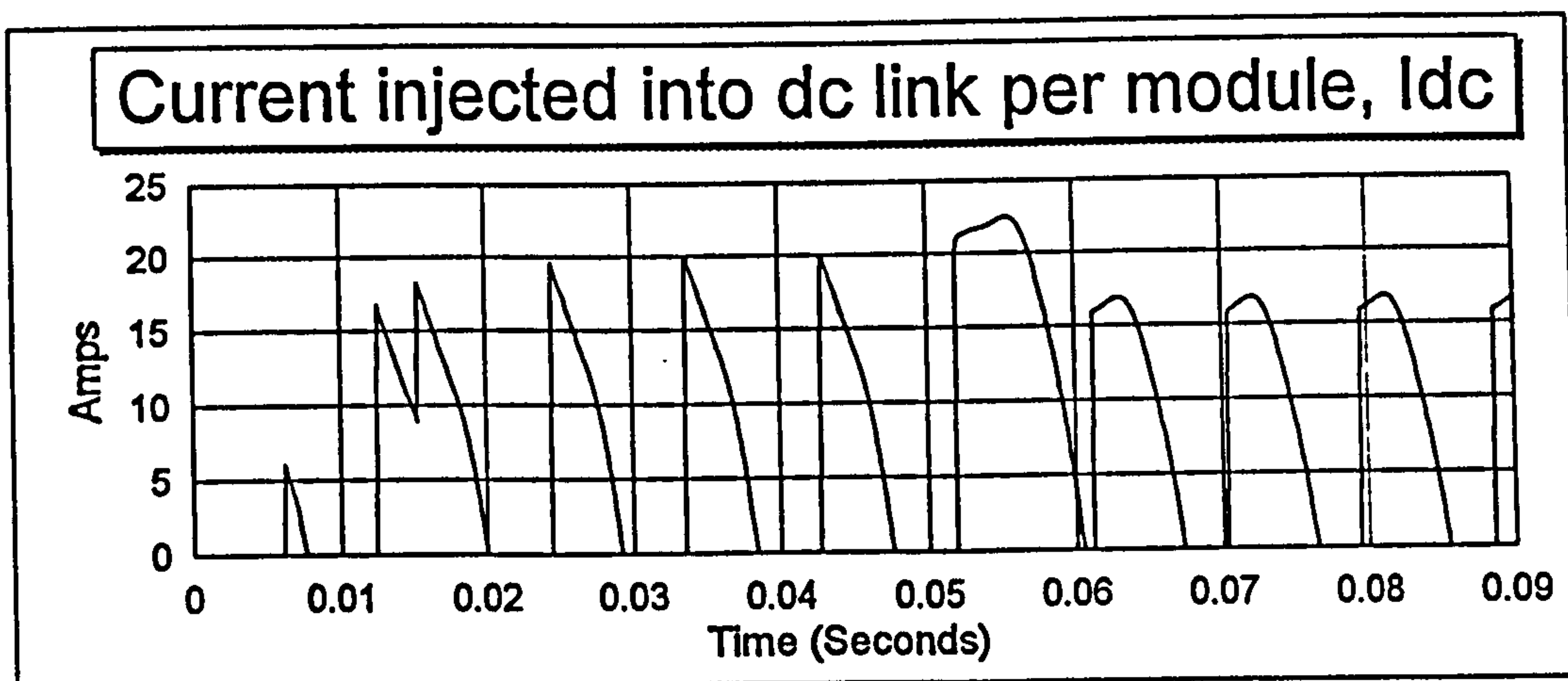


Figure 5.14: Current injected into the dc link after step down in V_{dc}

The results from WINDVARP have been validated using the PSPICE [98] electronics package. The generator parameters, returned from WINDVARD and WINDVARP, are presented in section 5.4 for a range of generator ratings typically found in wind turbines applications. The value of tuning capacitor is chosen to ensure that over the frequency range of interest the possible power transfer across the airgap matches the profile of the input mechanical power from the wind. This means that the size and frequency range of the resonant peak power transfer characteristic must be chosen carefully. Choosing too small

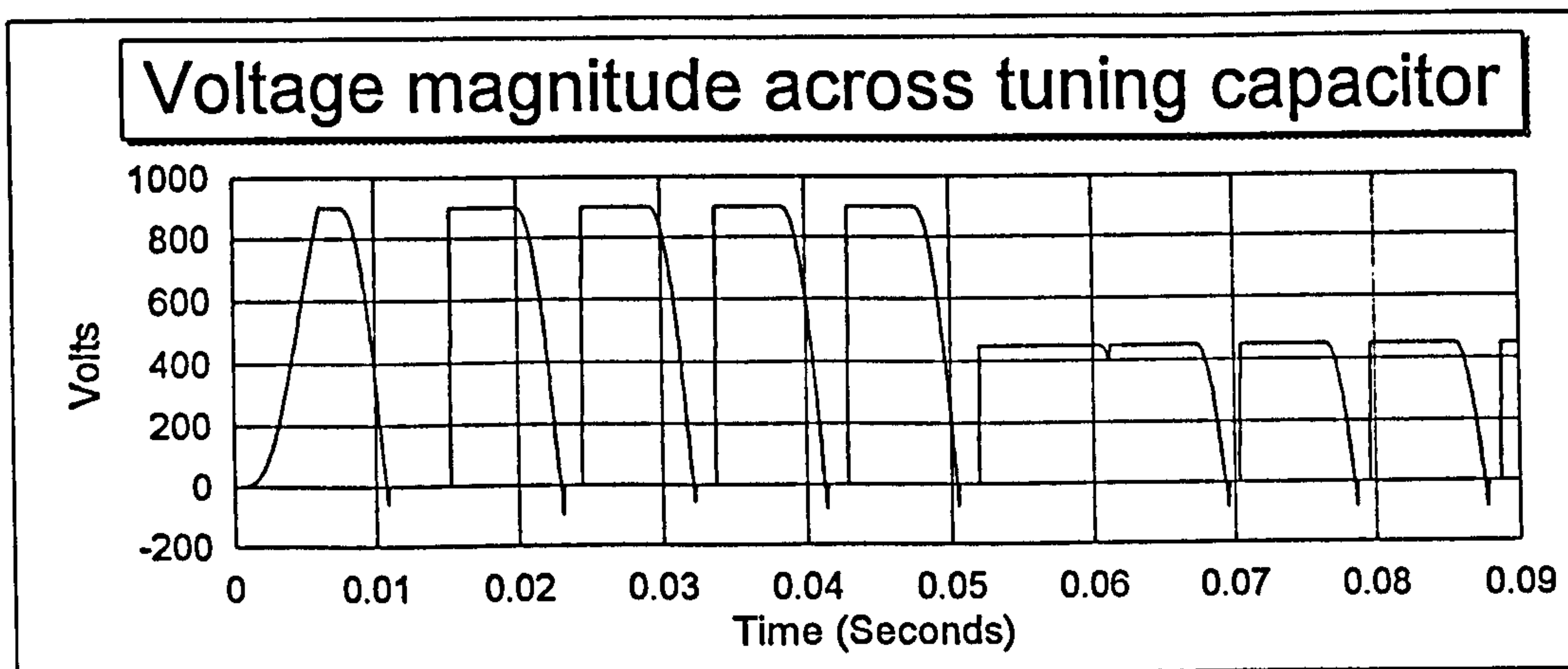


Figure 5.15: Voltage waveform across the tuning capacitance after step down in V_{dc}

a value of capacitance relative to the E-core inductance leads to only a small amount of resonance. Choosing too large a value of capacitance may lead to too much resonance with resulting control problems. The capacitances presented in section 5.4 have been chosen so that the resonance of the tuned circuit is matched to the input mechanical power of the wind turbine over the frequency of operation. WINDVARP returns values of steady state airgap power and dc link power as rotor speed and dc link voltage vary over the full range of operating wind speeds. These are transferred into MATLAB as 2D lookup tables referenced by rotor speed and dc link voltage. The injected dc link current, and not dc power, is the variable used in the MATLAB simulation and this is easily obtained by dividing the dc link power by the corresponding dc link voltage level it has been calculated at. The next section explains how these can be included in a SIMULINK model to represent the generator and rectifier.

5.3.6 Generator and rectifier combined model

The time taken for the resonant circuit to reach a steady value is about 0.5 seconds. But subsequently to that small changes in frequency or dc link voltage take only a few cycles to reach a steady value. Therefore it was assumed that the combined generator and rectifier could be modelled in a quasi-static way.

GENERATOR AND RECTIFIER MODELLING. The concepts for this were introduced in the previous section. The methodology used to develop a SIMULINK model is to carry out a quasi-static analysis to derive lookup tables for the airgap power transfer and

injected current into the dc link. These tables are referenced by rotor speed, ω_r , and the dc link voltage, V_{dc} , such that the airgap power and injected current per module is known for any value of ω and V_{dc} . As the modules are in parallel they share this airgap power equally and, for a fixed airgap power, they inject a steady mean value of current into the dc link. The same equation governing rotor movement as for the fixed speed case, equation 3.15, is then used to give a quasi-static method for establishing how the turbine rotor speed will change in response to any change in operating point. The SIMULINK implementation of the generator rotor swing equation and the injected dc link current can be seen in Figure 5.16 and Figure 5.17 respectively. In Figure 5.16 the block titled 'Generator and rectifier power transfer characteristic' contains the 2D lookup table for airgap power transfer which is derived in the next few paragraphs. The value for the power transferred across the airgap is compared against the mechanical power from the wind turbine model at each simulation step to determine changes in rotor speed. In Figure 5.17 the block titled 'Injected dc link current characteristic' contains the 2D lookup table returned from WINDVARP for the current injected per module into the dc link. This is compared against the current drawn by the inverter to determine changes in dc link voltage. Both lookup tables are referenced by dc link voltage and rotor speed.

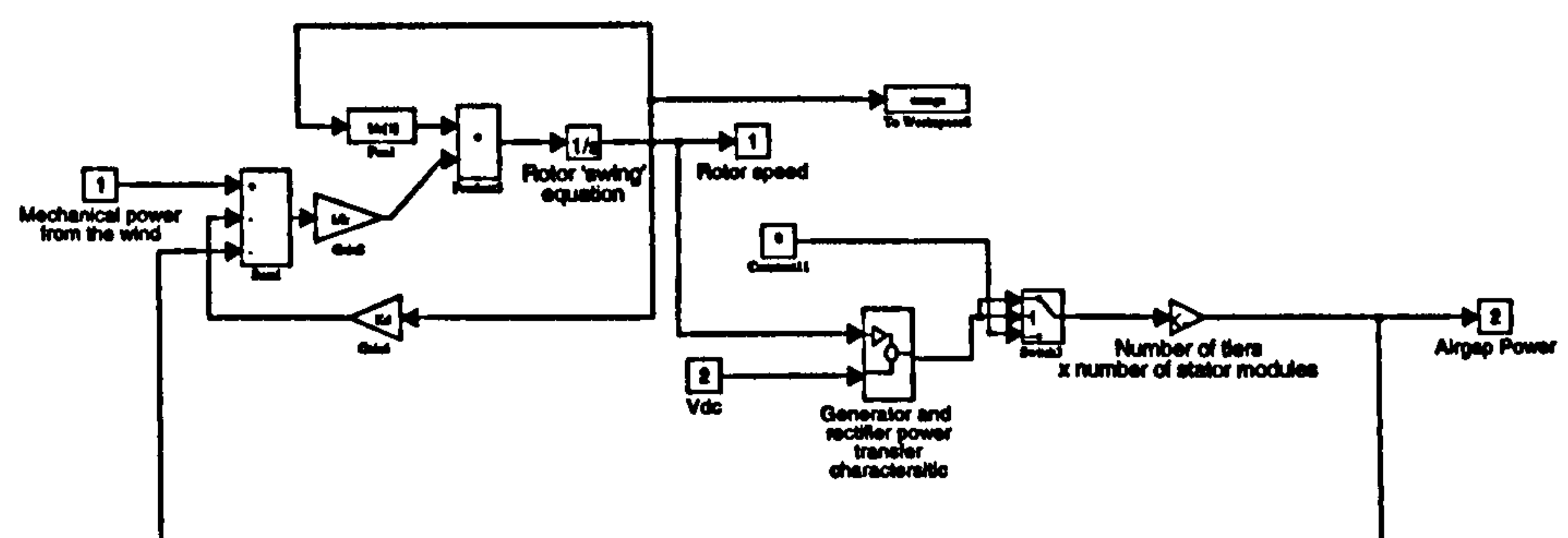


Figure 5.16: SIMULINK model for generator rotor equation

GENERATOR AND RECTIFIER POWER TRANSFER CHARACTERISTIC.

The E-core, tuning capacitor and rectifier power transfer characteristic is obtained by using a time stepping analysis, outlined in Appendix D, and the resulting power transfer performance calculated as rotor speed varies for fixed values of V_{dc} . The airgap power characteristic, P_{ac} , for a single module of the 455 kW generator can be seen in Figure 5.18.

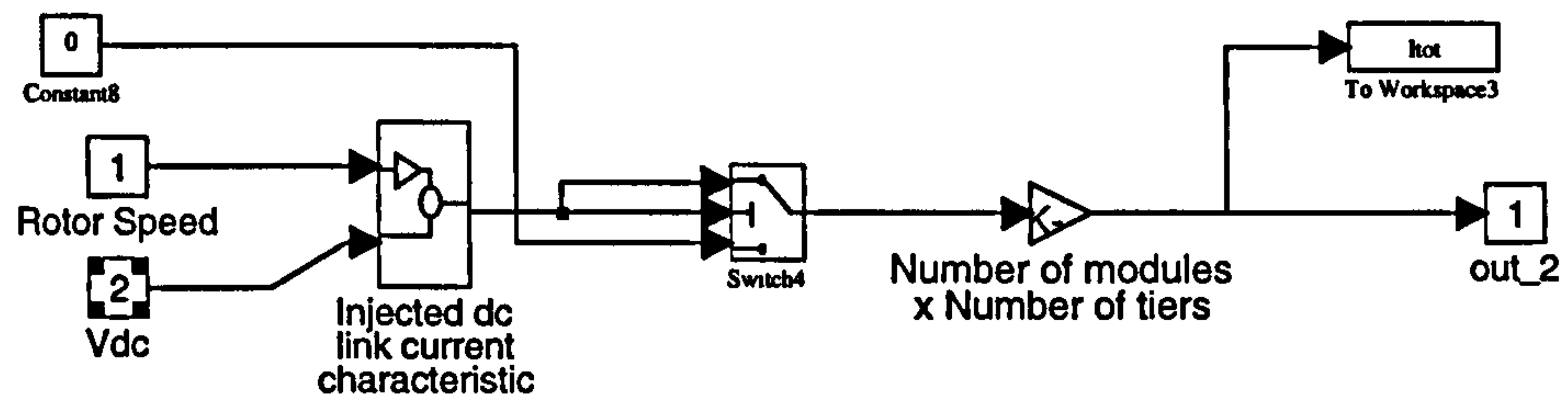


Figure 5.17: SIMULINK model for the injected dc link current

Each line on the figure represents the power transfer through a single E-core and rectifier module onto the dc link for a constant value of V_{dc} as the rotor speed varies. As the rotor speed increases from standstill the emf of the E-core increases and, coupled with an increase in the resonant effect with frequency, leads to higher dc link voltages at which power can be transferred. However power can only be transferred to the dc link when the absolute magnitude of the voltage across the diode bridge is greater than the dc link voltage and so for a higher dc link voltage a higher rotor speed is required to provide the necessary voltage magnitude. As the speed subsequently increases above the power transfer cut-in level, the steady state power transfer characteristic would follow line 1 for a low value of V_{dc} . The steady state power transfer at a given frequency is found from the analysis of the operation of the circuit in Figure 5.9. An explanation of this is given in section 5.3.5. The build up of line 1 depends upon the increasing conduction time per half cycle as E_f becomes larger and larger than the dc link voltage with rotor speed. An eventual maximum power transfer is reached and this can be explained with the use of the circuit shown in Figure 5.19.

An estimate for the maximum current from the E-core into the tuning capacitance and diode bridge circuit can be determined by considering the circuit shown in Figure 5.19 where the dc link voltage is zero. When the dc link voltage is zero, the tuning capacitor, C_{ac} , is effectively short circuited and the diode bridge will be in its continuous conduction mode. This circuit is governed by,

$$\lim_{V_{dc} \rightarrow 0} E_f = Z I_{lim} \quad (5.2)$$

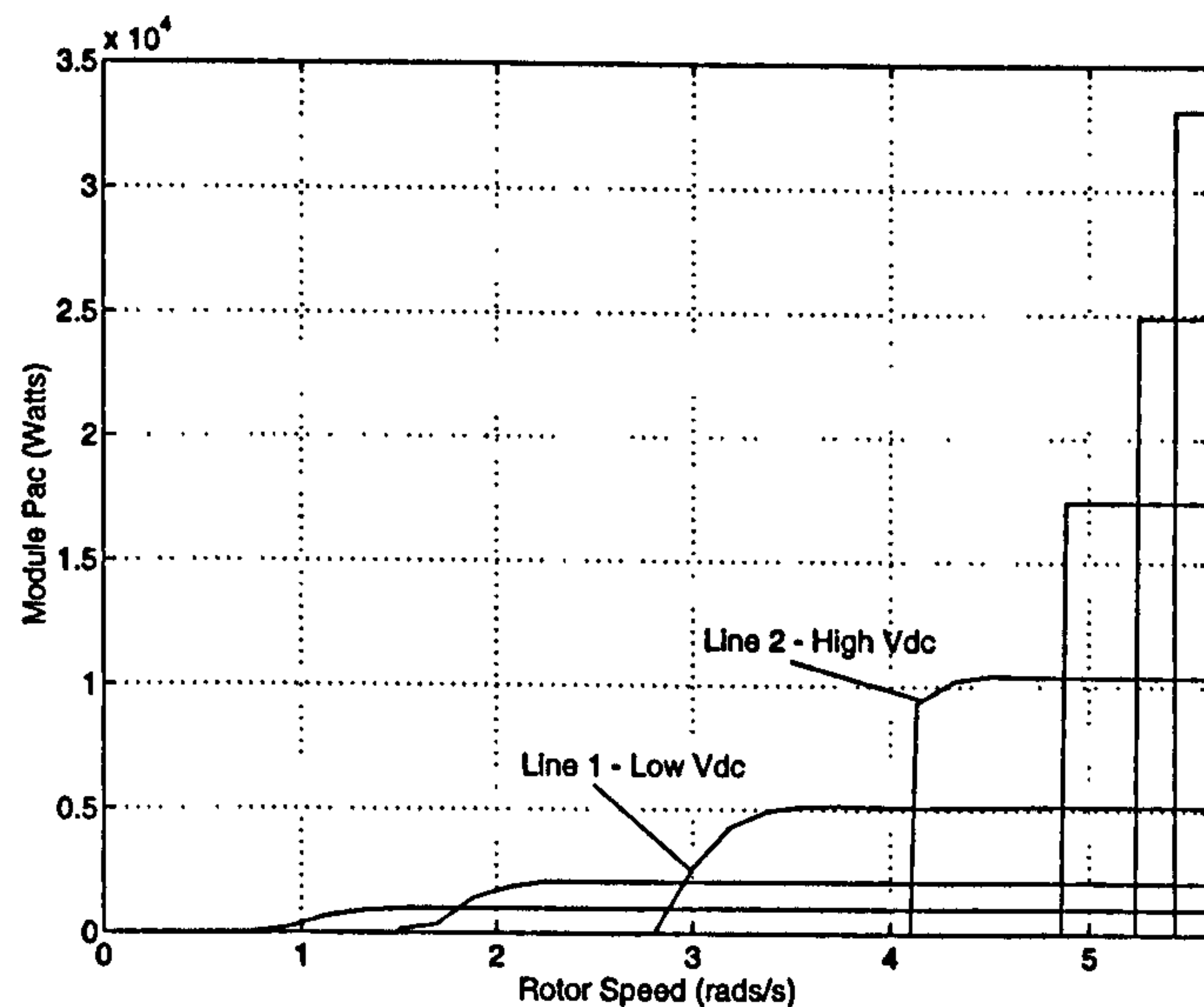


Figure 5.18: Airgap power as rotor speed varies for constant V_{dc}

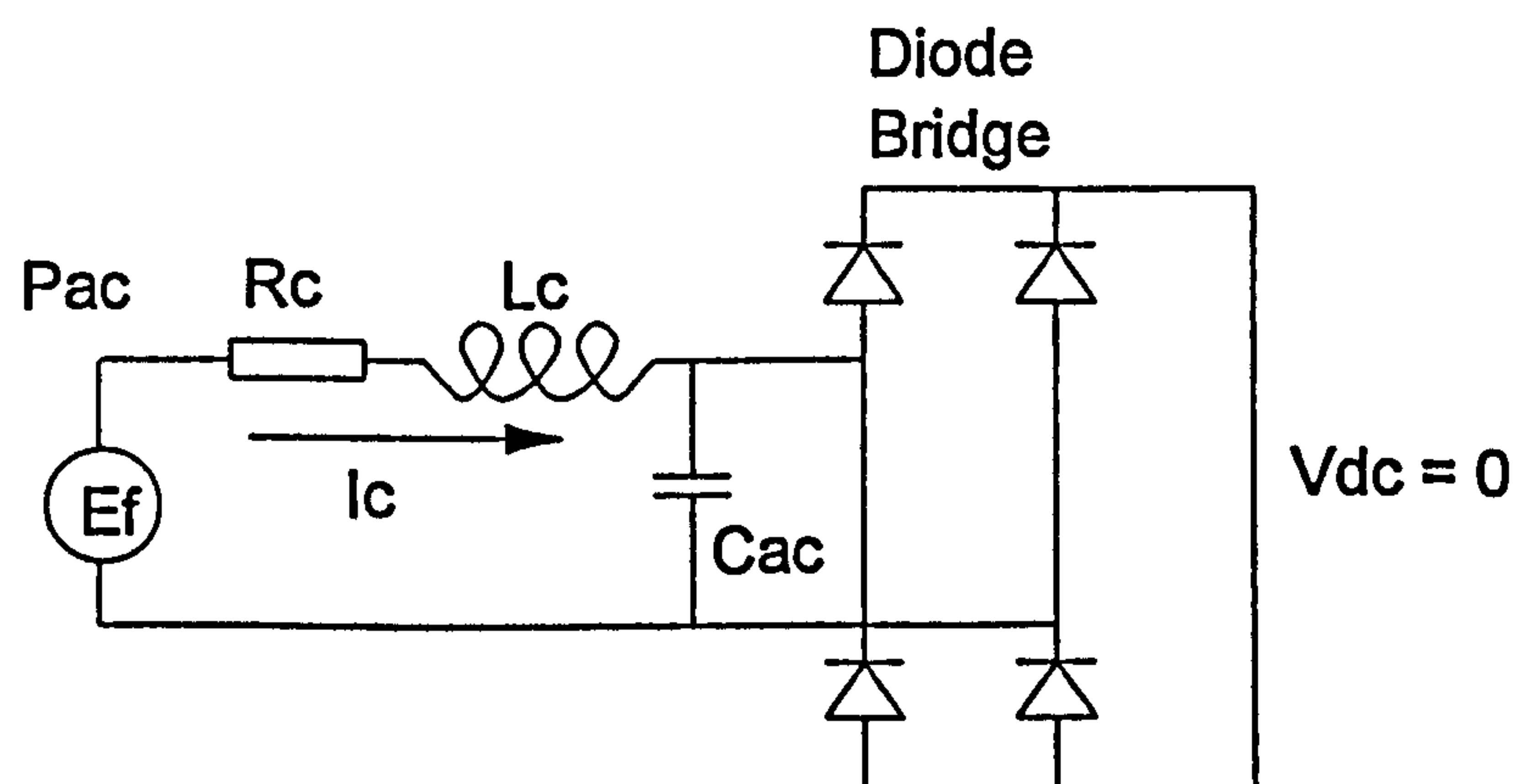


Figure 5.19: Maximum current from the E-core

Substituting expressions for the emf and impedance, assuming the resistance is much lower than the inductance, gives the following,

$$k\phi\omega = \omega L_c I_{lim} \quad (5.3)$$

L_c and $k\phi$ are constant values dependent on the design of the generator. Cancelling out the speed terms gives an expression for the maximum possible current from an E-core and into the dc link,

$$I_{lim} = \frac{k\phi}{L_c} \quad (5.4)$$

When V_{dc} is greater than zero but the E-core voltage is large enough to ensure virtually continuous conduction of the diodes at the equilibrium position then the maximum steady state power transfer through the E-core will be given by,

$$P_{lim} = V_{dc}I_{lim} + P_{losses} \quad (5.5)$$

The E-core and rectifier losses are comprised of the copper loss, diode loss and iron loss. The copper loss and diode loss are proportional to the rms current in the windings and mean injected current flowing into the dc link and dominate the iron loss. As the current flowing is constant these losses will be virtually constant and therefore the power transferred from the airgap is constant.

GENERATOR AND RECTIFIER MECHANICAL POWER INPUT CHARACTERISTIC. Similar curves can be derived from the C_p information for the input mechanical power, P_m , to a single module for a range of constant wind speeds as the rotor speed varies and these are shown in Figure 5.20 as solid lines. The dashed lines are the curves from the ac power transfer characteristic shown in Figure 5.18 for the low and high and high values of V_{dc} . During simulation the mechanical power to be balanced by each module is the power given by equation 5.1 divided by the number of stator modules.

5.3.7 Deriving the C_{pmax} tracking control law

Now the characteristic of the mechanical power input and airgap power of the generator versus rotor speed have been presented, it is possible to overlay the tables of Figure 5.18 and Figure 5.20 and obtain a C_{pmax} tracking control law. The wind turbine speed is controlled by balancing the electromagnetic reaction torque and the shaft torque. For example, if the control strategy is to keep V_{dc} constant, the generator airgap power might follow line 1 on Figure 5.20 as the rotor speed varies. A step up in windspeed of 8 to 12 m/s would result in the generator mechanical power moving vertically up from point A on the 8 m/s curve to point B on the 12 m/s curve and then on to point C because of the resulting

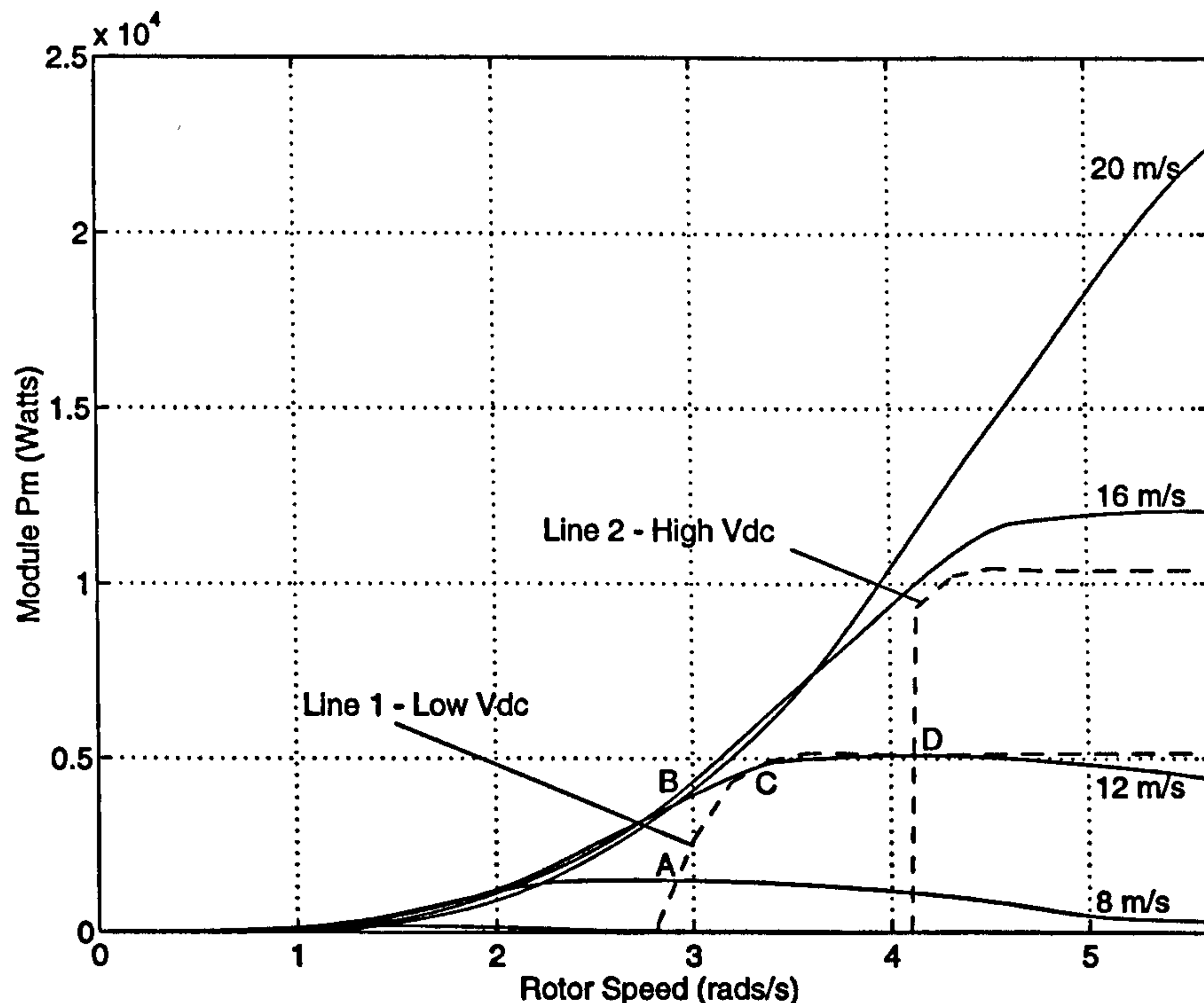


Figure 5.20: Mechanical power in as rotor speed varies for constant windspeed

acceleration due to the imbalance between P_m and P_{ac} . This would increase the rotor speed until balanced operation was again reached where P_m is equal to P_{ac} . However the resulting energy capture would be increased by about 10 % if a control strategy could be developed to change the level of V_{dc} to ensure point D is reached at C_{pmax} .

For maximum energy capture the speed should be controlled to follow the C_{pmax} curve. This curve can be derived from the two look up tables shown in Figure 5.18 and Figure 5.20. For any given wind and rotor speed a low and high value of V_{dc} exists such that point D, on Figure 5.20, is reached where the mechanical input power and the electrical power transfer capability balance with $C_p = C_{pmax}$. The low value of V_{dc} corresponds to line 1 on Figure 5.20 where the rectifier operates at high current and is inefficient. Extracting the relationship between rotor speed and the high value of V_{dc} for maximum power transfer leads to the graph shown in Figure 5.21 which can be used to determine the necessary V_{dc} setpoint for any particular rotor speed.

However this is a quasi-static method as in the presence of rapidly changing turbulence the operational state of the wind turbine is displaced from the curve since the powers can no longer be balanced due to the dynamic loads. This loss in performance could be

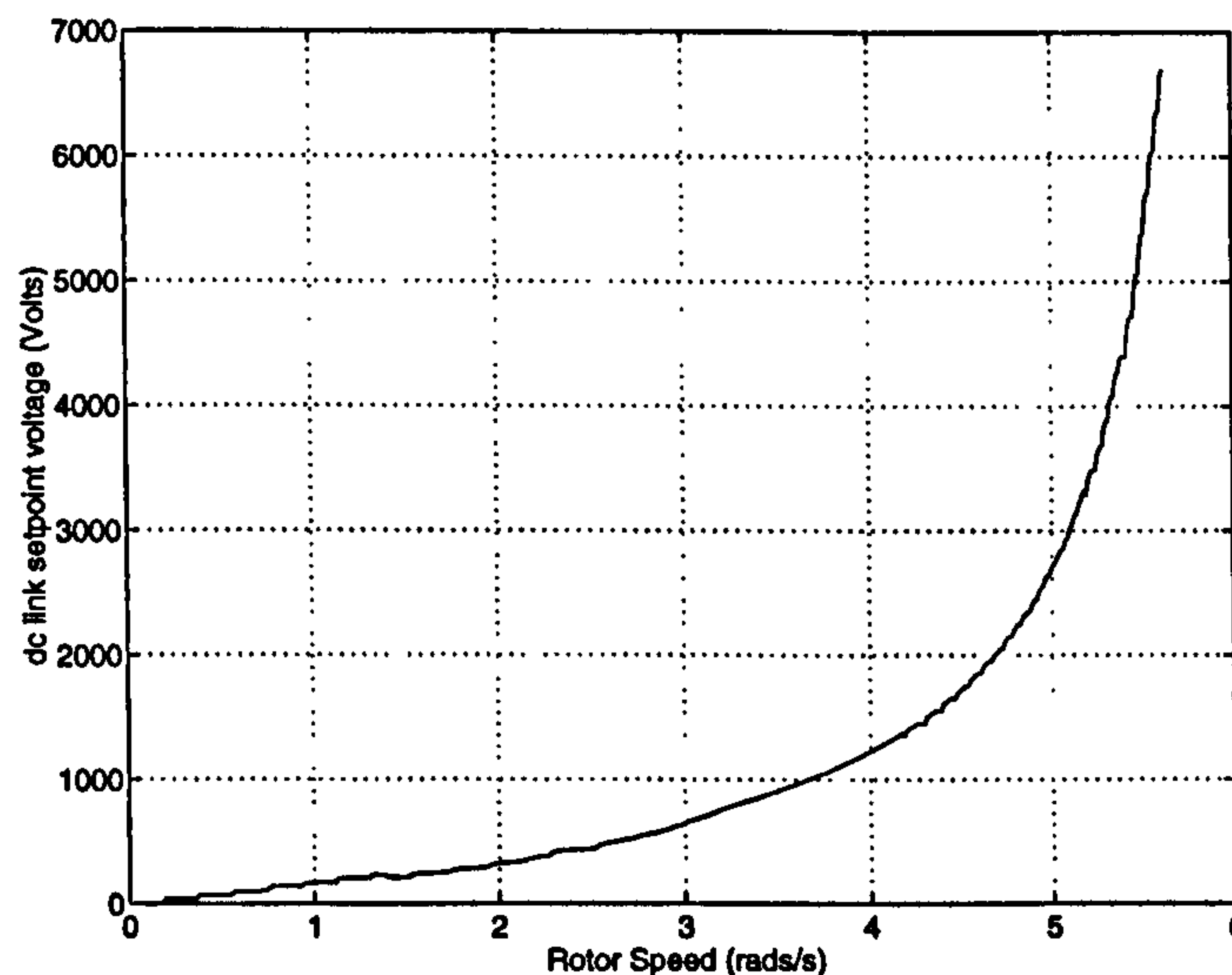


Figure 5.21: V_{dc} setpoint versus shaft speed for optimal C_{pmax} tracking

compensated for by using broad peaked C_p curve aerofoils. However the benefits when compared with the fixed speed case are also reduced. So an algorithm that will track the C_{pmax} curve despite the turbulence of the wind or the dynamics of the turbine must be derived.

A schematic of the control methodology can be seen in Figure 5.22. Below rated power the dc link voltage is altered to track maximum power with the pitch angle kept constant. Above rated power the controller will switch to the same pitch control algorithm, as outlined in Chapter 2, to ensure the generator is not overloaded. The relationship between the power angle controller and its usefulness in controlling the dc link voltage to achieve the required setpoint is outlined in section 5.3.12 after the dc link model and inverter models have been outlined. A further question now arises as to how to control V_{dc} during pitching action and this is discussed in detail in section 5.5.5. A dead band can be included to ensure a smooth transition between the two control options. The only measurement of wind velocity for this control scheme is to determine whether the wind is strong enough to make it economic to synchronise the generator to the grid or so strong that the generator must shut down for safety reasons.

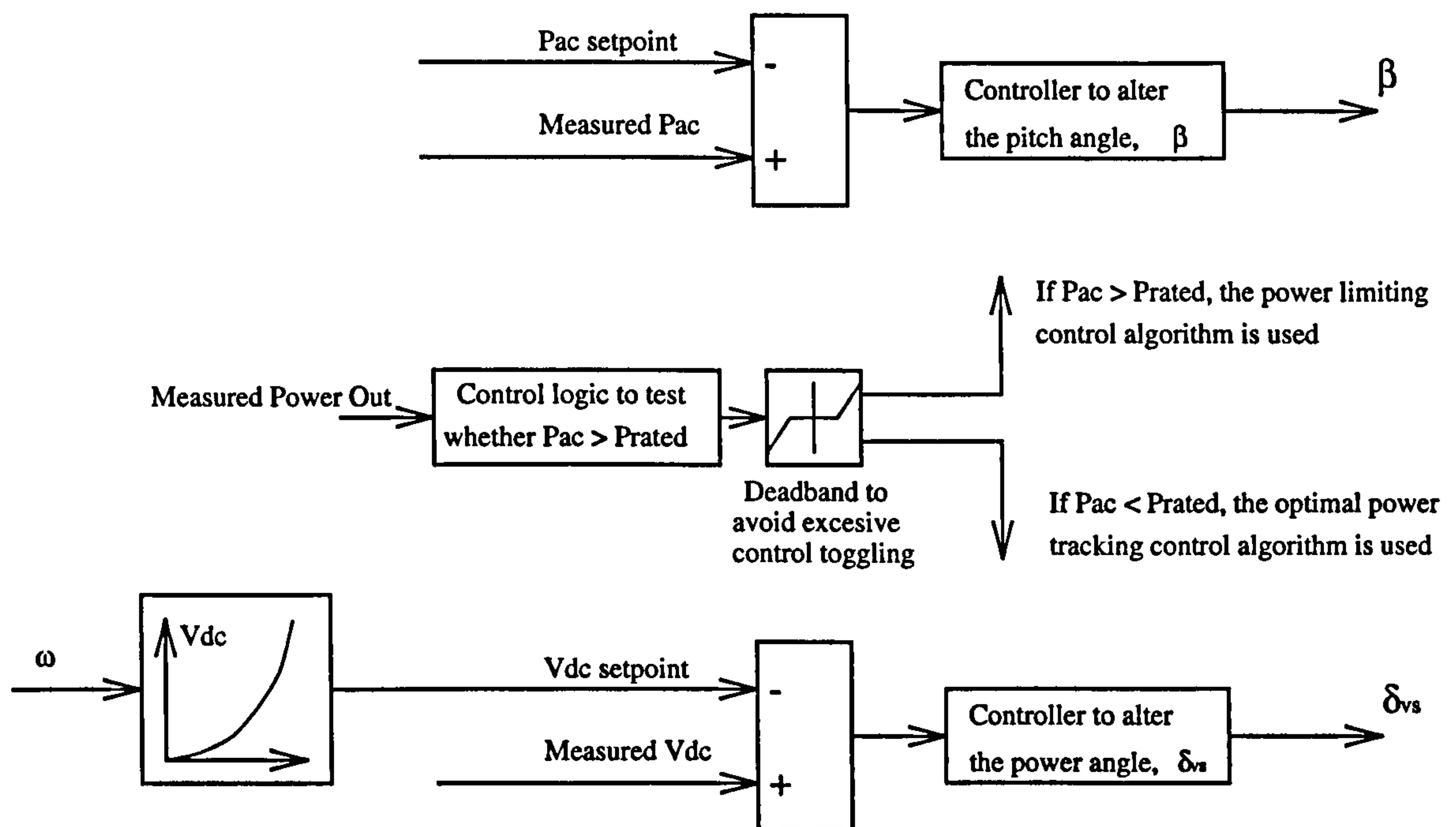


Figure 5.22: Variable Speed Control Architecture for constant control ratio

5.3.8 DC link modelling

The dc link, shown in Figure 5.9 is simply a capacitor and as such has the following equation governing the dc link voltage,

$$V_{dc} = \frac{1}{C_{dc}} \int I_{cap} dt \quad (5.6)$$

The input current to the dc link capacitor, I_{cap} , is the difference between the total current flowing into the dc link and the current flowing into the inverter. The current flowing into the link is the sum of the currents out of the generator and rectifier modules, I_{dc} , and the inverter current, I_{inv} , is determined by the power transfer into the grid. The initial dc link voltage is set so that the wind turbine is operating on the C_{pmax} curve at the initial windspeed.

DC LINK SIMULINK MODEL. The dc link voltage is governed by equation 5.6 and the implementation on SIMULINK can be seen in Figure 5.23 where the inverter current is calculated as presented in the next section. The initial value of the dc link voltage is set to equal the required value for C_{pmax} tracking, as shown in Figure 5.12.

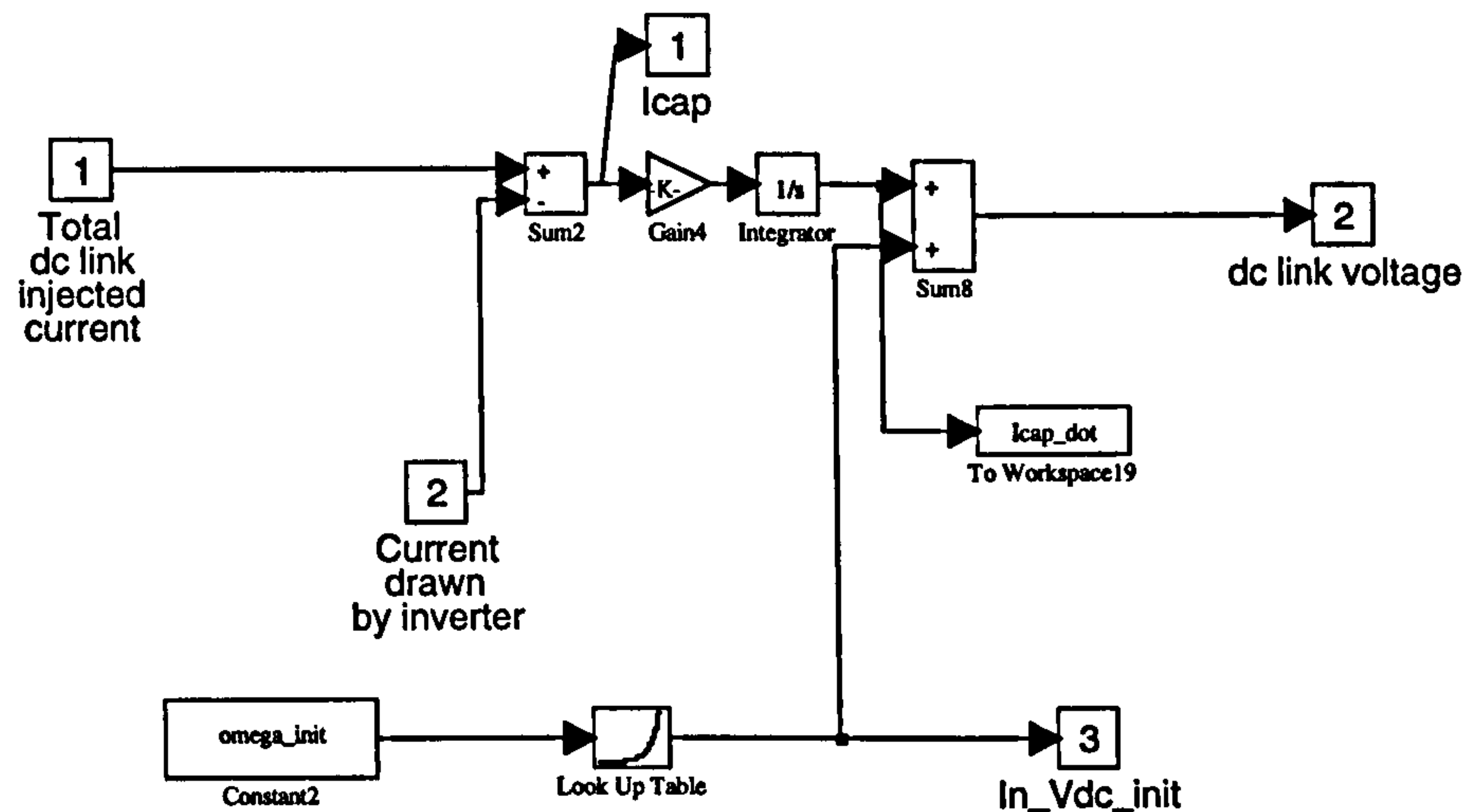


Figure 5.23: DC link SIMULINK model

5.3.9 Inverter configurations

It is unlikely that a single six pulse naturally commutated inverter using thyristor technology would satisfy the harmonic distortion levels for grid connection without further bulky and expensive filtering. Therefore a 6n pulse forced commutated voltage source inverter configuration using insulated gate bipolar transistor (IGBT) technology would be more appropriate. Many configurations exist and several of the most suitable for the permanent magnet generator and multi-pulse rectifier are compared in [96]. When considering each option to determine its performance and its applicability to the generator and multi-phase rectifier, there are three main considerations to take into account:

1. Setting of the dc link voltage level and corresponding transformer ratio.
2. Harmonic distortion of the terminal voltage and switching loss.
3. Overall frequency converter and transformer cost

The purpose of this thesis is not to ascertain which scheme is best but rather to develop a control methodology that will enable the fixed and variable speed operation of the permanent magnet generator to be compared. Overall the greater the number of six pulse inverters that are paralleled together and phase displaced, the lower the resulting total current harmonic distortion (TCHD) into the grid. For a twenty four pulse inverter, the TCHD is 1.545 % which compares with 8.326 % for a single inverter using selective harmonic elimination (SHE) as the means for reducing harmonic distortion. However the cost increases with

5.3 _____ Variable Speed Wind Turbine Modelling

each additional inverter and therefore a trade-off must be determined. The 12 and 24 pulse inverters and single SHE controlled inverter have a good mix of characteristics and are well suited to the proposed permanent magnet generator and multi-phase rectifier design. It is important to understand their operation and this is discussed in the next section for the case of an SHE controlled voltage source inverter using IGBT technology. The discussion is limited to this case as this is the model used in the simulations to derive suitable control strategies for the variable speed wind turbine. However the simulation model can easily be adapted to represent the case of the 12 and 24 pulse inverters by adjusting the relationship for the control ratio of the inverter.

5.3.10 Inverter modelling

An inverter requires several switching devices to operate in unison to sample a dc voltage in such a way that an alternating voltage waveform is created at the output terminals. Several families of semiconductor switching devices have been used in the past, based on both thyristors and transistors, but now the insulated gate bipolar transistor (IGBT) is coming into its own with good power and switching capabilities [99]. IGBT's have a simple gate firing control like MOSFET's [100] but have a much higher power capacity and are assumed as the basis for the discussion of inverters in this thesis [101].

The individual modelling of the IGBT's within the inverter is not strictly necessary to devise control strategies for the operation of the wind turbine as the time scale of control of the wind turbine is far greater than that of the individual switching of the transistors. However the rating of the transistors must not be exceeded to ensure the safe operation of the inverter and the mechanisms for controlling the power flow through the inverter must be understood to allow a suitable dynamic model to be developed.

IGBT PERFORMANCE. For present purposes the IGBT performance can be described in terms of a power transfer capacity and a voltage breakdown limit. Furthermore it is assumed that sufficient heat sinking is available so that the power dissipation of the IGBT's is not exceeded. The controller of the dc link voltage, described in section 5.3.11, must not act to exceed either of these two limits of the IGBT or the IGBT's performance would be compromised. This is the only consideration of the individual IGBT's in the thesis. Once the characteristic $\omega - V_{dc}$ curve for the setpoint of V_{dc} to track C_{pmax} has been evaluated an

IGBT module can be chosen to ensure its breakdown voltage is greater than the maximum required voltage for tracking C_{pmax} over the range of variable speed operation. The power and voltage breakdown capacity of an individual IGBT may be enhanced by the parallel and serial connection of several IGBT's to form a single firing leg of the inverter. This would however lead to a large increase in the required number of gates and driving circuitry and therefore proper sizing of the IGBT's is essential to keep costs down. This is discussed further in the next chapter.

SINGLE INVERTER DESCRIPTION. An equivalent circuit for a typical six pulse inverter can be seen in Figure 5.24. Each leg of this voltage controlled inverter can be fired separately to create a variety of waveforms by suitable switching of the individual transistors. The transistors are marked 1-6 in the order they are switched on and remain switched on for one half cycle. The potential at X, Y, Z will then be three square wave voltages with amplitude $\frac{V_{dc}}{2}$ phase displaced 120 degrees from each other. The potentials of the individual legs X, Y, Z of the inverter would change as shown in Figure 5.25.

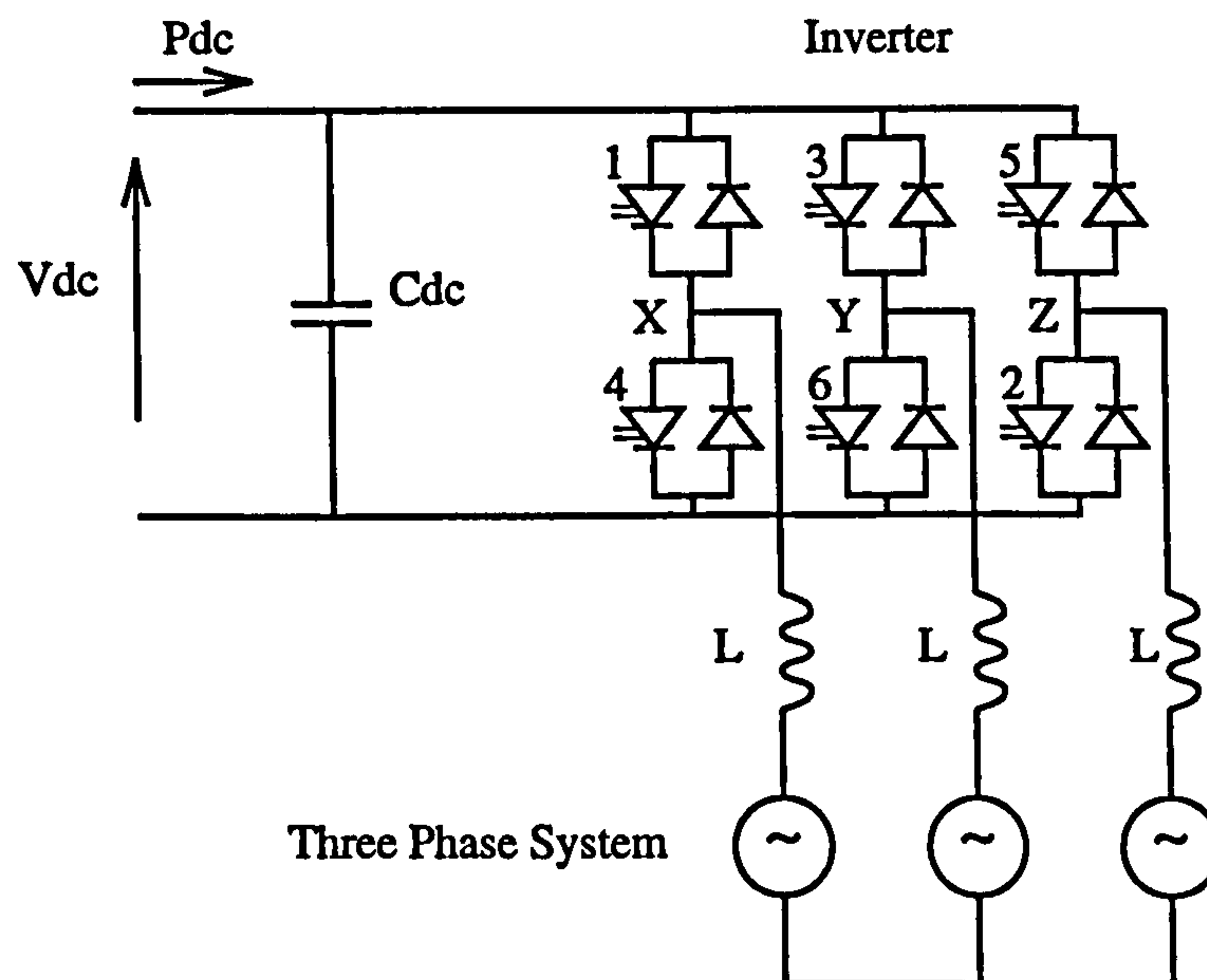


Figure 5.24: Equivalent Circuit for Inverter

PHASE CONTROL. By delaying the firing of each limb of the inverter the fundamental of the output voltage can have any phase delay between 0 and 360 degrees. This allows control of the real power flow into the grid.

OUTPUT HARMONIC CONTENT. Fourier analysis of the square wave phase voltages, presented in Figure 5.25, shows that they consist of odd harmonics with rms values

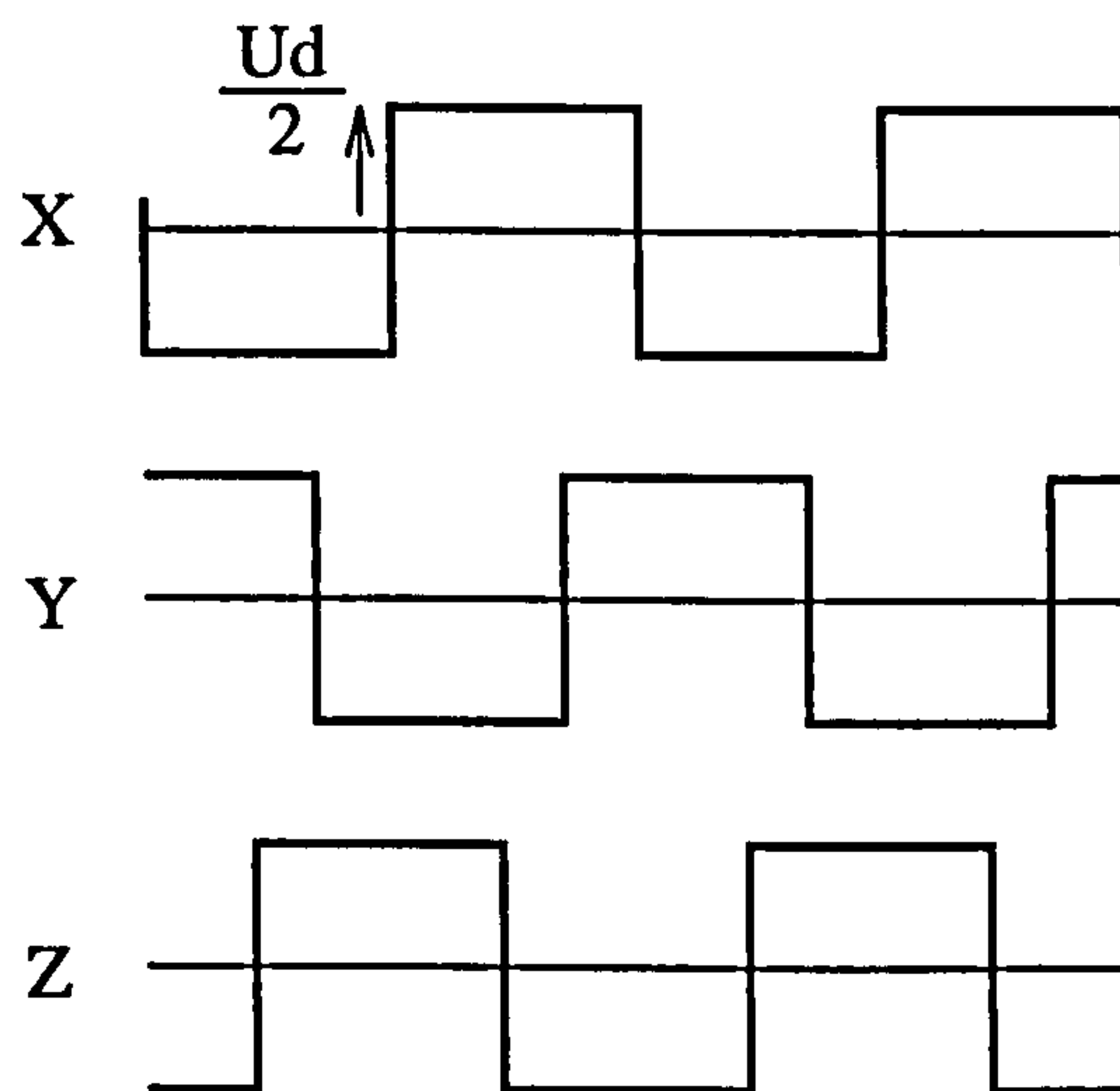


Figure 5.25: Potential Waveforms

given by,

$$V(n) = 0.9 \frac{V_{dc}}{2n} = \frac{0.45}{n} V_{dc} \quad n \text{ odd} \quad (5.7)$$

where n is the order of the harmonic and is always odd. The phase to phase voltages can be calculated as the difference between corresponding phase voltages and have the same harmonics as the phase voltages. When the output of the inverter is connected via a Δ -Wye transformer the triplen harmonics are eliminated and the output phase voltage is given by,

$$V(n) = \sqrt{3} \frac{0.45}{n} V_{dc} = \frac{0.78}{n} V_{dc} \quad n = 1, 5, 7, 11, 13, \dots \quad (5.8)$$

5.3.11 Harmonic output and voltage control

The low order harmonics present in the output from the inverter can cause damage and losses within the power network and the connection requirements of the National Grid Company limit the permissible level of the Total Harmonic Distortion (THD). There is also a limit on the allowable voltage fluctuation at the terminals of the transformer of between +6 and -10 % [93]. To reduce the level of harmonics and alter the output voltage level from the inverter to within the necessary range, the inverter can be further controlled in one of three ways:

1. Varying the input dc voltage by using a controlled rectifier.
2. Varying the output voltage by using some form of ac converter.
3. Waveform modulation which can either be achieved by building an output as a difference between two or more phase shifted voltages or by pulse width modulation.

The last control method and in particular pulse width modulation is a method which could easily be employed in wind turbine applications and will now be discussed in greater detail.

PULSE WIDTH MODULATION. Pulse width modulation implies that the square waveform of the output voltage is changed by additional commutations and that the phase potential will change sign several times during each half cycle. The main purpose of pulse width modulation is to change the ratio of the fundamental component of the ac voltage to the dc voltage. As this ratio decreases there will at the same time be an increase in the harmonic content of the output ac waveform. However with the use of a well designed switching strategy selective harmonics can be eliminated or reduced significantly. Individual harmonics are normally quoted as a percentage of the fundamental with a measure of the total harmonic distortion (THD) introduced given by,

$$k = \sqrt{\epsilon V_{(n)}^2} \quad (5.9)$$

with harmonics of order greater than 25 usually neglected. A typical allowed level for the THD at 10 kV is 3 % [102].

Several switching strategies are common in inverter control and each have their drawbacks and advantages. Firstly, simple strategies such as center and end pulse modulation of the waveform can be used to control the magnitude of the fundamental but the harmonic content of the output voltage cannot be controlled and is usually unacceptable unless some form of additional filtering is used. Secondly, selective harmonic elimination by means of voltage reversal can be used which allow the fundamental to be controlled and certain harmonics to be eliminated. Each voltage reversal gives one degree of freedom to eliminate a harmonic or control the fundamental. Finally sinusoidal pulse width modulation can be used where the level of certain low order harmonics are reduced whilst the less harmful high order harmonics are reinforced. The sinusoidal reference voltage and triangular voltage must have a high enough frequency ratio as this determines the order of the harmonics to be reinforced.

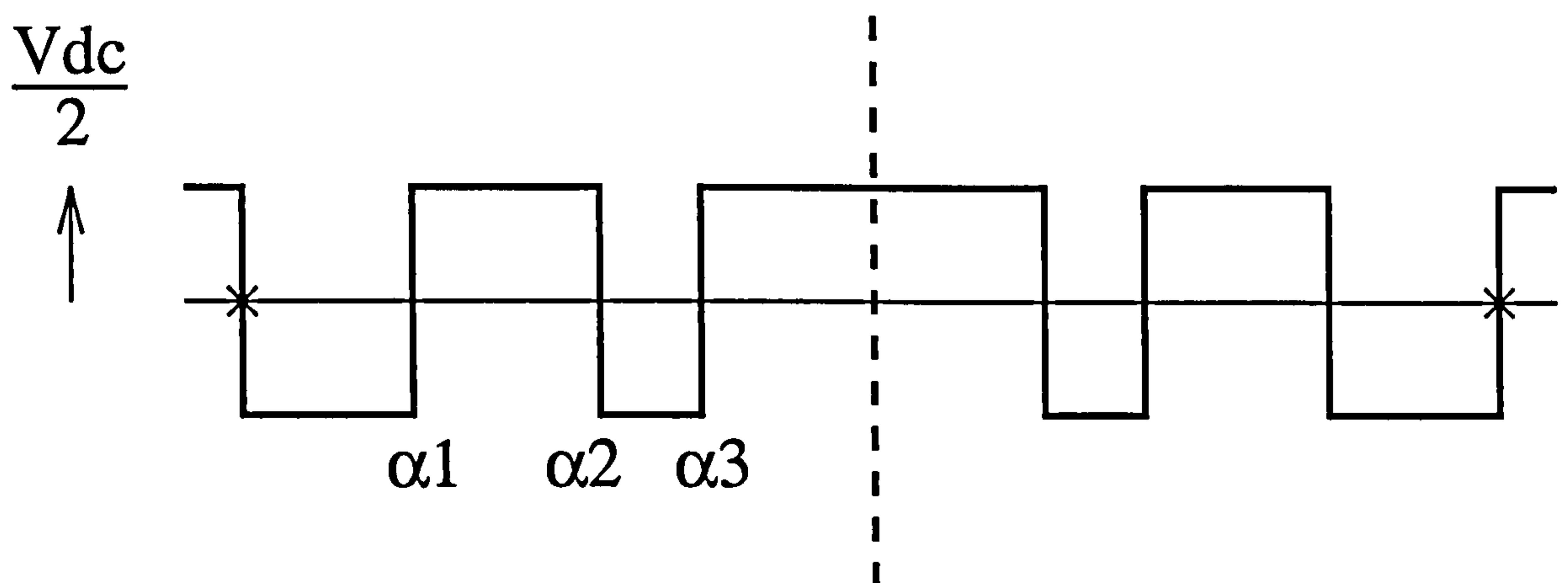


Figure 5.26: Voltage Reversals for Selective Harmonic Elimination

The two methods, selective harmonic elimination (SHE) and sinusoidal pulse width modulation (SPWM), are both used extensively to control the output of inverters [103] [104]. However SPWM was really devised with analogue switching devices in mind and the use of the new IGBT's with microprocessor control facilitates the storage of the switching strategies for SHE in the EPROM of the controller. An example of selective harmonic elimination will now be used to illustrate such inverter control.

SELECTIVE HARMONIC ELIMINATION. A switching strategy for the inverter of the type shown in Figure 5.24 is required for the elimination of the 5th and the 7th harmonics whilst retaining control of the fundamental. Three reversals of voltage per half cycle are required to give the necessary control of the fundamental and eliminate the two odd harmonics. A waveform of such a phase voltage can be seen in Figure 5.26. The notches are placed symmetrically about the centre line of the half cycle. The equation governing the rms value of the n^{th} harmonic of the waveform is,

$$V(n) = \frac{1}{\sqrt{2}} \frac{4}{\pi} \frac{V_{dc}}{2} \left[-\int_0^{\alpha_1} \sin n\alpha d\alpha + \int_{\alpha_1}^{\alpha_2} \sin n\alpha d\alpha + \cdots \int_{\alpha_p}^{90} \sin n\alpha d\alpha \right] \quad (5.10)$$

$$= \frac{0.45}{n} V_{dc} [2(\cos n\alpha_1 - \cos n\alpha_2 + \cos n\alpha_3 - \cdots) - 1] \quad (5.11)$$

Control of the fundamental and elimination of the 5th and 7th, will result in a system of transcendental equations which can be solved to give the required angles of reversal and the size of the 11th and 13th harmonic in relation to the fundamental as the control ratio is

changed. The control ratio, $K_{V_{dc}}$, is the ratio of the fundamental of the rms output voltage of the inverter to the fundamental of the unmodulated waveform and is the bracketed term of equation 5.11. So for a given control ratio the angles must be determined to eliminate the chosen harmonics and give the required control ratio. The fundamental of the unmodulated waveform is given by equation 5.11 with the bracket equal to one and $n = 1$ and hence the control ratio is defined as,

$$K_{V_{dc}} = \frac{V(1)}{0.45V_{dc}} \quad (5.12)$$

The variations of the required switching angles for elimination of the 5th and 7th harmonics versus control ratio are shown in Figure 5.27 [102]. The angles are undefined for control ratios greater than 0.9 and therefore the control ratio can be varied in the range 0 to 0.9. For selective harmonic elimination schemes the fundamental voltage at the output terminals of the inverter is always much less than the dc link voltage and therefore a larger turns ratio transformer is typically required to step up the voltage to the grid connection level than for other schemes.

Furthermore as the fundamental is controlled by varying the control ratio the next two highest harmonics will vary as a percentage of the fundamental as shown in Figure 5.28. This means that providing three suitable angles are chosen the 5th and 7th can be eliminated and the magnitude of the fundamental controlled. Such a scheme can be extended to eliminate as many harmonics as required with the only limitation being the switching loss and switching time, especially in higher power and frequency applications. The angles could be stored as a lookup table in the memory of the microprocessor control unit and an interpolation routine could be used to give intermediate points.

5.3.12 Overall inverter to grid representation

Now that the operation of a single inverter has been introduced it is necessary to outline how the output power can be transmitted to the grid. The overall description of the proposed dynamic representation of the inverter interaction with the infinite bus is the same as for an ideal synchronous machine. Therefore it can be represented by the phasor diagram of Figure 5.29.

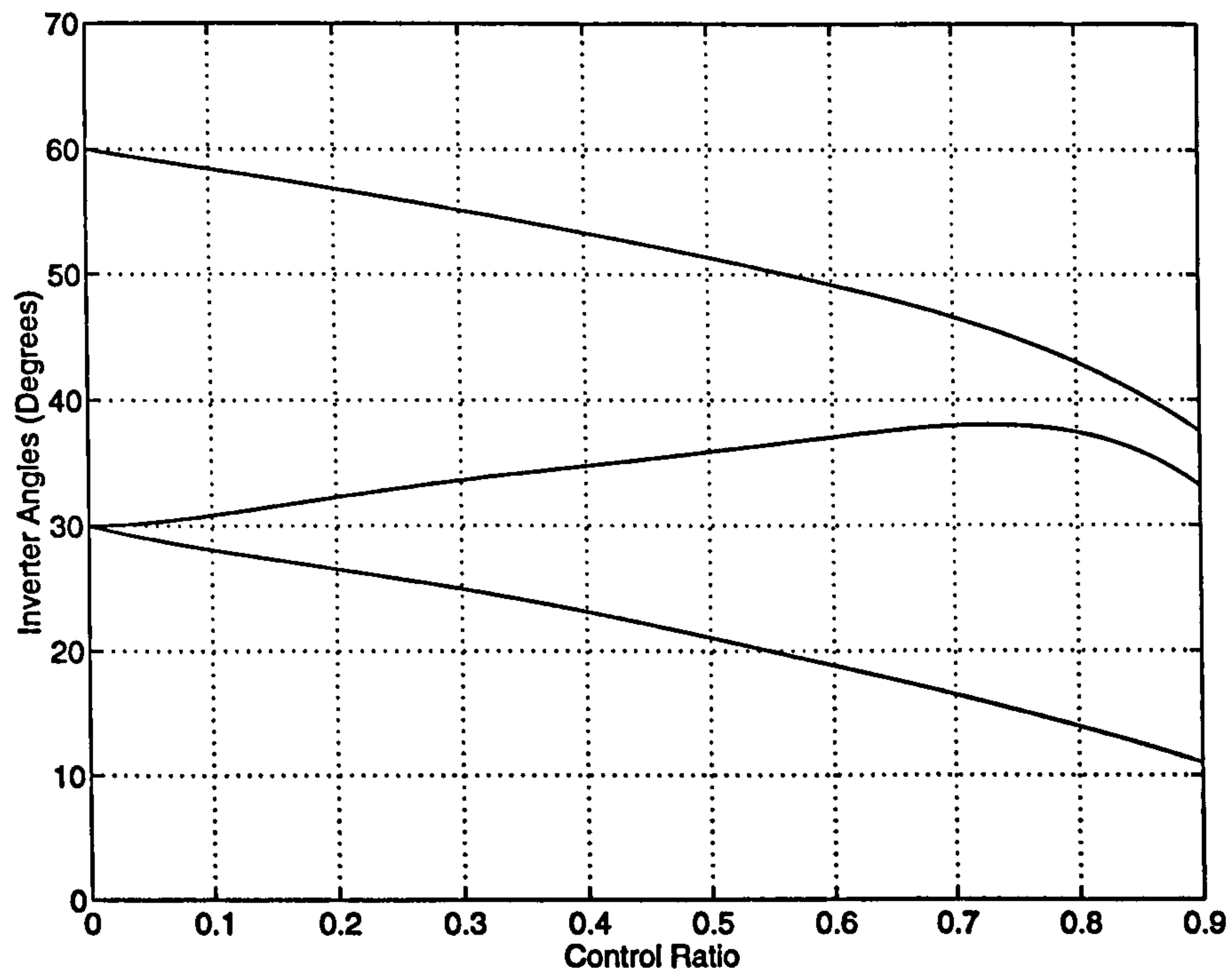


Figure 5.27: Switching angles for the elimination of the 5th and 7th harmonics with control of the fundamental by means of voltage reversal

REAL AND REACTIVE POWER CONTROL. The fundamental of the r.m.s terminal voltage of the inverter is represented as a variable proportion of the dc link voltage by the control ratio which leads to,

$$V(1) = 0.45K_{V_{dc}}V_{dc} \quad (5.13)$$

where $K_{V_{dc}}$ is the control ratio. Figure 5.28 shows the variation of the lowest of the remaining harmonics with control ratio which can be varied from 0 to 0.9 until the switching angles become undefined. The power angle, δ_{vs} , is defined for the variable speed case as the angle between the terminal voltage of the inverter and the infinite bus. The power angle, therefore, still sets the power flow into the grid. The power angle, and hence power flow into the grid, can be varied almost instantaneously, by adjusting the delay of the switching of the inverter firing angles. The firing angles are typically stored in a look up table and a delay is included in the model of the inverter to represent both the delay in accessing the table and the measurement by a zero crossing device to evaluate the power angle, δ_{vs} . The real three phase electrical power into the grid, assuming the transmission line can be

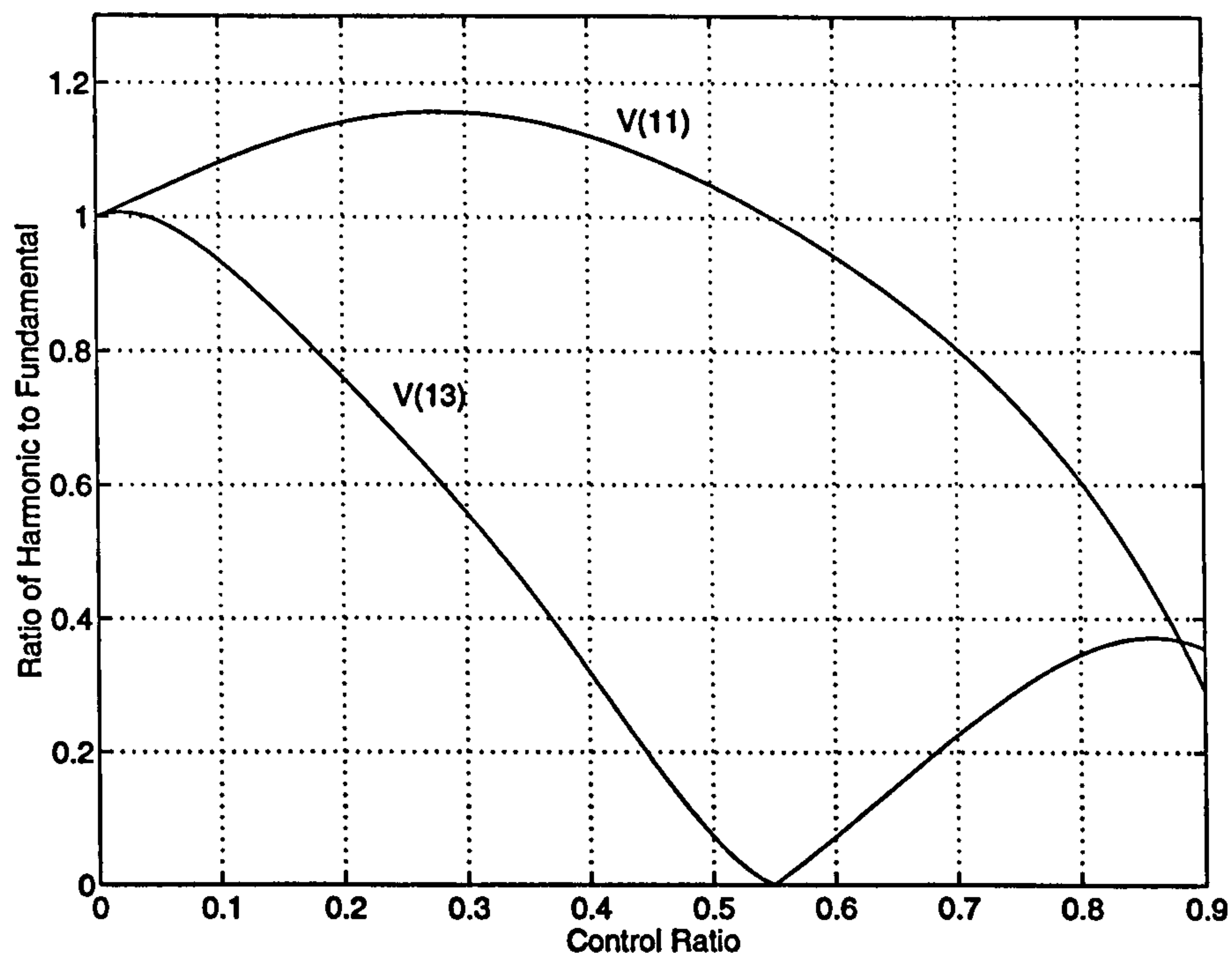


Figure 5.28: Variation of the 11th and 13th harmonics versus control ratio with elimination of the 5th and 7th harmonics using three switching angles

represented by a pure reactance, is given by,

$$P = \frac{3V(1)V_{sys}}{X_s} \sin \delta_{vs} \quad (5.14)$$

The reactive power flow, likewise, is governed by,

$$Q = \frac{3V_{sys}}{X_s} (V(1) \cos \delta_{vs} - V_{sys}) \quad (5.15)$$

It is the balance between controlling δ_{vs} and $V(1)$ that is important when looking at control techniques of the inverter.

INVERTER AND VARIABLE SPEED CONTROL. By controlling the start of the sequence of inverter firing angles it is possible to control the power output of the inverter to the grid. The phase of the fundamental of the terminal voltage of the inverter can be altered with respect to the measured phase of the infinite bus voltage and thus change the effective power angle, δ_{vs} , between the fundamental terminal voltage of the inverter and the infinite bus voltage. In one PWM switching scheme the zero crossing point of the

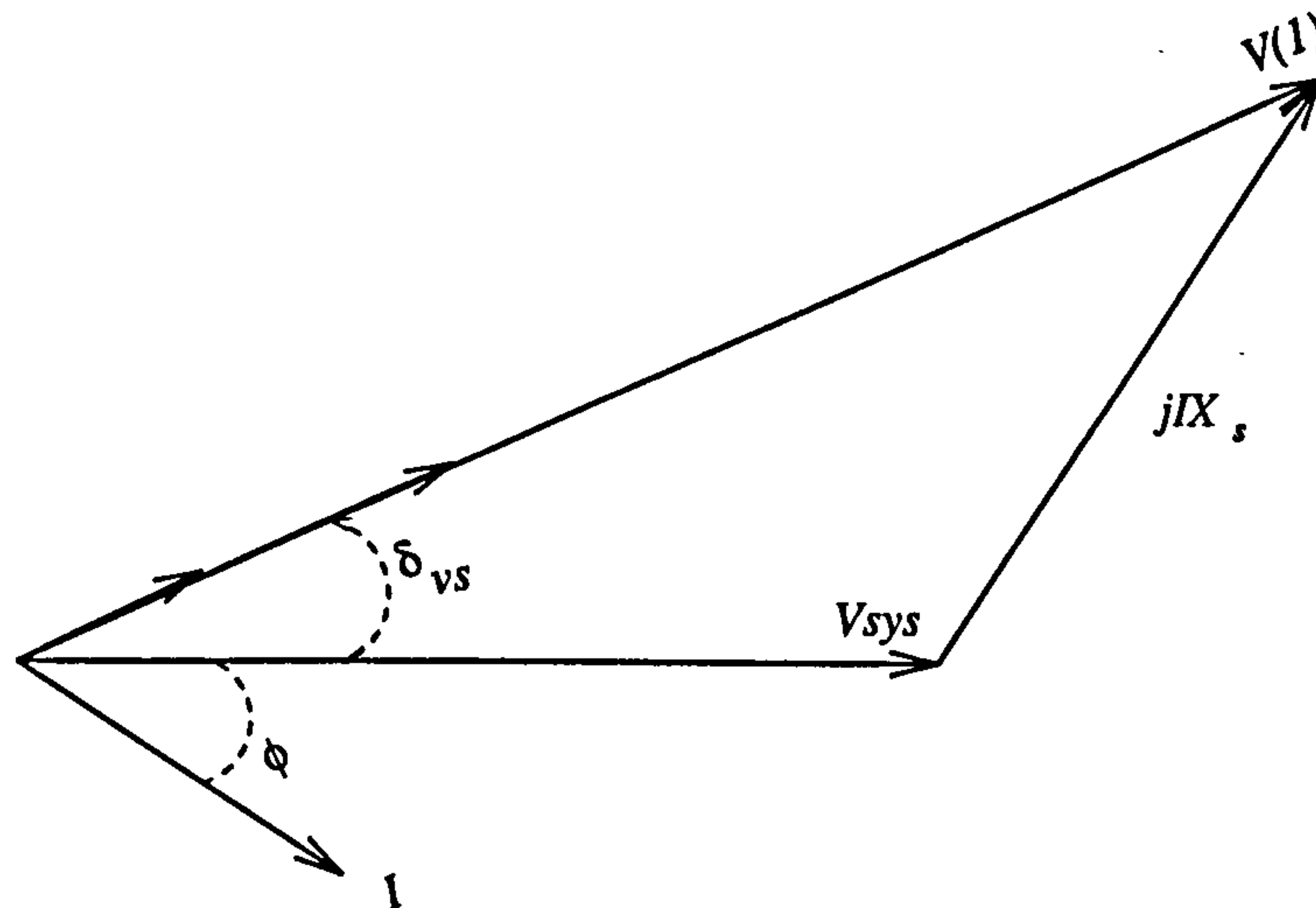


Figure 5.29: Phasor diagram of the inverter connected to the infinite bus

system voltage at the infinite bus is measured and transmitted to the inverter switching controller. This is then used to evaluate the required switching pattern. The power loss due to switching within the inverter is modelled by assuming a constant efficiency of 97%. The power transmitted to the grid by the generator is given by,

$$P = \frac{3V(1)V_{sys}}{X_s} \sin \delta_{vs} \quad (5.16)$$

where $V(1)$ is related to the dc link voltage, V_{dc} , and control ratio by equation 5.13 and X_s is the reactance of the transformer and transmission line to the infinite bus. The dc link voltage, V_{dc} , varies due to the charging current flowing into the capacitor which is calculated from the difference between I_{dc} and I_{inv} as shown in Figure 5.1. Changing the angle, δ_{vs} , alters the power flow into the grid and hence the required current flowing into the inverter. The relationship between the inverter current and power angle, δ_{vs} , can be found from a consideration of the power flow across the inverter, which must be balanced, and substituting in V_{dc} using equation 5.13. This gives,

$$P_{inv} = 0.97V_{dc}I_{inv} = \frac{3V(1)V_{sys}}{X_s} \sin \delta_{vs} \quad (5.17)$$

$$I_{inv} = \frac{1.31KV_{dc}V_{sys}}{X_s} \sin \delta_{vs} \quad (5.18)$$

A change in δ_{vs} leads to a change in I_{inv} which results in a change in V_{dc} , provided the control

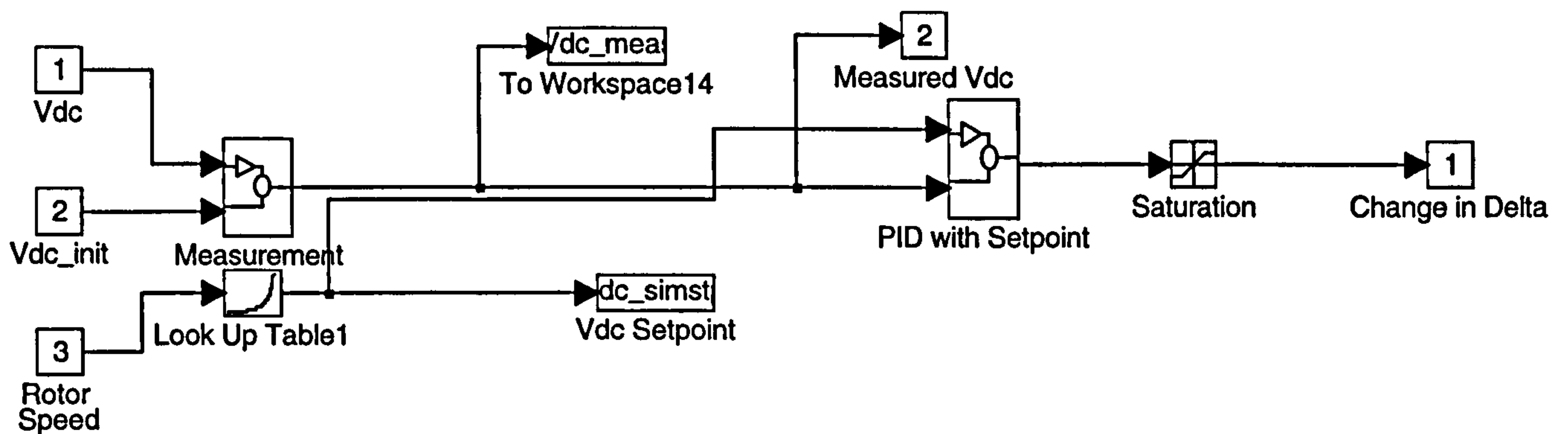


Figure 5.31: SIMULINK implementation of the V_{dc} setpoint controller

be operating at C_{pmax} and hence the required dc link voltage from the $\omega - V_{dc}$ characteristic. Once the value of ω and V_{dc} are known the values for the corresponding airgap power and current injected into the dc link can be found from interpolation within the 2D lookup tables discussed in section 5.3.6. The control ratio of the inverter is set to give nominal inverter terminal voltage. The inverter current is set to equal the current flowing into the dc link and substituting this value for I_{inv} into equation 5.18 gives the initial value for the power angle, δ_{vs} , between the inverter terminal voltage and the infinite bus. At each subsequent time step as the windspeed varies the power angle between the inverter and the infinite bus and the control ratio of the inverter are controlled to track C_{pmax} and maintain rated voltage. As ω and V_{dc} vary with the wind speed the values for the airgap power extracted from the shaft and the injected dc link current are evaluated from the 2D lookup tables and used to determine what change in rotor speed and dc link voltage occur.

One key aspect that must be addressed is the interpolation routine that is used to find values of airgap power, P_{ac} , and dc link current, I_{dc} , from the lookup-tables, described in the previous sections, as the rotor speed and dc link voltage change in response to the wind time history used as input to the model. This interpolation routine is essential for the accuracy and smooth running of the simulations.

INTERPOLATION TECHNIQUES. There are several interpolation techniques that are available in MATLAB and the one used is based on cubic spline interpolation. Some extrapolation of the performance data returned from WINDVARP is necessary to ensure accurate interpolation. Firstly the output data from WINDVARP was rearranged into two

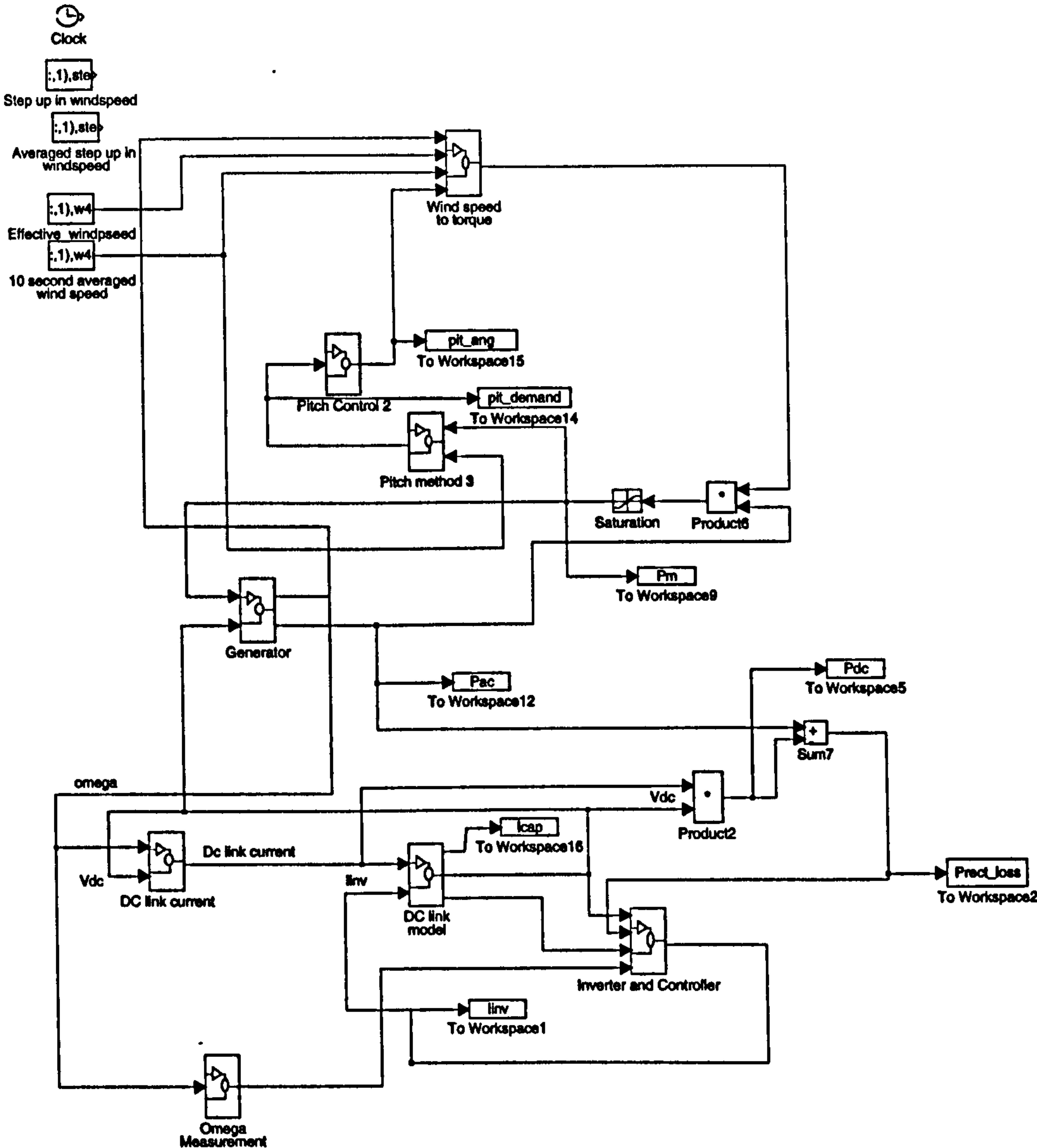


Figure 5.32: Variable speed wind turbine model

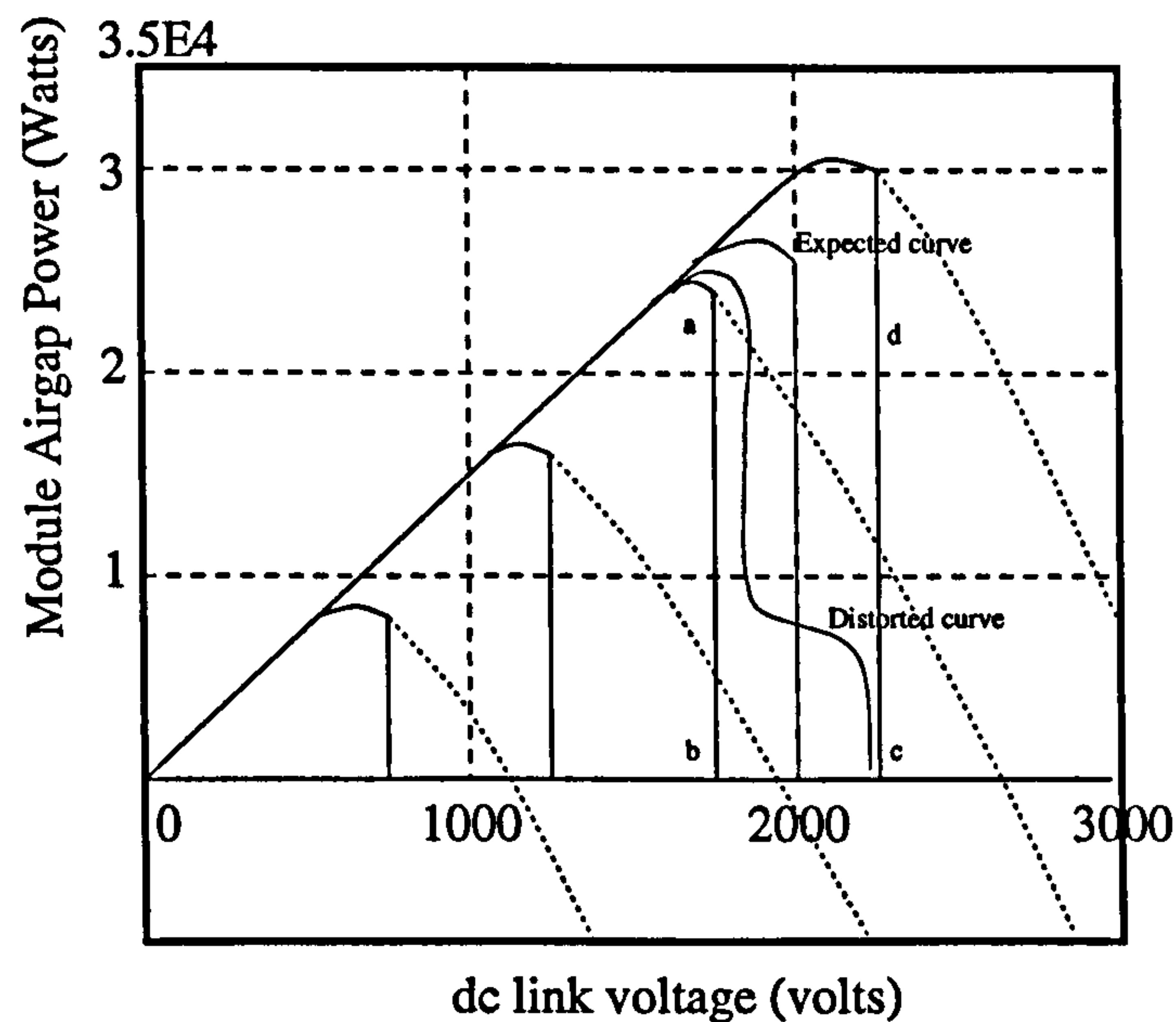


Figure 5.33: Extended power curves for accurate interpolation

2D tables representing the ac power transfer characteristic, P_{ac} , and the current injected into the dc link per module indexed by monotonically increasing rotor speed and dc link voltage indexes. Then the tables were expanded beyond the bounds of physical reality. This ensured that the interpolation space was sufficiently covered to minimise error. The type of error that can occur with a non-linear table can be seen in Figure 5.33.

The non-linearity causes the values returned from the interpolation routine in the region abcd on Figure 5.33 to follow the curve shown instead of bisecting the two characteristic curves either side as would be expected. Expanding the curves as shown, and being careful to set the output from the tables to zero when outside the bounds of physical reality, led to a reduction in this type of error.

5.4 The parameters of the variable speed system

The purpose of this section is to outline the derivation of the parameters for the permanent magnet generator and rectifier, dc link and inverter. The overall design procedure for the wind turbine is the same as outlined in Chapter 3 except now the tuning capacitance must be chosen to ensure an appropriate power transfer characteristic between the wind and the generator and rectifier unit. Several design drivers are identified and these are used to quantify the design interactions for generator ratings from 200 kW to 1.5 MW, a typical

5.4 _____ The parameters of the variable speed system

range for wind power applications.

5.4.1 Overall design procedure

The required diameter of the blades is found, as before, by rearranging the equation for the power in the wind to give,

$$\text{diameter} = \sqrt{\frac{8P_{nom}}{\rho V_{nom}^3 C_{p_{nom}} \pi}} \quad (5.19)$$

but with $C_{p_{nom}}$ set to equal $C_{p_{max}}$, assuming ideal tracking. This leads to blades with slightly less diameter than the fixed speed case being required for the same rating or what is more likely a slightly increased generator rating.

The cut-in wind speed is still determined by the level at which useful power is delivered to the grid which now depends not only on the losses in the generator but also on the losses of the rectifier and inverter. The cut-in wind speed also sets the minimum rotational speed of the rotor assuming the wind turbine operates at the optimum tip speed ratio. The minimum rotor speed as a function of rated rotor speed will be given by,

$$\frac{\omega_{min}}{\omega_{rated}} = \frac{V_{cut-in}}{V_{rated}} \quad (5.20)$$

The rated rotational speed of a wind turbine is still constrained by the tip speed which should be typically between 50 and 70 m/s for minimum noise generation. Hence, for a given nominal wind speed and the calculated diameter, a particular rated rotational speed is given by,

$$\frac{50}{\text{diameter}} \geq \omega_r \leq \frac{70}{\text{diameter}} \quad (5.21)$$

The maximum rotational speed is set such that the limits imposed by the insulation requirements for the generated voltage in the E-core and the power transfer capability are not violated. Furthermore as the rotor speed increases the dc link voltage increases for a given current limit in the tuning circuit to maintain the correct power transfer. Therefore the speed is restricted to prevent the dc link voltage from being so great as to break down the blocking voltage level of the IGBT's in the inverter.

The rated rotor speed fixes the number of pole pairs required to give 55 Hz generation

5.4 _____ The parameters of the variable speed system

and, using the magnetic circuit described in section 3.1.5, the outside diameter of the rotor. The maximum number of E-cores is given by dividing the circumference of the rotor by the standard E-core width of 75 mm. It is no longer necessary to arrange the winding connections to give a satisfactory output voltage or have a multiple of three E-cores and this gives more scope in sizing and setting out the E-cores, which are now uniformly distributed around the rotor.

5.4.2 WINDVARD, WINDVARP, WINDVOUT - A variable speed permanent magnet design suite

Three linked programs, WINDVARD, WINDVARP, WINDVOUT, that enable a full range of variable speed permanent magnet generators to be designed have been written by other members of the Wind Energy Research Group at Durham. The functionality of each program and how it has been used to generate suitable designs for range of typical wind turbines ratings is now outlined.

WINDVARD. The required specification in terms of the wind turbine blade diameter, rotational speed, mean windspeed at hub height and coefficient of performance data are entered first and a nominal power rating is found. One key difference between the fixed and variable speed design process is that the frequency is not limited to 50 Hz and for the reasons given in the first section of this chapter 55 Hz is considered a good value both in terms of reduced cost but also because a better power transfer characteristics is obtained for the tuning circuit. The standard module sizes for both the rotor and stator are then chosen from a selection which satisfy the design constraints of demagnetisation current, required frequency of operation and electric loading.

Once the basic design is entered a magnetic circuit analysis is carried out to find the values of generator reactance, resistance and the generated emf. A phasor analysis, assuming a sinusoidal E-core voltage, is then carried out to determine the level of power transfer per stator module at rated frequency for a range of tuning circuit capacitances. The method for this is given in Appendix D. The level of tuning capacitance is chosen so that the total power transfer for the given number of stator modules per ring satisfies the thermal loading of a whole generator ring. The minimum number of rings to satisfy the thermal loading is chosen by the user. This means that the variable speed generator design can be very

5.4 _____ The parameters of the variable speed system

economical in the material used for a given power rating. The program then moves onto the performance section.

WINDVARP. This program requires the user to enter a rotor speed range and a dc link voltage range to establish a prediction of the generator power transfer performance and, hence, ascertain the effectiveness of the design over the entered range. For every step in rotor speed through the range the program evaluates the level of the dc link voltage at which power is transferred and then outputs the variation as the dc link voltage is reduced from this value by a user defined decrement.

WINDVOUT. This program outputs all the values from WINDVARD and WINDVARP and returns values for the masses of the key generator parts. Weight is a crucial design criteria in wind turbines as a low tower head weight leads to a lighter tower structure and overall cost savings. The returned values for the weights are used to calculate the inertia of the rotary parts of the generator. This calculation is the same as presented in Chapter 2 except the stator inertia is not considered as it is stationary for the variable speed case.

5.4.3 Tier Number

As explained in Chapter 2 several tiers are mounted in parallel on the rotor shaft to enable the power to be transmitted to the grid without violating the thermal loading constraint on the E-core windings. The lack of a requirement to design for the compliant mounting means that the minimum number of tiers can be used. This leads to substantial weight savings. The number of tiers is incorporated into the variable speed model as the mechanical and electrical power per module must balance for steady state operation.

5.4.4 The choice of dc link capacitance

The dc link capacitance is chosen to be $4000\ \mu F$ as this is a sufficiently large value to ensure a smooth dc link voltage during switching transients. The variation of the performance as this value is varied is presented in Chapter 6.

5.4 _____ The parameters of the variable speed system

5.4.5 Variation with generator ratings

It is now appropriate to consider the change in the key parameters as the generator ratings vary for units which are considered to be well designed in light of the arguments presented in the previous sections. The key parameters for a range of variable speed generator ratings typically found in wind turbine applications can be seen in Table 5.2.

Rating	200 kW	455 kW	750 kW	1 MW	1.5 MW
Stator OD (m)	2.15	2.59	3.12	3.65	4.52
Design frequency	55	55	55	55	55
Rated rotor speed (rev/min)	44.8	36.1	29.1	25	20
No. of Poles	148	184	226	264	330
No. of Tiers	1	2	2	2	3
No of stator modules per tier	80	98	120	142	178
Tuning capacitance	25 μ F	33 μ F	33 μ F	33 μ F	33 μ F
Rotor inertia	38680	178400	649400	1139000	3185000
Total generator weight	3990	8270	12260	15630	28520

Table 5.2: Variable speed generator Parameters

As expected the stator diameter increases with generator rating because the lower rated rotational speed with generator rating requires more poles to generate a nominal 55 Hz. The generator weight also increases with generator ratings but, just as in the fixed speed case, the rotor inertia is dominated by the wind turbine blades and there is not much difference between the fixed and variable speed rotor inertias. However there is a marked difference in generator weight because of the reduced number of tiers and this is discussed in more detail in Chapter 7. The level of tuning capacitance is chosen to match the input power characteristic from the wind with the power characteristic across the E-core and rectifier modules of the generator. Further work could be carried out to optimise the capacitance level in terms of choosing the minimum cost capacitance that would achieve the desired tuning effect. The value of 33 μ F was found to be adequate across the range except for the 200 kW rated generator which needed less capacitance to avoid excessive resonance over the speed range of operation.

5.4.6 Data post-processing

The performance data output from WINDVOUT is post-processed both in EXCEL, as presented in Chapter 3, and also in MATLAB to create the lookup tables necessary for the

5.4 _____ The parameters of the variable speed system

variable speed simulation.

POST-PROCESSING ON EXCEL. The design data has again been implemented on a spreadsheet using Microsoft Excel [84] in a similar manner to that presented in Chapter 3. This simplifies the procedure for evaluating the necessary parameters for the Simulink models as just a few values from the printed output from WINDVOUT are required and the rest of the values are updated automatically using simple mathematical formulae. For instance equation 3.8 is used to calculate the rotor inertia. An example of the spreadsheet is included for completeness and can be seen in Figure 5.34. The values taken from the output of WINDVOUT are highlighted in bold.

3 GRP Blades, Design Vw=12	Variable	Variable	Variable	Variable	Variable
Generator Rating	200 kW	458.2 kW	791 kW	1000 kW	1500 kW
Rated Frequency	55 Hz	55 Hz	55 Hz	55 Hz	55 Hz
Rated Rotational Speed	44.80	36.00	29.10	25.00	20.00
Blade Diameter	24.00	36.00	46.00	62.00	66.00
Blade Weight	0.79	1.71	3.64	6.00	8.95
Blade Inertia at Rgy = 0.5L	8.49E+04	3.94E+05	1.45E+06	2.54E+06	7.09E+06
Check using rod	1.13E+05	8.26E+05	1.93E+06	3.38E+06	9.45E+06
Check with Rgy = Rod/3	3.77E+04	1.79E+05	6.42E+05	1.13E+06	3.18E+06
Hub Diameter	1.20	1.75	2.30	2.60	3.25
Hub Weight	0.59	1.29	2.73	3.75	6.71
Hub Inertia	8.49E+01	3.94E+02	1.45E+03	2.54E+03	7.09E+03
Number of Ribs	1.00	2.00	2.00	2.00	3.00
Rotor OD1	1.93	2.37	2.90	3.43	4.30
Rotor ID1	1.73	2.17	2.70	3.23	4.10
Rotor structure mass	3.53E+02	4.16E+02	5.01E+02	5.94E+02	6.81E+02
Total Rotor Weight	1.47E+03	3.19E+03	4.29E+03	5.16E+03	9.45E+03
Number of Poles	146	184	226	264	330
Module Weight	6.70	6.70	6.70	6.70	6.70
Total Module Mass	8.44E+02	2.10E+03	2.58E+03	3.01E+03	5.64E+03
Shaft Outer Diameter	0.21	0.28	0.36	0.40	0.60
Shaft Inner Diameter	0.10	0.14	0.18	0.20	0.25
Shaft Length	1.32	1.86	2.02	2.10	2.70
Shaft Weight	2.78E+02	6.74E+02	1.21E+03	1.55E+03	3.12E+03
Rotor Outer Weight	1.02E+03	2.31E+03	2.83E+03	3.31E+03	6.98E+03
Rotor Outer Inertia	8.58E+02	2.97E+03	5.54E+03	9.17E+03	2.64E+04
Number of Stator Modules per ring	80.00	96.00	120.00	142.00	178.00
Shaft Inertia	12.28	43.23	118.34	186.07	540.89
Total Inertia	3.87E+04	1.78E+05	6.49E+05	1.14E+06	3.18E+06
Airgap	0.002	0.002	0.003	0.003	0.003
Stator Outer Diameter	2.16	2.89	3.12	3.65	4.82
E - core Depth	0.06	0.06	0.06	0.06	0.06
Stator Module Mass	10.15	10.15	10.15	10.15	10.15
Stator Structure Mass	7.49E+02	1.20E+03	1.63E+03	2.28E+03	1.08E+03
Misc Mass	9.50E+02	1.89E+03	3.91E+03	6.31E+03	1.25E+04
Stator Mass	1.55E+03	3.19E+03	4.06E+03	6.16E+03	6.80E+03
Stator Inertia	1.71E+03	5.10E+03	9.53E+03	1.67E+04	3.24E+04
EMF Emf at Nominal speed	4.41E+02	6.03E+02	6.30E+02	7.08E+02	6.27E+02
System Voltage	1.27E+03	1.27E+03	1.27E+03	1.27E+03	1.27E+03
Tuning Capacitance	25 uF	33 uF	33 uF	33 uF	33 uF
Dc Link Capacitance	2000 uF	2000 uF	2000 uF	2000 uF	2000 uF
Total Weight	3.99E+03	8.27E+03	1.23E+04	1.56E+04	2.85E+04
Active Weight	1.66E+03	4.09E+03	5.01E+03	6.89E+03	1.11E+04
Structural Weight	2.33E+03	4.18E+03	7.26E+03	9.74E+03	1.79E+04
ECU per Kg Active weight	3.20	3.18	3.17	3.19	3.19
ECU per Kg Support weight	2.36	1.82	1.46	1.48	1.21
Cost of active structure	5.30E+03	1.30E+04	1.59E+04	1.88E+04	3.53E+04
Cost of support structure	5.80E+03	7.60E+03	1.05E+04	1.44E+04	2.12E+04
Rated Frequency	55	55	55	55	55
Total Cost	1.08E+04	2.06E+04	2.65E+04	3.32E+04	5.65E+04

Figure 5.34: Variable speed generator parameter spreadsheet

POST-PROCESSING ON MATLAB. The performance data output from WINDVOUT is used to form the power transfer characteristic and is discussed in the next section. To do this the data is read into MATLAB and rearranged from constant speed information

5.5 Further control issues for a variable speed wind generator

into constant voltage information. Further post-processing is also carried out to get the data into the monotonically increasing form that is required for accurate data interpolation.

5.5 Further control issues for a variable speed wind generator

It is now appropriate to consider the further control options that are necessary for a variable speed wind generator to ensure that the perceived advantages presented in the first section of this chapter can be realised. The major control aim is to track the C_p curve in below rated wind speeds to enhance the energy capture but equally as important is the need to control terminal voltage, reactive power and the interaction with the pitch controller.

5.5.1 Reactive power control for an embedded generator

So far the discussion on the control of the variable speed wind turbine has focussed on the ability to alter the real power flow through the inverter and thereby alter the rotor speed to track C_{pmax} . This is a very important facet of the inverter performance but equally important is the ability to alter the control ratio, K_{Vdc} , to maintain a constant terminal voltage even though the dc link voltage is varying. The wind turbine is typically considered to be an embedded generator, i.e. it is connected to the distribution network below 33 kV. An illustration representing the concept of embedded generation can be seen in Figure 5.35. Case (a) represents a direct connection to a fixed bus and case (b) shows the case where the generator is still connected to a fixed bus but there is a load tapped off before the connection to it. This places more stringent requirements on the quality of the generated power and voltage.

For the case of Figure 5.35 (a) neither the voltage nor the frequency of the grid can change and so the only question is how to maximize the power flow into the grid whilst minimising the cost of the reactive power. However for the case of Figure 5.35 (b) it is important that the voltage level at the load is within the statutory requirements of the connection agreement. In general the voltage level is not fixed for economic reasons but is allowed to vary in a tolerance band about a set of preferred levels. The performance of the distribution network is then measured in terms of freedom from interruptions and maintenance of satisfactory

5.5 Further control issues for a variable speed wind generator

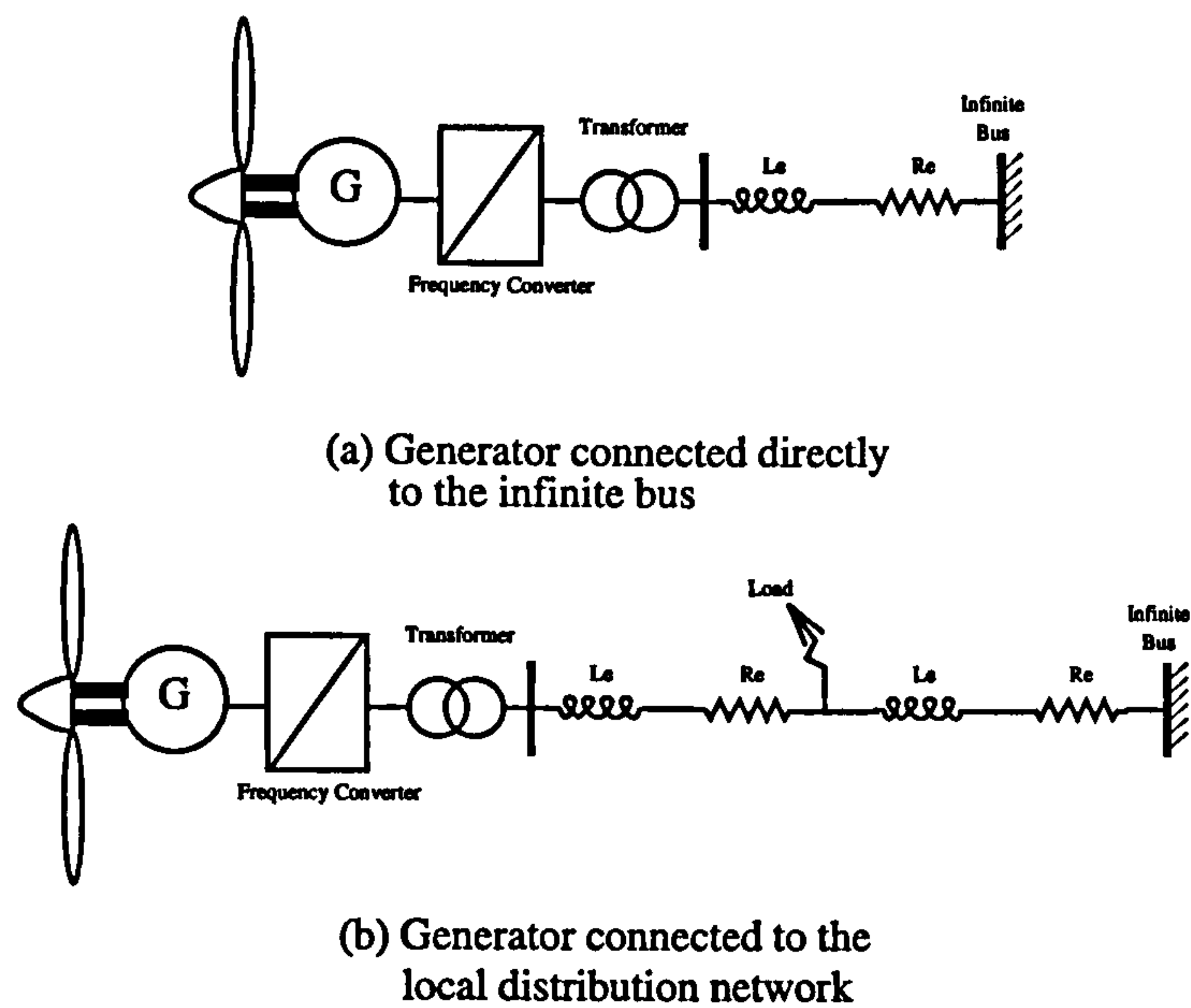


Figure 5.35: Grid Connection Configuration

voltage levels at the loads, i.e. customer's premises. Too high a steady state voltage will lead to reduced light bulb life, reduced life of electronic components and other types of apparatus. On the other hand too low a steady state voltage causes lowered illumination levels and problems with heating devices and motors.

Several methods exist for altering the voltage at the load, tap changing autotransformers, generator voltage regulation and capacitor correction. The permanent magnet, synchronous generator has no generator voltage regulator because of the permanent magnet excitation but the output voltage of the inverter can be altered by altering the control ratio.

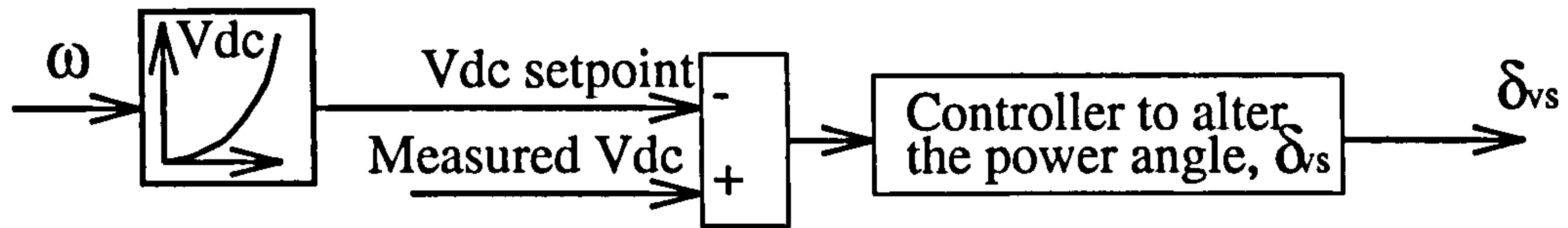
Considering the phasor diagram of power being transmitted along a short transmission line, whose sending end voltage is being controlled, gives the equation for reactive power as,

$$Q = \frac{3V_{sys}}{X_s} (V(1) \cos \delta_{vs} - V_{sys}) \quad (5.22)$$

There is no control of reactive power in the variable speed case presented in section 5.3 because $V(1)$ is proportional to V_{dc} which, with a constant control ratio, is proportional to the speed of the generator rotor via the $\omega - V_{dc}$ characteristic. The power angle, δ_{vs} , between the inverter terminal voltage and infinite bus voltage has a value which alters the current drawn by the inverter and thereby controls V_{dc} . However, when using voltage controlled inverters, the ratio between V_{dc} and $V(1)$ can also be changed and therefore the reactive

5.5 Further control issues for a variable speed wind generator

power, Q , can be altered. A control scheme of the form shown in Figure 5.36 might thus be likely depending on the value of supplying real or reactive power.



(a) Alter δ to track C_{pmax}



(b) Alter K_{Vdc} and hence $V(1)$ to maintain Q setpoint

Figure 5.36: Power Control Scheme

There are two control handles, $V(1)$ and δ_{vs} , and these are used to control the real power, P , and reactive power, Q . The Q setpoint could be set to balance the Q demand of the load and voltage drop due to the transmission line. The SIMULINK blocks for the K_{Vdc} controller can be seen in Figure 5.30.

5.5.2 Further control issues in variable speed operation

So far the main aim of the work in modelling the variable speed wind turbine has been to evaluate the effectiveness of a controller to track the C_{pmax} curve for maximum real power transfer into the grid and to ensure the output of the inverter remains within the statutory grid connection requirements. However there are several other control issues that must be addressed for the commercial operation of such a wind turbine.

1. What signal should be used to control V_{dc} whilst the pitch controller is in operation.
2. How can δ_{vs} be measured and incorporated effectively into a control hierarchy?
3. How valid are the assumptions made in developing the variable speed model.

The first two stem from the likely connection of such a system to the utility distribution network and not directly to the high voltage grid. The last point can only really be tackled through the use of test rig validation and this is discussed later.

CONTROLLING V_{dc} DURING PITCH CONTROL. It is imperative to limit the power out of the generator to its rated value to ensure safe and economic operation. To do this pitch control is used to limit the power into the main shaft. The question that has not been addressed yet is how to control the dc link voltage whilst in this mode of operation. The pitch actuator takes a finite time to respond to any demand and there will be changes in both rotor speed and hence the power transfer capability of the generator rectifier unit. Balanced operation still needs to be achievable and hence some control of V_{dc} must be maintained. Perhaps the easiest way to do this would be to keep V_{dc} constant above rated wind speed. Such operation can be seen in Figure 5.37 for a step increase in windspeed from the rated windspeed, 12 m/s, to 14 m/s.

Initially the generator is operating at point a which lies on the intersection of the C_{pmax} curve and the line representing the mechanical power at a windspeed of 12 m/s. At the instant of the step up in windspeed, the mechanical input power increases to point b on the 14 m/s curve. Without any pitch control and keeping V_{dc} constant above rated windspeed, the power imbalance between the mechanical power in and airgap power out of the generator would result in an increase in rotor speed. Eventually point c would be reached, where the mechanical power and airgap power are again balanced. If the pitch controller then operated to limit the power into the shaft, the 14 m/s power curve would be reduced by the pitch angle, β . If constant V_{dc} is still maintained, point d would then be reached at the intersection of the constant V_{dc} line and the curve for mechanical power at a windspeed of 14 m/s with a pitch angle of 4 degrees. This is, however, very close to the original rotor speed and V_{dc} level if the C_{pmax} tracking strategy for below rated windspeeds were maintained. This suggests a control scheme where no change should be made to the method of deriving the setpoint dc link voltage for above rated wind speed conditions, i.e. still base the setpoint dc link voltage on the one derived for C_{pmax} tracking. This would be an easy control scheme to implement and hopefully would not lead to large dc link voltage variations with good pitch control. A further benefit of this approach is that, when the windspeed reduced below rated windspeed subsequently, the voltage should already be right for C_{pmax} tracking. Alternatively similar curves to the $\omega - V_{dc}$ curve presented earlier to track C_{pmax} could be derived which are modified by the effect of the pitch angle, β . This would give the control scheme as seen in Figure 5.38. These strategies for controlling a pitch controlled wind turbine and variable speed operated generator are explored in more detail in Chapter 6.

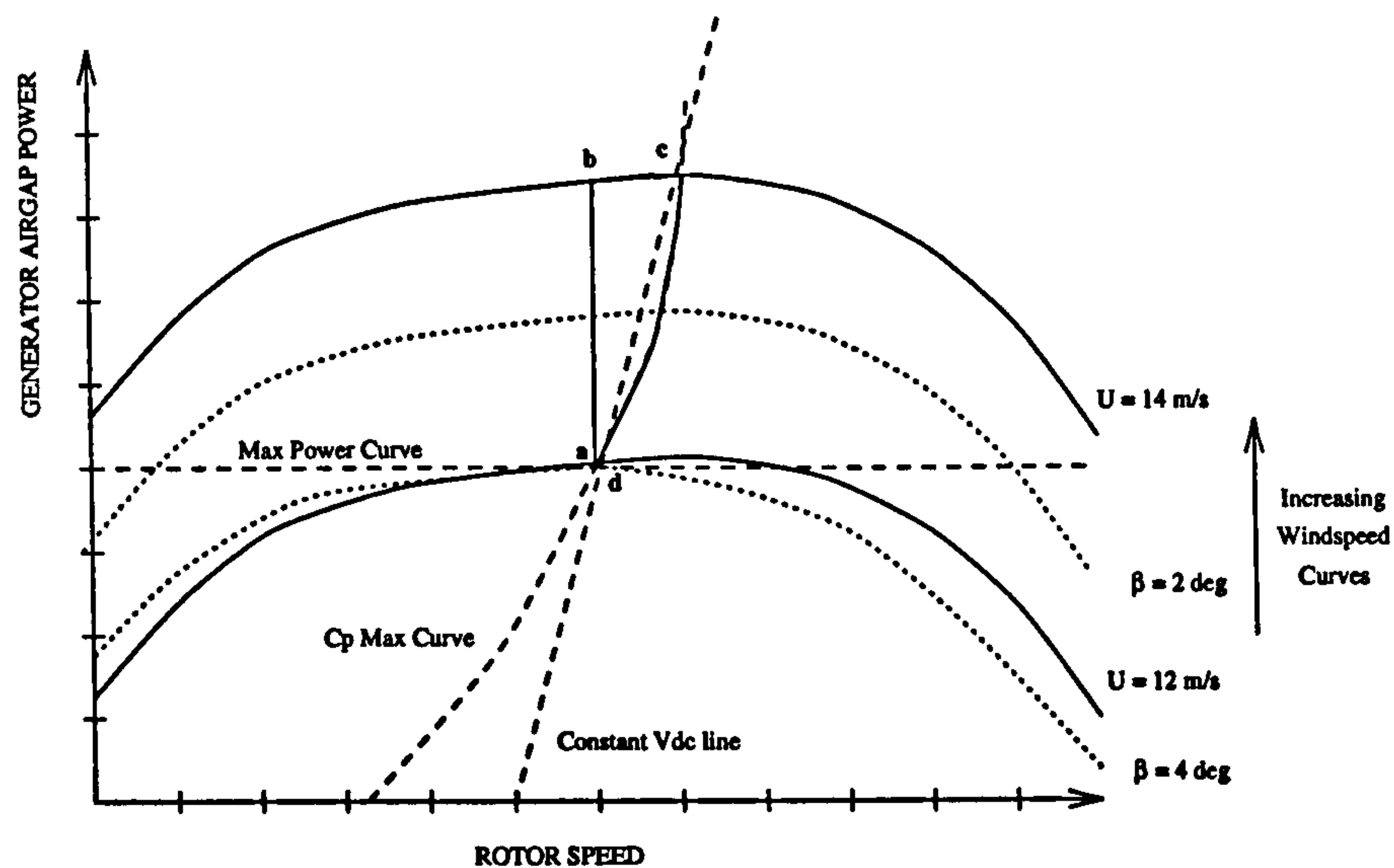


Figure 5.37: Maintaining V_{dc} constant during pitch control

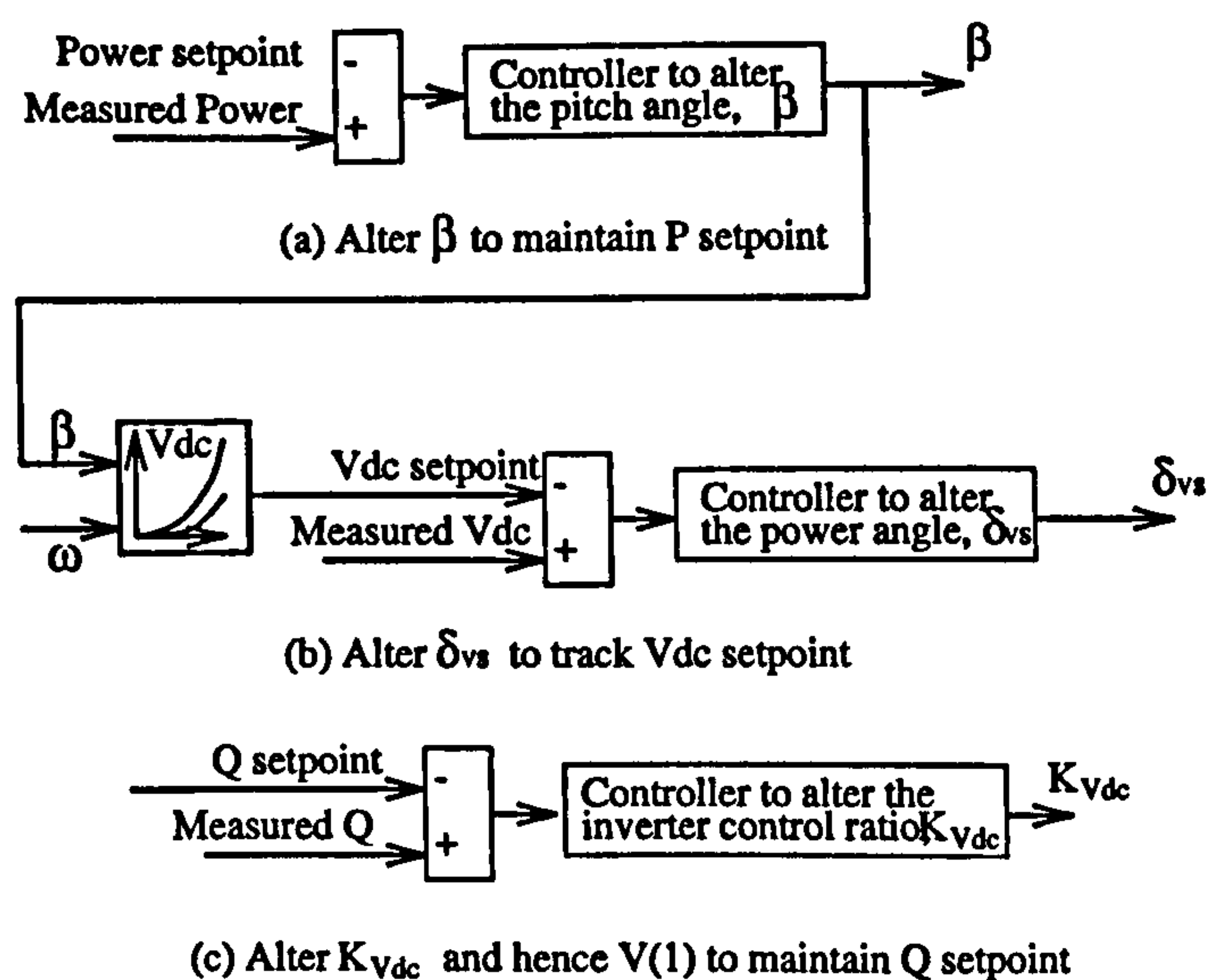


Figure 5.38: V_{dc} control during pitch control

5.5 Further control issues for a variable speed wind generator

MEASURING δ_{vs} . The control to maximize the real power into the grid described in the previous sections is dependent on measuring the zero crossing point of the infinite bus voltage to determine the delay time for the correct setting of δ_{vs} . The question arises as how can δ_{vs} be measured if access to the infinite bus which may be many miles away is limited?

If the zero crossing point of the system voltage is measured at some remote point to the wind turbine and relayed via a radio transmission link to it, there will be some finite measurement and transmission time delay resulting in an error in the value of the δ_{vs} . The reactance to the grid, X_s , which determines the power transfer capability of the generator will now be the total reactance to the point of measurement. The delay and error mean that the actual power delivered to the grid will in fact be slightly different to the power calculated from the δ_{vs} measurement. This means that some adaptive control for setting the firing angles of the inverter to give the correct δ_{vs} may be needed.

5.5.3 Overall proposed control scheme

The overall control scheme showing the key control loops can be seen in Figure 5.39. An over-speed condition is included to cater for variable speed wind turbines which have a limit on the upper speed because the extra cost to cater for the increased speed range does not outweigh the derived benefits.

The effective windspeed, U_w , which includes for the purposes of the schematic all the rotational effects, is substituted into equation 5.1 to evaluate the shaft power from the wind which is dependent on both tip speed ratio and pitch angle. The difference between the mechanical power in and electrical power out at the airgap determines the change in rotor speed which is then used to determine the new value of V_{dc} for maximum power tracking provided the power is below rated. Above rated power pitch control is used and C_p is no longer a maximum but is reduced by pitch the blades. The power angle is altered to effect this change in C_p and as the dc link voltage varies as a result of this control the control ratio of the inverter is altered to maintain either constant terminal voltage or a reactive power setpoint. The interactions within this control scheme are examined in the next chapter to show that neither the tracking of C_{pmax} for maximum power transfer nor the independent control of real and reactive power are easy to achieve.

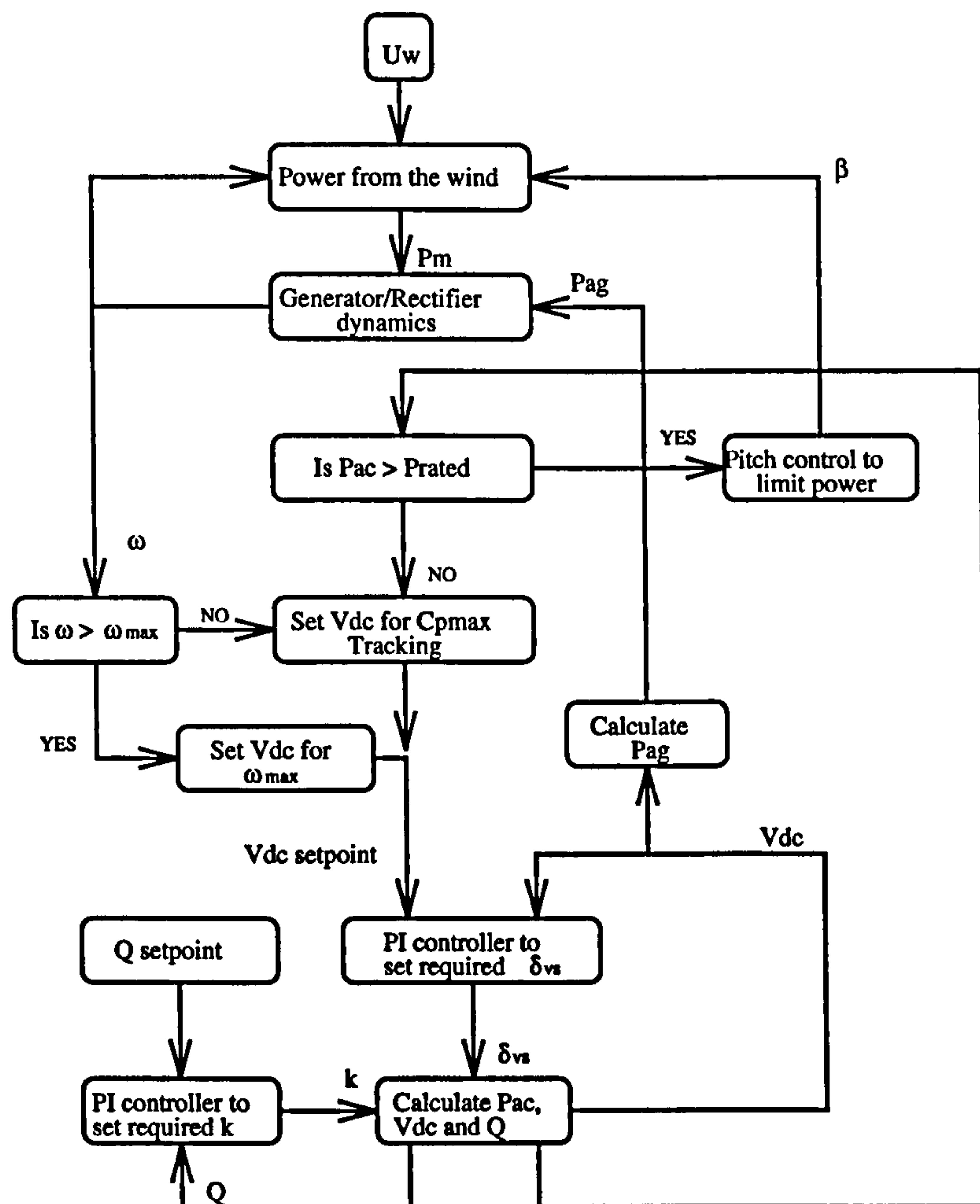


Figure 5.39: Overall Control Scheme

5.6 Concluding remarks

This chapter has described the theory and modelling effort that has been undertaken to develop a SIMULINK model of a variable speed, multi-pole, permanent magnet, synchronous generator and frequency converter suitable for a wind turbine. The key parameters for a range of generator ratings have been presented and the development of control strategies to gain as much advantage from variable speed operation as possible outlined with respect to a 455 kW rated generator. The performance of the generator with those control strategies is presented in the next chapter. The models presented in this chapter have been collated into the form of the SIMULINK library presented in Chapter 1 from which many configurations of variable speed wind turbine can be developed and their performance and control simulated easily.

Chapter 6

Variable Speed Results

In the last chapter the case for variable speed operation was presented in terms of increased energy capture, load alleviation, power smoothing and noise reduction. Several schemes for the frequency converter connection were identified and the modelling effort for the chosen scheme described. The control mechanisms and performance of that scheme are now outlined using several key results from the full non-linear simulation developed in section 5.3.

The main aim of this chapter is to explore the effects of the inverter control and pitch control on the performance of the variable speed wind turbine in order to develop the control strategy presented in section 5.5 and evaluate how the potential benefits of variable speed operation can be achieved. Therefore the results presented gradually build up the picture of the overall control interactions by introducing each controller in turn to the model. The performance can then be used to compare the fixed and variable speed designs and this is carried out in Chapter 7.

Firstly, results are presented for a series of step increases in windspeed with no rotational effects included for a 458 kW rated generator with values as shown in Figure 5.34 in below rated wind speeds. A constant ratio between V_{dc} and the fundamental voltage output from the inverter, V_1 , is assumed. The results demonstrate the ability to track the optimum value of C_p by altering the value of the dc link voltage, V_{dc} , by controlling the firing angle, α , of the inverter to change the power angle, δ_{vs} , between the output of the inverter and the grid. The rationale behind choosing the values for the PI controller for this control of the

power angle δ_{vs} is discussed. These step results indicate several problems with just tracking C_{pmax} without considering the grid connection of the wind turbine:

1. The first problem is that the dc link voltage setpoint gives a value for V_{dc} which exceeds the breakdown voltage of the individual IGBT's in each leg of the inverter and two methods for combatting this are presented.
2. The second problem is that a constant ratio between V_{dc} and the fundamental voltage output from the inverter, V_1 is assumed. If this ratio does not change then no control over the voltage level of the transmission line or reactive power flow is possible whilst tracking C_{pmax} . As section 5.3.12 shows by suitable switching of the inverter it is possible to alter the ratio between V_{dc} and V_1 and hence control reactive power and the transmission voltage. A method for keeping the fundamental voltage, $V(1)$, of the terminals of the inverter at unity is presented.

The first of the above problems can be solved relatively easily but the effect of changing the control ratio, $K_{V_{dc}}$, of the inverter to keep the terminal voltage of the inverter constant interacts in an adverse manner with the control of the power angle, δ_{vs} , to track C_{pmax} for reasons expanded in section 6.3.2. This method to maintain the terminal voltage at unity can be adapted so that instead of having a constant terminal voltage, $V(1)$, as the desired control aim, a constant reactive power setpoint can be evaluated and used as the control aim to set the value for $V(1)$. Results are presented showing how the reactive power setpoint is achieved.

All of the results described previously apply to operation in below rated wind speeds and as such pitch control has not been an issue. The next section discusses the relevance of pitching action on the results. Whilst pitching the blades the control of the dc link voltage by the inverter firing angle is not so important as the prime requirement of the control scheme is to limit the real power into the turbine to avoid any generator windings overheating or overstressing of the turbine shaft. The terminal voltage of the inverter must also be controlled to remain within the grid connection requirements and the breakdown limit of the individual IGBT's which was set to the highest value achievable at the time of the work, 1200 V [97]. Furthermore when the wind subsequently falls below rated wind speed and the pitch controller is no longer used then it would increase the energy capture if the dc

6.1 Tracking C_{pmax} with the control ratio, K_{Vdc} , constant

link voltage could be controlled to be at the right point for the entry back into the C_{pmax} tracking mode.

In the next section the results are extended to the full windy environment to show the difficulties in tracking C_{pmax} and controlling the connection voltage in such a turbulent environment. The energy captured is used to quantify the benefit returned by tracking C_{pmax} and compared against the theoretical maximum energy capture is the variable speed wind turbine could act instantaneously and with no other constraints.

The conclusions to the chapter discuss the implications of the operational control schemes outlined during the chapter and presents the final control method which would provide the best transient and economic performance for variable speed operation.

6.1 Tracking C_{pmax} with the control ratio, K_{Vdc} , constant

Results are presented in this section to demonstrate that if appropriate control of the power angle is achieved then C_{pmax} can be tracked. The benefit in terms of increase in energy capture for a variable speed operated generator over a fixed speed generator can only occur in below rated wind speeds because in above rated wind speeds power limiting is used. The first results are for a step up in wind speed from 8 to 12 m/s with no rotational effects included. These step results are included as it is easy to see what is happening in terms of the interactions between the system and control dynamics. The values for a well designed PI controller to alter the inverter firing angle, α , to control the power angle between the inverter and the grid, δ_{vs} , are then presented.

6.1.1 Control scheme

The control scheme to keep track C_{pmax} was introduced in Chapter 5 and can be seen in Figure 5.22. When, for instance, there is a step increase in the wind speed the rotor speed will increase and so will the required value of the V_{dc} setpoint according to the curve shown in Figure 5.21. This setpoint is then compared with the measured value of V_{dc} and a PI controller used to alter the power angle, δ_{vs} , to ensure the correct value of V_{dc} is attained. As the control ratio of the inverter, K_{Vdc} is unchanged during the simulation run the terminal voltage of the inverter will alter in the same manner as the dc link voltage, V_{dc} , according

6.1 Tracking C_{pmax} with the control ratio, K_{Vdc} , constant

to equation 5.6.

6.1.2 Step response with no control of the control ratio, K_{Vdc}

The wind steps from 8 m/s to 12 m/s and the required dc link voltage must increase to track C_{pmax} accordingly as the rotor speed increases due to the imbalance of input torque to reaction torque. The first set of results are included as the base reference case to show the key dynamic interactions.

The full set of results is discussed for this reference case and only the pertinent plots included for subsequent cases. Figure 6.1 shows the step increase in wind speed and the corresponding increase in the mechanical torque into the wind turbine. The overshoots in torque are due to the induction lag effect mentioned in Chapter 2. The run identifiers are also indicated to show the values of the various control parameters. The variable names for the PID gains of the 'delta' controller have the prefix 'V' because of their effect on the dc link voltage and as there is no control of the inverter control ratio, K_{Vdc} , for this run the values of the PID gains for this controller are all zero. Furthermore as there is no pitch control, the gain which amplifies the power error to a suitable pitch demand, K_{pitch} , is also zero.

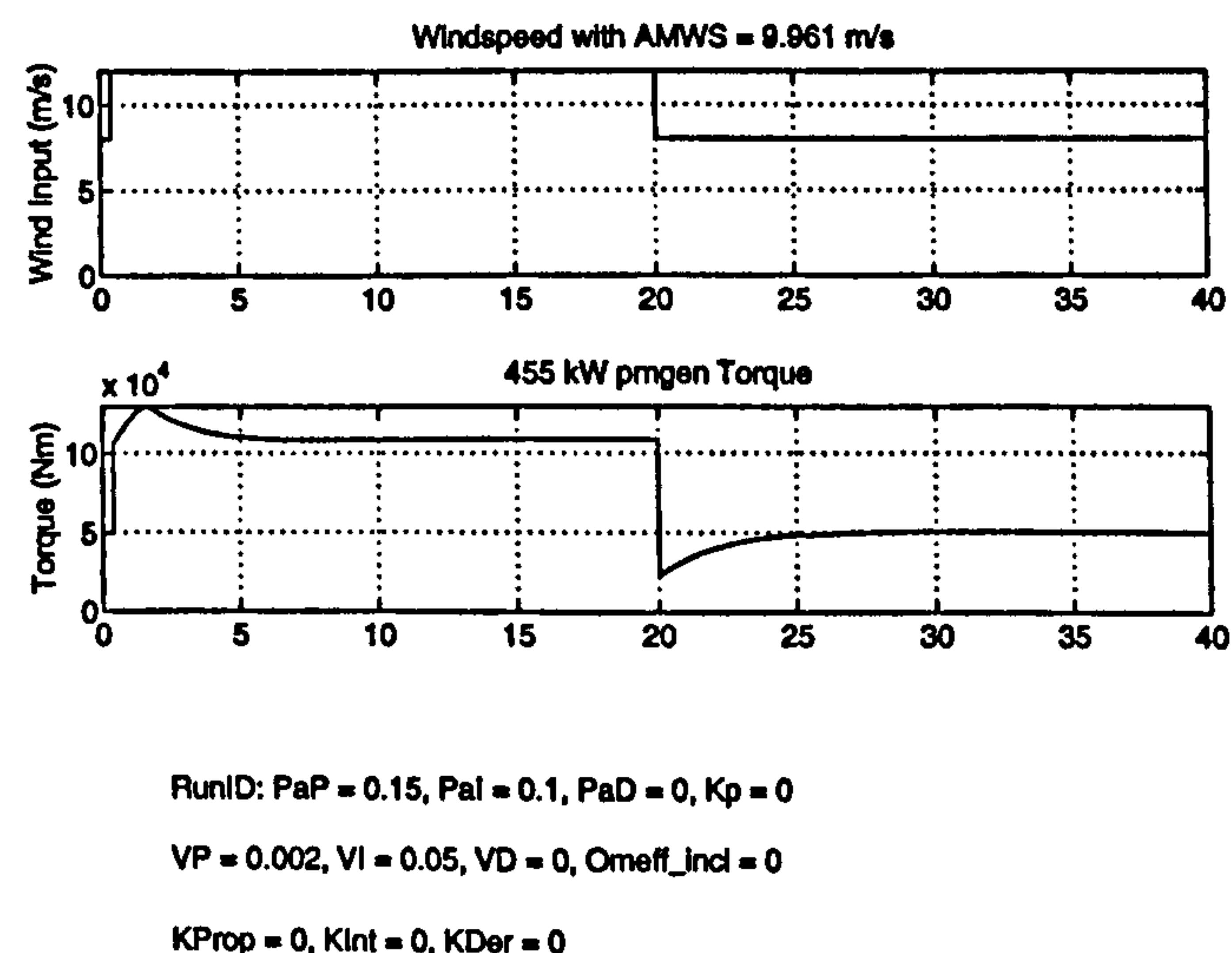


Figure 6.1: Step increase and corresponding input torque

The top trace of Figure 6.2 shows that no rotational effects have been included for this run. It is interesting to note that the power coefficient starts at 0.45 and then after the

6.1 Tracking C_{pmax} with the control ratio, $K_{V_{dc}}$, constant

wind speed steps to 12 m/s returns to the maximum value, thus demonstrating the ability to track C_{pmax} . This is because the tip speed ratio (TSR) which relates the rotor speed, ω , to the wind speed, U_w , is controlled to be at the value corresponding to C_{pmax} , i.e. $TSR = 6$, by the altering of the inverter power angle which changes V_{dc} and the power transferred from the rotor shaft to the grid.

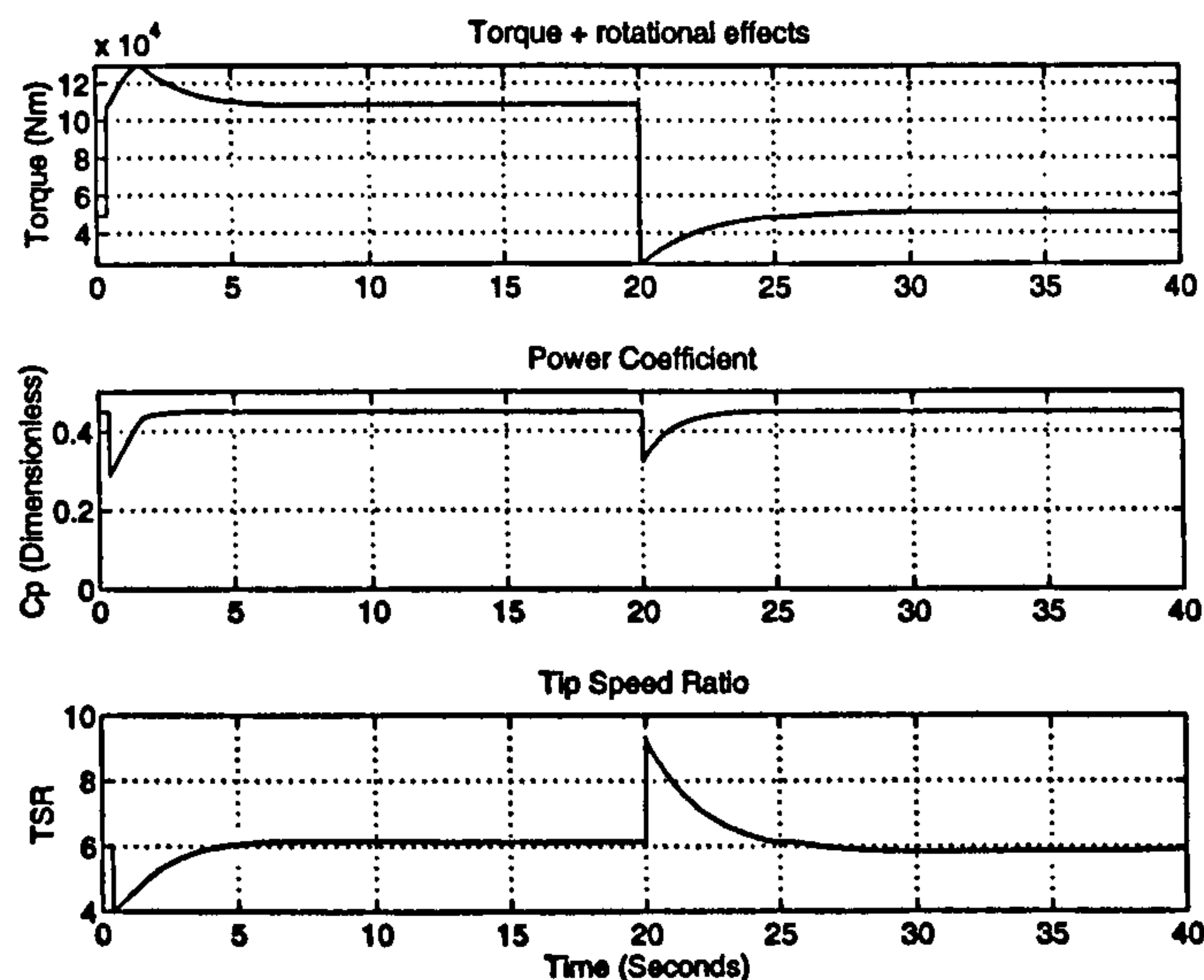


Figure 6.2: The resulting power coefficient and tip speed ratio

The mechanical power, P_m , from the wind turbine and the corresponding airgap power, P_{ac} , out into the E-core and rectifier arrangement can be seen in Figure 6.3. The dashed lines correspond to the variation of P_{ac} versus rotational speed for a range of constant dc link voltages. The solid lines correspond to the variation of the mechanical input power, P_m , versus rotational speed for a range of constant windspeeds. The mechanical power changes very quickly for the positive and negative steps in wind speed with the initial overshoot in mechanical power because of the induction lag effect introduced in section 2.2.3. The response of the airgap power transfer follows the response of the inverter control of the dc link voltage as rotor speed increases and clearly follows the C_{pmax} curve.

The mechanical power, P_m , can increase above the value predicted from conventional C_p theory which is based on conservation of momentum and actuator disc theory [41] because, as was explained in Chapter 2, for any change in the operating condition of the wind turbine the wake takes a finite time to adjust and leads to an effect known as induction lag. Taking for instance a step up in wind speed across the wind turbine blades, initially the upwind wind speed and the downwind wind speed are related by the amount of energy extracted

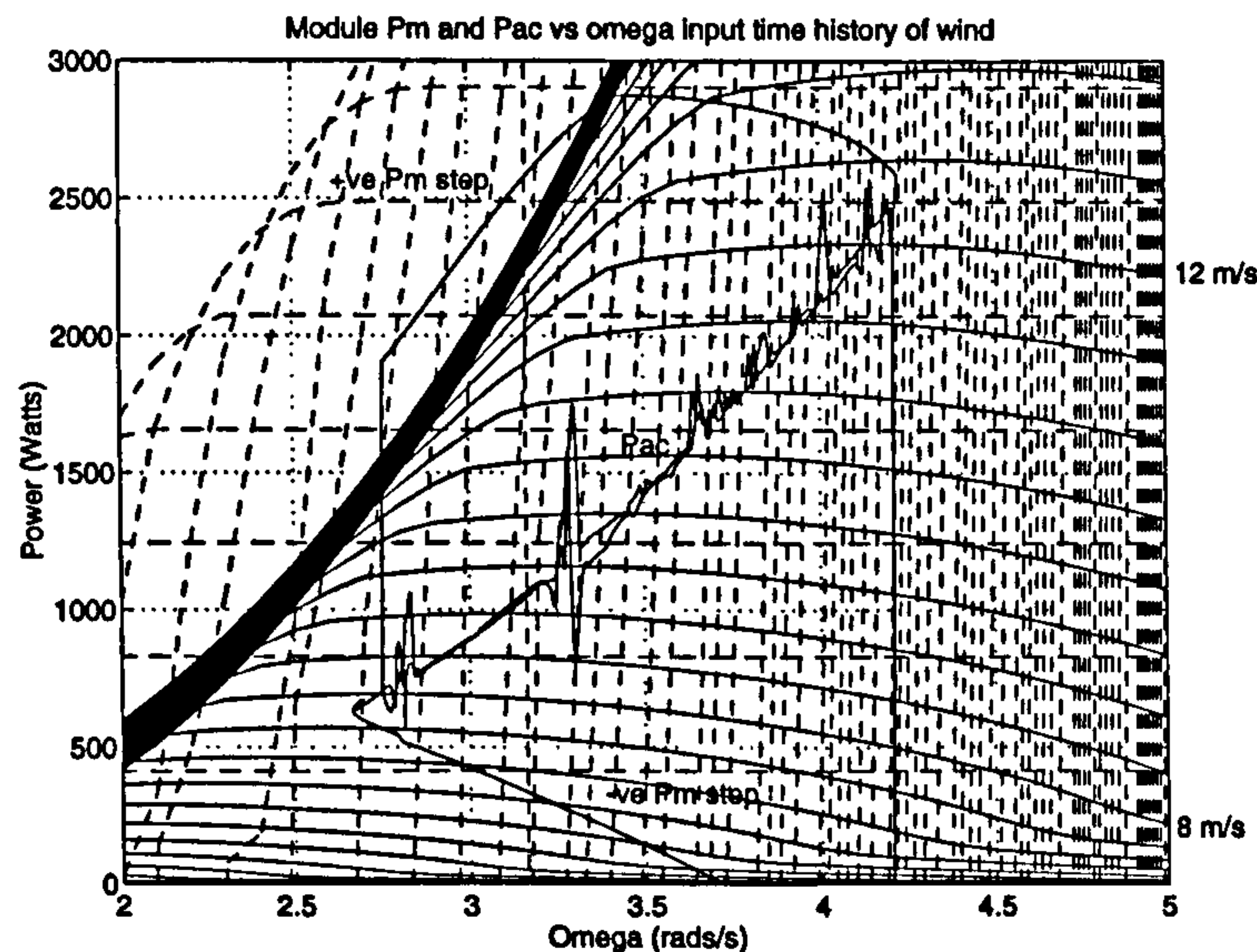


Figure 6.3: Module airgap and mechanical power

by the value given by C_p . However when the wind speed changes the downwind wind speed takes a finite time to change and for the energy across the wind turbine to balance more power must flow into the wind turbine until the up and down wind speeds equalise at the steady levels predicted by C_p .

Figure 6.4 shows the variation of the input power, the resulting airgap power, the variation of rotor speed and dc link voltage. There are two things to note about these plots. Firstly it should be noted that the airgap power, P_{ac} , rotor speed and dc link voltage take a finite time to respond to the step in the input mechanical power. This is because of the large inertia of the wind turbine blades and this leads to a reduction of energy when compared with the theoretical maximum. This is discussed further in section 6.5. Secondly the dc link voltage stays exceeds the 1200 V rating of the commercially available high power IGBT [97] and the breakdown limit is clearly compromised. Two solutions exist to combat this problem. Firstly the number of IGBT's per leg of the inverter could be increased by serial connection of the IGBT's leading to an increased voltage breakdown. For example, inserting two IGBT's per leg of the inverter would typically increase the breakdown limit of the inverter by slightly less than two because of the unequal sharing between the devices. However this leads to a doubling in component count and therefore increased cost and possible failure. A preferred alternative would be to include a limit on the allowed value of the dc link voltage setpoint. The effect of this is presented in the next section.

6.1 Tracking C_{pmax} with the control ratio, $K_{V_{dc}}$, constant

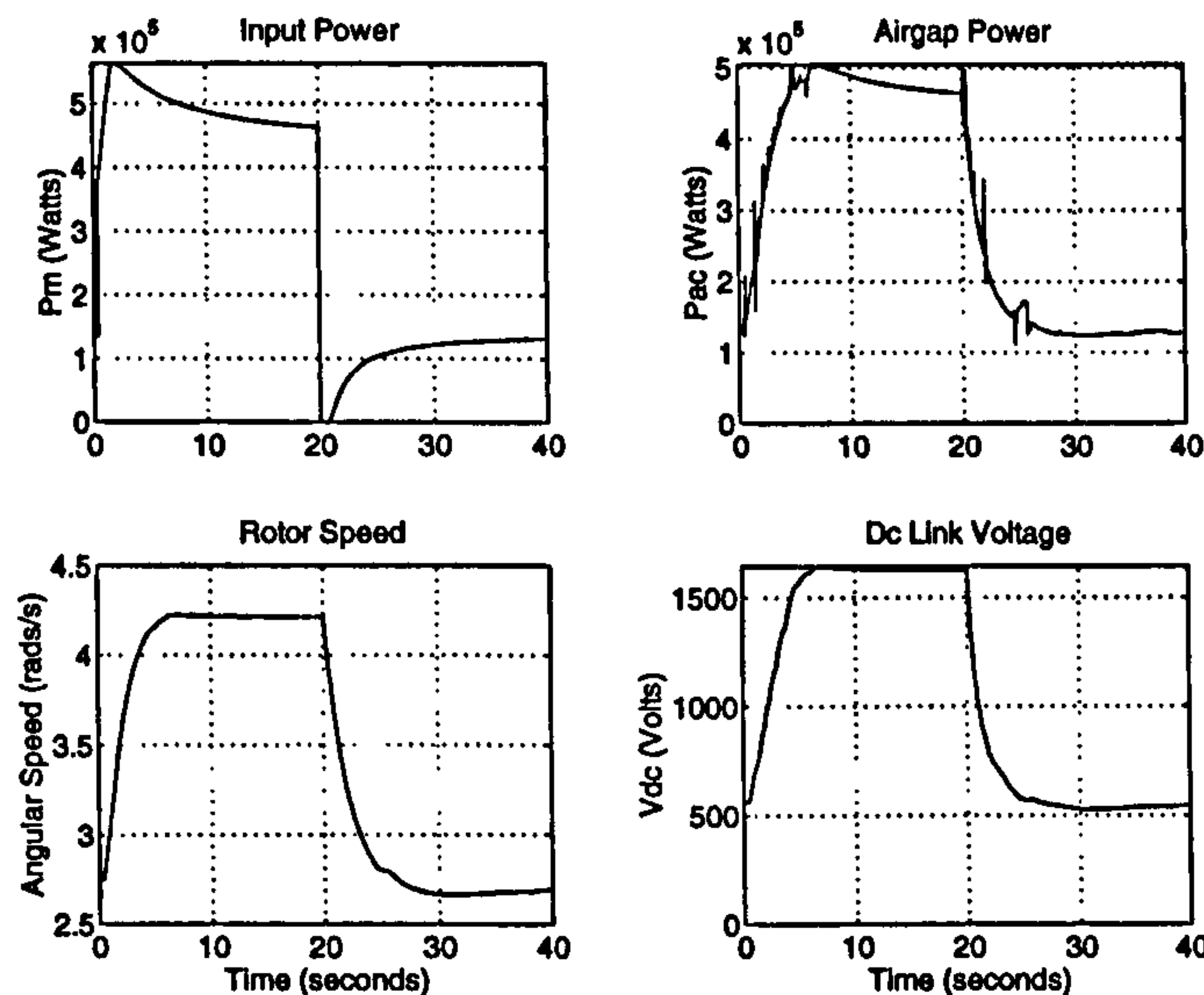


Figure 6.4: The input power, airgap power, rotor speed and dc link voltage

Figure 6.5 shows the current flowing into the inverter, the injected dc link current, the output electrical power into the grid and the overall power loss through the e-core, rectifier and inverter. The currents shown are indicative of the magnitude of the currents flowing through the dc link and it is assumed that the commutation time of the IGBT's is zero. The final value of output power is only 10 % below rated power leading to a loss of about 13 % when the simulation time is 20 seconds. This suggests that the generator should be rated at 1.1 times its output rating to ensure it delivers power appropriate to its registered capacity.

Figure 6.6 shows the variation of the measured dc link voltage and the dc link voltage setpoint from the $\omega - V_{dc}$ relationship to track C_{pmax} against time. The PI controller is so good at altering the inverter firing angle to control, δ_{vs} , that the error between the measured V_{dc} and the setpoint voltage from the $\omega - V_{dc}$ relationship is very small and the two plots are virtually indistinguishable.

The plots shown in Figure 6.7 are very important as they demonstrate the problem with keeping the inverter control ratio, $K_{V_{dc}}$, which links the dc link voltage and the fundamental line value of the inverter output voltage, constant. The initial value for $K_{V_{dc}}$ is chosen to give a terminal voltage of one per unit from equation 5.12. It is clear that as the dc link voltage increases in magnitude the required V_{dc} setpoint to maintain $V(1)$ at unity decreases and as there is no control of $K_{V_{dc}}$ for this run the reactive power increases dramatically.

6.1 Tracking C_{pmax} with the control ratio, K_{Vdc} , constant

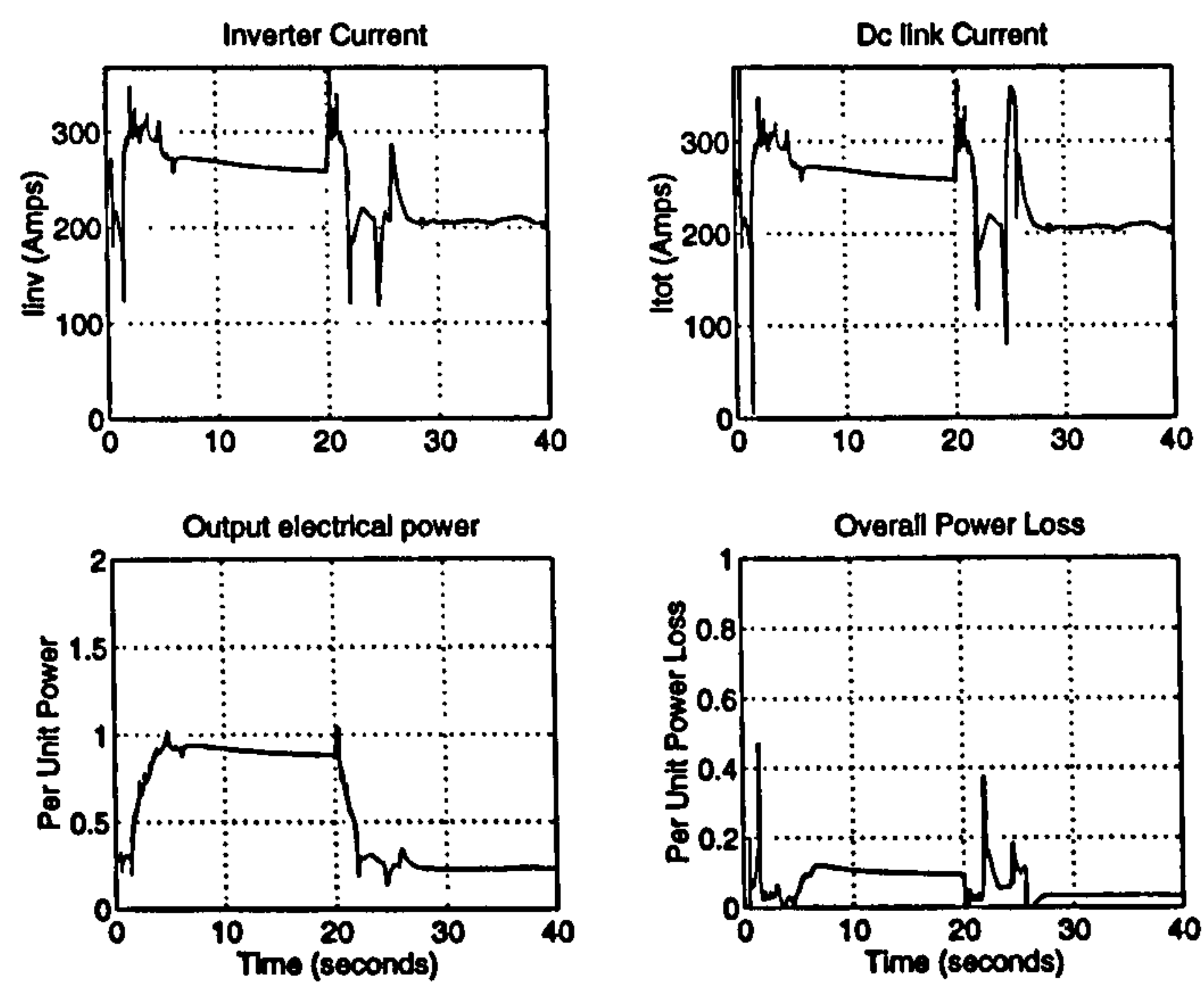


Figure 6.5: Inverter and dc link current and output power and overall power loss

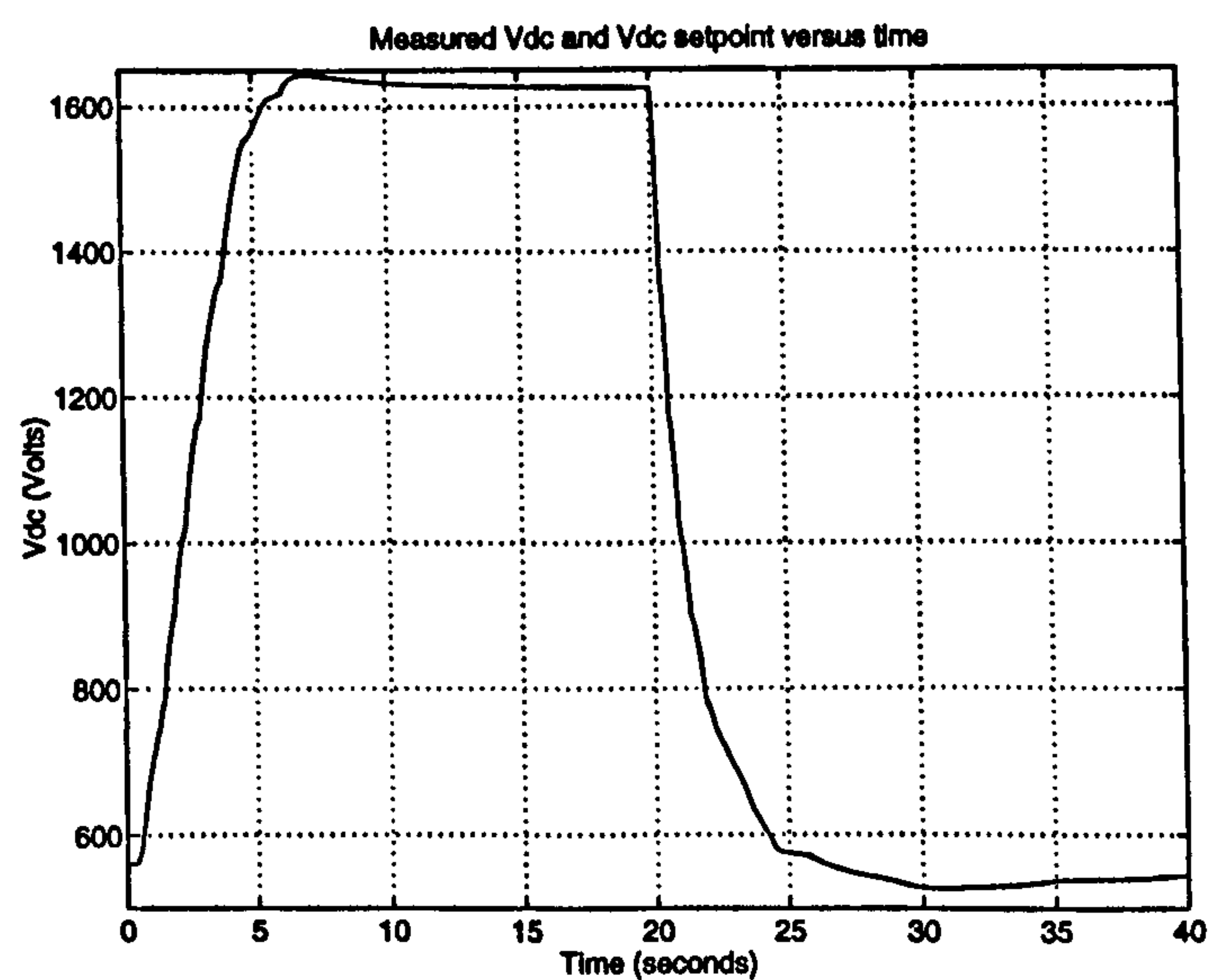


Figure 6.6: Measured and dc link setpoint voltage

6.1 Tracking C_{pmax} with the control ratio, K_{Vdc} , constant

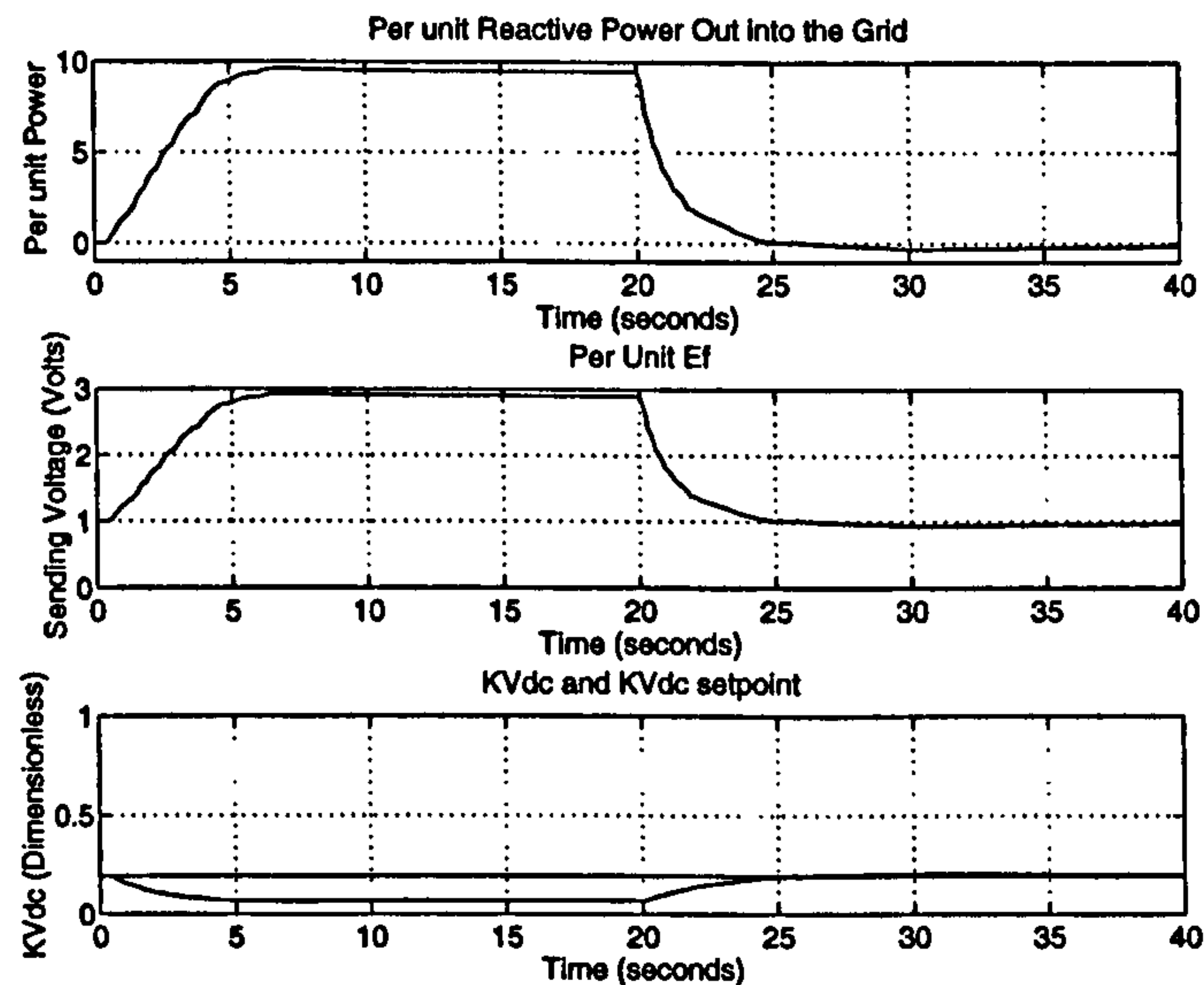


Figure 6.7: Reactive Power and voltage regulation

The equation governing the reactive power for an ideal reactive transmission line connected to an infinite bus is,

$$Q = \frac{V_{sys}}{X_s} (V(1) \cos \delta_{vs} - V_{sys}) \quad (6.1)$$

The reactance, X_s , for this case is very low in per unit terms because it only includes the value for the transformer and transmission line to the grid. This means that any small value from the bracket leads to a large value for the reactive power into the grid. As the per unit terminal voltage changes because it is not controlled the reactive power out is very large indeed - upto 10 per unit - and the voltage regulation along the line is very poor - about 3 times rated value. This would cause the problems mentioned in section 5.5.1 and is clearly unacceptable. This underlines the importance of controlling K_{Vdc} to ensure proper voltage regulation within +6 and -10 % of nominal terminal voltage.

6.1.3 Best values for PI controller

A PI controller is used to alter the firing angle of the inverter to change the power angle between the inverter terminal and the grid and effectively control the level of the dc link voltage at the setpoint for C_{pmax} tracking. This PI controller has the same architecture as shown in Figure 2.2.7 and is termed the power angle controller because that is what is

6.1 Tracking C_{pmax} with the control ratio, K_{Vdc} , constant

effectively being controlled. The control methodology for setting the values for P and I are based upon the best performance returned from several simulation runs as opposed to detailed conventional controller design techniques as introduced in Chapter 2 for the pitch controller. Again the reason for this are the large non-linearities involved in such controller design. The best values for the power angle controller are given in Table 6.1 and are used in every subsequent simulation run.

VProp	0.002
VInt	0.05
VDer	0

Table 6.1: PI controller values for power angle controller

6.1.4 Discussion

There are two key points that must be addressed from the results which have been presented. Firstly the breakdown voltage limit of the IGBT's of the legs of the inverter is violated for this generator design and, rather than redesign the generator or include extra IGBT's in each leg of the inverter, a V_{dc} limit must be introduced into the inverter power angle controller. Secondly the fundamental r.m.s. voltage at the output of the inverter, $V(1)$, which is presented in Figure 6.7, increases way above the +6 % of nominal level required for grid connection and therefore some control of the inverter control ratio is required. This will now be discussed.

It has been shown that it is possible to track C_{pmax} in response to a step increase in the windspeed. It is clear, however, that the inertia of the turbine blades limits the rate at which C_{pmax} can be tracked and this may lead to a reduction in the energy capture. This is considered in section 6.5 of this chapter but the first two major problems which have been identified must be addressed: namely the introduction of a limit on V_{dc} and secondly control of the inverter control ratio to limit $V(1)$.

6.2 Tracking C_{pmax} with $K_{V_{dc}}$ constant and V_{dc} limited to 1100 Volts

6.2 Tracking C_{pmax} with $K_{V_{dc}}$ constant and V_{dc} limited to 1100 Volts

Results are presented in this section for the same case as the section before but now including a limit on the allowed dc link voltage setpoint of 1100 Volts. It is desirable to look at the effect this would have on the dc link voltage to see if the controller has been effective and on the airgap power transfer to see how far off the C_{pmax} curve the wind turbine operates because of the dc link voltage limit.

6.2.1 Step response with no control of the control ratio, $K_{V_{dc}}$

The wind steps from 8 m/s to 12 m/s as in the previous case and no inverter control ratio or pitch control is used. The mechanical power, P_m , from the wind turbine and the corresponding airgap power, P_{ac} , out into the E-core and rectifier arrangement can be seen in Figure 6.8. The response of the airgap power transfer follows the response of the inverter control of the dc link voltage as rotor speed increases and clearly follows the C_{pmax} curve. Once the dc link voltage reaches 1100 V the P_{ac} transfer follows the constant V_{dc} line associated with 1100 Volts and this leads to a higher intercept with the mechanical power than for the previous case where no limit was present. This effect would be reduced by the pitch controller which limits the input power above rated.

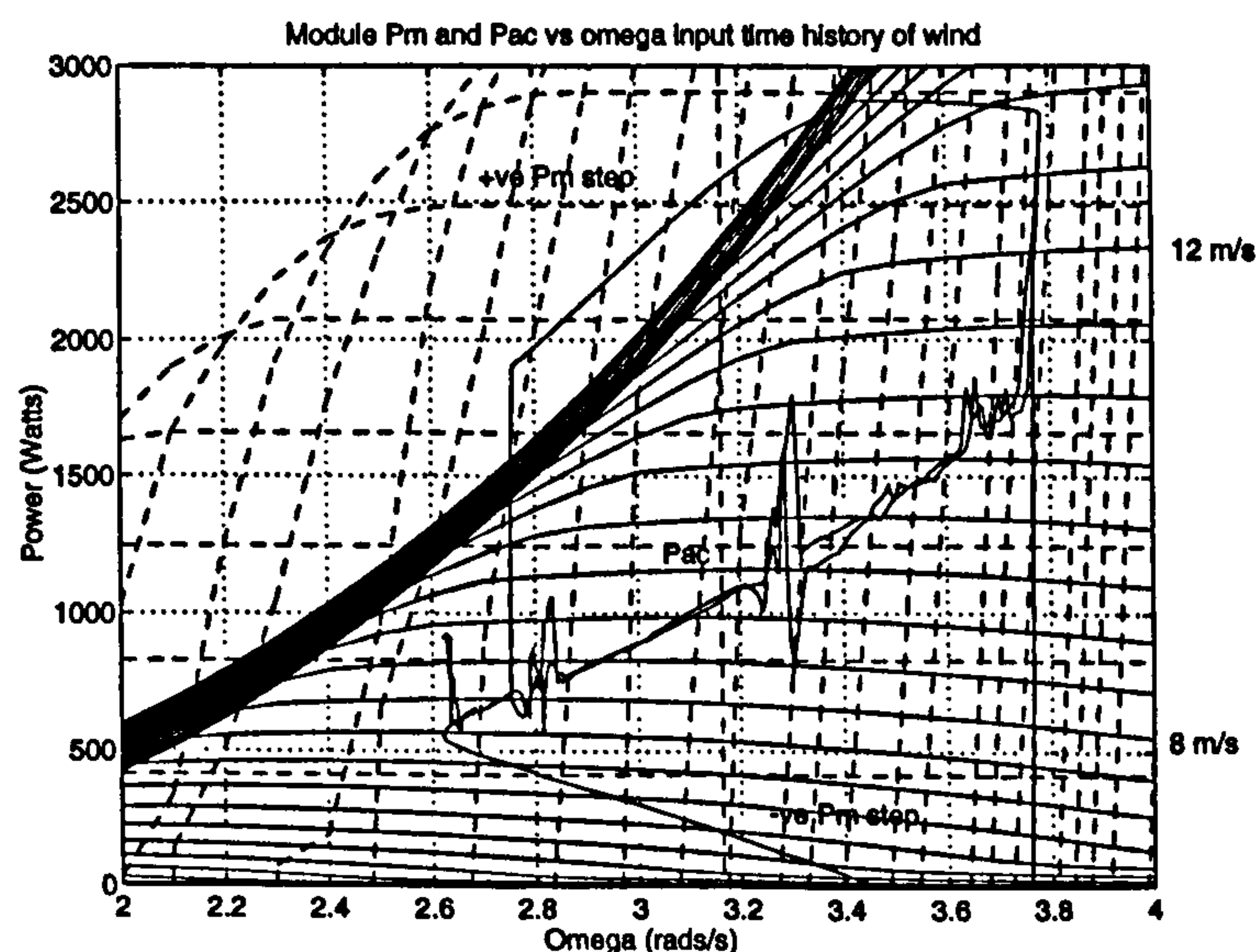


Figure 6.8: Module airgap and mechanical power

The input mechanical power, resulting airgap power, rotational speed, dc link voltage can be seen in Figure 6.9. Again the inertia of the turbine blades increases the time it takes for the rotor speed to respond. The key point to note about these plots is that the dc link voltage is limited to below 1200 V and therefore the IGBT's would not breakdown.

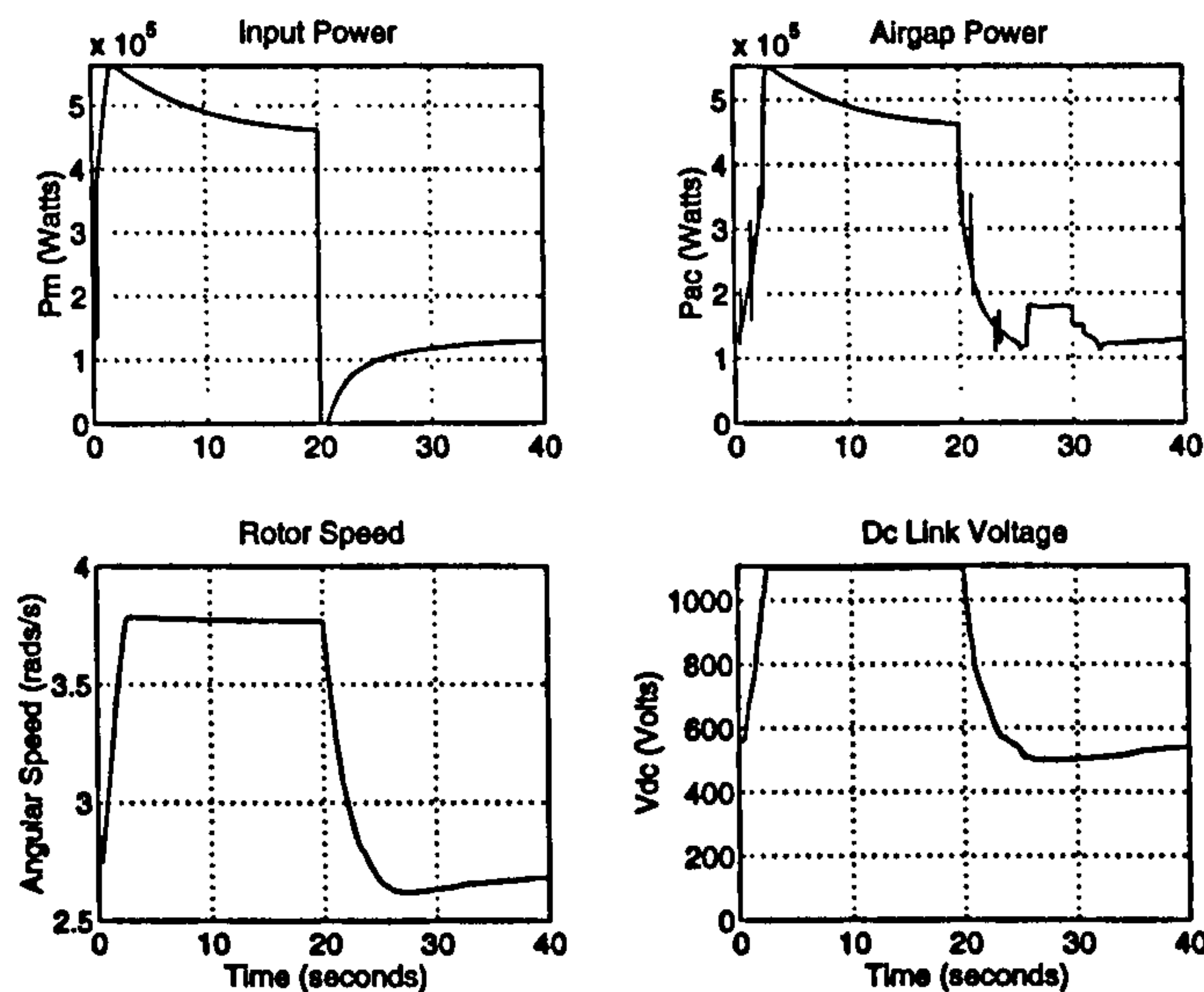


Figure 6.9: The input power, airgap power, rotor speed and dc link voltage

6.3 Maintaining V_1 constant as V_{dc} varies

The dc link voltage must be allowed to alter if C_{pmax} is to be tracked to increase the overall energy capture from the wind turbine blades. However if the proportion between V_{dc} and V_1 is kept constant, i.e. the control ratio of the inverter is kept the same, then the voltage at the sending end of the transmission line to the infinite bus will vary. This could cause problems in terms of protection devices, such as tap changing autotransformers, switching to maintain the voltage. Excessive tap-changing can cause problems and should be there to respond to system faults and not to poor control of the generator operation. Furthermore below the 33 KV level there is no continuous monitoring [105] [106] in UK distribution system which means embedded grid connected generation must be closely controlled. To this aim a scheme for maintaining $V(1)$ between +6 and -10 % of nominal is developed.

6.3.1 Control Scheme

The control scheme to keep $V(1)$ constant can be seen in Figure 5.36. When, for instance, there is a step increase in the value of V_{dc} the required value of $K_{V_{dc}}$ is calculated to keep $V(1)$ at the desired value, for this case unity, using equation 5.12. This $K_{V_{dc}}$ setpoint is then compared with the measured value of $K_{V_{dc}}$ and a PI controller used to ensure the correct value is attained.

6.3.2 Controlling $K_{V_{dc}}$ to keep $V(1)$ constant

Clearly when V_{dc} increases the inverter control ratio, $K_{V_{dc}}$, must decrease to keep $V(1)$ constant. Figure 6.10 shows the key result when the control scheme of Figure 5.36 is implemented. The first thing to note is that the reactive power is about 20 % of the reference case shown in Figure 6.7 and so the control of $V(1)$ is having the desired effect of reducing the output reactive power. However the bottom trace, which indicates the variation of the control ratio, $K_{V_{dc}}$, and its setpoint, still shows a large error between the required and actual value. This is reflected in the per unit value of the fundamental of the inverter terminal, $V(1)$, which violates the +6 and -10 % limits.

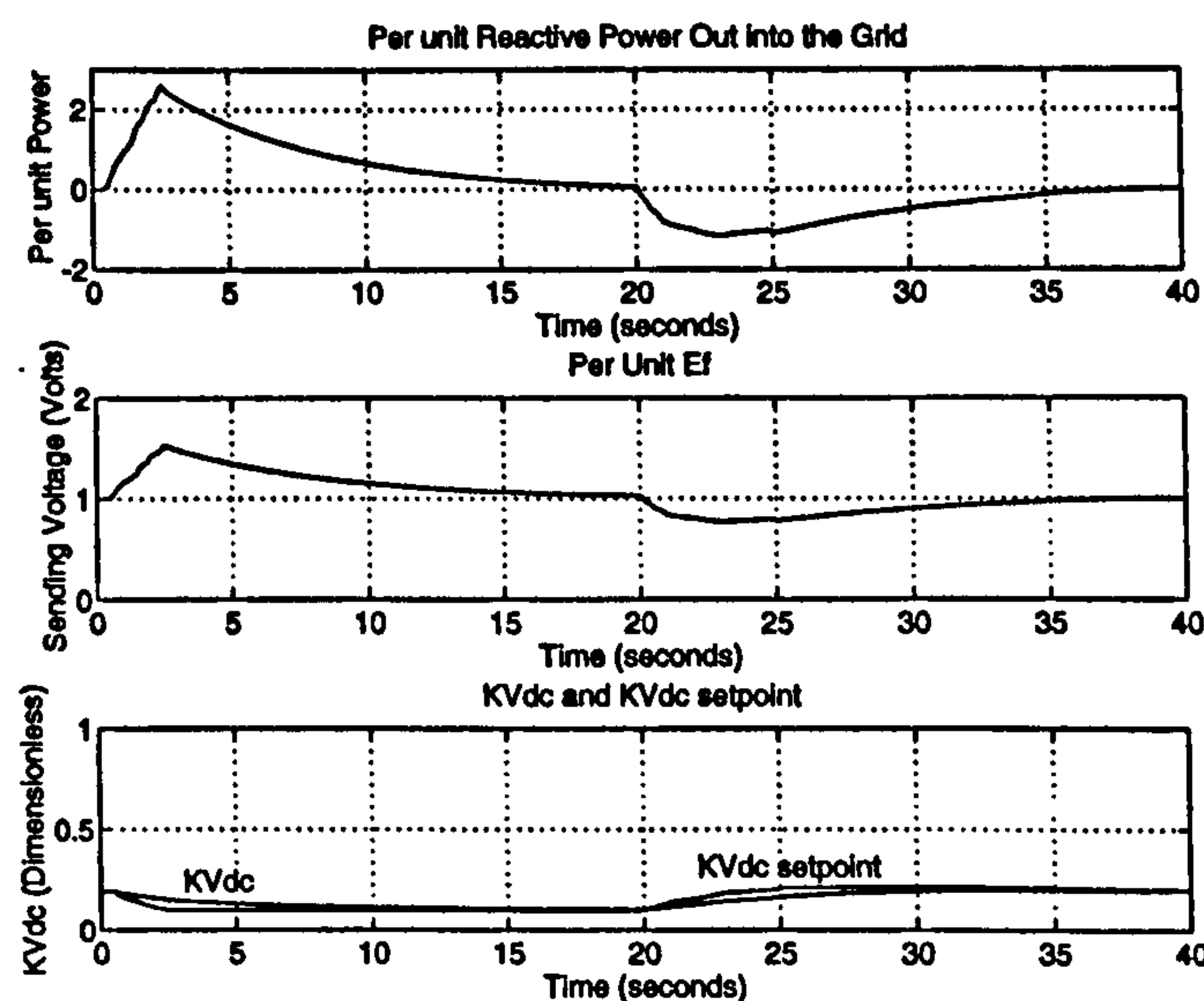


Figure 6.10: Response of Q , V_1 and $K_{V_{dc}}$ for step change in wind speed from 8 m/s to 12 m/s

The value of $K_{Prop} = 0.5$ and $K_{Int} = 0.25$ were used for this simulation and this gave a satisfactory response. However the reactive power out is still very large and this occurs for

two reasons.

1. Firstly there is a large error between the desired value $K_{V_{dc}}$ and the $K_{V_{dc}}$ setpoint. This is either because K_{Prop} is not a high enough value to limit the error sufficiently or because there is some coupling or interference between the $K_{V_{dc}}$ controller to maintain $V(1)$ constant and the controller that alters the inverter power angle, δ_{vs} , to track C_{pmax} .
2. Secondly although this error may not seem significant it has a major effect. This is because the reactance connecting the inverter to the grid is low, and the reactive power to the grid assuming no line resistance is given by Equation 6.1 Hence a small reactance leads to any slight difference between $V_1 \cos(\delta_{vs})$ and V_b being magnified. A value of 0.2 per unit is used in the simulations for the value for the reactance to the grid and so any difference in the bracketed term of Equation 6.1 is magnified five times if $V(1)$ is maintained at its rated value.

PI controller design to maintain $V(1)$ constant

Several simulation run throughs led to increasing K_{Prop} to 6 and K_{Int} to 0.25 as giving reasonable performance with the plots for the per unit reactive power, terminal voltage and $K_{V_{dc}}$ and $K_{V_{dc}}$ setpoint as seen in Figure 6.11. The reactive power is now about a third of that shown in Figure 6.10 and so the control of $V(1)$ is having the desired effect of reducing the output reactive power. There is also much less error between the required and actual value of $K_{V_{dc}}$. This is reflected in the per unit value of the fundamental of the inverter terminal, $V(1)$, which increases just above the 6 % limit, but such a step is unlikely and the response to real wind data shows that voltage regulation is adequate.

The value of $K_{Prop} = 6$ and $K_{Int} = 0.25$ are used for all subsequent simulation runs. Increasing K_{Prop} and K_{Int} much further leads to instability in the control ratio controller and therefore it is important to consider the second factor and the development of a control scheme to avoid interference between the inverter power angle and control ratio controllers will now be discussed.

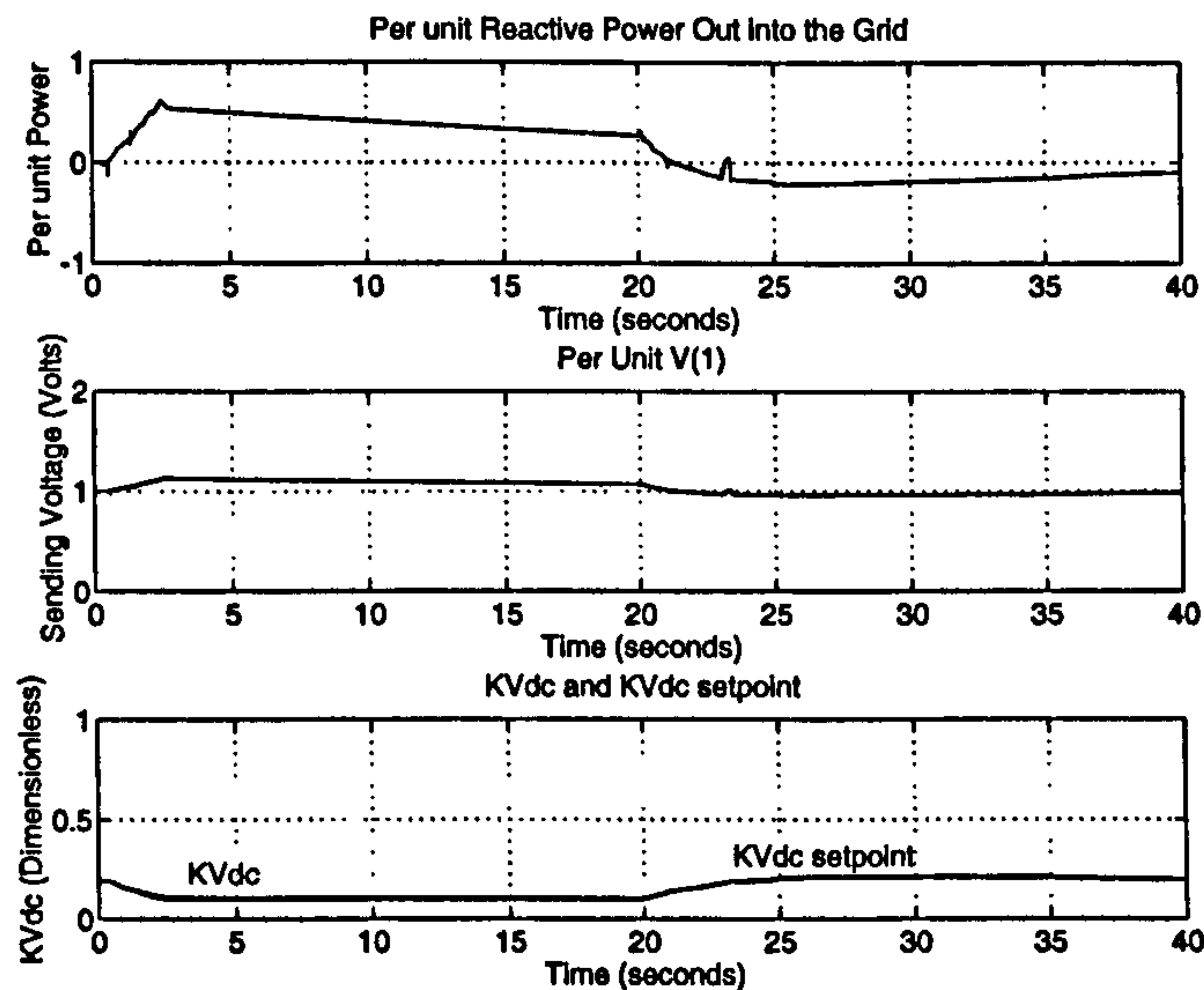


Figure 6.11: Response of Q , V_1 and $K_{V_{dc}}$ for step change in wind speed from 8 m/s to 12 m/s

Development of a suitable control scheme to avoid controller interference

The main problem with controlling both the output voltage level of the inverter to control reactive power and the real power flowing through the E-core to grid arrangement to maximise energy capture is that they are inextricably linked. If the power angle, δ_{vs} , is reduced as a response to the C_{pmax} controller action, less power would be extracted and therefore the current flowing into the inverter decreases and, providing the current flowing into the dc link is constant over the interval of this example, the dc link voltage level will increase. However if the dc link voltage rises the controller to keep $V(1)$ constant will reduce the control ratio, $K_{V_{dc}}$, to maintain $V(1)$ at its setpoint and thereby reduce the power extracted. This acts in unison with the effect of the C_{pmax} controller and so the control action is shared. However the results of Figure 6.10 show that the C_{pmax} tracking controller is more effective and hence $K_{V_{dc}}$ is not reduced enough which leads to excessive reactive power flowing into the system.

A control scheme could be developed to counteract this problem with the overriding aim of such control schemes being to limit the terminal voltage to within the limits laid down in the connection agreement with the local distribution company otherwise the generator would be penalised heavily or even disconnected. Thus the controller would act to keep $V(1)$ within the limits foremost and allow C_{pmax} tracking provided it is safe to do so.

6.3.3 Discussion

This section has outlined the problems with controlling both the firing angle and control ratio of the inverter to achieve control of both C_p and $V(1)$ respectively. A well designed controller has been found to minimise the interaction problems associated with the two control aims of changing δ_{vs} to alter V_{dc} to track C_{pmax} and changing $K_{V_{dc}}$ to maintain a constant $V(1)$ which tend to act to cancel one another out as explained in section 6.2.2. The terminal voltage has been kept within the limits imposed by the grid connection for an unusually large step in input wind speed and the scheme outlined in the previous section is considered adequate. Other schemes involving state space techniques to decouple the two controllers have been proposed [107] [108] but the scheme, outlined in the previous section, has a simple elegance that is easy to understand and implement and is therefore used subsequently. This method of controlling $K_{V_{dc}}$ to maintain the terminal voltage at its nominal value can be modified slightly to enable a reactive power setpoint to be used and the development of this slight adjustment to the $K_{V_{dc}}$ setpoint model is now presented.

6.4 Maintaining Q constant as V_{dc} varies

In the previous section the aim was to just maintain V_1 at a constant level, for example, at nominal value. This led to the reactive power being slightly negative due to the small power angle δ_{vs} . Now it would be advantageous to be able to deliver reactive power to the grid in response to some demand, i.e. a local induction motor switches on and requires reactive power to be supplied to it at a certain power factor. This would require the wind turbine to operate as a supplier of both real and reactive power. To achieve this a reactive power setpoint could be included in the control hierarchy.

6.4.1 Control scheme to include a reactive power setpoint

The control scheme necessary to include the reactive power setpoint in the control hierarchy of the wind turbine can be seen in Figure 5.36. Depending on the current value of the power angle, δ_{vs} , the $K_{V_{dc}}$ setpoint is altered to maintain Q at the setpoint. This is done by rearranging equation 6.1 and combining it with equation 5.6 to give the following expression

6.5 The effect of pitch action on variable speed operation

that gives K_{Vdc} in terms of the reactive power setpoint, Q_{spt} .

$$K_{Vdc} = \frac{0.45V(1)}{V_{dc}} \left(\frac{Q_{spt}X_s}{V_b \cos \delta_{vs}} + \frac{V_b}{\cos \delta_{vs}} \right) \quad (6.2)$$

6.4.2 Constant Q results

Again a step up in windspeed from 8 to 12 m/s is used as an example for demonstrating the principle of maintaining a reactive power setpoint. For the following results the Q setpoint is 0.2 per unit. The response of the reactive power, terminal voltage and K_{vdc} and its setpoint can be seen in Figure 6.12. The reactive power setpoint is maintained after the transient response is completed. The peak value of the reactive power transient is more than the corresponding value from keeping $V(1)$ at unity and this is because the initial $V(1)$ is at a higher initial value.

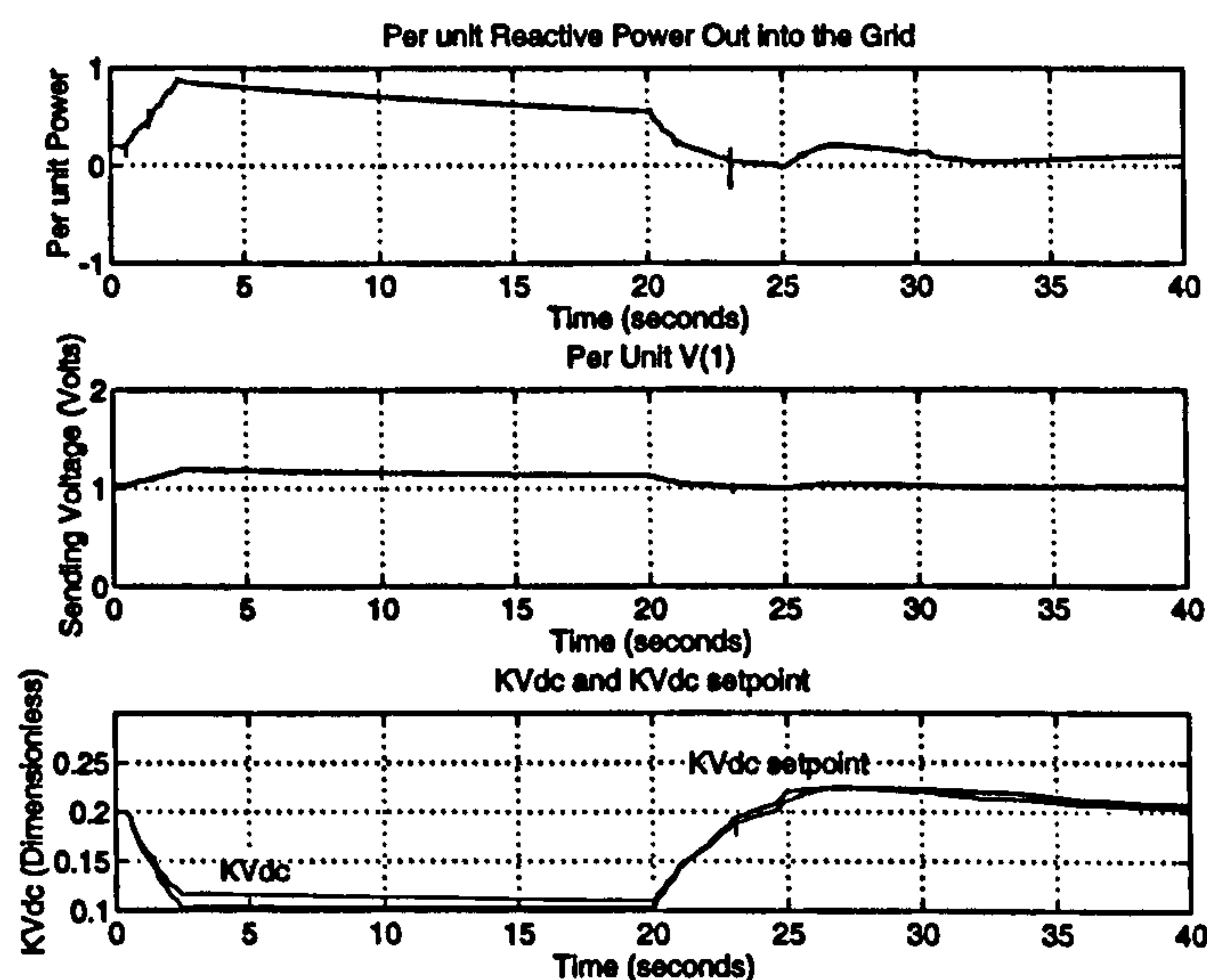


Figure 6.12: Response of Q , V_1 and K_{Vdc} for step change in wind speed from 8 m/s to 15 m/s

6.5 The effect of pitch action on variable speed operation

This section outlines the combining of the real and reactive power controllers to track C_{pmax} and limit Q into the grid with the pitch controller to limit power into the generator to avoid above rated operation.

6.5 _____ The effect of pitch action on variable speed operation

6.5.1 Suitable pitch control for variable speed operation

The operation of the wind generator at variable speed poses additional difficulties in the design of a suitable pitch control system. For the fixed speed case rated power occurs at rated torque and rated speed and in per unit terms power and torque are interchangeable because the speed is fixed by the grid. In variable speed operation, however, the speed is determined by tracking C_{pmax} below rated wind speed and used to limit power above rated subject to the constraint of the maximum allowable shaft torque. This can be qualified by the situation where the turbine is not at rated speed when a step into above rated wind speed occurs. At the instant of the step an over-torque situation arises even though the power may well be below rated. A controller therefore should act upon a signal of power and not torque in variable speed wind turbines. This leads to the same pitch demand as depicted in Figure 2.6 but now ensuring that power is used as the input variable. As such the same values as designed in Chapter 2 for the pitch controller and actuator are also used.

6.5.2 Step up and step down result

The effect of pitch action is best shown with respect to a step above rated wind speed followed by a step down in rated wind speed to determine the overall cycle and see how well the controller tracks the dc link setpoint voltage for C_{pmax} . The following results are for a step up followed by a step down from 12 to 13 and back to 12 m/s. The response of the mechanical and airgap power versus the rotor speed for this value of pitch control can be seen in Figure 6.13. The final value of P_m , after the initial overshoot due to the induction lag effect, is 1.14 of the rated value and the controller works well.

The controller works well upto the design windspeed of 13 m/s but above this value a larger error would be required to give the necessary blade pitch angle. This would lead to over rated operation of the generator in high windspeed condition and this is not desirable. Furthermore the measurement of shaft power is no easy process with both a speed and torque transducer required. These often prove unreliable and relatively expensive. Therefore not measuring shaft power may be advantageous.

6.6 Response of the 458 kW rated generator to simulated wind data

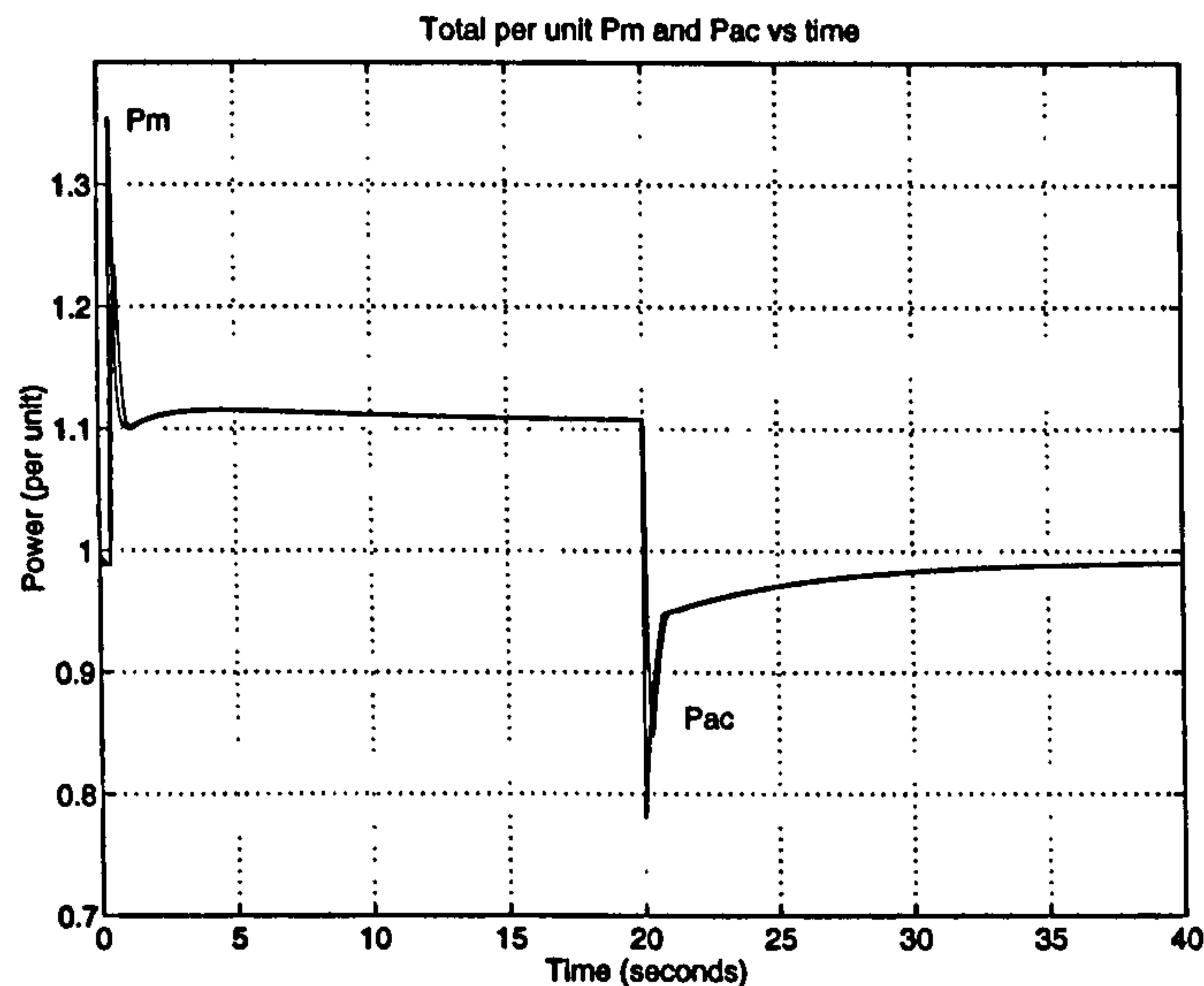


Figure 6.13: Response of P_m and P_{ag} for step up then step down in windspeed from 12 to 13 m/s

6.6 Response of the 458 kW rated generator to simulated wind data

The step response results are now extended to cover the case with simulated wind speed data from the spectral method including all rotational effects. These results show that the effect of the slow response of the rotor blades inertia to gusting and the transients introduced due to the rotational effects limit the effectiveness of the C_{pmax} tracking controller and, hence, the energy captured by the 458 kW rated generator. Possible solutions to this problem are proposed and further issues raised to indicate the problems associated with connecting the turbine to the grid.

This section also investigates how the value of the dc link capacitance, the equivalent parameter in the variable speed design to the compliant mounting of the fixed speed case, can be altered to improve the interaction of the complete wind turbine system in a typical windy environment and demonstrates the ability of the capacitance to limit any high frequency power oscillations and rotor movement. The pitch controller has the same values as designed in Chapter 2.

Five simulated wind speeds are generated by the spectral method and used to characterise the performance of the variable speed operated permanent magnet generator and assess

6.6 _____ Response of the 458 kW rated generator to simulated wind data

the impact of the pitch controller on the output power. These five wind speed variations correspond to the following cases:

1. **Cut in.** This corresponds to the synchronisation case presented in Chapter 4 and is not considered here because synchronisation of the variable speed system is unnecessary because of the presence of the frequency converter. This is a further advantage of variable speed control is that complicated monitoring and control equipment required for the synchronisation of the fixed speed wind turbine is no longer necessary.
2. **Below rated windspeed.** This is the most important region for the variable speed wind turbine and is presented as the base case for the windy simulations with a comparison with the fixed speed performance included in the next chapter.
3. **Below to above rated windspeed.** This is the key area for the pitch controller as the output power to the grid must be limited to rated value with the frequency converter ensuring smooth operation.
4. **Above rated windspeed.** Gradually the turbulence becomes stronger in the wind and the pitch controller must act more to maintain constant power out.
5. **Cut out.** Finally this time history demonstrates the fail safe pitching of the blade when the mean wind speed is greater than the designed cut-out value of 25 m/s the pitch controller must shut down the turbine and voltage control used to limit the dc link voltage to within the safe operational level.

The last four situations are now simulated for the 458 kW rated generator with the values for the different controllers as designed earlier and presented in Tables 2.3, 6.1 and 6.2. Then the effect of varying the dc link capacitance is demonstrated to show what happens when poor control of the dc link voltage occurs. This will vindicate the use of the 4000 μF dc link capacitance. Only the key results are included here.

6.6.1 Below rated wind speed response

The simulated wind speed with mean 9 m/s and the corresponding response of the mechanical torque due to the effective wind speed before the rotational torques have been added

6.6 _____ Response of the 458 kW rated generator to simulated wind data

can be seen in Figure 6.14. The run identifiers are also indicated to show the values of the various control parameters for the pitch angle, power angle and control ratio controllers.

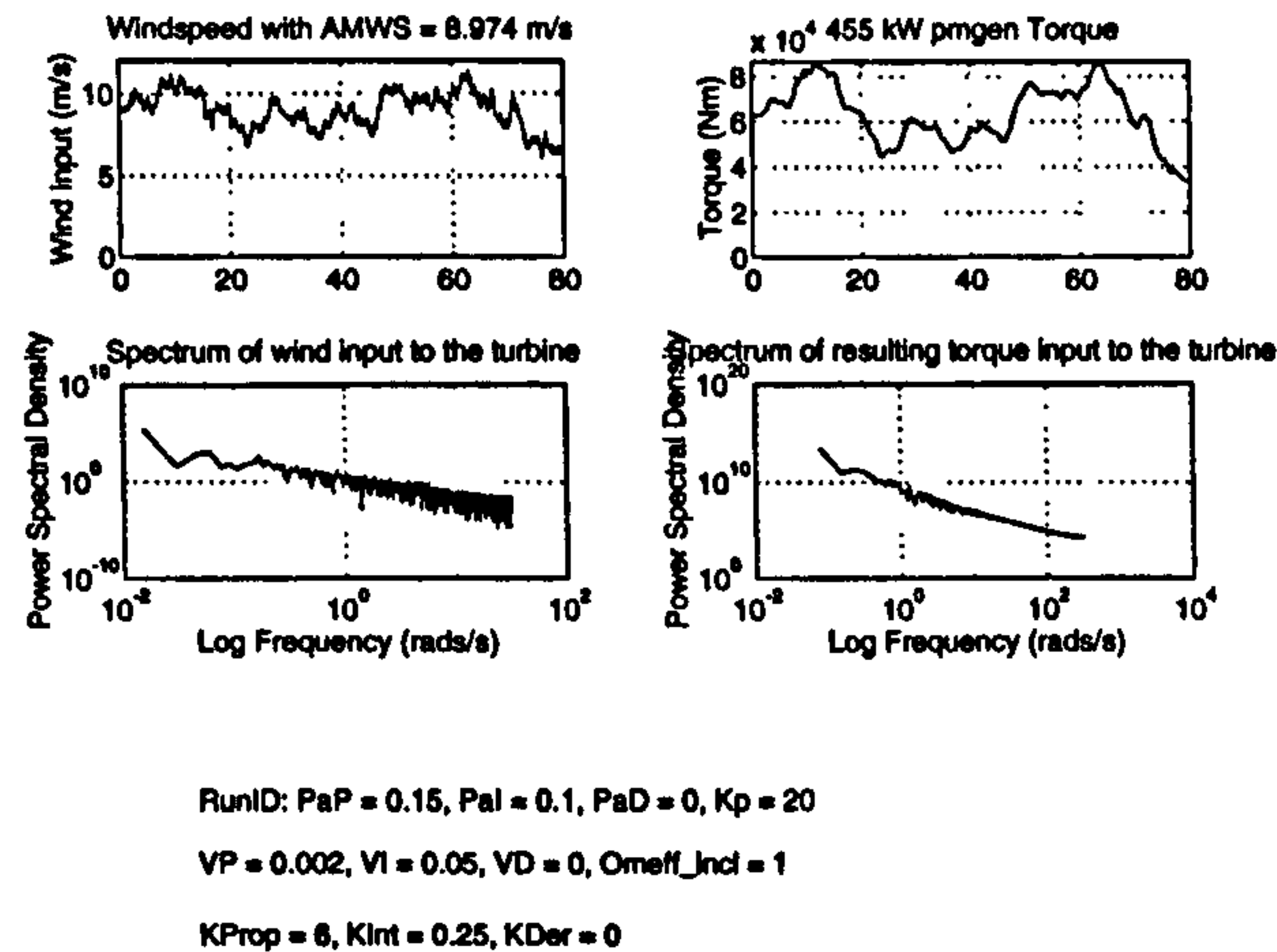


Figure 6.14: Simulated wind speed with AMWS of 9 m/s and the corresponding input torque

The top trace of Figure 6.15 shows that rotational effects have been included for this run through as it is now the response of the generator in simulated wind conditions that is required. It is interesting to note that the power coefficient starts at 0.45 and subsequently varies only very slightly about this maximum value as the V_{dc} controller attempts to alter the inverter firing angle and hence alter the power angle to track C_{pmax} . The spectrum of the total driving torque input to the generator can be seen in the third plot with two vertical straight lines indicating the $3\omega_r$ and $1\omega_r$ frequencies. As the wind speed does not change much in the interval of the simulation, the frequency of rotation of the generator does not vary as much as for a longer run. This means that the spectral peaks are still apparent even though on a longer simulation run where the wind turbine operated over its complete frequency range the peaks would be expected to blend into the overall spectrum and become less discernible.

The mechanical power, P_m , from the wind turbine blades and the corresponding airgap power, P_{ac} , out into the E-core and rectifier arrangement can be seen in Figure 6.16. The response of the airgap power follows the response of the inverter control of the dc link voltage as rotor speed increases, i.e. tracks C_{pmax} . The mechanical power into the wind turbine shows the oscillatory variations induced by the rotational effects and the changing wind speed input into the wind turbine.

6.6 _____ Response of the 458 kW rated generator to simulated wind data

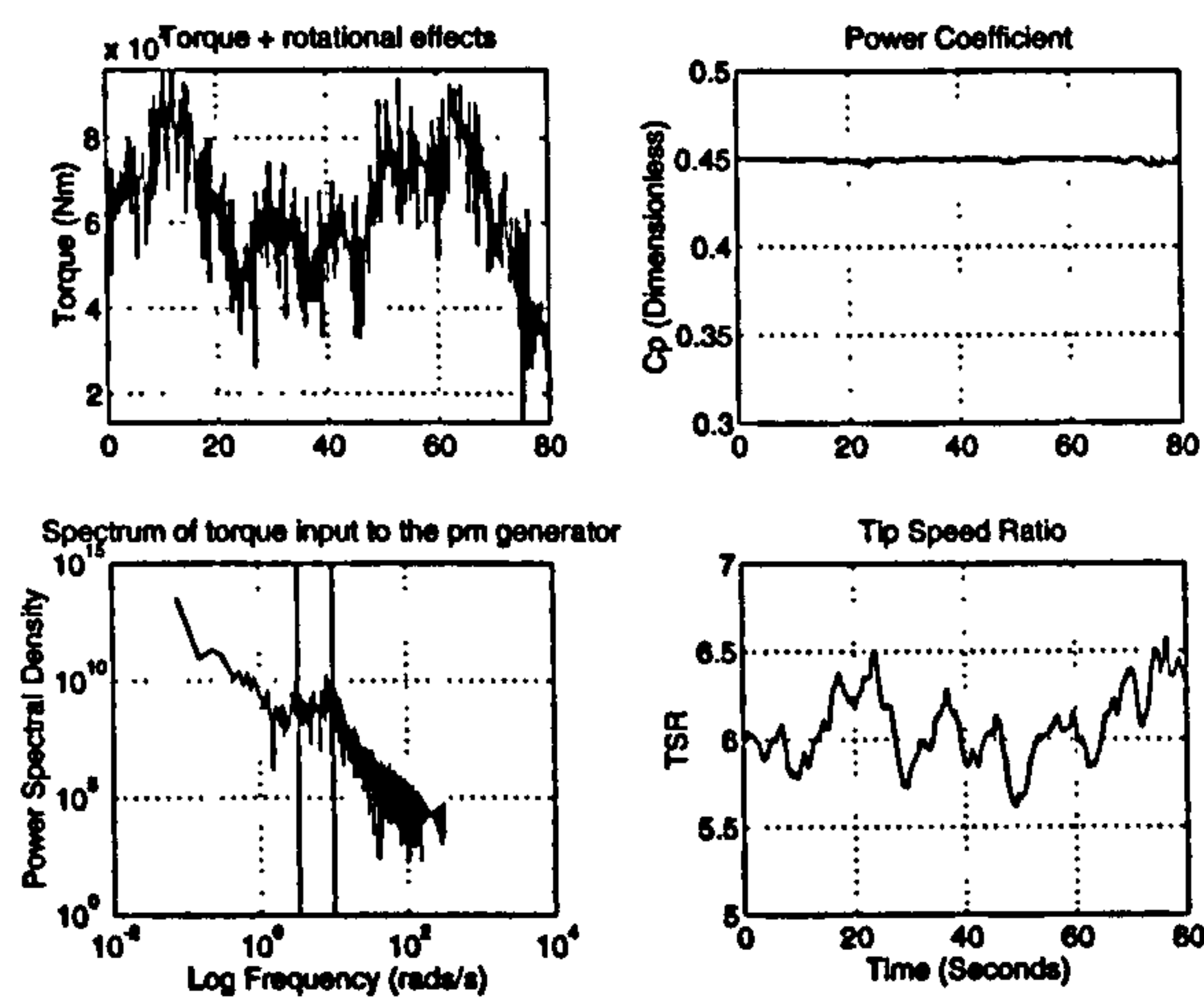


Figure 6.15: The resulting power coefficient and tip speed ratio

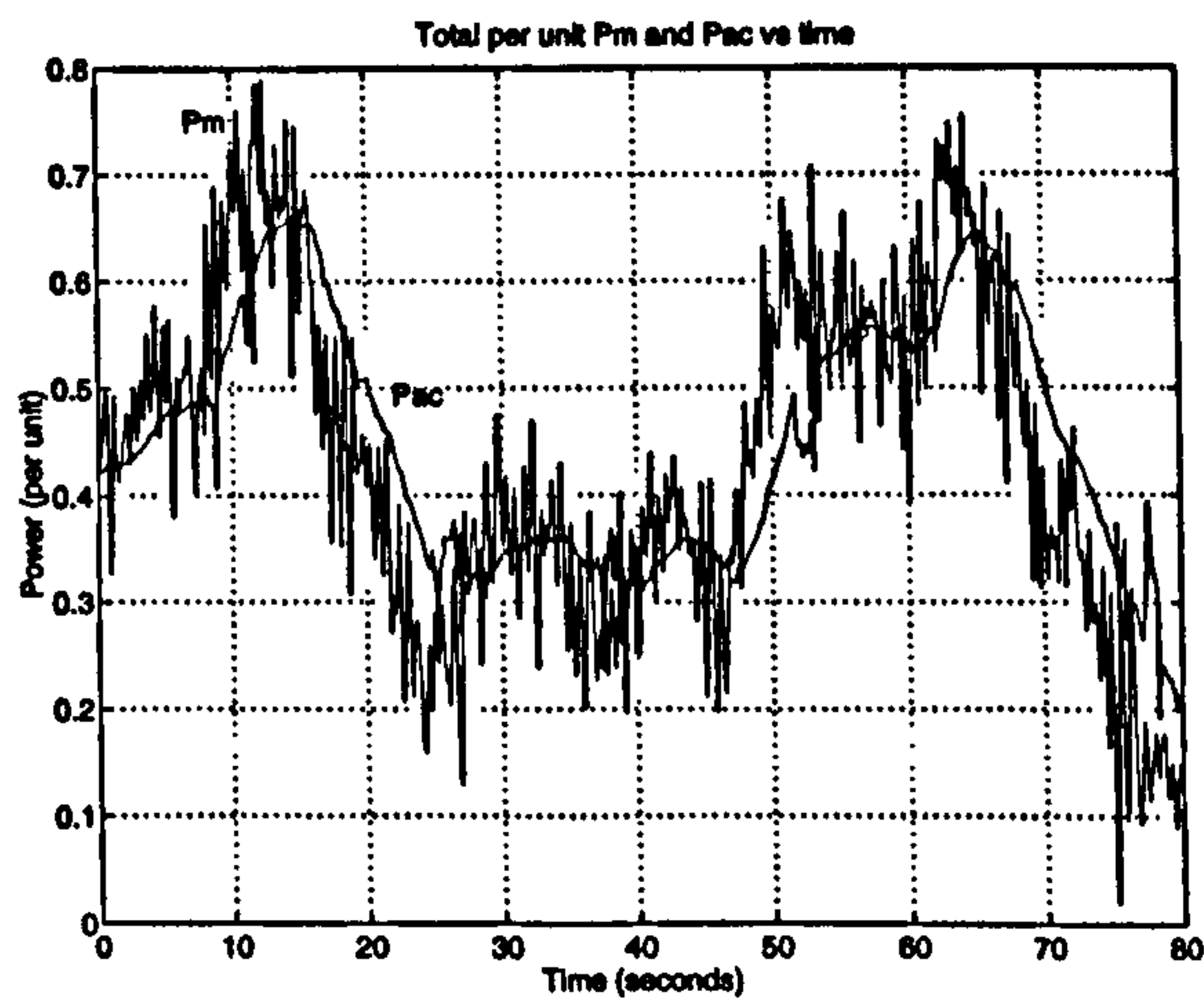


Figure 6.16: Module airgap and mechanical power

6.6 _____ Response of the 458 kW rated generator to simulated wind data

Figure 6.17 shows the variation of the input power, the resulting airgap power, the variation of rotor speed and dc link voltage. It should be noted that the dc link voltage stays within the 1200 V rating of the high power IGBT.

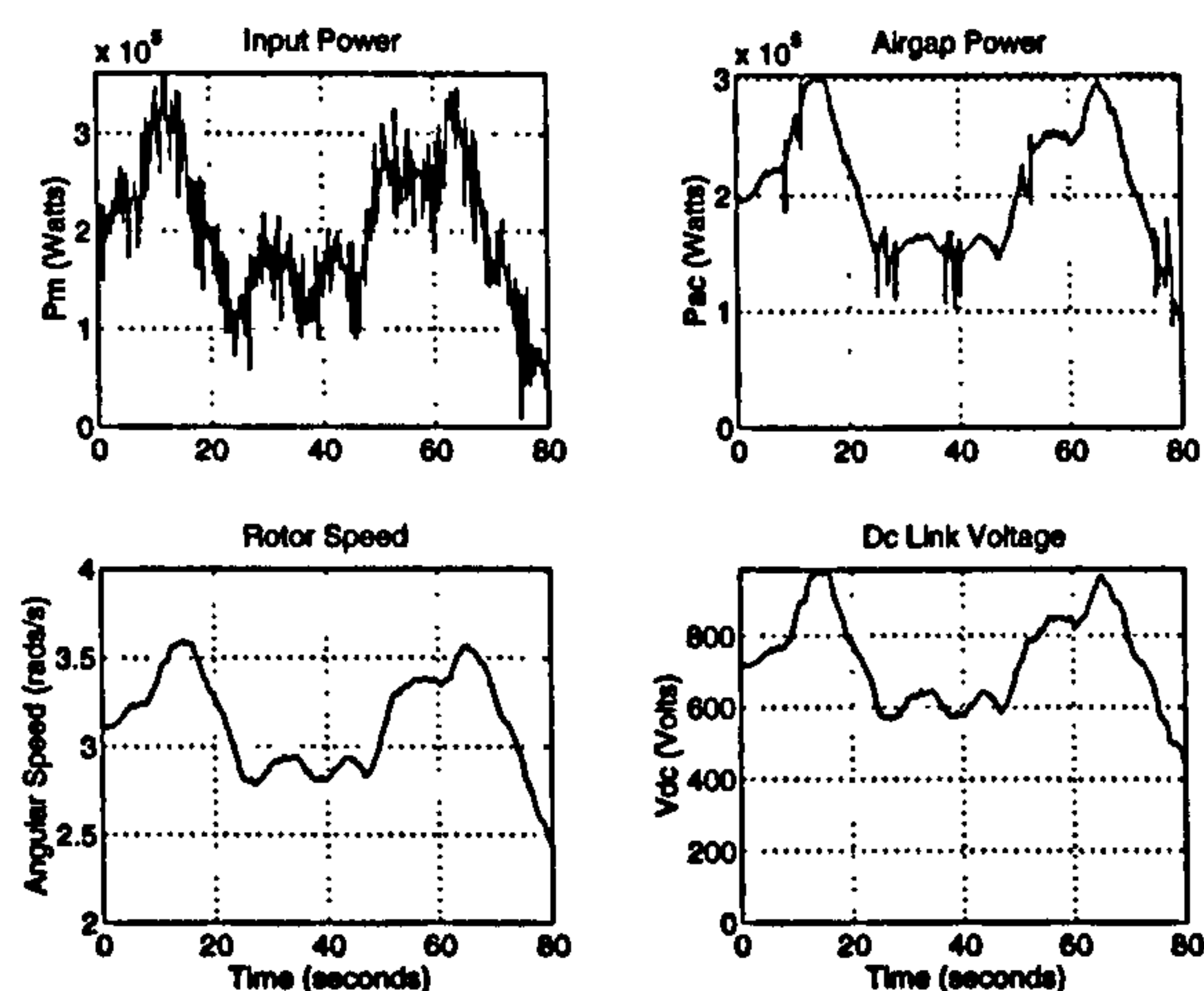


Figure 6.17: The input power, airgap power, rotor speed and dc link voltage

Figure 6.18 shows the current flowing into the inverter and the dc link current and the output electrical power into the grid and the overall power loss through the e-core, rectifier and inverter. The current plots are indicative of the magnitude of the current into and out of the dc link and inherent in the simulation method is that commutation of the IGBT's in the inverter is instantaneous.

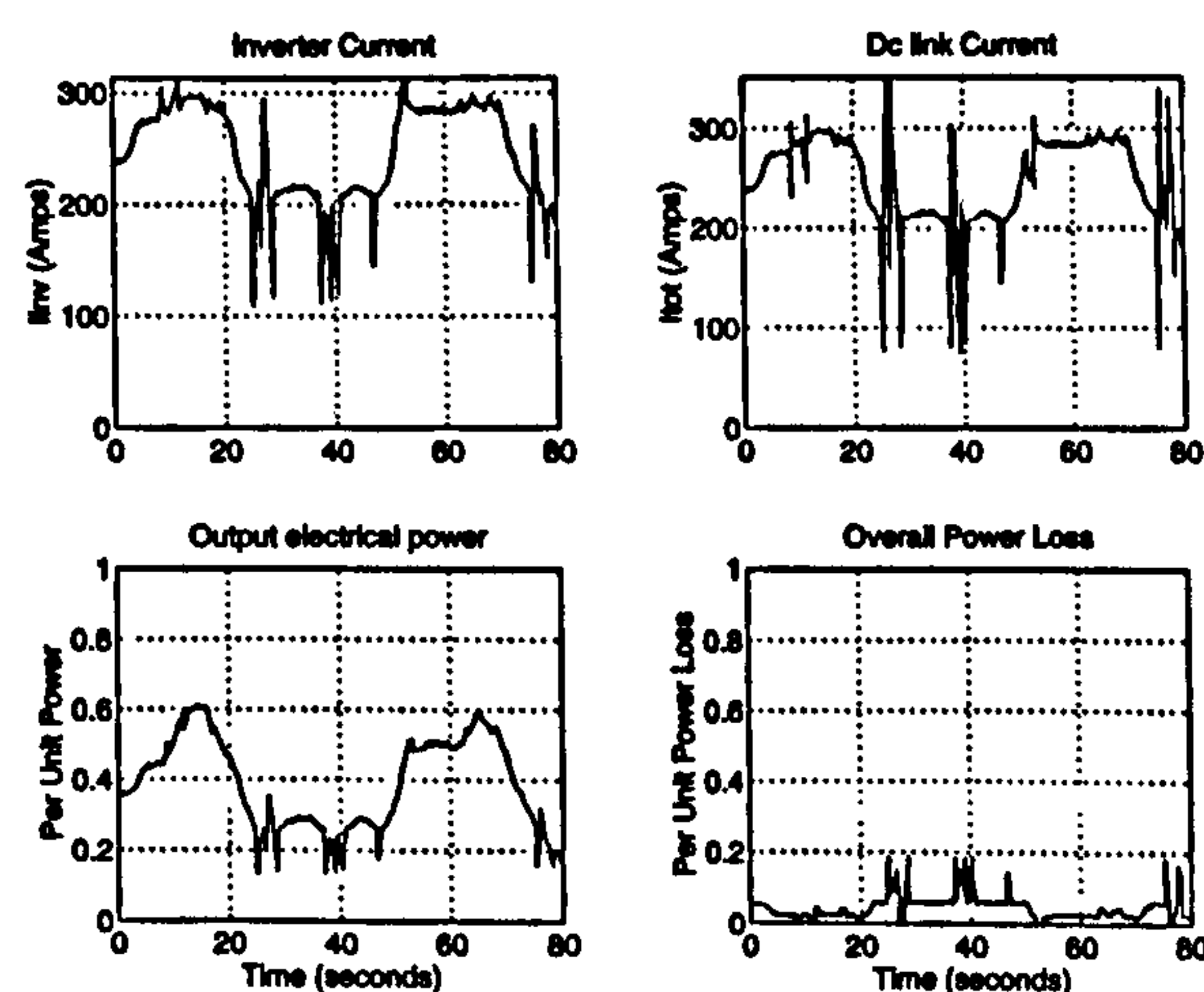


Figure 6.18: Inverter and dc link current and output power and overall power loss

Figure 6.19 shows the variation of the measured dc link voltage and the dc link voltage setpoint from the $\omega - V_{dc}$ relationship to track C_{pmax} against time. The power angle PI controller is sufficient to track this relationship accurately and for the case where only C_{pmax}

6.6 _____ Response of the 458 kW rated generator to simulated wind data

needs to be tracked the constraint of keeping V_{dc} within the required breakdown voltage limit of 1200 Volts is satisfied with only marginal loss in performance.

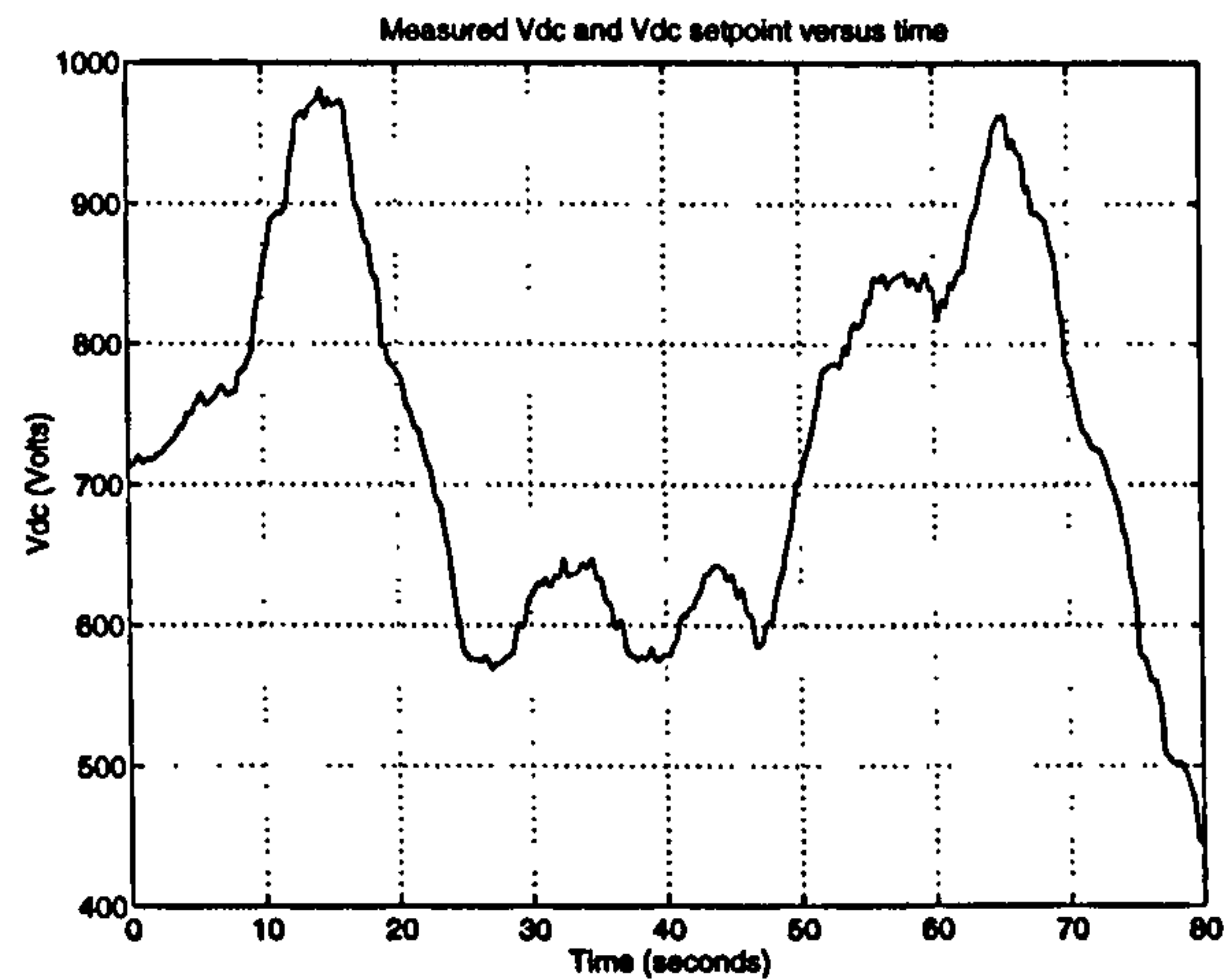


Figure 6.19: Measured and dc link setpoint voltage

The plots shown in Figure 6.20 are very important as they demonstrate the adequate control of the inverter control ratio, $K_{V_{dc}}$, at the required level to give the reactive power setpoint of 0.2 per unit in the windy environment. The terminal voltage does not fluctuate about its nominal value by more than the +6 and -10 % limit laid down for grid connection.

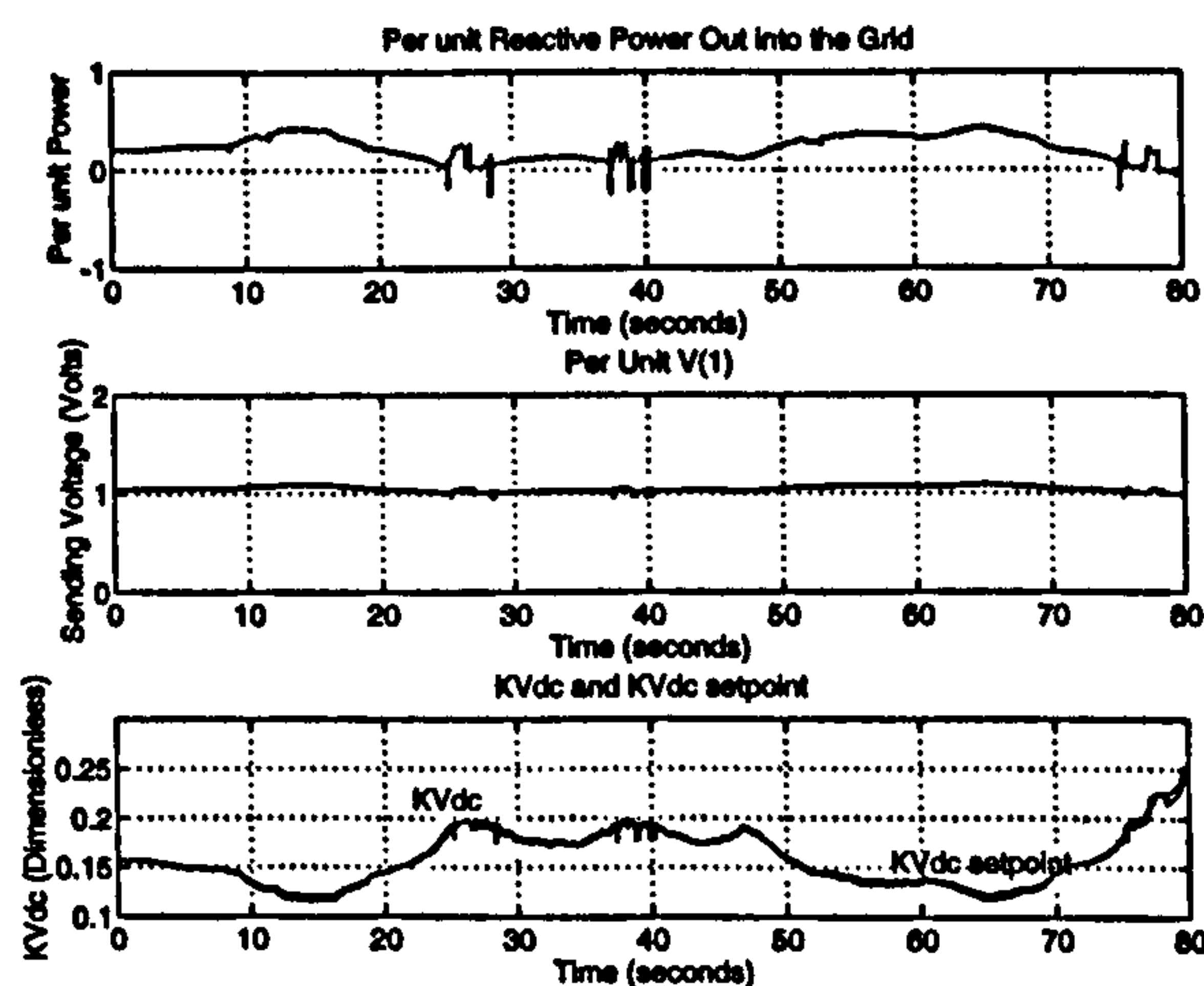


Figure 6.20: Reactive power and $K_{V_{dc}}$ setpoint

ENERGY CAPTURE ANALYSIS. An analysis of the energy flows within the variable speed wind turbine for the response to the wind speed time history with AMWS of 9 m/s can be seen in Table 6.2.

There are several points to be made about the figures presented in Table 6.2. Firstly the

6.6 ——— Response of the 458 kW rated generator to simulated wind data

Mechanical energy into turbine	4.45 kWh
Electrical energy out at the airgap	4.58 kWh
Max possible energy capture	4.48 kWh
Controller effectiveness	99.33 %
DC link energy	3.96 kWh
Generator and Rectifier Efficiency	89.2 %
Overall energy out to the grid	3.95 kWh
Overall Efficiency	86.5 %

Table 6.2: Energy capture analysis for the 458 kW rated variable speed generator

fact that the mechanical energy into the airgap is greater than the electrical power out of the airgap is due to the rotor slowing down over the simulation run. Secondly, although the wind changes speed during a gust far more quickly than the rotor speed can due to the large inertia of the rotor blades, the controller is still very effective at following the desired $\omega - V_{dc}$ characteristic to track C_{pmax} . This is in opposition to statements made in [91] where it was discovered that the turbine operated away from C_{pmax} for most of the time and there was a larger corresponding reduction in energy capture from the theoretical maximum. This difference could be due to the aerofoils used in this thesis having a different C_p curve. Aerofoil design is an issue in variable speed operation with broad C_p curves allowing C_{pmax} to be tracked easily. These broad curves however limit the advantage over fixed speed because these aerofoils are less effective and over the speed range of the variable speed turbine the change in C_p when compared with the fixed speed value would be reduced. The aerofoils used in this thesis lead to an energy capture which is 99.33 % of the theoretical maximum and, after including all the losses in the generator, rectifier and inverter, the variable speed wind turbine has an efficiency of 86.5 % over this simulation run with an AMWS of 9 m/s. The final point to make, therefore, is that despite good tracking of C_{pmax} significant energy losses are recorded from the airgap to the grid and a scheme which both tracked C_{pmax} and the efficiency of the generator could be more effective. This is discussed in Chapter 8 and a comparison of energy capture with the fixed speed case is discussed in Chapter 7.

6.6.2 Below to above rated wind speed response

The simulated wind speed with mean 12 m/s and the corresponding response of the mechanical torque into the wind turbine, before rotational effects are added can be seen in

6.6 ——— Response of the 458 kW rated generator to simulated wind data

Figure 6.21. The run identifiers are also indicated to show the values of the pitch angle, power angle and control ratio controller parameters.

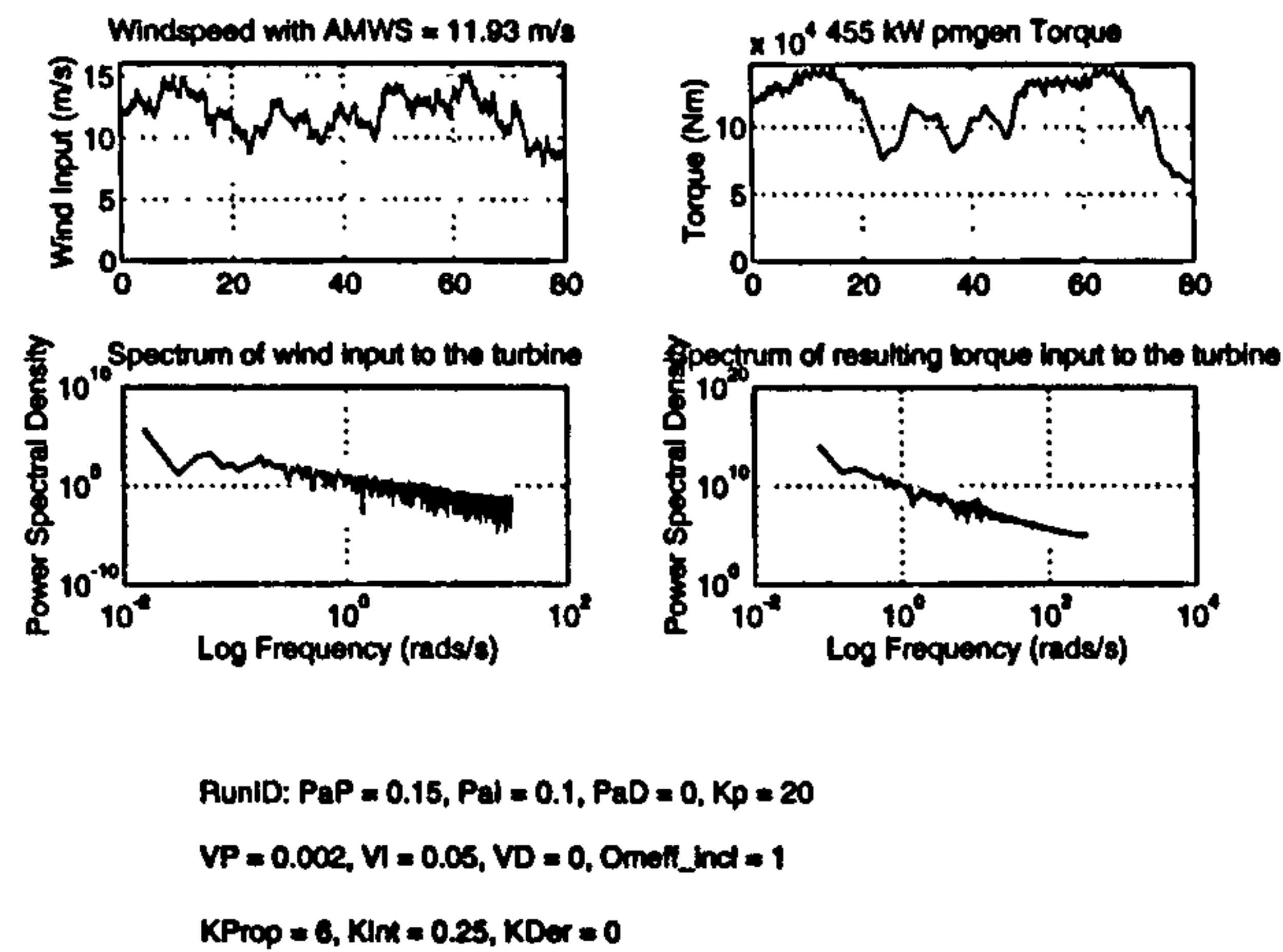


Figure 6.21: Simulated wind speed with AMWS of 12 m/s and the corresponding input torque

The top trace of Figure 6.22 shows that rotational effects have been included for this run through. It is interesting to note that the power coefficient starts at 0.45 for the intervals where the wind speed is below rated varies only slightly about this maximum value as the V_{dc} controller attempts to alter the inverter firing angle, and hence power angle, to track C_{pmax} . However when the wind speed is above rated the pitch controller begins to alter the pitch angle to maintain rated power and C_p reduces markedly. The spectral peaks in the induced hub torque are still apparent due to the short length of the simulation run.

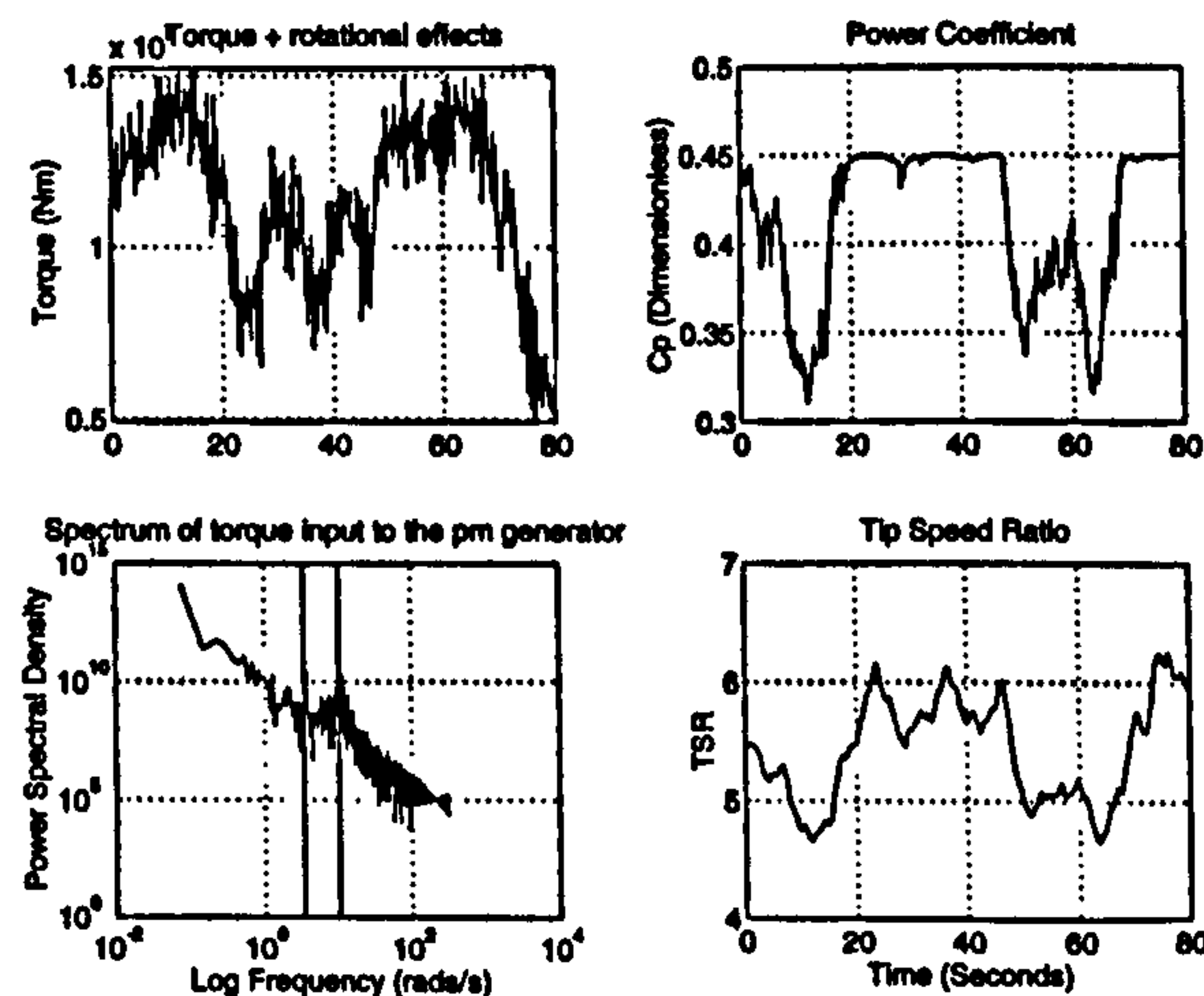


Figure 6.22: The resulting power coefficient and tip speed ratio

The mechanical power, P_m , from the wind turbine blades and the corresponding airgap

6.6 _____ Response of the 458 kW rated generator to simulated wind data

power, P_{ac} , out into the E-core and rectifier arrangement can be seen in Figure 6.23. The response of the airgap power follows the response of the inverter control of the dc link voltage as rotor speed increases, i.e. tracks C_{pmax} , in below rated wind speeds and is limited to 1.28 of rated value for wind speeds above rated. The mechanical power into the wind turbine shows the oscillatory variations induced by the rotational effects and the changing wind speed input into the wind turbine.

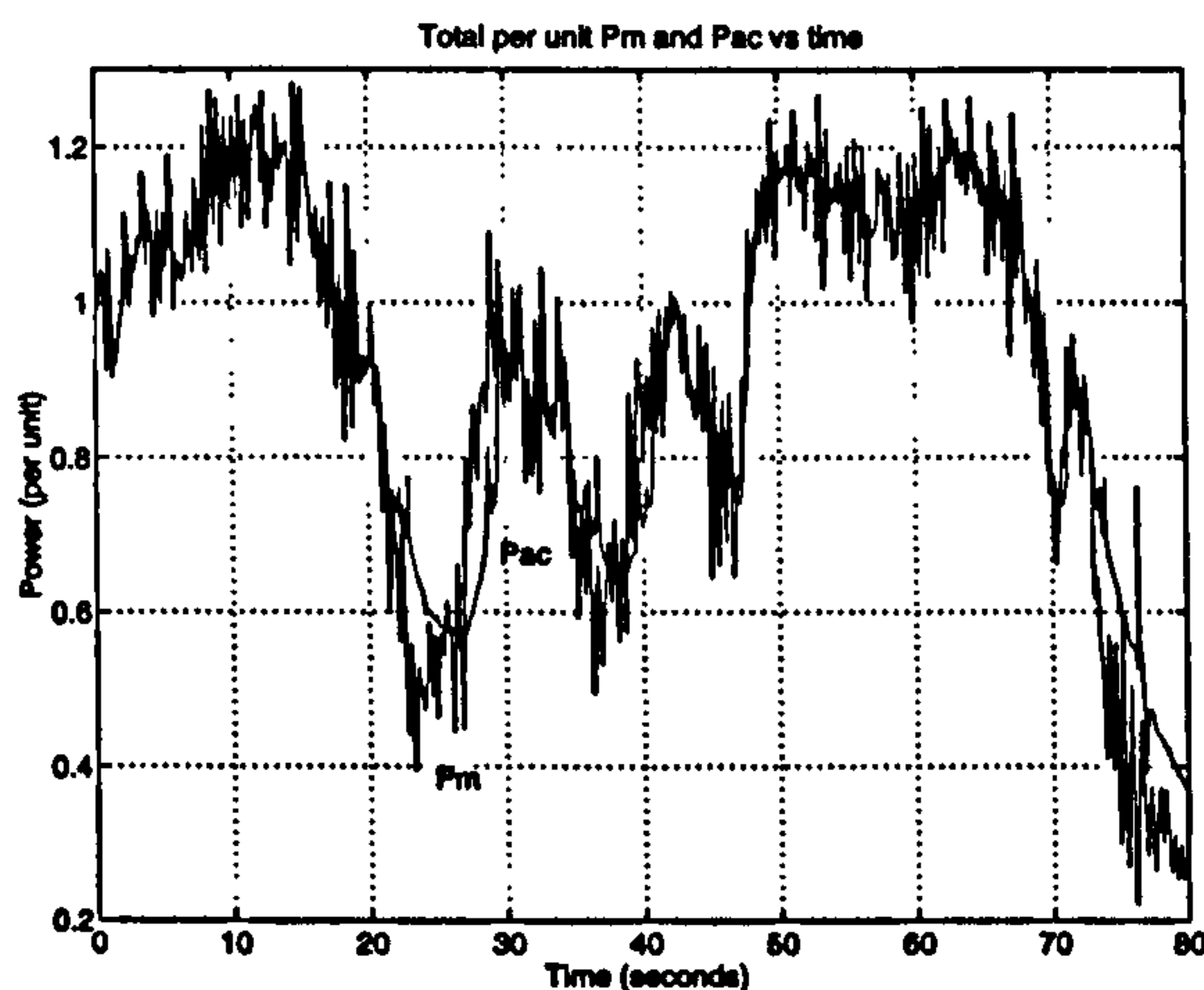


Figure 6.23: Module airgap and mechanical power

The pitch demand and pitch angle necessary to maintain the variable speed wind turbine at rated power in above rated wind speeds can be seen in Figure 6.24. As for the fixed speed case, the pitch angle is smoother than the pitch demand because the limits on both the rate and acceleration of the pitch actuator smooth out the power variations introduced by the rotational effects.

The plots shown in Figure 6.25 are very important as they demonstrate the adequate control of the inverter control ratio, K_{Vdc} , to keep the fundamental value of the inverter output voltage constant at its desired setpoint to give a reactive power of 0.2 per unit.

ENERGY CAPTURE ANALYSIS. An analysis of the energy flows within the variable speed wind turbine for the response to the wind speed time history with AMWS of 12 m/s can be seen in Table 6.3.

The effectiveness of the controller now includes the effect of pitch action as well as control of the inverter firing angle to track C_{pmax} for the periods below rated wind speed. Figure 6.23 shows that the mechanical power is above one per unit for much of the simulation run as the pitch controller is unable to limit the power to the desired rating and hence the effectiveness

6.6 _____ Response of the 458 kW rated generator to simulated wind data

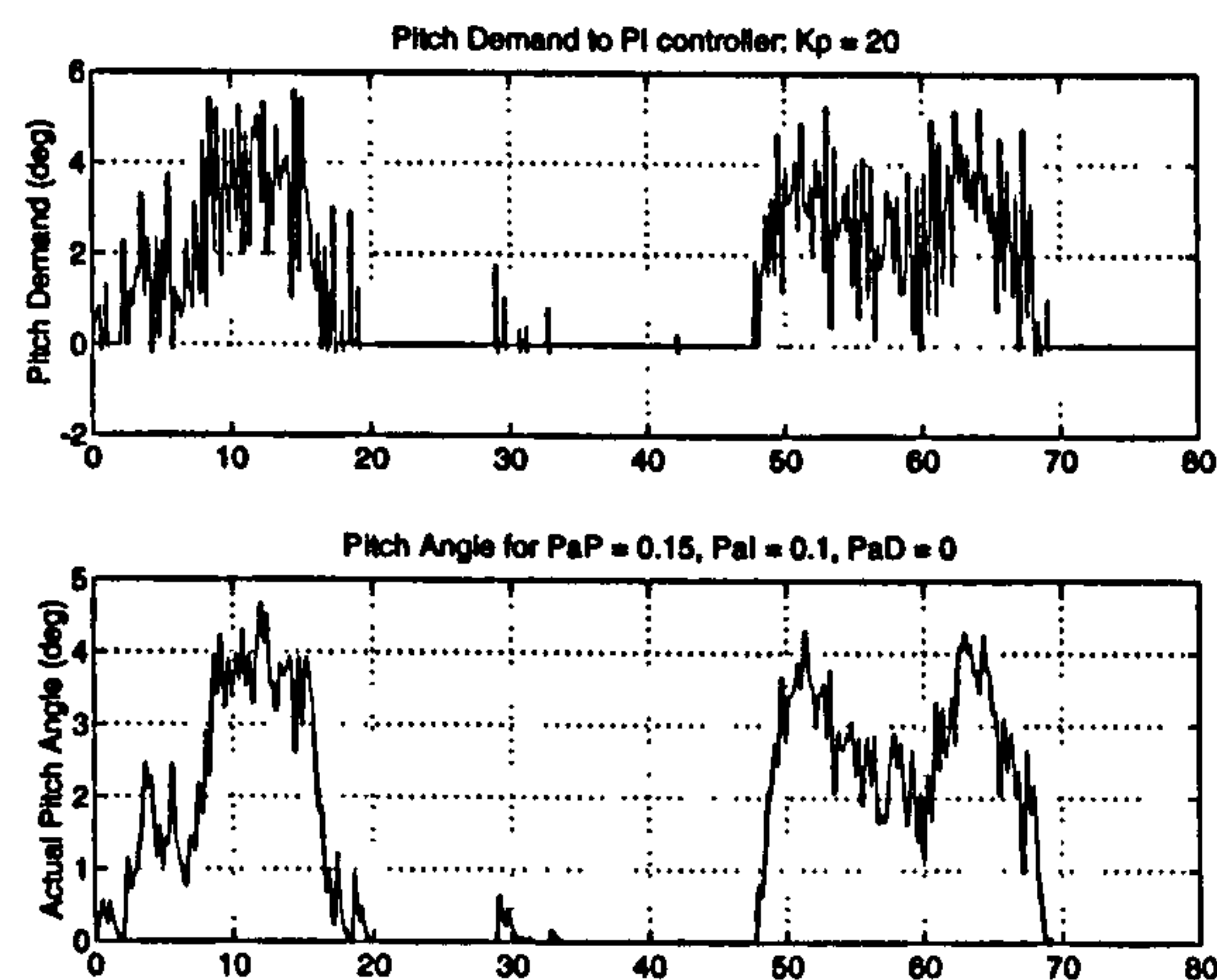


Figure 6.24: Pitch control and actuator response

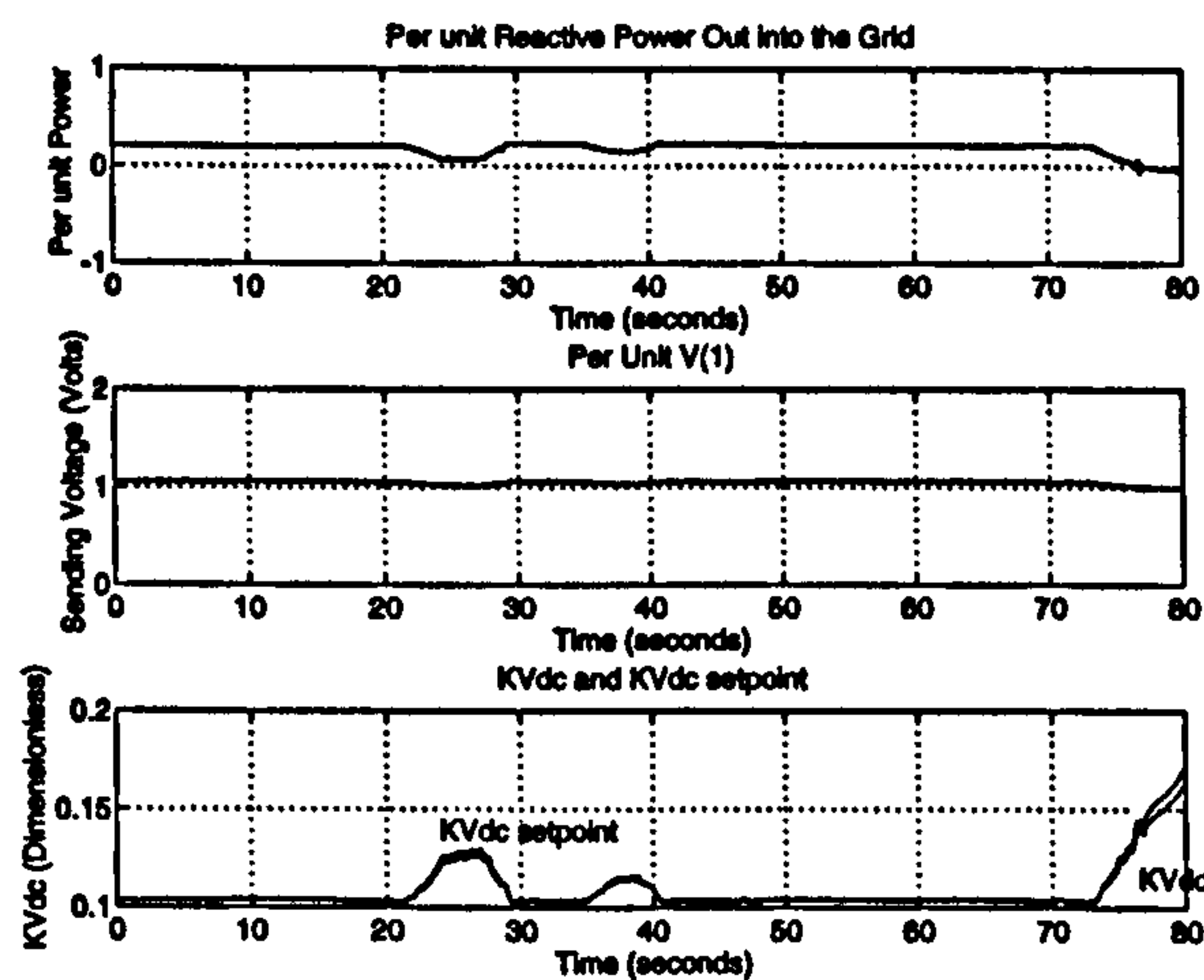


Figure 6.25: Reactive Power and voltage regulation

Mechanical energy into turbine	9.34 kWh
Electrical energy out at the airgap	9.48 kWh
Max possible energy capture	8.99 kWh
Controller effectiveness	1.04 %
Overall energy out to the grid	8.66 kWh
Overall Efficiency	91.4 %

Table 6.3: Energy capture analysis for the 458 kW rated variable speed generator

6.6 _____ Response of the 458 kW rated generator to simulated wind data

value is greater than unity. The overall efficiency is higher than that presented in Table 6.2 and highlights the need to track efficiency as well as C_{pmax} .

6.6.3 Above rated wind speed results

The simulated wind speed with mean 18 m/s and the corresponding response of the mechanical torque, before the addition of rotational effects, into the wind turbine can be seen in Figure 6.26. The run identifiers are also indicated.

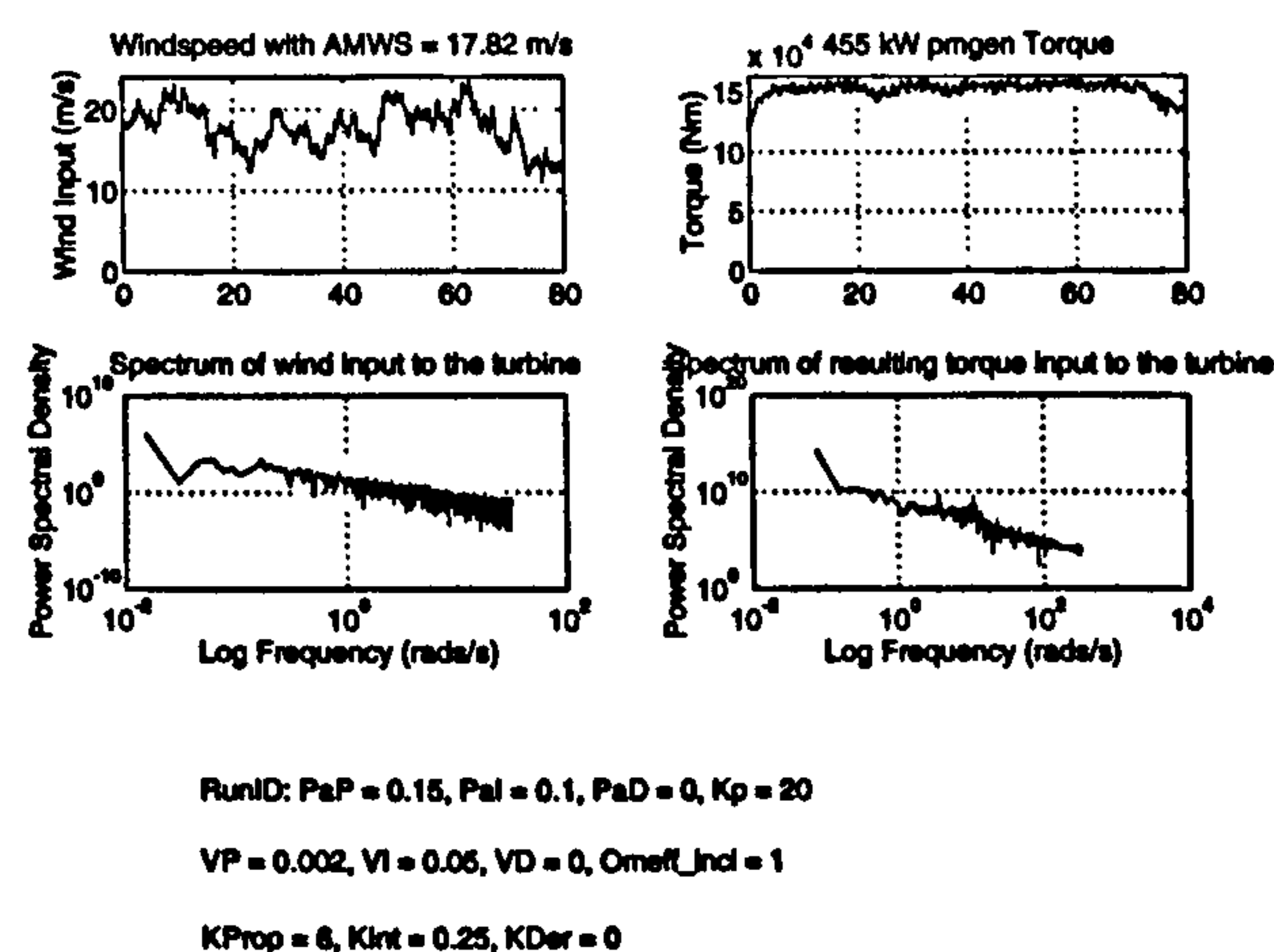


Figure 6.26: Simulated wind speed with AMWS of 18 m/s and the corresponding input torque

The top trace of Figure 6.27 shows that rotational effects have been included for this simulation run. The power coefficient starts at 0.09, the value which gives rated power at the start pitch angle corresponding to a wind speed of 18 m/s, and subsequently varies much below the maximum value, C_{pmax} , due to the action of the pitch controller. The tip speed ratio is much less than 6, the value corresponding to C_{pmax} , because of the high wind speed.

The mechanical power, P_m , from the wind turbine blades and the corresponding airgap power, P_{ac} , out into the E-core and rectifier arrangement can be seen in Figure 6.28. The response of the airgap power is limited to 1.45 of rated value as the wind speed is above rated. The mechanical power into the wind turbine shows the oscillatory variations induced by the rotational effects and the changing wind speed input into the wind turbine.

The pitch demand and pitch angle necessary to maintain the variable speed wind turbine at rated power in above rated wind speeds can be seen in Figure 6.29. There is now much

6.6 _____ Response of the 458 kW rated generator to simulated wind data

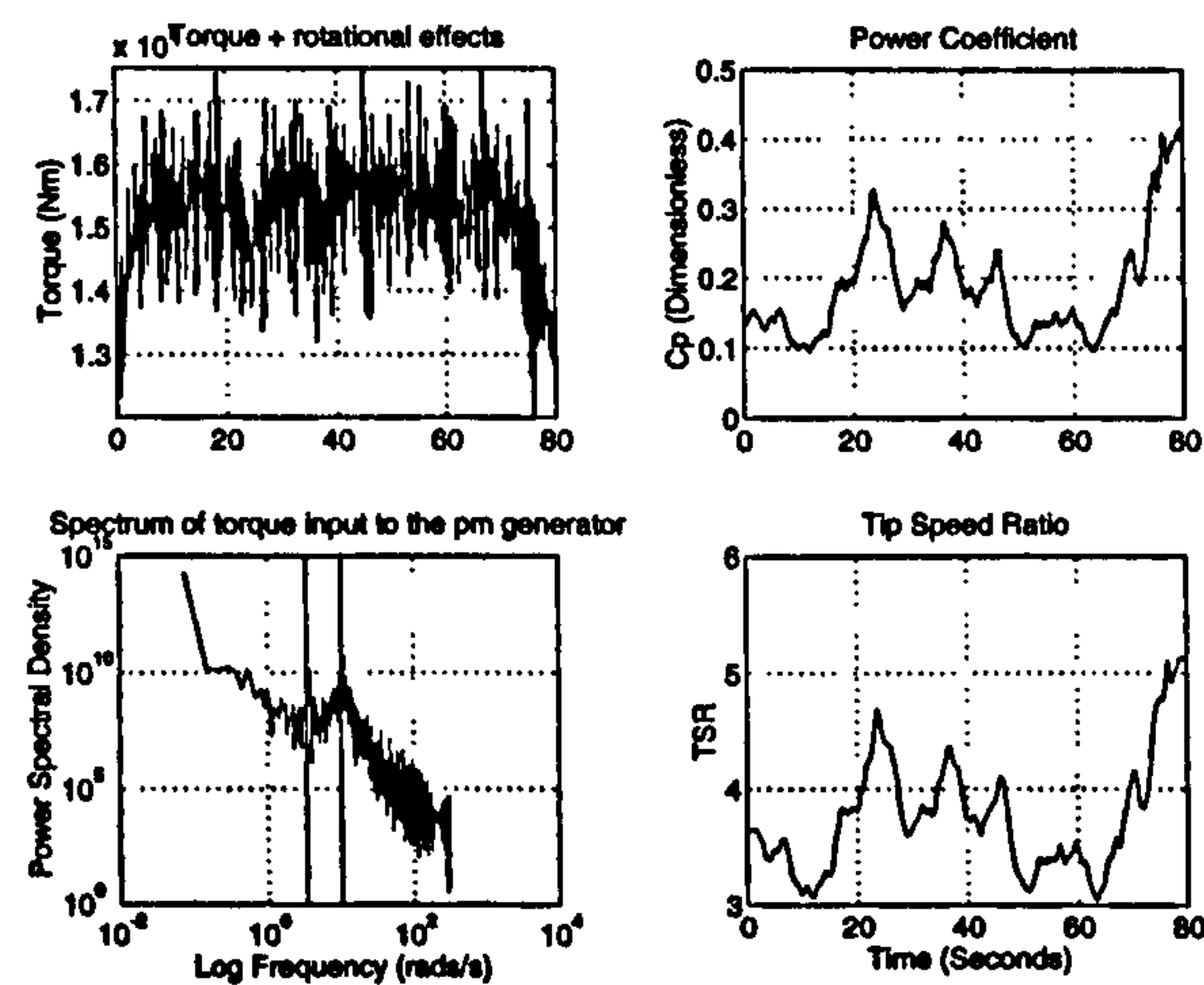


Figure 6.27: The resulting power coefficient and tip speed ratio

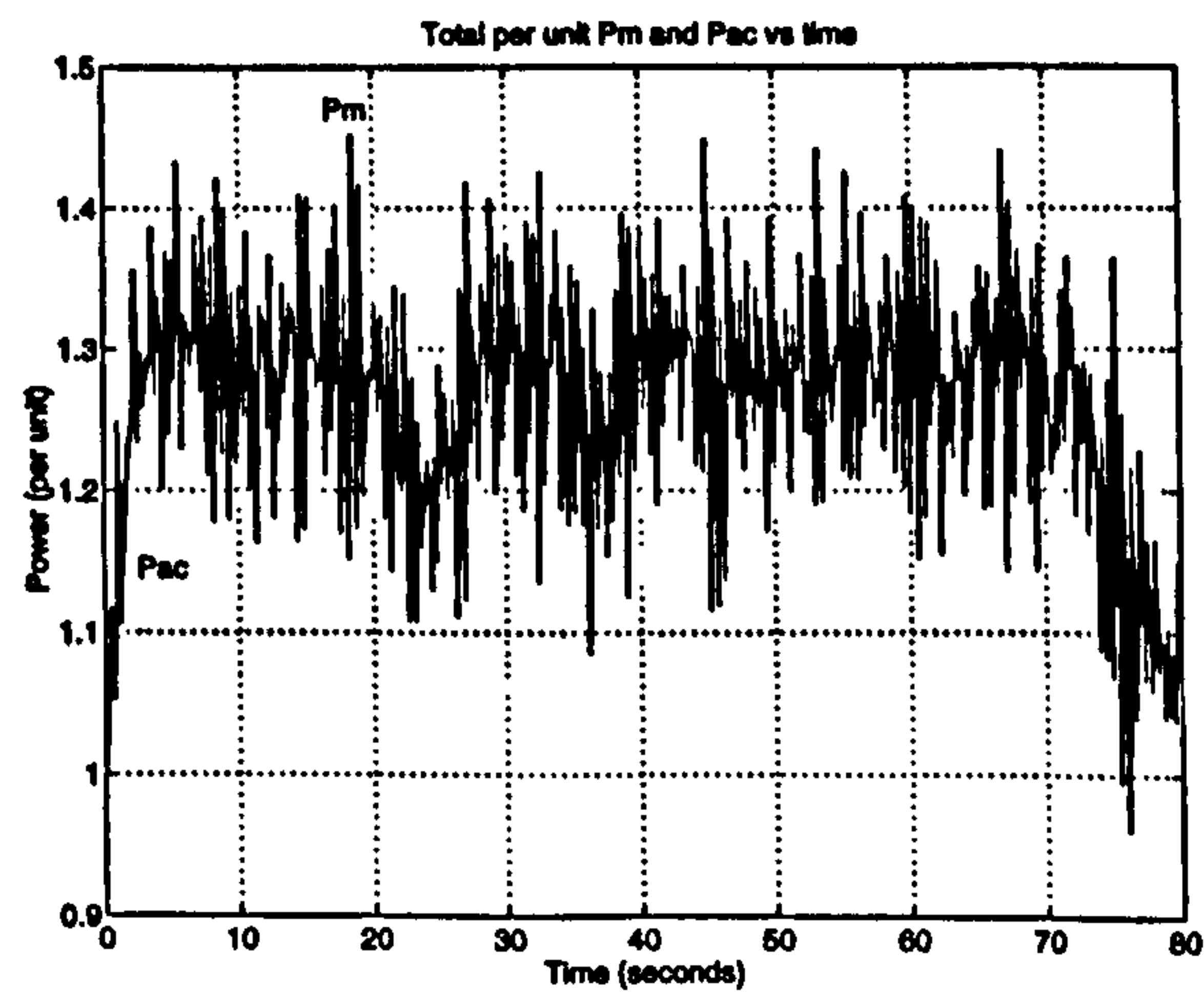


Figure 6.28: Module airgap and mechanical power

6.6 _____ Response of the 458 kW rated generator to simulated wind data

more pitch action than for the previous case because of the increased turbulence at the higher windspeed. The pitching duty is again reduced when compared with the equivalent fixed speed case because of the ability of the variable speed wind turbine to alter its speed.

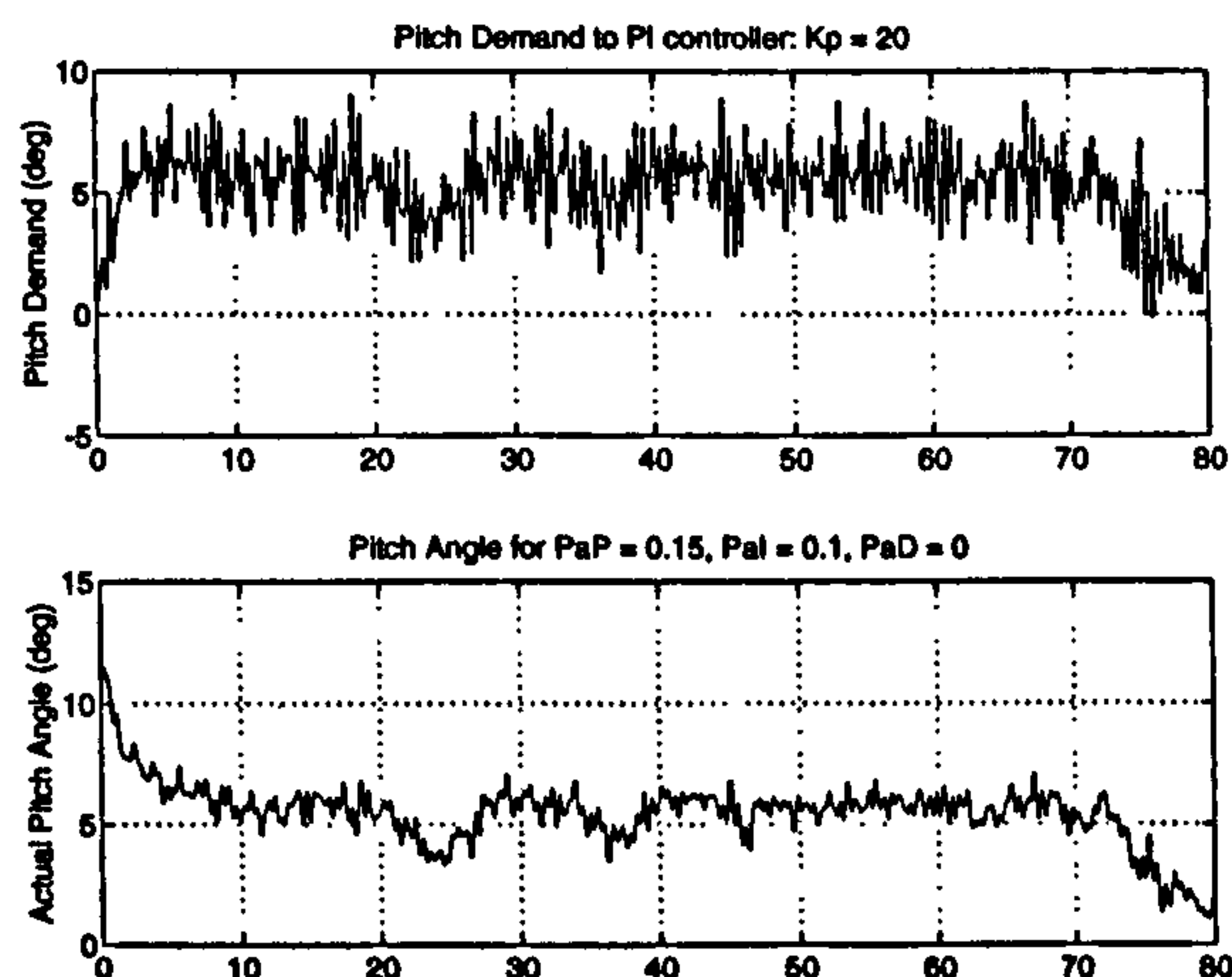


Figure 6.29: Pitch control and actuator response

The plots shown in Figure 6.30 are very important as they demonstrate the adequate control of the inverter control ratio, K_{Vdc} , to keep the fundamental value of the inverter output voltage constant at its desired setpoint to give a reactive power of 0.2 per unit.

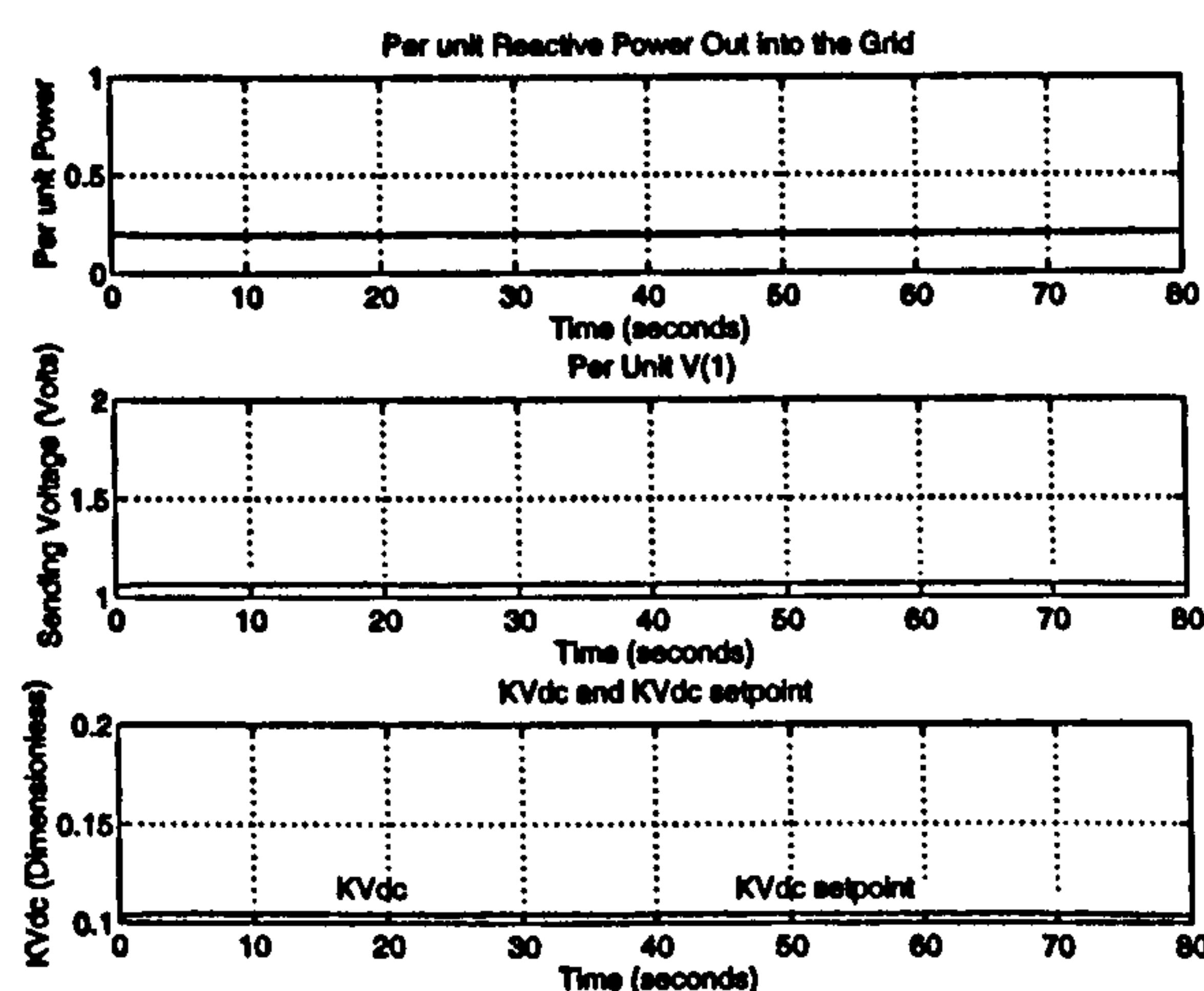


Figure 6.30: Reactive Power and voltage regulation

ENERGY CAPTURE ANALYSIS. An analysis of the energy flows within the variable speed wind turbine for the response to the wind speed time history with AMWS of 18 m/s can be seen in Table 6.4. Again the controller effectiveness is greater than unity indicating that the pitch controller is not limiting the power in to rated power and therefore suggesting that the generator be overrated to cope.

6.6 Response of the 458 kW rated generator to simulated wind data

Mechanical energy into turbine	12.86 kWh
Electrical energy out at the airgap	12.86 kWh
Max possible energy capture	10.18 kWh
Controller effectiveness	1.26
Overall energy out to the grid	11.86 kWh
Overall Efficiency	92.24 %

Table 6.4: Energy capture analysis for the 458 kW rated variable speed generator

6.6.4 Cut-out wind speed results

The simulated wind speed with mean 25 m/s and the corresponding response of the mechanical torque, without the addition of rotational effects, into the wind turbine can be seen in Figure 6.31. The run identifiers are also indicated to show the control parameter values.

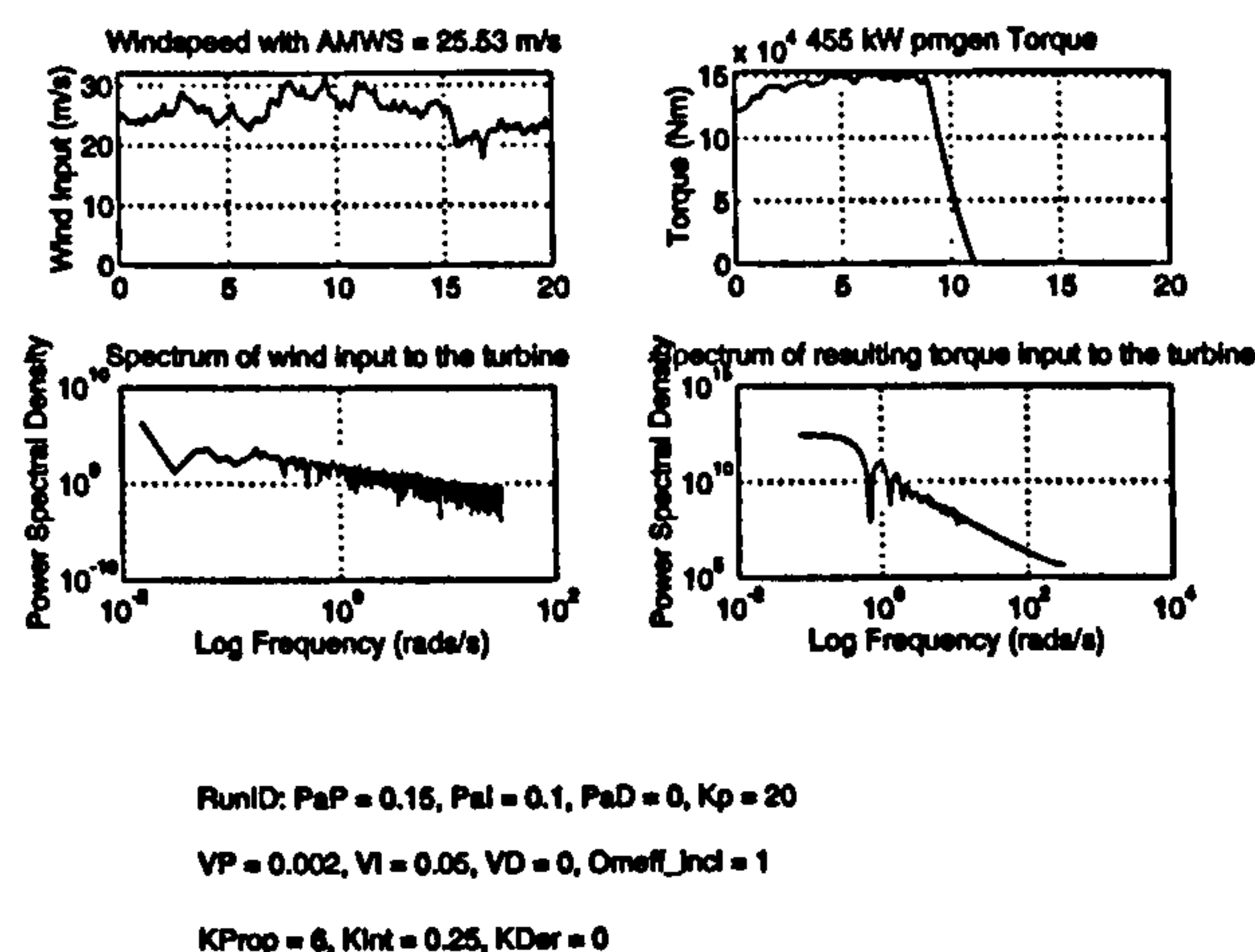


Figure 6.31: Simulated wind speed with AMWS of 25 m/s and the corresponding input torque

It is important to note the response of the pitch controller and the effect on the mechanical power into the turbine once the 'fail safe' flag indicator has been raised to indicate wind speeds above 25 m/s. This occurs at about 9 seconds into the simulation run and so only the first 15 seconds of the wind speed time history is used. The effect of reducing the power into the turbine to zero on the terminal voltage is also important in the shut down scenario as large voltage spikes into the network are undesirable.

The top trace of Figure 6.32 shows that rotational effects have been included for this simulation run. The power coefficient starts at 0.05, the value which gives rated power at the start pitch angle corresponding to a wind speed of 25 m/s, and subsequently varies much below the maximum value, C_{pmax} , due to the action of the pitch controller until the 'fail

6.6 _____ Response of the 458 kW rated generator to simulated wind data

safe' flag is raised. The pitch demand is then set to 90 degrees, full feather, and the power coefficient falls to zero as the blades attain this pitch angle. The tip speed ratio is also much less than 6, the value corresponding to C_{pmax} , because of the higher wind speed.

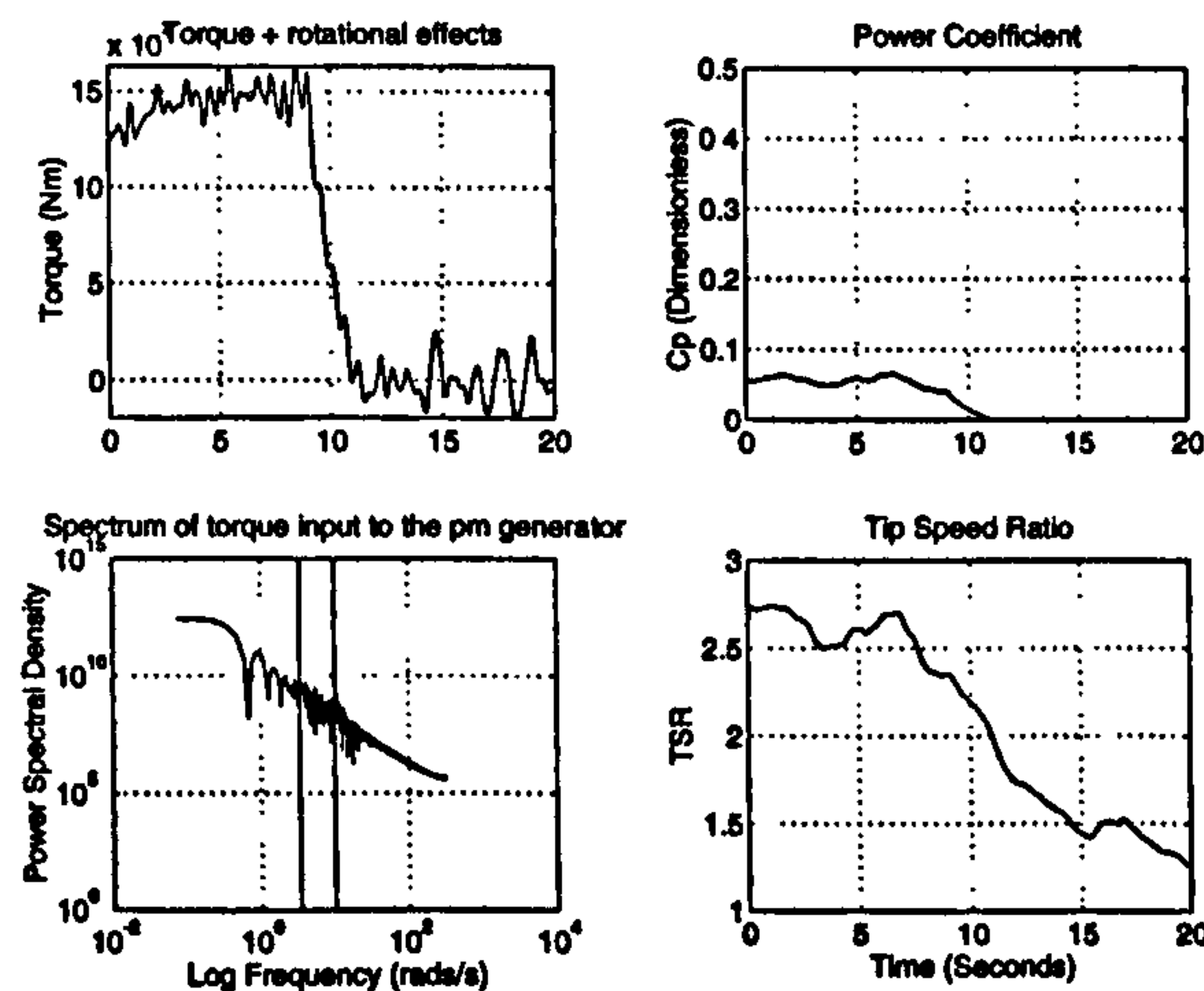


Figure 6.32: The resulting power coefficient and tip speed ratio

The mechanical power, P_m , from the wind turbine blades and the corresponding airgap power, P_{ac} , out into the E-core and rectifier arrangement can be seen in Figure 6.33. The response of the airgap power is limited to 1.25 of rated value as the wind speed is above rated and then reduces to zero as the blade pitch angle reaches 90 degrees. The mechanical power into the wind turbine shows the oscillatory variations induced by the rotational effects and the changing wind speed input into the wind turbine.

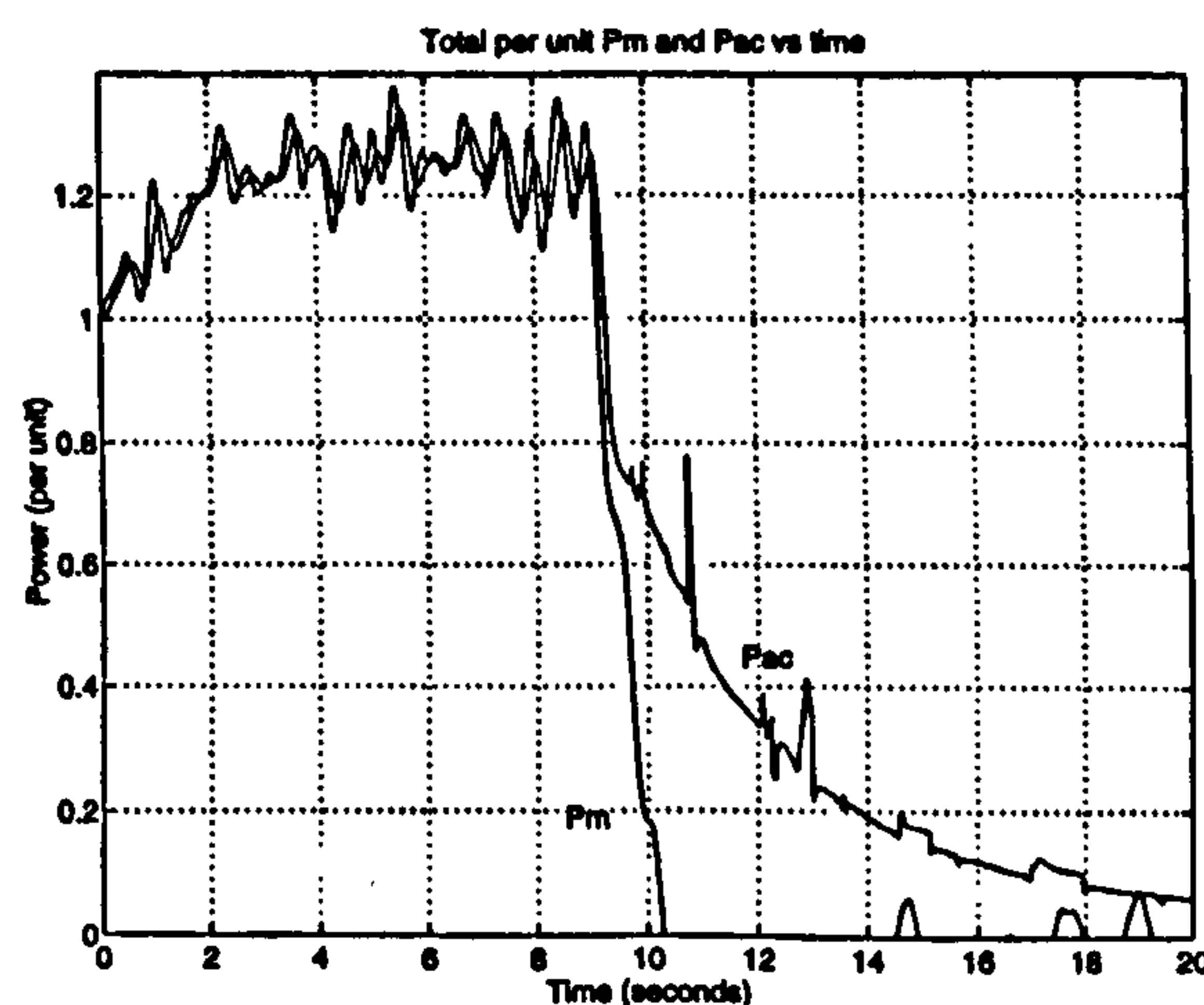


Figure 6.33: Module airgap and mechanical power

The pitch demand and pitch angle necessary to maintain the variable speed wind turbine at rated power in above rated wind speeds and then to shed all the power in the wind above

6.6 _____ Response of the 458 kW rated generator to simulated wind data

the cut-off windspeed can be seen in Figure 6.34. Once the wind speed measurement, which is a ten second averaged value, reaches 25 m/s the pitch demand is set to 90 degrees to limit the stress on the wind turbine structure as explained in Chapter 2. The pitching duty is again reduced when compared with the equivalent fixed speed case because of the ability of the variable speed wind turbine to alter its speed.

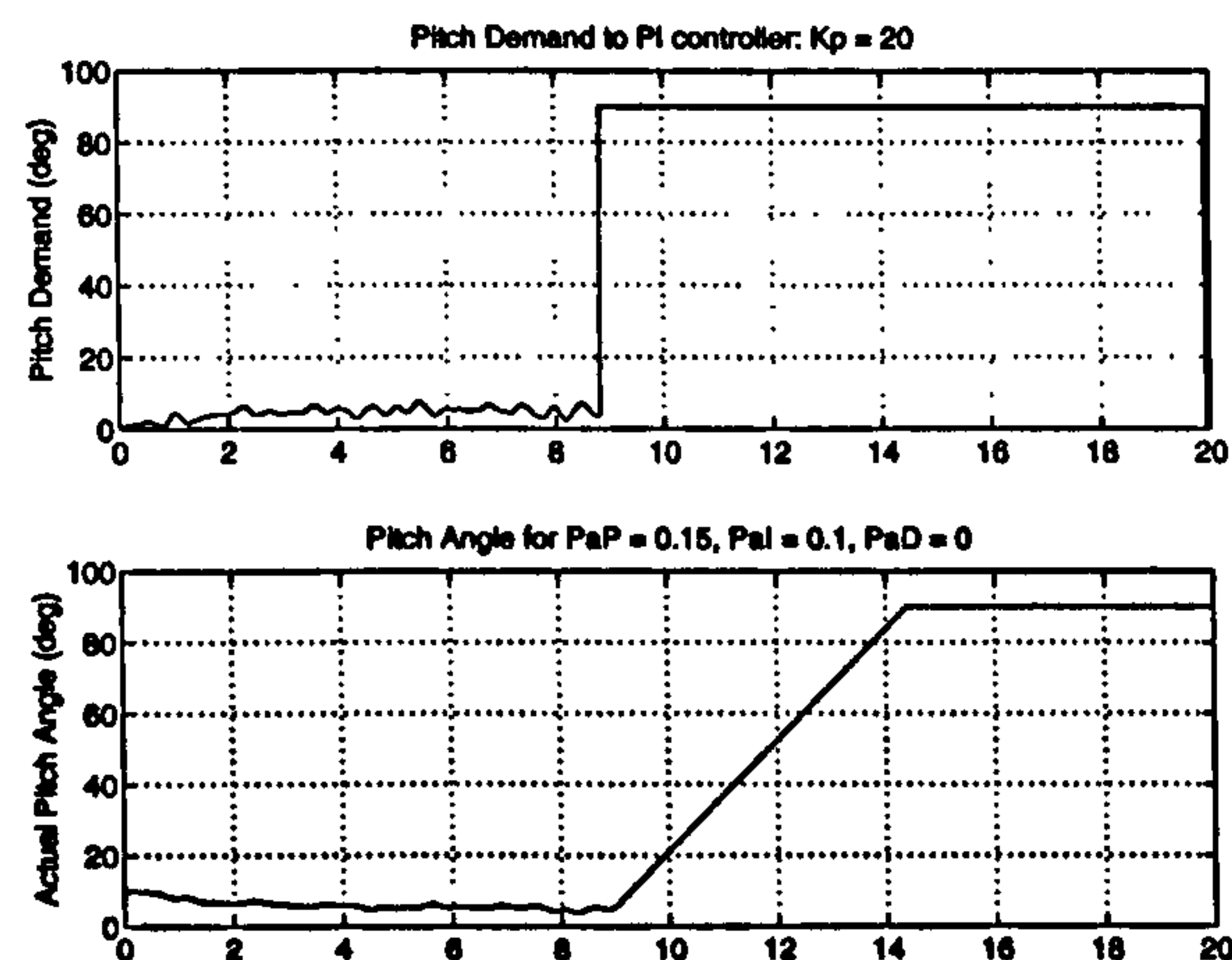


Figure 6.34: Pitch control and actuator response

The plots shown in Figure 6.35 demonstrate the adequate control of the inverter control ratio, $K_{V_{dc}}$, to keep the fundamental value of the inverter output voltage within the +6 and -10 % limits until the 'fail safe' signal occurs. Then the control of $K_{V_{dc}}$ to give a reactive power of 0.2 per unit is unable to cope with the large transient caused by setting the pitch angle to 90 degrees. The voltage begins to sag because the mechanical power into the system reduces far quicker than the power taken out of the inverter as the dc link voltage is still linked to the rotational speed of the rotor which can only change slowly. This imbalance of power reduces the speed of the rotor and hence the terminal voltage sags. The inverter control ratio increases to maintain the terminal voltage but the reduction in V_{dc} is too great for the setpoint to be maintained. The speed eventually levels out as the inverter switches off. A better control scheme would link the inverter controller to the fail safe such that the speed reduced to a safe level and then the inverter switched off.

If the wind speed persisted at a level greater than 25 m/s then some further control would act to bring the turbine to a complete rest and stop the inverter exporting power to the grid until a safe wind speed was recorded. Then the variable speed wind turbine could be restarted by disconnecting the parking brake and controlling the inverter to increase the

6.6 Response of the 458 kW rated generator to simulated wind data

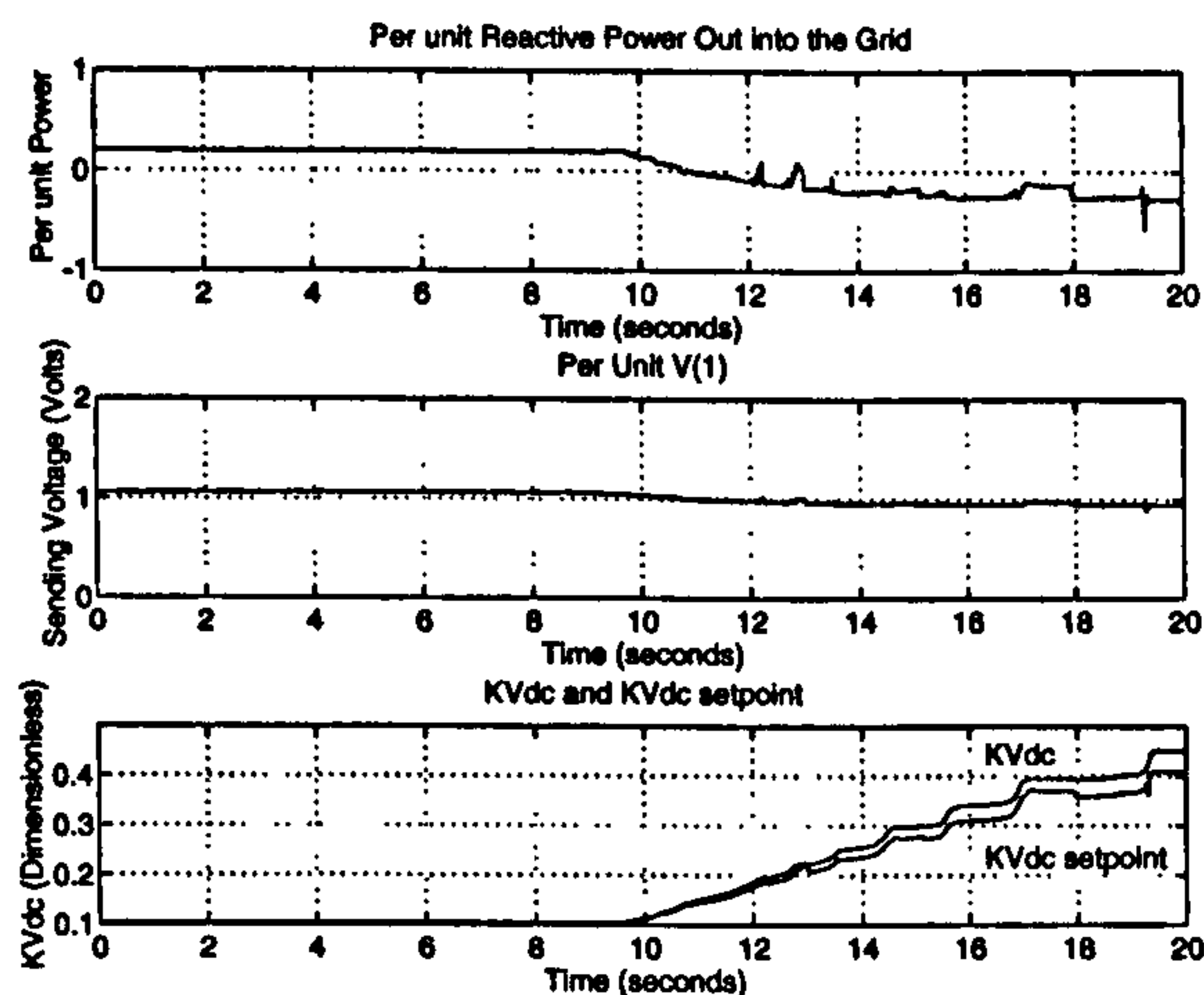


Figure 6.35: Reactive Power and voltage regulation

turbine speed to that required by the $\omega - V_{dc}$ characteristic and the wind speed.

6.6.5 Capacitance variation

The performance of the 458 kW rated variable speed generator will now be examined as the capacitance varies from $2000 \mu F$ to $8000 \mu F$. The 80 seconds of the simulated wind speed with mean 9 m/s is used for each simulation run and the corresponding response of the mechanical torque into the wind turbine can be seen in Figure 6.14.

2000 μF RESULTS. When the capacitance is reduced to $0.002 \mu F$ the control of the dc link voltage to track C_{pmax} becomes so difficult that large power spikes into the network are recorded and the simulation is unstable.

8000 μF RESULTS. The comparison between the performance with the $4000 \mu F$ and the $8000 \mu F$ capacitor is best undertaken by considering the energy captured and the standard deviation of the real and reactive power out to the grid as the plots are fairly similar. The values of these performance measures are shown in Table 6.5.

Capacitance	4000 μF	8000 μF
Energy capture	4.58 kWh	4.57 kWh
Energy to the grid	3.95 kWh	3.94 kWh
Standard deviation of real power	0.135 p.u.	0.134 p.u.
Standard deviation of reactive power	0.120 p.u.	0.124 p.u.

Table 6.5: Performance comparison between dc link with a capacitance of $4000 \mu F$ versus $8000 \mu F$

These values highlight the choice of design value for the dc link capacitance. Reducing the value of capacitance leads to poorer output power quality but an increase in the energy captured because the dc link voltage can change more quickly in response to the change in power angle of the inverter to track C_{pmax} and vice versa for higher values of capacitance.

6.7 Conclusions

This chapter has demonstrated the feasibility of controlling both the real and reactive power out into the grid from a permanent magnet synchronous generator operated at variable speed using a frequency converter. When no turbulence or rotational effects are included in the input to the wind turbine model the control scheme can follow C_{pmax} effectively. In the real windy situation the stochastic nature of the wind and the rotational effects introduced by the blades sampling the free wind stream contrive to move the wind turbine away from the maximum power coefficient operating point, C_{pmax} , and therefore energy is lost when compared with the maximum theoretical value.

The variable speed operation also leads to improved grid connection with the power delivered to the grid being far smoother than for the fixed speed case and this is expanded in the next chapter. The terminal voltage can be maintained at any setpoint required by the grid connection agreement, either at unity or at a value determined by the reactive power that the wind turbine is required to contribute. The dc link capacitance issue has been addressed with $4000 \mu F$ giving good overall controllability of the dc link voltage whereas $2000 \mu F$ is too low for power quality and $8000 \mu F$ too high for C_{pmax} tracking.

The results presented in this chapter rely on a quasi-static method for simulating a permanent magnet generator coupled to the grid via a rectifier and voltage controlled inverter arrangement. Interpolation techniques were used at each iteration step to track through look-up tables representing the airgap power transfer and injected dc link current and power transfer used to represent the inverter. The main reason for such an approach was the predicted simulation time savings and the main difficulty encountered was interpolating accurately and quickly. The time savings presented in section 5.3.2 did not materialise as 80 seconds of simulation took about 5 hours to run. This was still four times quicker than a full non-linear simulation would take. The difficulties with interpolation arose because of the non-linear nature and steep gradients present in the look-up tables. The airgap power

transfer table is plotted out versus rotor speed for constant values of the dc link voltage in Figure 6.36.

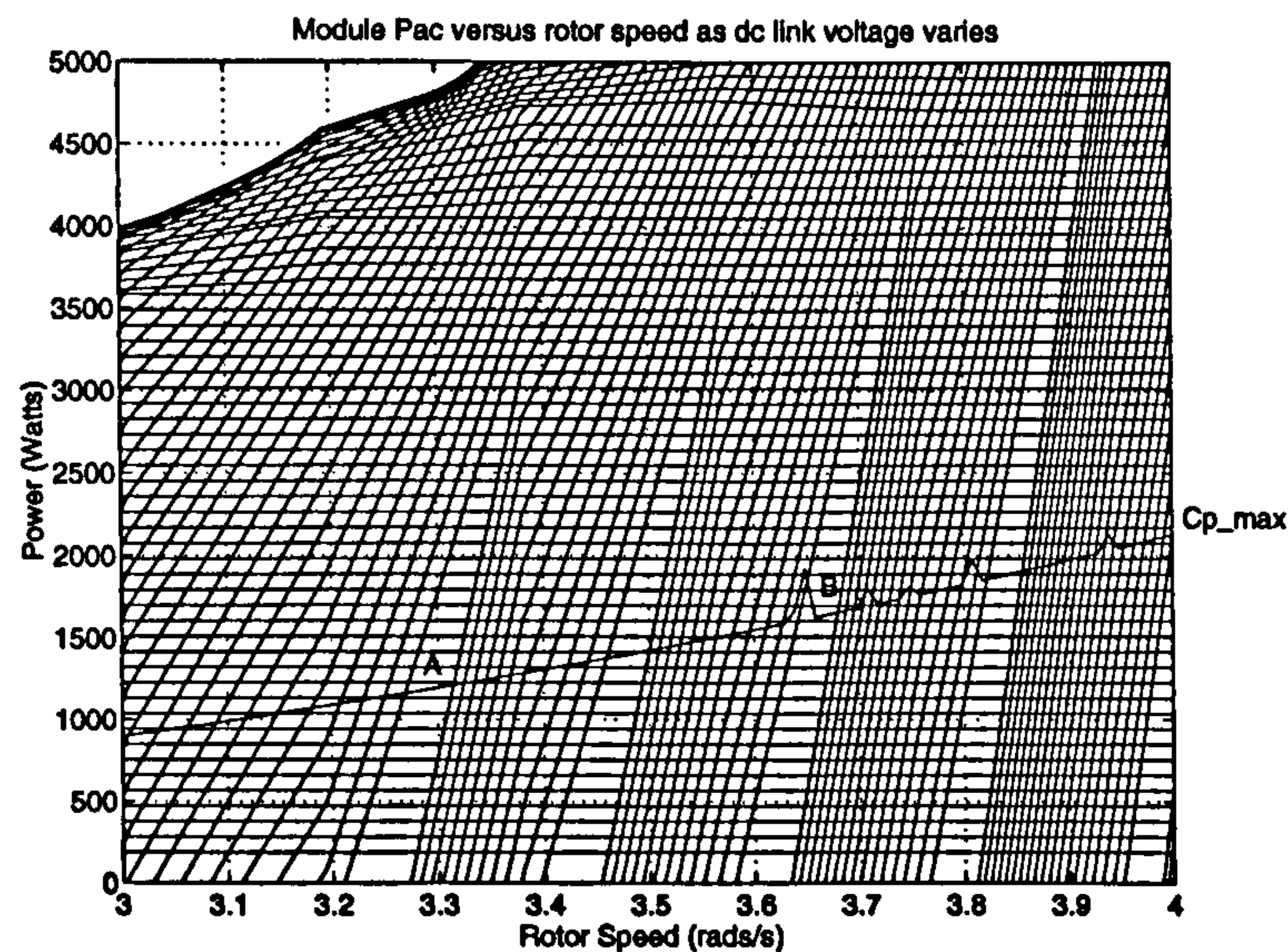


Figure 6.36: Airgap Transfer Table

Taking the case of the mechanical input and airgap power output for the windspeed of 9 m/s shown in Figure 6.17. At a time of about 10 seconds a large spike can be seen on the second plot which occurred at a rotational speed, shown on the third plot, of between 3.2 and 3.3 rads/s. This corresponds to point A on Figure 6.36. Further work is required to control this simulation error by ensuring the data in the look-up tables is more evenly spaced and highlights the fact that a simulation is only as good as the data entered into it. This concludes the variable speed modelling and a comparison between the fixed and variable speed operation of the permanent magnet, synchronous generator with each other and the industry standard gearbox and induction generator is presented in the next chapter.

Chapter 7

Comparison between fixed and variable speed operation of the permanent magnet generator

This chapter describes a comparison between the performance and system cost of the fixed and variable speed operation of the permanent magnet, synchronous generator to identify the key criteria for improving each design and to discuss which is the best mode of operation for such a generator.

The perceived advantages of operating the wind turbine at fixed or variable speed in terms of energy capture, smoother power, load alleviation and generator design freedom were introduced in Chapter 5 and used to develop designs for a range of variable speed generators. The performance of the 458 kW rated, variable speed, permanent magnet generator was examined in Chapter 6 and it is now necessary to compare and contrast the designs and their performance with the fixed speed generator designs developed in Chapters 3 and 4.

Each of the perceived advantages is compared using the modelled designs and their performance to assess to what extent the arguments hold. The fixed and variable speed designs are compared in terms of weight, cost and reliability to ascertain which is the most likely mode of operation to be pursued further. The designs are then compared with the industry standard gearbox driven induction generator design to assess the benefits of the direct drive generator. Finally the key design drivers for both systems are identified and areas which

Variable speed	4.56 kWh
Fixed speed	4.108 kWh
Energy capture increase	.453 kWh

Table 7.1: A comparison of energy capture

should be targeted for re-design to improve the performance are explored. The conclusion to the chapter presents whether the direct drive generator is the way forward in terms of wind turbine re-design and if so which mode of operation should be used.

7.1 A comparison of energy capture

In the last chapter energy capture information with the C_{pmax} and reactive power setpoint controller was presented for the variable speed operated multi-pole, permanent magnet synchronous generator for a wind time series history with an AMWS of 9 m/s. This wind time series history will now be used to compare the energy capture performance of the fixed and variable speed operated generator and is shown in Figure 7.1 with the resulting airgap power histories in Figure 7.2. The resulting energy capture at the airgap during the fifty seconds of wind data is presented in Table 7.1.

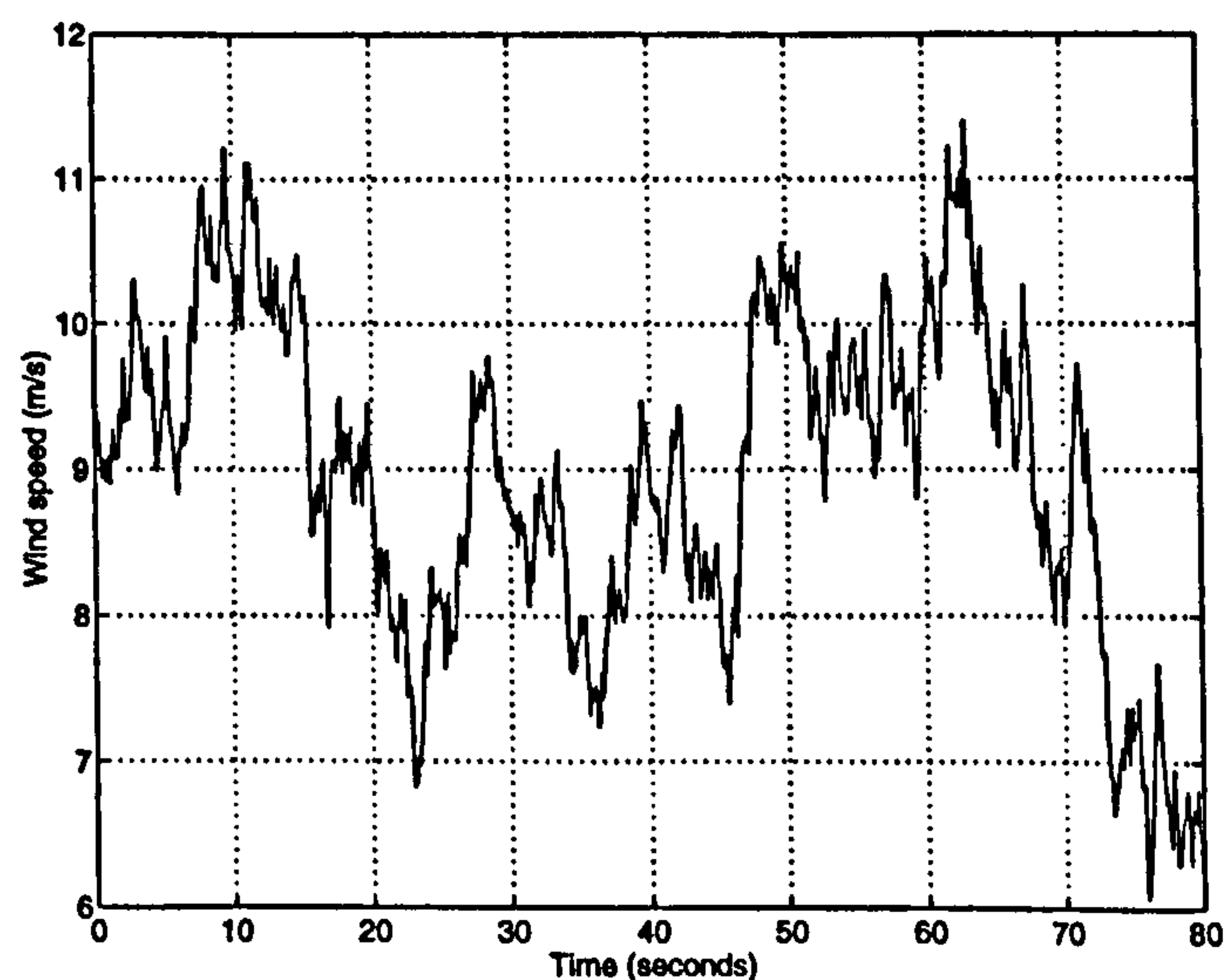


Figure 7.1: Windspeed time history input to the models

There is a clear increase of 11.2 % in the energy captured by the wind turbine at the airgap of the variable speed generator when compared with the fixed speed case. However it is

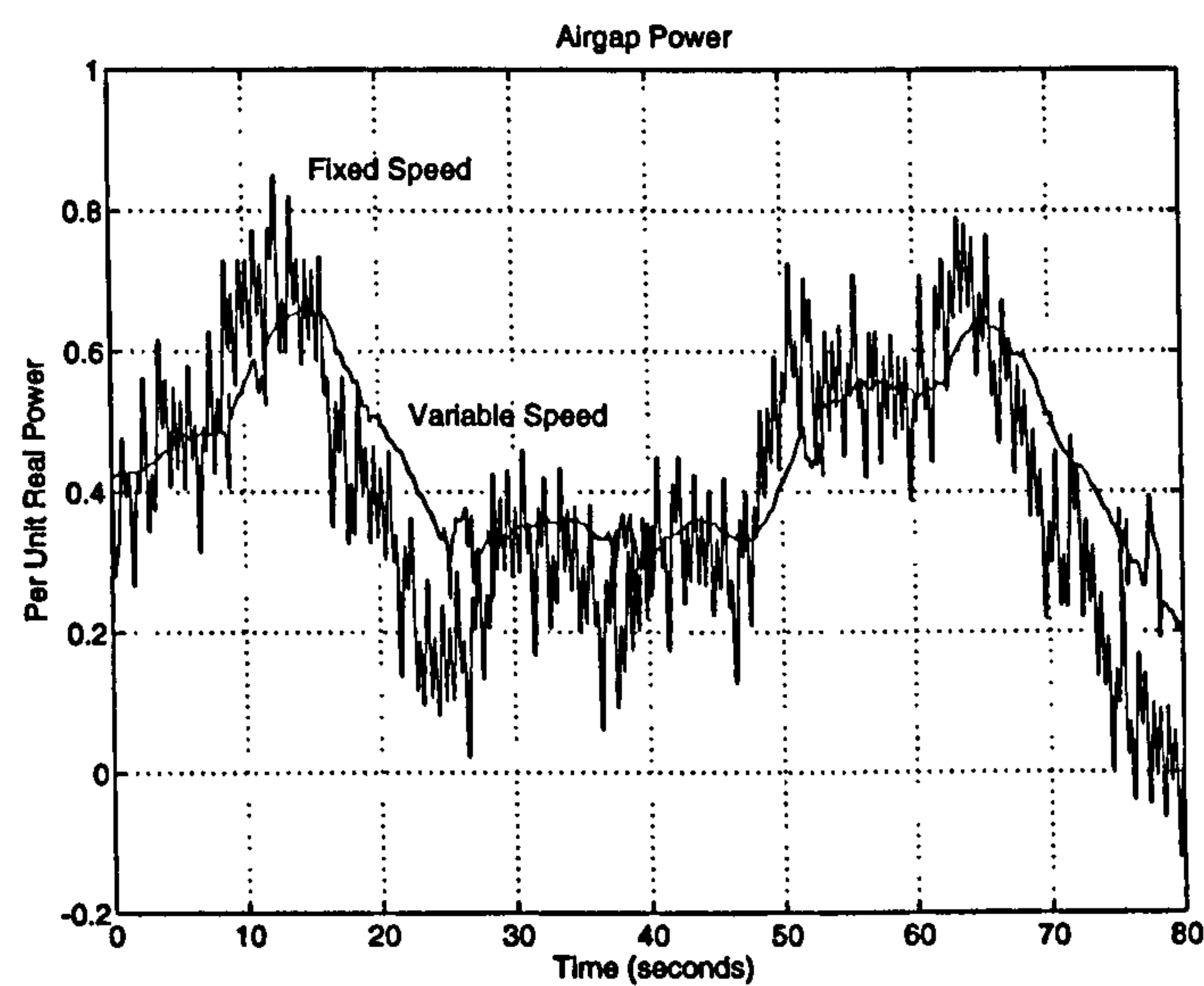


Figure 7.2: The airgap power for the fixed and variable speed case

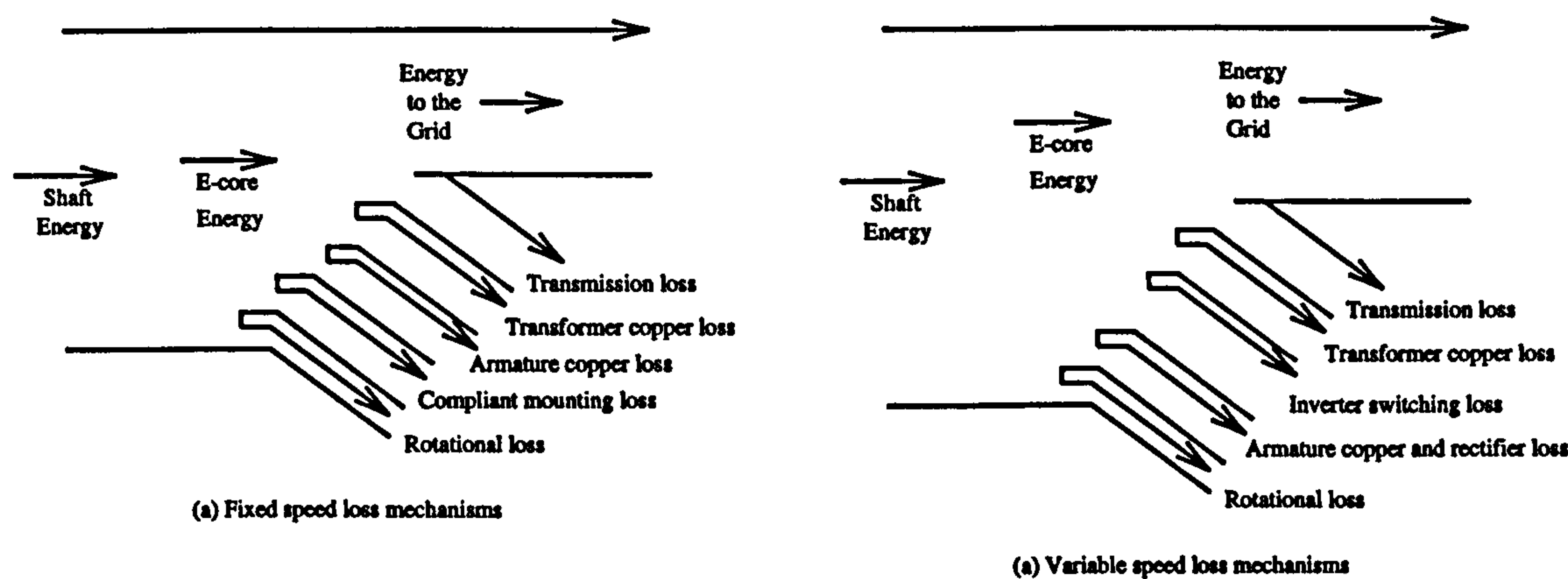


Figure 7.3: The loss mechanisms for the fixed and variable speed case

the power out of the generator terminals, i.e. at the point of the grid connection metering, which is important in terms of evaluating the increased revenue stream generated by the variable speed operation. This power out is determined by the losses present from the airgap power to the grid connection. These loss mechanisms can be seen in Figure 7.3.

Taking these loss mechanisms into account gives rise to the responses seen in Figure 7.4 for the resulting output power to the grid. The resulting energy input to the grid and the revenue returned, assuming a flat rate of 4 p/kWh, can be seen in Table 7.2. The values for the energy capture can be converted to a value for the revenue earned over the simulation run by converting from kJ to kWh and multiplying by the flat rate.

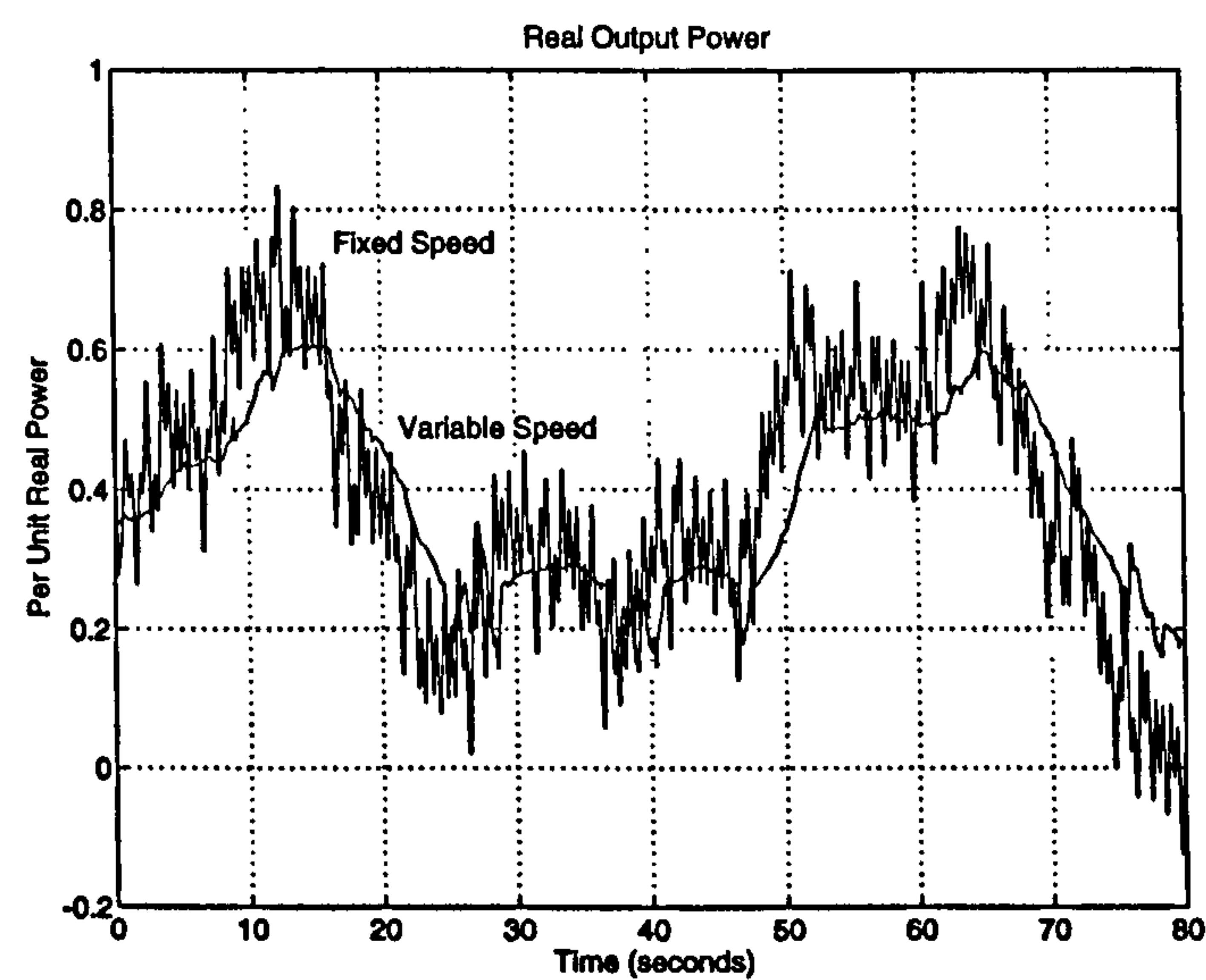


Figure 7.4: The delivered power for the fixed and variable speed case

Variable speed	3.95 kWh
Fixed speed	3.947 kWh
Energy capture increase	0.003 kWh
Variable speed revenue	15.81 p
Fixed speed revenue	15.80 p
Increase in revenue	0.01 p

Table 7.2: A comparison of delivered energy and revenue

7.1.1 Application to yearly energy delivered to the grid

The problem, now, is how can the effectiveness of the variable speed wind turbine over the fixed speed turbine at capturing the energy in this 80 seconds of wind time series information be applied to the comparison presented in section 5.1.2 and a figure established for the yearly energy delivered to the grid. The Raleigh distribution assumes that the variable speed wind turbine is always operating at C_{pmax} for wind speeds below rated and furthermore does not take into account switching losses in the inverter or losses in the generator itself.

Two programs have been written to analyse the energy flows from the wind turbine blades to the energy transmitted to the grid which includes all the relevant losses for the fixed and variable speed simulation models. The results for the energy captured and the energy transmitted to the grid, after all the losses have been taken into account, can be used to get overall efficiencies for the wind turbine, operating at fixed or variable speed, based on runs at different wind speeds. These can be used to ascertain the effective loss from that predicted by the Raleigh distribution. The energy flow analysis gives rise to a series of effective efficiencies versus wind speed and these once multiplied by the result for the energy at a given wind speed from the Raleigh distribution give an approximate method for obtaining the operational energy delivered by the 455 kW fixed and variable speed wind turbines to the grid. These yearly figures for energy delivered to the grid and resulting revenues are presented in Table 7.3. The revenues are again evaluated for the energy delivered to the grid over the year at a flat rate of 4 p/kWh.

Variable Speed	1403.1 MWhr/yr
Fixed Speed	1383.9 MWhr/yr
Energy delivered increase	20 MWhr/yr
Variable speed revenue	£56156 /yr
Fixed speed revenue	£55356 /yr
Increase in revenue	£800 /yr

Table 7.3: Comparison of yearly energy delivered to the grid and resulting revenues

7.1.2 Discussion

The 1.4% increase in energy delivered to the grid and resulting revenue of the variable speed over the fixed speed case would lead to an increased revenue per year of £800 with the assumptions made above. However this increase in yearly revenue would be partially

7.2 _____ The grid connection performance comparison

offset by the cost of the rectifier and inverter equipment. A discounted cash flow analysis [109] [110] is carried out in section 7.4.4 between both the fixed and variable speed wind turbines and also for a induction generator and gearbox arrangement to see which is the most cost effective. Furthermore the increased component count for the rectifier and inverter system might lead to more down time for maintenance. However the smoother power flow and the reduced number of tiers for the variable speed case would lead to a lighter generator and lower tower costs.

7.2 The grid connection performance comparison

As was mentioned in the previous section, the increase in energy capture of the variable speed over the fixed speed case will lead to a slight increase in revenue stream over the lifetime of the plant but more important now is the improvement in the quality of the real and reactive power into the grid. The reactive power flow for the fixed speed case is uncontrollable when compared with the variable speed case and the real power transfer is much more variable. However the voltage regulation is not an issue for a well designed fixed speed turbine which generates one per unit emf at rated speed and is more of a control problem for the variable speed case. Each of the these points will now be discussed.

7.2.1 Reactive power flow for simulated wind speed of AMWS 9 m/s

A comparison of the reactive power flow for the fixed and variable speed case can be seen in Figure 7.5. It is clear that the reactive power for the fixed speed case is uncontrollable yet the low reactance between the inverter and the grid means that the variable speed case is far worse in terms of the fluctuations. The standard deviation of the reactive power for the fixed speed case is only 0.029 per unit whilst that for the variable speed case is 0.12 per unit. This clearly needs to be improved through better control of the dc link voltage.

However the bonus for the variable speed case in that for a setpoint of 0.2 per unit the mean of the reactive power for the variable speed case is 0.22 whereas there can be no setpoint for the fixed speed case and it has a mean of -0.15. The effect of this on the cost of connecting such a wind turbine to the grid would be to increase the revenue from the National Grid Company for the reactive power supplied for the variable speed case and a penalty for the

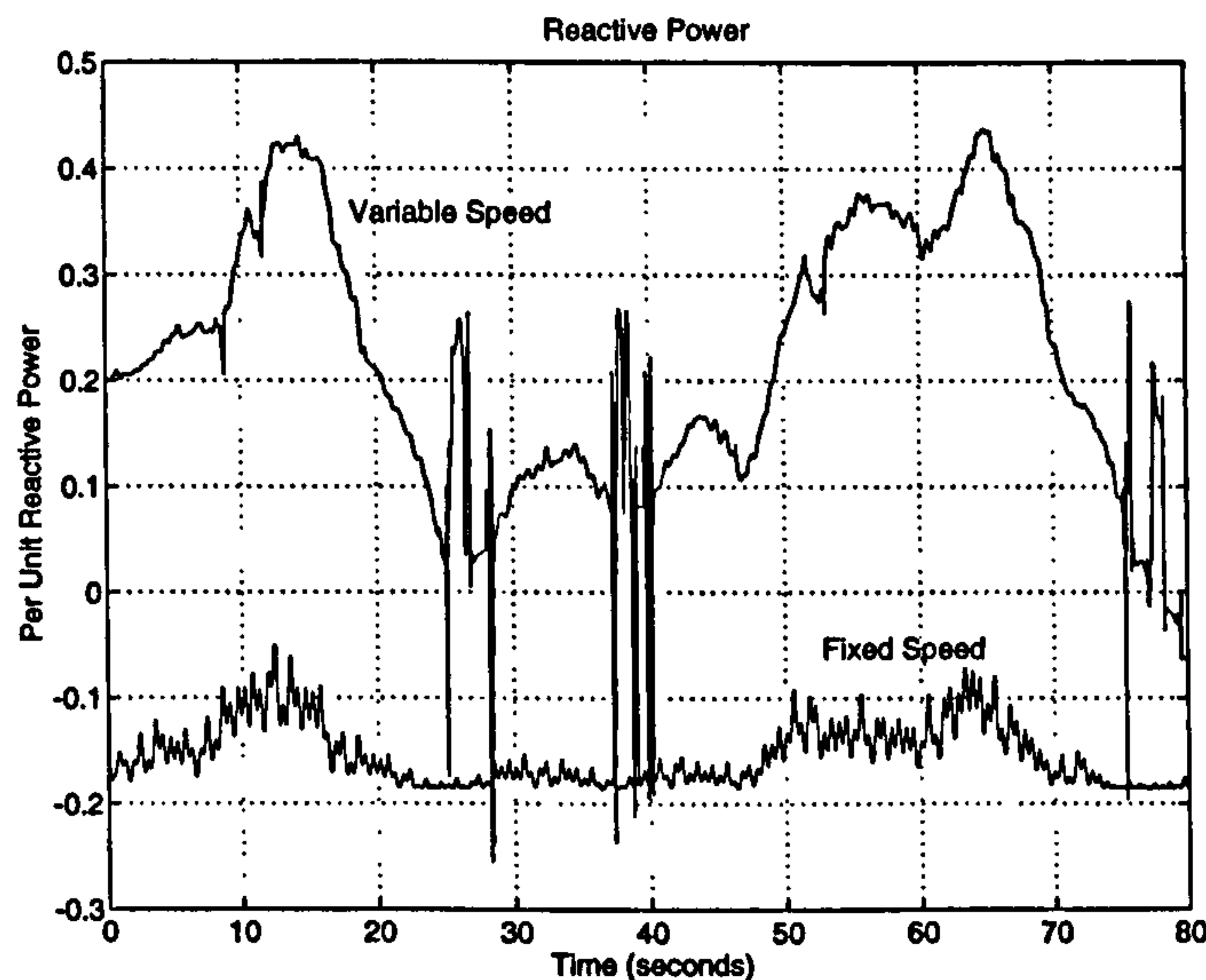


Figure 7.5: Reactive power comparison between fixed and variable speed case for wind speed with AMWS of 9 m/s

reactive power consumed by the fixed speed case [105].

7.2.2 Real power quality for simulated wind speed of AMWS 9 m/s

A comparison of the real power flow out into the grid for the fixed and variable speed case can be seen in Figure 7.4. It is clear that the real power flowing into the grid is much less smooth for the fixed speed case and therefore the variable speed case is far better. In fact the standard deviation of the real power transmitted to the grid for the fixed speed case is 0.18 which is far worse than for the variable speed case which is only 0.13 per unit, an improvement of about 26.4 %. This figure underestimates the possible improvements because of the extra variation introduced by interpolation problems and the improvement is more likely to be around 40 % in the real system. The effect of this on the cost of connecting such a wind turbine to the grid needs to be quantified, but it would certainly result in much less fatiguing of the components of the wind turbine and could be used to justify extending the turbine's working life which is typically about 20 to 25 years at present.

7.2 The grid connection performance comparison

7.2.3 Voltage regulation for simulated wind speed of AMWS 9 m/s

A comparison of the per unit voltage regulation for the fixed and variable speed case can be seen in Figure 7.6. It is clear that the voltage regulation is better for the fixed speed case in this instance and the variable speed case is little worse. This is undoubtedly due to the poor performance of the PI controllers used which cannot track ramp like functions particularly well and the steepness of the power transfer against dc link voltage characteristic. As the rotor speed to dc link voltage setpoint for C_{pmax} ramps up with increase in rotor speed and the setpoint lies on the steep portion of the curve for efficient operation of the generator and rectifier any slight error leads to a degradation in voltage control. Furthermore there is an increase in error due to the poor level of decoupling between the maximum power controller and the V_{dc} setpoint controller. However both controllers would be within the limits imposed by a REC. Further work is required in this area to reduce the coupling and this is discussed in the next chapter. The overall standard deviation for the terminal voltage of the variable speed case is 0.026 per unit, thirty times larger than that of the fixed speed case. However the terminal voltage of the fixed speed case would deteriorate in a weak grid as the frequency, and hence terminal voltage, of the generator could alter. The voltage regulation of the variable speed case should remain at a similar level in this situation.

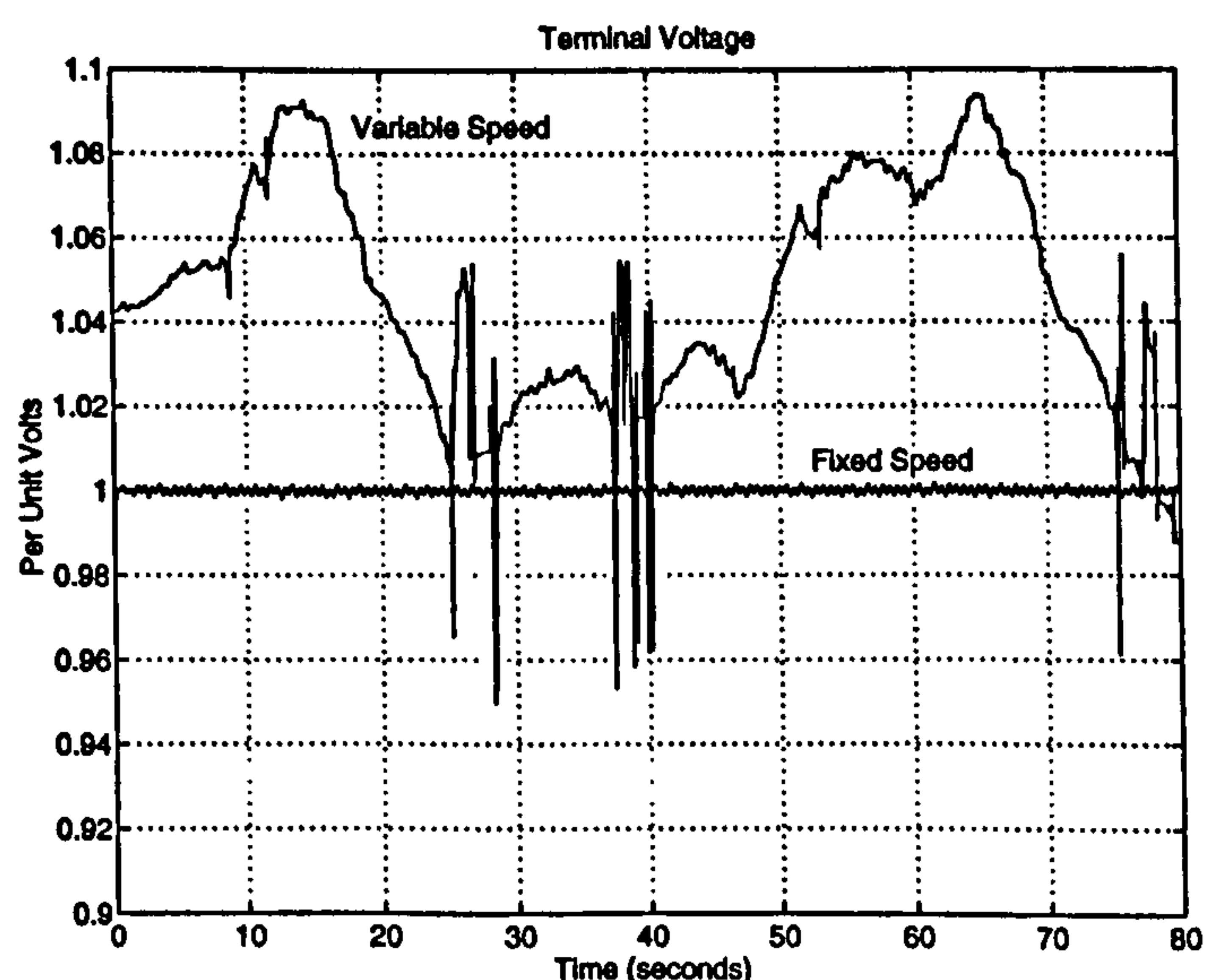


Figure 7.6: Voltage regulation comparison between fixed and variable speed case for wind speed with AMWS of 9 m/s

The effect of this on the cost of connecting a variable speed wind turbine to the grid would

be dramatic because if the generator voltage could not be controlled sufficiently it would be disconnected leading to zero revenue stream. The voltage control is improved with increase in the dc link capacitor but again this would increase the cost of the whole system.

7.3 Comparison of design values and cost

The preceding sections showed the definite advantage of operating the wind turbine at variable speed in terms of the quality and quantity of the real power. However the fixed speed case comes out well in terms of voltage regulation and, although the fixed speed generator absorbs reactive power, it has a much reduced fluctuation when compared with the variable speed case. It is now necessary to compare the designs themselves and see if they are actually cost effective.

7.3.1 Comparison of generator weight

A comparison of the overall weights of the fixed and variable speed designs can be seen in Figure 7.7. It is clear that the variable speed generator itself will be lighter than its equivalent rated fixed speed generator.

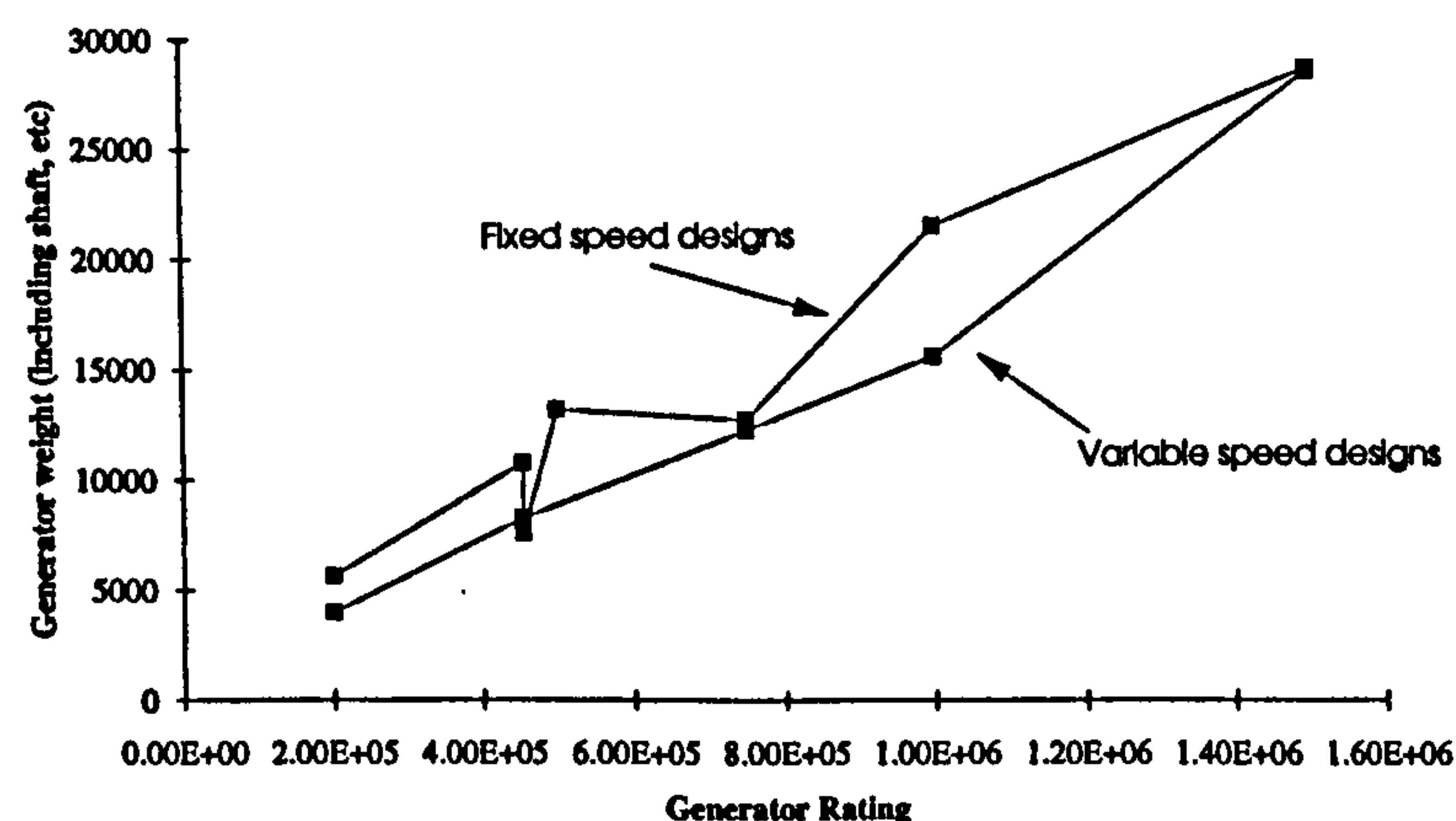


Figure 7.7: Weight comparison between the fixed and variable speed case

7.3.2 Comparison of resulting capital cost

A comparison of the corresponding material costs, neglecting construction costs which are considered to be the same proportion extra for each case, for the fixed and variable speed designs can be seen in Figure 7.8. It is clear that the variable speed generator itself will be cheaper than its equivalent rated fixed speed generator.

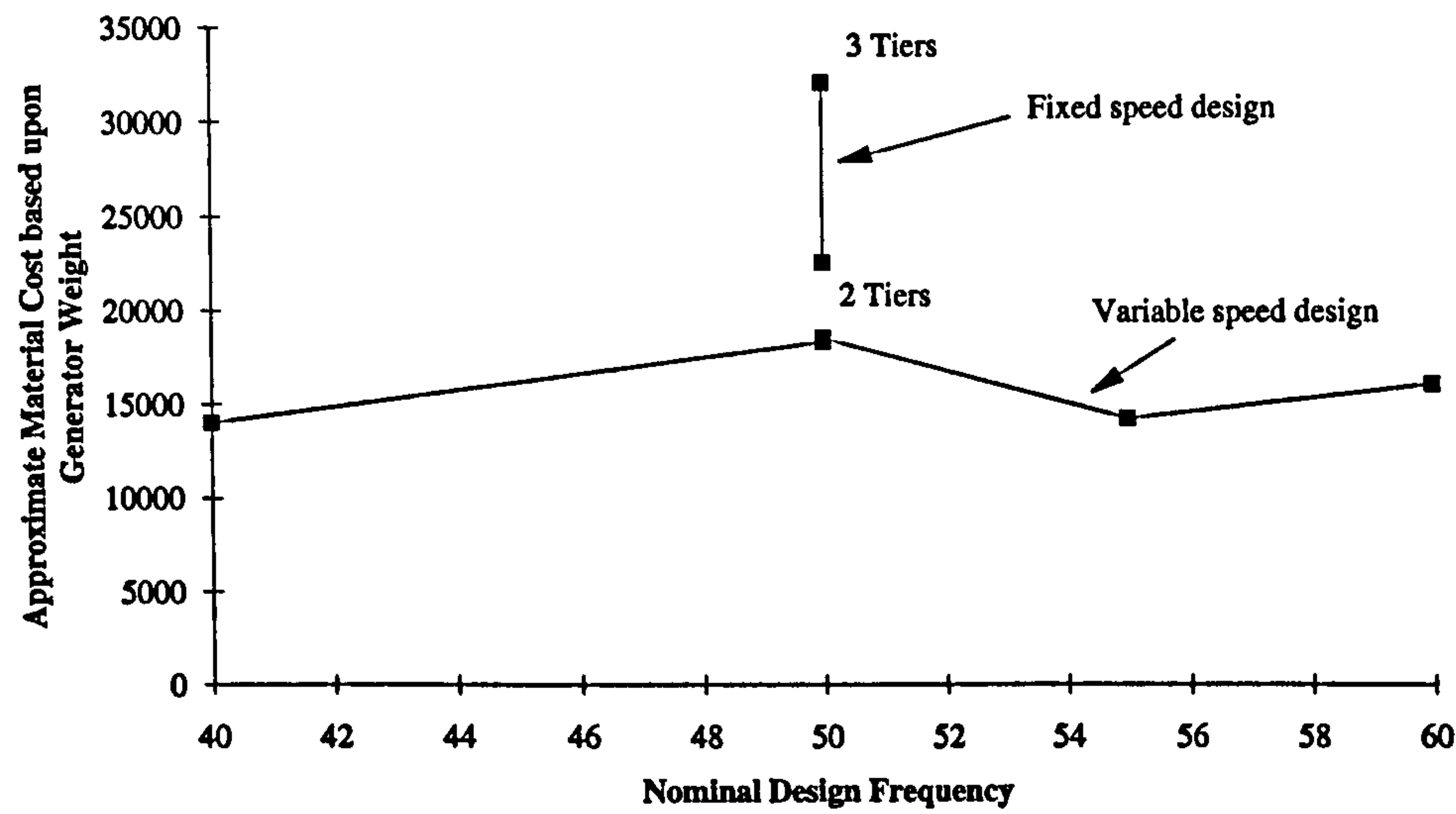


Figure 7.8: Cost comparison between the fixed and variable speed case

However the capital cost of the variable speed generator would be considerably increased by the cost of the inverter. Such a cost cannot be estimated because of the lack of detailed information and therefore what can be said is that the rectifier, tuning capacitors, dc link capacitor and inverter must be less than 40 % of the capital cost of the variable speed generator on average for the capital costs to be equivalent to the fixed speed case across the range. Costing does, however, not merely depend on the initial capital cost but also on the expected revenue stream over the lifetime of the plant and this can be calculated by using a discounted cash flow rate of return analysis. This is carried out in section 7.4.4. This would be the tool that investors would use to evaluate the relative merits of a project, but it is heavily dependent on the assumed interest rate and lifetime of the plant. If the advantage accrued from the increased revenue stream for the variable speed case and cost due to the inverter and rectifier did not lead to a pay back until after the lifetime of the plant then this arrangement would be unsuitable.

7.4 — Comparison against the gearbox and induction generator configuration

7.4 Comparison against the gearbox and induction generator configuration

Again there are two key areas where comparison must be made between the industry standard fixed speed gearbox and induction generator arrangement and the fixed speed and variable speed direct drive generator: firstly, performance in the windy environment in terms of the quality of the power out and, secondly, comparison on weight, cost and reliability. However to do this requires a simulation model for such a standard induction generator and gearbox. The development of such a model will now be described and then the key comparisons, mentioned above, will be carried out to determine which is the best step forward to take in terms of this avenue of wind turbine design.

7.4.1 Induction generator plus gearbox model

A simple representation of an induction generator plus gearbox drive train can be seen in Figure 7.9. This simplified representation is adequate for the dynamic modelling of the wind turbine in the time scales required for a comparison of control action and resulting energy capture [65].

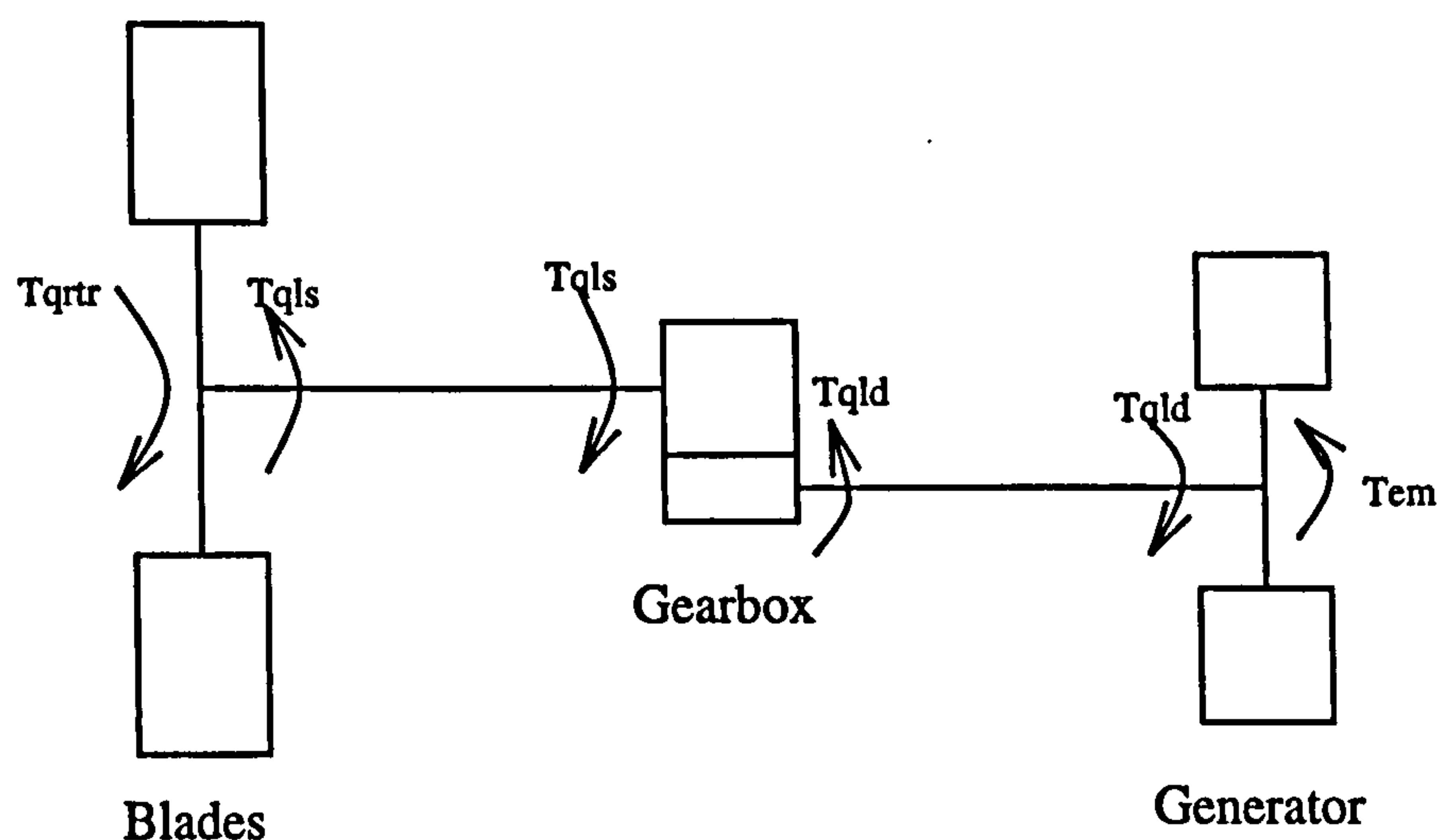


Figure 7.9: Induction generator and gearbox model representation

GOVERNING EQUATIONS. The system shown in Figure 7.9 can be represented by a fourth order model comprising four first order differential equations which govern the behaviour of the low speed shaft torque and rotational speed and the electrical reaction

7.4 — Comparison against the gearbox and induction generator configuration

torque and rotational speed. These equations are now listed.

The low speed shaft speed is governed by the equation,

$$\dot{\omega}_{ls} = \frac{1}{J_{ls}} (T_{q_{rtr}} - T_{q_{ls}} - c_{ls}\omega_{ls}) \quad (7.1)$$

The low speed torque is determined by,

$$T_{q_{ls}} = \frac{k_{ls} (\omega_{ls} - \frac{\omega_{ld}}{N})}{1 + \frac{k_{ls}}{k_{hs}N^2}} \quad (7.2)$$

The high speed torque is found from,

$$T_{q_{ld}} = \frac{1}{\tau_{ld}} (T_{q_{spcvslip}} - T_{q_{ld}}) \quad (7.3)$$

Finally the high speed shaft rotational speed is given by,

$$\dot{\omega}_{ld} = \frac{1}{J_{hs}} \left(\frac{T_{q_{ls}}}{N} - T_{q_{ld}} - c_{hs}\omega_{ld} \right) \quad (7.4)$$

Inherent in the above set of equations is the linking between the inertias and speeds of the low and high speed by the correct use of the gearbox gear ratio, N . Furthermore the induction generator is assumed to operate at fairly low values of slip and therefore the torque-speed curve of the induction generator can be approximated by a straight line with the generator reaction torque given by,

$$T_{em} = T_{q_{spcv}} \times \text{slip} \quad (7.5)$$

The derivation of the above equations and the method for setting up the initial conditions of the wind turbine driven induction generator and gearbox are included in Appendix E.

SIMULINK IMPLEMENTATION. This fourth order representation has been coded into a SIMULINK model. A schematic of the SIMULINK system can be seen in Figure 7.10 showing how each equation relates to the others.

INCORPORATION INTO THE WIND TURBINE MODEL. The schematic of the SIMULINK model shown in Figure 7.10 can be incorporated easily into the SIMULINK model of the three blade, partial span pitch controlled, wind turbine introduced in Chapter

7.4 — Comparison against the gearbox and induction generator configuration

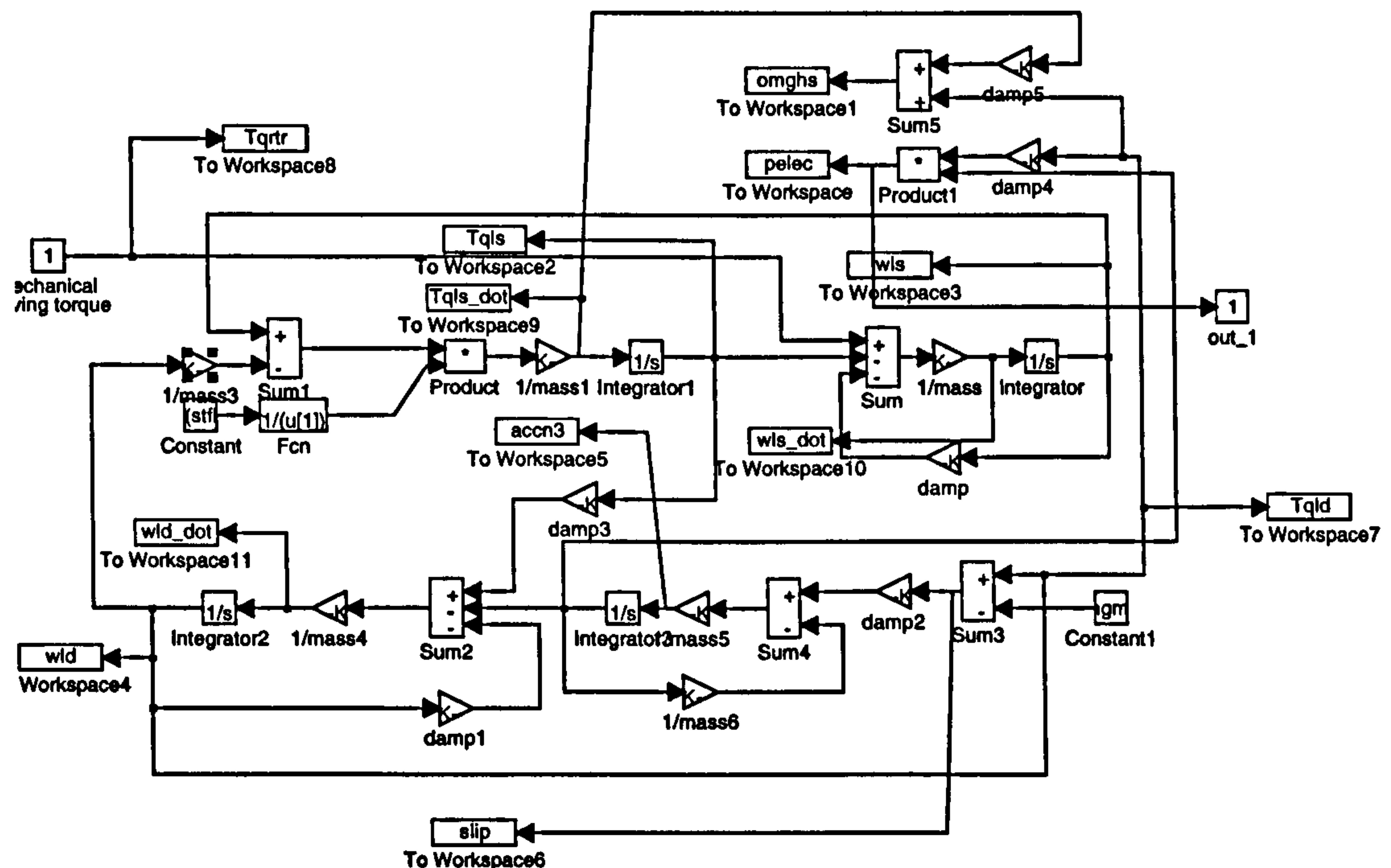


Figure 7.10: SIMULINK model of the induction generator plus gearbox

2. Again the spectral method is used to generate the wind speed variation used for the comparison with the direct drive generator. The model representing the induction generator and gearbox is placed where the sixth order model of the direct drive permanent magnet synchronous generator is shown in Figure 2.32 and this leads to the overall simulation model shown in Figure 7.11. The same values for the pitch controller and pitch actuation models are also assumed as those presented in Chapter 2 so a fair comparison can be made.

INDUCTION GENERATOR AND GEARBOX VALUES. The values for an induction generator designed for 50 Hz grid connection at the same designed rotational speed of the wind turbine blades as for the fixed speed case can be seen in Table 7.4. The values are suitably modified from those presented by Leithead for a 300 kW rated induction generator plus gearbox [65] to uprate them to the 455 kW power rating.

SETTING UP THE INITIAL CONDITIONS. The initial conditions for the induction generator plus gearbox model are set up in a very similar manner to the fixed speed case. The power in the wind is calculated from the rated value of power coefficient and wind speed. An iterative approach is then used to evaluate the required value of rotor torque, found from the wind speed and power coefficient, and corresponding amount of slip to give

7.4 — Comparison against the gearbox and induction generator configuration

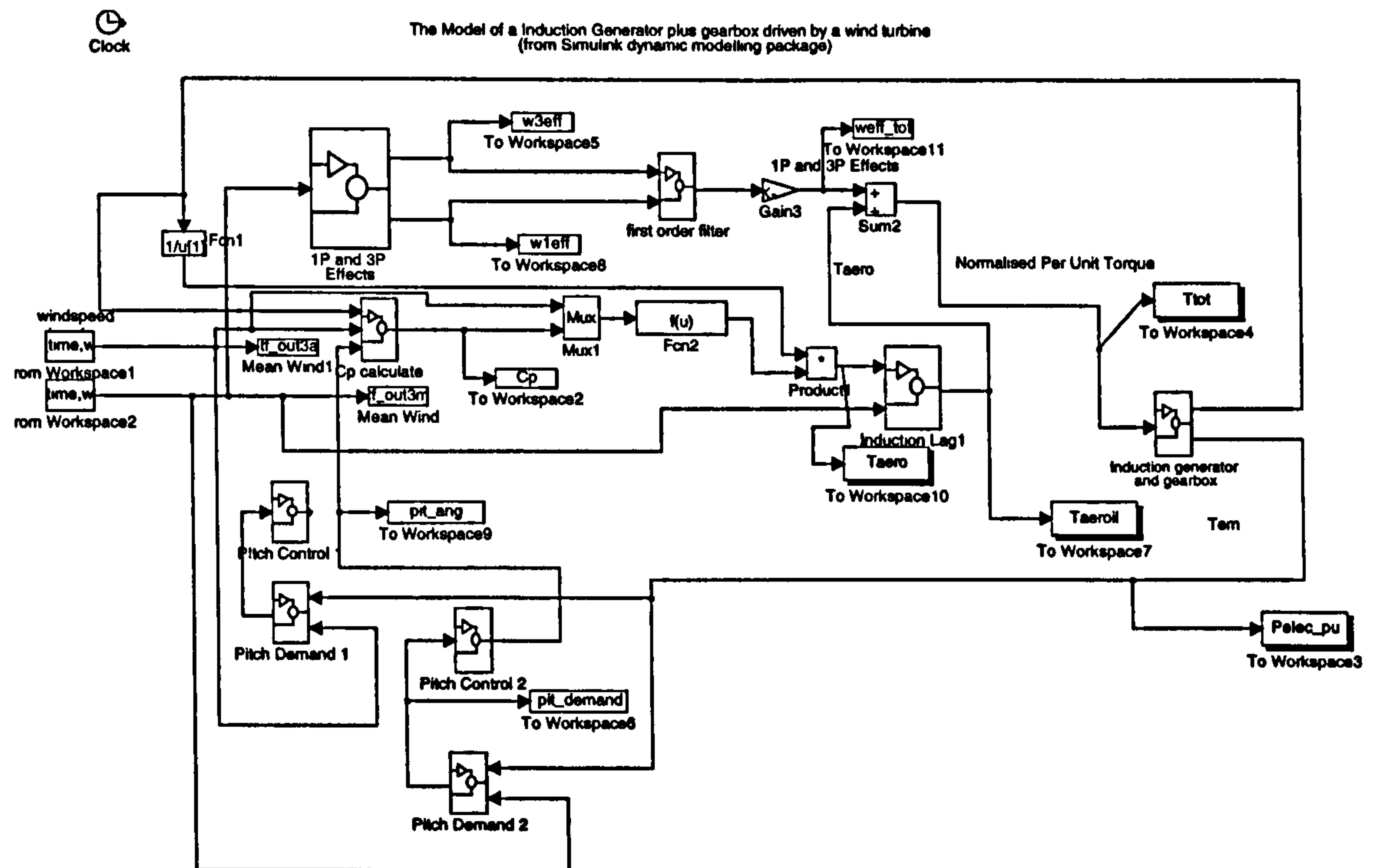


Figure 7.11: SIMULINK model of wind turbine driven induction generator plus gearbox

balanced operation. This procedure is outlined in Appendix E.

7.4.2 Induction generator plus gearbox performance

The basic performance of the simplified induction generator plus gearbox model is now presented for both a step change in the input torque level and in response to the torques generated in windy conditions.

STEP RESPONSE. The response of the induction generator plus gearbox can be seen in Figure 7.12 for a one per unit step change in input torque. The resulting oscillations clearly last for far longer than the equivalent oscillations shown for the power angle of the compliant mounted permanent magnet generator in Figure 4.3.

RESPONSE TO THE WIND SPEED WITH AMWS OF 9 m/s. The wind time history and corresponding power spectra can be seen in Figure 7.13. The run identifiers show that the same values for the pitch controller have been used as for all the previous results although during this simulation run as it is for below rated wind speeds there is no pitch action.

7.4 — Comparison against the gearbox and induction generator configuration

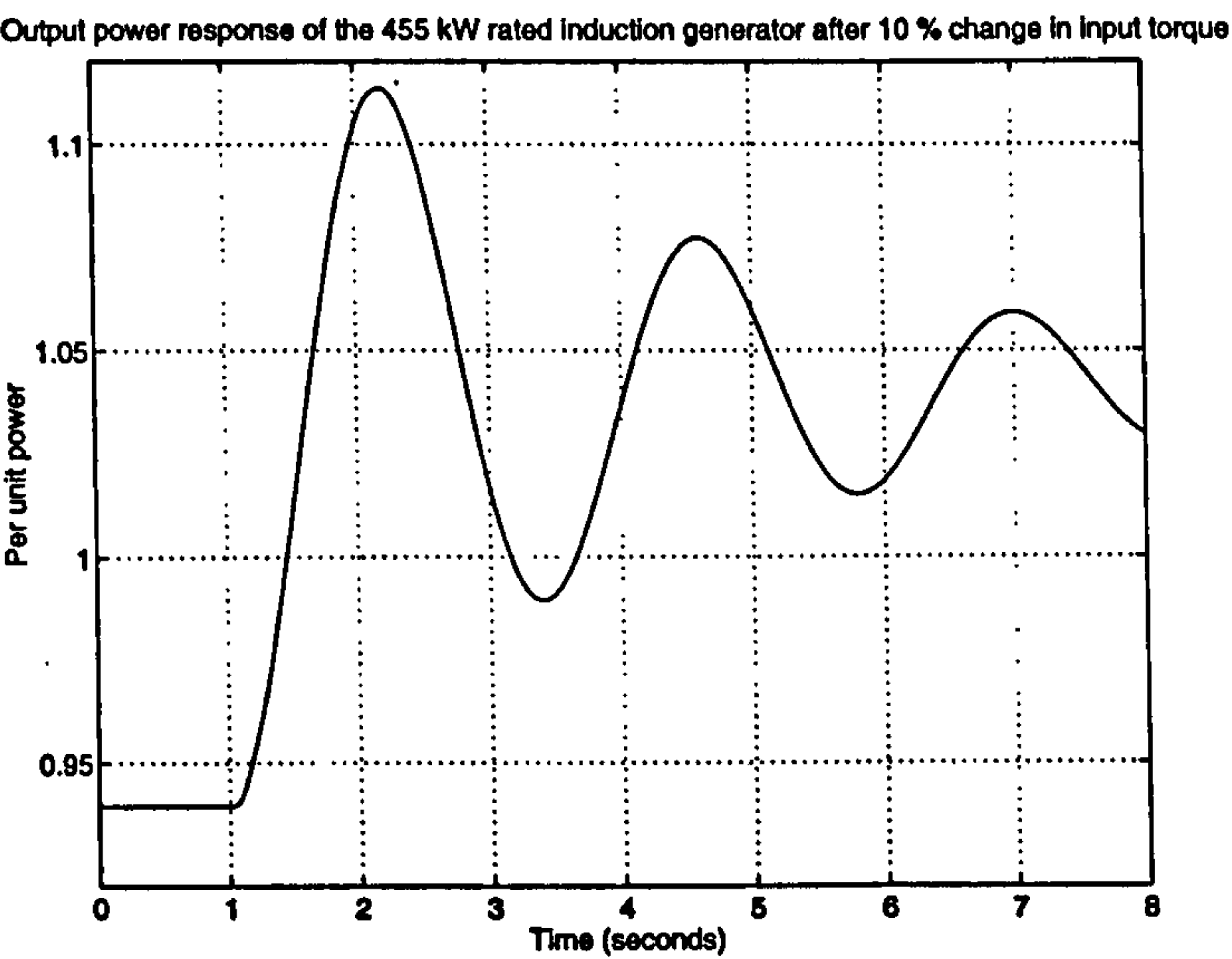


Figure 7.12: Induction generator plus gearbox step response

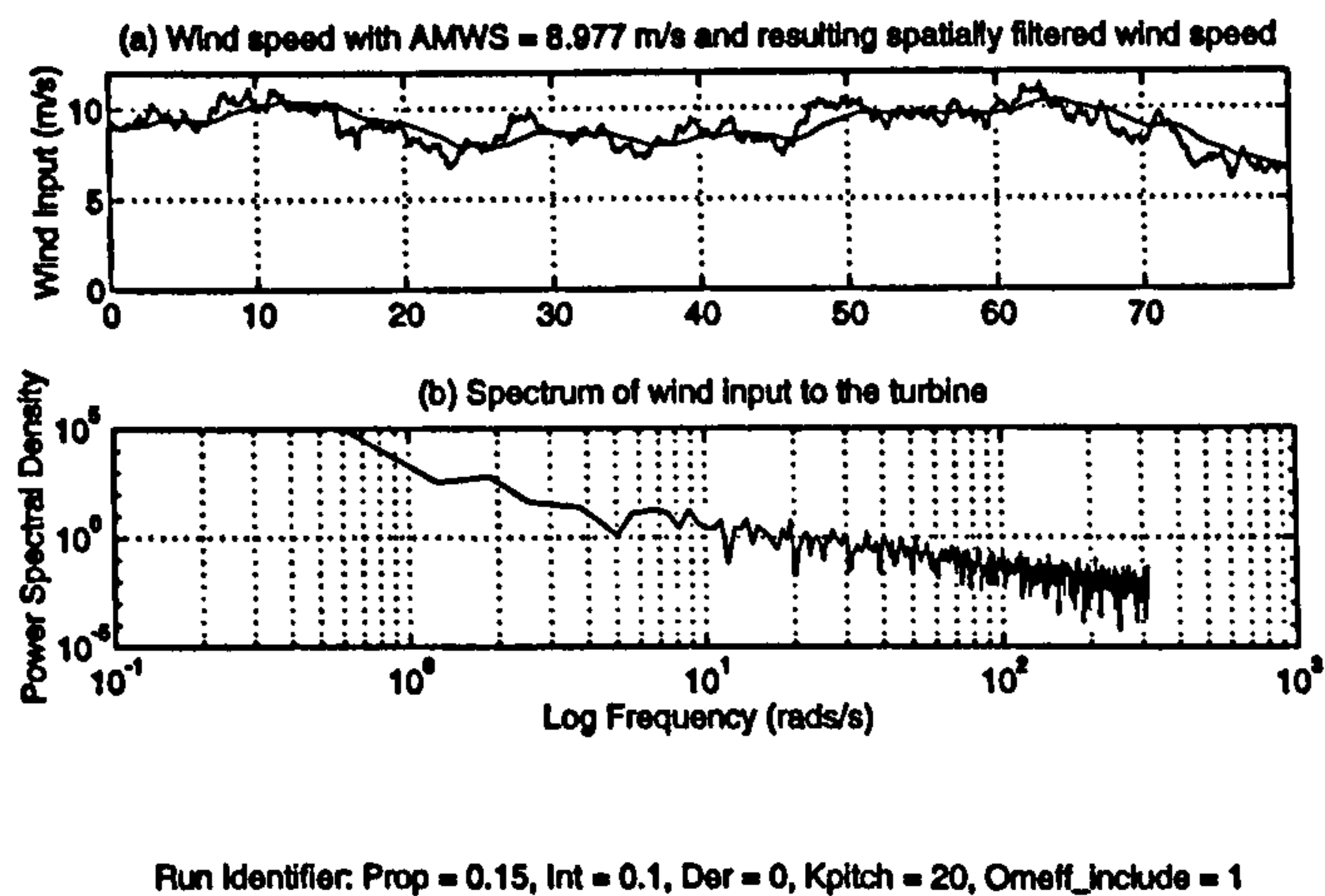


Figure 7.13: Wind speed and and corresponding power spectra

7.4 — Comparison against the gearbox and induction generator configuration

Rated Power	455 kW
Blade plus low speed shaft inertia	175E3 Kgm^{-2}
High speed shaft inertia	5.7 Kgm^{-2}
Low speed shaft stiffness	1.5E6 Nm/rad
High speed shaft stiffness	7.5E4 Nm/rad
High speed shaft damping	0.3 Nm/rads/s
Low speed shaft damping	1470 Nm/rads/s
Number of pole pairs	2
Grid frequency	50 Hz
Efficiency	0.95
Rated slip	1.5 %
Gearbox ratio	42.1
Rated rotational speed	3.79 rads/s
Electrical Torque coefficient	1275 Nm/rads/s
Rated electrical torque	3004 Nm

Table 7.4: Induction generator plus gearbox values

The resulting power coefficient, torque before and after the effect of induction lag, torque including rotational effects and resulting power spectrum showing the typical rotational peaks can be seen in Figure 7.14. This is very similar in essence to the performance of the fixed speed wind turbine and a comparison of the key performance indicators is included in the next section.

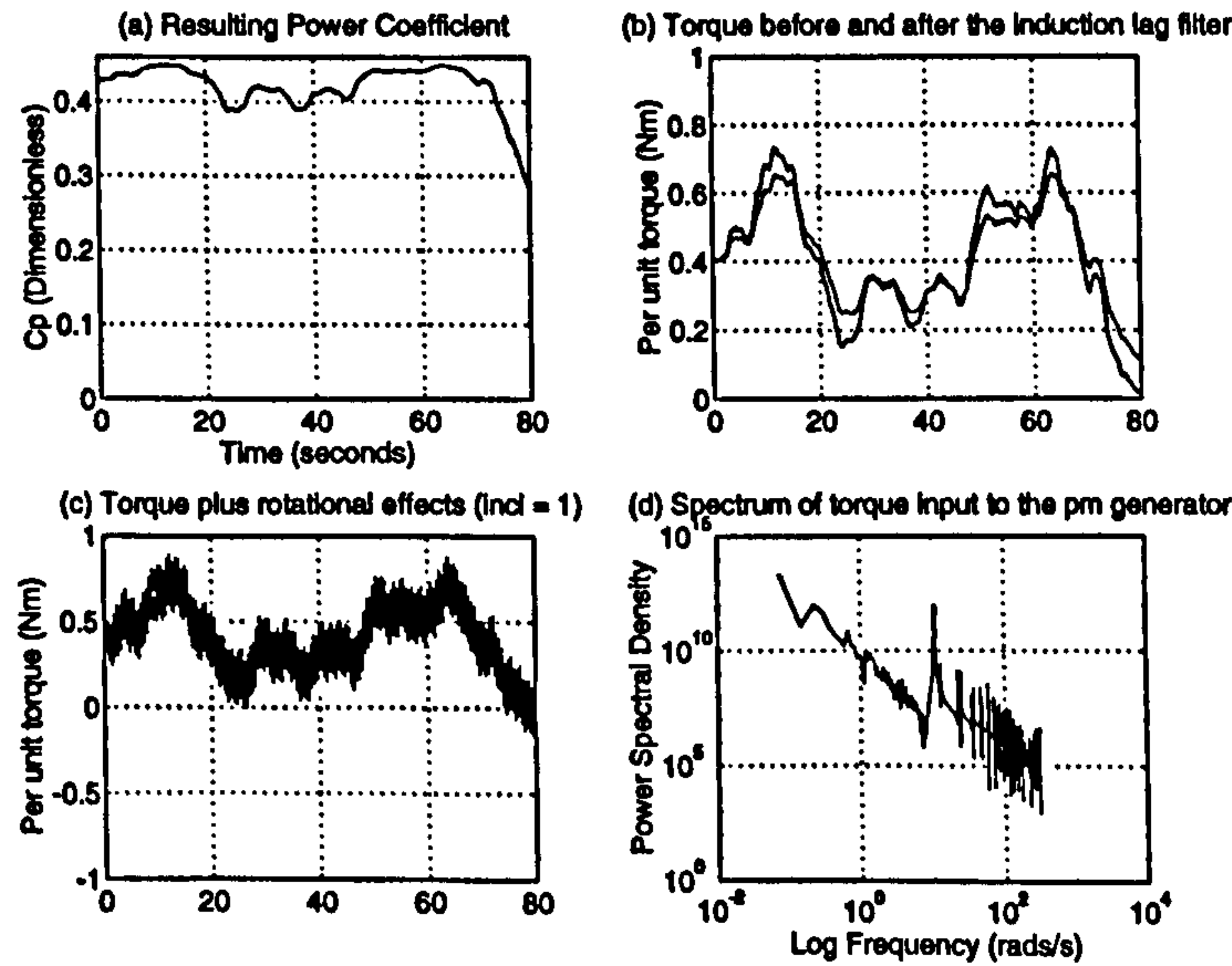


Figure 7.14: Power coefficient, aerodynamic torque and corresponding power spectrum

The resulting induction generator slip, low and high speed shaft rotational speeds and tip speed ratio can be seen in Figure 7.15. These plots generally show the increased variation in angular speed for the induction generator arrangement when compared with the fixed speed,

7.4 — Comparison against the gearbox and induction generator configuration

grid connected, permanent magnet, synchronous generator. This could lead to increased fatiguing of the shaft and increased likelihood of dynamic resonances occurring.

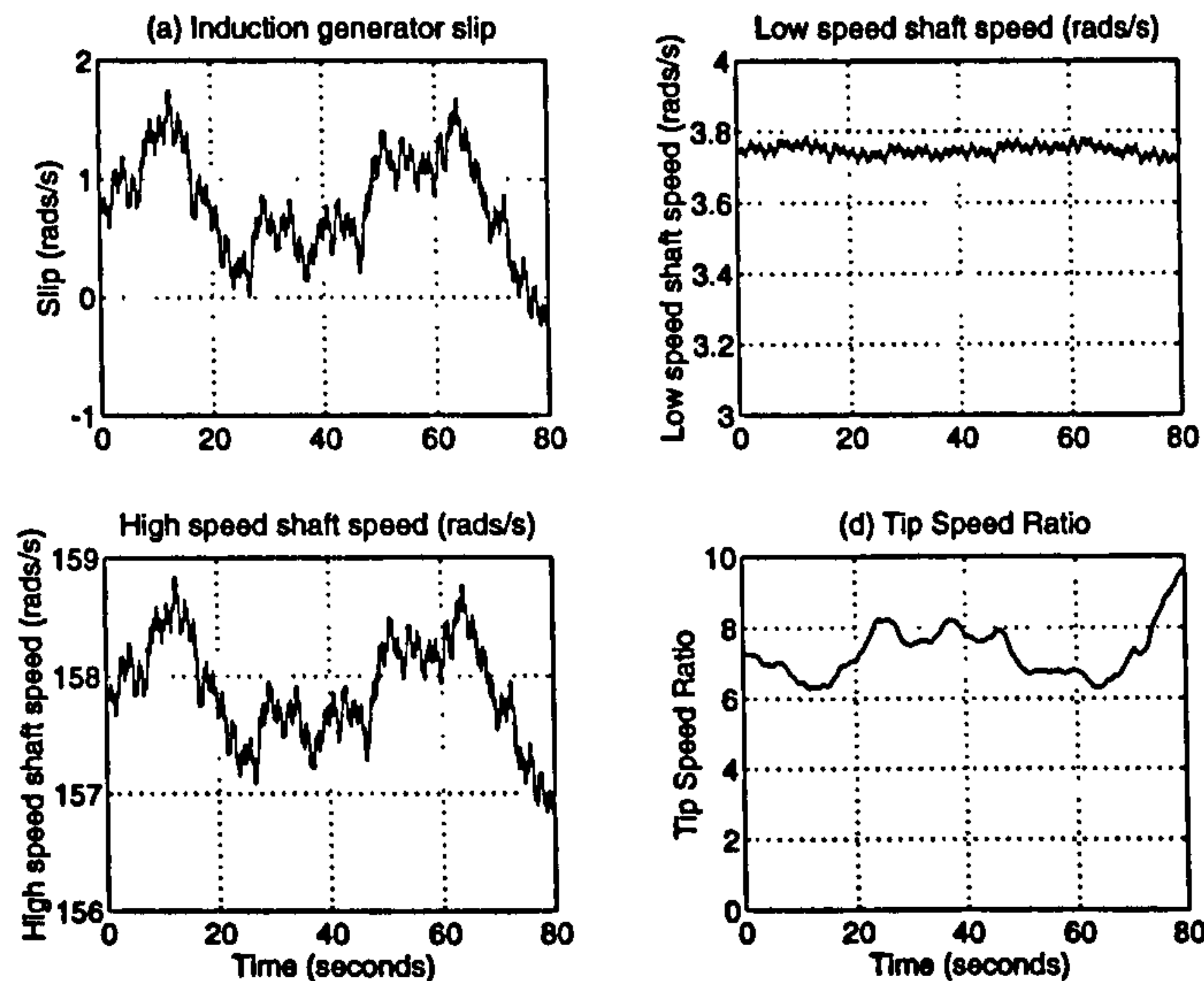


Figure 7.15: Induction generator slip, low and high speed shaft rotational speeds and tip speed ratio

The input mechanical power, the real power out to the grid and overall power loss can be seen in Figure 7.16. Comparing plots 1 and 2 with Figures 7.2 and 7.4 shows that the ability of the induction generator to change speed slightly with relation to the grid allows far greater power smoothing than for the fixed speed case but not as much as for the variable speed case. This is again examined at greater length in the next section.

7.4.3 Comparison of the transient performance

The step performance of the induction generator and gearbox system will first be compared against the fixed speed, permanent magnet, synchronous generator system. Then the comparison will be extended to the full wind turbine simulation and include the performance of the variable speed permanent magnet generator configuration.

Firstly comparing the step response of the output power to the grid of the induction generator and gearbox arrangement, shown in Figure 7.12 against the step response for the well designed fixed speed operated, permanent magnet, synchronous generators, shown in Figure 4.3, it is clear that the induction generator performance is far worse with a settling time of greater than 7 seconds as opposed to 2 seconds and a peak overshoot of 50 % compared

7.4 — Comparison against the gearbox and induction generator configuration

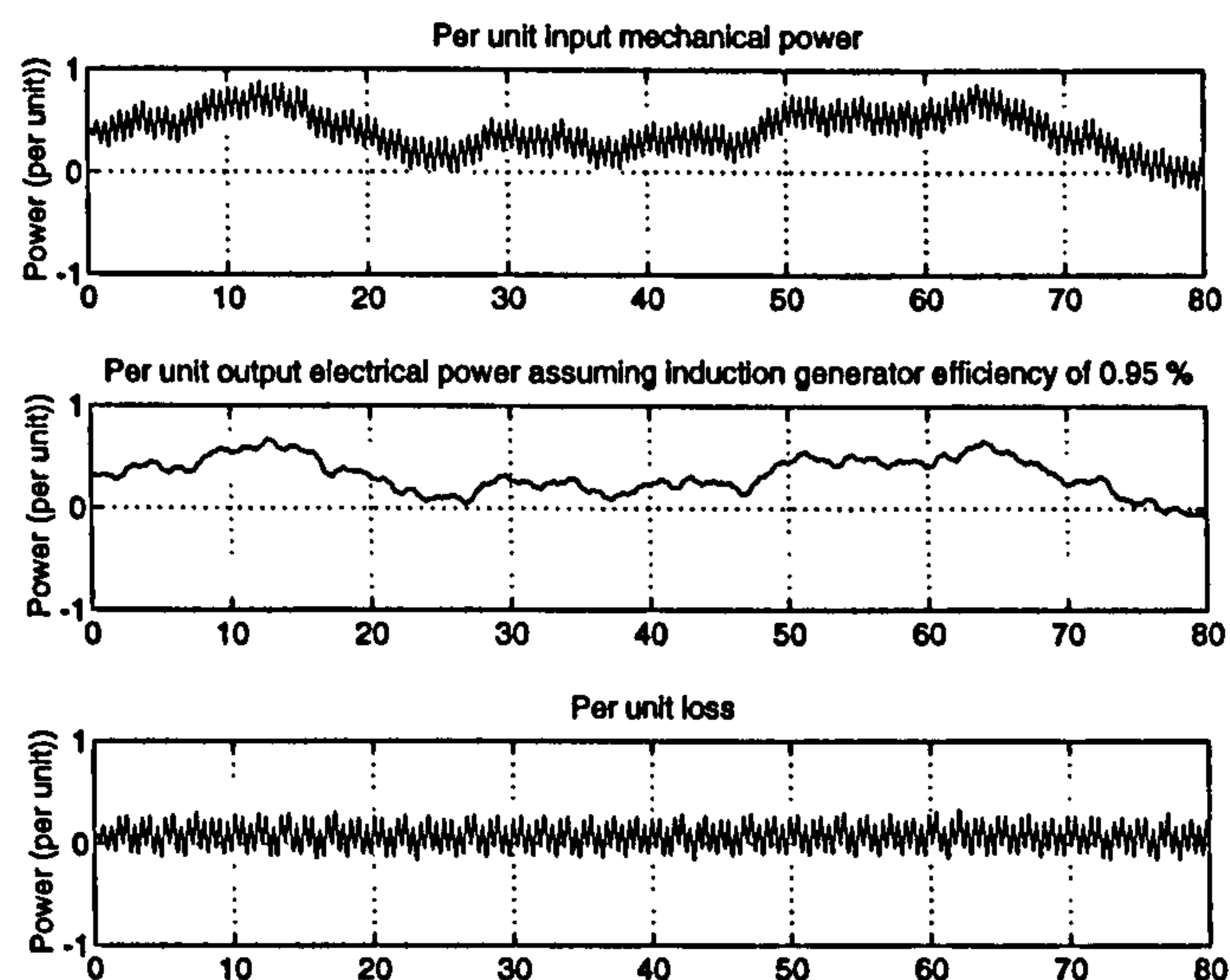


Figure 7.16: Mechanical power input, real power out to the grid and power loss with 25 %.

Secondly comparing the performance in the windy environment in terms of the energy captured and the standard deviation of the power delivered to the grid, it is clear that the induction generator has lesser power swings but is worse at capturing the energy available in the free wind stream than the compliantly mounted, fixed speed, permanent magnet generator. The values for the energy captured and standard deviation of the real power to the grid for the 80 seconds of simulated wind speed with an AMWS of 9 m/s can be seen in Table 7.5.

Gen. Type	Induction	Fixed speed PM Gen.	Variable speed PM Gen.
Energy Captured	4.13 kWh	4.11 kWh	4.56 kWh
Energy out to the grid	3.34 kWh	3.95 kWh	3.95 kWh
Stdev. of output power	.17 p.u.	0.18 p.u.	0.13 p.u.

Table 7.5: Comparison of performance in the windy environment

Clearly the variable speed operated permanent magnet generator is the best in terms of energy captured, energy delivered to the grid and the power quality during this simulation run. The advantages of the fixed speed permanent magnet generator over the induction generator is more difficult to judge and is really dependent on the capital cost and resulting revenue from the yearly delivered energy to the grid. Figures for this yearly delivered energy and the resulting revenue based on 4.5 p/kWh have been calculated for the induction generator using the same method from section 7.1.1 and are presented in Table 7.6.

7.4 — Comparison against the gearbox and induction generator configuration

These figures are used for comparison in the full discounted cash flow analysis presented in section 7.4.4.

Energy to the grid	1277.4 MWh/yr
Resulting Revenue	£51096 /yr

Table 7.6: Comparison of yearly energy capture

7.4.4 Comparison on weight, cost and reliability

The information for the comparison presented here between those values predicted for the direct drive generator by WINDGEN2 and WINDVARD and its geared industry equivalent comes from an exhaustively validated cost modelling program written by Harrison [36].

WEIGHT COMPARISON. Figure 7.17 shows the same weight results presented in the previous section but now with the industry standard weights for drive train and induction generator included. Clearly the fixed speed direct drive option is as light as its industrial equivalent at low ratings and the variable speed generator even lighter. However as the ratings increase this advantage reduces such that the gearbox and induction generator arrangement is lighter than both the fixed and variable speed permanent magnet synchronous generator. This reduction in advantage can be explained due to the increase in tier number as the permanent magnet synchronous generator increases in rating and corresponding increase in the weight of magnetic and structural material required. For the fixed speed case the tier number increases more with rating than the variable speed case because of the need to design the generator to allow enough scope to design the values for the compliant mounting to operate satisfactorily. For the variable speed case it is merely the fact that synchronous generators tend to be heavier and bulkier than an equivalent rated induction generator. Therefore weight should not really be put forward as the key argument for implementing the direct drive permanent magnet synchronous generator designs as opposed to the induction generator plus gearbox arrangement.

CAPITAL COST COMPARISON. Figure 7.18 shows the same capital cost results presented in Figure 7.8 with the cost of the industry standard induction generator and gearbox arrangement also included. Clearly the fixed speed direct drive option is cheaper than its industrial equivalent and the main reason for this is the increase in gearbox cost as rating increases. The cyclic loads on the gearbox and the large torque rating for wind

7.4 — Comparison against the gearbox and induction generator configuration

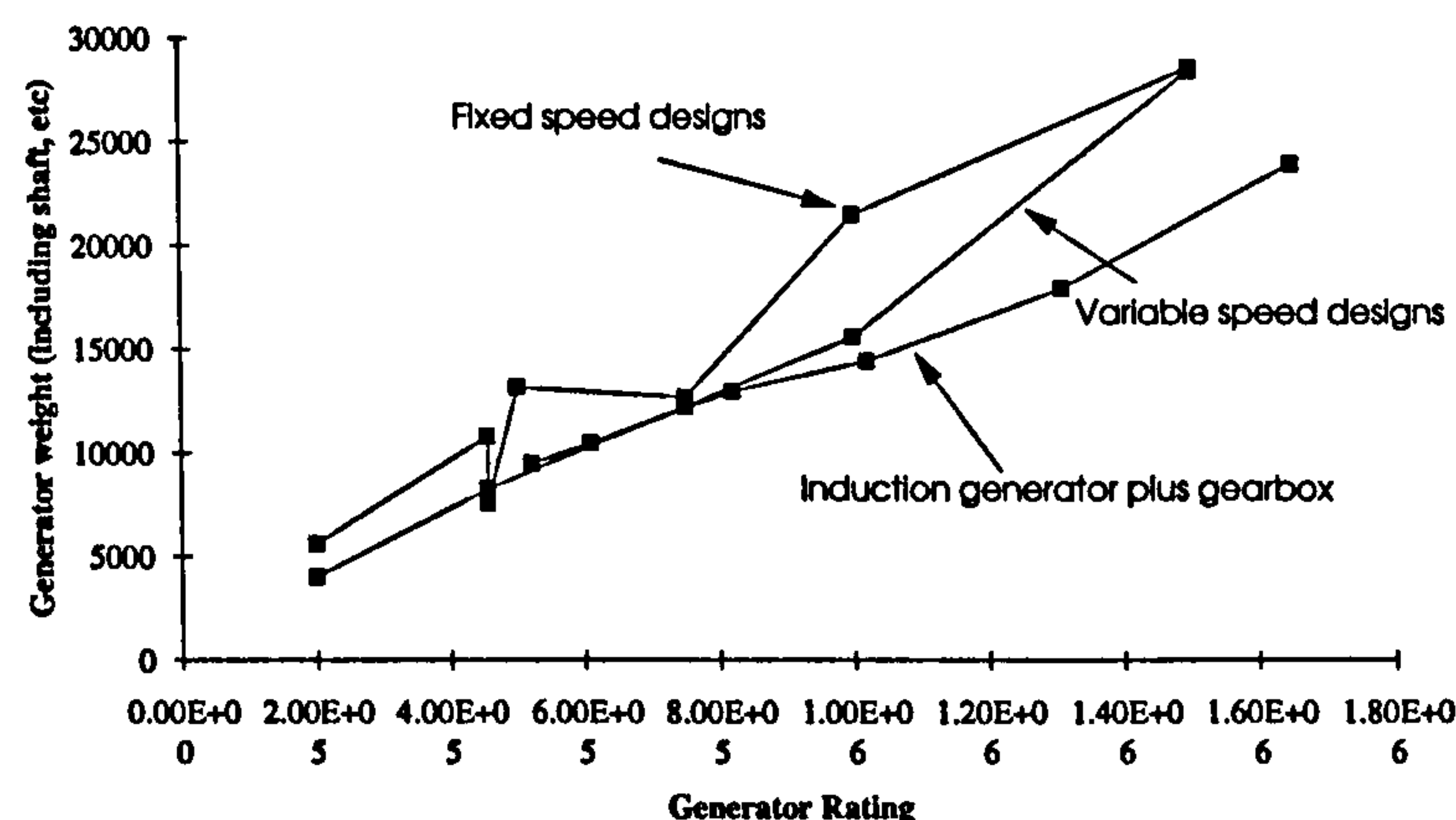


Figure 7.17: Weight comparison between fixed and variable speed case and industrial standard model

turbines with large power ratings and low rotational speeds lead to very expensive gearbox designs. The variable speed generator cost is shown without including the cost of the inverter and rectifier as these costs are difficult to quantify at present.

DISCOUNTED CASH FLOW RATE OF RETURN ANALYSIS. This form of accounting analysis allows factors such as interest rates, lifetime of plant and differences in revenue earned to be included in the costing process. The solution to the complex procedure gives an indication of the cost effectiveness of different configurations in an equivalent sum relative to today's prices and allows a direct comparison to be made. Performing this analysis for the 455 kW rated wind turbine configurations gives the figures shown in Table 7.6 for the relative net present value of the revenue earned over the twenty five year lifetime of the plant assuming a discount rate of 10 %. Also implicit in this calculation is that the value of electricity generated and the cost of the wind turbine attached to the generator remains the same for all three types of generator configuration. The total cost of current wind turbines is about £1000 per kW installed and this figure is modified by the differential between the capital cost of the permanent magnet generator versus the standard induction generator plus gearbox to give the total turbine cost. The cost of the rectifier and inverter is neglected for this comparison of capital cost.

Clearly from this analysis the induction generator plus gearbox arrangement is only just viable at 4 p/kWh and will be unlikely to return as good a payback until the price awarded

7.4 — Comparison against the gearbox and induction generator configuration

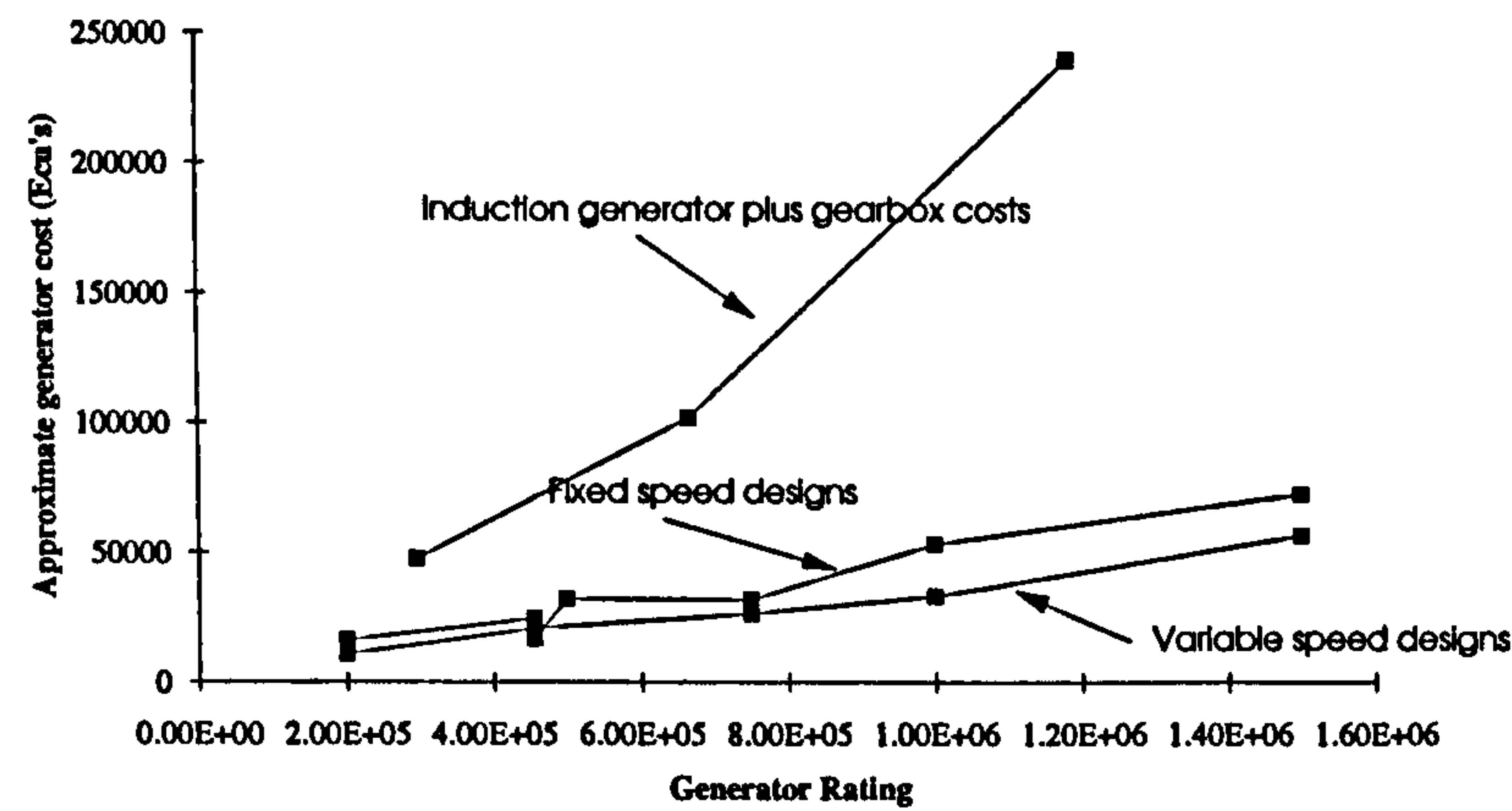


Figure 7.18: Weight comparison between fixed and variable speed case and industrial standard model

Gen. Type	Induction plus gearbox	Fixed speed PM Gen.	Variable Speed PM Gen.
Cost	£70525	£66430	£34125
Net present value	£463,660	£502,470	£509,730
Total turbine cost	£455,000	£450,905	£418600

Table 7.7: Comparison of cost versus net present value

to wind farms under the various NFFO agreements falls to a more realistic figure. The fixed speed permanent magnet has a better future with a return on investment of 11.4 %. The variable speed permanent magnet generator has an even better return on investment of 21.8 % but this fails to include the capital cost of the rectifier and inverter. This is likely to be anywhere upto 20 % of the capital cost of the wind turbine . Performing a sensitivity analysis by taking this figure and a figure of 10 % of capital cost gives a return on investment of about 1.5 % and 10.7 % respectively. Both of these values are less than for the fixed speed case. However the above analysis has failed to recognise the revenue which could be earned by the variable speed wind turbine in ancillary contracts, e.g. supplying reactive power.

RELIABILITY COMPARISON. One of the key arguments put forward for the direct drive option is the fact that eliminating the gearbox would lead to increased reliability and reduced time for maintenance. This was more valid for the early gearboxes used in wind turbines but a greater understanding of the cyclic forces acting on the gear boxes has led to better designs which function well. However maintenance is still required for lubrication

7.5 ————— Design comparison of the fixed and variable speed wind turbines

change which is not a problem for the direct drive generator. Furthermore the modular arrangement means that if one stator module is broken it can easily be replaced. In fact for the variable speed case the generator could continue to operate with several broken E-cores until a regular planned maintenance stop. This is incorporated into the design by the fact that the use of an integral number of tiers usually leads to about 15 % over design and hence 15 % of the E-cores could fail and the machine still transmit rated power.

7.5 Design comparison of the fixed and variable speed wind turbines

The key design drivers for the fixed and variable speed operated permanent magnet generators were outlined in Chapters 3 and 5 respectively and used to develop an understanding of the performance of a range of generators. It is important to understand which drivers have the effect of increasing the weight and cost of each mode of operation and which have the effect of reducing performance. This analysis can be used to recommend avenues for further design enhancement to the multi-pole, permanent magnet synchronous generator. To this aim the key design drivers of each mode of operation are discussed and the limits on further development outlined.

7.5.1 Fixed speed operation

The biggest design driver for the fixed speed operation of the permanent magnet generator is to match the synchronous reactance of the generator to the parameters of the compliant mounting that is required for the necessary stability and performance to connect it safely to the grid. The compliant mounting design requirements are such that a heavier generator is needed than a generator designed purely from thermal considerations. The compliant mounting is also expensive leading to the cost of the compliantly mounted 455 kW generator being £146 per installed kilowatt [47]. So to improve the fixed speed arrangement's cost further would require eliminating the compliant mounting or redesigning it.

The first option, that of eliminating the compliant mounting completely, would require a larger pole pitch, thus allowing room for conventional damper windings or another form of damping altogether. The former option could only be achieved by larger generator di-

7.5 ————— Design comparison of the fixed and variable speed wind turbines

ameters or higher rotational speeds. A larger generator diameter, of similar radius to the Enercon E40 [55], would allow a fundamental redesign of the permanent magnet generator configuration. However for this to be more economic would require that the damper windings could be inserted easily and a low synchronous reactance from a lesser number of stator tiers. This is becoming more like a conventional generator which has been shown to be unlikely to suit the wind turbine application and still be economic [47]. The second option of increasing the rotational speed would still require the insertion of damper windings but would also need a speed increasing gearbox. Including a gearbox would reverse the step forward taken in this thesis and is therefore unacceptable. However a case could be made for a single stage, low ratio gearbox, say 2:1, which would be relatively light, cheap and easy to maintain [36], coupled to a redesigned generator with half the number of poles and therefore twice the pole pitch. This could lead to cost savings but is speculative and would have to be the subject for further work.

The second option, changing the compliant mounting arrangement, would not necessarily lead to any real cost saving. The requirement for a low synchronous reactance is fundamental to the peak power that can be delivered to the grid and therefore a larger number of tiers is still required. However changing to say a hysteretic rubber mounting arrangement or active damping [88], might lead to a reduction in the compliant mounting cost. This kind of arrangement would have a non-linear damping response perhaps proportional to the stator velocity squared. This would change the eigenvalue analysis presented in chapter 4 as now the $c\delta_s$ terms would become $c\dot{\delta}_s^2$ terms. When linearised this would mean that the effect of the compliant mounting, c , would be twice as much as before. The effect on this on the overall generator performance and design could also be the subject of further work but it is felt that any performance improvement would be marginal and that the overall cost of the generator would only reduce slightly.

7.5.2 Variable speed operation

The largest benefit of the variable speed operation of the permanent magnet generator is not, as has been thought of for some time, energy capture but the increased control of the output power to the grid and the reduced overall weight when compared with the fixed speed case. The main design driver in terms of low capital cost is the expense of the frequency

converter. The inverter is likely to be the predominant cost of the frequency converter and therefore work to reduce the number of IGBT's required and their associated driver circuitry whilst maintaining the controllability and restricting the harmonic distortion of the terminal voltage is required. The generator could also be redesigned to use different numbers of magnet blocks per module as there is no restriction of frequency. The effect of both of these areas on system cost and performance needs to be assessed.

7.6 Conclusions

These conclusions are really included to re-emphasise the point that there is a hierarchy to the scale of engineering and cost when moving between the different designs and the resultant changes in overall performance should justify the increased cost and design effort.

When comparing the fixed speed, direct drive, multi-pole, permanent magnet, synchronous generator against the standard induction generator plus gearbox arrangements, both designs have a similar cost but the former design wins on performance and loses on weight as the rating increases. Therefore if fixed speed operation is desired the compliantly mounted, permanent magnet, generator is the preferred option for the future. However there are improvements to be made in terms of better power quality and reduced weight when moving to the variable speed case with an increased revenue stream but quite a large question mark over the cost improvement due to the uncertain data about inverter costs. A presenter at the Clean Power 2001 conference in 1993 answered the question on cost with a figure of 20 % of the total capital cost of a wind turbine. As the generator is only 5 to 10 % of the capital cost of a wind turbine this would lead to an increase in cost from the variable to fixed speed turbine of 11 %, excluding any benefits from tower or blade redesign, with only a slight increase in return on investment over the lifetime of the plant. Therefore the fixed speed option is preferred until the capital cost of the inverter reduces to a low enough level.

Comparing a variable speed induction generator plus gearbox against the variable speed permanent magnet generator there is a definite cost advantage for the permanent magnet generator as both would use similar costing equipment for the frequency converter and, assuming similar energy capture, the differential in capital cost for the generators would be the only real difference between the two schemes. Hence the variable speed permanent magnet generator is preferred costing about 8 % less.

Chapter 8

Conclusions and further work

The key points of chapters 1 to 7 are first summarised and then overall conclusions for the thesis presented. These conclusions show that a valuable tool for simulating and comparing the operation of fixed and variable speed multi-pole permanent magnet synchronous generators for wind turbine applications has been developed. Several areas where further work is needed to take the results presented in the thesis and apply them to the real wind turbine design situation are then presented. The original contribution of the author is discussed with reference to several published papers and the chapter concludes the thesis with a brief summary of the benefits derived from this work.

8.1 Chapter summary and key conclusions

Each chapter of the thesis has been devoted to developing arguments in support of the use of the direct drive, multi-pole, permanent magnet, synchronous generator to bring down the overall complexity, weight, cost and improve the performance of wind turbines. It is now appropriate to include a section which summarises the key points raised and attempts to assess whether the aims of the research presented in section 1.3 have been achieved.

CHAPTER 1. The first key point that was raised in this chapter was that wind produced electricity has a very low environmental impact and is one of the most economic of all the renewables with a predicted cost of generated electricity of 3.5 p/kWh by the year 2000. Furthermore arguments were presented which concluded that the industry standard wind

turbine that would be simulated as a test bed for the permanent magnet generator was a three blade, partial span pitch controlled, upwind, horizontal axis, wind turbine.

CHAPTER 2. Firstly, methods for representing the complex nature of the wind interaction with the turbine blades were presented in this chapter to obtain a method for deriving suitable simulation models for the developed shaft torque of three blade wind turbines. The discrete spectral methods proposed by [58] [65] and discrete point wind speed models of [40] were implemented and compared. The comparison revealed that the spectral method was necessary for simulation of the real wind situation and the point wind speed model required for preliminary understanding of the dynamic interactions within the turbine and the design of suitable controllers, which is most easily achieved using step response information. The spectral method was validated against wind data provided by NREL with good correlation. Secondly, the modelling of a suitable pitch control strategy for limiting the power into the wind turbine to ensure rated operation of the generator was presented and the methods for designing a suitable pitch controller and actuator discussed. The resulting power curve versus wind speed was validated for a 500 kW rated wind turbine against the Vesta's 500 and reasonable agreement reached.

CHAPTER 3. The design, theory, modelling and validation of the fixed speed, direct drive, multi-pole, permanent magnet, synchronous generator was presented in this chapter. The operation of the compliant mounting to provide suitable level of damping was introduced and a sixth order model representing the situation developed. A testrig at UMIST was then used to validate the model using both linearisation and simulation. The measured transient responses of the resulting stator movement and armature current for both step changes in input torque and after synchronisation to the grid were compared and good agreement reached.

CHAPTER 4. Firstly, the key dynamic interactions between a generator rated at 455 kW and the compliant mounting were analysed using eigenvalue techniques and full non-linear simulation to match the proposed modes of oscillation to the system. These showed that it was necessary to design the generator to have a low value of synchronous reactance to ensure mode 1 operation (where the generator rotor and stator oscillate together against the anchor point with a frequency of response determined by the spring stiffness, k , and damping coefficient, c , of the compliant mounting). For the generator to have a low synchronous

reactance it is necessary to typically have an extra tier than is required from consideration of the electric loading alone. Therefore fixed speed and hence compliantly mounted generators are heavy and over rated to fulfill the damping requirements for stability and good transient performance. Furthermore the manufacture of the compliant mounting and the flexibility associated with it leads to a high cost of generator of the order £146 per installed kilowatt. This is however comparable with the cost of an induction generator plus gearbox which would cost in the range £155 per installed kilowatt for the same rating [36]. The eigenvalue analysis was then extended to a range of generators with ratings typical of the wind power application from 200 kW to 1.5 MW. Across the range the same design requirements applied and 'best' designs for each rating were presented.

Secondly, the synchronisation requirements of the 455 kW generator were explored through full non-linear simulation and it was found that the generator would synchronise to the grid at large values of speed and angular mismatch. The implementation in the real wind situation was then considered and again the pitch controller could act to ensure successful synchronisation. This is an important result because the only control over the permanent magnet generator is the pitch control as there is no automatic voltage regulator.

Finally, the dynamic interactions between the generator and the wind turbine were examined with key results presented for the cases with wind speeds below and above rated levels. It is clear that the performance is satisfactory. The effect of the varying shaft torque from the wind on the performance of the compliantly mounted, permanent magnet, synchronous generator was shown to depend on the values for the compliant mounting. This vindicated the design procedure based on eigenvalues and step response information from full non-linear simulation as a means to design for the windy environment.

Chapter 4 clearly demonstrated the viability of the fixed speed, multi-pole, permanent magnet, synchronous generator for wind power applications but problems associated with the operation of the compliant mounting mean that the cost, weight, and performance advantages over the industrial standard case of a gearbox and induction generator, although good, are not as great as at first thought and therefore the variable speed case was considered.

CHAPTER 5. The theory, design and modelling of suitable schemes for the variable speed operation of such a multi-pole, permanent magnet, synchronous generator was introduced in Chapter 5. The lack of a compliant mounting in this system, as damping at the

generator is no longer needed, and the freedom to design at any frequency, because of the introduction of a frequency converter between the generator and the grid, led to generator designs which were up to a third lighter and therefore considerably cheaper. However the frequency converter brings cost and complexity penalties which were difficult to quantify and therefore a performance comparison was carried out. To compare the fixed and variable speed systems required new control aims to be developed for the frequency converter to demonstrate the perceived performance advantages of the variable speed system. These were again implemented on SIMULINK.

The method of simulating the variable speed generator and frequency converter as several lookup tables representing power transfer and control loops representing the action of the inverter whilst ignoring any detailed modelling of the E-core, rectifier and inverter small time scale transients meant that longer time simulations could be carried out more easily and overall control strategies developed. It is considered to be a valid approach to assess the performance at this time scale level.

CHAPTER 6. The performance of a 455 kW variable speed operated wind turbine was assessed in this chapter with key results presented for below and above rated wind speed levels. Control strategies to track C_{pmax} , maintain the terminal voltage of the inverter at rated value and even to maintain a reactive power setpoint were developed and tested using step responses with good overall demonstration of the powerful capabilities of the frequency converter.

The operation at variable speed leads to only a 1.2 % increase in delivered energy to the grid, but does lead to a 26.4 % reduction in the standard deviation of power into the grid and allows a reactive power setpoint to be implemented. However the variable speed operation does lead to a degradation in the standard deviation of reactive power flow into the grid over the fixed speed case due to the low value of transmission reactance and better control of the terminal voltage is required. Once sorted this would lead to an increased revenue stream for the variable speed over the fixed speed case. The effect of the dc link capacitance was not that marked in terms of power quality and controllability of the dc link voltage with the value of 4000 μF a reasonable choice.

CHAPTER 7. Firstly, the performance, weight and cost of the fixed speed and variable speed generators were compared across the range of generator ratings to assess which

mode of operation was the most likely to lead to substantial reductions in the cost of generated electricity over the lifetime of a wind energy conversion system. The discounted cash flow analysis and performance comparison concluded that for fixed or variable speed operation the permanent magnet generator is an improvement over the induction generator and gearbox arrangement but that when comparing fixed or variable speed operation of the permanent magnet generator the cost of the inverter was critical.

8.1.1 Key conclusions

To sum up then, the direct drive permanent magnet generator is an important step in the development of wind energy conversion systems. It combines the elegance of removing the gearbox from the overall drive train of the wind turbine with a very practical solution in terms of low cost, good performance and a well thought out manufacturable design. Both the fixed speed and variable speed operation of such a turbine are an improvement over the equivalent competition, the industrial standard induction generator and gearbox arrangement. However further comparison must be made to justify the increase in revenue stream of the variable speed over the fixed speed operation of the generator versus the increase in cost due to the inverter. The author feels that the costs of IGBT's will reduce considerably as increasing design knowledge is gained and at the same time ratings will increase dramatically as module technology is matured. This will lead to the variable speed operation of the generator as being the preferred mode of operation.

8.2 Suggestions for further work

It is important in any piece of work to realise the constraints of time and the need to deliver some concrete conclusions and therefore many promising avenues of research have had to be curtailed to keep the main thread focussed. The suggestions for further work logically break into three main areas: firstly enhancements to the wind turbine model, secondly fixed speed operation, and thirdly variable speed operation. These will now be discussed in greater detail.

8.2.1 Enhancements to the wind turbine model

There are several possible enhancements to the wind turbine model which would make it more accurate and enable other design issues to be addressed.

TOWER AND BLADE STRUCTURAL MODELLING. The incorporation of tower and blade structural modelling into the SIMULINK model would add to its complexity considerably but would also allow the two dynamic interactions not considered so far to be analysed and total wind turbine design would be possible. This is particularly important in reducing the overall costs of wind turbines as ‘soft-soft’ designs are a lot lighter and can therefore be built with taller towers and capture even more energy [36] [50].

The effect of tower movement would be to alter the dynamic performance of the compliant mounting and the effect of blade movement would be to alter the effective wind speed seen by the blades. These two effects would be represented by lumped mass, spring and damper systems with values derived from finite element work. These effects could be incorporated into the SIMULINK model as a time variation superimposed on the stator rotational speed effective wind speed respectively. This would allow a consideration of the tower and blade bending moments and resulting fatiguing to be introduced into the models.

STALL REGULATION. Stall regulation is becoming more in vogue as a simple method to limit the power input to the wind turbine hub shaft because the understanding of the shock loading on the turbine blades is increasing due to the large research effort in this area. Stall regulation can easily be incorporated into the wind turbine model. Instead of a pitch controller and 2d-lookup table referenced by tip speed ratio and pitch angle to determine the power coefficient, C_p , a single function dependent on the tip speed ratio and derived from manufacturer’s measured power curve data for a stall regulated wind turbine could be used. This process has already been mostly implemented with data from [55] but was considered not appropriate to this thesis because of the chosen test bed design. However it would be useful to compare the pitch and stall regulation for both fixed and variable speed operation to see which offered superior performance.

ADVANCED PITCH MECHANISMS. Models for advanced pitch mechanisms and their control algorithms could be tried and tested using the simulation libraries of the wind turbine to establish better ways of moderating the power into the shaft of the wind turbine.

8.2.2 Fixed speed operation

The main area that needs to be improved here is the incorporation and modelling of other damping mechanisms which may lead to better modes of oscillation and the elimination of the requirement to have an extra generator tier.

OTHER DAMPING MECHANISMS. Other damping mechanisms have been reported for this kind of compliantly mounted permanent magnet generator [88] but only perfect viscous dampers have been modelled in this thesis. One favourable idea is to use hysteretic rubber mountings which would fulfill both the support, stiffness and damping roles in one simple to manufacture block and could lead to cost savings and increased system simplicity.

8.2.3 Variable speed operation

There are three main areas where further work is required. Firstly and most importantly validation and implementation of a variable speed test rig, secondly development of better control algorithms and finally an in-depth look at the possible redesign of the generator.

VALIDATION. The most important further work that must be carried out here is the validation of the assumptions presented in Chapter 5 in developing the variable speed. The key assumptions that switching transients can be ignored over the timescales of the wind induced dynamic interactions must be validated either through a CASED simulation [111] or by suitable control of the dc motor driven variable speed test rig in the laboratory [96].

CONTROL ALGORITHMS. The control algorithms presented for the control of the inverter to decouple the real and reactive power control are easy to implement and to understand. However more advance state space techniques to decouple these two control requirements exist [108] [107]. The benefit in terms of reduced voltage regulation by continually adjusting the inverter control ratio, $K_{V_{dc}}$, and power angle, δ , as opposed to changing the control ratio discretely as presented in Chapter 6 could be considerable.

GENERATOR REDESIGN. There are no restrictions placed on the variable speed generator in terms of either design for the compliant mounting nor frequency of operation and therefore some substantial cost savings could be introduced if the generator were redesigned to be lighter or more easy to manufacture. This re-design process should focus on the size of the E-cores and the number of magnet blocks per rotor module. The arrangement used

in the thesis used two block per magnet module but there is no reason why this could not be extended to four or six and would lead to an increase in the airgap size which could ease manufacture and assembly considerably. Furthermore redistribution and resizing of the E-cores may lead to a reduction in the minimum tier number to satisfy the electric loading. These redesigns should, however, maintain the modularity of the generator which is key to many of the performance enhancements seen in the thesis.

8.3 Original contribution

The author feels that his original contribution to this thesis can be split into several areas relating both to the development of the simulation models for the fixed and variable speed operation of the generator and the theory of their operation. This next section outlines the author's contribution to each simulation model and its performance in turn. Firstly the wind model will be discussed, then the compliant mounting and fixed speed permanent magnet generator and finally the variable speed generator and frequency converter.

8.3.1 Wind Modelling

Although the wind model has been developed from work into effective wind speed models [58] it has never been implemented on SIMULINK nor applied to the variable speed case.

8.3.2 Fixed speed generator modelling and performance

The design program and values it returned for the fixed speed design of generator was written by Prof.E. Spooner [76] and the values for the wind turbine were found from [36]. The simulation of a permanent magnet generator has been carried out before [78] [46] but not using SIMULINK and certainly not one which was compliantly mounted apart from [88] which is DC motor driven and not wind turbine driven. Eigenvalue analysis of the type carried out for the generator and presented in [112] [51] has also not been undertaken except in [88]. Furthermore the modes of oscillation analysis and presentation of the design drivers for a fixed speed, wind turbine driven, compliantly mounted, multi-pole, permanent magnet, synchronous generator has not been done before [113].

8.3.3 Wind turbine driving the fixed speed, permanent magnet, generator model

Leithead has developed a model for coupling a wind model to an induction generator but this differs in both simulation language and generator model so that although pretty similar to the model developed in Chapter 2 and 3 in overall nature they are considerably different in actual design. This has not been done elsewhere and therefore the simulation is novel.

8.3.4 Variable speed wind generator modelling and performance

The modelling of the variable speed generator has not been done elsewhere using the techniques used in this thesis. A mixed signal simulator such as SABER or dedicated suite of user written 'C' programs are typically used for modelling systems like the wind driven permanent magnet generator and frequency converter and these tend to be very expensive both in terms of time and money. Using the steady state characteristics for power transfer out of the generator and rectifier, although slightly inaccurate, has allowed suitable control strategies to be developed quite easily and their performance analysed quickly [114].

8.4 Benefits and final conclusions

To conclude then, the author feels that his original contribution to this thesis has led to an increased understanding of the modelling, dynamics, and control of direct drive, multi-pole, permanent magnet, synchronous generators for wind turbine applications. The study of the performance and likely comparative costs between fixed and variable speed operation of such a turbine has indicated variable speed operation as the way forward. However the fixed speed operation of the wind turbine should not be discounted where the cost of maintaining and installing the inverter is too prohibitive, for instance in offshore structures, nor if the predicted price reductions of IGBT technology do not materialise. A suite of simulation programs have been built and validated as much as possible which can now be used as a basis for a variety of projects to enhance the fixed or variable speed designs options further. Future work for the first option should concentrate on generator redesign to reduce the number of tiers to give mode 1 operation and concentrate on control strategies and inverter topologies that will require the least silicon for the second option.

References

- [1] P.B. Simpson, "Developments in Wind Turbine Technolgy," in *Proceedings of the Wind Energy Conference 94*, 1994.
- [2] E.W. Golding, *The Generation of Electricity by Wind Power*. Spon, 1976.
- [3] P.J.Musgrove, "Wind energy conversion-an introduction," *IEE Proceedings*, vol. 130, pp. 506-516, December 1983.
- [4] ETSU, "Strategic review of the renewable energy technologies - an economic review," tech. rep., ETSU report R13, 1982.
- [5] Various, "NFFO News," *Review*, vol. 21, pp. 16-17, December 1993.
- [6] Various, "NFFO News," *Review*, vol. 21, pp. 16-17, May 1995.
- [7] G.W. Braun and D.R. Smith, "Commercial Wind Power - Recent Experience in the United States," *Annual review of energy and the environment*, vol. 17, pp. 97-121, 1992.
- [8] Meridian, "Energy System Emissions and Material Requirements," tech. rep., DOE, 1989.
- [9] Various, "Wind Energy In the News," *Wind Directions*, vol. 8, no. 3, p. 16, 1994.
- [10] Various, "Wind Energy In the News," *Wind Directions*, vol. 14, no. 1, p. 11, 1994.
- [11] C. Stanton, "The visual impact and design of wind farms in the landscape," in *Proceedings of BWEA Annual Conference*, pp. 249-255, 1994.
- [12] A.R. McKenzie, "Assessment of tonal noise from wind turbines," in *Proceedings of the Wind Energy Conference 94*, 1994.

- [13] P. Gipe, "Apercu sur l'energie eolienne en Europe," *Systemes Solaires*, Paris 1994.
- [14] North Energy Associates, "Planners, academics and engineers on wind farm study tour," *Wind Directions*, vol. 14, no. 1, p. 10, 1994.
- [15] M. Trinick, "Best Practice in planning for wind energy development," in *Proceedings of BWEA Annual Conference*, pp. 155–157, 1994.
- [16] B.H. Chowdhury, "Assessment of the economic Value of Wind Generated Power to Electric Utilities," *Electric Power Systems Research*, vol. 21, pp. 33–42, 1991.
- [17] Editorial, "Wind Energy Economics," tech. rep., British Wind Energy Association, 1992.
- [18] Sorensen, *Renewable Energy*. Academic Press, 1979.
- [19] Andrew Garrad, *Wind Energy in Europe*. European Wind Energy Association, 1991.
- [20] I. Van Der Hoven, "Power spectrum of horizontal wind speeds in the frequency range from 0.0007 to 900 cycles per hour," *International Meteorology*, vol. 4, pp. 160–164, 1957.
- [21] F.Bonanno et al, "Analysis of hybrid generation system configurations utilising renewable sources," in *Proceedings of the 30th Universities Power Engineering Conference*, 1995.
- [22] J.G.F.Holland and G. Cramer, "Rathlin Island Wind/Diesel/Battery System," in *Proceedings of the International Conferenece on Renewable Energy*, 1993.
- [23] Editorial, "A comparison of several renewable energy sources," *Review*, November 1990.
- [24] D. Macnaughton, "Tidal Stream Turbine Development," in *Proceedings of the International Conference on Renewable Energy - Clean Power 2001*, pp. 67–71, 1993.
- [25] F.Barthorpe, "Wave power plugs into the grid," *Professional Engineering*, vol. 8, p. 25, August 1995.
- [26] Editorial, "Sunken Osprey gets a relacement," *Professional Engineering*, vol. 8, p. 5, September 1995.

- [27] Associated Press, "Australia points to a bright future for solar power," *Guardian Newspaper*, p. 17, November 1993.
- [28] R.J.Wheatley and J.J. Hedgecock, "Waste to energy in south east London," in *Proceedings of the International Conference on Renewable Energy - Clean Power 2001*, pp. 49-54, 1993.
- [29] S.H. Salter, "Changing the 1981 Spine Based Ducks," in *International Conference on Renewable Energy*, 1993.
- [30] R.A. Abduras, "Economic Aspects of Solar Technologies for Power Generation," in *International Conference on Renewable Energy*, 1993.
- [31] S. Collett, "The Wyre Barrage: The Pros and Cons," *Review*, vol. 19, pp. 14-16, Summer 1992.
- [32] G. Piepers, "News from Denmark," *Wind Directions*, vol. XIII, no. 3, pp. 20-21, 1994.
- [33] T.L. Shaw, "Present status and prospects for hydro-power generation in England and Wales," in *International Conference on Renewable Energy*, 1993.
- [34] P. Gipe, "Overview of worldwide wind generation," *Windnet*, April 1995.
- [35] D.J. Milborrow, "Wind energy economics," in *Proceedings of BWEA Annual Conference*, pp. 13-18, 1994.
- [36] R Harrison and G Jenkins, "Cost Modelling of Horizontal Axis Wind Turbines," tech. rep., Renewable Energy Centre, University of Sunderland, 1992.
- [37] Editorial Team, "WEG turbines fail in storm," *Wind Directions*, vol. 13, no. 3, p. 14, 1994.
- [38] W.E. Leithead, "A Comparison of the Performance of Constant Speed HAWT'S," in *Proceedings of the International Conferenece on Renewable Energy*, 1993.
- [39] *Proceedings of seminar on prospects and cost benefits of advanced HAWTS*, ETSU, 1994.
- [40] P.M. Anderson and A. Bose, "Stability Simulation of Wind Turbine Systems," *IEEE Transactions on Power Apparatus and Systems*, vol. 102, pp. 3791-3795, December 1983.

- [41] D.Spera, *Wind Turbine Technology*. ASME Press, 1994.
- [42] E. Spooner and A.C Williamson, "Permanent-Magnet Generators for Wind Power Applications," in *International Conference on Electrical Machines*, 1992.
- [43] E. Spooner, A.C Williamson, and L. Thompson, "Direct Drive, Grid Connected, Modular Permanent-Magnet Generators," in *Proceedings of the Wind Energy Conference 94*, 1994.
- [44] J. Hicklin and A. Grace, *Simulink*. Math Works INC., 1992.
- [45] E. Spooner and A.C Williamson, "Direct-Coupled, Permanent-Magnet Generators for Wind Turbine Applications," in *IEE-Proceedings B, Electric Power Applications*, Submitted 1994.
- [46] T.Alasuvanto and T. Jokinen, "Comparison of four different Permanent Magnet Rotor Constructions," in *International Conference on Electrical Machines*, pp. 1034–1039, 1990.
- [47] E. Spooner et al, "Development of a direct drive generator for wind energy applications." Final Report, January 1994.
- [48] Various, "North Wind 250," tech. rep., Northern Power Systems, 1994.
- [49] W.E. Leithead, "Dynamic characteristics of the drive-train: causes and effects," in *Proceedings of the 16th BWEA Wind Energy Conference*, 1994.
- [50] C.Zhang et al, "Simulation of dynamic electromechanical behaviour of a compliant wind power system," in *Proceedings of the Wind Energy Conference 94*, 1994.
- [51] A.J.G. Westlake and J.R.Bumby, "Design interactions of a flexible mounting for a permanent magnet, synchronous generator," in *7th International Conference on Electrical Machines and Drives*, 1995.
- [52] P. Jamieson and D. Mcleish, "The Howden-300 Wind Turbine," *IEE Proceedings - Part A*, vol. 130, pp. 550–554, December 1983.
- [53] E.J. Fordham, "The spatial structure of turbulence in the atmospheric boundary layer," *Wind Engineering*, vol. 9, no. 2, pp. 95–133, 1985.

- [54] D.M. Stoddard and F.S. Stoddard, *Wind Turbine Engineering Design*. Van Nostrand Reinhold, 1987.
- [55] Several, "European Wind Turbine Catalogue," tech. rep., Energy Centre, Denmark, 1994.
- [56] J.R. Connell, "The spectrum of wind speed fluctuations encountered by a rotating blade of a wind energy conversion system," *Solar Energy*, vol. 29, pp. 363–375, 1982.
- [57] Leif Kristensen and Sten Frandsen, "Model for the Power Spectra of the Blade of a Wind Turbine Measured from the Moving Frame of Reference," *Journal of Wind Engineering and Industrial Aerodynamics*, vol. 10, pp. 249–262, February 1982.
- [58] W.E. Leithead, "Effective Wind Speed Models for simple Wind Turbine Simulations," in *Proceedings of the 14th BWEA Wind Energy Conference*, 1992.
- [59] D.J. Sharpe, "Layman's guide to the aerodynamics of wind turbines," in *Proceedings of the International Symposium on Wind energy Systems*, pp. 229–242, September 1982.
- [60] O. Wasynczuk, D.T. Man, and J.P. Sullivan, "Dynamic Behaviour of a class of Wind Turbine Generator during random Wind Fluctuations," *IEEE Trans. on Power Apparatus and Systems*, vol. 100, pp. 2837–2845, June 1981.
- [61] A.G. Davenport, "Spectrum of horizontal gustiness near the ground in high winds," *Quarterly journal of the Royal Meteorological Society*, vol. 87, no. 3, pp. 194–211, 1961.
- [62] W.E. Holley et al, "Wind Turbulence Inputs for Horizontal Axis Wind Turbines," in *Proceedings of the Wind Turbine Dynamics Conference*, pp. 101–112, 1981.
- [63] J.C. Kaimal, "Turbulence spectra, Lebght scales and structure parameters in the stable surface layer," *Boundary Layer Meterology*, vol. 4, pp. 289–309, 1973.
- [64] S.Frandsen, "Flapwise extreme response of wind turbine blades to turbulence loading," in *Proceedings of BWEA Annual Conference*, 1988.
- [65] W.E. Leithead et al, "Wind Turbine Control Systems Modelling and Design Phase I and II - Appendix D," tech. rep., Industrial Control Unit, Univ. of Strathclyde, 1992.

- [66] E. Muljadi, "Wind data from 42m mast at NREL." Private communication, October 1995.
- [67] Stig-Øye, "Unsteady Wake Effects caused by pitch-angle changes," tech. rep., Technical University of Denmark, 1986.
- [68] S.J.R. Powles, *Horizontal Axis Wind Turbines*. PhD thesis, School of Engineering, Cambridge, 1983.
- [69] P.H. Madsen and Sten Frandsen, "Pitch Angle for Power Limitation," in *European Wind Energy Conference, Hamburg*, pp. 612-619, October 1984.
- [70] W.E. Leithead et al, "Wind Turbine Control Systems Modelling and Design Phase I and II," tech. rep., Industrial Control Unit, Univ. of Strathclyde, 1992.
- [71] E.A. Bossanyi, "Adaptive Pitch Control of a 250 Kw Wind Turbine," in *BWEA Conference on Wind Energy Conversion*, 1992.
- [72] W.E. Leithead, S. Delasalle, and D. Reardon, "Classical Control of Active Pitch Regulation of Constant Speed horizontal Axis Wind Turbines," *International Journal of Control*, vol. 55, no. 4, pp. 845-876, 1992.
- [73] N.Nise, *Control Systems Engineering*. The Benjamin/Cummings Publishing Company, 1992.
- [74] J. E. Slotine and L. Weiping, *Applied nonlinear control*. Prentice-Hall, 1991.
- [75] W.E. Leithead et al, "Simulation and investigation of the control dynamics of the Richborough HWP 55/1000," tech. rep., Industrial Control Unit, Univ. of Strathclyde, 1992.
- [76] E.Spooner, "WINDGEN2." Software program, September 1994.
- [77] M.Sarma, *Synchronous Machines - Theory and Stability*. Wiley, 1977.
- [78] H.Weih et al, "Design concepts and force generation in inverter fed synchronous machines with permanent magnet excitation," *IEEE Transactions on Magnetics*, vol. 20, pp. 1756-1761, September 1984.
- [79] G.R. Slemon and A. Straughen, *Electric Machines*. Addison Wesley, 1980.

- [80] McPherson and Laramore, *An introduction to electrical machines and transformers*. Wiley, 1990.
- [81] E. Spooner, A.C Williamson, and G. Catto, "Modular design of permanent-Magnet generators for wind turbines," in *IEE Proc.-Electr. Power Appl.*, Vol 143, No. 5, 1996.
- [82] J.Kirtley, "Armature motion damping for superconducting generators," *IEEE Transactions on Power Apparatus and Systems*, vol. 100, no. 100, pp. 2870–2877, 1981.
- [83] E. Spooner et al, "Development of a direct drive generator for wind energy applications." Intermediate Report, March 1992.
- [84] *EXCEL - Version 4.0*. MICROSOFT, 1992.
- [85] N.N. Hancock, *Matrix analysis of electrical machinery*. Pergamon Press, 1964.
- [86] A.Consoli and G Renna, "Interior type permanent magnet synchronous motor analysis by equivalent circuits," *IEEE Transactions on Energy Conversion*, vol. 4, pp. 681–689, December 1989.
- [87] F.Parasiliti and P. Poitet, "A model for saturation in high field permanent magnet synchronous motors," *IEEE Transactions on Energy Conversion*, vol. 4, pp. 487–494, December 1989.
- [88] G. Catto, *Direct Coupled Permanent Magnet Synchronous Generators*. PhD thesis, University of Manchester, Institute of Technology, 1994.
- [89] M.G. Say, *Alternating Current Machines*. Pitman International, 1978.
- [90] P.M. Anderson and A.A Fouad, *Power Systems Control and Stability*. Iowa State University Press, 1977.
- [91] J. Hicklin and A. Grace, *Control Systems Toolbox*. Math Works INC., 1992.
- [92] G. Catto, A.C Williamson, and E. Spooner, "Stabilising of Slow Speed Permanent Magnet Synchronous Generators by means of Mechanical Damping," in *International Conference on Electrical Machines*, Accepted for the 1994 conference.
- [93] System development consultancy group, "Engineering recommendation G59: recommendations for the connection of private generating plant to the electricity board's

- distribution systems,” tech. rep., The Electricity Council Chief Engineer’s Conference, 1985.
- [94] W.E. Leithead, “Dependence of performance of variable speed wind turbines on the turbulence, dynamics and control,” *IEE Proceedings*, vol. 137, pp. 403–413, November 1990.
 - [95] M.V. Lowson, “A new prediction model for wind turbine noise,” in *Proceedings of the International Conference on Renewable Energy - Clean Power 2001*, pp. 177–182, 1993.
 - [96] Z. Chen and E. Spooner, “A variable speed Permanent magnet wind turbine generator and it’s control,” in *30th Universities Power Engineering Conference*, vol. 2, pp. 517–520, 1995.
 - [97] Z. Chen and E. Spooner, “A modular, permanent-magnet generator for variable speed wind turbines,” in *Seventh International Conference on Electrical Machines and Drives*, 1995.
 - [98] *PSPICE*. Microsim Corporation, 1992.
 - [99] R.Jones and G.A. Smith, “High quality mains power from variable speed wind turbines,” in *Proceedings of the International Conference on Renewable Energy - Clean Power 2001*, pp. 202–206, 1993.
 - [100] B.W. Williams, *Power Electronics - Second Edition*. MacMillan, 1992.
 - [101] *IGBT rectifier handbook*. 1995.
 - [102] K. Thorborg, *Power Electronics*. Prentice Hall, 1988.
 - [103] Mohan et al, *Power Electronics: converters, applications and design*. Wiley, 1989.
 - [104] J.G. Kassakian et al, *Principles of Power Electronics*. Addison Wesley, 1991.
 - [105] N. Jenkins, “Embedded Generation,” *Power Engineering Journal*, vol. 9, no. 3, pp. 145–150, 1995.
 - [106] D. Milborrow, “What happens when the wind stops blowing,” *Wind Directions*, vol. XIV, no. 3, pp. 6–7, 1995.

- [107] Y. Tang and L. Xu, "A flexible active and reactive power control strategy for a variable speed constant frequency generating system," *IEEE Transactions on Power Electronics*, vol. 10, pp. 472–478, July 1995.
- [108] P. Novak et al, "Modeling and control of variable speed wind turbine drive system dynamics," *IEEE Control Systems*, pp. 28–37, August 1995.
- [109] Moscovice et al, *Cost Accounting with managerial applications - 5th Ed.* Houghton Mifflin, 1986.
- [110] F.P. Langley and G.S. Howdem, *Introduction to accounting for business - 5th Ed.* Butterworths, 1993.
- [111] M. McCulloch, *CASED*. M. McCulloch, 1995.
- [112] A. Westlake et al, "Damping the rotor angle oscillations of a permanent magnet wind generator," in *28th Universities Power Engineering Conference*, vol. 1, pp. 190–193, 1993.
- [113] A. Westlake, J.Bumby, and E.Spooner, "Damping power angle oscillations of a Permanent Magnet Generator with particular reference to Wind Turbine applications," in *IEE-Proceedings B, Electric Power Applications*, To be published 1996.
- [114] A. Westlake and J.R. Bumby, "Modelling a variable speed permanent magnet wind generator," in *30th Universities Power Engineering Conference*, vol. 1, pp. 29–32, 1995.
- [115] Vaicaitis, Rimas, Masanoba Shinozuka, and Masaru Takeno, "Parameter Study of Wind Loading on Structures," *Journal of the Structural Div., ASCE*, vol. 1, pp. 453–468, March 1973.

Appendix A

Wind Modelling Equations

This appendix contains all the key equations for the aerodynamic modelling of the wind and its interaction with a three blade wind turbine. Firstly the point wind speed equations are developed and secondly the spectral method is described.

A.1 Discrete Point Wind Model Equations

The total wind speed is given by,

$$U_{Wind} = U_{Base} + U_{Gust} + U_{Ramp} + U_{Noise} \quad (A.1)$$

The base wind component is given by,

$$U_{Base} = K_{Bm/s} \quad (A.2)$$

The gust wind component is described by the equation,

$$U_{Gust} = \begin{cases} 0 & t < T_{1G} \\ U_{cos} & T_{1G} < t < T_{2G} \\ 0 & t > T_{2G} \end{cases} \quad (A.3)$$

where,

$$\begin{aligned}
 U_{cos} &= (MAXG/2)(1 - \cos 2\pi[\frac{t}{T_G} - \frac{T_{1G}}{T_G}]) \\
 T_G &= \text{gust period in secs} \\
 T_{1G} &= \text{gust starting time in secs} \\
 MAXG &= \text{gust peak in m/s} \\
 t &= \text{time in secs}
 \end{aligned}$$

The ramp wind component is described by the equation,

$$U_{Ramp} = \begin{cases} 0 & t < T_{1R} \\ U_R & T_{1R} < t < T_{2R} \\ 0 & t > T_{2R} \end{cases} \quad (A.4)$$

where,

$$\begin{aligned}
 U_R &= MAXR(1 - \frac{t - T_{2R}}{T_{1R} - T_{2R}}) \\
 MAXR &= \text{ramp maximum in m/s} \\
 T_{1R} &= \text{ramp start time in secs} \\
 T_{2R} &= \text{ramp end time in secs}
 \end{aligned}$$

The noisy component is generated by a function of the form,

$$U_{Noise} = 2 \sum_{i=1}^N [S_v(\omega_i) \Delta\omega]^{0.5} \cos(\omega_i t + \phi_i) \quad (A.5)$$

where,

$$\omega_i = (i - 0.5)\Delta\omega \quad (A.6)$$

$$\phi_i = \text{random variable with uniform probability density on the interval } 0 \text{ to } 2\pi \quad (A.7)$$

and the function $S_v(\omega_i)$ is the spectral density function defined by Vaicaitis et al [115] by the equation,

$$S_v(\omega_i) = \frac{2K_N F^2 |\omega_i|}{\pi^2 [1 + (\frac{F\omega_i}{\mu\pi})^2]^{\frac{4}{3}}} \quad (\text{A.8})$$

where,

$$K_N = \text{surface drag coefficient} = 0.004$$

$$F = \text{turbulence scale, ft} = 2000$$

$$\mu = \text{mean speed of the wind at reference height, ft/s}$$

Various studies have shown that values of $N = 50$ and $\Delta\omega = 0.5 - 2.0\text{rad/s}$ provide results of excellent accuracy. The power from the wind is found by substituting the derived value of windspeed into the following equation with C_p evaluated at the correct value of tip speed ratio,

$$P_{shaft} = \frac{1}{2} \rho A C_p U_{wind}^3 \quad (\text{A.9})$$

A.2 Spectral method equations

The derivation of the spectral equations that are not included in the text are derived from [65] and the reader should consult this report for a full explanation as the derivations are quite complicated. However the necessary equations for the implementation on SIMULINK are now presented for completeness.

A.2.1 Spectral point wind speed equations

The spectral point wind speed is found from passing white noise through a first order filter which approximates the Von Karman spectrum. The Von Karman spectrum is given by,

$$S_u(\omega) = 0.475 \sigma_u^2 \frac{L\bar{U}^{-1}}{[1 + (\omega L\bar{U} - 1)^2]^{\frac{5}{6}}} \quad (\text{A.10})$$

The filter can be converted into a transfer function by substituting the laplace operator, s , in place of the $j\omega$ terms of the filter and this can then be implemented in the time domain as a series of interconnected integrators. The following first order differential equation can

be derived which represents the first order filter, W_{FS} , as introduced in section 2.1.7,

$$\dot{U}_{FS} = b_t W - a_t U_{FS} \quad (\text{A.11})$$

where U_{FS} is the wind output from the first order filter, b_t and a_t are coefficients as explained in Chapter 2 and W is the output from a white noise source with a variance of 1 and mean of zero.

The point wind speed is then given by,

$$U = U_{base} + U_{FS} \quad (\text{A.12})$$

A.2.2 Derivation of time domain equivalent of the spatial filter

The wind speed time history, U , is then passed through a spatial filter to represent the averaging of the free wind stream by the turbine blades. The spatial filter is given by,

$$W_{AV} = \frac{(\sqrt{2} + \lambda s)}{(\sqrt{2} + \sqrt{a}\lambda s)(1 + \frac{\lambda s}{\sqrt{a}})} \quad (\text{A.13})$$

and its conversion to a time domain equivalent is quite involved. The equation can be made equivalent to,

$$\frac{y_{out}}{y_{in}} = \frac{1 + T_1 s}{(1 + T_2 s)(1 + T_3 s)} \quad (\text{A.14})$$

where $T_{1,2,3}$ are factors evaluated for each mean windspeed according to the equation in Chapter 2 for λ . This equation can be multiplied out to give,

$$T_2 T_3 s^2 y_{out} + (T_2 + T_3) s y_{out} + y_{out} = y_{in} + T_1 s y_{in} \quad (\text{A.15})$$

This can be represented by the two first order differential equations,

$$\dot{x}_1 = \frac{y_{in}(T_2 T_3 - T_1(T_2 + T_3))}{(T_2 T_3)^2} - \frac{y_{out}}{T_2 T_3} - x_1 \frac{T_2 + T_3}{T_2 T_3} \quad (\text{A.16})$$

$$\dot{y}_{out} = x_1 + y_{in} \frac{T_1}{T_2 T_3} \quad (\text{A.17})$$

where x_1 is an intermediate state variable as a result of the second order transfer function. This has been implemented on SIMULINK and the model is shown in Figure A.1. The

effective wind speed experienced by the wind turbine blades is thus the output from the spatial filter, y_{out} . $T1t$, $T2t$, and $T3t$ are implemented as look up tables referenced by the mean wind speed. The rest of the functionality is there to implement equations A.16 and A.17.

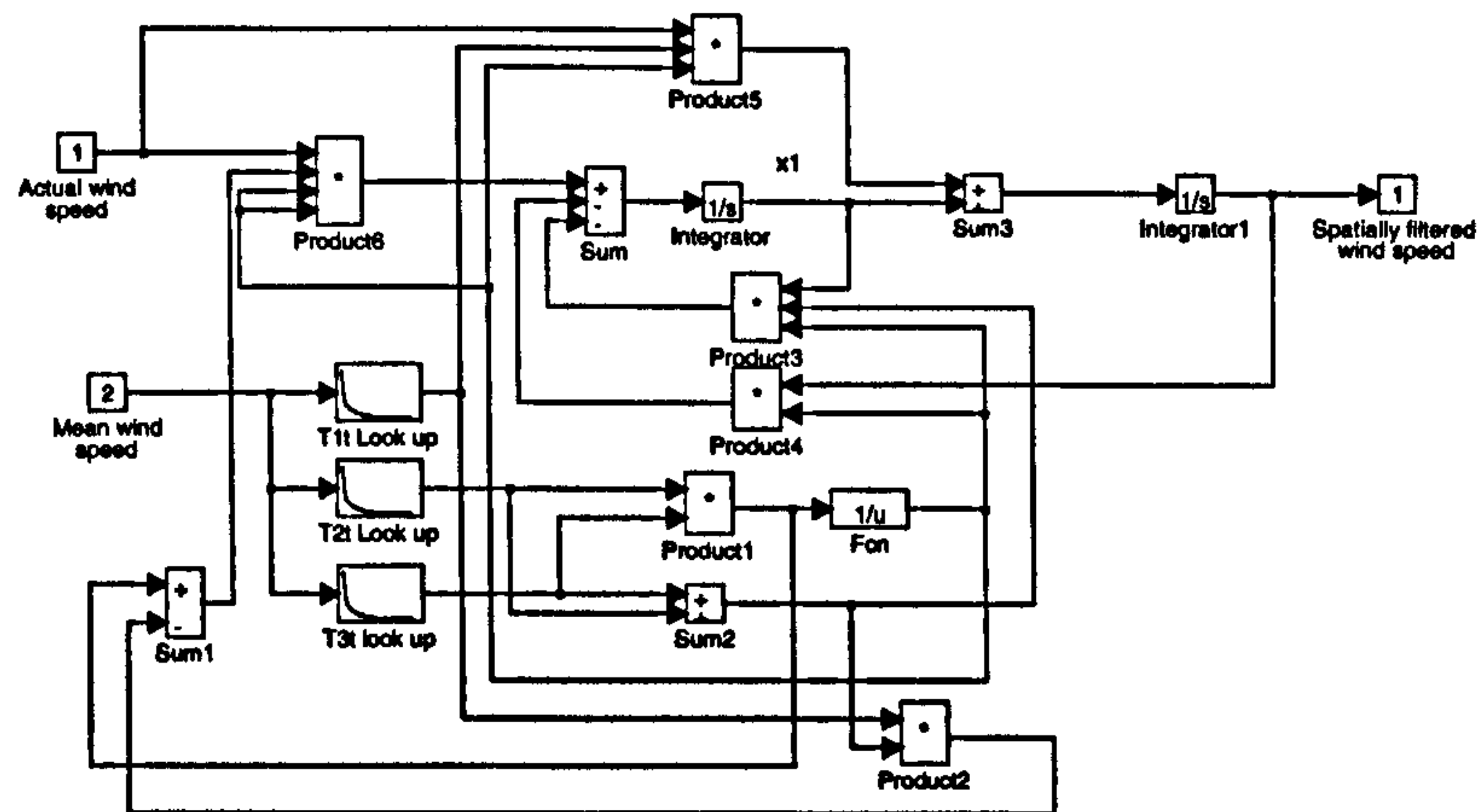


Figure A.1: SIMULINK model for the spatial filter

A.2.3 Power in the wind

The power from the wind is calculated in the same way as for the discrete model by substituting the derived value of the effective windspeed into the following equation with C_p evaluated at the correct value of tip speed ratio,

$$P_{shaft} = \frac{1}{2} \rho A C_p U_{wind}^3 \quad (A.18)$$

However two further effects can also be easily incorporated into the spectral method and the equations for these two effects will now be introduced.

A.2.4 Induction Lag

Induction lag is a first order effect and can be modelled by the transfer function of the form,

$$I = \frac{1 + As}{1 + \tau s} \quad (A.19)$$

which can be converted to,

$$\dot{x}_1 = -0.5\tau T_{hub} - \tau x_1 \quad (\text{A.20})$$

$$T_{ind} = x_1 + 1.5T_{hub} \quad (\text{A.21})$$

where τ is dependent on the blade radius and mean wind speed. This effect can be included in both the discrete and spectral point wind speed methods. The SIMULINK model for the induction lag effect is shown in Figure A.2.

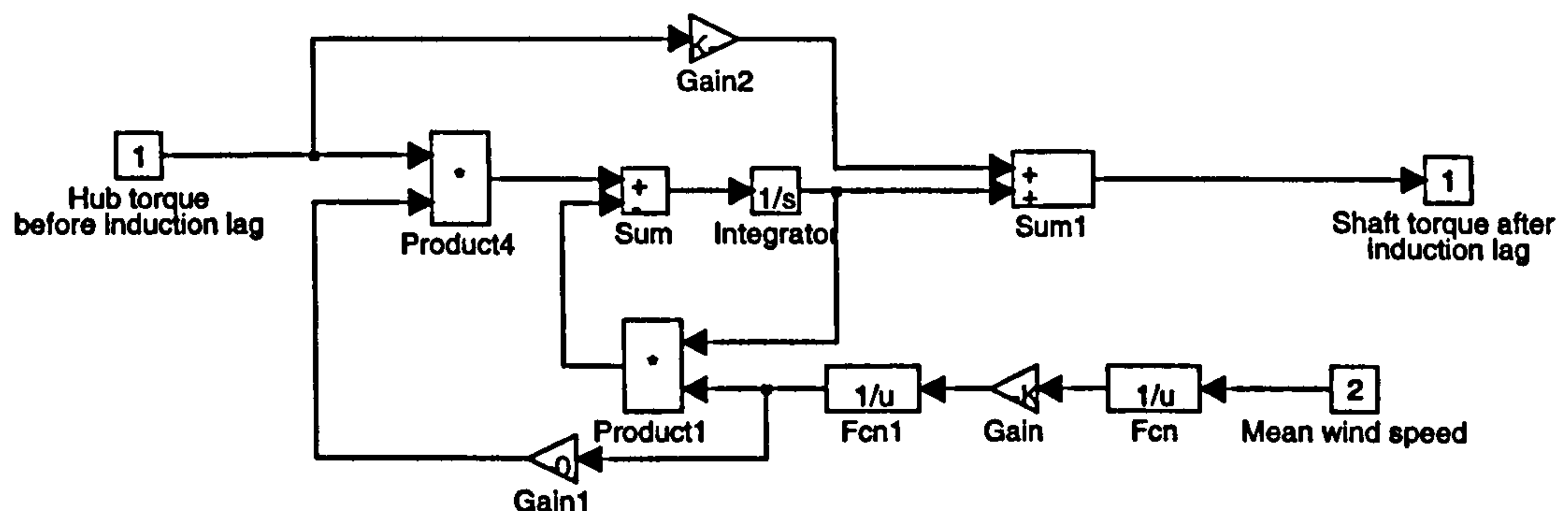


Figure A.2: SIMULINK model for the induction lag

A.2.5 Rotational Sampling

The rotational sampling of the free wind stream by the blades introduces spectral peaks into the spectrum of the induced torque at intervals of the blade rotational frequency. A pure sinusoidal oscillation of the form,

$$T = A \sin \omega_r \quad (\text{A.22})$$

has a spectrum which is a vertical line at the frequency of oscillation, ω_r , and would contribute the following variance,

$$Var = \frac{A^2}{2} \quad (\text{A.23})$$

However the effect of turbulence on the rotational sampling at $3\omega_r$ is spread about the spike at $3\omega_r$ and a method for determining the contribution to the variance of such a spread and its implementation on SIMULINK needs to be considered.

The rotational sampling at $3\omega_r$ can be represented by [65],

$$U_{3r}(t) = (A_{3r} + \epsilon_\alpha(t)) \cos 3\omega_r t + (A_{3r} + \epsilon_\beta(t)) \sin 3\omega_r t \quad (\text{A.24})$$

where A_{3r} is a constant and $\epsilon_\alpha(t)$ and $\epsilon_\beta(t)$ are the outputs of first order differential equations both driven by white noise,

$$\dot{\epsilon}_\alpha(t) = -a_{3r}\epsilon_\alpha(t) + b_{3r}W_\alpha(t) \quad (\text{A.25})$$

$$\dot{\epsilon}_\beta(t) = -a_{3r}\epsilon_\beta(t) + b_{3r}W_\beta(t) \quad (\text{A.26})$$

The reason for $\epsilon_\alpha(t)$ and $\epsilon_\beta(t)$ is to add random noise to the signal at $3\omega_r$ to achieve the desired spread in the power spectrum. The constants A_{3r} , a_{3r} , and b_{3r} are chosen to produce a power spectrum that agrees with representative site data. The variance contribution of the deterministic and stochastic peaks are given by,

$$Var_{peak} = A_{3r}^2 \quad (\text{A.27})$$

$$Var_{stch} = \frac{b_{3r}^2}{2a_{3r}} \quad (\text{A.28})$$

Therefore once the overall contribution to the variance of the individual components of the rotational sampling has been determined, usually by examining measured site data, it is quite a simple procedure to evaluate the component values from the above equations. The width of the stochastic spread about $3\omega_r$ is determined by a_{3r} and a value of 1.5 rads is typical. The SIMULINK block diagram for this effect is shown in Chapter 2.

Appendix B

The derivation of the governing equations of a permanent magnet, synchronous generator

This appendix contains the rigorous derivations of the multi-pole, permanent magnet, synchronous generator. The per unit system used in the following derivations is first outlined and then per unit model which includes all frequency effects is developed from the equations of the five winding model.

B.1 Per Units

The principle equations for the per unit system used in the fixed speed modelling of the permanent magnet synchronous generator are derived in the following sections for both the electrical and mechanical design variables.

B.1.1 Electrical per units

The two principle base quantities are for the voltage and power and are chosen as the r.m.s. voltage and rated three phase power respectively. These can then used to define the per

unit voltage and current,

$$V_{pu} = \frac{V_t}{V_{r.m.s}} \quad (B.1)$$

$$I_{pu} = \frac{S_{base}}{3V_{r.m.s}} \quad (B.2)$$

The equation for the per unit current is found from the governing equation for apparent power in a three phase system,

$$S = 3VI \quad (B.3)$$

This demonstrates the freedom in choosing the first base quantities and then the restrictions in specifying the subsequent values. The rest of the per unit relations will now be derived. From Ohm's Law the impedance base can now be defined,

$$Z_{base} = \frac{V_{base}}{I_{base}} \quad (B.4)$$

Hence the per unit reactances and resistances can be defined,

$$X_{dpu} = \frac{X_d}{Z_{base}} \quad (B.5)$$

$$X_{qpu} = \frac{X_q}{Z_{base}} \quad (B.6)$$

$$R_{pu} = \frac{R}{Z_{base}} \quad (B.7)$$

B.1.2 Mechanical per units

There are four variables that need to be converted to per units: the inertias of the stator and the rotor and the stiffness and damping of the compliant mounting.

The inertias are converted to per units by the following expression,

$$H_{pu} = \frac{\text{The sum of the kinetic energy of the rotating mass}}{S_{base}} \quad (B.8)$$

This leads to,

$$H_{pu} = \frac{0.5J\omega^2}{S_{base}} \quad (B.9)$$

B.2 --- Five winding governing equations

where the synchronous speed of the generator is given by,

$$\omega = \frac{2\omega_s}{n_p} \quad (\text{B.10})$$

The stiffness and the damping of the compliant mounting are defined in per unit terms as the torque per electrical radian and the torque per electrical radian per second. This is to fit into the torque equation properly. Hence converting from linear stiffness and damping to per unit values uses the following expression,

$$k_{pu} = \frac{k_{linear}}{r^2 T_r n_p} \quad (\text{B.11})$$

$$c_{pu} = \frac{c_{linear}}{r^2 T_r n_p} \quad (\text{B.12})$$

The rated torque is defined from the relation between mechanical power and angular speed.

$$T_r = \frac{S_{base}}{\omega_s} \quad (\text{B.13})$$

From this point forward all capitalised variables are per unit values on the r.m.s. base and all lower case variables are instantaneous values on the per unit r.m.s base.

B.2 Five winding governing equations

Assuming per unit notation and the current into the winding as positive, i.e. motor action, the flux linkages for the windings of the five winding model can be written,

For the armature:

$$\psi_d = L_{ad}i_f + L_{akd}i_{kd} + L_d i_d \quad (\text{B.14})$$

$$\psi_q = L_{akq}i_{kq} + L_q i_q \quad (\text{B.15})$$

For the rotor:

$$\psi_f = L_f i_f + L_{ad}i_d + L_{fkd}i_{kd} \quad (\text{B.16})$$

$$\psi_{kd} = L_{kd}i_{kd} + L_{fkd}i_f + L_{akd}i_d \quad (\text{B.17})$$

$$\psi_{kq} = L_{kq}i_{kq} + L_{akq}i_q \quad (\text{B.18})$$

while the voltage equations are,

$$v_f = r_f i_f + p\psi_f \quad (\text{B.19})$$

$$v_{kd} = r_{kd} i_{kd} + p\psi_{kd} \quad (\text{B.20})$$

$$v_{kq} = r_{kq} i_{kq} + p\psi_{kq} \quad (\text{B.21})$$

$$v_d = r_a i_d + p\psi_d - \omega\psi_q \quad (\text{B.22})$$

$$v_q = r_a i_q + p\psi_q + \omega\psi_d \quad (\text{B.23})$$

where the p operator denotes differential operation. Now often the reactance is used instead of inductance in the flux linkage equations. If this is done it is necessary to divide all the inductances in the above voltage equations by ω_0 to give,

$$v_f = r_f i_f + \frac{1}{\omega_0} p\psi_f \quad (\text{B.24})$$

$$v_{kd} = r_{kd} i_{kd} + \frac{1}{\omega_0} p\psi_{kd} \quad (\text{B.25})$$

$$v_{kq} = r_{kq} i_{kq} + \frac{1}{\omega_0} p\psi_{kq} \quad (\text{B.26})$$

$$v_d = r_a i_d + \frac{1}{\omega_0} p\psi_d - \frac{\omega}{\omega_0} \psi_q \quad (\text{B.27})$$

$$v_q = r_a i_q + p\psi_q + \frac{\omega}{\omega_0} \psi_d \quad (\text{B.28})$$

B.3 Three winding governing equations

The five winding model is reduced to a three winding model which represents the permanent magnet generator without damper windings. Assuming standard notation and the current into the winding as negative, i.e. generating action, the flux equations from the standard five winding model become,

$$\psi_d = K\phi_f + L_d i_d \quad (\text{B.29})$$

$$\psi_q = L_q i_q \quad (\text{B.30})$$

B.3 --- Three winding governing equations

and the voltage equations,

$$v_d = -r_a i_d - p\psi_d - \omega\psi_q \quad (\text{B.31})$$

$$v_q = -r_a i_q - p\psi_q + \omega\psi_d \quad (\text{B.32})$$

where all values are instantaneous values and from the phasor diagram and including the $dq0$ to abc transformation factor,

$$i_d = \sqrt{\frac{3}{2}}\sqrt{2}I_d = \sqrt{3}I_d \quad (\text{B.33})$$

$$i_q = \sqrt{\frac{3}{2}}\sqrt{2}I_q = \sqrt{3}I_q \quad (\text{B.34})$$

$$v_d = \sqrt{\frac{3}{2}}\sqrt{2}V_d = -\sqrt{3}V_b \sin \delta \quad (\text{B.35})$$

$$v_q = \sqrt{\frac{3}{2}}\sqrt{2}V_q = \sqrt{3}V_b \cos \delta \quad (\text{B.36})$$

Substituting the flux equations into the voltage equations and converting to reactances gives,

$$v_d = -r_a i_d - p(k\phi_f + \frac{1}{\omega_0}X_d i_d) - \frac{\omega}{\omega_0}X_q i_q \quad (\text{B.37})$$

$$v_q = -r_a i_q - p\frac{1}{\omega_0}X_q i_q + \omega k\phi_f + \frac{\omega}{\omega_0}X_d i_d \quad (\text{B.38})$$

leading to,

$$v_d = -r_a i_d - p\frac{1}{\omega_0}X_d i_d - \frac{\omega}{\omega_0}X_q i_q \quad (\text{B.39})$$

$$v_q = -r_a i_q - p\frac{1}{\omega_0}X_q i_q + \omega k\phi_f + \frac{\omega}{\omega_0}X_d i_d \quad (\text{B.40})$$

as the flux, $k\phi_f$, is constant with respect to time.

B.3.1 Derivation of expressions for pi_d and pi_q

The above voltage equations can be rearranged to give expressions for the first order differential equations governing i_d and i_q . Furthermore the relation between v_d and v_q to the

B.3 _____ Three winding governing equations

infinite bus voltage can also be incorporated leading to,

$$p_{i_d} = -\frac{\omega_0 r_a i_d}{X_d} - \frac{\omega X_q i_q}{X_d} + \frac{\omega_0 \sqrt{3} V_b \sin \delta}{X_d} \quad (\text{B.41})$$

$$p_{i_q} = -\frac{\omega_0 r_a i_q}{X_q} + \frac{\omega X_d i_d}{X_q} + \frac{\omega e}{X_q} - \frac{\omega_0 \sqrt{3} V_b \cos \delta}{X_q} \quad (\text{B.42})$$

where $e = k\phi_f \omega$ is the instantaneous emf generated by the magnets.

B.3.2 Electromagnetic Torque

The electromagnetic torque is found from a consideration of the electric power generated at the airgap. The instantaneous per unit power at the generator terminals is given by,

$$p_e = (v_d i_d + v_q i_q) \quad (\text{B.43})$$

assuming balanced operation. Substituting the expressions for v_d and v_q gives,

$$p_e = ((p\psi_d i_d + p\psi_q i_q) + r_a(i_d^2 + i_q^2) + (\psi_d i_q - \psi_q i_d)\omega) \quad (\text{B.44})$$

The first bracket term corresponds to the rate of change of the magnetic energy with respect to time, the second represents the stator resistance loss and the last represents the power transferred across the airgap. The airgap power is therefore given by,

$$p_{ag} = \omega_{ag}(\psi_d i_q - \psi_q i_d) \quad (\text{B.45})$$

Substituting the flux equations into this equation and converting to reactances leads to,

$$p_{ag} = \left(e i_q - i_q i_d (X_d - X_q) \frac{\omega_{ag}}{\omega_0} \right) \quad (\text{B.46})$$

The airgap power and electromagnetic torque are related by,

$$\tau_{ag} = \frac{p_{ag}}{\omega_{ag}} \quad (\text{B.47})$$

where the airgap rotational speed is given in mechanical radians as,

$$\omega_{ag} = \frac{1}{n_p} \left(\omega_0 + [\dot{\delta}_r - \dot{\delta}_s] \right) \quad (\text{B.48})$$

This leads to the expression for the airgap torque as,

$$\tau_{ag} = e i_q - i_q i_d (X_d - X_q) \frac{\omega_{ag}}{\omega_0} \quad (\text{B.49})$$

B.4 Initial Conditions

The derivation of the initial conditions for the non-linear simulation and linearisations is presented in the next few sections.

B.4.1 Initial values of i_d and i_q

The derivation of the initial values for the simulation is included here for the r.m.s. phasor currents which are related to i_{d_0} and i_{q_0} by,

$$i_{d_0} = \sqrt{3} I_{d_0} \quad (\text{B.50})$$

$$i_{q_0} = \sqrt{3} I_{q_0} \quad (\text{B.51})$$

The phasor diagram for the single wind turbine infinite bus system can be seen in Figure B.1.

Resolving in the d- and q-axis directions gives,

$$0 = V_b \sin \delta - I_d R - I_q X_q \quad (\text{B.52})$$

$$0 = E - V_b \cos \delta - I_q R + I_d X_d \quad (\text{B.53})$$

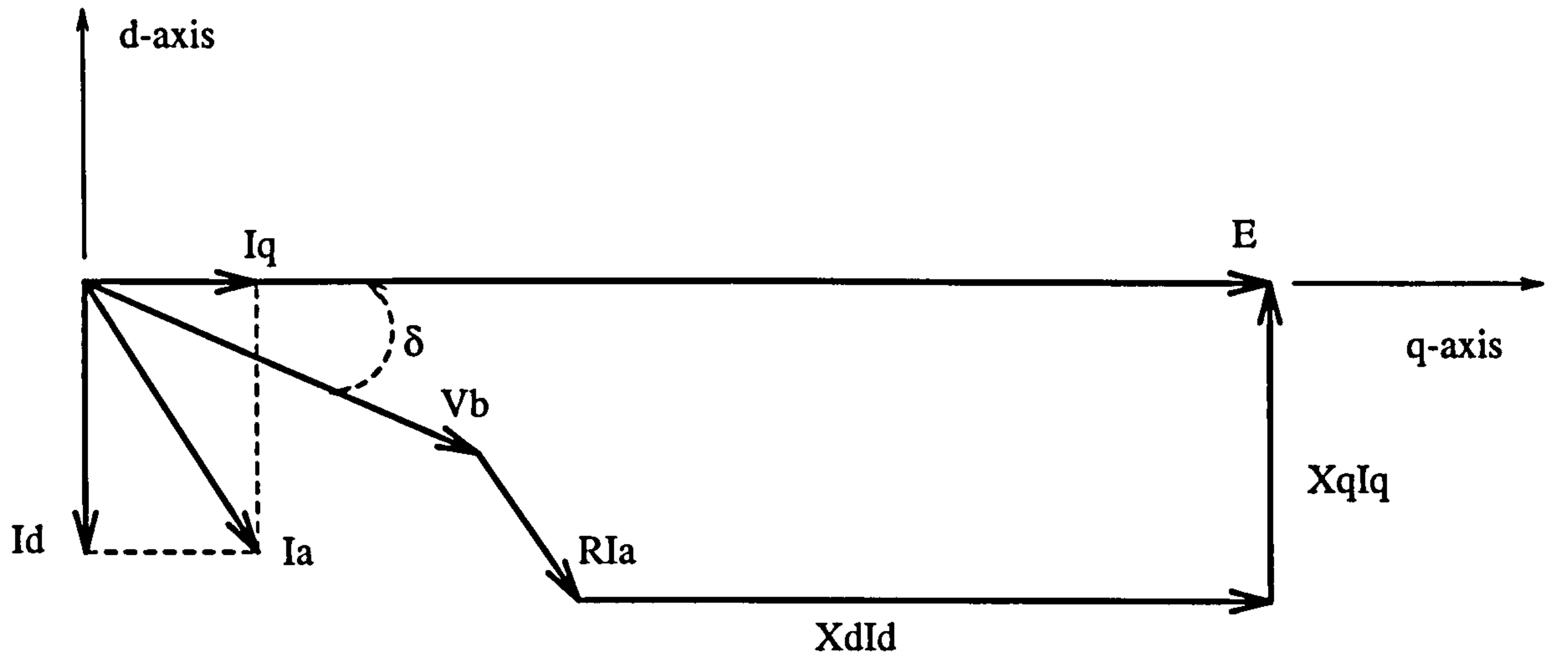


Figure B.1: The phasor diagram for single wind turbine infinite bus system

Multiplying the second equation by R/X_d gives,

$$\frac{RE}{X_d} - \frac{V_b R \cos \delta}{X_d} - \frac{I_q R^2}{X_d} + I_d R = 0 \quad (\text{B.54})$$

Adding this to the first equation gives,

$$V \sin \delta - I_q X_q + \frac{RE}{X_d} - \frac{V_b R \cos \delta}{X_d} - \frac{I_q R^2}{X_d} = 0 \quad (\text{B.55})$$

which rearranges to give an expression for I_q ,

$$I_q = \frac{X_d V_b \sin \delta + RE - V_b R \cos \delta}{X_q X_d + R^2} \quad (\text{B.56})$$

Rearranging the first equation gives an expression for I_d ,

$$I_d = -\frac{I_q X_q - V_b \sin \delta}{R} \quad (\text{B.57})$$

Substituting Equation B.56 gives,

$$I_d = -\frac{\left(\frac{X_d V_b \sin \delta + RE - V_b R \cos \delta}{X_q X_d + R^2}\right) X_q - V_b \sin \delta}{R} \quad (\text{B.58})$$

This can be rearranged to give,

$$I_d = -\frac{EX_q - V_b X_q \cos \delta - V_b R \sin \delta}{R^2 + X_d X_q} \quad (\text{B.59})$$

$$I_{q0} = \frac{X_d V_b \sin \delta_0 + R E - V_b R \cos \delta_0}{X_q X_d + R^2} \quad (\text{B.60})$$

$$I_{d0} = -\frac{E X_q - V_b X_q \cos \delta_0 - V_b R \sin \delta_0}{X_d X_q + R^2} \quad (\text{B.61})$$

where from now on the 0 subscript denotes an initial value.

B.4.2 Initial value of τ_{ag}

This can be calculated by substitution of i_{q0} and i_{d0} into equation B.49. For steady state conditions the mechanical driving torque equals the electromagnetic torque.

B.4.3 Initial value of δ_r and δ_s

At steady state the $\dot{\delta}$ and $\ddot{\delta}$ terms equal zero and hence the equation governing the stator reduces to,

$$0 = \frac{\omega_0}{2H_s} (\tau_{ag0} - k\delta_{s0}) \quad (\text{B.62})$$

i.e. the following holds true,

$$\delta_{s0} = \frac{\tau_{ag0}}{k} \quad (\text{B.63})$$

The initial rotor angle, δ_{r0} , is evaluated by definition as,

$$\delta_{r0} = \delta_0 + \delta_{s0} \quad (\text{B.64})$$

Appendix C

The theory behind linearisation

This appendix discusses the key approaches that can be used in finding some understanding of transient stability from the state space equations of any system but in particular synchronous machines.

C.1 Linearising the governing equations of a synchronous machine

Synchronous machines are non-linear devices due to the form of the output power equation and the effect of magnetic saturation. In order to study problems associated with dynamic stability a model linearised about some operating point is generally used [90].

When a power system is subjected to a small change in load it tends to acquire a new operating state. During the transition between the initial state and the new state the system behaviour is oscillatory. If the two states are such that all the state variables change only slightly (i.e., the variable x_i changes from x_{i0} to $x_{i0} + x_{i\Delta}$ where $x_{i\Delta}$ is a small change in x_i), the system is operating near the initial state. The initial state may be considered as the quiescent operating condition for the system.

To examine the behaviour of the system when it is perturbed such that the new and old equilibrium states are nearly equal, the system equations are linearised about the quiescent operating point, i.e. first order approximations are made for the system equations. The

C.1 ————— Linearising the governing equations of a synchronous machine

new linear equations are assumed to be valid near to the quiescent operating point.

The dynamic response of a linear system is determined by its characteristic equation. Both the forced response and the free response are decided by the roots of this equation. From a point of view of stability the free response gives the needed information. If it is stable any bounded input will give a bounded and therefore stable output.

The synchronous machine model developed earlier in the chapter has two types of nonlinearities: product nonlinearities and trigonometric functions. The first order approximations that hold for these are outlined below.

As an example of product linearities consider the term $x_i x_j$. Let the state variables have the initial values denoted x_{i0} and x_{j0} . Thus for a small change we get,

$$(x_{i0} + x_{i\Delta})(x_{j0} + x_{j\Delta}) = x_{i0}x_{j0} + x_{i0}x_{j\Delta} + x_{j0}x_{i\Delta} + x_{i\Delta}x_{j\Delta} \quad (\text{C.1})$$

The last term is a second order term which is assumed to be negligibly small. Thus as a first order approximation this equation becomes,

$$(x_{i0} + x_{i\Delta})(x_{j0} + x_{j\Delta}) = x_{i0}x_{j0} + x_{i0}x_{j\Delta} + x_{j0}x_{i\Delta} \quad (\text{C.2})$$

The trigonometric nonlinearities can be treated the same way as

$$\cos(\delta_0 + \delta_\Delta) = \cos \delta_0 \cos \delta_\Delta - \sin \delta_0 \sin \delta_\Delta \quad (\text{C.3})$$

with $\cos \delta_\Delta \cong 1$ and $\sin \delta_\Delta \cong \delta_{\Delta}$. Hence the incremental change in $\cos \delta$ is given by,

$$\cos(\delta_0 + \delta_\Delta) - \cos \delta_0 \cong -\sin \delta_0 \delta_\Delta \quad (\text{C.4})$$

Similarly for $\sin \delta$,

$$\sin(\delta_0 + \delta_\Delta) - \sin \delta_0 \cong \cos \delta_0 \delta_\Delta \quad (\text{C.5})$$

Now having defined a state space, x_0 , at time $t = t_0$ at the occurrence of a small disturbance the states will change slightly from their previous position or values. Thus,

$$x = x_0 + x_\Delta \quad (\text{C.6})$$

C.2 --- Linearising the three winding model

The state space model is in the form,

$$\dot{x} = f(x, t) \quad (\text{C.7})$$

which on substituting C.6 gives,

$$\dot{x}_0 + \dot{x}_\Delta = f(x_0 + x_\Delta, t) \quad (\text{C.8})$$

Expanding this and ignoring second order terms leads to the equation,

$$\dot{x}_0 + \dot{x}_\Delta \cong f(x_0, t) + A(x_0)x_\Delta + B(x_0)u \quad (\text{C.9})$$

from which the linearised state space equation is found to be,

$$\dot{x}_\Delta = A(x_0)x_\Delta + B(x_0)u \quad (\text{C.10})$$

The elements of the A matrix depend upon the initial conditions of the state vector x_0 . The dynamic properties of the system are determined from the nature of the eigenvalues of the A matrix.

C.2 Linearising the three winding model

The governing equations presented in Appendix C for the three winding model of a permanent magnet, synchronous generator can be linearised according to the methods laid out in the previous section to develop the state space expression,

$$\dot{x} = [A]x + [B]u \quad (\text{C.11})$$

where the state variables are defined,

$$x_1 = i_d \quad (\text{C.12})$$

$$x_2 = i_q \quad (\text{C.13})$$

$$x_3 = \delta \quad (\text{C.14})$$

$$x_4 = \dot{\delta} \quad (\text{C.15})$$

$$x_5 = \delta_s \quad (C.16)$$

$$x_6 = \dot{\delta}_s \quad (C.17)$$

$$(C.18)$$

The linearised governing equations are,

$$\Delta v_d = -\sqrt{3}V_b \cos \delta \quad (C.19)$$

$$\Delta v_q = -\sqrt{3}V_b \sin \delta \quad (C.20)$$

$$\Delta \dot{i}_d = -\frac{\omega_0 r_a}{X_d} \Delta i_d - \frac{\omega_0 X_q}{X_d} \Delta i_q - \frac{X_q \sqrt{3} I_{q0}}{X_d} \Delta \omega + \frac{\omega_0 \sqrt{3} V_b \cos \delta_0}{X_d} \Delta \delta \quad (C.21)$$

$$\Delta \dot{i}_q = -\frac{\omega_0 r_a}{X_q} \Delta i_q + \frac{\sqrt{3} E}{X_q} \Delta \omega + \frac{\omega_0 X_d}{X_q} \Delta i_d - \frac{X_d \sqrt{3} I_{d0}}{X_q} \Delta \omega + \frac{\omega_0 \sqrt{3} V_b \sin \delta_0}{X_q} \Delta \delta \quad (C.22)$$

$$\Delta \tau_{ag} = [\sqrt{3} E \Delta i_q - \sqrt{3} I_{d0} \Delta i_q (X_d - X_q) - \Delta i_d \sqrt{3} I_{q0} (X_d - X_q)] \quad (C.23)$$

$$\Delta \ddot{\delta} = \frac{\omega_0}{2H_r} (\Delta \tau_m - \Delta \tau_{ag}) - \frac{\omega_0}{2H_s} (\Delta \tau_{ag} - c \Delta \dot{\delta}_s - k \Delta \delta_s) \quad (C.24)$$

$$\Delta \ddot{\delta}_s = \frac{\omega_0}{2H_s} (\Delta \tau_{ag} - c \Delta \dot{\delta}_s - k \Delta \delta_s) \quad (C.25)$$

$$\Delta \delta = \Delta \delta_r - \Delta \delta_s \quad (C.26)$$

These equations can be expressed in the standard form of equation C.11 with the plant matrix, $[A]$, given by, Putting this correction into the state space form gives,

$$[A] = \begin{bmatrix} -\frac{\omega_0 r_a}{X_d} & -\frac{X_q \omega_0}{X_d} & \frac{\omega_0 \sqrt{3} V_b \cos \delta_0}{X_d} & -\frac{X_q \sqrt{3} I_{q0}}{X_d} & 0 & 0 \\ \frac{\omega_0 X_d}{X_q} & -\frac{\omega_0 r_a}{X_q} & \frac{\omega_0 \sqrt{3} V_b \sin \delta_0}{X_q} & \frac{E + X_d \sqrt{3} I_{d0}}{X_q} & 0 & 0 \\ 0 & 0 & 0 & 1 & 0 & 0 \\ \frac{\omega_0}{2} (\frac{1}{H_r} + \frac{1}{H_s}) \sqrt{3} I_{q0} (X_d - X_q) & \frac{\omega_0}{2} (\frac{1}{H_r} + \frac{1}{H_s}) \sqrt{3} E - \sqrt{3} I_{d0} (X_d - X_q) & 0 & 0 & \frac{\omega_0 k}{2H_s} & \frac{\omega_0 c}{2H_s} \\ 0 & 0 & 0 & 0 & 0 & 1 \\ -\frac{\omega_0 \sqrt{3} I_{q0} (X_d - X_q)}{2H_s} & \frac{\omega_0 (\sqrt{3} E - \sqrt{3} I_{d0} (X_d - X_q))}{2H_s} & 0 & 0 & \frac{-\omega_0 k}{2H_s} & \frac{-\omega_0 c}{2H_s} \end{bmatrix} \quad (C.27)$$

whilst the driving matrix, $[B]$, is given by,

$$[B] = \begin{bmatrix} 0 \\ 0 \\ 0 \\ \frac{\omega_0 \Delta \tau_m}{2H_r} \\ 0 \\ 0 \end{bmatrix} \quad (C.28)$$

Appendix D

The theory of a variable speed operated generator

This appendix contains equations for the variable speed operated permanent magnet generator and in particular the equations for the modelling of the capacitor compensated E-core and rectifier circuit. These equations are contained in WINDVARD and WINDVARP, the programs used to design and predict the performance of the variable speed operated permanent magnet generator.

D.1 Power flow by the phasor method

In order to choose a suitable value for the tuning capacitance in the circuit of Figure 5.9, it is necessary to find a method to simulate the performance of the circuit at rated frequency and power for a range of capacitance values. This method should be quick and easy to compute and provide an estimate for the power flow into and out of the E-core, tuning capacitor and rectifier arrangement. This can be done by constructing and then analysing the phasor diagram of the circuit assuming that all the real current flows into the rectifier and therefore only reactive current flows in the tuning capacitor. The phasor diagram can be seen in Figure D.1. The analysis of the phasor diagram assumes a sinusoidal E-core emf, \bar{E}_f , and this is adequate for such an estimation.

To solve this phasor diagram for \bar{I}_c and ϕ and thus the rated and peak power of the E-core

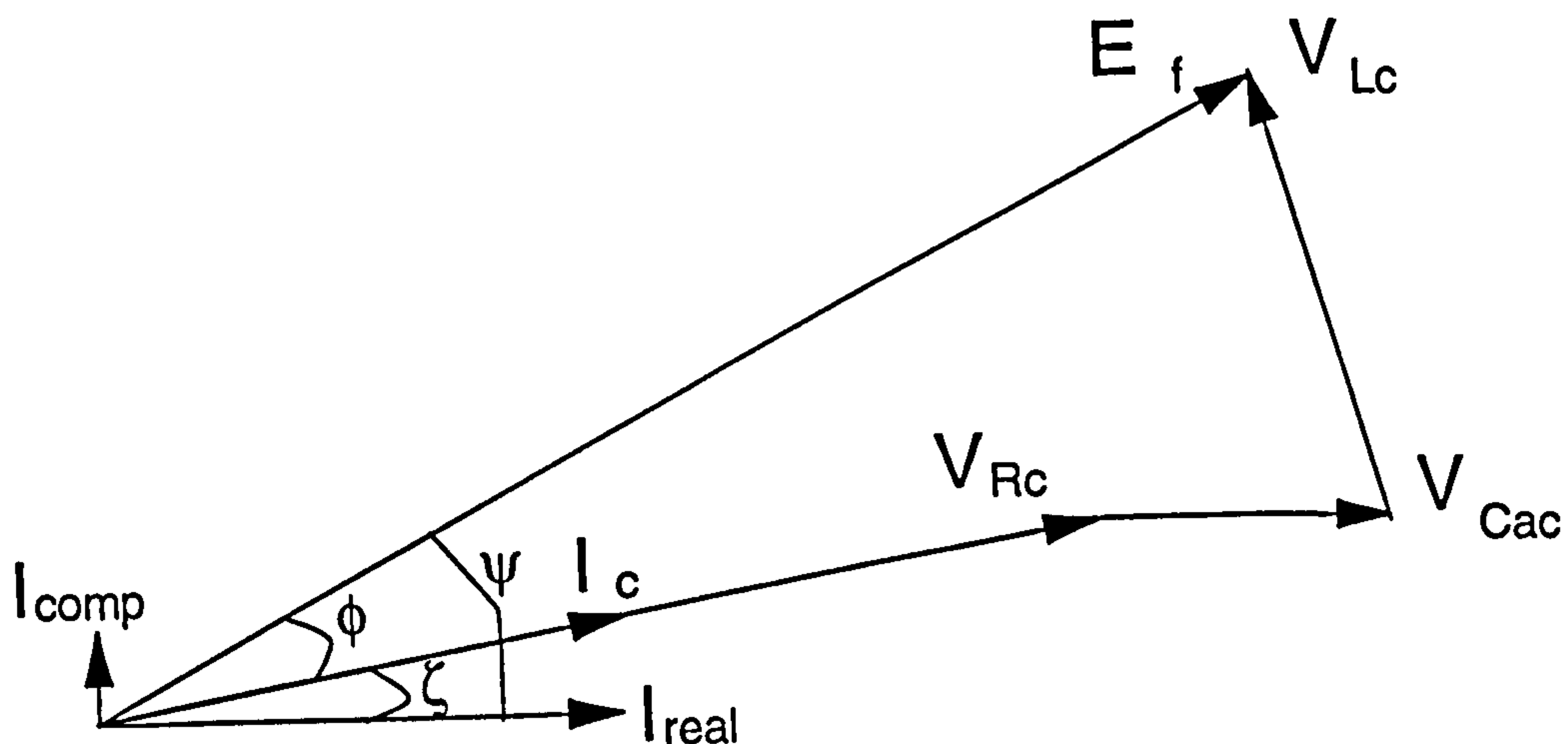


Figure D.1: Phasor diagram of the E-core and tuning capacitor circuit

at rated frequency requires an iterative process to determine the balanced conditions of the circuit. The governing equation of the phasor diagram is found from a consideration of the voltage balance in the circuit and this is given by,

$$\bar{E}_f = \bar{V}_{Cac} + \bar{V}_{Rc} + \bar{V}_{Lc} \quad (D.1)$$

The magnitude of \bar{E}_f is set to equal the rated module emf at rated frequency. This is calculated from the magnetic circuit analysis. The initial values of \bar{V}_{Cac} , \bar{V}_{Rc} and \bar{V}_{Lc} must be set and then the value for \bar{V}_{Cac} changed at each iteration step to determine the voltage balance. This voltage balance is made more complicated by the phase relation between each of the voltage phasors and the current, \bar{I}_c , flowing in the circuit. The current flowing within the circuit must not exceed the rated module current from thermal considerations. In the first iteration, it is assumed that the real part of the complex current \bar{I}_c is given by,

$$I_{real} = \frac{E_f}{R_c} \quad (D.2)$$

The impedance of the inductance and capacitance can be evaluated for rated frequency. Then the voltage drop across the resistance is given by,

$$V_{R_c} = I_{real} * R_c \quad (D.3)$$

Assuming that initially the complex part of \bar{I}_c equals half the real part, the magnitude of the voltages across the capacitor and inductance are given by,

$$V_{C_{ac}} = \frac{I_{real}}{\pi f C_{ac}} \quad (D.4)$$

$$V_{L_c} = I_{real} \pi f L_c \quad (D.5)$$

At every subsequent iteration step, $V_{C_{ac}}$ is altered either up or down depending on the balance between the right hand and left hand sides of equation D.1. The initial iteration step size is half the value of $V_{C_{ac}}$ and this is reduced by half at the end of each iteration. The magnitude of the complex current is calculated by,

$$I_{comp} = V_{C_{ac}} 2\pi f C_{ac} \quad (D.6)$$

If the complex current flowing in the circuit is greater than the maximum rated thermal current, $V_{C_{ac}}$ is reduced and the next iteration is initiated. This ensures that a voltage balance is avoided where no real current could flow without violating the thermal limit of the module. If the complex current is less than the limit, the corresponding real current is calculated, assuming that full rated current is flowing by,

$$I_{real} = \sqrt{I_{therm}^2 - I_{comp}^2} \quad (D.7)$$

A voltage balance is then performed by comparing the square of the left and right hand sides of equation D.1. If the right hand side is greater than the left, $V_{C_{ac}}$ is reduced by the iteration voltage step and vice versa. The iteration voltage step is then reduced by half, the real and imaginary parts of current, \bar{I}_c , are recalculated and the process repeated until the value of \bar{I}_c flowing in the circuit equals the rated thermal current of the E-core and the equation D.1 is balanced. The rated thermal current is found from a consideration of the size of the E-core, the heat dissipated in the winding, the capacity of the conduction

paths to remove this generated heat and the maximum allowed operating temperature of the E-core. The power in the E-core is then given by,

$$P_{therm} = E_f I_c \cos(\phi) \quad (D.8)$$

The angle ϕ can be calculated by the expression,

$$\phi = \psi - \zeta \quad (D.9)$$

where ψ and ζ are given by,

$$\zeta = \arctan\left(\frac{I_{comp}}{I_{real}}\right) \quad (D.10)$$

$$\psi = \arctan\left(\frac{RI_{comp} + X_{Lc}I_{real}}{I_{real}R_c + V_{Cac} - X_{Lc}I_{comp}}\right) \quad (D.11)$$

The maximum possible power that can be transmitted through the E-core and rectifier arrangement can then be found from a consideration of the Thevenin equivalent of the circuit shown in Figure 5.9. The peak power can be calculated from,

$$P_{max} = \frac{V_{thev}^2}{Z_{thev}} \quad (D.12)$$

where V_{thev} is the Thevenin equivalent source voltage and Z_{thev} is the equivalent impedance of the tuning circuit.

Once the rated and peak power of the E-core have been estimated for a range of capacitance values, a value for the tuning capacitance can be chosen. This value is chosen to match the required rated power per module at rated frequency to the power per module from the shaft and provide a reasonable peak power transfer capability. A more accurate prediction of the performance of the capacitor compensated E-core and rectifier, over the full operating range of the wind turbine, can then be determined from non-linear simulations with the tuning capacitance at the chosen value.

D.2 Time stepping solution of the capacitor compensated E-core and rectifier

D.2 Time stepping solution of the capacitor compensated E-core and rectifier

The equations for the time stepping procedure that is used to predict the accurate performance of the capacitor compensated E-core and rectifier arrangement are outlined in this section. The program WINDVARD performs this analysis at each desired step in rotor speed and dc link voltage over the user specified range. The equation governing the performance of the circuit shown in Figure 5.9 can be arranged to be of the form,

$$\frac{dI_c}{dt} = \frac{1}{L_c}(E_f - V_{Cac} - I_c R_c) \quad (D.13)$$

This differential equation for I_c needs to be solved together with the differential equation for the voltage across the capacitor, V_{Cac} and taking into account the operation of the bridge rectifier. The differential equation for V_{Cac} is,

$$\frac{dV_{Cac}}{dt} = \frac{I_c}{2\pi f C_{ac}} \quad (D.14)$$

The solution for the system is not as simple as finding the solution to the RLC circuit because the rectifier has several modes of operation, forward or reverse bias and switched on or off. This means that at every time interval the state of the rectifier must be determined and the governing equations altered accordingly. This is done by comparing the voltage across the capacitor with the dc link voltage and, depending on whether I_c is positive or negative, determining the switch on and off point of the rectifier. The differential equations are solved using an Euler integration routine. The instantaneous value for E_f is found at each time interval by summing the contribution of the odd harmonic voltages, predicted by the magnetic circuit analysis, at the phase angle corresponding to the elapsed simulation time.

Initially the currents are all set to zero. The equations are solved using 100 steps per half cycle. Once the mean value for I_c and that injected into the dc link, I_{dc} , has built up and stabilised at a steady value the values for power flow within the circuit can be found. Firstly the values for I_c^2 and I_{dc} are averaged over the last half cycle to give the rms and mean values respectively. These are then used in the following equations to give the values

D.2 Time stepping solution of the capacitor compensated E-core and rectifier

for the power flow through the module,

$$P_{out} = V_{dc}I_{dc} \quad (D.15)$$

$$P_{copper} = I_c^2 R_c \quad (D.16)$$

$$P_{iron} = \frac{\text{Feloss} * \text{freq}}{\text{Nominal Frequency}} \quad (D.17)$$

$$P_{diode} = I_{dc}V_{diode} \quad (D.18)$$

$$P_{in} = P_{out} + P_{copper} + P_{iron} + P_{diode} \quad (D.19)$$

$$effy = \frac{P_{out}}{P_{in}} \quad (D.20)$$

The quantity, Feloss, is the calculated iron loss at rated frequency due to the fluxes flowing in the ferromagnetic material of the E-core. It is assumed that this varies proportionally with frequency. The steady state values for the power flow within the E-core and rectifier are then formed into 2D lookup tables, indexed by rotor speed and dc link voltage, and are used in the simulation of the variable speed permanent magnet generator as described in Chapter 5. The airgap power table is created from the values stored in P_{in} and the injected dc link current table can be calculated by dividing the P_{out} table by the corresponding dc link voltage.

Appendix E

The derivation of the governing equations of an induction generator plus gearbox

This appendix contains the derivations of the governing equations of an induction generator plus gearbox taken from [65]. The key equations which model the system are first outlined and then the derivation of the initial conditions for the simulation model is presented.

E.1 Governing equations

The low speed shaft speed is governed by the standard equation from Newtons second law applied to rotational systems,

$$\dot{\omega}_{ls} = \frac{1}{J_{ls}} (T_{q_{rtr}} - T_{q_{ls}} - c_{ls}\omega_{ls}) \quad (\text{E.1})$$

where the difference in driving torque and reaction torque referred to the low speed side of the gearbox, $T_{q_{rtr}} - T_{q_{ls}}$, divided by the low speed inertia, which includes the inertia of the turbine blades, gives the shaft acceleration. A low speed shaft damping factor is included to represent friction and other losses in the drive train. The reaction torque is converted to

the driving torque side of the wind turbine gearbox, the low speed shaft torque, by,

$$\dot{T}_{qls} = \frac{k_{ls} (\omega_{ls} - \frac{\omega_{ld}}{N})}{1 + \frac{k_{ls}}{k_{hs} N^2}} \quad (\text{E.2})$$

This equation is derived by considering the linked torsional system of the low and high speed shafts and the gearbox coupling. It assumes that the difference in rotational speeds of the low speed shaft compared to the high speed shaft referred to the low speed side is small. The high speed shaft torque is found from standard induction motor theory assuming very low slip and a torque-speed curve which is linear in this region with gradient T_{qspcv} . This leads to,

$$\dot{T}_{qld} = \frac{1}{\tau_{ld}} (T_{qspcvslip} - T_{qld}) \quad (\text{E.3})$$

The induction generator's electrical time constant, τ_{ld} , determines the rate at which the high speed shaft torque can change. Finally the high speed shaft speed is given by Newton's Second Law but now for the generator and high speed shaft,

$$\dot{\omega}_{ld} = \frac{1}{J_{hs}} \left(\frac{T_{qls}}{N} - T_{qld} - c_{hs} \omega_{ld} \right) \quad (\text{E.4})$$

E.2 Initial conditions

The initial conditions for the induction generator plus gearbox arrangement driven by a wind turbine are set by following this procedure. Firstly the initial power in the wind is found from,

$$P_0 = 0.5 \rho A C_p U_{w_0}^3 \quad (\text{E.5})$$

which corresponds to a rotor driving torque of,

$$T_{q_{rtr0}} = \frac{P}{\omega_{ls0}} \quad (\text{E.6})$$

where the 0 denotes an initial condition. Now the reaction torque to balance this driving torque is dependent on the slip of the induction generator and therefore an iterative process

is required to find the shaft speed, ω_{ls_0} , that gives the required slip.

The initial conditions from equation D.1 to D.4 are found from rearranging,

$$(T_{q_{rtr_0}} - T_{q_{ls_0}} - c_{ls}\omega_{ls_0}) = 0 \quad (\text{E.7})$$

$$\omega_{ls_0} - \frac{\omega_{ld_0}}{N} = 0 \quad (\text{E.8})$$

$$(T_{q_{spcv}} \times \text{slip}_0 - T_{q_{ld_0}}) = 0 \quad (\text{E.9})$$

$$\left(\frac{T_{q_{ls_0}}}{N} - T_{q_{ld_0}} - c_{hs}\omega_{ld_0} \right) = 0 \quad (\text{E.10})$$

and solving by a process of substitution to give,

$$\omega_{ld_0} = \frac{T_{q_{rtr_0}} + NT_{q_{spcv}}\omega}{(Nc_{hs} + \frac{c_{ls}}{N} + NT_{q_{spcv}})} \quad (\text{E.11})$$

from which all the other initial conditions can be found by iterating until the initial conditions for D.1 balance.

